

**INTERNATIONAL COUNCIL FOR RESEARCH AND INNOVATION
IN BUILDING AND CONSTRUCTION**

WORKING COMMISSION W18 - TIMBER STRUCTURES

CIB - W18

MEETING FORTY-THREE

NELSON

NEW ZEALAND

AUGUST 2010

Ingenieurholzbau und Baukonstruktionen
Karlsruhe Institute of Technology
Germany
Compiled by Rainer Görlacher
2010

ISSN 1864-1784

CONTENTS

1. Chairman's Introduction
2. General Topics
3. Loading Codes
4. Test Methods
5. Serviceability
6. Glued Joints
7. Fire
8. Structural Stability
9. Laminated Members
10. Timber Joints and Fasteners
11. Stresses for Solid Timber
12. Stress Grading
13. Any Other Business
14. Venue and Program for Next Meeting
15. Close
16. Peer Review of Papers for the CIB-W18 Proceedings
17. List of CIB-W18 Papers Nelson, New Zealand 2010
18. Current List of CIB-W18 Papers

CIB-W18 Papers 43-5-1 up to 43101-1

0 List of Participants

**INTERNATIONAL COUNCIL FOR RESEARCH AND INNOVATION
IN BUILDING AND CONSTRUCTION
WORKING COMMISSION W18 - TIMBER STRUCTURES**

**MEETING FORTY-THREE
Nelson, New Zealand, 22 - 26 August 2010**

LIST OF PARTICIPANTS

AUSTRALIA

K Crews	University of Technology, Dural
L Daziel	CADE Systems, Koo Wee Rup
C Gerber	University of Technology, Sydney
T Gibney	Timber Imagineering, Melbourne
R Nestic	Tim Gibney and Associates, Melbourne

DENMARK

H J Larsen	Copenhagen
J Munch-Andersen	Danish Timber Information, Lyngby

FINLAND

T Poutanen	Tampere University of Technology
------------	----------------------------------

FRANCE

C Faye	FCBA, Bordeaux
F Rouger	FCBA, Paris

GERMANY

S Aicher	MPA University Stuttgart
H J Blaß	Karlsruhe Institute of Technology (KIT)
M Frese	Karlsruhe Institute of Technology (KIT)
R Görlacher	Karlsruhe Institute of Technology (KIT)
P Schädle	Karlsruhe Institute of Technology (KIT)
P Stapel	TU München
T Uibel	Karlsruhe Institute of Technology (KIT)
S Winter	TU München

ITALY

A Ceccotti	IVALSA-CNR
M Fragiaco	University of Sassari, Alghero

JAPAN

M Yasumura	Shizuoka University
------------	---------------------

NEW ZEALAND

M Ardalany	University of Canterbury, Christchurch
W Banks	Carter Holt Havey, Auckland
G Beattie	BRANZ, Porirua
A Buchanan	University of Canterbury, Christchurch
D Carradine	University of Canterbury, Christchurch
M Cusiel	University of Canterbury, Christchurch
B Franke	University of Auckland
S Franke	University of Auckland
S Giorgini	University of Canterbury, Christchurch
M Jamil	University of Auckland
J Jensen	University of Auckland
H Morris	University of Auckland
P Moss	University of Canterbury, Christchurch
J O'Neill	University of Canterbury, Christchurch
A Palermo	University of Canterbury, Christchurch
P Quenneville	University of Auckland
C Rodger	CHH Woodproducts, Auckland
F Scheibmair	University of Auckland
W Van Beerschoten	University of Canterbury, Christchurch
B Walford	SCIOIN Rotorua
P Zarnami	University of Auckland

SWEDEN

R Crocetti	Lund University
J Schmid	SP Trätek, Stockholm

SWITZERLAND

T Tannert	Berner Fachhochschule, Biel
-----------	-----------------------------

THE NETHERLANDS

A Jorissen	TU Eindhoven
------------	--------------

UNITED KINGDOM

R Harris	University of Bath
----------	--------------------

USA

T Skaggs	American Plywood Association, Tacoma
B Yeh	American Plywood Association, Tacoma

- 1. Chairman's Introduction**
- 2. General Topics**
- 3. Loading Codes**
- 4. Test Methods**
- 5. Serviceability**
- 6. Glued Joints**
- 7. Fire**
- 8. Structural Stability**
- 9. Laminated Members**
- 10. Timber Joints and Fasteners**
- 11. Stresses for Solid Timber**
- 12. Stress Grading**
- 13. Any Other Business**
- 14. Venue and Program for Next Meeting**
- 15. Close**
- 16. Peer Review of Papers for the
CIB-W18 Proceedings**

**INTERNATIONAL COUNCIL FOR RESEARCH AND INNOVATION
IN BUILDING AND CONSTRUCTION**

WORKING COMMISSION W18 - TIMBER STRUCTURES

MEETING FORTY-THREE

NELSON, NEW ZEALAND

22 AUGUST – 26 AUGUST 2010

**MINUTES
(P Quenneville)**

1 CHAIRMAN'S INTRODUCTION

H Blass welcomed the delegates to the 43rd CIB-W18 Meeting in Nelson, New Zealand. He thanked Andy Buchanan and David Carradine for hosting the meeting.

Twenty seven papers will be presented this year. The presentations are limited to 20 minutes each, allowing time for meaningful discussions after each paper. The Chair asked the presenters to conclude the presentation with a general proposal or statements concerning impact of the research results on existing or future potential application and development in codes and standards. R Görlacher will deal with questions regarding the meeting proceedings.

Papers brought directly to the meeting would not be accepted for presentation, discussions, or publication. Papers presented by non-authors or non-co-authors are not recommended except in exceptional situations because the discussion process might be compromised.

2 GENERAL TOPICS

H Larsen made a proposal regarding research notes:

One of the reasons for the high quality of the CIB-W18 papers and the success of the meetings is the strict procedures that have been established: papers shall relate to Eurocode 5 or other design codes, summaries are required for acceptance 6 months before the next meetings, there are good editorial guidelines for the papers and final papers are (after being checked by the secretariat) available for downloading a month before the meeting, there is a reasonable time for presenting and discussing the papers, and the papers are made available in proceedings where also the minutes are summarised. The quality is also documented by the fact that many papers later appear in peer-reviewed journals.

The established procedures have, however, also drawbacks. Some are: If you find out that you would rather present some newer ideas or findings you have to wait another year and you have to enlarge interesting ideas to a 10- pages scientific paper.

I, therefore, suggest that we introduce a new type of papers that could be called Notes and allow time for discussing them, e.g. 2 hours allowing presentation of up to 8 notes. The author should bring copies of the notes for distribution at the beginning of the meeting and they should be included in the Proceedings.

As examples may be mentioned:

- *Information on the background for Eurocode 5 clauses where they are not based on CIB-W18 work. Clause 6.18 for example gives a shape factor for torsion that is in conflict with the only CIB W18 Paper, viz. Paper 7-6-1: K Möhler, Strength and long-term behaviour of lumber and glued laminated timber under torsion loads.*
- *Papers that only contain information but not knowledge. As an example may be mentioned test result for basic properties, e.g. embedding strength. The results are very valuable and should be reported in a CIB-paper, but the scientific content is meagre.*
- *Proposals for new research.*
- *Information about new materials and fasteners and their properties.*
- *New design methods.*

H Blass recommended considering H Larsen's proposal. Authors are being notified about the new possibility by the minutes of CIB-W18. The working commission will observe how it develops in the coming years.

A Jorissen gave an overview regarding the Structural Eurocodes. He described the schedule of changes, the maintenance procedures and publications related to the Eurocodes as well as the future developments. J Munch-Andersen mentioned the topic of robustness with regard to the Eurocodes.

S Winter gave an overview regarding European Standardisation on the supporting standards (CEN TC 124). The following topics were discussed:

- list of all standards
- status of harmonization
- examples (shear) on consequences of each of harmonization.

P Quenneville asked whether there will be a central authority in Europe. S Winter answered that this is lacking. A Jorissen sees a move towards central jurisdiction. A Palermo mentioned EN standards and EC5. A Jorissen stated that some countries did already accept EC5 others are still to follow. H Blass mentioned the positive effect of moving towards one EC. This has caused the national design codes to become much more similar. A complete harmonisation is not there yet but there is a move in this direction.

3 LOADING CODES

43 - 101- 1 Dependant versus Independent Loads in Structural Design - T Poutanen

Presented by T Poutanen

T Poutanen said that there are mistakes in the paper but that the presentation content is correct.

A Buchanan asked whether the author had this discussion about dependant and independent loads with other materials organizations. What was the response? T Poutanen answered he had presented it in May but without response and dialogue.

J Munch-Andersen: I still do not understand that loads are to be dependant on strength. T Poutanen: those do not believe in this can have a look at reliability book and will see that loads are not independent. Loads are dependent on the structure.

T Tannert: if considering loads independent is unsafe, why are we not experiencing more failures? T Poutanen: At most 20% unsafe. Therefore failures are not observe in practice.

S Winter: Will the paper be corrected? T Poutanen: Yes.

4 TEST METHODS

43 - 21 - 1 Estimation of Load-Bearing Capacity of Timber Connections - J Munch-Andersen, J D Sørensen, F Sørensen

Presented by J Munch-Andersen

A Jorissen: Questioned non-safety of D-8 in EC. J Munch-Andersen: Eurocode method allows connections to be taken into account.

H Blass: how to standardize smart, honest and stupid sampling? J Munch-Andersen: that is impossible and to be avoided.

H Larsen: that proposal is too late as new approach (unsafe) is already adopted.

43 - 21 - 2 A New Method to Determine Suitable Spacings and Distances for Self-tapping Screws - T Uibel, H J Blass

Presented by T Uibel

B Walford: Did he check crack growth and weathering? T Uibel: No, only cracks due to insertion and short term behaviour were studied.

A Jorissen: Will distances recommendation be made? H Blass: This procedure is already in place in a CUAP for ETAs for self-drilling screws.

P Quenneville: what about multi-screw in a row? T. Uibel: Procedure works also for multiple screws in rows or columns.

S Aicher: Crack growth and in-service crack growth: have you addressed this? H Blass: no, only short term behaviour was studied.

J Schmidt: effect of density? Why results not symmetrical? T. Uibel: density is not known in service. The screw was inserted between the end grain and the second screw.

H Morris: dye in split sample - How is it done? T Uibel: remove screw and insert ink.

S Franke: diagram difference between predicted and actual split. T Uibel: caused by natural variability.

R Harris: EC rule about row screw offset and effect. H Blass: No influence of offset.

R Harris: effect of grain direction - is it investigated? T Uibel: tests were performed with different grain directions. Influence is about 10%.

F Rouger: how to simulate split area? T Uibel: Using springs representing cracking behaviour.

J Munch-Andersen: drilling tips and effect. T Uibel: not significant.

S Winter: good method and danger of providing very detailed spacing recommendations. H Blass: producers want detailed rules for non-pre-drilled screws.

S Aicher: single screw results and offset effect: he recommends offset. H. J. Blass: The offset certainly does not harm and is beneficial for nails and screws in non-predrilled holes.

5 SERVICEABILITY

43 - 20 - 1 The Long Term Instrumentation of a Timber Building in Nelson NZ - the Need for Standardisation - H W Morris, S R Uma, K Gledhill, P Omenzetter, M Worth

Presented by H W Morris

B Yeh: how is segregation of vertical movement done? H W Morris: can't be done in current set up.

B Yeh: history of vertical movement?

A Buchanan: is moisture content of wood measured?

A Ceccotti: how do dissipating devices work? H W Morris describes the principle and refers to explanations during the visit of the building site.

A Palermo: moisture and creep measurements? H W Morris: will be difficult.

M Fragiaco: long-term measurements of MC for LVL and experience are available at Canterbury.

P Schädle: Is a performance-based or a force-based design in use? A Palermo: displacement-based design has been used in this case.

M Fragiaco comments about flexibility of joint at portal frames and his experience at University of Canterbury.

M Frese asks about slide 18 – compression stress distribution at bottom of shear wall?

A Palermo states that a uniform stress under pre-stress and a linear distribution under rocking were assumed.

S Aicher: maximum stress at corner. Design or ultimate strength? A Buchanan: ask designer in afternoon presentation

6 **GLUED JOINTS**

43 - 18 - 1 Comparison of API, RF and MUF Adhesives Using a Draft Australian/New Zealand Standard - B Walford

Presented by B Walford

S Aicher: why re-invent new classification system and not adapt from European ones? B Walford: not reinvention but borrowing from others.

7 **FIRE**

43 - 16 - 2 Fire Exposed Cross-Laminated Timber - Modelling and Tests - J Schmid, J König

Presented by J Schmid

H Blass: one dimensional model should not apply to lintel. J Schmid: It does not.

S Winter does not agree with statement that EC5 is unsafe. Fire design always is rough prediction and 10% difference should be acceptable. In multi-span, d_0 would be different for tension and compression portion; this would be too complicated. J Schmid: this is what is done for concrete design.

S Winter: predictions are for strength. What about deflection governed designs?

S Aicher: do figures apply to CLT with glued edges? J Schmid: if edges are opened, charring rate increases.

S Winter: charring rate is hard to establish. Higher if edges are open but char expands and closes gaps.

B Yeh: is the delamination layer important? J Schmid: Yes, as the charring rate will increase for a while.

43 - 16 - 3 Timber-Concrete Composite Floors in Fire - J O'Neill, D Carradine, R Dhakal, P J Moss, A H Buchanan, M Fragiaco

Presented by D Carradine

S Winter: how were LVL beams connected? D Carradine: screwed together

S Winter: where were screws located? D Carradine: too low! ~ 75 mm from the bottom. It is also important to use fully-threaded screws.

B Yeh: why use size of LVL and not 200 mm to verify theory developed? D Carradine: users of this technology wanted to verify the fire rating for cold designs.

B Yeh: fire regulation would not let extrapolation of results from 400 to 200. A Buchanan: in NZ, extrapolation is possible.

T Gibney: why use so much reinforcing steel in concrete topping? A Buchanan: to satisfy seismic design.

A Palermo: what about continuous slabs and the connection concrete/wood? D. Carradine: not to be considered at the moment (Need to assess priority of next variable).

43 - 16 - 4 Light Timber Frame Construction with Solid Timber Members – Application of the Reduced Cross-section Method - J König, J Schmid

Presented by J Schmid

No Questions

8 STRUCTURAL STABILITY

43 - 15 - 1 Influence of the Boundary Conditions on the Racking Strength of Shear Walls with an Opening - M Yasumura

Presented by M Yasumura

L Dalziel: What are consequences of multiple openings? M Yasumura: would be more complicated. Not being studied.

L Dalziel: Software was developed for multiple openings.

S Franke: does model allow “negative” uplift? M Yasumura: negative uplift is for sheeting only.

H Blass: springs elements for sheeting connections? M Yasumura: yes, and polygonal.

T Gibney: Where tie-down forces measured and what were they? M Yasumura: No, forces where not measured.

T Gibney: were lateral displacements measured? M Yasumura: Yes and always good correlation with model.

S Aicher: Why tension force is approximately constant? M Yasumura: Longer walls can resist higher lateral forces and tensile forces are more or less constant.

43 - 15 - 2 Influence of Different Standards on the Determination of Earthquake Properties of Timber Shear Wall Systems - P Schädle, H Blass

Presented by P Schädle

A Ceccotti: Congratulations for nice work. H Blass should ask TC250 for a new proposal for timber construction for EC 8.

A Jorissen: Is it possible to have a uniform test method for timber elements? P Schädle: Yes, two tests are needed – connector and entire wall.

A Palermo: One should not refer to 1st cycle, only to 2nd and 3rd because of strength degradation. Were simulated earthquakes reflecting the requirements of EC 8? P Schädle: Yes.

A Palermo: Why use force-based analysis? P Schädle - test standard in Germany is still force based.

M Fragiacomio: were tests performed with wall components? P Schädle: No, with entire shear walls.

43 - 15 - 4 Optimized Anchor-Bolt Spacing for Structural Panel Shearwalls Subjected to Combined Shear and Wind Uplift Forces - B Yeh, E Keith, T Skaggs

Presented by B Yeh

P Quenneville: what is the effect of doubling the sill plate? B Yeh: it would work but construction industry does not want to trim all studs.

M Yasumura: In tests, how do you control the vertical forces? B Yeh: Lateral and vertical forces can be controlled to remain constant. There are no standard test methods but perhaps ISO can initiate this.

H Morris: Was the 1.2m spacing tested? B Yeh: It has been in use for almost 50 years.

43 - 15 - 5 Full-Scale Shear Wall Tests for Force Transfer around Openings - T Skaggs, B Yeh, F Lam

Presented by T Skaggs

L Daziel: Are the forces measured in the opening where the strap is loaded in compression only? T Skaggs: No. sometimes in tension and also shear as well. It is also a cycle test. When in compression, the straps are not mobilized.

R Crocetti: Are straps only on one side (outside)? T Skaggs: Yes, only on the outside

P Schädle: Testing method. How much time does it take for the entire test? T Skaggs: from 2 sec – 2 mins. At slow rate, strap forces are a bit less but this is not due to rate.

G Beattie: Modelling wood and earthquake. I recommend the fast loading.

L Daziel: was there any difference in strap forces for different opening size? T Skaggs: this effect has not been analyzed yet. It will be available in the future.

9 LAMINATED MEMBERS

43 – 12 – 1 Fatigue Behaviour of Finger Jointed Lumber - S Aicher, G Stapf

Presented by S Aicher

R Crocetti: were failures in joints or in lumber? S Aicher: Mostly (about 90%) in joints. Some were in lumber at knots.

R Crocetti: The ratio is closer to 0 for lumber. Why use 0.5? S Aicher: Design offices for roller coaster asked for testing at this value. Testing currently being done is at 0.1

T Poutanen: for other glues, would results be different? S Aicher: 1 comp. Polyurethane performs better.

J Schmid: for joint failures, are they due to glue? S Aicher: no, always in the fingers.

T Tannert: do you have indication that moisture factor proposed is dependant on moisture cycling? S Aicher: hard to say but moisture content factor is based on average moisture content.

43 - 12 - 3 *System Effects in Glued Laminated Timber in Tension and Bending* - M Frese, H Blass

Presented by M Frese

A Jorissen: Is the length factor (observed for tension members) valid for bending as well?

M Frese: No. Length factor is for tension only.

R Nestic: In the numerical model, did lamination have different behaviour. M Frese: Yes, each 150mm segments behave differently

S Aicher: What is failure? M Frese: Failure in outer lamination (bending) in lumber or finger – joint.

S Winter: Is the effect really a volume effect for which the tension is the main significant one?

T Poutanen: How do you model the timber in compression? M Frese: the behaviour is modelled as linear-elastic.

T Poutanen: do you assume that failure occurs in compression? H Blass: No. It does not make a difference in the 5th% value. Tension failure is critical on the 5%-level.

L Daziel: Is the multiple-span factor a recommendation? M Frese: Yes! What about spans of different length? M Frese: We do not know at this point what the effect of different span length is.

43 - 12 - 4 *Experimental Investigations on Mechanical Behaviour of Glued Solid timber* - C Faye, F Rouger, P Garcia

Presented by C Faye

H Larsen: Why are the E values higher for some of the configuration? C Faye: It may be due to system effect.

H Larsen: Since averages are taken, E should not change.

R Crocetti: In transversely pre-stressed bridge decks, higher E values are also obtained.

43 - 12 - 5 *Experimental and Numerical Investigation on the Shear Strength of Glulam* - R Crocetti, P J Gustafsson, H Danielsson, A Emilsson, S Ormarsson

Presented by R Crocetti

H Larsen: Tests should be done using EN408 so that results can be corrected. Other methods are more complicated and EN408 is the simplest. R Crocetti: You may be right but EN408 method is not always successful.

R Nestic: Have you compared results with ASTM tests? R Crocetti: No, but beam tests method is higher than small specimens' tests

B Yeh: People assume that glulam shear values are for ASTM method but this is not the case. How to induce shear in a beam with overhangs when there are no shear within these parts? R Crocetti: It does occur.

S Aicher: Did you try to evaluate k_{cr} value for specimens with cracks? R Crocetti: It was not our intention.

T Poutanen: Shear values obtained look high in comparison to the ones in use. Do you agree? R Crocetti: No.

A Manoorchehr: How is the notch made in the specimens?

R Crocetti: using band saw. The cracks forces the stresses to start

L Daziel: When putting UDL on un-glued laminations, the same capacity was obtained because of friction. The shear capacity was observed as negligible.

10 TIMBER JOINTS AND FASTENERS

43 - 7 - 1 *Probabilistic Capacity Prediction of Timber Joints under Brittle Failure Modes* - **T Tannert, T Vallée, and F Lam**

Presented by T Tannert

H Blass: Did you consider failure in header for dovetail joint? T Tannert: we avoided it in our testing program to verify the method.

H Larsen: Anisotropic materials are nasty materials. Anisotropy introduces secondary stresses. One must start and evaluate material parameters every time. T Tannert: Yes, FE analyses are very complex but material parameters do not have to be evaluated every time. Material parameters can be taken from tables.

H Larsen: why calling it probabilistic? T Tannert: It is more stochastic and certainly not deterministic.

S Aicher: What is sensitivity to volume? T Tannert: not sensitive if one changes volume and scales material parameters accordingly.

43 - 7 - 2 *Ductility in Timber Structures* - **A Jorissen, M Fragiaco**

Presented by A Jorissen

H Larsen: Not in agreement with capacity based concept.

A Palermo: It is good to have presentation like this but what about structural systems?

H Blass: how does one expect to have large moments and ductility in beam as shown in Gerber system?

T Poutanen: Assuming 2 structures and one is brittle and one ductile. How much is the ductile one better? A Jorissen: hard to put a number but the steel and concrete industry are using this concept.

P Quenneville: how to force connections to control this design? M Fragiaco: the ductility is to be forced only through system design, not component design.

A Ceccotti: In EC 8, safety coefficient for timber is to be 1 for brittle, 1.3 ductile.

A Buchanan: Not in agreement with paper. The authors are trying to use seismic concepts in non seismic situations.

43 - 7 - 3 *Design of Mechanically Jointed Composite Concrete-Timber Beams Taking into Account the Plastic Behaviour of the Fasteners* - **H J Larsen, A Ceccotti, H Riberholt**

Presented by H Larsen

H Blass: Discrepancy between interpretations of some of the behaviour of some connectors. H Larsen: Will be reviewed.

B Walford: Not a good idea to have plastic behaviour of connector for bridges. H Larsen: this is a suggestion for the design, not the actual behaviour.

43 - 7 - 4 *Design of Timber-Concrete Composite Beams with Notched Connections* - **M Fragiaco, D Yeoh**

Presented by M Fragiaco

R Nistic: What about long term? M Fragiaco: There are long term tests in progress and results will be published.

H Larsen: This concept is hard to use as fasteners are far too strong and stiff. Notches suggested are expensive as well.

H Blass: Some of the data used in reference was done with shear strength of 1/3 the characteristic values for shear.

A Palermo: How will MC and fatigue affect serviceability issues? M Fragiaco: MC increase is not substantial in wood.

S Franke: Tests in Weimar showed that MC increase is not deep in timber. M Fragiaco: Increase in MC in wood is not a problem for wood, but loss of moisture from concrete is a problem.

43 - 7 - 5 *Development of Design Procedures for Timber Concrete Composite Floors in Australia and New Zealand* - **K Crews, C Gerber**

Presented by C Gerber

H Blass: what is an S notch? C Gerber: A notch with rounded edges. A diagram will be added to the paper.

P Quenneville: What is a batten connection? C Gerber: A diagram will be added to the paper.

S Aicher: How to derive the K stiffness for the fasteners? C Gerber: From connection tests. Linear regression from separate results, not floor test.

S Winter: Hard to get information from paper and presentation. More information is needed to follow procedures. K Crews: An 80 page report will be available.

H Larsen: why would one want a simplified method? C Gerber: in Australia, they want simple methods. K Crews: A design tool is needed and will be made available.

T Tannert: We also teach TCC and suggest getting away from Gamma Method as it is too complicated. K Crews: A method in a design tool (spreadsheet) will be what is used.

M Fragiaco: Length will influence some factors. Some values in tables are not

compatible with NZ Design. How to explain? C Gerber: Tabled values were adjusted between Australia and NZ.

43 - 7 - 6 Failure Behaviour and Resistance of Dowel-Type Connections Loaded Perpendicular to Grain - B Franke, P Quenneville

Presented by P Quenneville

A Jorissen: Is there still splitting at $a/h = 0.7$? P Quenneville: there could be. Model gives proper load-slip curve and failure criterion is used (first occurrence of splitting or 5% offset).

R Crocetti: Laboratory results may be simulated, but in practice this type of connection should be avoided. P Quenneville: Reinforcement will be avoided due to cost.

T Tannert: Numerical study is 2D. What would be the influence of 3D? P Quenneville: 3D would be more favourable to a ductile behaviour.

R Görlacher: Have you compared results to the C1B- paper of 1989? B Franke: No, comparison was to code equations.

M Yasumura: What is the failure criterion? B Franke: failure (in splitting) is maximum load when crack becomes unstable.

L Daziel: here Steel-Wood-Steel connection is shown, in practice Steel-Wood is often used. What will be the influence? P Quenneville: Possible embedment and 3D model would be needed.

A Palermo: How did you verify the model for the cohesive part? B Franke: No calibration was carried out, average values for Canadian glulam code were used.

A Manoorchehr: What was the thickness of the cohesive elements? B Franke: no thickness at all.

P Schädle: which element type was used? B Franke: Element no.174 in ANSYS.

43 - 7 - 7 Post-Tensioned Timber Frames and Beams - S Giorgini, A Neale, A Palermo, D Carradine, S Pampanin, A H Buchanan

Presented by A Palermo

B Yeh: What about moisture effects? A Palermo: Some experimental work is being done where moisture is being monitored but this is taken care in k_{def} .

A Jorissen: You are introducing aging effect. Why? A Palermo: The procedure is borrowed from concrete technology. Integration of pre-stress and losses is taken into account with time and this allows one not to do experimental tests.

T Gibney: What strands are being used? A Palermo: 7-wire strands

S Aicher: any monitoring of pool post-tensioned beams? A Palermo: No. Not allowed.

S Winter: What about corrosion prevention in pool building? A Palermo: Grease and plastic membrane were used.

T Poutanen: Is there economical benefit analysis to this technology? A Palermo: Done for a bridge deck. Same costs. Some reduction in timber section size.

R Crocetti: Should look at what has been done in timber bridge decks to minimize pre-stress losses. A Palermo: Agree. Several stressing cycles may be required and this may be difficult for frames. To be considered.

M Fragiaco: experimental data for frames is required to confirm analytical work. A Palermo: agree, especially for frames.

43 - 7 - 8 Simplified Design of Post-tensioned Timber Buildings - M Newcombe, M Cusiél, S Pampanin, A Palermo, A H Buchanan

Presented by M Cusiél

L Daziel: How significant are the plates to limit the crushing at the columns? M Cusiél: It provides a stiffer connection. Better to use flexibility in member than plasticity in connection.

A Ceccotti: Why was this system not used in the NMIT building? A Buchanan: It was not in the winning bid.

A Ceccotti: How much crushing is allowed in seismic design (due to pre-stress)? How much pre-stress losses? M Cusiél: none.

M Fragiaco: Do dissipators help? M Cusiél: connections are stiffer and dissipators are not engaged. Uneconomical.

11 STRESSES FOR SOLID TIMBER

43 - 6 - 1 The Bearing Strength of Timber Beams on Discrete Supports - A Jorissen, B de Leijer, A Leijten

Presented by A Jorissen

R Crocetti: The beam shown in picture is a good example of a bad design. Bearing plate should be as wide as beam. A Jorissen: this is just an example

H Blass: is the 10% failure criteria too relaxed?

H Larsen: did you design this beam? A Jorissen: No.

S Franke: this is local effect which depends on growth ring orientation.

L Daziel: About example of failure. Was this a deviation in planned construction? A Jorissen: No.

12 STRESS GRADING

43 - 5 - 1 Quality Control Methods - Application to Acceptance Criteria for a Batch of Timber - F Rouger

Presented by F Rouger

H Larsen: why do we have acceptance criteria on timber acceptance? The situation described does not exist. F Rouger: I do not agree. In glulam industry in France, each lamination must be checked. In EN 384, the acceptance criterion was a rule-of-thumb.

J Munch-Andersen: This new rule must comply with Eurocode 0. F Rouger: The method in itself is not new for engineering but new for timber.

43 - 5 - 2 Influence of Origin and Grading Principles on the Engineering Properties of European Timber - P Stapel, J W v. d. Kuilen, A Rais

Presented by P Stapel

H Larsen: I support the recommendation of eliminating the depth effect.

L Daziel: was visual grading done by supplier? P. Stapel: No.

13 ANY OTHER BUSINESS

S Winter: H Blass will be honoured with the Wallenberg prize in September. We wish to congratulate him for his achievements.

14 VENUE AND PROGRAMME FOR NEXT MEETING

2011 - University of Sassari, Alghero, Italy (28 Aug – 1 Sept)

2012 - Linnaeus University, Växjö, Sweden

15 CLOSE

The chair thanked the speakers for their presentations and the delegates for their participation. He also thanked the host team for their efforts to organize an excellent meeting.

**16. Peer Review of Papers for the
CIB-W18 Proceedings**

16. Peer review of papers for the CIB-W18 Proceedings

Experts involved:

Members of the CIB-W18 “Timber Structures” group are a community of experts in the field of timber engineering.

Procedure of peer review

- Submission of manuscripts: all members of the CIB-W18 group attending the meeting receive the manuscripts of the papers at least four weeks before the meeting. Everyone is invited to read and review the manuscripts especially in their respective fields of competence and interest.
- Presentation of the paper during the meeting by the author
- Comments and recommendations of the experts, discussion of the paper
- Comments, discussion and recommendations of the experts are documented in the minutes of the meeting and are printed on the front page of each paper.
- Final acceptance of the paper for the proceedings with
 - no changes
 - minor changes
 - major changes
 - or reject
- Revised papers are to be sent to the editor of the proceedings and the chairman of the CIB-W18 group
- Editor and chairman check, whether the requested changes have been carried out.

**17. List of CIB-W18 Papers,
Nelson, New Zealand 2010**

List of CIB-W18 Papers, Nelson, New Zealand 2010

- 43 - 5 - 1 Quality Control Methods - Application to Acceptance Criteria for a Batch of Timber - **F Rouger**
- 43 - 5 - 2 Influence of Origin and Grading Principles on the Engineering Properties of European Timber - **P Stapel, J W v. d. Kuilen, A Rais**
- 43 - 6 - 1 The Bearing Strength of Timber Beams on Discrete Supports - **A Jorissen, B de Leijer, A Leijten**
- 43 - 7 - 1 Probabilistic Capacity Prediction of Timber Joints under Brittle Failure Modes - **T Tannert, T Vallée, and F Lam**
- 43 - 7 - 2 Ductility in Timber Structures - **A Jorissen, M Fragiaco**
- 43 - 7 - 3 Design of Mechanically Jointed Concrete-Timber Beams Taking into Account the Plastic Behaviour of the Fasteners - **H J Larsen, H Riberholt, A Ceccotti**
- 43 - 7 - 4 Design of Timber-Concrete Composite Beams with Notched Connections - **M Fragiaco, D Yeoh**
- 43 - 7 - 5 Development of Design Procedures for Timber Concrete Composite Floors in Australia and New Zealand - **K Crews, C Gerber**
- 43 - 7 - 6 Failure Behaviour and Resistance of Dowel-Type Connections Loaded Perpendicular to Grain - **B Franke, P Quenneville**
- 43 - 7 - 7 Predicting Time Dependent Effects in Unbonded Post-Tensioned Timber Beams and Frames - **S Giorgini, A Neale, A Palermo, D Carradine, S Pampanin, A H Buchanan**
- 43 - 7 - 8 Simplified Design of Post-tensioned Timber Frames - **M Newcombe, M Cusi, S Pampanin, A Palermo, A H Buchanan**
- 43 - 12 - 1 Fatigue Behaviour of Finger Jointed Lumber - **S Aicher, G Stapf**
- 43 - 12 - 2 Experimental and Numerical Investigation on the Shear Strength of Glulam - **R Crocetti, P J Gustafsson, H Danielsson, A Emilsson, S Ormarsson**
- 43 - 12 - 3 System Effects in Glued Laminated Timber in Tension and Bending - **M Frese, H J Bläß**
- 43 - 12 - 4 Experimental Investigations on Mechanical Behaviour of Glued Solid timber - **C Faye, F Rouger, P Garcia**
- 43 - 15 - 1 Influence of the Boundary Conditions on the Racking Strength of Shear Walls with an Opening - **M Yasumura**
- 43 - 15 - 2 Influence of Different Standards on the Determination of Earthquake Properties of Timber Shear Wall Systems - **P Schädle, H J Bläß**
- 43 - 15 - 3 Full-Scale Shear Wall Tests for Force Transfer Around Openings - **T Skaggs, B Yeh, F Lam**
- 43 - 15 - 4 Optimized Anchor-Bolt Spacing for Structural Panel Shearwalls Subjected to Combined Shear and Wind Uplift Forces - **B Yeh, E Keith, T Skaggs**

- 43 - 16 - 1 Light Timber Frame Construction with Solid Timber Members – Application of the Reduced Cross-section Method - **J König, J Schmid**
- 43 - 16 - 2 Fire Exposed Cross-Laminated Timber - Modelling and Tests - **J Schmid, J König, J Köhler**
- 43 - 16 - 3 Timber-Concrete Composite Floors in Fire - **J O'Neill, D Carradine, R Dhakal, P J Moss, A H Buchanan, M Fragiaco**
- 43 - 18 - 1 Comparison of API, RF and MUF Adhesives Using a Draft Australian/New Zealand Standard - **B Walford**
- 43 - 20 - 1 The Long Term Instrumentation of a Timber Building in Nelson NZ - the Need for Standardisation - **H W Morris, S R Uma, K Gledhill, P Omenzetter, M Worth**
- 43 - 21 - 1 Estimation of Load-Bearing Capacity of Timber Connections - **J Munch-Andersen, J D Sørensen, F Sørensen**
- 43 - 21 - 2 A New Method to Determine Suitable Spacings and Distances for Self-tapping Screws - **T Uibel, H J Blaß**
- 43 - 101- 1 Dependant Versus Independent Loads in Structural Design - **T Poutanen**

18. Current List of CIB-W18(A) Papers

CURRENT LIST OF CIB-W18(A) PAPERS

Technical papers presented to CIB-W18(A) are identified by a code CIB-W18(A)/a-b-c, where:

a denotes the meeting at which the paper was presented.

- 1 Princes Risborough, England; March 1973
- 2 Copenhagen, Denmark; October 1973
- 3 Delft, Netherlands; June 1974
- 4 Paris, France; February 1975
- 5 Karlsruhe, Federal Republic of Germany; October 1975
- 6 Aalborg, Denmark; June 1976
- 7 Stockholm, Sweden; February/March 1977
- 8 Brussels, Belgium; October 1977
- 9 Perth, Scotland; June 1978
- 10 Vancouver, Canada; August 1978
- 11 Vienna, Austria; March 1979
- 12 Bordeaux, France; October 1979
- 13 Otaniemi, Finland; June 1980
- 14 Warsaw, Poland; May 1981
- 15 Karlsruhe, Federal Republic of Germany; June 1982
- 16 Lillehammer, Norway; May/June 1983
- 17 Rapperswil, Switzerland; May 1984
- 18 Beit Oren, Israel; June 1985
- 19 Florence, Italy; September 1986
- 20 Dublin, Ireland; September 1987
- 21 Parksville, Canada; September 1988
- 22 Berlin, German Democratic Republic; September 1989
- 23 Lisbon, Portugal; September 1990
- 24 Oxford, United Kingdom; September 1991
- 25 Åhus, Sweden; August 1992
- 26 Athens, USA; August 1993
- 27 Sydney, Australia; July 1994
- 28 Copenhagen, Denmark; April 1995
- 29 Bordeaux, France; August 1996
- 30 Vancouver, Canada; August 1997
- 31 Savonlinna, Finland; August 1998
- 32 Graz, Austria, August 1999
- 33 Delft, The Netherlands; August 2000
- 34 Venice, Italy; August 2001
- 35 Kyoto, Japan; September 2002
- 36 Colorado, USA; August 2003
- 37 Edinburgh, Scotland, August 2004
- 38 Karlsruhe, Germany, August 2005
- 39 Florence, Italy, August 2006
- 40 Bled, Slovenia, August 2007
- 41 St. Andrews, Canada 2008
- 42 Dübendorf, Switzerland 2009
- 43 Nelson, New Zealand 2010

b denotes the subject:

- 1 Limit State Design
- 2 Timber Columns
- 3 Symbols
- 4 Plywood
- 5 Stress Grading
- 6 Stresses for Solid Timber
- 7 Timber Joints and Fasteners
- 8 Load Sharing
- 9 Duration of Load
- 10 Timber Beams
- 11 Environmental Conditions
- 12 Laminated Members
- 13 Particle and Fibre Building Boards
- 14 Trussed Rafters
- 15 Structural Stability
- 16 Fire
- 17 Statistics and Data Analysis
- 18 Glued Joints
- 19 Fracture Mechanics
- 20 Serviceability
- 21 Test Methods
- 100 CIB Timber Code
- 101 Loading Codes
- 102 Structural Design Codes
- 103 International Standards Organisation
- 104 Joint Committee on Structural Safety
- 105 CIB Programme, Policy and Meetings
- 106 International Union of Forestry Research Organisations

c is simply a number given to the papers in the order in which they appear:

Example: CIB-W18/4-102-5 refers to paper 5 on subject 102 presented at the fourth meeting of W18.

Listed below, by subjects, are all papers that have to date been presented to W18. When appropriate some papers are listed under more than one subject heading.

LIMIT STATE DESIGN

- 1-1-1 Limit State Design - H J Larsen
- 1-1-2 The Use of Partial Safety Factors in the New Norwegian Design Code for Timber Structures - O Brynildsen
- 1-1-3 Swedish Code Revision Concerning Timber Structures - B Noren
- 1-1-4 Working Stresses Report to British Standards Institution Committee BLCP/17/2
- 6-1-1 On the Application of the Uncertainty Theoretical Methods for the Definition of the Fundamental Concepts of Structural Safety - K Skov and O Ditlevsen
- 11-1-1 Safety Design of Timber Structures - H J Larsen
- 18-1-1 Notes on the Development of a UK Limit States Design Code for Timber - A R Fewell and C B Pierce
- 18-1-2 Eurocode 5, Timber Structures - H J Larsen
- 19-1-1 Duration of Load Effects and Reliability Based Design (Single Member) - R O Foschi and Z C Yao
- 21-102-1 Research Activities Towards a New GDR Timber Design Code Based on Limit States Design - W Rug and M Badstube
- 22-1-1 Reliability-Theoretical Investigation into Timber Components Proposal for a Supplement of the Design Concept - M Badstube, W Rug and R Plessow
- 23-1-1 Some Remarks about the Safety of Timber Structures - J Kuipers
- 23-1-2 Reliability of Wood Structural Elements: A Probabilistic Method to Eurocode 5 Calibration - F Rouger, N Lheritier, P Racher and M Fogli
- 31-1-1 A Limit States Design Approach to Timber Framed Walls - C J Mettem, R Bainbridge and J A Gordon
- 32 -1-1 Determination of Partial Coefficients and Modification Factors- H J Larsen, S Svensson and S Thelandersson
- 32 -1-2 Design by Testing of Structural Timber Components - V Enjily and L Whale
- 33-1-1 Aspects on Reliability Calibration of Safety Factors for Timber Structures – S Svensson and S Thelandersson
- 33-1-2 Sensitivity studies on the reliability of timber structures – A Ranta-Maunus, M Fonselius, J Kurkela and T Toratti
- 41-1-1 On the Role of Stiffness Properties for Ultimate Limit State Design of Slender Columns– J Köhler, A Frangi, R Steiger

TIMBER COLUMNS

- 2-2-1 The Design of Solid Timber Columns - H J Larsen
- 3-2-1 The Design of Built-Up Timber Columns - H J Larsen
- 4-2-1 Tests with Centrally Loaded Timber Columns - H J Larsen and S S Pedersen
- 4-2-2 Lateral-Torsional Buckling of Eccentrically Loaded Timber Columns- B Johansson
- 5-9-1 Strength of a Wood Column in Combined Compression and Bending with Respect to Creep - B Källsner and B Norén
- 5-100-1 Design of Solid Timber Columns (First Draft) - H J Larsen
- 6-100-1 Comments on Document 5-100-1, Design of Solid Timber Columns - H J Larsen and E Theilgaard
- 6-2-1 Lattice Columns - H J Larsen
- 6-2-2 A Mathematical Basis for Design Aids for Timber Columns - H J Burgess

6-2-3	Comparison of Larsen and Perry Formulas for Solid Timber Columns- H J Burgess
7-2-1	Lateral Bracing of Timber Struts - J A Simon
8-15-1	Laterally Loaded Timber Columns: Tests and Theory - H J Larsen
17-2-1	Model for Timber Strength under Axial Load and Moment - T Poutanen
18-2-1	Column Design Methods for Timber Engineering - A H Buchanan, K C Johns, B Madsen
19-2-1	Creep Buckling Strength of Timber Beams and Columns - R H Leicester
19-12-2	Strength Model for Glulam Columns - H J Blaß
20-2-1	Lateral Buckling Theory for Rectangular Section Deep Beam-Columns- H J Burgess
20-2-2	Design of Timber Columns - H J Blaß
21-2-1	Format for Buckling Strength - R H Leicester
21-2-2	Beam-Column Formulae for Design Codes - R H Leicester
21-15-1	Rectangular Section Deep Beam - Columns with Continuous Lateral Restraint - H J Burgess
21-15-2	Buckling Modes and Permissible Axial Loads for Continuously Braced Columns - H J Burgess
21-15-3	Simple Approaches for Column Bracing Calculations - H J Burgess
21-15-4	Calculations for Discrete Column Restraints - H J Burgess
22-2-1	Buckling and Reliability Checking of Timber Columns - S Huang, P M Yu and J Y Hong
22-2-2	Proposal for the Design of Compressed Timber Members by Adopting the Second-Order Stress Theory - P Kaiser
30-2-1	Beam-Column Formula for Specific Truss Applications - W Lau, F Lam and J D Barrett
31-2-1	Deformation and Stability of Columns of Viscoelastic Material Wood - P Becker and K Rautenstrauch
34-2-1	Long-Term Experiments with Columns: Results and Possible Consequences on Column Design – W Moorkamp, W Schelling, P Becker, K Rautenstrauch
34-2-2	Proposal for Compressive Member Design Based on Long-Term Simulation Studies – P Becker, K Rautenstrauch
35-2-1	Computer Simulations on the Reliability of Timber Columns Regarding Hygrothermal Effects- R Hartnack, K-U Schober, K Rautenstrauch
36-2-1	The Reliability of Timber Columns Based on Stochastic Principles - K Rautenstrauch, R Hartnack
38-2-1	Long-term Load Bearing of Wooden Columns Influenced by Climate – View on Code - R Hartnack, K Rautenstrauch

SYMBOLS

3-3-1	Symbols for Structural Timber Design - J Kuipers and B Norén
4-3-1	Symbols for Timber Structure Design - J Kuipers and B Norén
28-3-1	Symbols for Timber and Wood-Based Materials - J Kuipers and B Noren
1	Symbols for Use in Structural Timber Design

PLYWOOD

- 2-4-1 The Presentation of Structural Design Data for Plywood - L G Booth
- 3-4-1 Standard Methods of Testing for the Determination of Mechanical Properties of Plywood - J Kuipers
- 3-4-2 Bending Strength and Stiffness of Multiple Species Plywood - C K A Stieda
- 4-4-4 Standard Methods of Testing for the Determination of Mechanical Properties of Plywood - Council of Forest Industries, B.C.
- 5-4-1 The Determination of Design Stresses for Plywood in the Revision of CP 112 - L G Booth
- 5-4-2 Veneer Plywood for Construction - Quality Specifications - ISO/TC 139. Plywood, Working Group 6
- 6-4-1 The Determination of the Mechanical Properties of Plywood Containing Defects - L G Booth
- 6-4-2 Comparison of the Size and Type of Specimen and Type of Test on Plywood Bending Strength and Stiffness - C R Wilson and P Eng
- 6-4-3 Buckling Strength of Plywood: Results of Tests and Recommendations for Calculations - J Kuipers and H Ploos van Amstel
- 7-4-1 Methods of Test for the Determination of Mechanical Properties of Plywood - L G Booth, J Kuipers, B Norén, C R Wilson
- 7-4-2 Comments Received on Paper 7-4-1
- 7-4-3 The Effect of Rate of Testing Speed on the Ultimate Tensile Stress of Plywood - C R Wilson and A V Parasin
- 7-4-4 Comparison of the Effect of Specimen Size on the Flexural Properties of Plywood Using the Pure Moment Test - C R Wilson and A V Parasin
- 8-4-1 Sampling Plywood and the Evaluation of Test Results - B Norén
- 9-4-1 Shear and Torsional Rigidity of Plywood - H J Larsen
- 9-4-2 The Evaluation of Test Data on the Strength Properties of Plywood - L G Booth
- 9-4-3 The Sampling of Plywood and the Derivation of Strength Values (Second Draft) - B Norén
- 9-4-4 On the Use of the CIB/RILEM Plywood Plate Twisting Test: a progress report - L G Booth
- 10-4-1 Buckling Strength of Plywood - J Dekker, J Kuipers and H Ploos van Amstel
- 11-4-1 Analysis of Plywood Stressed Skin Panels with Rigid or Semi-Rigid Connections- I Smith
- 11-4-2 A Comparison of Plywood Modulus of Rigidity Determined by the ASTM and RILEM CIB/3-TT Test Methods - C R Wilson and A V Parasin
- 11-4-3 Sampling of Plywood for Testing Strength - B Norén
- 12-4-1 Procedures for Analysis of Plywood Test Data and Determination of Characteristic Values Suitable for Code Presentation - C R Wilson
- 14-4-1 An Introduction to Performance Standards for Wood-base Panel Products - D H Brown
- 14-4-2 Proposal for Presenting Data on the Properties of Structural Panels - T Schmidt
- 16-4-1 Planar Shear Capacity of Plywood in Bending - C K A Stieda
- 17-4-1 Determination of Panel Shear Strength and Panel Shear Modulus of Beech-Plywood in Structural Sizes - J Ehlbeck and F Colling
- 17-4-2 Ultimate Strength of Plywood Webs - R H Leicester and L Pham

- 20-4-1 Considerations of Reliability - Based Design for Structural Composite Products - M R O'Halloran, J A Johnson, E G Elias and T P Cunningham
- 21-4-1 Modelling for Prediction of Strength of Veneer Having Knots - Y Hirashima
- 22-4-1 Scientific Research into Plywood and Plywood Building Constructions the Results and Findings of which are Incorporated into Construction Standard Specifications of the USSR - I M Guskov
- 22-4-2 Evaluation of Characteristic values for Wood-Based Sheet Materials - E G Elias
- 24-4-1 APA Structural-Use Design Values: An Update to Panel Design Capacities - A L Kuchar, E G Elias, B Yeh and M R O'Halloran

STRESS GRADING

- 1-5-1 Quality Specifications for Sawn Timber and Precision Timber - Norwegian Standard NS 3080
- 1-5-2 Specification for Timber Grades for Structural Use - British Standard BS 4978
- 4-5-1 Draft Proposal for an International Standard for Stress Grading Coniferous Sawn Softwood - ECE Timber Committee
- 16-5-1 Grading Errors in Practice - B Thunell
- 16-5-2 On the Effect of Measurement Errors when Grading Structural Timber- L Nordberg and B Thunell
- 19-5-1 Stress-Grading by ECE Standards of Italian-Grown Douglas-Fir Dimension Lumber from Young Thinnings - L Uzielli
- 19-5-2 Structural Softwood from Afforestation Regions in Western Norway - R Lackner
- 21-5-1 Non-Destructive Test by Frequency of Full Size Timber for Grading - T Nakai
- 22-5-1 Fundamental Vibration Frequency as a Parameter for Grading Sawn Timber - T Nakai, T Tanaka and H Nagao
- 24-5-1 Influence of Stress Grading System on Length Effect Factors for Lumber Loaded in Compression - A Campos and I Smith
- 26-5-1 Structural Properties of French Grown Timber According to Various Grading Methods - F Rouger, C De Lafond and A El Quadrani
- 28-5-1 Grading Methods for Structural Timber - Principles for Approval - S Ohlsson
- 28-5-2 Relationship of Moduli of Elasticity in Tension and in Bending of Solid Timber - N Burger and P Glos
- 29-5-1 The Effect of Edge Knots on the Strength of SPF MSR Lumber - T Courchene, F Lam and J D Barrett
- 29-5-2 Determination of Moment Configuration Factors using Grading Machine Readings - T D G Canisius and T Isaksson
- 31-5-1 Influence of Varying Growth Characteristics on Stiffness Grading of Structural Timber - S Ormarsson, H Petersson, O Dahlblom and K Persson
- 31-5-2 A Comparison of In-Grade Test Procedures - R H Leicester, H Breitingner and H Fordham
- 32-5-1 Actual Possibilities of the Machine Grading of Timber - K Frühwald and A Bernasconi
- 32-5-2 Detection of Severe Timber Defects by Machine Grading - A Bernasconi, L Boström and B Schacht
- 34-5-1 Influence of Proof Loading on the Reliability of Members – F Lam, S Abayakoon, S Svensson, C Gyamfi
- 36-5-1 Settings for Strength Grading Machines – Evaluation of the Procedure according to prEN 14081, part 2 - C Bengtsson, M Fonselius

- 36-5-2 A Probabilistic Approach to Cost Optimal Timber Grading - J Köhler, M H Faber
- 36-7-11 Reliability of Timber Structures, Theory and Dowel-Type Connection Failures - A Ranta-Maunus, A Kevärinmäki
- 38-5-1 Are Wind-Induced Compression Failures Grading Relevant - M Arnold, R Steiger
- 39-5-1 A Discussion on the Control of Grading Machine Settings – Current Approach, Potential and Outlook - J Köhler, R Steiger
- 39-5-2 Tensile Proof Loading to Assure Quality of Finger-Jointed Structural timber - R Katzengruber, G Jeitler, G Schickhofer
- 40-5-1 Development of Grading Rules for Re-Cycled Timber Used in Structural Applications - K Crews
- 40-5-2 The Efficient Control of Grading Machine Settings - M Sandomeer, J Köhler, P Linsenmann
- 41-5-1 Probabilistic Output Control for Structural Timber - Fundamental Model Approach – M K Sandomeer, J Köhler, M H Faber
- 42-5-1 Machine Strength Grading – a New Method for Derivation of Settings - R Ziethén, C Bengtsson
- 43-5-1 Quality Control Methods - Application to Acceptance Criteria for a Batch of Timber - F Rouger
- 43-5-2 Influence of Origin and Grading Principles on the Engineering Properties of European Timber - P Stapel, J W v. d. Kuilen, A Rais

STRESSES FOR SOLID TIMBER

- 4-6-1 Derivation of Grade Stresses for Timber in the UK - W T Curry
- 5-6-1 Standard Methods of Test for Determining some Physical and Mechanical Properties of Timber in Structural Sizes - W T Curry
- 5-6-2 The Description of Timber Strength Data - J R Tory
- 5-6-3 Stresses for EC1 and EC2 Stress Grades - J R Tory
- 6-6-1 Standard Methods of Test for the Determination of some Physical and Mechanical Properties of Timber in Structural Sizes (third draft) - W T Curry
- 7-6-1 Strength and Long-term Behaviour of Lumber and Glued Laminated Timber under Torsion Loads - K Möhler
- 9-6-1 Classification of Structural Timber - H J Larsen
- 9-6-2 Code Rules for Tension Perpendicular to Grain - H J Larsen
- 9-6-3 Tension at an Angle to the Grain - K Möhler
- 9-6-4 Consideration of Combined Stresses for Lumber and Glued Laminated Timber - K Möhler
- 11-6-1 Evaluation of Lumber Properties in the United States - W L Galligan and J H Haskell
- 11-6-2 Stresses Perpendicular to Grain - K Möhler
- 11-6-3 Consideration of Combined Stresses for Lumber and Glued Laminated Timber (addition to Paper CIB-W18/9-6-4) - K Möhler
- 12-6-1 Strength Classifications for Timber Engineering Codes - R H Leicester and W G Keating
- 12-6-2 Strength Classes for British Standard BS 5268 - J R Tory
- 13-6-1 Strength Classes for the CIB Code - J R Tory
- 13-6-2 Consideration of Size Effects and Longitudinal Shear Strength for Uncracked Beams - R O Foschi and J D Barrett

13-6-3	Consideration of Shear Strength on End-Cracked Beams - J D Barrett and R O Foschi
15-6-1	Characteristic Strength Values for the ECE Standard for Timber - J G Sunley
16-6-1	Size Factors for Timber Bending and Tension Stresses - A R Fewell
16-6-2	Strength Classes for International Codes - A R Fewell and J G Sunley
17-6-1	The Determination of Grade Stresses from Characteristic Stresses for BS 5268: Part 2 - A R Fewell
17-6-2	The Determination of Softwood Strength Properties for Grades, Strength Classes and Laminated Timber for BS 5268: Part 2 - A R Fewell
18-6-1	Comment on Papers: 18-6-2 and 18-6-3 - R H Leicester
18-6-2	Configuration Factors for the Bending Strength of Timber - R H Leicester
18-6-3	Notes on Sampling Factors for Characteristic Values - R H Leicester
18-6-4	Size Effects in Timber Explained by a Modified Weakest Link Theory- B Madsen and A H Buchanan
18-6-5	Placement and Selection of Growth Defects in Test Specimens - H Riberholt
18-6-6	Partial Safety-Coefficients for the Load-Carrying Capacity of Timber Structures - B Norén and J-O Nylander
19-6-1	Effect of Age and/or Load on Timber Strength - J Kuipers
19-6-2	Confidence in Estimates of Characteristic Values - R H Leicester
19-6-3	Fracture Toughness of Wood - Mode I - K Wright and M Fonselius
19-6-4	Fracture Toughness of Pine - Mode II - K Wright
19-6-5	Drying Stresses in Round Timber - A Ranta-Maunus
19-6-6	A Dynamic Method for Determining Elastic Properties of Wood - R Görlacher
20-6-1	A Comparative Investigation of the Engineering Properties of "Whitewoods" Imported to Israel from Various Origins - U Korin
20-6-2	Effects of Yield Class, Tree Section, Forest and Size on Strength of Home Grown Sitka Spruce - V Picardo
20-6-3	Determination of Shear Strength and Strength Perpendicular to Grain - H J Larsen
21-6-1	Draft Australian Standard: Methods for Evaluation of Strength and Stiffness of Graded Timber - R H Leicester
21-6-2	The Determination of Characteristic Strength Values for Stress Grades of Structural Timber. Part 1 - A R Fewell and P Glos
21-6-3	Shear Strength in Bending of Timber - U Korin
22-6-1	Size Effects and Property Relationships for Canadian 2-inch Dimension Lumber - J D Barrett and H Griffin
22-6-2	Moisture Content Adjustements for In-Grade Data - J D Barrett and W Lau
22-6-3	A Discussion of Lumber Property Relationships in Eurocode 5 - D W Green and D E Kretschmann
22-6-4	Effect of Wood Preservatives on the Strength Properties of Wood - F Ronai
23-6-1	Timber in Compression Perpendicular to Grain - U Korin
24-6-1	Discussion of the Failure Criterion for Combined Bending and Compression - T A C M van der Put
24-6-3	Effect of Within Member Variability on Bending Strength of Structural Timber - I Czmocho, S Thelandersson and H J Larsen

- 24-6-4 Protection of Structural Timber Against Fungal Attack Requirements and Testing- K Jaworska, M Rylko and W Nozynski
- 24-6-5 Derivation of the Characteristic Bending Strength of Solid Timber According to CEN- Document prEN 384 - A J M Leijten
- 25-6-1 Moment Configuration Factors for Simple Beams- T D G Canisius
- 25-6-3 Bearing Capacity of Timber - U Korin
- 25-6-4 On Design Criteria for Tension Perpendicular to Grain - H Petersson
- 25-6-5 Size Effects in Visually Graded Softwood Structural Lumber - J D Barrett, F Lam and W Lau
- 26-6-1 Discussion and Proposal of a General Failure Criterion for Wood - T A C M van der Put
- 27-6-1 Development of the "Critical Bearing": Design Clause in CSA-086.1 - C Lum and E Karacabeyli
- 27-6-2 Size Effects in Timber: Novelty Never Ends - F Rouger and T Fewell
- 27-6-3 Comparison of Full-Size Sugi (*Cryptomeria japonica* D.Don) Structural Performance in Bending of Round Timber, Two Surfaces Sawn Timber and Square Sawn Timber - T Nakai, H Nagao and T Tanaka
- 28-6-1 Shear Strength of Canadian Softwood Structural Lumber - F Lam, H Yee and J D Barrett
- 28-6-2 Shear Strength of Douglas Fir Timbers - B Madsen
- 28-6-3 On the Influence of the Loading Head Profiles on Determined Bending Strength - L Muszyński and R Szukala
- 28-6-4 Effect of Test Standard, Length and Load Configuration on Bending Strength of Structural Timber- T Isaksson and S Thelandersson
- 28-6-5 Grading Machine Readings and their Use in the Calculation of Moment Configuration Factors - T Canisius, T Isaksson and S Thelandersson
- 28-6-6 End Conditions for Tension Testing of Solid Timber Perpendicular to Grain - T Canisius
- 29-6-1 Effect of Size on Tensile Strength of Timber - N Burger and P Glos
- 29-6-2 Equivalence of In-Grade Testing Standards - R H Leicester, H O Breitingner and H F Fordham
- 30-6-1 Strength Relationships in Structural Timber Subjected to Bending and Tension - N Burger and P Glos
- 30-6-2 Characteristic Design Stresses in Tension for Radiata Pine Grown in Canterbury - A Tsehay, J C F Walker and A H Buchanan
- 30-6-3 Timber as a Natural Composite: Explanation of Some Peculiarities in the Mechanical Behaviour - E Gehri
- 31-6-1 Length and Moment Configuration Factors - T Isaksson
- 31-6-2 Tensile Strength Perpendicular to Grain According to EN 1193 - H J Blaß and M Schmid
- 31-6-3 Strength of Small Diameter Round Timber - A Ranta-Maunus, U Saarelainen and H Boren
- 31-6-4 Compression Strength Perpendicular to Grain of Structural Timber and Glulam - L Damkilde, P Hoffmeyer and T N Pedersen
- 31-6-5 Bearing Strength of Timber Beams - R H Leicester, H Fordham and H Breitingner
- 32-6-1 Development of High-Resistance Glued Robinia Products and an Attempt to Assign Such Products to the European System of Strength Classes - G Schickhofer and B Obermayr

- 32-6-2 Length and Load Configuration Effects in the Code Format - T Isaksson
- 32-6-3 Length Effect on the Tensile Strength of Truss Chord Members - F Lam
- 32-6-4 Tensile Strength Perpendicular to Grain of Glued Laminated Timber - H J Blaß and M Schmid
- 32-6-5 On the Reliability-based Strength Adjustment Factors for Timber Design - T D G Canisius
- 34-6-1 Material Strength Properties for Canadian Species Used in Japanese Post and Beam Construction - J D Barrett, F Lam, S Nakajima
- 35-6-1 Evaluation of Different Size Effect Models for Tension Perpendicular to Grain Design - S Aicher, G Dill-Langer
- 35-6-2 Tensile Strength of Glulam Perpendicular to Grain - Effects of Moisture Gradients - J Jönsson, S Thelandersson
- 36-6-1 Characteristic Shear Strength Values Based on Tests According to EN 1193 - P Glos, J Denzler
- 37-6-1 Tensile Strength of Nordic Birch - K H Solli
- 37-6-2 Effect of Test Piece Orientation on Characteristic Bending Strength of Structural Timber - P Glos, J K Denzler
- 37-6-3 Strength and Stiffness Behaviour of Beech Laminations for High Strength Glulam - P Glos, J K Denzler, P W Linsenmann
- 37-6-4 A Review of Existing Standards Related to Calculation of Characteristic Values of Timber - F Rouger
- 37-6-5 Influence of the Rolling-Shear Modulus on the Strength and Stiffness of Structural Bonded Timber Elements - P Fellmoser, H J Blass
- 38-6-1 Design Specifications for Notched Beams in AS:1720 - R H Leicester
- 38-6-2 Characteristic Bending Strength of Beech Glulam - H J Blaß, M Frese
- 38-6-3 Shear Strength of Glued Laminated Timber - H Klapp, H Brüninghoff
- 39-6-1 Allocation of Central European hardwoods into EN 1912 - P Glos, J K Denzler
- 39-6-2 Revisiting EN 338 and EN 384 Basics and Procedures - R Steiger, M Arnold, M Fontana
- 40-6-1 Bearing Strength Perpendicular to the Grain of Locally Loaded Timber Blocks - A J M Leijten, J C M Schoenmakers
- 40-6-2 Experimental Study of Compression and Shear Strength of Spruce Timber - M Poussa, P Tukiainen, A Ranta-Maunus
- 40-6-3 Analysis of Tension and Bending strength of Graded Spruce Timber - A Hanhijärvi, A Ranta-Maunus, H Sarkama, M Kohsaku, M Poussa, J Puttonen
- 41-6-1 Design of Inclined Glulam Members with an End Notch on the Tension Face - A Asiz, I Smith
- 41-6-2 A New Design Approach for End-notched Beams - View on Code - K Rautenstrauch, B Franke, S Franke, K U Schober
- 41-6-3 The Design Rules in Eurocode 5 for Compression Perpendicular to the Grain - Continuous Supported Beams - H J Larsen, T A C M van der Put, A J M Leijten
- 41-6-4 Size Effects in Bending – J K Denzler, P Glos
- 42-6-1 Variability of Strength of European Spruce - A Ranta-Maunus, J K Denzler
- 42-6-2 Impact Loaded Structural Timber Elements Made from Swiss Grown Norway Spruce - R Widmann, R Steiger
- 42-6-3 Modelling the Bending Strength of Timber Components –Implications to Test Standards - J Köhler, M Sandomeer, T Isaksson, B Källsner

- 43-6-1 The Bearing Strength of Timber Beams on Discrete Supports - A Jorissen, B de Leijer, A Leijten

TIMBER JOINTS AND FASTENERS

- 1-7-1 Mechanical Fasteners and Fastenings in Timber Structures - E G Stern
- 4-7-1 Proposal for a Basic Test Method for the Evaluation of Structural Timber Joints with Mechanical Fasteners and Connectors - RILEM 3TT Committee
- 4-7-2 Test Methods for Wood Fasteners - K Möhler
- 5-7-1 Influence of Loading Procedure on Strength and Slip-Behaviour in Testing Timber Joints - K Möhler
- 5-7-2 Recommendations for Testing Methods for Joints with Mechanical Fasteners and Connectors in Load-Bearing Timber Structures - RILEM 3 TT Committee
- 5-7-3 CIB-Recommendations for the Evaluation of Results of Tests on Joints with Mechanical Fasteners and Connectors used in Load-Bearing Timber Structures - J Kuipers
- 6-7-1 Recommendations for Testing Methods for Joints with Mechanical Fasteners and Connectors in Load-Bearing Timber Structures (seventh draft) - RILEM 3 TT Committee
- 6-7-2 Proposal for Testing Integral Nail Plates as Timber Joints - K Möhler
- 6-7-3 Rules for Evaluation of Values of Strength and Deformation from Test Results - Mechanical Timber Joints - M Johansen, J Kuipers, B Norén
- 6-7-4 Comments to Rules for Testing Timber Joints and Derivation of Characteristic Values for Rigidity and Strength - B Norén
- 7-7-1 Testing of Integral Nail Plates as Timber Joints - K Möhler
- 7-7-2 Long Duration Tests on Timber Joints - J Kuipers
- 7-7-3 Tests with Mechanically Jointed Beams with a Varying Spacing of Fasteners - K Möhler
- 7-100-1 CIB-Timber Code Chapter 5.3 Mechanical Fasteners; CIB-Timber Standard 06 and 07 - H J Larsen
- 9-7-1 Design of Truss Plate Joints - F J Keenan
- 9-7-2 Staples - K Möhler
- 11-7-1 A Draft Proposal for International Standard: ISO Document ISO/TC 165N 38E
- 12-7-1 Load-Carrying Capacity and Deformation Characteristics of Nailed Joints - J Ehlbeck
- 12-7-2 Design of Bolted Joints - H J Larsen
- 12-7-3 Design of Joints with Nail Plates - B Norén
- 13-7-1 Polish Standard BN-80/7159-04: Parts 00-01-02-03-04-05.
"Structures from Wood and Wood-based Materials. Methods of Test and Strength Criteria for Joints with Mechanical Fasteners"
- 13-7-2 Investigation of the Effect of Number of Nails in a Joint on its Load Carrying Ability - W Nozynski
- 13-7-3 International Acceptance of Manufacture, Marking and Control of Finger-jointed Structural Timber - B Norén
- 13-7-4 Design of Joints with Nail Plates - Calculation of Slip - B Norén
- 13-7-5 Design of Joints with Nail Plates - The Heel Joint - B Källsner
- 13-7-6 Nail Deflection Data for Design - H J Burgess
- 13-7-7 Test on Bolted Joints - P Vermeyden

13-7-8	Comments to paper CIB-W18/12-7-3 "Design of Joints with Nail Plates"- B Norén
13-7-9	Strength of Finger Joints - H J Larsen
13-100-4	CIB Structural Timber Design Code. Proposal for Section 6.1.5 Nail Plates - N I Bovim
14-7-1	Design of Joints with Nail Plates (second edition) - B Norén
14-7-2	Method of Testing Nails in Wood (second draft, August 1980) - B Norén
14-7-3	Load-Slip Relationship of Nailed Joints - J Ehlbeck and H J Larsen
14-7-4	Wood Failure in Joints with Nail Plates - B Norén
14-7-5	The Effect of Support Eccentricity on the Design of W- and WW-Trussed with Nail Plate Connectors - B Källsner
14-7-6	Derivation of the Allowable Load in Case of Nail Plate Joints Perpendicular to Grain - K Möhler
14-7-7	Comments on CIB-W18/14-7-1 - T A C M van der Put
15-7-1	Final Recommendation TT-1A: Testing Methods for Joints with Mechanical Fasteners in Load-Bearing Timber Structures. Annex A Punched Metal Plate Fasteners - Joint Committee RILEM/CIB-3TT
16-7-1	Load Carrying Capacity of Dowels - E Gehri
16-7-2	Bolted Timber Joints: A Literature Survey - N Harding
16-7-3	Bolted Timber Joints: Practical Aspects of Construction and Design; a Survey - N Harding
16-7-4	Bolted Timber Joints: Draft Experimental Work Plan - Building Research Association of New Zealand
17-7-1	Mechanical Properties of Nails and their Influence on Mechanical Properties of Nailed Timber Joints Subjected to Lateral Loads - I Smith, L R J Whale, C Anderson and L Held
17-7-2	Notes on the Effective Number of Dowels and Nails in Timber Joints - G Steck
18-7-1	Model Specification for Driven Fasteners for Assembly of Pallets and Related Structures - E G Stern and W B Wallin
18-7-2	The Influence of the Orientation of Mechanical Joints on their Mechanical Properties - I Smith and L R J Whale
18-7-3	Influence of Number of Rows of Fasteners or Connectors upon the Ultimate Capacity of Axially Loaded Timber Joints - I Smith and G Steck
18-7-4	A Detailed Testing Method for Nailplate Joints - J Kangas
18-7-5	Principles for Design Values of Nailplates in Finland - J Kangas
18-7-6	The Strength of Nailplates - N I Bovim and E Aasheim
19-7-1	Behaviour of Nailed and Bolted Joints under Short-Term Lateral Load - Conclusions from Some Recent Research - L R J Whale, I Smith and B O Hilson
19-7-2	Glued Bolts in Glulam - H Riberholt
19-7-3	Effectiveness of Multiple Fastener Joints According to National Codes and Eurocode 5 (Draft) - G Steck
19-7-4	The Prediction of the Long-Term Load Carrying Capacity of Joints in Wood Structures - Y M Ivanov and Y Y Slavic
19-7-5	Slip in Joints under Long-Term Loading - T Feldborg and M Johansen
19-7-6	The Derivation of Design Clauses for Nailed and Bolted Joints in Eurocode 5 - L R J Whale and I Smith

- 19-7-7 Design of Joints with Nail Plates - Principles - B Norén
- 19-7-8 Shear Tests for Nail Plates - B Norén
- 19-7-9 Advances in Technology of Joints for Laminated Timber - Analyses of the Structural Behaviour - M Piazza and G Turrini
- 19-15-1 Connections Deformability in Timber Structures: A Theoretical Evaluation of its Influence on Seismic Effects - A Ceccotti and A Vignoli
- 20-7-1 Design of Nailed and Bolted Joints-Proposals for the Revision of Existing Formulae in Draft Eurocode 5 and the CIB Code - L R J Whale, I Smith and H J Larsen
- 20-7-2 Slip in Joints under Long Term Loading - T Feldborg and M Johansen
- 20-7-3 Ultimate Properties of Bolted Joints in Glued-Laminated Timber - M Yasumura, T Murota and H Sakai
- 20-7-4 Modelling the Load-Deformation Behaviour of Connections with Pin-Type Fasteners under Combined Moment, Thrust and Shear Forces - I Smith
- 21-7-1 Nails under Long-Term Withdrawal Loading - T Feldborg and M Johansen
- 21-7-2 Glued Bolts in Glulam-Proposals for CIB Code - H Riberholt
- 21-7-3 Nail Plate Joint Behaviour under Shear Loading - T Poutanen
- 21-7-4 Design of Joints with Laterally Loaded Dowels. Proposals for Improving the Design Rules in the CIB Code and the Draft Eurocode 5 - J Ehlbeck and H Werner
- 21-7-5 Axially Loaded Nails: Proposals for a Supplement to the CIB Code - J Ehlbeck and W Siebert
- 22-7-1 End Grain Connections with Laterally Loaded Steel Bolts A draft proposal for design rules in the CIB Code - J Ehlbeck and M Gerold
- 22-7-2 Determination of Perpendicular-to-Grain Tensile Stresses in Joints with Dowel-Type Fasteners - A draft proposal for design rules - J Ehlbeck, R Görlacher and H Werner
- 22-7-3 Design of Double-Shear Joints with Non-Metallic Dowels A proposal for a supplement of the design concept - J Ehlbeck and O Eberhart
- 22-7-4 The Effect of Load on Strength of Timber Joints at high Working Load Level - A J M Leijten
- 22-7-5 Plasticity Requirements for Portal Frame Corners - R Gunnewijk and A J M Leijten
- 22-7-6 Background Information on Design of Glulam Rivet Connections in CSA/CAN3-086.1-M89 - A proposal for a supplement of the design concept - E Karacabeyli and D P Janssens
- 22-7-7 Mechanical Properties of Joints in Glued-Laminated Beams under Reversed Cyclic Loading - M Yasumura
- 22-7-8 Strength of Glued Lap Timber Joints - P Glos and H Horstmann
- 22-7-9 Toothed Rings Type Bistyp 075 at the Joints of Fir Wood - J Kerste
- 22-7-10 Calculation of Joints and Fastenings as Compared with the International State - K Zimmer and K Lissner
- 22-7-11 Joints on Glued-in Steel Bars Present Relatively New and Progressive Solution in Terms of Timber Structure Design - G N Zubarev, F A Boitemirov and V M Golovina
- 22-7-12 The Development of Design Codes for Timber Structures made of Composite Bars with Plate Joints based on Cylindrical Nails - Y V Piskunov
- 22-7-13 Designing of Glued Wood Structures Joints on Glued-in Bars - S B Turkovsky

- 23-7-1 Proposal for a Design Code for Nail Plates - E Aasheim and K H Solli
- 23-7-2 Load Distribution in Nailed Joints - H J Blass
- 24-7-1 Theoretical and Experimental Tension and Shear Capacity of Nail Plate Connections - B Källsner and J Kangas
- 24-7-2 Testing Method and Determination of Basic Working Loads for Timber Joints with Mechanical Fasteners - Y Hirashima and F Kamiya
- 24-7-3 Anchorage Capacity of Nail Plate - J Kangas
- 25-7-2 Softwood and Hardwood Embedding Strength for Dowel type Fasteners - J Ehlbeck and H Werner
- 25-7-4 A Guide for Application of Quality Indexes for Driven Fasteners Used in Connections in Wood Structures - E G Stern
- 25-7-5 35 Years of Experience with Certain Types of Connectors and Connector Plates Used for the Assembly of Wood Structures and their Components- E G Stern
- 25-7-6 Characteristic Strength of Split-ring and Shear-plate Connections - H J Blass, J Ehlbeck and M Schlager
- 25-7-7 Characteristic Strength of Tooth-plate Connector Joints - H J Blass, J Ehlbeck and M Schlager
- 25-7-8 Extending Yield Theory to Screw Connections - T E McLain
- 25-7-9 Determination of k_{def} for Nailed Joints - J W G van de Kuilen
- 25-7-10 Characteristic Strength of UK Timber Connectors - A V Page and C J Mettem
- 25-7-11 Multiple-fastener Dowel-type Joints, a Selected Review of Research and Codes - C J Mettem and A V Page
- 25-7-12 Load Distributions in Multiple-fastener Bolted Joints in European Whitewood Glulam, with Steel Side Plates - C J Mettem and A V Page
- 26-7-1 Proposed Test Method for Dynamic Properties of Connections Assembled with Mechanical Fasteners - J D Dolan
- 26-7-2 Validatory Tests and Proposed Design Formulae for the Load-Carrying Capacity of Toothed-Plate Connected Joints - C J Mettem, A V Page and G Davis
- 26-7-3 Definitions of Terms and Multi-Language Terminology Pertaining to Metal Connector Plates - E G Stern
- 26-7-4 Design of Joints Based on in V-Shape Glued-in Rods - J Kangas
- 26-7-5 Tests on Timber Concrete Composite Structural Elements (TCCs) - A U Meierhofer
- 27-7-1 Glulam Arch Bridge and Design of it's Moment-Resisting Joints - K Komatsu and S Usuku
- 27-7-2 Characteristic Load - Carrying Capacity of Joints with Dowel - type Fasteners in Regard to the System Properties - H Werner
- 27-7-3 Steel Failure Design in Truss Plate Joints - T Poutanen
- 28-7-1 Expanded Tube Joint in Locally DP Reinforced Timber - A J M Leijten, P Ragupathy and K S Virdi
- 28-7-2 A Strength and Stiffness Model for the Expanded Tube Joint - A J M Leijten
- 28-7-3 Load-carrying Capacity of Steel-to Timber Joints with Annular Ring Shank Nails. A Comparison with the EC5 Design Method - R Görlacher
- 28-7-4 Dynamic Effects on Metal-Plate Connected Wood Truss Joints - S Kent, R Gupta and T Miller
- 28-7-5 Failure of the Timber Bolted Joints Subjected to Lateral Load Perpendicular to Grain - M Yasumura and L Daudeville

- 28-7-6 Design Procedure for Locally Reinforced Joints with Dowel-type Fasteners - H Werner
- 28-7-7 Variability and Effects of Moisture Content on the Withdrawal Characteristics for Lumber as Opposed to Clear Wood - J D Dolan and J W Stelmokas
- 28-7-8 Nail Plate Capacity in Joint Line - A Kevarinmäki and J Kangas
- 28-7-9 Axial Strength of Glued-In Bolts - Calculation Model Based on Non-Linear Fracture Mechanics - A Preliminary Study - C J Johansson, E Serrano, P J Gustafsson and B Enquist
- 28-7-10 Cyclic Lateral Dowel Connection Tests for seismic and Wind Evaluation - J D Dolan
- 29-7-1 A Simple Method for Lateral Load-Carrying Capacity of Dowel-Type Fasteners - J Kangas and J Kurkela
- 29-7-2 Nail Plate Joint Behaviour at Low Versus High Load Level - T Poutanen
- 29-7-3 The Moment Resistance of Tee and Butt - Joint Nail Plate Test Specimens - A Comparison with Current Design Methods - A Reffold, L R J Whale and B S Choo
- 29-7-4 A Critical Review of the Moment Rotation Test Method Proposed in prEN 1075 - M Bettison, B S Choo and L R J Whale
- 29-7-5 Explanation of the Translation and Rotation Behaviour of Prestressed Moment Timber Joints - A J M Leijten
- 29-7-6 Design of Joints and Frame Corners using Dowel-Type Fasteners - E Gehri
- 29-7-7 Quasi-Static Reversed-Cyclic Testing of Nailed Joints - E Karacabeyli and A Ceccotti
- 29-7-8 Failure of Bolted Joints Loaded Parallel to the Grain: Experiment and Simulation - L Davenne, L Daudeville and M Yasumura
- 30-7-1 Flexural Behaviour of GLT Beams End-Jointed by Glued-in Hardwood Dowels - K Komatsu, A Koizumi, J Jensen, T Sasaki and Y Iijima
- 30-7-2 Modelling of the Block Tearing Failure in Nailed Steel-to-Timber Joints - J Kangas, K Aalto and A Kevarinmäki
- 30-7-3 Cyclic Testing of Joints with Dowels and Slotted-in Steel Plates - E Aasheim
- 30-7-4 A Steel-to-Timber Dowelled Joint of High Performance in Combination with a High Strength Wood Composite (Parallam) - E Gehri
- 30-7-5 Multiple Fastener Timber Connections with Dowel Type Fasteners - A Jorissen
- 30-7-6 Influence of Ductility on Load-Carrying Capacity of Joints with Dowel-Type Fasteners - A Mischler
- 31-7-1 Mechanical Properties of Dowel Type Joints under Reversed Cyclic Lateral Loading - M Yasumura
- 31-7-2 Design of Joints with Laterally Loaded Dowels - A Mischler
- 31-7-3 Flexural Behaviour of Glulam Beams Edge-Jointed by Lagscrews with Steel Splice Plates - K Komatsu
- 31-7-4 Design on Timber Capacity in Nailed Steel-to-Timber Joints - J Kangas and J Vesa
- 31-7-5 Timber Contact in Chord Splices of Nail Plate Structures - A Kevarinmäki
- 31-7-6 The Fastener Yield Strength in Bending - A Jorissen and H J Blaß
- 31-7-7 A Proposal for Simplification of Johansen's Formulae, Dealing With the Design of Dowelled-Type Fasteners - F Rouger

- 31-7-8 Simplified Design of Connections with Dowel-type fasteners - H J Blaß and J Ehlbeck
- 32-7-1 Behaviour of Wood-Steel-Wood Bolted Glulam Connections - M Mohammad and J H P Quenneville
- 32-7-2 A new set of experimental tests on beams loaded perpendicular-to-grain by dowel-type joints- M Ballerini
- 32-7-3 Design and Analysis of Bolted Timber Joints under Lateral Force Perpendicular to Grain - M Yasumura and L Daudeville
- 32-7-4 Predicting Capacities of Joints with Laterally Loaded Nails - I Smith and P Quenneville
- 32-7-5 Strength Reduction Rules for Multiple Fastener Joints - A Mischler and E Gehri
- 32-7-6 The Stiffness of Multiple Bolted Connections - A Jorissen
- 32-7-7 Concentric Loading Tests on Girder Truss Components - T N Reynolds, A Reffold, V Enjily and L Whale
- 32-7-8 Dowel Type Connections with Slotted-In Steel Plates - M U Pedersen, C O Clorius, L Damkilde, P Hoffmeyer and L Esklidsen
- 32-7-9 Creep of Nail Plate Reinforced Bolt Joints - J Vesa and A Kevarinmäki
- 32-7-10 The Behaviour of Timber Joints with Ring Connectors - E Gehri and A Mischler
- 32-7-11 Non-Metallic, Adhesiveless Joints for Timber Structures - R D Drake, M P Ansell, C J Mettem and R Bainbridge
- 32-7-12 Effect of Spacing and Edge Distance on the Axial Strength of Glued-in Rods - H J Blaß and B Laskewitz
- 32-7-13 Evaluation of Material Combinations for Bonded in Rods to Achieve Improved Timber Connections - C J Mettem, R J Bainbridge, K Harvey, M P Ansell, J G Broughton and A R Hutchinson
- 33-7-1 Determination of Yield Strength and Ultimate Strength of Dowel-Type Timber Joints – M Yasumura and K Sawata
- 33-7-2 Lateral Shear Capacity of Nailed Joints – U Korin
- 33-7-3 Height-Adjustable Connector for Composite Beams – Y V Piskunov and E G Stern
- 33-7-4 Engineering Ductility Assessment for a Nailed Slotted-In Steel Connection in Glulam– L Stehn and H Johansson
- 33-7-5 Effective Bending Capacity of Dowel-Type Fasteners - H J Blaß, A Bienhaus and V Krämer
- 33-7-6 Load-Carrying Capacity of Joints with Dowel-Type Fasteners and Interlayers - H J Blaß and B Laskewitz
- 33-7-7 Evaluation of Perpendicular to Grain Failure of Beams caused by Concentrated Loads of Joints – A J M Leijten and T A C M van der Put
- 33-7-8 Test Methods for Glued-In Rods for Timber Structures – C Bengtsson and C J Johansson
- 33-7-9 Stiffness Analysis of Nail Plates – P Ellegaard
- 33-7-10 Capacity, Fire Resistance and Gluing Pattern of the Rods in V-Connections – J Kangas
- 33-7-11 Bonded-In Pultrusions for Moment-Resisting Timber Connections – K Harvey, M P Ansell, C J Mettem, R J Bainbridge and N Alexandre
- 33-7-12 Fatigue Performance of Bonded-In Rods in Glulam, Using Three Adhesive Types - R J Bainbridge, K Harvey, C J Mettem and M P Ansell
- 34-7-1 Splitting Strength of Beams Loaded by Connections Perpendicular to Grain, Model Validation – A J M Leijten, A Jorissen
- 34-7-2 Numerical LEFM analyses for the evaluation of failure loads of beams loaded perpendicular-to-grain by single-dowel connections – M Ballerini, R Bezzi

- 34-7-3 Dowel joints loaded perpendicular to grain - H J Larsen, P J Gustafsson
- 34-7-4 Quality Control of Connections based on in V-shape glued-in Steel Rods – J Kangas, A Kevarinmäki
- 34-7-5 Testing Connector Types for Laminated-Timber-Concrete Composite Elements – M Grosse, S Lehmann, K Rautenstrauch
- 34-7-6 Behaviour of Axially Loaded Glued-in Rods - Requirements and Resistance, Especially for Spruce Timber Perpendicular to the Grain Direction – A Bernasconi
- 34-7-7 Embedding characteristics on fibre reinforcement and densified timber joints - P Haller, J Wehsener, T Birk
- 34-7-8 GIROD – Glued-in Rods for Timber Structures – C Bengtsson, C-J Johansson
- 34-7-9 Criteria for Damage and Failure of Dowel-Type Joints Subjected to Force Perpendicular to the Grain – M Yasumura
- 34-7-10 Interaction Between Splitting and Block Shear Failure of Joints – A J M Leijten, A Jorissen, J Kuipers
- 34-7-11 Limit states design of dowel-fastener joints – Placement of modification factors and partial factors, and calculation of variability in resistance – I Smith, G Foliente
- 34-7-12 Design and Modelling of Knee Joints - J Nielsen, P Ellegaard
- 34-7-13 Timber-Steel Shot Fired Nail Connections at Ultimate Limit States - R J Bainbridge, P Larsen, C J Mettem, P Alam, M P Ansell
- 35-7-1 New Estimating Method of Bolted Cross-lapped Joints with Timber Side Members - M Noguchi, K Komatsu
- 35-7-2 Analysis on Multiple Lag Screwed Timber Joints with Timber Side Members - K Komatsu, S Takino, M Nakatani, H Tateishi
- 35-7-3 Joints with Inclined Screws - A Kevarinmäki
- 35-7-4 Joints with Inclined Screws - I Bejtka, H J Blaß
- 35-7-5 Effect of distances, Spacing and Number of Dowels in a Row on the Load Carrying Capacity of Connections with Dowels failing by Splitting - M Schmid, R Frasson, H J Blaß
- 35-7-6 Effect of Row Spacing on the Capacity of Bolted Timber Connections Loaded Perpendicular-to-grain - P Quenneville, M Kasim
- 35-7-7 Splitting Strength of Beams Loaded by Connections, Model Comparison - A J M Leijten
- 35-7-8 Load-Carrying Capacity of Perpendicular to the Grain Loaded Timber Joints with Multiple Fasteners - O Borth, K U Schober, K Rautenstrauch
- 35-7-9 Determination of fracture parameter for dowel-type joints loaded perpendicular to wooden grain and its application - M Yasumura
- 35-7-10 Analysis and Design of Modified Attic Trusses with Punched Metal Plate Fasteners - P Ellegaard
- 35-7-11 Joint Properties of Plybamboo Sheets in Prefabricated Housing - G E Gonzalez
- 35-7-12 Fiber-Reinforced Beam-to-Column Connections for Seismic Applications - B Kasal, A Heiduschke, P Haller
- 36-7-1 Shear Tests in Timber-LWAC with Screw-Type Connections - L Jorge, H Cruz, S Lopes
- 36-7-2 Plug Shear Failure in Nailed Timber Connections: Experimental Studies - H Johansson
- 36-7-3 Nail-Laminated Timber Elements in Natural Surface-Composite with Mineral Bound Layer - S Lehmann, K Rautenstrauch
- 36-7-4 Mechanical Properties of Timber-Concrete Joints Made With Steel Dowels - A Dias, J W G van de Kuilen, H Cruz

- 36-7-5 Comparison of Hysteresis Responses of Different Sheating to Framing Joints - B Dujič, R Zarnić
- 36-7- 6 Evaluation and Estimation of the Performance of the Nail Joints and Shear Walls under Dry/Humid Cyclic Climate - S Nakajima
- 36-7-7 Beams Transversally Loaded by Dowel-Type Joints: Influence on Splitting Strength of Beam Thickness and Dowel Size - M Ballerini, A Giovanella
- 36-7-8 Splitting Strength of Beams Loaded by Connections - J L Jensen
- 36-7-9 A Tensile Fracture Model for Joints with Rods or Dowels loaded Perpendicular-to-Grain - J L Jensen, P J Gustafsson, H J Larsen
- 36-7-10 A Numerical Model to Simulate the Load-Displacement Time-History of Mutiple-Bolt Connections Subjected to Various Loadings - C P Heine, J D Dolan
- 36-7-11 Reliability of Timber Structures, Theory and Dowel-Type Connection Failures - A Ranta-Maunus, A Kevarinmäki
- 37-7-1 Development of the "Displaced Volume Model" to Predict Failure for Multiple-Bolt Timber Joints - D M Carradine, J D Dolan, C P Heine
- 37-7-2 Mechanical Models of the Knee Joints with Cross-Lapped Glued Joints and Glued in Steel Rods - M Noguchi, K Komatsu
- 37-7-3 Simplification of the Neural Network Model for Predicting the Load-Carrying Capacity of Dowel-Type Connections - A Cointe, F Rouger
- 37-7-4 Bolted Wood Connections Loaded Perpendicular-to-Grain- A Proposed Design Approach - M C G Lehoux, J H P Quenneville
- 37-7-5 A New Prediction Formula for the Splitting Strength of Beams Loaded by Dowel Type Connections - M Ballerini
- 37-7-6 Plug Shear Failure: The Tensile Failure Mode and the Effect of Spacing - H Johnsson
- 37-7-7 Block Shear Failure Test with Dowel-Type Connection in Diagonal LVL Structure - M Kairi
- 37-7-8 Glued-in Steel Rods: A Design Approach for Axially Loaded Single Rods Set Parallel to the Grain - R Steiger, E Gehri, R Widmann
- 37-7-9 Glued in Rods in Load Bearing Timber Structures - Status regarding European Standards for Test Procedures - B Källander
- 37-7-10 French Data Concerning Glued-in Rods - C Faye, L Le Magorou, P Morlier, J Surleau
- 37-7-11 Enhancement of Dowel-Type Fasteners by Glued Connectors - C O Clorius, A Højman
- 37-7-12 Review of Probability Data for Timber Connections with Dowel-Type Fasteners - A J M Leijten, J Köhler, A Jorissen
- 37-7-13 Behaviour of Fasteners and Glued-in Rods Produced From Stainless Steel - A Kevarinmäki
- 37-7-14 Dowel joints in Engineered Wood Products: Assessment of Simple Fracture Mechanics Models - M Snow, I Smith, A Asiz
- 37-7-15 Numerical Modelling of Timber and Connection Elements Used in Timber-Concrete-Composite Constructions - M Grosse, K Rautenstrauch
- 38-7-1 A Numerical Investigation on the Splitting Strength of Beams Loaded Perpendicular-to-grain by Multiple-dowel Connections – M Ballerini, M Rizzi
- 38-7-2 A Probabilistic Framework for the Reliability Assessment of Connections with Dowel Type Fasteners - J Köhler
- 38-7-3 Load Carrying Capacity of Curved Glulam Beams Reinforced with self-tapping Screws - J Jönsson, S Thelandersson
- 38-7-4 Self-tapping Screws as Reinforcements in Connections with Dowel-Type Fasteners- I Bejtka, H J Blaß

- 38-7-5 The Yield Capacity of Dowel Type Fasteners - A Jorissen, A Leijten
- 38-7-6 Nails in Spruce - Splitting Sensitivity, End Grain Joints and Withdrawal Strength - A Kevarinmäki
- 38-7-7 Design of Timber Connections with Slotted-in Steel Plates and Small Diameter Steel Tube Fasteners - B Murty, I Smith, A Asiz
- 39-7-1 Effective in-row Capacity of Multiple-Fastener Connections - P Quenneville, M Bickerdike
- 39-7-2 Self-tapping Screws as Reinforcements in Beam Supports - I Bejtka, H J Blaß
- 39-7-3 Connectors for Timber-concrete Composite-Bridges - A Döhrer, K Rautenstrauch
- 39-7-4 Block Shear Failure at Dowelled Double Shear Steel-to-timber Connections - A Hanhijärvi, A Kevarinmäki, R Yli-Koski
- 39-7-5 Load Carrying Capacity of Joints with Dowel Type Fasteners in Solid Wood Panels - T Uibel, H J Blaß
- 39-7-6 Generalised Canadian Approach for Design of Connections with Dowel Fasteners - P Quenneville, I Smith, A Asiz, M Snow, Y H Chui
- 40-7-1 Predicting the Strength of Bolted Timber Connections Subjected to Fire - M Fragiaco, A Buchanan, D Carshalton, P Moss, C Austruy
- 40-7-2 Edge Joints with Dowel Type Fasteners in Cross Laminated Timber - H J Blaß, T Uibel
- 40-7-3 Design Method against Timber Failure Mechanisms of Dowelled Steel-to-Timber Connections - A Hanhijärvi, A Kevarinmäki
- 40-7-4 A EYM Based Simplified Design Formula for the Load-carrying Capacity of Dowel-type Connections - M Ballerini
- 40-7-5 Evaluation of the Slip Modulus for Ultimate Limit State Verifications of Timber-Concrete Composite Structures - E Lukaszewska, M Fragiaco, A Frangi
- 40-7-6 Models for the Predictions of the Ductile and Brittle Failure Modes (Parallel-to-Grain) of Timber Rivet Connections - M Marjerrison, P Quenneville
- 40-7-7 Creep of Timber and Timber-Concrete Joints. - J W G van de Kuilen, A M P G Dias
- 40-7-8 Lag Screwed Timber Joints with Timber Side Members- K Komatsu, S Takino, H Tateishi
- 41-7-1 Applicability of Existing Design Approaches to Mechanical Joints in Structural Composite Lumber - M Snow, I Smith, A Asiz, M Ballerini
- 41-7-2 Validation of the Canadian Bolted Connection Design Proposal - P Quenneville, J Jensen
- 41-7-3 Ductility of Moment Resisting Dowelled Joints in Heavy Timber Structures - A Polastri, R Tomasi, M Piazza, I Smith
- 41-7-4 Mechanical Behaviour of Traditional Timber Connections: Proposals for Design, Based on Experimental and Numerical Investigations. Part I: Birdsmouth - C Faye, P Garcia, L Le Magorou, F Rouger
- 41-7-5 Embedding Strength of European Hardwoods - U Hübner, T Bogensperger, G Schickhofer
- 42-7-1 Base Parameters of Self-tapping Screws - G Pirnbacher, R Brandner, G Schickhofer
- 42-7-2 Joints with Inclined Screws and Steel Plates as Outer Members - H Krenn, G Schickhofer
- 42-7-3 Models for the Calculation of the Withdrawal Capacity of Self-tapping Screws - M Frese, H J Blaß
- 42-7-4 Embedding Strength of New Zealand Timber and Recommendation for the NZ Standard - S Franke, P Quenneville
- 42-7-5 Load Carrying Capacity of Timber-Wood Fiber Insulation Board – Joints with Dowel Type Fasteners - G Gebhardt, H J Blaß

- 42-7-6 Prediction of the Fatigue Resistance of Timber-Concrete-Composite Connections - U Kuhlmann, P Aldi
- 42-7-7 Using Screws for Structural Applications in Laminated Veneer Lumber - D M Carradine, M P Newcombe, A H Buchanan
- 42-7-8 Influence of Fastener Spacings on Joint Performance - Experimental Results and Codification - E Gehri
- 42-7-9 Connections with Glued-in Hardwood Rods Subjected to Combined Bending and Shear Actions - J L Jensen, P Quenneville
- 43-7-1 Probabilistic Capacity Prediction of Timber Joints under Brittle Failure Modes - T Tannert, T Vallée, and F Lam
- 43-7-2 Ductility in Timber Structures - A Jorissen, M Fragiaco
- 43-7-3 Design of Mechanically Jointed Concrete-Timber Beams Taking into Account the Plastic Behaviour of the Fasteners - H J Larsen, H Riberholt, A Ceccotti
- 43-7-4 Design of Timber-Concrete Composite Beams with Notched Connections - M Fragiaco, D Yeoh
- 43-7-5 Development of Design Procedures for Timber Concrete Composite Floors in Australia and New Zealand - K Crews, C Gerber
- 43-7-6 Failure Behaviour and Resistance of Dowel-Type Connections Loaded Perpendicular to Grain - B Franke, P Quenneville
- 43-7-7 Predicting Time Dependent Effects in Unbonded Post-Tensioned Timber Beams and Frames - S Giorgini, A Neale, A Palermo, D Carradine, S Pampanin, A H Buchanan
- 43-7-8 Simplified Design of Post-tensioned Timber Frames - M Newcombe, M Cusiél, S Pampanin, A Palermo, A H Buchanan

LOAD SHARING

- 3-8-1 Load Sharing - An Investigation on the State of Research and Development of Design Criteria - E Levin
- 4-8-1 A Review of Load-Sharing in Theory and Practice - E Levin
- 4-8-2 Load Sharing - B Norén
- 19-8-1 Predicting the Natural Frequencies of Light-Weight Wooden Floors - I Smith and Y H Chui
- 20-8-1 Proposed Code Requirements for Vibrational Serviceability of Timber Floors - Y H Chui and I Smith
- 21-8-1 An Addendum to Paper 20-8-1 - Proposed Code Requirements for Vibrational Serviceability of Timber Floors - Y H Chui and I Smith
- 21-8-2 Floor Vibrational Serviceability and the CIB Model Code - S Ohlsson
- 22-8-1 Reliability Analysis of Viscoelastic Floors - F Rouger, J D Barrett and R O Foschi
- 24-8-1 On the Possibility of Applying Neutral Vibrational Serviceability Criteria to Joisted Wood Floors - I Smith and Y H Chui
- 25-8-1 Analysis of Glulam Semi-rigid Portal Frames under Long-term Load - K Komatsu and N Kawamoto
- 34-8-1 System Effect in Sheathed Parallel Timber Beam Structures – M Hansson, T Isaksson
- 35-8-1 System Effects in Sheathed Parallel Timber Beam Structures part II. - M Hansson, T Isaksson
- 39-8-1 Overview of a new Canadian Approach to Handling System Effects in Timber Structures - I Smith, Y H Chui, P Quenneville

DURATION OF LOAD

- 3-9-1 Definitions of Long Term Loading for the Code of Practice - B Norén
- 4-9-1 Long Term Loading of Trussed Rafters with Different Connection Systems - T Feldborg and M Johansen
- 5-9-1 Strength of a Wood Column in Combined Compression and Bending with Respect to Creep - B Källsner and B Norén
- 6-9-1 Long Term Loading for the Code of Practice (Part 2) - B Norén
- 6-9-2 Long Term Loading - K Möhler
- 6-9-3 Deflection of Trussed Rafters under Alternating Loading during a Year - T Feldborg and M Johansen
- 7-6-1 Strength and Long Term Behaviour of Lumber and Glued-Laminated Timber under Torsion Loads - K Möhler
- 7-9-1 Code Rules Concerning Strength and Loading Time - H J Larsen and E Theilgaard
- 17-9-1 On the Long-Term Carrying Capacity of Wood Structures - Y M Ivanov and Y Y Slavic
- 18-9-1 Prediction of Creep Deformations of Joints - J Kuipers
- 19-9-1 Another Look at Three Duration of Load Models - R O Foschi and Z C Yao
- 19-9-2 Duration of Load Effects for Spruce Timber with Special Reference to Moisture Influence - A Status Report - P Hoffmeyer
- 19-9-3 A Model of Deformation and Damage Processes Based on the Reaction Kinetics of Bond Exchange - T A C M van der Put
- 19-9-4 Non-Linear Creep Superposition - U Korin
- 19-9-5 Determination of Creep Data for the Component Parts of Stressed-Skin Panels - R Kliger
- 19-9-6 Creep an Lifetime of Timber Loaded in Tension and Compression - P Glos
- 19-1-1 Duration of Load Effects and Reliability Based Design (Single Member) - R O Foschi and Z C Yao
- 19-6-1 Effect of Age and/or Load on Timber Strength - J Kuipers
- 19-7-4 The Prediction of the Long-Term Load Carrying Capacity of Joints in Wood Structures - Y M Ivanov and Y Y Slavic
- 19-7-5 Slip in Joints under Long-Term Loading - T Feldborg and M Johansen
- 20-7-2 Slip in Joints under Long-Term Loading - T Feldborg and M Johansen
- 22-9-1 Long-Term Tests with Glued Laminated Timber Girders - M Badstube, W Rug and W Schöne
- 22-9-2 Strength of One-Layer solid and Lengthways Glued Elements of Wood Structures and its Alteration from Sustained Load - L M Kovaltchuk, I N Boitemirova and G B Uspenskaya
- 24-9-1 Long Term Bending Creep of Wood - T Toratti
- 24-9-2 Collection of Creep Data of Timber - A Ranta-Maunus
- 24-9-3 Deformation Modification Factors for Calculating Built-up Wood-Based Structures - I R Kliger
- 25-9-2 DVM Analysis of Wood. Lifetime, Residual Strength and Quality - L F Nielsen
- 26-9-1 Long Term Deformations in Wood Based Panels under Natural Climate Conditions. A Comparative Study - S Thelandersson, J Nordh, T Nordh and S Sandahl

- 28-9-1 Evaluation of Creep Behavior of Structural Lumber in Natural Environment - R Gupta and R Shen
- 30-9-1 DOL Effect in Tension Perpendicular to the Grain of Glulam Depending on Service Classes and Volume - S Aicher and G Dill-Langer
- 30-9-2 Damage Modelling of Glulam in Tension Perpendicular to Grain in Variable Climate - G Dill-Langer and S Aicher
- 31-9-1 Duration of Load Effect in Tension Perpendicular to Grain in Curved Glulam - A Ranta-Maunus
- 32-9-1 Bending-Stress-Redistribution Caused by Different Creep in Tension and Compression and Resulting DOL-Effect - P Becker and K Rautenstrauch
- 32-9-2 The Long Term Performance of Ply-Web Beams - R Grantham and V Enjily
- 36-9-1 Load Duration Factors for Instantaneous Loads - A J M Leijten, B Jansson
- 39-9-1 Simplified Approach for the Long-Term Behaviour of Timber-Concrete Composite Beams According to the Eurocode 5 Provisions - M Fragiaco, A Ceccotti

TIMBER BEAMS

- 4-10-1 The Design of Simple Beams - H J Burgess
- 4-10-2 Calculation of Timber Beams Subjected to Bending and Normal Force - H J Larsen
- 5-10-1 The Design of Timber Beams - H J Larsen
- 9-10-1 The Distribution of Shear Stresses in Timber Beams - F J Keenan
- 9-10-2 Beams Notched at the Ends - K Möhler
- 11-10-1 Tapered Timber Beams - H Riberholt
- 13-6-2 Consideration of Size Effects in Longitudinal Shear Strength for Uncracked Beams - R O Foschi and J D Barrett
- 13-6-3 Consideration of Shear Strength on End-Cracked Beams - J D Barrett and R O Foschi
- 18-10-1 Submission to the CIB-W18 Committee on the Design of Ply Web Beams by Consideration of the Type of Stress in the Flanges - J A Baird
- 18-10-2 Longitudinal Shear Design of Glued Laminated Beams - R O Foschi
- 19-10-1 Possible Code Approaches to Lateral Buckling in Beams - H J Burgess
- 19-2-1 Creep Buckling Strength of Timber Beams and Columns - R H Leicester
- 20-2-1 Lateral Buckling Theory for Rectangular Section Deep Beam-Columns - H J Burgess
- 20-10-1 Draft Clause for CIB Code for Beams with Initial Imperfections - H J Burgess
- 20-10-2 Space Joists in Irish Timber - W J Robinson
- 20-10-3 Composite Structure of Timber Joists and Concrete Slab - T Poutanen
- 21-10-1 A Study of Strength of Notched Beams - P J Gustafsson
- 22-10-1 Design of Endnotched Beams - H J Larsen and P J Gustafsson
- 22-10-2 Dimensions of Wooden Flexural Members under Constant Loads - A Pozgai
- 22-10-3 Thin-Walled Wood-Based Flanges in Composite Beams - J König
- 22-10-4 The Calculation of Wooden Bars with flexible Joints in Accordance with the Polish Standard Code and Strict Theoretical Methods - Z Mielczarek
- 23-10-1 Tension Perpendicular to the Grain at Notches and Joints - T A C M van der Put

- 23-10-2 Dimensioning of Beams with Cracks, Notches and Holes. An Application of Fracture Mechanics - K Riipola
- 23-10-3 Size Factors for the Bending and Tension Strength of Structural Timber - J D Barret and A R Fewell
- 23-12-1 Bending Strength of Glulam Beams, a Design Proposal - J Ehlbeck and F Colling
- 23-12-3 Glulam Beams, Bending Strength in Relation to the Bending Strength of the Finger Joints - H Riberholt
- 24-10-1 Shear Strength of Continuous Beams - R H Leicester and F G Young
- 25-10-1 The Strength of Norwegian Glued Laminated Beams - K Solli, E Aasheim and R H Falk
- 25-10-2 The Influence of the Elastic Modulus on the Simulated Bending Strength of Hyperstatic Timber Beams - T D G Canisius
- 27-10-1 Determination of Shear Modulus - R Görlacher and J Kürth
- 29-10-1 Time Dependent Lateral Buckling of Timber Beams - F Rouger
- 29-10-2 Determination of Modulus of Elasticity in Bending According to EN 408 - K H Solli
- 29-10-3 On Determination of Modulus of Elasticity in Bending - L Boström, S Ormarsson and O Dahlblom
- 29-10-4 Relation of Moduli of Elasticity in Flatwise and Edgewise Bending of Solid Timber - C J Johansson, A Steffen and E W Wormuth
- 30-10-1 Nondestructive Evaluation of Wood-based Members and Structures with the Help of Modal Analysis - P Kuklik
- 30-10-2 Measurement of Modulus of Elasticity in Bending - L Boström
- 30-10-3 A Weak Zone Model for Timber in Bending - B Källsner, K Salmela and O Ditlevsen
- 30-10-4 Load Carrying Capacity of Timber Beams with Narrow Moment Peaks - T Isaksson and J Freysoldt
- 37-10-1 Design of Rim Boards for Use with I-Joists Framing Systems - B Yeh, T G Williamson
- 40-10- 1 Extension of EC5 Annex B Formulas for the Design of Timber-concrete Composite Structures - J Schänzlin, M Fragiaco
- 40-10-2 Simplified Design Method for Mechanically Jointed Beams - U A Girhammar
- 41-10-1 Composite Action of I-Joist Floor Systems - T G Williamson, B Yeh
- 41-10-2 Evaluation of the Prestressing Losses in Timber Members Prestressed with Unbonded Tendons - M Fragiaco, M Davies
- 41-10-3 Relationship Between Global and Local MOE – J K Denzler, P Stapel, P Glos
- 42-10-1 Relationships Between Local, Global and Dynamic Modulus of Elasticity for Soft- and Hardwoods – G J P Ravenshorst, J W G van de Kuilen

ENVIRONMENTAL CONDITIONS

- 5-11-1 Climate Grading for the Code of Practice - B Norén
- 6-11-1 Climate Grading (2) - B Norén
- 9-11-1 Climate Classes for Timber Design - F J Keenan
- 19-11-1 Experimental Analysis on Ancient Downgraded Timber Structures - B Leggeri and L Paolini
- 19-6-5 Drying Stresses in Round Timber - A Ranta-Maunus

22-11-1	Corrosion and Adaptation Factors for Chemically Aggressive Media with Timber Structures - K Erler
29-11-1	Load Duration Effect on Structural Beams under Varying Climate Influence of Size and Shape - P Galimard and P Morlier
30-11-1	Probabilistic Design Models for the Durability of Timber Constructions - R H Leicester
36-11-1	Structural Durability of Timber in Ground Contact – R H Leicester, C H Wang, M N Nguyen, G C Foliente, C McKenzie
38-11-1	Design Specifications for the Durability of Timber – R H Leicester, C-H Wang, M Nguyen, G C Foliente
38-11-2	Consideration of Moisture Exposure of Timber Structures as an Action - M Häglund, S Thelandersson

LAMINATED MEMBERS

6-12-1	Directives for the Fabrication of Load-Bearing Structures of Glued Timber - A van der Velden and J Kuipers
8-12-1	Testing of Big Glulam Timber Beams - H Kolb and P Frech
8-12-2	Instruction for the Reinforcement of Apertures in Glulam Beams - H Kolb and P Frech
8-12-3	Glulam Standard Part 1: Glued Timber Structures; Requirements for Timber (Second Draft)
9-12-1	Experiments to Provide for Elevated Forces at the Supports of Wooden Beams with Particular Regard to Shearing Stresses and Long-Term Loadings - F Wassipaul and R Lackner
9-12-2	Two Laminated Timber Arch Railway Bridges Built in Perth in 1849 - L G Booth
9-6-4	Consideration of Combined Stresses for Lumber and Glued Laminated Timber - K Möhler
11-6-3	Consideration of Combined Stresses for Lumber and Glued Laminated Timber (addition to Paper CIB-W18/9-6-4) - K Möhler
12-12-1	Glulam Standard Part 2: Glued Timber Structures; Rating (3rd draft)
12-12-2	Glulam Standard Part 3: Glued Timber Structures; Performance (3 rd draft)
13-12-1	Glulam Standard Part 3: Glued Timber Structures; Performance (4th draft)
14-12-1	Proposals for CEI-Bois/CIB-W18 Glulam Standards - H J Larsen
14-12-2	Guidelines for the Manufacturing of Glued Load-Bearing Timber Structures - Stevin Laboratory
14-12-3	Double Tapered Curved Glulam Beams - H Riberholt
14-12-4	Comment on CIB-W18/14-12-3 - E Gehri
18-12-1	Report on European Glulam Control and Production Standard - H Riberholt
18-10-2	Longitudinal Shear Design of Glued Laminated Beams - R O Foschi
19-12-1	Strength of Glued Laminated Timber - J Ehlbeck and F Colling
19-12-2	Strength Model for Glulam Columns - H J Blaß
19-12-3	Influence of Volume and Stress Distribution on the Shear Strength and Tensile Strength Perpendicular to Grain - F Colling
19-12-4	Time-Dependent Behaviour of Glued-Laminated Beams - F Zaupa
21-12-1	Modulus of Rupture of Glulam Beam Composed of Arbitrary Laminae - K Komatsu and N Kawamoto

- 21-12-2 An Appraisal of the Young's Modulus Values Specified for Glulam in Eurocode 5- L R J Whale, B O Hilson and P D Rodd
- 21-12-3 The Strength of Glued Laminated Timber (Glulam): Influence of Lamination Qualities and Strength of Finger Joints - J Ehlbeck and F Colling
- 21-12-4 Comparison of a Shear Strength Design Method in Eurocode 5 and a More Traditional One - H Riberholt
- 22-12-1 The Dependence of the Bending Strength on the Glued Laminated Timber Girder Depth - M Badstube, W Rug and W Schöne
- 22-12-2 Acid Deterioration of Glulam Beams in Buildings from the Early Half of the 1960s - Preliminary summary of the research project; Overhead pictures - B A Hedlund
- 22-12-3 Experimental Investigation of normal Stress Distribution in Glue Laminated Wooden Arches - Z Mielczarek and W Chanaj
- 22-12-4 Ultimate Strength of Wooden Beams with Tension Reinforcement as a Function of Random Material Properties - R Candowicz and T Dziuba
- 23-12-1 Bending Strength of Glulam Beams, a Design Proposal - J Ehlbeck and F Colling
- 23-12-2 Probability Based Design Method for Glued Laminated Timber - M F Stone
- 23-12-3 Glulam Beams, Bending Strength in Relation to the Bending Strength of the Finger Joints - H Riberholt
- 23-12-4 Glued Laminated Timber - Strength Classes and Determination of Characteristic Properties - H Riberholt, J Ehlbeck and A Fewell
- 24-12-1 Contribution to the Determination of the Bending Strength of Glulam Beams - F Colling, J Ehlbeck and R Görlacher
- 24-12-2 Influence of Perpendicular-to-Grain Stressed Volume on the Load-Carrying Capacity of Curved and Tapered Glulam Beams - J Ehlbeck and J Kürth
- 25-12-1 Determination of Characteristic Bending Values of Glued Laminated Timber. EN-Approach and Reality - E Gehri
- 26-12-1 Norwegian Bending Tests with Glued Laminated Beams-Comparative Calculations with the "Karlsruhe Calculation Model" - E Aasheim, K Solli, F Colling, R H Falk, J Ehlbeck and R Görlacher
- 26-12-2 Simulation Analysis of Norwegian Spruce Glued-Laminated Timber - R Hernandez and R H Falk
- 26-12-3 Investigation of Laminating Effects in Glued-Laminated Timber - F Colling and R H Falk
- 26-12-4 Comparing Design Results for Glulam Beams According to Eurocode 5 and to the French Working Stress Design Code (CB71) - F Rouger
- 27-12-1 State of the Art Report: Glulam Timber Bridge Design in the U.S. - M A Ritter and T G Williamson
- 27-12-2 Common Design Practice for Timber Bridges in the United Kingdom - C J Mettem, J P Marcroft and G Davis
- 27-12-3 Influence of Weak Zones on Stress Distribution in Glulam Beams - E Serrano and H J Larsen
- 28-12-1 Determination of Characteristic Bending Strength of Glued Laminated Timber - E Gehri
- 28-12-2 Size Factor of Norwegian Glued Laminated Beams - E Aasheim and K H Solli
- 28-12-3 Design of Glulam Beams with Holes - K Riipola
- 28-12-4 Compression Resistance of Glued Laminated Timber Short Columns- U Korin
- 29-12-1 Development of Efficient Glued Laminated Timber - G Schickhofer

- 30-12-1 Experimental Investigation and Analysis of Reinforced Glulam Beams - K Oiger
- 31-12-1 Depth Factor for Glued Laminated Timber-Discussion of the Eurocode 5 Approach - B Källsner, O Carling and C J Johansson
- 32-12-1 The bending stiffness of nail-laminated timber elements in transverse direction- T Wolf and O Schäfer
- 33-12-1 Internal Stresses in the Cross-Grain Direction of Wood Induced by Climate Variation – J Jönsson and S Svensson
- 34-12-1 High-Strength I-Joist Compatible Glulam Manufactured with LVL Tension Laminations – B Yeh, T G Williamson
- 34-12-2 Evaluation of Glulam Shear Strength Using A Full-Size Four-Point Test Method – B Yeh, T G Williamson
- 34-12-3 Design Model for FRP Reinforced Glulam Beams – M Romani, H J Blaß
- 34-12-4 Moisture induced stresses in glulam cross sections – J Jönsson
- 34-12-5 Load Carrying Capacity of Nail-Laminated Timber under Concentrated Loads – V Krämer, H J Blaß
- 34-12-6 Determination of Shear Strength Values for GLT Using Visual and Machine Graded Spruce Laminations – G Schickhofer
- 34-12-7 Mechanically Jointed Beams: Possibilities of Analysis and some special Problems – H Kreuzinger
- 35-12-1 Glulam Beams with Round Holes – a Comparison of Different Design Approaches vs. Test Data - S Aicher L Höfflin
- 36-12-1 Problems with Shear and Bearing Strength of LVL in Highly Loaded Structures - H Bier
- 36-12-2 Weibull Based Design of Round Holes in Glulam - L Höfflin, S Aicher
- 37-12-1 Development of Structural LVL from Tropical Wood and Evaluation of Their Performance for the Structural Components of Wooden Houses. Part-1. Application of Tropical LVL to a Roof Truss - K Komatsu, Y Idris, S Yuwasdiki, B Subiyakto, A Firmanti
- 37-12-2 Reinforcement of LVL Beams With Bonded-in Plates and Rods - Effect of Placement of Steel and FRP Reinforcements on Beam Strength and Stiffness - P Alam, M P Ansell, D Smedley
- 39-12-1 Recommended Procedures for Determination of Distribution Widths in the Design of Stress Laminated Timber Plate Decks - K Crews
- 39-12-2 In-situ Strengthening of Timber Structures with CFRP - K U Schober, S Franke, K Rautenstrauch
- 39-12-3 Effect of Checking and Non-Glued Edge Joints on the Shear Strength of Structural Glued Laminated Timber Beams - B Yeh, T G Williamson, Z A Martin
- 39-12-4 A Contribution to the Design and System Effect of Cross Laminated Timber (CLT) - R Jöbstl, T Moosbrugger, T Bogensperger, G Schickhofer
- 39-12-5 Behaviour of Glulam in Compression Perpendicular to Grain in Different Strength Grades and Load Configurations - M Augustin, A Ruli, R Brandner, G Schickhofer
- 40-12-1 Development of New Constructions of Glulam Beams in Canada - F Lam, N Mohadevan
- 40-12-2 Determination of Modulus of Shear and Elasticity of Glued Laminated Timber and Related Examination - R Brandner, E Gehri, T Bogensperger, G Schickhofer
- 40-12-3 Comparative Examination of Creep of GTL and CLT-Slabs in Bending - R A Jöbstl, G Schickhofer,
- 40-12-4 Standard Practice for the Derivation of Design Properties of Structural Glued Laminated Timber in the United States - T G Williamson, B Yeh

- 40-12-5 Creep and Creep-Rupture Behaviour of Structural Composite Lumber Evaluated in Accordance with ASTM D 6815 - B Yeh, T G Williamson.
- 40-12-6 Bending Strength of Combined Beech-Spruce Glulam - M Frese, H J Blaß
- 40-12-7 Quality Control of Glulam: Shear Tests of Glue Lines - R Steiger, E Gehri
- 41-12-1 Paper withdrawn by the author
- 41-12-2 Bending Strength of Spruce Glulam: New Models for the Characteristic Bending Strength - M Frese, H J Blass,
- 41-12-3 In-Plane Shear Strength of Cross Laminated Timber - R A Joebstl, T Bogensperger, G Schickhofer
- 41-12-4 Strength of Glulam Beams with Holes - Tests of Quadratic Holes and Literature Test Results Compilation - H Danielsson, P J Gustafsson
- 42-12-1 Glulam Beams with Holes Reinforced by Steel Bars – S Aicher, L Höfflin
- 42-12-2 Analysis of X-lam Panel-to-Panel Connections under Monotonic and Cyclic Loading - C Sandhaas, L Boukes, J W G van de Kuilen, A Ceccotti
- 42-12-3 Laminating Lumber and End Joint Properties for FRP-Reinforced Glulam Beams - T G Williamson, B Yeh
- 43-12-4 Validity of Bending Tests on Strip-Shaped Specimens to Derive Bending Strength and Stiffness Properties of Cross-Laminated Solid Timber (CLT) - R Steiger, A Gülzow
- 42-12-5 Mechanical Properties of Stress Laminated Timber Decks - Experimental Study - K Karlsson, R Crocetti, R Kliger
- 43-12-1 Fatigue Behaviour of Finger Jointed Lumber - S Aicher, G Stapf
- 43-12-2 Experimental and Numerical Investigation on the Shear Strength of Glulam - R Crocetti, P J Gustafsson, H Danielsson, A Emilsson, S Ormarsson
- 43-12-3 System Effects in Glued Laminated Timber in Tension and Bending - M Frese, H J Blaß
- 43-12-4 Experimental Investigations on Mechanical Behaviour of Glued Solid timber - C Faye, F Rouger, P Garcia

PARTICLE AND FIBRE BUILDING BOARDS

- 7-13-1 Fibre Building Boards for CIB Timber Code (First Draft)- O Brynildsen
- 9-13-1 Determination of the Bearing Strength and the Load-Deformation Characteristics of Particleboard - K Möhler, T Budianto and J Ehlbeck
- 9-13-2 The Structural Use of Tempered Hardboard - W W L Chan
- 11-13-1 Tests on Laminated Beams from Hardboard under Short- and Longterm Load - W Nozynski
- 11-13-2 Determination of Deformation of Special Densified Hardboard under Long-term Load and Varying Temperature and Humidity Conditions - W Halfar
- 11-13-3 Determination of Deformation of Hardboard under Long-term Load in Changing Climate - W Halfar
- 14-4-1 An Introduction to Performance Standards for Wood-Base Panel Products - D H Brown
- 14-4-2 Proposal for Presenting Data on the Properties of Structural Panels - T Schmidt
- 16-13-1 Effect of Test Piece Size on Panel Bending Properties - P W Post
- 20-4-1 Considerations of Reliability - Based Design for Structural Composite Products - M R O'Halloran, J A Johnson, E G Elias and T P Cunningham
- 20-13-1 Classification Systems for Structural Wood-Based Sheet Materials - V C Kearley and A R Abbott

21-13-1	Design Values for Nailed Chipboard - Timber Joints - A R Abbott
25-13-1	Bending Strength and Stiffness of Izopanel Plates - Z Mielczarek
28-13-1	Background Information for "Design Rated Oriented Strand Board (OSB)" in CSA Standards - Summary of Short-term Test Results - E Karacabeyli, P Lau, C R Henderson, F V Meakes and W Deacon
28-13-2	Torsional Stiffness of Wood-Hardboard Composed I-Beam - P Olejniczak

TRUSSED RAFTERS

4-9-1	Long-term Loading of Trussed Rafters with Different Connection Systems - T Feldborg and M Johansen
6-9-3	Deflection of Trussed Rafters under Alternating Loading During a Year - T Feldborg and M Johansen
7-2-1	Lateral Bracing of Timber Struts - J A Simon
9-14-1	Timber Trusses - Code Related Problems - T F Williams
9-7-1	Design of Truss Plate Joints - F J Keenan
10-14-1	Design of Roof Bracing - The State of the Art in South Africa - P A V Bryant and J A Simon
11-14-1	Design of Metal Plate Connected Wood Trusses - A R Egerup
12-14-1	A Simple Design Method for Standard Trusses - A R Egerup
13-14-1	Truss Design Method for CIB Timber Code - A R Egerup
13-14-2	Trussed Rafters, Static Models - H Riberholt
13-14-3	Comparison of 3 Truss Models Designed by Different Assumptions for Slip and E-Modulus - K Möhler
14-14-1	Wood Trussed Rafter Design - T Feldborg and M Johansen
14-14-2	Truss-Plate Modelling in the Analysis of Trusses - R O Foschi
14-14-3	Cantilevered Timber Trusses - A R Egerup
14-7-5	The Effect of Support Eccentricity on the Design of W- and WW-Trusses with Nail Plate Connectors - B Källsner
15-14-1	Guidelines for Static Models of Trussed Rafters - H Riberholt
15-14-2	The Influence of Various Factors on the Accuracy of the Structural Analysis of Timber Roof Trusses - F R P Pienaar
15-14-3	Bracing Calculations for Trussed Rafter Roofs - H J Burgess
15-14-4	The Design of Continuous Members in Timber Trussed Rafters with Punched Metal Connector Plates - P O Reece
15-14-5	A Rafter Design Method Matching U.K. Test Results for Trussed Rafters - H J Burgess
16-14-1	Full-Scale Tests on Timber Fink Trusses Made from Irish Grown Sitka Spruce - V Picardo
17-14-1	Data from Full Scale Tests on Prefabricated Trussed Rafters - V Picardo
17-14-2	Simplified Static Analysis and Dimensioning of Trussed Rafters - H Riberholt
17-14-3	Simplified Calculation Method for W-Trusses - B Källsner
18-14-1	Simplified Calculation Method for W-Trusses (Part 2) - B Källsner
18-14-2	Model for Trussed Rafter Design - T Poutanen
19-14-1	Annex on Simplified Design of W-Trusses - H J Larsen

- 19-14-2 Simplified Static Analysis and Dimensioning of Trussed Rafters - Part 2 - H Riberholt
- 19-14-3 Joint Eccentricity in Trussed Rafters - T Poutanen
- 20-14-1 Some Notes about Testing Nail Plates Subjected to Moment Load - T Poutanen
- 20-14-2 Moment Distribution in Trussed Rafters - T Poutanen
- 20-14-3 Practical Design Methods for Trussed Rafters - A R Egerup
- 22-14-1 Guidelines for Design of Timber Trussed Rafters - H Riberholt
- 23-14-1 Analyses of Timber Trussed Rafters of the W-Type - H Riberholt
- 23-14-2 Proposal for Eurocode 5 Text on Timber Trussed Rafters - H Riberholt
- 24-14-1 Capacity of Support Areas Reinforced with Nail Plates in Trussed Rafters - A Kevarinmäki
- 25-14-1 Moment Anchorage Capacity of Nail Plates in Shear Tests - A Kevarinmaki and J. Kangas
- 25-14-2 Design Values of Anchorage Strength of Nail Plate Joints by 2-curve Method and Interpolation - J Kangas and A Kevarinmaki
- 26-14-1 Test of Nail Plates Subjected to Moment - E Aasheim
- 26-14-2 Moment Anchorage Capacity of Nail Plates - A Kevarinmäki and J Kangas
- 26-14-3 Rotational Stiffness of Nail Plates in Moment Anchorage - A Kevarinmäki and J Kangas
- 26-14-4 Solution of Plastic Moment Anchorage Stress in Nail Plates - A Kevarinmäki
- 26-14-5 Testing of Metal-Plate-Connected Wood-Truss Joints - R Gupta
- 26-14-6 Simulated Accidental Events on a Trussed Rafter Roofed Building - C J Mettem and J P Marcroft
- 30-14-1 The Stability Behaviour of Timber Trussed Rafter Roofs - Studies Based on Eurocode 5 and Full Scale Testing - R J Bainbridge, C J Mettern, A Reffold and T Studer
- 32-14-1 Analysis of Timber Reinforced with Punched Metal Plate Fasteners- J Nielsen
- 33-14-1 Moment Capacity of Timber Beams Loaded in Four-Point Bending and Reinforced with Punched Metal Plate Fasteners – J Nielsen
- 36-14-1 Effect of Chord Splice Joints on Force Distribution in Trusses with Punched Metal Plate Fasteners - P Ellegaard
- 36-14-2 Monte Carlo Simulation and Reliability Analysis of Roof Trusses with Punched Metal Plate Fasteners - M Hansson, P Ellegaard
- 36-14-3 Truss Trouble – R H Leicester, J Goldfinch, P Paevere, G C Foliente
- 40-14-1 Timber Trusses with Punched Metal Plate Fasteners - Design for Transport and Erection - H J Blaß

STRUCTURAL STABILITY

- 8-15-1 Laterally Loaded Timber Columns: Tests and Theory - H J Larsen
- 13-15-1 Timber and Wood-Based Products Structures. Panels for Roof Coverings. Methods of Testing and Strength Assessment Criteria. Polish Standard BN-78/7159-03
- 16-15-1 Determination of Bracing Structures for Compression Members and Beams - H Brüninghoff
- 17-15-1 Proposal for Chapter 7.4 Bracing - H Brüninghoff
- 17-15-2 Seismic Design of Small Wood Framed Houses - K F Hansen

18-15-1	Full-Scale Structures in Glued Laminated Timber, Dynamic Tests: Theoretical and Experimental Studies - A Ceccotti and A Vignoli
18-15-2	Stabilizing Bracings - H Brüninghoff
19-15-1	Connections Deformability in Timber Structures: a Theoretical Evaluation of its Influence on Seismic Effects - A Ceccotti and A Vignoli
19-15-2	The Bracing of Trussed Beams - M H Kessel and J Natterer
19-15-3	Racking Resistance of Wooden Frame Walls with Various Openings - M Yasumura
19-15-4	Some Experiences of Restoration of Timber Structures for Country Buildings - G Cardinale and P Spinelli
19-15-5	Non-Destructive Vibration Tests on Existing Wooden Dwellings - Y Hirashima
20-15-1	Behaviour Factor of Timber Structures in Seismic Zones. - A Ceccotti and A Vignoli
21-15-1	Rectangular Section Deep Beam - Columns with Continuous Lateral Restraint - H J Burgess
21-15-2	Buckling Modes and Permissible Axial Loads for Continuously Braced Columns- H J Burgess
21-15-3	Simple Approaches for Column Bracing Calculations - H J Burgess
21-15-4	Calculations for Discrete Column Restraints - H J Burgess
21-15-5	Behaviour Factor of Timber Structures in Seismic Zones (Part Two) - A Ceccotti and A Vignoli
22-15-1	Suggested Changes in Code Bracing Recommendations for Beams and Columns - H J Burgess
22-15-2	Research and Development of Timber Frame Structures for Agriculture in Poland- S Kus and J Kerste
22-15-3	Ensuring of Three-Dimensional Stiffness of Buildings with Wood Structures - A K Shenghelia
22-15-5	Seismic Behavior of Arched Frames in Timber Construction - M Yasumura
22-15-6	The Robustness of Timber Structures - C J Mettem and J P Marcroft
22-15-7	Influence of Geometrical and Structural Imperfections on the Limit Load of Wood Columns - P Dutko
23-15-1	Calculation of a Wind Girder Loaded also by Discretely Spaced Braces for Roof Members - H J Burgess
23-15-2	Stability Design and Code Rules for Straight Timber Beams - T A C M van der Put
23-15-3	A Brief Description of Formula of Beam-Columns in China Code - S Y Huang
23-15-4	Seismic Behavior of Braced Frames in Timber Construction - M Yasumara
23-15-5	On a Better Evaluation of the Seismic Behavior Factor of Low-Dissipative Timber Structures - A Ceccotti and A Vignoli
23-15-6	Disproportionate Collapse of Timber Structures - C J Mettem and J P Marcroft
23-15-7	Performance of Timber Frame Structures During the Loma Prieta California Earthquake - M R O'Halloran and E G Elias
24-15-2	Discussion About the Description of Timber Beam-Column Formula - S Y Huang
24-15-3	Seismic Behavior of Wood-Framed Shear Walls - M Yasumura
25-15-1	Structural Assessment of Timber Framed Building Systems - U Korin

- 25-15-3 Mechanical Properties of Wood-framed Shear Walls Subjected to Reversed Cyclic Lateral Loading - M Yasumura
- 26-15-1 Bracing Requirements to Prevent Lateral Buckling in Trussed Rafters - C J Mettem and P J Moss
- 26-15-2 Eurocode 8 - Part 1.3 - Chapter 5 - Specific Rules for Timber Buildings in Seismic Regions - K Becker, A Ceccotti, H Charlier, E Katsaragakis, H J Larsen and H Zeitter
- 26-15-3 Hurricane Andrew - Structural Performance of Buildings in South Florida - M R O'Halloran, E L Keith, J D Rose and T P Cunningham
- 29-15-1 Lateral Resistance of Wood Based Shear Walls with Oversized Sheathing Panels - F Lam, H G L Prion and M He
- 29-15-2 Damage of Wooden Buildings Caused by the 1995 Hyogo-Ken Nanbu Earthquake - M Yasumura, N Kawai, N Yamaguchi and S Nakajima
- 29-15-3 The Racking Resistance of Timber Frame Walls: Design by Test and Calculation - D R Griffiths, C J Mettem, V Enjily, P J Steer
- 29-15-4 Current Developments in Medium-Rise Timber Frame Buildings in the UK - C J Mettem, G C Pitts, P J Steer, V Enjily
- 29-15-5 Natural Frequency Prediction for Timber Floors - R J Bainbridge, and C J Mettem
- 30-15-1 Cyclic Performance of Perforated Wood Shear Walls with Oversize Oriented Strand Board Panels - Ming He, H Magnusson, F Lam, and H G L Prion
- 30-15-2 A Numerical Analysis of Shear Walls Structural Performances - L Davenne, L Daudeville, N Kawai and M Yasumura
- 30-15-3 Seismic Force Modification Factors for the Design of Multi-Storey Wood-Frame Platform Construction - E Karacabeyli and A Ceccotti
- 30-15-4 Evaluation of Wood Framed Shear Walls Subjected to Lateral Load - M Yasumura and N Kawai
- 31-15-1 Seismic Performance Testing On Wood-Framed Shear Wall - N Kawai
- 31-15-2 Robustness Principles in the Design of Medium-Rise Timber-Framed Buildings - C J Mettem, M W Milner, R J Bainbridge and V. Enjily
- 31-15-3 Numerical Simulation of Pseudo-Dynamic Tests Performed to Shear Walls - L Daudeville, L Davenne, N Richard, N Kawai and M Yasumura
- 31-15-4 Force Modification Factors for Braced Timber Frames - H G L Prion, M Popovski and E Karacabeyli
- 32-15-1 Three-Dimensional Interaction in Stabilisation of Multi-Storey Timber Frame Buildings - S Andreasson
- 32-15-2 Application of Capacity Spectrum Method to Timber Houses - N Kawai
- 32-15-3 Design Methods for Shear Walls with Openings - C Ni, E Karacabeyli and A Ceccotti
- 32-15-4 Static Cyclic Lateral Loading Tests on Nailed Plywood Shear Walls - K Komatsu, K H Hwang and Y Itou
- 33-15-1 Lateral Load Capacities of Horizontally Sheathed Unblocked Shear Walls – C Ni, E Karacabeyli and A Ceccotti
- 33-15-2 Prediction of Earthquake Response of Timber Houses Considering Shear Deformation of Horizontal Frames – N Kawai
- 33-15-3 Eurocode 5 Rules for Bracing – H J Larsen
- 34-15-1 A simplified plastic model for design of partially anchored wood-framed shear walls – B Källsner, U A Girhammar, Liping Wu
- 34-15-2 The Effect of the Moisture Content on the Performance of the Shear Walls – S Nakajima

- 34-15-3 Evaluation of Damping Capacity of Timber Structures for Seismic Design – M Yasumura
- 35-15-1 On test methods for determining racking strength and stiffness of wood-framed shear walls - B Källsner, U A Girhammar, L Wu
- 35-15-2 A Plastic Design Model for Partially Anchored Wood-framed Shear Walls with Openings - U A Girhammar, L Wu, B Källsner
- 35-15-3 Evaluation and Estimation of the Performance of the Shear Walls in Humid Climate - S Nakajima
- 35-15-4 Influence of Vertical Load on Lateral Resistance of Timber Frame Walls - B Dujič, R Žarnić
- 35-15-5 Cyclic and Seismic Performances of a Timber-Concrete System - Local and Full Scale Experimental Results - E Fournely, P Racher
- 35-15-6 Design of timber-concrete composite structures according to EC5 - 2002 version - A Ceccotti, M Fragiaco, R M Gutkowski
- 35-15-7 Design of timber structures in seismic zones according to EC8- 2002 version - A Ceccotti, T Toratti, B Dujič
- 35-15-8 Design Methods to Prevent Premature Failure of Joints at Shear Wall Corners - N Kawai, H Okiura
- 36-15-1 Monitoring Light-Frame Timber Buildings: Environmental Loads and Load Paths – I Smith et al.
- 36-15-2 Applicability of Design Methods to Prevent Premature Failure of Joints at Shear Wall Corners in Case of Post and Beam Construction - N Kawai, H Isoda
- 36-15-3 Effects of Screw Spacing and Edge Boards on the Cyclic Performance of Timber Frame and Structural Insulated Panel Roof Systems - D M Carradine, J D Dolan, F E Woeste
- 36-15-4 Pseudo-Dynamic Tests on Conventional Timber Structures with Shear Walls - M Yasumura
- 36-15-5 Experimental Investigation of Laminated Timber Frames with Fiber-reinforced Connections under Earthquake Loads - B Kasal, P Haller, S Pospisil, I Jirovsky, A Heiduschke, M Drdacky
- 36-15-6 Effect of Test Configurations and Protocols on the Performance of Shear Walls - F Lam, D Jossen, J Gu, N Yamaguchi, H G L Prion
- 36-15-7 Comparison of Monotonic and Cyclic Performance of Light-Frame Shear Walls - J D Dolan, A J Toothman
- 37-15-1 Estimating 3D Behavior of Conventional Timber Structures with Shear Walls by Pseudodynamic Tests - M Yasumura, M Uesugi, L Davenne
- 37-15-2 Testing of Racking Behavior of Massive Wooden Wall Panels - B Dujič, J Pucelj, R Žarnić
- 37-15-3 Influence of Framing Joints on Plastic Capacity of Partially Anchored Wood-Framed Shear Walls - B Källsner, U A Girhammar
- 37-15-4 Bracing of Timber Members in Compression - J Munch-Andersen
- 37-15-5 Acceptance Criteria for the Use of Structural Insulated Panels in High Risk Seismic Areas - B Yeh, T D Skaggs, T G Williamson Z A Martin
- 37-15-6 Predicting Load Paths in Shearwalls - Hongyong Mi, Ying-Hei Chui, I Smith, M Mohammad
- 38-15-1 Background Information on ISO STANDARD 16670 for Cyclic Testing of Connections - E Karacabeyli, M Yasumura, G C Foliente, A Ceccotti
- 38-15-2 Testing & Product Standards – a Comparison of EN to ASTM, AS/NZ and ISO Standards – A Ranta-Maunus, V Enjily

- 38-15-3 Framework for Lateral Load Design Provisions for Engineered Wood Structures in Canada - M Popovski, E Karacabeyli
- 38-15-4 Design of Shear Walls without Hold-Downs - Chun Ni, E Karacabeyli
- 38-15-5 Plastic design of partially anchored wood-framed wall diaphragms with and without openings - B Källsner, U A Girhammar
- 38-15-6 Racking of Wooden Walls Exposed to Different Boundary Conditions - B Dujič, S Aicher, R Žarnić
- 38-15-7 A Portal Frame Design for Raised Wood Floor Applications - T G Williamson, Z A Martin, B Yeh
- 38-15-8 Linear Elastic Design Method for Timber Framed Ceiling, Floor and Wall Diaphragms - Jarmo Leskelä
- 38-15-9 A Unified Design Method for the Racking Resistance of Timber Framed Walls for Inclusion in EUROCODE 5 - R Griffiths, B Källsner, H J Blass, V Enjily
- 39-15-1 Effect of Transverse Walls on Capacity of Wood-Framed Wall Diaphragms - U A Girhammar, B Källsner
- 39-15-2 Which Seismic Behaviour Factor for Multi-Storey Buildings made of Cross-Laminated Wooden Panels? - M Follesa, M P Lauriola, C Minowa, N Kawai, C Sandhaas, M Yasumura, A Ceccotti
- 39-15-3 Laminated Timber Frames under dynamic Loadings - A Heiduschke, B Kasal, P Haller
- 39-15-4 Code Provisions for Seismic Design of Multi-storey Post-tensioned Timber Buildings - S Pampanin, A Palermo, A Buchanan, M Fragiaco, B Deam
- 40-15-1 Design of Safe Timber Structures – How Can we Learn from Structural Failures? - S Thelandersson, E Frühwald
- 40-15-2 Effect of Transverse Walls on Capacity of Wood-Framed Wall Diaphragms—Part 2 - U A Girhammar, B Källsner
- 40-15-3 Midply Wood Shear Wall System: Concept, Performance and Code Implementation - Chun Ni, M Popovski, E Karacabeyli, E Varoglu, S Stierner
- 40-15-4 Seismic Behaviour of Tall Wood-Frame Walls - M Popovski, A Peterson, E Karacabeyli
- 40-15-5 International Standard Development of Lateral Load Test Method for Shear Walls - M Yasumura, E Karacabeyli
- 40-15-6 Influence of Openings on Shear Capacity of Wooden Walls - B Dujič, S Klobcar, R Žarnić
- 41-15-1 Need for a Harmonized Approach for Calculations of Ductility of Timber Assemblies - W Muñoz, M Mohammad, A Salenikovitch, P Quenneville
- 41-15-2 Plastic Design of Wood Frame Wall Diaphragms in Low and Medium Rise Buildings - B Källsner, U A Girhammar
- 41 15-3 Failure Analysis of Light Wood Frame Structures under Wind Load - A Asiz, Y H Chui, I Smith
- 41-15-4 Combined Shear and Wind Uplift Resistance of Wood Structural Panel Shearwalls B Yeh, T G Williamson
- 41-15-5 Behaviour of Prefabricated Timber Wall Elements under Static and Cyclic Loading – P Schädle, H J Blass
- 42-15-1 Design Aspects on Anchoring the Bottom Rail in Partially Anchored Wood-Framed Shear Walls - U A Girhammar, B Källsner
- 42-15-2 New Seismic Design Provisions for Shearwalls and Diaphragms in the Canadian Standard for Engineering Design in Wood - M Popovski, E Karacabeyli, Chun Ni, P Lepper, G Doudak

- 42-15-3 Stability Capacity and Lateral Bracing Force of Metal Plate Connected Wood Truss Assemblies - Xiaobin Song, F Lam, Hao Huang, Minjuan He
- 42-15-4 Improved Method for Determining Braced Wall Requirements for Conventional Wood-Frame Buildings - Chun Ni, H Rainer, E Karacabeyli
- 43-15-1 Influence of the Boundary Conditions on the Racking Strength of Shear Walls with an Opening - M Yasumura
- 43-15-2 Influence of Different Standards on the Determination of Earthquake Properties of Timber Shear Wall Systems - P Schädle, H J Blaß
- 43-15-3 Full-Scale Shear Wall Tests for Force Transfer Around Openings - T Skaggs, B Yeh, F Lam
- 43-15-4 Optimized Anchor-Bolt Spacing for Structural Panel Shearwalls Subjected to Combined Shear and Wind Uplift Forces - B Yeh, E Keith, T Skaggs
- FIRE**
- 12-16-1 British Standard BS 5268 the Structural Use of Timber: Part 4 Fire Resistance of Timber Structures
- 13-100-2 CIB Structural Timber Design Code. Chapter 9. Performance in Fire
- 19-16-1 Simulation of Fire in Tests of Axially Loaded Wood Wall Studs - J König
- 24-16-1 Modelling the Effective Cross Section of Timber Frame Members Exposed to Fire - J König
- 25-16-1 The Effect of Density on Charring and Loss of Bending Strength in Fire - J König
- 25-16-2 Tests on Glued-Laminated Beams in Bending Exposed to Natural Fires - F Bolonius Olesen and J König
- 26-16-1 Structural Fire Design According to Eurocode 5, Part 1.2 - J König
- 31-16-1 Revision of ENV 1995-1-2: Charring and Degradation of Strength and Stiffness - J König
- 33-16-1 A Design Model for Load-carrying Timber Frame Members in Walls and Floors Exposed to Fire - J König
- 33-16-2 A Review of Component Additive Methods Used for the Determination of Fire Resistance of Separating Light Timber Frame Construction - J König, T Oksanen and K Towler
- 33-16-3 Thermal and Mechanical Properties of Timber and Some Other Materials Used in Light Timber Frame Construction - B Källsner and J König
- 34-16-1 Influence of the Strength Determining Factors on the Fire Resistance Capability of Timber Structural Members – I Totev, D Dakov
- 34-16-2 Cross section properties of fire exposed rectangular timber members - J König, B Källsner
- 34-16-3 Pull-Out Tests on Glued-in Rods at High Temperatures – A Mischler, A Frangi
- 35-16-1 Basic and Notional Charring Rates - J König
- 37 - 16 - 1 Effective Values of Thermal Properties of Timber and Thermal Actions During the Decay Phase of Natural Fires - J König
- 37 - 16 - 2 Fire Tests on Timber Connections with Dowel-type Fasteners - A Frangi, A Mischler
- 38-16-1 Fire Behaviour of Multiple Shear Steel-to-Timber Connections with Dowels - C Erchinger, A Frangi, A Mischler
- 38-16-2 Fire Tests on Light Timber Frame Wall Assemblies - V Schleifer, A Frangi
- 39-16-1 Fire Performance of FRP Reinforced Glulam - T G Williamson, B Yeh
- 39-16-2 An Easy-to-use Model for the Design of Wooden I-joists in Fire - J König, B Källsner

- 39-16-3 A Design Model for Timber Slabs Made of Hollow Core Elements in Fire - A Frangi, M Fontana
- 40-16-1 Bonded Timber Deck Plates in Fire - J König, J Schmid
- 40-16-2 Design of Timber Frame Floor Assemblies in Fire - A Frangi, C Erchinger
- 41-16-1 Effect of Adhesives on Finger Joint Performance in Fire - J König, J Norén, M Sterley
- 42-16-1 Advanced Calculation Method for the Fire Resistance of Timber Framed Walls -S Winter, W Meyn
- 42-16-2 Fire Design Model for Multiple Shear Steel-to-Timber Dowelled Connections - C Erchinger, A Frangi, M Fontana
- 42-16-3 Comparison between the Conductive Model of Eurocode 5 and the Temperature Distribution Within a Timber Cross-section Exposed to Fire - M Fragiaco, A Menis, P Moss, A Buchanan, I Clemente
- 43-16-1 Light Timber Frame Construction with Solid Timber Members – Application of the Reduced Cross-section Method - J König, J Schmid
- 43-16-2 Fire Exposed Cross-Laminated Timber - Modelling and Tests - J Schmid, J König, J Köhler
- 43-16-3 Timber-Concrete Composite Floors in Fire - J O'Neill, D Carradine, R Dhakal, P J Moss, A H Buchanan, M Fragiaco

STATISTICS AND DATA ANALYSIS

- 13-17-1 On Testing Whether a Prescribed Exclusion Limit is Attained - W G Warren
- 16-17-1 Notes on Sampling and Strength Prediction of Stress Graded Structural Timber - P Glos
- 16-17-2 Sampling to Predict by Testing the Capacity of Joints, Components and Structures - B Norén
- 16-17-3 Discussion of Sampling and Analysis Procedures - P W Post
- 17-17-1 Sampling of Wood for Joint Tests on the Basis of Density - I Smith, L R J Whale
- 17-17-2 Sampling Strategy for Physical and Mechanical Properties of Irish Grown Sitka Spruce - V Picardo
- 18-17-1 Sampling of Timber in Structural Sizes - P Glos
- 18-6-3 Notes on Sampling Factors for Characteristic Values - R H Leicester
- 19-17-1 Load Factors for Proof and Prototype Testing - R H Leicester
- 19-6-2 Confidence in Estimates of Characteristic Values - R H Leicester
- 21-6-1 Draft Australian Standard: Methods for Evaluation of Strength and Stiffness of Graded Timber - R H Leicester
- 21-6-2 The Determination of Characteristic Strength Values for Stress Grades of Structural Timber. Part 1 - A R Fewell and P Glos
- 22-17-1 Comment on the Strength Classes in Eurocode 5 by an Analysis of a Stochastic Model of Grading - A proposal for a supplement of the design concept - M Kiesel
- 24-17-1 Use of Small Samples for In-Service Strength Measurement - R H Leicester and F G Young
- 24-17-2 Equivalence of Characteristic Values - R H Leicester and F G Young
- 24-17-3 Effect of Sampling Size on Accuracy of Characteristic Values of Machine Grades - Y H Chui, R Turner and I Smith
- 24-17-4 Harmonisation of LSD Codes - R H Leicester
- 25-17-2 A Body for Confirming the Declaration of Characteristic Values - J Sunley

- 25-17-3 Moisture Content Adjustment Procedures for Engineering Standards - D W Green and J W Evans
- 27-17-1 Statistical Control of Timber Strength - R H Leicester and H O Breitingen
- 30-17-1 A New Statistical Method for the Establishment of Machine Settings - F Rouger
- 35-17-1 Probabilistic Modelling of Duration of Load Effects in Timber Structures - J Köhler, S Svenson
- 38-17-1 Analysis of Censored Data - Examples in Timber Engineering Research - R Steiger, J Köhler
- 39-17-1 Possible Canadian / ISO Approach to Deriving Design Values from Test Data - I Smith, A Asiz, M Snow, Y H Chui

GLUED JOINTS

- 20-18-1 Wood Materials under Combined Mechanical and Hygral Loading - A Martensson and S Thelandersson
- 20-18-2 Analysis of Generalized Volkersen - Joints in Terms of Linear Fracture Mechanics - P J Gustafsson
- 20-18-3 The Complete Stress-Slip Curve of Wood-Adhesives in Pure Shear - H Wernersson and P J Gustafsson
- 22-18-1 Perspective Adhesives and Protective Coatings for Wood Structures - A S Freidin
- 34-18-1 Performance Based Classification of Adhesives for Structural Timber Applications - R J Bainbridge, C J Mettem, J G Broughton, A R Hutchinson
- 35-18-1 Creep Testing Wood Adhesives for Structural Use - C Bengtsson, B Källander
- 38-18-1 Adhesive Performance at Elevated Temperatures for Engineered Wood Products - B Yeh, B Herzog, T G Williamson
- 39-18-1 Comparison of the Pull-out Strength of Steel Bars Glued in Glulam Elements Obtained Experimentally and Numerically - V Rajčić, A Bjelanović, M Rak
- 39-18-2 The Influence of the Grading Method on the Finger Joint Bending Strength of Beech - M Frese, H J Blaß
- 43-18-1 Comparison of API, RF and MUF Adhesives Using a Draft Australian/New Zealand Standard - B Walford

FRACTURE MECHANICS

- 21-10-1 A Study of Strength of Notched Beams - P J Gustafsson
- 22-10-1 Design of Endnotched Beams - H J Larsen and P J Gustafsson
- 23-10-1 Tension Perpendicular to the Grain at Notches and Joints - T A C M van der Put
- 23-10-2 Dimensioning of Beams with Cracks, Notches and Holes. An Application of Fracture Mechanics - K Riipola
- 23-19-1 Determination of the Fracture Energie of Wood for Tension Perpendicular to the Grain - W Rug, M Badstube and W Schöne
- 23-19-2 The Fracture Energy of Wood in Tension Perpendicular to the Grain. Results from a Joint Testing Project - H J Larsen and P J Gustafsson
- 23-19-3 Application of Fracture Mechanics to Timber Structures - A Ranta-Maunus
- 24-19-1 The Fracture Energy of Wood in Tension Perpendicular to the Grain - H J Larsen and P J Gustafsson

- 28-19-1 Fracture of Wood in Tension Perpendicular to the Grain: Experiment and Numerical Simulation by Damage Mechanics - L Daudeville, M Yasumura and J D Lanvin
- 28-19-2 A New Method of Determining Fracture Energy in Forward Shear along the Grain - H D Mansfield-Williams
- 28-19-3 Fracture Design Analysis of Wooden Beams with Holes and Notches. Finite Element Analysis based on Energy Release Rate Approach - H Petersson
- 28-19-4 Design of Timber Beams with Holes by Means of Fracture Mechanics - S Aicher, J Schmidt and S Brunold
- 30-19-1 Failure Analysis of Single-Bolt Joints - L Daudeville, L Davenne and M Yasumura
- 37 - 19 - 1 Determination of Fracture Mechanics Parameters for Wood with the Help of Close Range Photogrammetry - S Franke, B Franke, K Rautenstrauch
- 39-19-1 First Evaluation Steps of Design Rules in the European and German codes of Transverse Tension Areas - S Franke, B Franke, K Rautenstrauch

SERVICEABILITY

- 27-20-1 Codification of Serviceability Criteria - R H Leicester
- 27-20-2 On the Experimental Determination of Factor k_{def} and Slip Modulus k_{ser} from Short- and Long-Term Tests on a Timber-Concrete Composite (TCC) Beam - S Capretti and A Ceccotti
- 27-20-3 Serviceability Limit States: A Proposal for Updating Eurocode 5 with Respect to Eurocode 1 - P Racher and F Rouger
- 27-20-4 Creep Behavior of Timber under External Conditions - C Le Govic, F Rouger, T Toratti and P Morlier
- 30-20-1 Design Principles for Timber in Compression Perpendicular to Grain - S Thelandersson and A Mårtensson
- 30-20-2 Serviceability Performance of Timber Floors - Eurocode 5 and Full Scale Testing - R J Bainbridge and C J Mettem
- 32-20-1 Floor Vibrations - B Mohr
- 37 - 20 - 1 A New Design Method to Control Vibrations Induced by Foot Steps in Timber Floors - Lin J Hu, Y H Chui
- 37 - 20 - 2 Serviceability Limit States of Wooden Footbridges. Vibrations Caused by Pedestrians - P Hamm
- 43-20-1 The Long Term Instrumentation of a Timber Building in Nelson NZ - the Need for Standardisation - H W Morris, S R Uma, K Gledhill, P Omenzetter, M Worth

TEST METHODS

- 31-21-1 Development of an Optimised Test Configuration to Determine Shear Strength of Glued Laminated Timber - G Schickhofer and B Obermayr
- 31-21-2 An Impact Strength Test Method for Structural Timber. The Theory and a Preliminary Study - T D G Canisius
- 35-21-1 Full-Scale Edgewise Shear Tests for Laminated Veneer Lumber- B Yeh, T G Williamson
- 39-21-1 Timber Density Restrictions for Timber Connection Tests According to EN28970/ISO8970 - A Leijten, J Köhler, A Jorissen
- 39-21-2 The Mechanical Inconsistence in the Evaluation of the Modulus of Elasticity According to EN384 - T Bogensperger, H Unterwieser, G Schickhofer

- 40 - 21 - 1 ASTM D198 - Interlaboratory Study for Modulus of Elasticity of Lumber in Bending - A Salenikovich
- 40 - 21 - 2 New Test Configuration for CLT-Wall-Elements under Shear Load - T Bogensperger, T Moosbrugger, G Schickhofer
- 41-21-1 Determination of Shear Modulus by Means of Standardized Four-Point Bending Tests - R Brandner, B Freytag, G Schickhofer
- 43-21-1 Estimation of Load-Bearing Capacity of Timber Connections - J Munch-Andersen, J D Sørensen, F Sørensen
- 43-21-2 A New Method to Determine Suitable Spacings and Distances for Self-tapping Screws - T Uibel, H J Blaß

CIB TIMBER CODE

- 2-100-1 A Framework for the Production of an International Code of Practice for the Structural Use of Timber - W T Curry
- 5-100-1 Design of Solid Timber Columns (First Draft) - H J Larsen
- 5-100-2 A Draft Outline of a Code for Timber Structures - L G Booth
- 6-100-1 Comments on Document 5-100-1; Design of Solid Timber Columns - H J Larsen and E Theilgaard
- 6-100-2 CIB Timber Code: CIB Timber Standards - H J Larsen and E Theilgaard
- 7-100-1 CIB Timber Code Chapter 5.3 Mechanical Fasteners; CIB Timber Standard 06 and 07 - H J Larsen
- 8-100-1 CIB Timber Code - List of Contents (Second Draft) - H J Larsen
- 9-100-1 The CIB Timber Code (Second Draft)
- 11-100-1 CIB Structural Timber Design Code (Third Draft)
- 11-100-2 Comments Received on the CIB Code - U Saarelainen; Y M Ivanov, R H Leicester, W Nozynski, W R A Meyer, P Beckmann; R Marsh
- 11-100-3 CIB Structural Timber Design Code; Chapter 3 - H J Larsen
- 12-100-1 Comment on the CIB Code - Sous-Commission Glulam
- 12-100-2 Comment on the CIB Code - R H Leicester
- 12-100-3 CIB Structural Timber Design Code (Fourth Draft)
- 13-100-1 Agreed Changes to CIB Structural Timber Design Code
- 13-100-2 CIB Structural Timber Design Code. Chapter 9: Performance in Fire
- 13-100-3a Comments on CIB Structural Timber Design Code
- 13-100-3b Comments on CIB Structural Timber Design Code - W R A Meyer
- 13-100-3c Comments on CIB Structural Timber Design Code - British Standards Institution
- 13-100-4 CIB Structural Timber Design Code. Proposal for Section 6.1.5 Nail Plates - N I Bovim
- 14-103-2 Comments on the CIB Structural Timber Design Code - R H Leicester
- 15-103-1 Resolutions of TC 165-meeting in Athens 1981-10-12/13
- 21-100-1 CIB Structural Timber Design Code. Proposed Changes of Sections on Lateral Instability, Columns and Nails - H J Larsen
- 22-100-1 Proposal for Including an Updated Design Method for Bearing Stresses in CIB W18 - Structural Timber Design Code - B Madsen
- 22-100-2 Proposal for Including Size Effects in CIB W18A Timber Design Code - B Madsen

- 22-100-3 CIB Structural Timber Design Code - Proposed Changes of Section on Thin-Flanged Beams - J König
- 22-100-4 Modification Factor for "Aggressive Media" - a Proposal for a Supplement to the CIB Model Code - K Erler and W Rug
- 22-100-5 Timber Design Code in Czechoslovakia and Comparison with CIB Model Code - P Dutko and B Kozelouh

LOADING CODES

- 4-101-1 Loading Regulations - Nordic Committee for Building Regulations
- 4-101-2 Comments on the Loading Regulations - Nordic Committee for Building Regulations
- 37-101-1 Action Combination Processing for the Eurocodes Basis of Software to Assist the Engineer - Y Robert, A V Page, R Thépaut, C J Mettem
- 43-101-1 Dependant Versus Independent Loads in Structural Design - T Poutanen

STRUCTURAL DESIGN CODES

- 1-102-1 Survey of Status of Building Codes, Specifications etc., in USA - E G Stern
- 1-102-2 Australian Codes for Use of Timber in Structures - R H Leicester
- 1-102-3 Contemporary Concepts for Structural Timber Codes - R H Leicester
- 1-102-4 Revision of CP 112 - First Draft, July 1972 - British Standards Institution
- 4-102-1 Comparison of Codes and Safety Requirements for Timber Structures in EEC Countries - Timber Research and Development Association
- 4-102-2 Nordic Proposals for Safety Code for Structures and Loading Code for Design of Structures - O A Brynildsen
- 4-102-3 Proposal for Safety Codes for Load-Carrying Structures - Nordic Committee for Building Regulations
- 4-102-4 Comments to Proposal for Safety Codes for Load-Carrying Structures - Nordic Committee for Building Regulations
- 4-102-5 Extract from Norwegian Standard NS 3470 "Timber Structures"
- 4-102-6 Draft for Revision of CP 112 "The Structural Use of Timber" - W T Curry
- 8-102-1 Polish Standard PN-73/B-03150: Timber Structures; Statistical Calculations and Designing
- 8-102-2 The Russian Timber Code: Summary of Contents
- 9-102-1 Svensk Byggnorm 1975 (2nd Edition); Chapter 27: Timber Construction
- 11-102-1 Eurocodes - H J Larsen
- 13-102-1 Program of Standardisation Work Involving Timber Structures and Wood-Based Products in Poland
- 17-102-1 Safety Principles - H J Larsen and H Riberholt
- 17-102-2 Partial Coefficients Limit States Design Codes for Structural Timberwork - I Smith
- 18-102-1 Antiseismic Rules for Timber Structures: an Italian Proposal - G Augusti and A Ceccotti
- 18-1-2 Eurocode 5, Timber Structures - H J Larsen
- 19-102-1 Eurocode 5 - Requirements to Timber - Drafting Panel Eurocode 5
- 19-102-2 Eurocode 5 and CIB Structural Timber Design Code - H J Larsen

19-102-3	Comments on the Format of Eurocode 5 - A R Fewell
19-102-4	New Developments of Limit States Design for the New GDR Timber Design Code - W Rug and M Badstube
19-7-3	Effectiveness of Multiple Fastener Joints According to National Codes and Eurocode 5 (Draft) - G Steck
19-7-6	The Derivation of Design Clauses for Nailed and Bolted Joints in Eurocode5 - L R J Whale and I Smith
19-14-1	Annex on Simplified Design of W-Trusses - H J Larsen
20-102-1	Development of a GDR Limit States Design Code for Timber Structures - W Rug and M Badstube
21-102-1	Research Activities Towards a New GDR Timber Design Code Based on Limit States Design - W Rug and M Badstube
22-102-1	New GDR Timber Design Code, State and Development - W Rug, M Badstube and W Kofent
22-102-2	Timber Strength Parameters for the New USSR Design Code and its Comparison with International Code - Y Y Slavik, N D Denesh and E B Ryumina
22-102-3	Norwegian Timber Design Code - Extract from a New Version - E Aasheim and K H Solli
23-7-1	Proposal for a Design Code for Nail Plates - E Aasheim and K H Solli
24-102-2	Timber Footbridges: A Comparison Between Static and Dynamic Design Criteria - A Ceccotti and N de Robertis
25-102-1	Latest Development of Eurocode 5 - H J Larsen
25-102-1A	Annex to Paper CIB-W18/25-102-1. Eurocode 5 - Design of Notched Beams - H J Larsen, H Riberholt and P J Gustafsson
25-102-2	Control of Deflections in Timber Structures with Reference to Eurocode 5 - A Martensson and S Thelandersson
28-102-1	Eurocode 5 - Design of Timber Structures - Part 2: Bridges - D Bajolet, E Gehri, J König, H Kreuzinger, H J Larsen, R Mäkipuro and C Mettem
28-102-2	Racking Strength of Wall Diaphragms - Discussion of the Eurocode 5 Approach - B Källsner
29-102-1	Model Code for the Probabilistic Design of Timber Structures - H J Larsen, T Isaksson and S Thelandersson
30-102-1	Concepts for Drafting International Codes and Standards for Timber Constructions - R H Leicester
33-102-1	International Standards for Bamboo – J J A Janssen
35-102-1	Design Characteristics and Results According to EUROCODE 5 and SNIIP Procedures - L Ozola, T Keskküla
35-102-2	Model Code for the Reliability-Based Design of Timber Structures - H J Larsen
36-102-1	Predicted Reliability of Elements and Classification of Timber Structures - L Ozola, T Keskküla
36-102-2	Calibration of Reliability-Based Timber Design Codes: Choosing a Fatigue Model - I Smith
38-102-1	A New Generation of Timber Design Practices and Code Provisions Linking System and Connection Design - A Asiz, I Smith
38-102-2	Uncertainties Involved in Structural Timber Design by Different Code Formats - L Ozola, T Keskküla

- 38-102-3 Comparison of the Eurocode 5 and Actual Croatian Codes for Wood Classification and Design With the Proposal for More Objective Way of Classification - V Rajcic A Bjelanovic
- 39-102-1 Calibration of Partial Factors in the Danish Timber Code - H Riberholt
- 41 - 102 - 1 Consequences of EC 5 for Danish Best Practise - J Munch-Andersen
- 41 - 102 - 2 Development of New Swiss standards for the Assessment of Existing Load Bearing Structures – R Steiger, J Köhler
- 41 – 102 - 3 Measuring the CO2 Footprint of Timber Buildings – A Buchanan, S John

INTERNATIONAL STANDARDS ORGANISATION

- 3-103-1 Method for the Preparation of Standards Concerning the Safety of Structures (ISO/DIS 3250) - International Standards Organisation ISO/TC98
- 4-103-1 A Proposal for Undertaking the Preparation of an International Standard on Timber Structures - International Standards Organisation
- 5-103-1 Comments on the Report of the Consultation with Member Bodies Concerning ISO/TC/P129 - Timber Structures - Dansk Ingeniorforening
- 7-103-1 ISO Technical Committees and Membership of ISO/TC 165
- 8-103-1 Draft Resolutions of ISO/TC 165
- 12-103-1 ISO/TC 165 Ottawa, September 1979
- 13-103-1 Report from ISO/TC 165 - A Sorensen
- 14-103-1 Comments on ISO/TC 165 N52 "Timber Structures; Solid Timber in Structural Sizes; Determination of Some Physical and Mechanical Properties"
- 14-103-2 Comments on the CIB Structural Timber Design Code - R H Leicester
- 21-103-1 Concept of a Complete Set of Standards - R H Leicester

JOINT COMMITTEE ON STRUCTURAL SAFETY

- 3-104-1 International System on Unified Standard Codes of Practice for Structures - Comité Européen du Béton (CEB)
- 7-104-1 Volume 1: Common Unified Rules for Different Types of Construction and Material - CEB
- 37-104-1 Proposal for a Probabilistic Model Code for Design of Timber Structures - J Köhler, H Faber

CIB PROGRAMME, POLICY AND MEETINGS

- 1-105-1 A Note on International Organisations Active in the Field of Utilisation of Timber - P Sonnemans
- 5-105-1 The Work and Objectives of CIB-W18-Timber Structures - J G Sunley
- 10-105-1 The Work of CIB-W18 Timber Structures - J G Sunley
- 15-105-1 Terms of Reference for Timber - Framed Housing Sub-Group of CIB-W18
- 19-105-1 Tropical and Hardwood Timbers Structures - R H Leicester
- 21-105-1 First Conference of CIB-W18B, Tropical and Hardwood Timber Structures Singapore, 26 - 28 October 1987 - R H Leicester

**INTERNATIONAL COUNCIL FOR RESEARCH AND INNOVATION
IN BUILDING AND CONSTRUCTION**

WORKING COMMISSION W18 - TIMBER STRUCTURES

**QUALITY CONTROL METHODS:
APPLICATION TO ACCEPTANCE CRITERIA FOR A BATCH OF TIMBER**

F Rouger
FCBA

FRANCE

**MEETING FORTY THREE
NELSON
NEW ZEALAND
AUGUST 2010**

Presented by F Rouger

H Larsen: why do we have acceptance criteria on timber acceptance? The situation described does not exist. F Rouger: I do not agree. In glulam industry in France, each lamination must be checked. In EN 384, the acceptance criterion was a rule-of-thumb.

J Munch-Andersen: This new rule must comply with Eurocode 0. F Rouger: The method in itself is not new for engineering but new for timber.

Quality control methods:

Application to acceptance criteria for a batch of timber

ROUGER Frédéric

FCBA, France

1 Abstract

In the ratified version EN 384, a method was stated in section 9, regarding quality verification of a batch of timber. This paper aims at showing that the current approach is not correct, and proposes a new approach that is in line with existing theories. This new method is based on quality control concepts. For stiffness control, average quality criterion has to be used, whereas for strength control, fraction defective criterion shall be applied.

Both criteria use a risk concept:

- The risk for the producer, denoted α , is the risk that a batch is rejected by the consumer whereas it is correct
- The risk for the consumer, denoted β , is the risk that the consumer accepts the batch whereas it is not correct

This paper firstly describes the theory, and illustrates the efficiency of the method on simulated and real experimental data sets. It also demonstrates the inefficiency of standardized approach. As a conclusion, the proposal based on this investigation, and which has been incorporated in the new version of EN 384 is briefly described.

2 Introduction

EN 384 mainly aims at deriving characteristic values for timber samples. But an interesting section, namely section 9, is dedicated to “acceptance criteria for a batch”.

This section can be used for instance by a consumer that receives a batch of timber, and wishes to check whether or not this batch meets the declared characteristic values.

The current standardized approach was established more or less as a “rule of thumb”. It is therefore necessary to come back to the theory, and establish rules which are technically correct and practically useable.

This procedure is related to quality control concepts. Two kinds of quality control approaches are available:

- Sampling by variables: we wish to check a numerical value against a declared one.
- Sampling by attributes: we wish to check a label attached on the product.

Since the checking is done on strength and stiffness values, we talk about quality control based on sampling by variables. Sampling by attributes is not dealt with in this paper, but could also be used for checking for example that a visual grading is made correctly.

Since the control is applied on both mean MOE and characteristic strength values, two approaches have to be used:

- For the mean MOE, we talk about average quality criterion
- For characteristic strengths, we talk about fraction defective criterion

Both approaches use a risk concept:

- The risk for the producer, denoted α , is the risk that a population is rejected by the consumer whereas it is correct
- The risk for the consumer, denoted β , is the risk that the consumer accepts the population whereas it is not correct

In ISO 12491, it is recommended that:

- $\alpha = 0,15; 0,25; 0,40; 0,65; 1,0; 1,5; 2,5; 4,0$
- $\beta = 0,65; 1,0; 1,5; 2,5; 4,0; 6,5; 10,0; 15,0$

Usually, we take $\alpha = 0,05$ and $\beta = 0,10$, but the method can be used for other sets of values

3 Check of mean MOE: Control by variables

From the population, a sample of size n is tested. The purpose of the control is, based on the sample result, to guess if the population (or lot) is correct.

Let us define some variables:

The sample mean is denoted as \bar{X} . The standard deviation is denoted σ . The coefficient of variation is denoted CV .

Let us define the mean of a “good” quality lot as μ_a . For example, if we want to check a C24 strength class, $\mu_a = 11 \text{ MPa}$

The mean of a sample from this lot can be demonstrated as Gaussian, given by:

$$\bar{X} = N(\mu_a, \sigma / \sqrt{n}) \quad (1)$$

Let us define the mean of a “bad” quality lot as μ_t . This value can be expressed as a shift from the good population:

$$\mu_t = \delta \mu_a \quad (2)$$

For example, we can take $\delta = 0.9$, which means that a drop of more than 10% is not acceptable.

The purpose is now to fix a limit to the sample mean, in such a way that the producer’s risk and the consumer’s risk are met.

Let us call this limit L . It can be also expressed as ratio of the target mean of the lot:

$$L = k_q \mu_a \quad (3)$$

Let us assume that the distribution is Gaussian.

The producer's risk, α , is defined as the probability that the sample mean \bar{X} is less than the limit (which means that the lot will be rejected), knowing that the population mean is correct ($= \mu_a$).

The consumer's risk, β , is defined as the probability that the sample mean \bar{X} is larger than the limit (which means that the lot will be accepted), knowing that the population mean is not correct ($= \mu_t$).

These two statements can be expressed in a mathematical form:

$$\begin{cases} P(\bar{X} < L | \mu_a) = \Phi\left(\frac{L - \mu_a}{\sigma / \sqrt{n}}\right) = \alpha \\ P(\bar{X} > L | \mu_t) = 1 - \Phi\left(\frac{L - \mu_t}{\sigma / \sqrt{n}}\right) = \beta \end{cases} \quad (4)$$

or

$$\begin{cases} \frac{\mu_a (k_q - \delta)}{\sigma / \sqrt{n}} = \Phi^{-1}(\alpha) \\ \frac{\mu_a (1 - \delta)}{\sigma / \sqrt{n}} = \Phi^{-1}(1 - \beta) \end{cases} \quad (5)$$

Solving the system of equations in (5), and using substitutions of equations (2) and (3) leads to the expressions for k_q and n :

$$k_q = \frac{\Phi^{-1}(1 - \beta) - \Phi^{-1}(\alpha) \delta}{\Phi^{-1}(1 - \beta) - \Phi^{-1}(\alpha)} \quad (6)$$

$$n = \left[\frac{CV(\Phi^{-1}(1 - \beta) - \Phi^{-1}(\alpha))}{1 - \delta} \right]^2 \quad (7)$$

It is very important to note that k_q only depends on α , β and δ . It does not depend on n , neither on CV . If we fix $\delta = 0.9$, we have the following values for k_q :

	alpha		
beta	0,050	0,100	0,150
0,050	0,950	0,956	0,961
0,100	0,944	0,950	0,955
0,150	0,939	0,945	0,950

Table 1 : k_q values for $\delta = 0.9$

The bolded value, $k_q = 0.944$, corresponds to target producer's and consumer's risks of 5% and 10%.

When looking at EN 384, k_q ranges from 0.8 to 0.9, which is totally unacceptable for two reasons:

- k_q should not depend on n ,
- Such values would lead to unacceptable risks :
 - A value of 0.9 means a consumer's risk of 50%, regardless of the producer's risk
 - A value of 0.8 means a consumer's risk of 55% and a producer's risk of 40%

These conclusions would lead to even stronger conclusion: please do not make any test, since a simple lottery guess is even safer.

The values of n , as seen in equation(7), also depend on the coefficient of variation. The following tables give results for different figures of the coefficient of variation.

CV = 0.4				CV = 0.3			
alpha				alpha			
Beta	0,050	0,100	0,150	beta	0,050	0,100	0,150
0,050	173	137	115	0,050	97	77	65
0,100	137	105	86	0,100	77	59	48
0,150	115	86	69	0,150	65	48	39

alpha			
CV= 0.2			
beta	0,050	0,100	0,150
0,050	43	34	29
0,100	34	26	21
0,150	29	21	17

Table 2 : n values for different values of CV

The proposal to be inserted in EN 384 could be the following:

- Take 34 pieces, and evaluate the mean MOE and its CV
- If $CV \leq 0.2$, OK
- If $0.2 \leq CV \leq 0.25$, increase the sample size to 54, and evaluate again the mean MOE
- Etc.
- If $0.35 \leq CV$, an alternative approach is to increase the consumer's risk, in order to minimize the sample size.
- The mean MOE should verify $\overline{MOE} \geq k_q MOE_{\text{target}}$ with $k_q = 0.944$

4 Check of characteristic strengths: Control by proportion

By assuming a normal distribution, the general equation for a proportion of the random variable X is given by:

$$P(X < x_k) = \Phi\left(\frac{x_k - \bar{X}}{\sigma}\right) \quad (8)$$

Where:

X is the random variable

x_k is the characteristic value

\bar{X} is the mean value of X

σ is the standard variation of X

Let us define a “correct” proportion for X as p_a . Typically, we can choose $p_a = 0.05$. In that case, the mean value of the correct lot, according to equation(8), is given by:

$$\mu_a = x_k - \sigma \cdot \Phi^{-1}(p_a) \quad (9)$$

The target proportion for the check is denoted as M .

The producer’s risk is defined as:

$$P(p > M) = P\left[\Phi\left(\frac{x_k - \bar{X}}{\sigma}\right) > M\right] = P\left[\bar{X} < x_k - \sigma \cdot \Phi^{-1}(M)\right] = \alpha \quad (10)$$

The sample mean is Gaussian (see equation (1)), and given by:

$$\bar{X} = N(\mu_a, \sigma / \sqrt{n}) = N(x_k - \sigma \cdot \Phi^{-1}(p_a), \sigma / \sqrt{n}) \quad (11)$$

$$P(\bar{X} < \xi) = \Phi\left(\frac{\xi - \mu_a}{\sigma / \sqrt{n}}\right) \quad (12)$$

Therefore, y combining equations (10) and (12), we obtain:

$$\Phi\left[\sqrt{n}\{\Phi^{-1}(p_a) - \Phi^{-1}(M)\}\right] = \alpha \quad (13)$$

Similarly, regarding the consumer’s risk, we get:

$$1 - \Phi\left[\sqrt{n}\{\Phi^{-1}(p_t) - \Phi^{-1}(M)\}\right] = \beta \quad (14)$$

Equations (13) and (14) can be solved to get n and M :

$$n = \left[\frac{\Phi^{-1}(1 - \beta) - \Phi^{-1}(\alpha)}{\Phi^{-1}(p_t) - \Phi^{-1}(p_a)} \right]^2 \quad (15)$$

$$M = \Phi\left(\Phi^{-1}(p_a) - \frac{\Phi^{-1}(\alpha)}{\sqrt{n}}\right) \quad (16)$$

To get p_t (proportion for a bad quality lot), let us assume a shift on the mean of δ (For EN 384, we propose $\delta = 0.2$). The value of p_t is given by:

$$p_t = \Phi \left(\frac{x_k - \delta \bar{X}}{CV \cdot \delta \bar{X}} \right) \quad (17)$$

where

$$\bar{X} = \frac{x_k}{1 + \Phi^{-1}(0.05) \cdot CV} \quad (18)$$

This is illustrated in Figure 1.

If we take $\alpha = 0.05$ and $\beta = 0.10$, we can calculate the values of n and M . They are reported in Table 3, which constitutes the basis for EN 384.

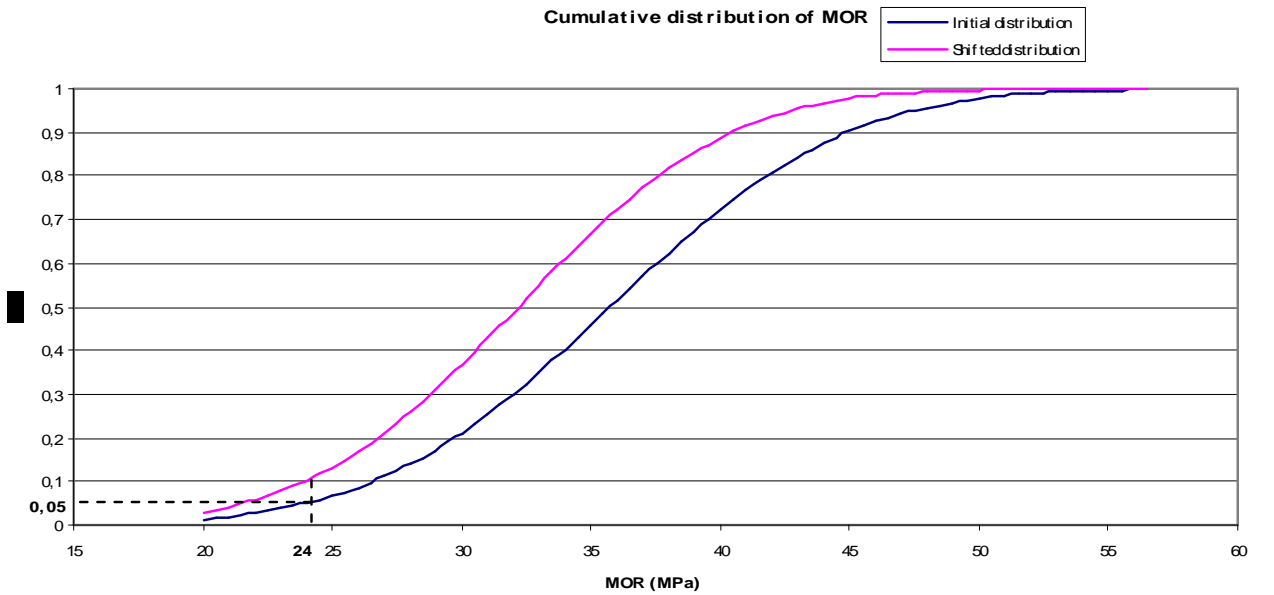


Figure 1 : Shift on the MOR distribution; effect on p_t

CV	n	M (p_{lim} in EN 384)
0,25	25	9.44%
0,30	48	7.96%
0,35	93	7%

Table 3 : Values for n and M (p_{lim} in EN 384)

If $CV > 0.35$, the sample size becomes prohibitive at a customer's risk of 10% (the sample size reaches 187 pieces for $CV = 0.4$). An option can be to increase the consumer's and producer's risks.

5 Numerical example

5.1 Database and methodology

A database was constituted by grouping Spruce, Scots Pine and Fir in order to have a large sample size within each grade. The total size is 3623 pieces. The calculations have been made on three visual grades (STI→C30; STII→C24; STIII→ C18). The strength and stiffness distributions are given in the following table.

	n	MOE (Gpa)		MOR (Mpa)		
		Mean	COV	Mean	COV	5%
ST1	733	13,69	22%	60,6	25%	34,9
ST2	1782	12,79	24,7%	49	32,3%	24,67
ST3	1108	11,9	25,2%	41	31,7%	22,2

Table 4 : strength and stiffness distributions of the database

The calculations have been made according to the following methodology for each grade:

- 500 samples have been iteratively taken from the parent sample
- For each sample, the sample size has been adjusted according to the principles stated in the proposal:
 - An initial guess for the COV (20% for MOE, 25% for MOR)
 - A first calculation for the characteristic value (mean value for MOE, 5% for MOR)
 - An adjustment of the sample size according to the actual COV, by using equations (7) and (15)
 - The characteristic values have been re-calculated
 - The check of acceptance has been made according to the proposal (k_q ratio for MOE, p_{lim} for MOR)
 - The proportion of acceptance has been calculated.

5.2 Results for the old method

In this context, figure 2 of EN 384 has been used to evaluate k_q . Since this factor depends on the sample size in the current text, the sample sizes in calculations described above have been used to derive k_q .

The first check is made on the population without any shift: the proportion of acceptance should correspond to the producer's risk.

The results are summarized in Table 5

Grade	Rejection Rate on MOE	Rejection rate on MOR
ST1	0,0%	2,4%
ST2	0,0%	0,2%
ST3	0,0%	0,0%
Mean	0,0%	0,9%

Table 5 : Verification on parent population

The percentage of acceptance is 100% for MOEs and 99% for MORs. This verification cannot be correct, since the producer's risk cannot be zero.

To look at the consumer's risks, we applied successive shifts to the parent population:

- For the MOE, two shifts were applied: 10% and 20%
- For the MOR, two shifts were applied: 20% and 30%

The results are summarized in Table 6.

	MOE shift		MOR shift	
	10%	20%	20%	30%
ST1	99,8%	41,2%	64,6%	31,8%
ST2	99,8%	31,8%	43,8%	12,8%
ST3	100,0%	31,6%	49,4%	9,0%
Mean	99,9%	34,9%	52,6%	17,9%

Table 6 : Acceptance rates for various shifts on MOEs and MORs

Some remarks can be made:

- A shift of 10% on the MOE is not detected (100% of acceptance).
- A shift of 20% on the MOE (e.g. from C30 to C18) is accepted in 1/3 of the cases.
- A shift of 20% on the MOR is accepted in more than 1/2 of the cases
- A shift of 30% on the MOR is still accepted in 1/5 of the cases

Clearly, these proportions of acceptance are not correct, and justify that the current approach of the standard should be left out.

5.3 Results for the new proposal

The initial check on the parent population has similarly been carried out with the new approach.

The results are summarized in Table 7.

It can be clearly seen that the percentage of non acceptance (4.7% and 7.8%) are very close to the producer's risk (5%), which is in line with the basic assumptions of the method.

Grade	Rejection Rate on MOE	Rejection rate on MOR
ST1	4,4%	9,4%
ST2	5,6%	7,4%
ST3	4,2%	6,6%
Mean	4,7%	7,8%

Table 7 : Verification on parent population

To look at the consumer's risks, we applied successive shifts to the parent population:

- For the MOE, two shifts were applied: 10% and 15%
- For the MOR, three shifts were applied: 20%, 25% and 30%

The results are summarized in Table 8.

	MOE shift		MOR shift		
	10%	15%	20%	25%	30%
ST1	3,2%	0,0%	29,8%	12,0%	1,0%
ST2	7,0%	0,2%	13,6%	3,6%	1,6%
ST3	6,8%	0,0%	5,8%	1,2%	0,0%
Mean	5,7%	0,1%	16,4%	5,6%	0,9%

Table 8 : Acceptance rates for various shifts on MOEs and MORs

Several remarks can be made:

- When the shifts correspond to the limits, the percentage of acceptance is in average (11.4%) close to the target consumer's risk of 10% (slightly non conservative for MOR, and slightly conservative for MOE)
- If the shifts are 5% further than the limits, the percentage of acceptance is well below the target risk.

This section concludes that the proposal has a very good behaviour, corresponding to the expectations of the theory.

6 Conclusions

Theoretical concepts of quality control have been successfully applied on the acceptance criteria for a batch of timber. Numerical investigations on “real data” clearly show that the existing approach of the standard is not correct, and that the new approach gives very good results. This justifies the revision which has been incorporated in the new version of the standard which is going to be ratified in a close future.

7 References

Tang A.H.S and Tang W.H. Probability concepts in engineering planning and design. John Wiley & Sons. 1975

EN 384 Timber Structures – Determination of characteristic values of mechanical properties and density

ISO 12491 Statistical methods for quality control of building materials and components

**INTERNATIONAL COUNCIL FOR RESEARCH AND INNOVATION
IN BUILDING AND CONSTRUCTION**

WORKING COMMISSION W18 - TIMBER STRUCTURES

**INFLUENCE OF ORIGIN AND GRADING PRINCIPLES ON THE
ENGINEERING PROPERTIES OF EUROPEAN TIMBER**

P Stapel

J.-W G v. d. Kuilen

A Rais

Holzforschung München, Technische Universität München
GERMANY

MEETING FORTY THREE

NELSON

NEW ZEALAND

AUGUST 2010

Presented by P Stapel

H Larsen: I support the recommendation of eliminating the depth effect.

L Daziel: was visual grading done by supplier? P. Stapel: No.

Influence of origin and grading principles on the engineering properties of European timber

P. Stapel¹, J.-W. G. v. d. Kuilen^{1,2}, A. Rais¹

¹ Holzforschung München, Technische Universität München, Germany

² Delft University of Technology, the Netherlands

1 Introduction

Due to increasing effort of grading machine manufacturers the amount of timber which can be used for approvals according to European standard EN 14081 increases. The available data can be used to obtain uniform settings that cover large parts of Europe. The European standard for machine approval EN 14081-Part 2/3 was developed when much less data was available. Alternative methods for machine grading in Europe have recently been proposed by SANDOMEER ET. AL (2008), ZIETHÉN AND BENGTTSSON (2009) and RANTA-MAUNUS AND TURK (2010). This paper deals with the current system. The improved experience in deriving machine settings of today, allows a critical analysis of the rules and methods decided upon at the time. This can be tested today, as a dataset of almost 5000 boards is available. The approval procedure requires the use of modification factors from a number of standards, of which EN 408 and EN 384 are the most important.

Timber quality (in terms of bending strength, modulus of elasticity and density) influences the settings for the machine. Low quality timber usually leads to higher settings and vice versa. However, the settings are not defined on the basis of the weakest sample only, but on a mean value of all sub-samples used in the approval procedure. The origin of the trees has an important influence on the mechanical properties of the sawn timber. If the user of a grading machine uses timber from the same sources and in a similar proportion as used for the derivation of settings, the output material can be safe. On the contrary, if a sawmill only uses timber from a limited radius around the production site, the results can be far from safe when the original approval testing covered a much larger area. If the incoming material is of low quality only, the graded material will not meet the required characteristic values on a regular basis.

Factors used in the derivation of settings include a depth factor k_h and a k_v - factor, which will be discussed in more detail. According to Eurocode 5, the depth effect may be applied on beams with a depth less than 150 mm. For depths above 150 mm, no correction for strength is required. However, during the derivation of characteristic values according to EN 384, the characteristic 5th-percentile value of sub-samples with a depth of more than 150 mm, shall be increased with the depth factor k_h given as:

$$k_h = \left(\frac{150}{h} \right)^{-0.2} \quad (1)$$

It means that characteristic values in accordance with the dotted line in Figure 1, will be used by designers as being in accordance with the continuous line. A discrepancy of around 10% can be observed for beam depths typically used for floors (> 200 mm).

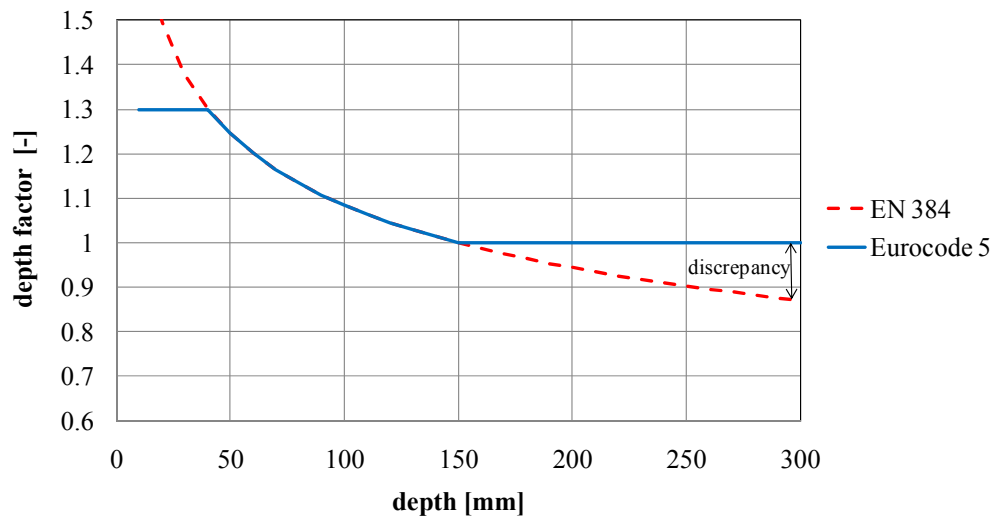


Figure 1: Discrepancy in the depth effect between EC 5 and EN 384.

In addition to the depth effect, EN 384 allows a k_v -factor to be applied on the characteristic value of the samples graded by a machine for strength classes up to C30 according to EN 338. The value of k_v is set fixed at 1.12, independent of the quality of the machine or strength class combination. The idea behind this factor is that the variation of the characteristic values of sub-samples is smaller for machine graded timber as compared to visually graded timber.

Other factors that influence the quality of visual and machine grading are the length of the pieces that were used in the analysis [ISAKSSON AND THELANDERSSON (1995), ØVRUM ET AL (2008), RAIS ET AL (2010)] as compared to the lengths used in practice. Other than the influence of the length of the pieces during the bending tests according to EN 408 / EN 384, length effects have not been taken into account here.

As no pan-European rules are used for visual grading of timber, EN 1912 regulates the application area of national grading rules. These grading areas are usually interpreted very wide. If visual grading is not sensible to the timber origin, this can be justified. The objectives and the analysis given in this paper can be summarized as:

- I) What is the influence of the origin and the grading principle on the characteristic value of the bending strength using the European standards EN 14081 and EN 384, after testing in accordance with EN 408?
- II) Does visual grading allow large growth areas like indicated in EN 1912?
- III) EN 384 and EN 14081 allow the use of some adjustment factors as mentioned previously:
 - i. To what extend do these factors influence the grading output?
 - ii. Is the k_v -factor ($k_v = 1.12$) justified by a lower variation of machine graded timber compared to visual graded timber?
 - iii. Is the variation in 5th-percentile values of sub-samples such, that different safety factors can be justified depending on the type of grading?

2 Material and method

2.1 Material

The dataset comprises a total of 4893 specimens. The analysis is based on Norway spruce (*Picea abies*) from Europe. As it is shown in Table 1, spruce data covers many parts of Central, North and Eastern Europe. 10 sub-samples were formed according to geographical aspects. The sampling was carried out in different regions within 11 different countries. It is assumed that the sampling is representative for the timber source from the according region. The cross section also covers a broad range: the thickness varies from 20 to 167 mm and the width (depth) from 63 to 284 mm.

The amount of boards of each sub-sample is sufficient to derive settings according to the current European standard EN 14081. The standard requires a minimum number of 100 pieces in a sub-sample. The numbers of pieces in each sub-sample vary from 204 to 1337. This was done in order to follow the origin of the boards.

One part of the complete dataset originates from the database of Holzforschung München. These 2617 boards are mostly data of recent projects. The other part of the dataset contains 2276 boards of the European “Gradewood”-Project. Common aim of the European joint-project “Gradewood – Grading of timber for engineered wood products” is to improve strength grading.

All destructive tests were performed according to EN 408. The factors given in EN 384 (k_h -factor, k_l -factor) were applied. Due to the k_h -factor the edgewise bending strength values (MoR) were adjusted to a depth of 150 mm. At 1091 boards the bending strength values were adjusted to the normal test arrangement (k_l -factor): a symmetrical two point loading over a span of 18 times the depth is used for the determination of bending strength. If possible the weakest section along the beam axis was tested. The orientation of the board in edgewise bending tests was chosen randomly. The static bending modulus of elasticity (MoE) is adjusted to a moisture content of 12 % by 2 % change for every percentage point difference in moisture content.

Moisture content measurements were carried out on small samples, free of defects and cut out close to failure, by oven dry method according EN 13183-1. Density (ρ) measurements were performed on the same samples. Table 1 summarizes mean values and coefficients of variation of the grade determining properties (bending strength - MoR, bending static modulus of elasticity - MoE, and density - ρ) as well as of the machine data (dynamic modulus of elasticity - MoE dynamic, tKAR).

The non-destructive data used in the analysis were not recorded by a grading machine. Rather, the machine data such as density, eigenfrequency or the knot value are detected under laboratory conditions. These data are recorded at eight different European research institutes. To achieve comparable results between the institutes, round robin tests were carried out before the laboratory measurements to ensure comparable destructive and non-destructive test data.

The tKAR is defined as the knot area within 150 mm projected on the end grain divided by the area of the cross section. Overlapping areas are only counted once. The tKAR-value shows a slightly better coefficient of determination to strength in comparison to the usually used knot parameters in visual grading. In return, visual grading rules also contain other parameters for predicting the strength class: slope of grain, pith, rate of growth, fissures, wane, warp or compression wood. All in all, the prediction accuracy of the chosen visual approach is comparable to the visual grading in practise.

Table 1: The dataset comprises timber from 10 geographical regions.

sub-sample	region	n	MoR		MoE		ρ		MoE, dynamic		tKAR	
			mean in N/mm ²	cov in %	mean in kN/mm ²	cov in %	mean in kg/m ³	cov in %	mean in kN/mm ²	cov in %	mean	cov in %
A	Slovenia	1126	43.4	30.7	11.2	20.5	445	9.9	12.8	19.4	0.25	39.9
B	Western Germany	1337	42.2	32.2	11.5	20.3	435	10.5	12.3	17.9	0.24	42.5
C	North Germany	511	36.6	36.0	10.6	22.8	447	12.6	11.2	21.3	0.26	45.3
D	Austria Czech Rep.	298	36.7	35.5	10.5	25.3	440	13.2	12.3	23.7	0.31	44.3
E	Belgium	262	41.4	25.4	11.0	15.6	437	9.3	12.1	15.4	0.26	38.2
F	Luxembourg	209	40.0	27.1	10.7	16.1	434	9.1	11.9	16.2	0.26	38.8
G	Poland	433	38.5	31.4	10.8	20.6	440	10.8	11.7	20.4	0.32	31.9
H	Romania Slovakia	303	37.0	30.6	9.7	18.1	397	9.2	10.6	18.4	0.29	34.0
I	Sweden	210	42.5	35.2	10.7	21.8	435	11.9	12.0	20.9	0.22	44.3
J	Ukraine	204	36.2	29.4	9.6	18.7	389	9.5	10.5	18.8	0.28	36.4
	Total sample	4893	40.6	32.4	10.9	21.0	435	11.2	12.0	20.1	0.26	41.4

2.2 Method

Model

Based on the total sample two different models are calculated by means of (multiple) linear regression analysis. The first model contains only the tKAR-value and simulates a visual grading. This is similar to most visual grading rules that predict the strength on the basis of knot size and knot location. The second model contains the tKAR-value and additionally the dynamic modulus of elasticity (MoE, dynamic). The dynamic modulus of elasticity is calculated using the eigenfrequency, the density, and the length. Equation (2) and (3) show the regression coefficients used in the regression model.

$$\text{visual model} \quad IP_1 = 58.2 - 67.4 * tKAR \quad (2)$$

$$\text{machine model} \quad IP_2 = 9.4 + 0.00334 * MoE_{dyn} - 34.4 * tKAR \quad (3)$$

The relationship between indicating property and bending strength is shown for both models in Figure 2.

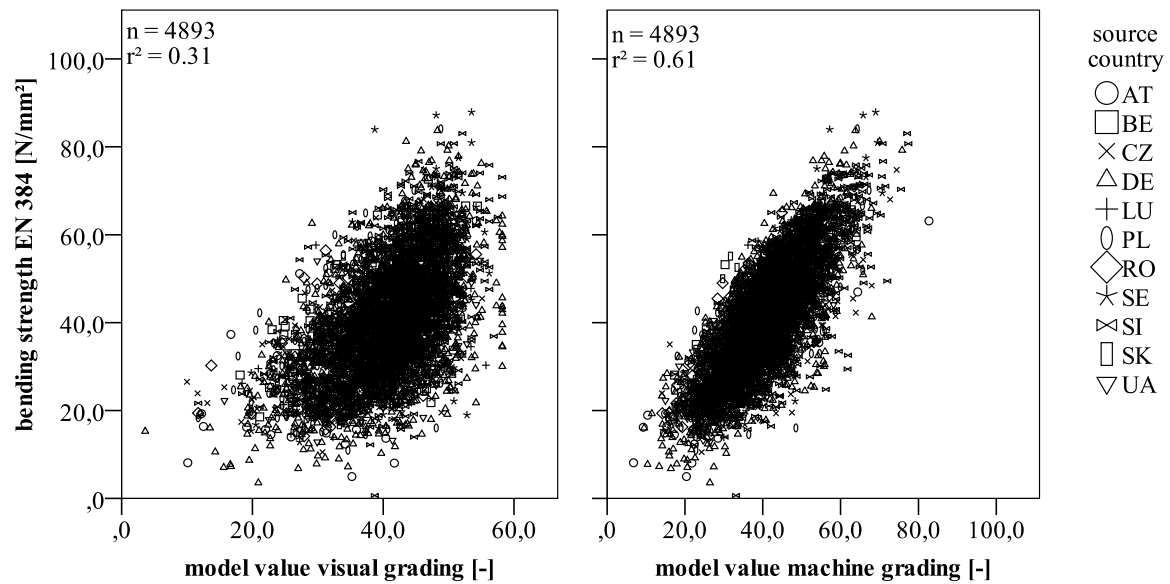


Figure 2: The indicating property of the two models plotted against the bending strength.

Table 2: Required characteristic values of European C-classes according to EN 338.

grade	MoR N/mm ²	MoR / k _v N/mm ²	MoE _{mean} N/mm ²	0.95 * MoE _{mean} N/mm ²	ρ ₁₂ kg/m ³
C40	40.0	40.0	14 000	13 300	420
C35	35.0	35.0	13 000	12 350	400
C30	30.0	26.8	12 000	11 400	380
C24	24.0	21.4	11 000	10 450	350
C18	18.0	16.1	9 000	8 550	320

Settings

The required characteristic values for the European C-classes are shown in Table 2, taking into account the 95% factor on mean bending modulus of elasticity given in EN 338 and the k_v-factor on the characteristic bending strength given in EN 384. Characteristic density is determined by ranking method. The k_v-factor used for reducing the strength requirements on the 5th-percentile level for strength classes C30 and below, needs to be kept in mind, as the graded material will not reach the strength values given in EN 338.

The settings were derived for a so called "machine controlled system" in compliance with the current standard EN 14081. This method is denoted the "cost matrix method" which was presented by Rouger (1997). The settings are derived maximising the yield of the highest grades and not minimising the reject. For each sub-sample the setting is determined from a sample comprising the remaining sub-samples ("excluded sub-sample" method).

Optimum grading provides the optimum assignment of strength class to the tested boards. These are assignments that would be made by a fictitious perfect grading machine. The calculation is not such a trivial task because all three properties (MoR, MoE, and ρ) should be optimized simultaneously according to algorithms from EN 14081-2. Currently there are two possible calculation routines for optimum grades. The method applied here for the optimum grade is given in clause 6.2.4.5 of EN 14081, note 2.

Material safety factors

In order to find out whether the given safety factor for sawn timber in Eurocode 5 is appropriate (advised γ_M value = 1.3, but may be specified on a national basis), the variation of the characteristic bending strength value of the sub-sample is studied. This is done using

an equation taken from ISO 2394, a standard partly influenced by the work of the JCSS [VROUWENVELDER]. A similar description can be found in EN 1990 – Eurocode - Basis of design. The required safety factor γ_M is specified as follows:

$$\gamma_M = \frac{R_k}{R_d} = \frac{1 - kV_R}{1 - \alpha_R \beta V_R} \quad (4)$$

Where:

R_k = characteristic value from the test data;

R_d = required design value;

$k = 1.64$ for samples with a large number of specimens ($n \gg 30$);

$\alpha_R = 3.8$ for normal structures with a reference period of 50 years;

$\beta = 0.8$ for the governing load.

Equation 4 is sensitive for high coefficients of variation (V_R) in combination with reliability index values (α_R) larger than 3.5. In most cases the coefficient of variation of graded timber is larger than 0.25. The derived value of γ_M according to Equation (4) includes the in Annex D of EN 1990 mentioned factor η , taking into account specific material effects, such as the modification factor k_{mod} . As a consequence the derived safety factors are no proposals for safety factors to be included in EC5, but are merely used to analyse any safety differences in batches of timber graded either visually or by machine.

3 Results

While all three grade determining properties were considered when deriving settings, the results focus on bending strength, as it proofed to be the crucial property in most cases. The effect of k_v will be considered throughout the results part. In order to limit the amount of variables used, k_h will be taken into account in the first part only.

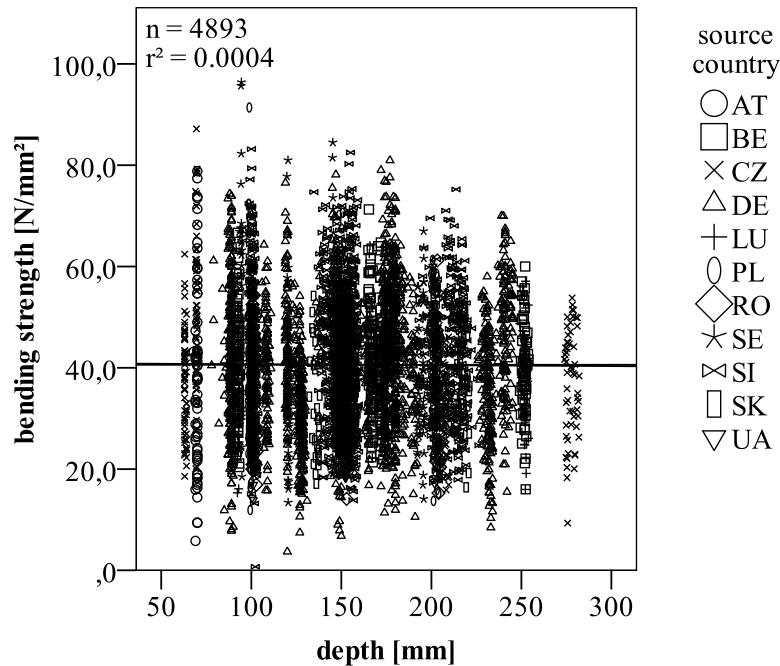


Figure 3: Bending strength not corrected by k_h as required by EN 384.

For the tested 4893 specimens nothing like a depth effect on the bending strength can be recognized. Figure 3 shows the pure test values corrected by the length (k_l) where necessary. The 4893 specimens from all over Europe cover all depths normally applied in

practice. The coefficient of determination ($r^2=0.0004$) does not indicate any correlation between depth and bending strength. The effect was also checked within different grades. There were no effects obvious which would conflict this general statement.

As described before, large depths lead to increased strength values if k_h is applied - also during deriving settings and grading. Combined with the k_v -factor used in machine grading, strength values could become more than 20 % below required values for depths exceeding 250 mm.

Figure 4 illustrates target values for timber graded using both factors. For strength class C35 and up to a depth of 150 mm the target values are as high as the according bending strength values given in EN 338. For larger depths the strength is reduced by k_h .

However, there is a jump for strength values independent of the depths when grading strength classes equal or below C30 caused by k_v for machine graded timber. Independent from the strength class the expected 5th-percentile bending strength value decreases with increasing depth.

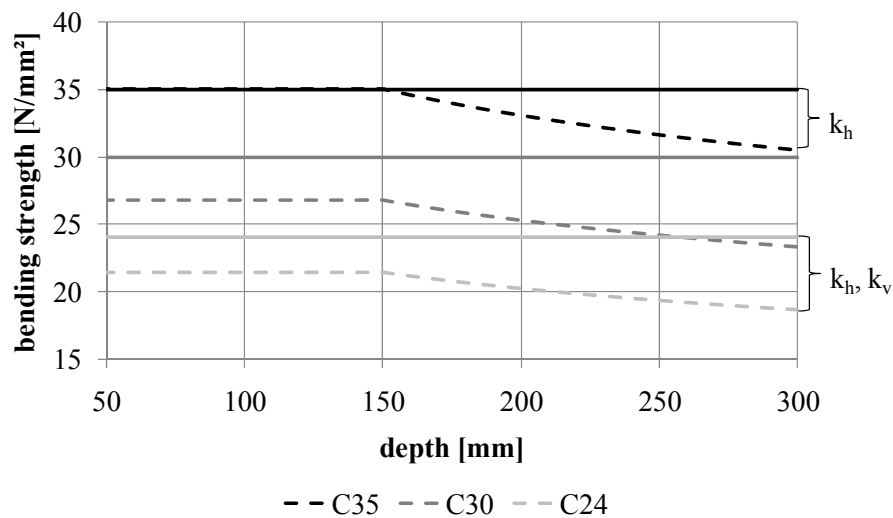


Figure 4: Expected 5th-percentile bending strength dependent on the depth of the member if k_v (EN 14081) and k_h (EN 384) are used, compared to strength values given EN 338.

Table 3 shows the 5th-percentile strength values for the grades C30 and C24, respectively. For C24 the yield reaches a maximum of 99 % for the undivided dataset in the optimum grade if the k_v -factor is used for the derivation of settings. A grading machine would assign almost the same amount of timber into C24 (98 %). The yield for visual grading drops to 79%, but the scatter in strength values for the single sub-samples is comparable to that graded by machine. The minimum strength value can be found for visual graded timber for sub-sample J (20.9 N/mm²). Only 18.9 N/mm² is reached in subsample D if k_v is applied when the machine settings are derived for C24.

For C30 the difference in yield between machine grading with and without k_v and visual grading increases. The assignment to C30 drops from 74 % (using k_v) to 56 % (without k_v), reaching a minimum of 6 % for visual grading. For visual grading no 5th-percentile values are given in table for six sub-samples, as less than 10 specimens were available in these cases. The lowest values for machine graded timber can again be found in sub-sample D (25.8 N/mm² and 23.3 N/mm²).

For C24 and C30 comparing the optimum grade (OG) considering k_v to the optimum grade neglecting k_v , shows an offset of exactly 12 % ($k_v=1.12$) for the undivided sample. However, when single sub-samples are compared this offset increases.

Table 3: Characteristic strength values. For the single sub-samples divided by grades, grading principles and the use of the k_v factor. Characteristic strength (N/mm^2) and yield for the undivided sample.

grade - C30						
principle / grade		OG	OG	machine	machine	visual
k_v		no	yes	no	yes	no
	sub-sample					
Characteristic strength [N/mm^2]	A	30.2	27.4	29.4	26.0	36.9
	B	30.3	27.4	31.2	27.8	33.3
	C	28.2	25.4	28.5	26.5	30.9
	D	30.1	25.9	25.8	23.3	-*
	E	30.5	28.0	31.9	27.8	-*
	F	29.4	27.0	32.6	28.0	-*
	G	30.5	26.9	31.6	27.8	-*
	H	29.6	26.3	34.4	24.5	-*
	I	28.8	26.6	27.7	25.3	20.4
	J	30.4	26.6	30.5	26.2	-*
	all	30.0	26.8	30.0	27.0	31.9
yield	all	78%	85%	56%	74%	6%
* too few data available						
grade - C24						
principle / grade		OG	OG	machine	machine	visual
k_v		no	yes	no	yes	no
	sub-sample					
Characteristic strength [N/mm^2]	A	25.3	23.1	24.5	22.6	25.1
	B	24.5	22.3	24.0	21.8	25.0
	C	23.3	20.0	22.3	18.9	22.0
	D	23.0	20.4	22.6	19.3	21.6
	E	26.4	24.5	27.5	24.9	27.7
	F	24.0	24.8	26.6	23.0	27.4
	G	23.2	21.4	23.9	21.2	23.9
	H	22.5	20.9	23.4	21.2	22.8
	I	24.6	21.3	22.2	21.7	21.9
	J	23.7	20.0	23.9	19.5	20.9
	all	24.0	21.4	24.0	21.4	24.0
yield	all	94%	99%	89%	98%	79%

Table 4: $\gamma_{M,mean}$ as the mean γ_M - value for the sub-samples. For different grades resulting from different grade class combinations using different grading principles and partly the k_v - factor.

grade	grade class combination	k_v	principle / grade	yield	$\gamma_{M,avg.}$ (ISO-2394)	$\gamma_{M,Std.}$ (ISO-2394)
C24	C24-rej	no	OG	4611	2.60	0.63
		no	machine	4338	2.61	1.00
		no	visual	3858	2.74	1.15
		yes	machine	4773	3.96	1.77
	C35-C24-rej	no	machine	2339	1.70	0.18
		yes	machine	2377	1.71	0.18
C30	C30-rej	no	machine	2720	1.76	0.37
		yes	machine	3622	2.36	1.23
C35	C35-rej	no	machine	1391	1.50	0.22
C40	C40-rej	no	machine	492	1.38	0.15

Where 30 N/mm^2 is required, sub-sample C has the lowest characteristic value of all, namely 28.2 N/mm^2 . This drops to a value of only 25.4 N/mm^2 when the k_v -factor is applied. For C24 similar effects can be observed.

In Table 4 the required γ_M values are given on the basis of equation 4. The given value is the average of the values of the individual sub-samples for each strength class. The scatter in terms of the standard deviation is also given.

4 Discussion

One major problem of machine strength grading in accordance with EN 14081 and underlying standards is visualized in Figure 4. The target strength value for machine graded timber lies clearly below the value an engineer is going to use for his design. The grading according to the current version of EN 14081 allows strength values which can additionally vary from this target value as the method does not require that each individual sub-sample meets the minimum strength requirements.

Even without considering the k_h -factor, which could additionally lower the strength values (depth $> 150 \text{ mm}$), the strength values for individual sub-samples can still become as low as 23.3 N/mm^2 where C30 is the target, and 18.9 N/mm^2 for C24.

If k_v is not applied for machine grading, the characteristic values obviously increase. In almost all cases the sub-sample strength values are even above the strength values for the optimum grade with k_v -factor included. Only for sub-sample D the value reaches 86 % of the required value for C30. In all other cases the values are at least 90 % of the required strength. While it is obvious that eliminating k_v leads to more reliable values, the aim of the paper is also to compare the reliability of machine grading with visual grading at the 5th-percentile strength level. This comparison can only be made for strength class C24, for which visual grading gives a yield of 79 %. The strength of visually graded C24 material is clearly above the values for machine graded timber if k_v is used. This proves at least that the k_v value is too high. Compared to machine grading without k_v differences are becoming small when looking at the 5th-percentile values of the individual subsamples; the yield in visual grading is 10 % lower.

From the results of γ_M for strength class C24, it can be clearly seen that a positive effect of machine grading can only be obtained if C24 is graded in a grade combination with C35 or higher. Otherwise, the characteristic strength of samples graded by a machine is not much better than when graded visually. The k_v -factor has a rather surprising effect on the characteristic values of the subsamples. The required safety factor for machine graded timber where settings are derived including the k_v -factor is higher. The reason for this is that with lowering the required value from 24 to $24/1.12 = 21.6$, a large number of test results with low strength are included in the sample, increasing the coefficient of variation of the sub-sample. As a consequence, the k_v -factor as currently applied cannot be justified.

The results indicate further that visual grading of C30 is very difficult if not impossible. For several sub-samples it is not possible to calculate reliable 5th-percentile strength values due to the number of pieces in the grades per sub-sample. With a yield of only 6 % it seems as if visual grading in higher strength classes is not realistic.

For higher strength classes, machine grading shows a clear benefit in terms of lower required γ_M values. Also the scatter on sub-samples is smaller. If graded in a combination with class C35 or higher, a lower γ_M value can also be justified for C24 timber.

The extreme low strength results could further decrease, if the k_h -factor is considered. Although values visualized in Figure 4 only appear if the worst comes to the worst, this factor can increase the risk for very low strength values of graded timber. As no correlation

can be shown based on the material used in this study, it is proposed to delete the depth factor from both EN 384 as well as EC5. DENZLER AND GLOS (2008) already gave the same suggestion using a different dataset.

5 Conclusions

Visual grading of wood into strength class C30 seems not to be justifiable, certainly not for the application range (growth areas) given in EN 1912. The coefficient of variation of the 5th-percentile strength values is such that higher safety factors need to be applied than currently specified in Eurocode 5. In addition, in some sub-samples the yield is so low that no characteristic values can be determined.

Visual grading into strength class C24 is possible on its own, leads however to a large scatter in 5th-percentile strength values for the different sub-samples. This in return would require high γ_M values, much higher than currently specified.

When only C24 is graded, also machine grading leads to a large variation in characteristic strength values within the grade (sub-sample level). When grading C24 by machine, a higher strength grade should be produced at the same time, increasing the threshold value for C24 and decreasing the variation within the grade. Grading of only one strength class by a machine should not be permitted, unless higher safety factors are prescribed for such material.

Adjustment factors given in EN 384 and EN 14081 intensify the problems caused by deriving settings for large areas according to the current standard. Therefore it is proposed to delete the k_v -factor from EN 384/14081-2. The k_v - factor allows more test results from the low strength range to become part of the sub-sample, having a higher scatter and consequently requires higher safety factors. The k_h -factor from EN 384/EC 5 should also be deleted. Apart from the fact that no evidence of its existence is found in the test results, there is a clear inconsistency in the standards. When deriving settings according to EN 14081 the weakest sub-sample should be taken into account and limits on the allowable deviation from the target value should be specified.

The advantage of machine grading (i.e. more reliable material with smaller scatter in strength properties) should lead to the specification of different safety factors for visual and machine graded timber. For grades C30, C35 and C40 produced by a machine, there is clearly a much lower scatter at characteristic strength level, justifying a difference in safety factor between visual grading and machine grading. This could be done by specifying different γ_M values, but another option is the specification of a modification factor, taking into account the difference in variability between visual and machine grading.

Acknowledgement

This research is partly based on a feasibility study made by the European wood industries under the Roadmap 2010 Building With Wood programme, and this project is supported by the industry via CEI-Bois. CEI-Bois is the main industrial financier of this project.

The Gradewood-project is realised by eight research institutes: Technische Universität München, VTT Technical Research Centre of Finland, BRE, FCBA, SP Wood Technology, HFA Holzforschung Austria, University of Ljubljana, and Swiss Federal Institute of Technology ETH. It belongs to the Wood Wisdom.Net-programme and is funded by national technology development bodies: Federal Ministry of Education and Research (Germany), Tekes Finnish Funding Agency for Technology and Innovation (Finland), Vinnova (Sweden), Ministry of Agriculture (France), and Slovenian Research

Agency (Slovenia). The contributions from funding organisations and other support are gratefully acknowledged.

Members of TC 124 / TG 1 are thanked for fruitful discussions during meetings.

6 Literature

Denzler J.K., Glos P.: Size effects in bending, CIB W18, proceedings paper 41-5-1, St. Andrews, Canada, 2008.

EN 338: FprEN 338: 2009 Structural timber - Strength classes. CEN, Brussels, 2009.

EN 384: FprEN 384: 2009 Structural timber - Determination of characteristic values of mechanical properties and density. CEN, Brussels, 2009.

EN 408: prEN 408: 2009 Timber structures - Structural timber and glued laminated timber - Determination of some physical and mechanical properties. CEN, Brussels, 2009.

EN 1912: EN 1912: 2004+A4: 2009 Structural timber - Strength classes - Assignment of visual grades and species. CEN, Brussels, 2009.

EN 1990 – Eurocode - Basis of structural design. CEN, Brussels, 2002.

EN 1995: EN 1995-1-1: 2004 Eurocode 5 - Design of timber structures, part 1-1: General - Common rules and rules for buildings. CEN, Brussels, 2004.

EN 14081-2: FprEN 14081-2: 2010 Timber structures – Strength graded structural timber with rectangular cross section – Part 2: Machine grading; additional requirements for initial type testing. CEN, Brussels, 2010.

EN 14081-3: prEN 14081-3: 2010 Timber structures – Strength graded structural timber with rectangular cross section – Part 3: Machine grading; additional requirements for factory production control. CEN, Brussels, 2010.

Isaksson T., Thelandersson S.: Effect of test standard, length and load configuration on bending strength of structural timber. CIB-W18 paper 28-6-4, Copenhagen, Denmark, 1995.

ISO 2394 General principles on reliability for structures, 1998.

Øvrum A., Vestøl G.I., Høibø O.A.: Modeling the longitudinal variation of sawn timber grades in Norway spruce (*Picea abies* (L.) Karst.), *Holz als Roh- und Werkstoff* 66(3): 219–227, 2008. DOI: 10.1007/s00107-008-0237-5.

Rais A., Stapel P., van de Kuilen, J.-W.: Assessment of local timber defects during testing and grading as influenced by machine approval procedure, proceedings WCTE 2010, Riva del Garda, Italy.

Ranta-Maunus A., Turk G.: Approach of dynamic production settings for machine strength grading, proceedings WCTE 2010, Riva del Garda, Italy.

Rouger, F.: A new statistical method for the establishment of machine settings, CIB W18, proceedings paper 30-17-1, Vancouver, Canada, 1997.

Sandomeer M., Köhler J., Faber M. H.: Probabilistic output control for structural timber – modelling approach, CIB W18, proceedings paper 41-5-1, St. Andrews, Canada, 2008.

Vrouwenvelder T.: http://www.rilem.net/tc_jcsspub.pdf, accessed 17.07.2010.

Ziethén R, Bengtsson C.: Machine strength grading – a new method for derivation of settings, CIB W18, proceedings paper 42-5-1, Dübendorf, Switzerland, 2009.

**INTERNATIONAL COUNCIL FOR RESEARCH AND INNOVATION
IN BUILDING AND CONSTRUCTION**

WORKING COMMISSION W18 - TIMBER STRUCTURES

THE BEARING STRENGTH OF TIMBER BEAMS ON DISCRETE SUPPORTS

A Jorissen

A Leijten

University of Technology, Eindhoven

Bas de Leijer

De Groot Vroomshoop, Vroomshoop

THE NETHERLANDS

MEETING FORTY THREE

NELSON

NEW ZEALAND

AUGUST 2010

Presented by A Jorissen

R Crocetti: The beam shown in picture is a good example of a bad design. Bearing plate should be as wide as beam. A Jorissen: this is just an example

H Blass: is the 10% failure criteria too relaxed?

H Larsen: did you design this beam? A Jorissen: No.

S Franke: this is local effect which depends on growth ring orientation.

L Daziel: About example of failure. Was this a deviation in planned construction? A Jorissen: No.

The bearing strength of timber beams on discrete supports

André Jorissen ⁽¹⁾ Ad Leijten ⁽²⁾ and Bas de Leijer ⁽³⁾

⁽¹⁾ University of Technology, Eindhoven and SHR, Wageningen, the Netherlands

⁽²⁾ University of Technology, Eindhoven, the Netherlands

⁽³⁾ De Groot Vroomshoop, Vroomshoop, the Netherlands

1 Abstract

The bearing strength capacity at discrete intermediate or/and end supports or areas of load introduction are the focus of this paper. Experimental research backed up by FEM and optical techniques have been used to assess and quantify the strength affecting parameters. It is demonstrated that the stress dispersion model by Van der Put is very well suited for strength predicting associated with 10% deformation.

2 Introduction

Many authors have tested and reported compressive perpendicular to grain tests, which is an issue as old as a beam on two supports. With the introduction of the railway ties many tests in the 19e century have most probably focused on the bearing resistance although the authors are unaware of any publications. In the early 20th century the engineered wood structures, like the platform method, developed where timber beams are continuous supported and loaded by studs as shown in Figure 2. The permissible strength design method, based on the proportional strength limit, Kolmann et al.[1], was used. An historic overview of some late 19e century, early 20e century efforts in search for the parameters of influence is given by H. Kühne [2]. Gehri [3], in his overview, focuses on the relation of compressive strength and density. He argues that differences in the determination methods and strength definition of test standards around the globe, lead to a confusing situation due to differences in specimen geometry and load configuration. For this reason test data is incompatible. Since engineered wood structures demand design rules, many have tried to develop models for strength and stiffness prediction. The complexity of the problem resulted in empirical models.

Recently, a successful attempt was made to apply an elastic-full plastic stress dispersion model by Van der Put [4]. Initially the model was only applied to solve the bearing



Figure 1: Continuous supported timber beams as

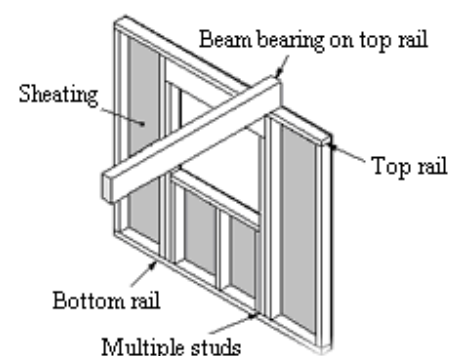


Figure 2: Vertical studs transfer the load from top the bottom rail.

strength capacity of dowel type fasteners in particle board; it was later used for continuous loaded timber beams loaded perpendicular to grain. Evaluation of additional tests added more credibility to this model, Leijten et al. [6]. It was concluded that the model is a potential candidate for future structural design codes adoption. The model reads according to equation (1).

$$\frac{F_d}{bl} = \sqrt{\frac{l_{ef}}{l}} f_{c,90} = k_{c,90} f_{c,0} \quad (1)$$

with:

- F_d is the load for a given deformation, in N
- l is the contact length of the applied load in grain direction, in mm
- b the width of the beam, in mm
- l_{ef} is the effective length at the bearing or support, in mm
- $f_{c,90}$ is the standard compressive strength perpendicular to the grain, in N/mm².

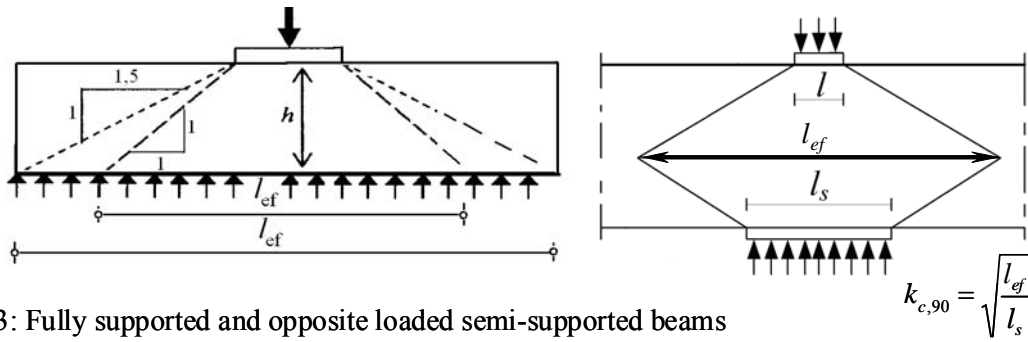


Fig. 3: Fully supported and opposite loaded semi-supported beams

The depth to width ratio should be limited to 4 in order to prevent other type of premature failure mechanism such as rolling shear, Basta [7].

A second category of beams were the compressive or bearing strength capacity is important are beams loaded at discrete locations, Figure 4. This paper concentrates on application of the stress dispersion model for these particular situations.

3 Beams loaded at discrete locations

Some examples of beams loaded at discrete locations are shown in Figure 4 and 5. In fact there is no difference between the load situation of a beam running over a (intermediate) support and a load introduce between two end supports of a single supported beam. In both cases a force is



Figure 4: Load transfer by perpendicular to grain stresses



Figure 5: Plastic failure mode

transmitted to one side (top) of the beam not finding direct support on the other side (bottom) of the beam, Figure 6.

Van der Put [5] indicates an option to apply his stress dispersion theory to a case with opposite loads, Figure 3. However, it is questioned if this approach is valid for small loaded areas or high beams despite the empirical limits set to $k_{c,90}$.

4 Tests on discrete loaded beams

A Master research project was set up and carried out by De Leier [8] to evaluate the stress dispersion method for discrete supported beams. Laboratory experiments, extended with optical measurements using the ESPI system, were complimented by numerical theoretical calculations. A summary of the results are presented below.

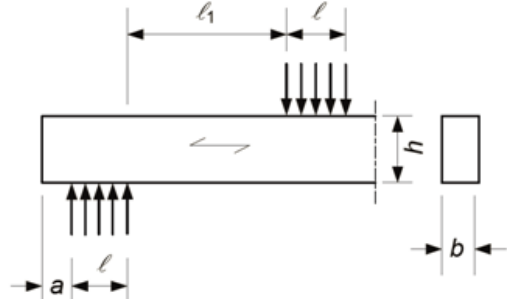


Figure 6: Discrete support

4.1 Wood species

The wood species used was Spruce with a mean density and modulus of elasticity of 437 kg/m^3 , 1016 N/mm^2 and 447 kg/m^3 , 12538 N/mm^2 for sawn and glued laminated test pieces, respectively. The modulus of elasticity was determined using the Timber Grader by Brookhuis Electronics (based on dynamic wave propagation technology). The grade assigned by the Timber Grader was C24 for the sawn timber and G24h for the glued laminated pieces.

4.2 Test program

The background for the choice of test specimen dimensions was that neither bending nor shear failure should govern but only the bearing capacity. This is achieved by taking a mid span loaded length of 100 mm over the full beam width and beam sizes as given in tables 1 and 2. The specimens were cut from 3000 mm length pieces taking as much different specimens per Series per board.

An overview of the different test pieces is given in figures 7 and 8 and tables 1 and 2.

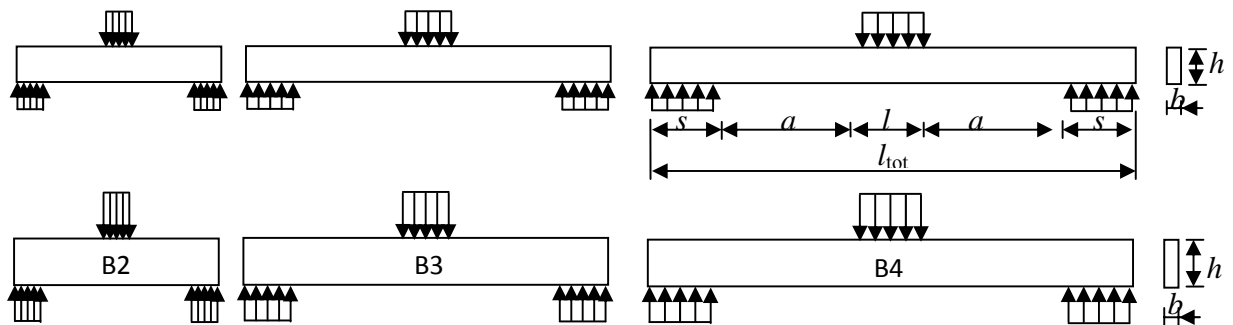


Figure 7: Overview of test specimen Series of sawn timber

Table 1: Dimension of Figure 7 test Series (sawn timber)

Specimen Series n=4	Width b [mm]	Depth h [mm]	Beam length l_{tot} [mm]	Support s [mm]	a [mm]	Loaded length l [mm]	$(l_{tot}-s)/\text{depth}$ ratio
A2	40	145	590	100	145	100	3,4
A3			880		290		5,4
A4			1170		435		6,7
B2	40	220	590	100	145	100	2,2
B3			880		290		3,5
B4			1170		435		4,9

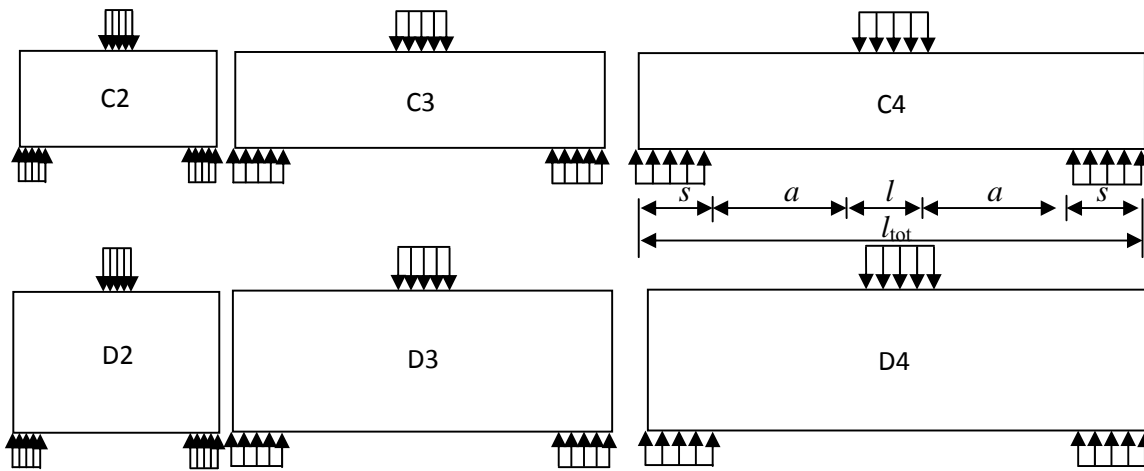


Figure 8: Overview of test specimen Series of glued laminated timber

Table 2: Dimensions of Figure 8 specimen Series (glued laminated timber)

Specimen Series n=4	Width b [mm]	Depth h [mm]	Beam length l_{tot} [mm]	Support s [mm]	a [mm]	Loaded length l [mm]	$(l_{tot}-s)/\text{depth}$ ratio
C2	80	400	590	100	145	100	1,2
C3			880		290		2,0
C4			1170		435		2,7
D2	80	600	590	100	145	100	0,8
D3			880		290		1,3
D4			1170		435		1,8

5 Numerical modeling, optical verification and laboratory tests

To examine stress dispersion perpendicular to grain numerically for continuously supported beams is not new. Madsen et al [9] performed numerical simulations and concluded that the bearing stresses dispersed not beyond 1,5 times the beam depth, which exactly corresponds to what Van der Put derived theoretically, Figure 3. The same was concluded by Riberholt [10].

The question is if the same applies for not continuous supported beams. To investigate this, De Leier [8] build a model using the FEM program Abaqus. This choice was made based on its user friendliness and the available expertise in our research group. After initial tests where the load displacement curve of the standard compressive tests perpendicular to grain according to EN 408 (cube tests with fully loaded surface) is simulated and compared to test results, the simulation considered the test series A to D. Hill's yield criterion was applied and despite its shortcomings to represent the timber behavior in detail, the final results corresponded well with previous reported simulations, Lum and Karacebeyli [11].

The analyses by De Leier [9] aimed at answering the question to what extend the bearing stresses disperse in discrete supported beams. Limits were set by the maximum bending stress (C24) or by 10% beam depth indentation. To determine the stress dispersion phenomenon in both parallel to grain and perpendicular to grain direction the deformation patterns were examined.

To investigate the indentation depth of the bearing stresses, the deformations at regular spaced cross-sections along the span were studied. In Figure 9 the vertical axis represent the indentation with respect to the top edge of the beam while horizontally the distance to the top edge of the beam is set of respective cross-section spaced along the beam.

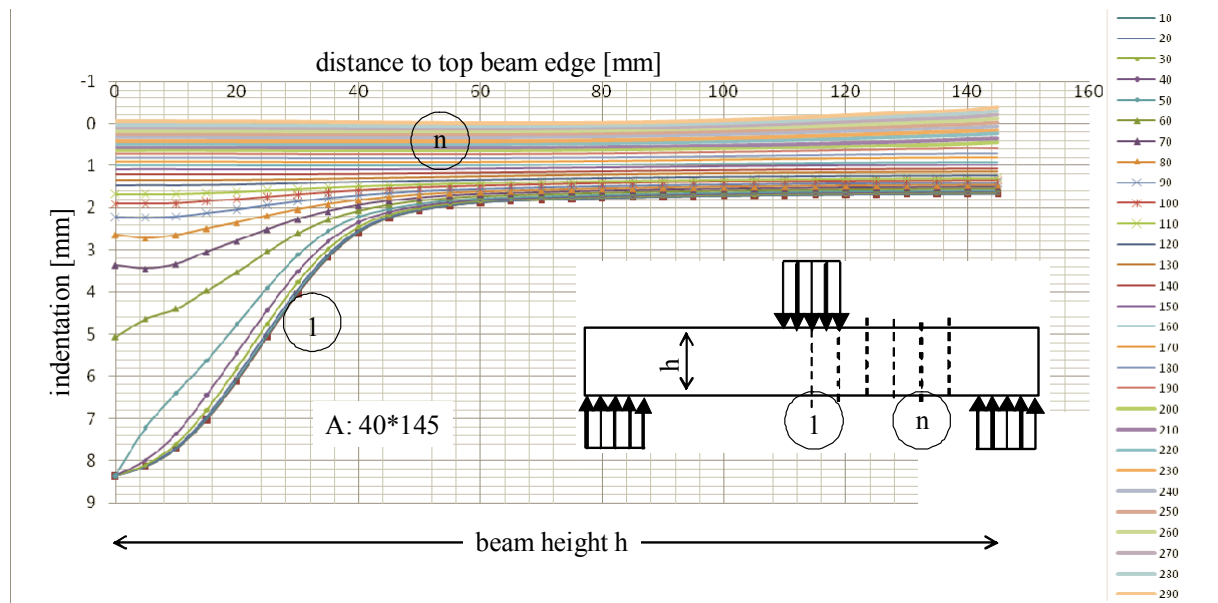


Figure 9: Penetration depth of bearing stresses in respective cross-sections for Series A2

The bottom line (1) in Figure 9 shows how the timber fibres of the mid span cross-section are affected by the bearing stress. As the figure reads the 8,4 mm indentation at the surface (distance to top edge 0 mm) drops to 2 mm at 50 mm depth from the top. Fibres situated closer to the lower beam edge are apparently hardly affected by the bearing stress at the top. The other lines of the graph represent the behaviour for cross-sections spaced at increments of 10 mm for the mid span cross-section. The line that represents a cross-section at 120 mm distance from mid span does not show any indentation where only bending deformation remains.

For verification of the FEM deformations the optical ESPI laser technique was used during the laboratory tests. After data processing graphs like Figure 10 are found. This graph is specific for the third specimen of Series A2 but all others are similar. On the vertical axis the deflection by

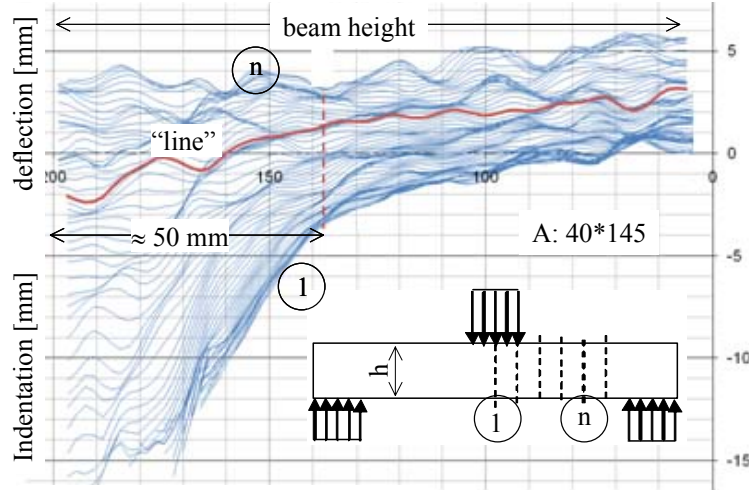


Figure 10: ESPI data of Series A2

bending is added compared to Figure 9. It is concluded that Figures 9 and 10 are in good agreement. Both show that at a certain depth the indentation by bearing stresses perpendicular to the grain is vanished and all that remains are bending deflection deformations. In Figure 10 this is given by the “line”.

The same numerical procedure is followed and backed up by the optical detection method, for the specimen Series A, B, C and D, which results in Figure 11 only showing the mid span cross-sections indentation. Although the indentations at the surface increase up to 35 mm for Series D, the indentation depth does not increase but attains a maximum of 140 mm.

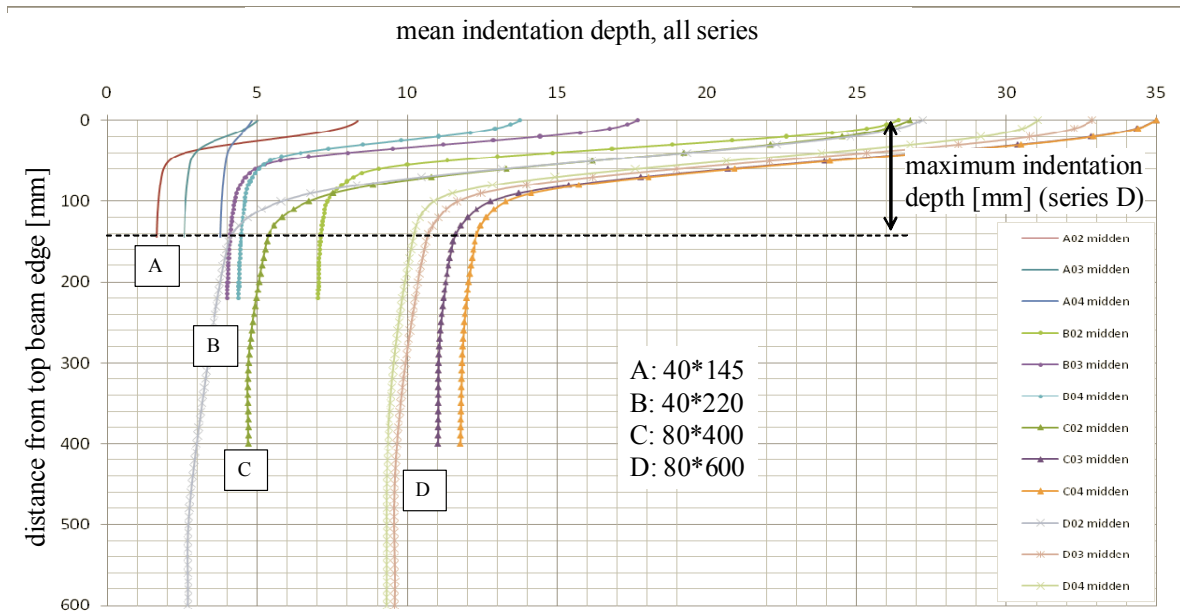


Figure 11: Summary of penetration depth at mid span cross-section.

In the same way as for Series A, horizontal sections spaced over the depth of the beam show how far the bearing stresses reach outside the loaded area, Figure 12. The top line is the indentation at

the top edge of the beam, which obviously is straight for 50 mm being half the bearing length. The bottom line shows clearly bending deflection only. Again at a certain depth added to the bending deflections the indentation by bearing stresses appears. The boundary is 50 mm from the top edge while the indentation length in grain direction is 120 mm from mid span, dotted vertical line in Figure 12. Both values are observed for a load level when the bending strength governed.

The results of the optical ESPI test method for a Series A2 specimen 3 is shown in Figure 13, which shows the indentation on left and right side of the loaded area. Evaluation shows both Figure 12 and 13 to be in close agreement.

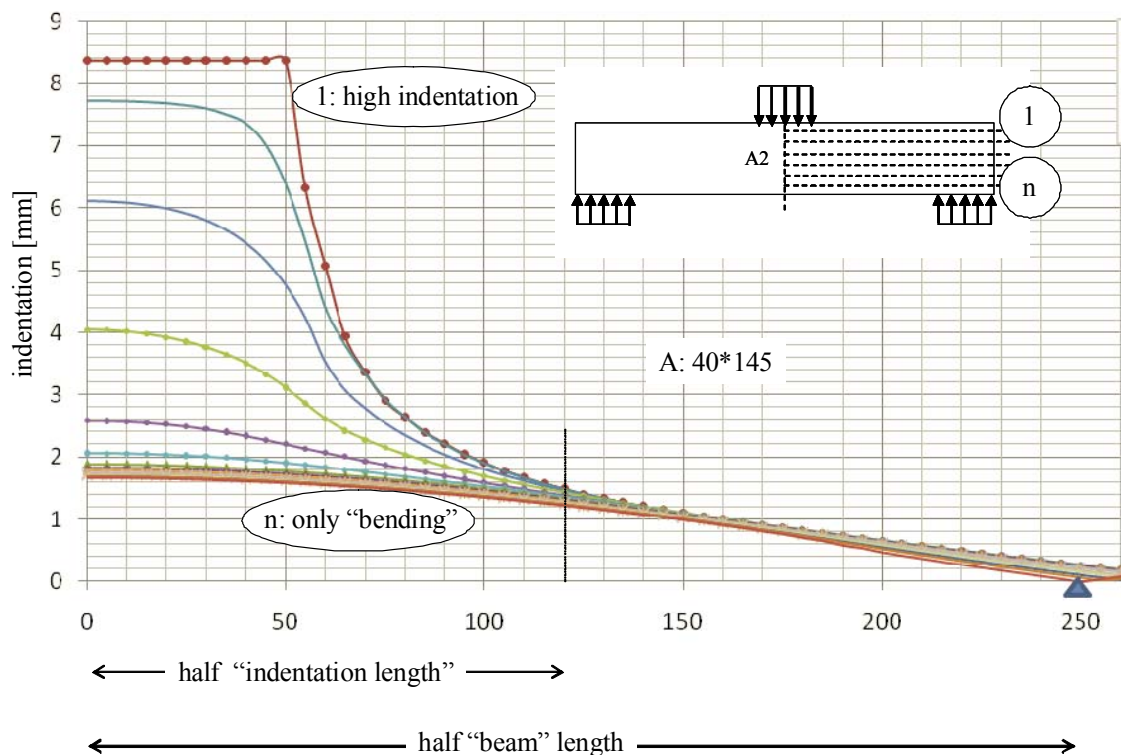


Figure 12: Indentation length of bearing stresses along the grain for series A2.

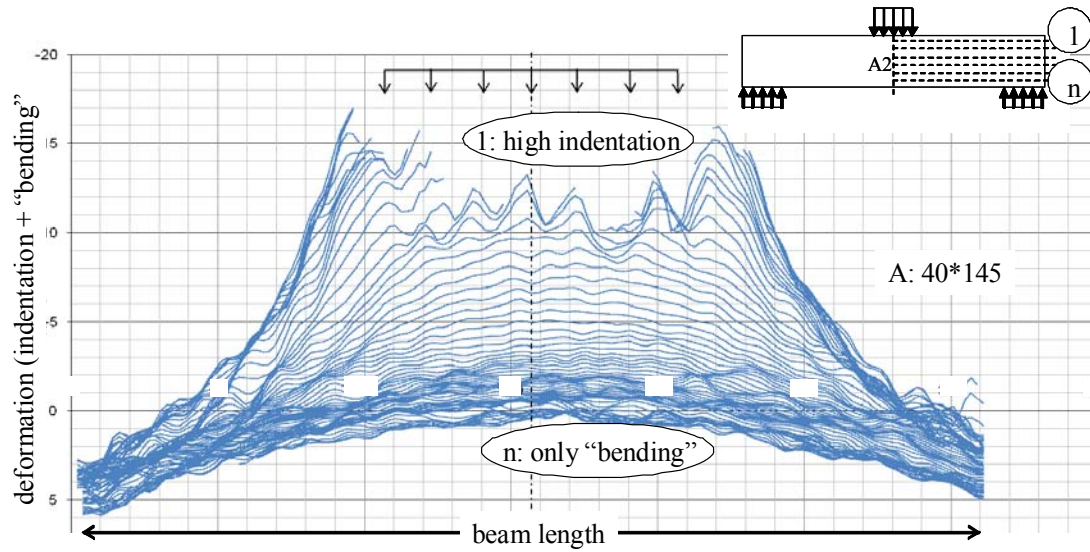


Figure 13: ESPI data of vertical deformation along the grain, Series A2

The same procedure was followed for the other test Series, B, C and D and an overview is given in Figure 14. The distance of the indentation affected areas is indicated by dotted lines for respective test Series. In the same way as for the indentation depth the indentation length reached a limit despite the increasing specimen dimensions indicated by the vertical dotted lines.

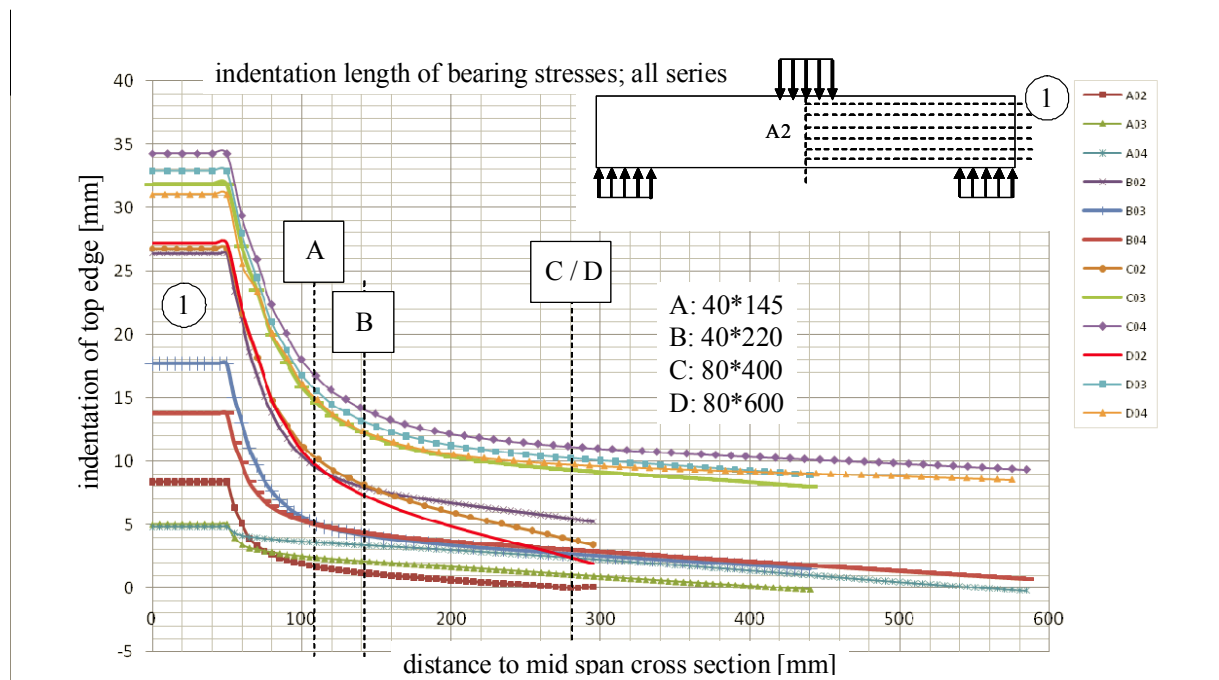


Fig. 14: Overview of edge fiber indentation versus mid span distance of all test Series

The numerically predicted indentation area expressed in depth and distance along the grain was confirmed optically, Table 3. The dispersion angle of bearing stress is derived based on these results. The mean compares very well with the theoretical value of 1,5 by Van der Put [5]. When the bending deflection become smaller it becomes more difficult to determine where the bending deformations are taken over by indentation. In other words the interpretation of the ESPI test results is less successful for the Series C and D. Figure 15 shows the indentation depth versus beam depth.

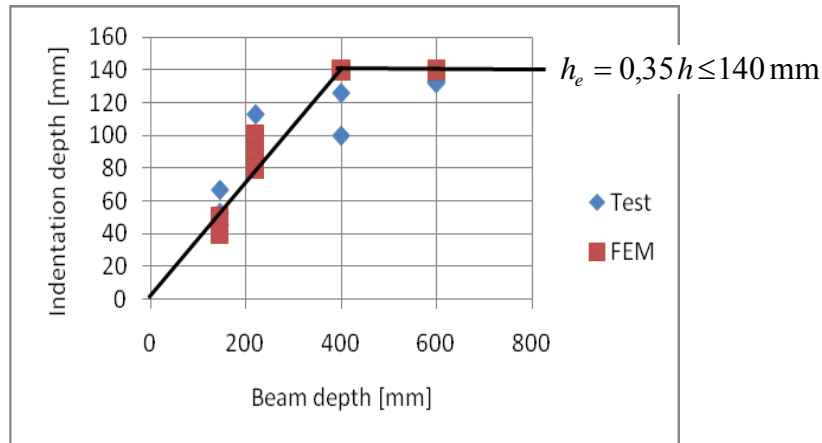


Figure 15: Indentation depth versus beam depth

Table 3: Overview of mean indentation depth and mean indentation length and $k_{c,90}$

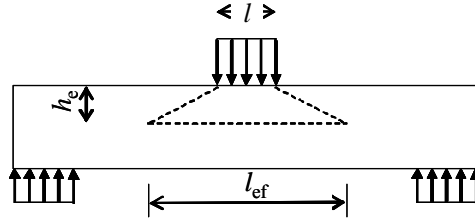
Specimen Series & Number of tests n	Width b [mm]	Depth h [mm]	Indentation depth [mm]		Tot. Indent. Length= l_{ef} [mm]		Dispersion angle [tan α]
			FEM	Test	FEM	Test	FEM
A2 n=9	40	144	50	53	240	233	1.4
A3 n=7			50	67	240	211	1.4
A4 n=8			40	46	240	200	1.75
B2 n=9	40	220	100	100	400	-	1.5
B3 n=9			90	113	320	250*	1.22
B4 n=8			80	87	320	320*	1.38
C2 n=8	80	400	140	140	320	450*	1.36
C3 n=8			140	126	480	560*	1.64
C4 n=8			140	100	560	560*	1.64
D2 n=4	80	600	140	133	560	454*	1.36
D3 n=4			140	132	480	540*	1.57
D4 n=4			140	140	540	560*	1.64
mean							1,49

*) reduced number of data available

Because the FEM results correspond well for the Series A and B more credibility is given to the FEM results were the tests become doubtful as for Series C and D. The following relations for the maximum indentation depth, h_e and length, l_{ef} are derived:

$$h_e = 0,35 h \leq 140 \text{ mm}$$

$$l_{ef} = l + 2 * 1,5 h_e = l + 3 h_e$$



This model can be applied for the prediction of the load, according to equation (2), which results in 10% deformation of the indentation depth, being 5,8 mm, 8,8 mm for Series A and B and 14 mm for Series C and D.

$$F = \sqrt{\frac{l_{ef}}{l}} f_{c,90} * b l \leq 4 f_{c,90} * b l \quad (2)$$

With b = beam width [mm]
 $f_{c,90}$ = compression perpendicular to the grain strength determined according to EN 408.

Finally, the experimental results are plotted in figure 16 together with the results according to the presented model and according to the present Eurocode 5, amendment A1, equations.

Compression strength at 10% deformation determined for each test specimen; average values

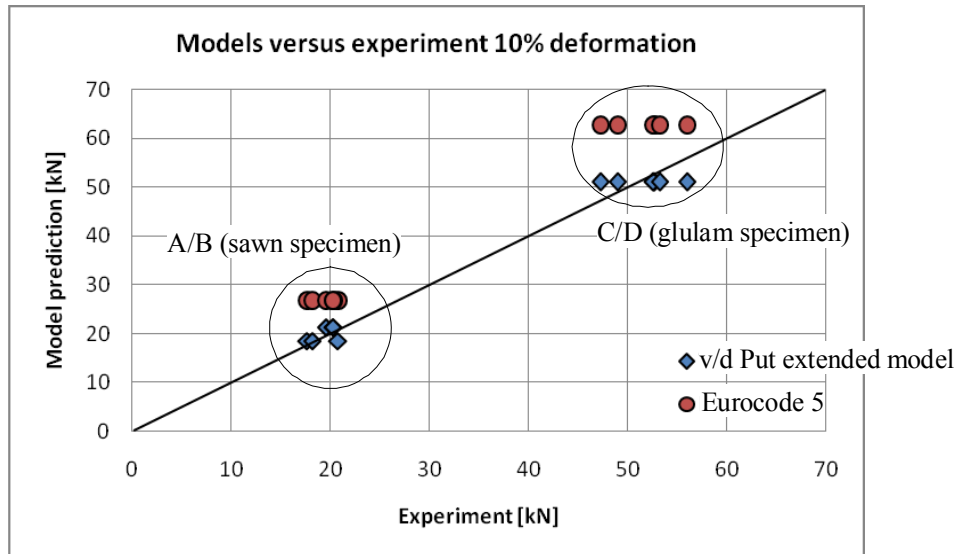


Figure 16: Experimental results compared to the model predictions according to the model presented in this paper (v/d Put extended model) and according to Eurocode 5

6 Conclusion

Using both numerical and optical techniques, it has been shown that for non-continuous supported beams loaded perpendicular to grain the dispersion of bearing stresses are limited to a certain area. For coniferous wood (Spruce) the bearing area is restricted to 35% of the beam depth with a maximum of 140 mm.

7 References

- [1] Kollmann/Côté (1984) Principles of Wood Science and Technology, Springer-Verlag, Volume 1.
- [2] Kühne H. (1956) Über den Einfluß von Wassergehalt, raumgewicht, faserstellung und Jahrringstellung auf die Festigkeit und Verformbarkeit Schweizerischen Fichten, Tannen, Lärchen, Rotbuchen und Eichenholz, Bericht 183, EMPA, Zürich.
- [3] Gehri E (1997) Timber in Compression perpendicular to Grain, In: Proceedings of the International Conference of IUFRO-S5.02. Copenhagen Denmark, June 16-17.
- [4] Van der Put T.A.C.M. (2008) Explanation of the embedding strength of particle board, Holz Roh. Werkst. 66: 259-265, DOI 10.1007/s00107-008-0234-8.
- [5] Van der Put T.A.C.M. (2008) Derivation of the bearing strength perpendicular to grain of locally loaded timber blocks, European Journal of Wood and Wood Products, 66: no.6 409-417.
- [6] Leijten, A J M, Larsen H J, Van der Put T C A M. (2010), Structural design for compression strength perpendicular to the grain of timber beams, Construction and Building Materials, 24, pp. 252-257 DOI information: 10.1016/j.conbuildmat.2009.08.042
- [7] Basta, C.T. (2005), Characterizing Perpendicular-to-Grain Compression in Wood Construction, Master thesis, Oregon State University, September 21, 2005.
- [8] De Leier, B.J.C. (2010) Het loodrecht op druk belasten van de houtvezel bij discreet ondersteunde balken, Master Thesis (in Dutch), Eindhoven University of Technology, 2010-1-CPS/A-2010.2.
- [9] Madsen B, Hooley R.F. and Hall C.P. (1982) A design method for bearing stresses in wood, Canadian Journal of Civil Engineering, 9, 338-349.
- [10] Riberholt H (2000) Compression perpendicular to the grain, Documentation of the strength, COWI –report June 2000.
- [11] Lum C, Karacebeyli E (1994) Development of the critical bearing design clause in CSA-086.1, In: Proceedings of CIB-W18, paper 27-6-1.

**INTERNATIONAL COUNCIL FOR RESEARCH AND INNOVATION
IN BUILDING AND CONSTRUCTION**

WORKING COMMISSION W18 - TIMBER STRUCTURES

**PROBABILISTIC CAPACITY PREDICTION OF TIMBER JOINTS
UNDER BRITTLE FAILURE MODES**

T Tannert

Bern University of Applied Sciences, Biel

T Vallée

College of Engineering and Architecture, Fribourg

SWITZERLAND

Frank Lam

University of British Columbia, Vancouver

CANADA

MEETING FORTY THREE

NELSON

NEW ZEALAND

AUGUST 2010

Presented by T Tannert

H Blass: Did you consider failure in header for dovetail joint? T Tannert: we avoided it in our testing program to verify the method.

H Larsen: Anisotropic materials are nasty materials. Anisotropy introduces secondary stresses. One must start and evaluate material parameters every time. T Tannert: Yes, FE analyses are very complex but material parameters do not have to be evaluated every time. Material parameters can be taken from tables.

H Larsen: why calling it probabilistic? T Tannert: It is more stochastic and certainly not deterministic.

S Aicher: What is sensitivity to volume? T Tannert: not sensitive if one changes volume and scales material parameters accordingly

Probabilistic capacity prediction of timber joints under brittle failure modes

Thomas Tannert¹, Till Vallée², Frank Lam³

¹Bern University of Applied Sciences, Biel, Switzerland

²College of Engineering and Architecture, Fribourg, Switzerland

³University of British Columbia, Vancouver, Canada

1 Introduction

To connect load bearing timber structures, practitioners have at their disposal a series of methods; a first fraction of them rely on mechanical fasteners, a second type of connections achieves load transmission by means of direct contact between timber members, and a third increasingly considered option is adhesively bonding, including welding of wood as a subcategory. All these connection methods have in common that their geometries generate stress singularities, for which "*traditional*" timber engineering design, based on stress or strain criteria, has proven to be of no use [1]. Additional complexity arises from the anisotropic nature of the material, its brittle failure modes under tension and shear loading, the complex multi-axial stress distribution, and the uncertainties regarding the associated material strength.

The capacity determination of joints exhibiting brittle failure has, for a long time, been solved using empirical methods. Mechanical problems involving stress singularities can be better solved using fracture mechanics. Most commonly used are linear elastic fracture mechanics (LEFM), which require a pre-existing crack. The failure criterion is either expressed in terms of energy release during crack propagation or a stress intensity factor. Dimensioning methods based on LEFM require the constitutive material behaviour, often idealized by a linear-elastic stress-strain curve up to the maximum stress followed by a strain softening relation from which the fracture energy is derived. This formulation has been extended to include more complex and realistic strain softening models; this generalised LEFM, e.g. [2] allows lifting the restrictions of the pre-existing cracks, and enables its application to arbitrary geometries, making it potentially interesting for practical cases. However, all methods derived from LEFM usually require an extensive and often tricky mechanical characterisation of material behaviour; furthermore, the implementation of LEFM-based methods into actionable design routines is by far not straightforward.

For materials that can be clearly defined as brittle, thus subject to significant size effects, besides LEFM based methods, Weibull weakest link theory [3] can potentially be used to overcome most of the difficulties encountered when implementing LEFM. Already forty years ago, Weibull theory has been successfully applied to characterize the magnitude of size effects on the brittle failure of timber in bending [4], tension perpendicular to grain [5] and shear [6]. It used to be difficult to analyse components with stress concentrations using Weibull theory [7] and capacity predictions were usually made for only one stress component at a time, and for stress states that exhibit elastic-brittle characteristics.

It has been shown on several occurrences that any attempt to predict the capacity of joints failing in a brittle manner and exhibiting stress peaks using a stress-based metric is deemed to fail, i.e. for adhesively bonded FRP joints [8]. To overcome the problematic associated to the sharp stress peaks of a combination of stresses, the concept of stress volume integrals was proposed [9]. A more elegant approach using a probabilistic dimensioning method was successfully developed and tested against experimental data for adhesively bonded FRP joints [10] and subsequently validated on timber joints [11-14].

Although no conclusive evidence has yet arisen for the accuracy of probabilistic strength theories to describe the size in the strength of timber, the existence of significant size effects is largely accepted. It is the purpose of this article to show that previously stated limitations “*Weibull theory suffers from similar limitations as stress or strain criteria*” [1] can be lifted. This paper describes a probabilistic method and its implementation in an actionable routine; the results are benchmarked by a direct comparison with the experimental results on three different types of joints: (i) adhesively bonded double lap joints; (ii) CNC fabricated rounded dovetail joints; and (iii) welded wood joints.

2 Probabilistic capacity prediction of timber joints

The following issues have to be addressed in the framework of a probabilistic approach to predict the capacity of timber joints under brittle failure: (2.1) determining the stress state; (2.2) identifying the failure mechanism and the associated failure criterion; (2.3) addressing the brittle nature of timber by in terms of size effects and its relation to material strength; and lastly, (2.4), implementing (2.1)–(2.3) into an actionable routine.

2.1 Stress state inside the joint

The determination of stresses inside bonded joints has been first considered on a purely analytical basis [15-16]. Analytical formulæ however are tributary to idealizations, i.e. isotropic material properties. It is thus almost impossible to achieve an accurate stress estimate, when deviating from the latter, as it is the case with timber. To overcome the limitations of analytical models, FEA has proven to be particularly effective [17].

2.2 Failure criterion of the involved materials

In the context of timber joints, the stress state is characterized by a superposition of multiple stress components acting simultaneously, making it critical to consider their combined effect on material strength. A number of failure criteria applicable to timber have been developed, and various in depth reviews were published, e.g. [18]. A commonly applied criterion was proposed by Norris [19], see Equation (1):

$$\begin{aligned} \left(\frac{\sigma_X}{f_X}\right)^2 - \left(\frac{\sigma_X \sigma_Y}{f_X f_Y}\right) + \left(\frac{\sigma_Y}{f_Y}\right)^2 + \left(\frac{\tau_{XY}}{f_{XY}}\right)^2 &= 1 \\ \left(\frac{\sigma_Y}{f_Y}\right)^2 - \left(\frac{\sigma_Y \sigma_Z}{f_Y f_Z}\right) + \left(\frac{\sigma_Z}{f_Z}\right)^2 + \left(\frac{\tau_{YZ}}{f_{YZ}}\right)^2 &= 1 \\ \left(\frac{\sigma_Z}{f_Z}\right)^2 - \left(\frac{\sigma_Z \sigma_X}{f_Z f_X}\right) + \left(\frac{\sigma_X}{f_X}\right)^2 + \left(\frac{\tau_{ZX}}{f_{ZX}}\right)^2 &= 1 \end{aligned} \quad (1)$$

where σ_X , σ_Y , σ_Z and τ_{XY} , τ_{YZ} , τ_{ZX} are the normal and shear stresses, respectively and f_X , f_Y , f_Z , f_{XY} , f_{YZ} , f_{ZX} are the material strength parameters.

2.3 Size effects and its relation to material strength

Failure of timber, when submitted to tensile or shear stresses, can be characterized as being extremely brittle. Such failure is conceptually considered to be triggered by a single weak element, i.e. a defect, randomly distributed in the material; thus the probability that such a defect is encountered in a structural element increases with its size. This is in essence the definition of size effects, which has been formalized by Weibull [3], by offering a straightforward quantifiable relationship between the size of material samples and their respective failure strength. The cumulative survival probability P_S of a volume V subjected to a non-uniform stress distribution is given by Equation (2):

$$P_S = \exp \left[- \int_V \left(\frac{\sigma}{m} \right)^k dV \right] \quad (2)$$

where, σ is the stress acting over a volume V , m is the characteristic stress or scale parameter and k is the shape parameter that gives a measure of the strength variability, with low values of k corresponding to a high variability in material properties and large size effects. One consequence of Equation (2) is that for two volumes V_1 and V_2 submitted to constant stresses σ_1 and σ_2 at failure, assuming equal P_S , a relationship is obtained that allows implementing size effects in numerical procedures: $\sigma_1 / \sigma_2 = (V_2 / V_1)^{1/k}$

2.4 Capacity prediction algorithm

As timber joints fail under a combination of the stresses, σ_1 , σ_2 , and τ_{12} , it is necessary to extend the concept of the Weibull distribution towards stresses acting conjunctly. For this purpose, it was rationally decided to consider the Norris criterion from Equation (1) modified in such a way, that only those stresses that cause brittle failure are considered; the stress operator can be replaced by a failure criterion, defined as follows:

$$\phi_F^2 = \min \left\{ \begin{aligned} & \left(\frac{\sigma_X}{f_X} \right)^2 - \left(\frac{\sigma_X \sigma_Y}{f_X f_Y} \right) + \left(\frac{\sigma_Y}{f_Y} \right)^2 + \left(\frac{\tau_{XY}}{f_{XY}} \right)^2 \\ & \left(\frac{\sigma_Y}{f_Y} \right)^2 - \left(\frac{\sigma_Y \sigma_Z}{f_Y f_Z} \right) + \left(\frac{\sigma_Z}{f_Z} \right)^2 \\ & \left(\frac{\sigma_Z}{f_Z} \right)^2 - \left(\frac{\sigma_Z \sigma_X}{f_Z f_X} \right) + \left(\frac{\sigma_X}{f_X} \right)^2 + \left(\frac{\tau_{ZX}}{f_{ZX}} \right)^2 \end{aligned} \right. \quad (3)$$

In the latter definition, $\phi_F^2 = 1$ defines failure, for which the subscript F stands, at the investigated scale. Idealizing the joint member under consideration as being constituted by n elements, which for practical reasons corresponds with the finite elements used in the FEA, its survival depends on the simultaneous non-failure of all elements $i \leq n$. As a result, for a given applied load, F , the probability of survival can be calculated by Equation (4):

$$P_S(F) = \prod_{i=1}^n P_{S,i}(F) \quad (4)$$

Where $P_{S,i}(F)$ is the probability of survival of the constituent element i associated with the applied load F , which can be calculated using Equation (2). Consequently, if each element i , with a volume V_i is subjected to a constant value of the failure function $\phi_{F,i}^2$, the probability of survival of the whole joint member is given by Equation (5):

$$P_S = \prod_{i=1}^n \exp \left[-\frac{V_i}{V_0} \cdot \left(\frac{\phi_{F,i}}{m} \right)^k \right] = \exp \sum_{i=1}^n \left[-\frac{V_i}{V_0} \cdot \left(\frac{\phi_{F,i}}{m} \right)^k \right] \quad (5)$$

To compare predictions with mean values of experimental results, a standard probability of survival of $P_S = 0.5$ has to be considered [20]; the corresponding value of F_{PRED} thus is the predicted capacity. As the approach is probabilistic, deterministic failure predictions cannot be given. To determine a strength value used by practitioners for design purposes, the strength value corresponding to a probability of failure of 5% and labelled herein $F_{\text{PRED},k}$.

3 Adhesively bonded timber joints

Adhesive bonding can provide an efficient and durable method, both in repair and in new-build applications, provided that the joints are correctly designed using an appropriate structural approach, that suitable materials and specifications are adopted, that the work is done by experienced operatives; and that strict quality control is exercised [21]. Adhesively bonded joints exhibit higher strengths and stiffnesses than mechanical connectors, the latter being of particular importance when the governing factor is serviceability limit state.

3.1 Investigations

The joints consisted of two outer ($t = 38\text{mm}$) and two inner boards ($t = 19\text{ mm}$ each) bonded with a stiff and brittle 2C epoxy adhesive, see Figure 1 left. The specimen width and the adhesive layer thickness were kept constant with 50 mm and 1.0 mm, respectively. The overlap length L was varied (40 to 280 mm in steps of 40 mm). The timber species was Spruce (*Picea abies*) cut from high quality defect-free boards, conditioned to 12% moisture content. The mechanical properties required were determined on off-axis small clear specimens (Figure 2) cut from the same boards used to produce the joints.



Figure 1: Adhesively bonded double lap joint: test specimen (left) and close-up at the locus of failure initiation after testing (right)

All experiments were performed as quasi-static axial tensile tests. To allow for the tensile forces to be introduced, the specimens had to be cut in dog-bones shapes, for all specimens, the maximum load (F_{EXP}) was recorded. All joints collapsed in a brittle manner and almost always failed by splitting just below the end of the overlap. In all cases failure was triggered by a crack developing from the surface, illustrated by Figure 1 right.

To determine the material strength parameters needed (f_x, f_y, f_{xy}) to formulate the failure criterion, axial tension tests were performed on dog-bone shaped specimens exhibiting different orientations, α , relatively to the grain, see Figure 2. Four series were performed: 0° , 10° ; 45° and 90° . Previous studies [22] showed that 2D modelling of adhesively bonded joints is accurate enough, thus 2D 8-node elements and symmetry conditions were used.

3.2 Results

A stress transformation on the results from the off-axis tests delivered the following strength: $f_X = 98.21$ MPa, $f_Y = 4.46$ MPa and $f_{XY} = 13.66$ MPa, and a regression procedure on the probability distribution yielded the Weibull parameters: $k = 3.717$ and $m = 1.124$.

Figure 3 displays the average and characteristic values of the experiments: joint capacity is positively correlated with the overlap length, however it can also be seen that the increase is not linear but seems to asymptotically approach a maximum value. The capacity prediction procedure was performed; the results for F_{PRED} which correspond to the 50%-quantile, and the lower 5%-quantile values $F_{\text{PRED},k}$ are also displayed in Figure 3 and exhibit very good agreement with the experimentally determined values.

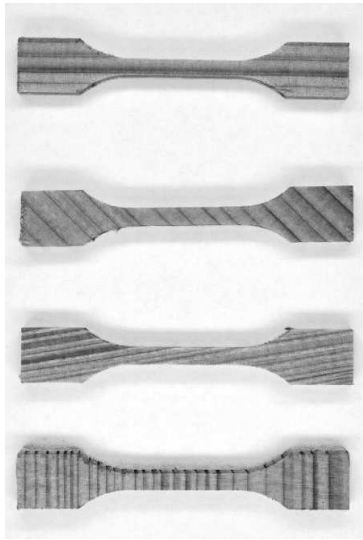


Figure 2: Determination of material parameters

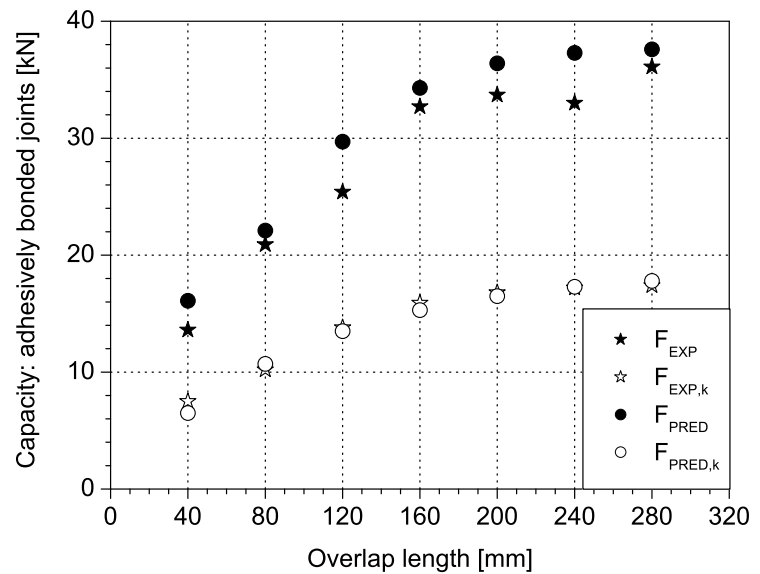


Figure 3: Experimental vs. predicted joint capacities for adhesively bonded joints

4 Rounded dovetail wood-to-wood joints

The Rounded Dovetail Joint (RDJ), named after the rounded shape similar to a dovetail (Figure 4 left) is adapted to be produced with a CNC-timber processor. A number of experimental studies on RDJ provided valuable insight, revealing that failure under shear loading was typically brittle, and occurred in the elastic range of the load deformation curve, e.g. [23-24]. Although RDJ were shown to be able to undergo large rotations before failing, the brittle nature of failure was independent of loading for similar joint geometries.

4.1 Investigations

The brittle material strength properties were determined according to ASTM-D143. A total of 480 individual tests were carried out, 160 for each of the material properties. These test series were performed on samples exhibiting different shapes and volumes (Figure 5).

RDJ geometries with varied dovetail flange angle and dovetail height were investigated resulting in different dovetail areas; subsequently used as a measure of joint size. Kiln-dried Western hemlock (*Tsuga heterophylla*) was used with average values of moisture content and apparent density of 12.6% and 495 kg/m³, respectively. The capacity at rupture of the joint (F_{EXP}) was determined.

The detailed specimen description, experimental set up and subsequent 3D FEA have been described previously [11]. The good agreement between experimentally and numerically obtained load deformation curves allowed the results to be used to obtain input data for the capacity predictions.

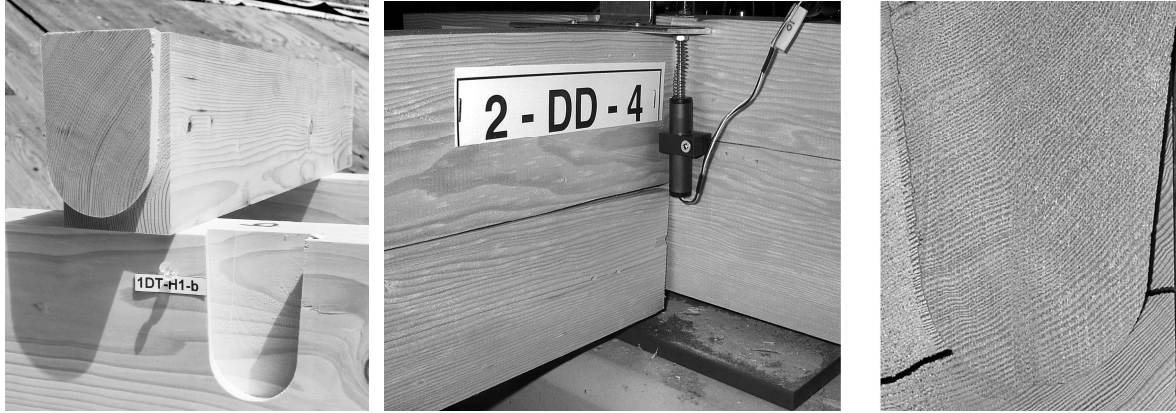


Figure 4: Rounded dovetail joint: specimen (left) and typical failure (right)

4.2 Results

The experimentally determined mean values of the material strengths were $f_x = 77.4$ MPa, $f_y = 2.92$ MPa and $f_{xy} = 7.80$ MPa, respectively. As the specimens exhibited different sizes for the different tests, the corresponding failure stresses could not be used in one single series. To overcome this formal issue, all values were first related to a reference volume. This procedure resulted in a homogeneous set of data, with $k = 4.55$ and $m = 1.122$.

Within the range of geometric parameters, loading and support conditions investigated, failure was always brittle, occurred in the elastic range, and initiated at the bottom of the dovetail of the joist member (Figure 4 right). Figure 6 illustrates the results of the recorded capacities, F_{EXP} , in function of the dovetail area and indicates that capacity does not increase proportionally with joint size. Also the predicted capacities, F_{PRED} , and the lower 5%-quantile values, $F_{EXP,k}$ and $F_{PRED,k}$ are displayed, exhibiting sufficient accuracy.

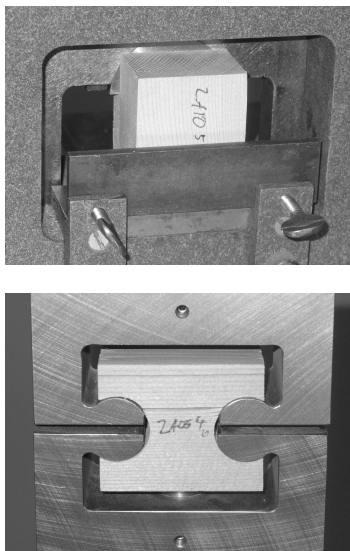


Figure 5: Determination of material parameters

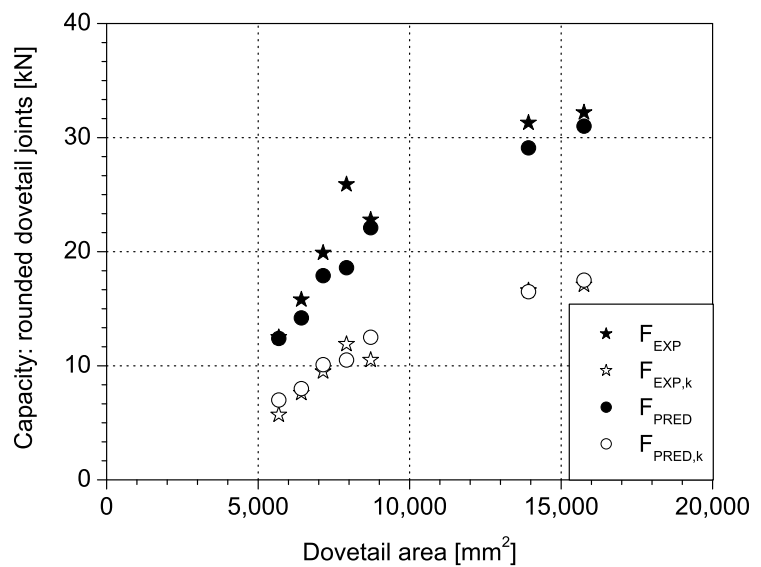


Figure 6: Experimental vs. predicted joint capacities for rounded dovetail joints

5 Welded wood joints

Wood joints by means of welding are an innovative connection, holding high potential for development. To achieve welded joints, the adherends are pressed against each other; rapidly vibrating melts the material at the interface within few seconds. Once the motion stops, after cooling down, a solid bond is formed [25]. The question to which extent welded joints can be considered for load bearing in structural timber engineering, and if, how such joints can be dimensioned, remains open and research has just begun to investigate all aspects governing strength and durability.

5.1 Investigations

A series of single-lap welded joints was manufactured in which the sole varied parameter was the overlap length. The timber species used was spruce (*Picea abies*) cut from high quality almost defect-free boards. The joints, shown in Figure 7 left, were manufactured by welding together two timber boards (700 mm x 60 mm x 15 mm) by means of a Branson M-DT24L linear vibration machine. Subsequently, a groove up to the wood weld was cut in each of the connected boards; the distance between the two grooves defined the overlap length (varied from 100 mm to 400 mm in steps of 100 mm). Each overlap length was manufactured, and subsequently tested, five times.

The determination of the stresses along the welded overlap line was achieved by using 2D 8-node elements; the timber was modelled using the same properties as used for the adhesively bonded joints, as the specimens were produced from the same batch of material. Following the experimental observations, the wood weld was modelled as being fully rigid.

Regarding failure criteria for interfaces of wood welded surfaces, no generalized theories exist, and preliminary investigations were carried out. The mechanical resistance of the interface with regard to simultaneously acting stresses (tension parallel to the weld line, σ_X , perpendicular to the weld line, σ_Y , and shear acting on the interface, τ_{XY}) was determined. To experimentally handle the determination of the corresponding strength data in one consistent test-setup, it was decided to perform off-axis tests. Five different sets of off-axis angles were considered, ranging from $\alpha = 0^\circ$ to $\alpha = 60^\circ$ in steps of 15° . A subset of the resulting specimens is depicted in Figure 8.

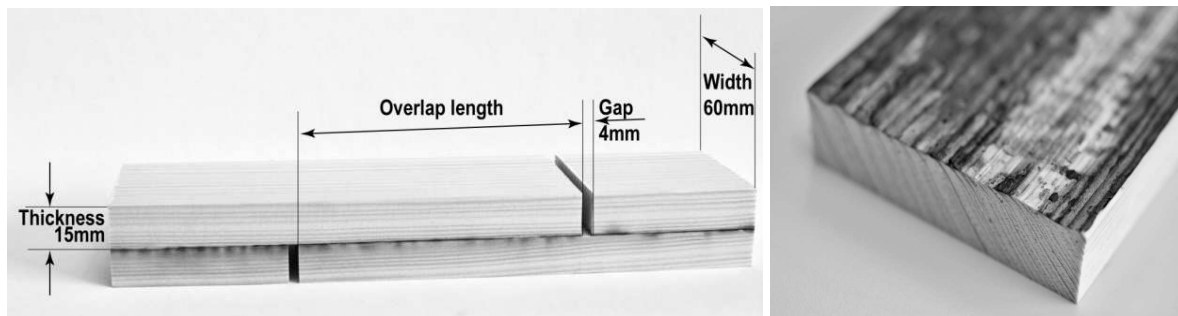


Figure 7: Welded wood joint: specimen (left) and typical failure (right)

5.2 Results

The off-axis samples on the welded interface exhibited almost linear load-displacement behaviour, and failure occurred in a brittle manner. Following a similar failure criteria formulation as for timber, the influence of the longitudinal stress, σ_X , was found to be negligible. By means of a subsequent statistical analysis, it was found that the off-axis data is best modelled by Equation (6):

$$\sigma_{F,W}^2 = \left(\frac{\sigma_Y}{f_{W,Y}} \right)^2 + \left(\frac{\tau_{XY}}{f_{W,XY}} \right)^2 = 1 \quad (6)$$

The strength parameters were found equal to $f_{W,Y} = 0.61$ MPa and $f_{W,XY} = 1.07$ MPa and the corresponding statistical parameters were estimated as $k = 3.68$, resp. $m = 1.15$.

All wood welded single lap joints exhibited almost perfectly linear-elastic load-displacement behaviour, and failed in a brittle manner. A closer post-failure observation indicates that the welding process did not always yield in perfectly welded surfaces, see Figure 7 right. The experimental results are displayed in Figure 9, where test results are plotted against the overlap length showing that the capacity of the welded joints increases with overlap length, but that the increase is limited, indicating a critical overlap length. The predictions of the mean values F_{PRED} and the lower 5%-quantile values $F_{\text{PRED},k}$ are also plotted in Figure 9. Sufficiently accurate agreement with the experiments was obtained.



Figure 8: Determination of material parameters

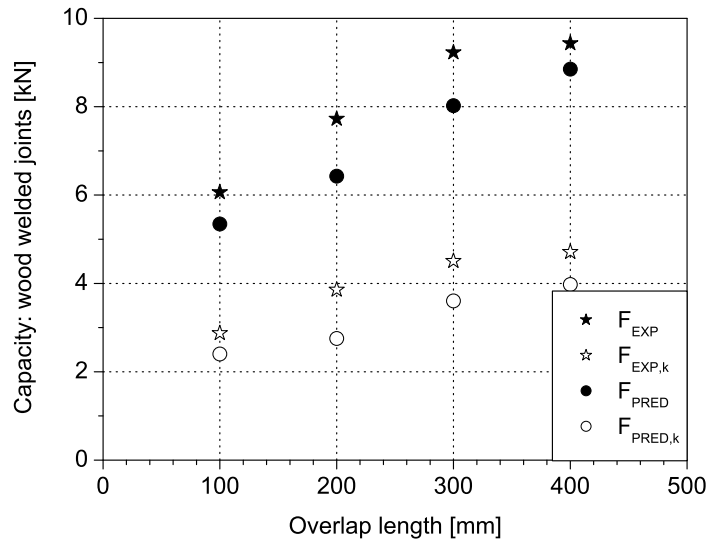


Figure 9: Experimental vs. predicted joint capacities for welded joints

6 Discussion and Conclusions

The capacity prediction of timber joints is difficult due to the anisotropic nature of the material, its brittle failure under tension and shear loading, the complex stress distribution as well as the uncertainties regarding the associated material resistance. This paper describes a probabilistic method to predict the capacity of timber joints under brittle failure modes. The method considers the statistical variation and the size effect in the strength of timber using a Weibull statistical function. The approach presents an explanation for the increased resistance of local zones subjected to high stress peaks as it takes into account not only the magnitude of the stress distributions, but also the volume over which they act. The method, besides yielding accurate predictions, has the additional benefit of relying solely on objective geometrical and mechanical parameters, excluding empirical input.

The method was applied to three different types of joints: (i) adhesively bonded double lap joints; (ii) CNC fabricated rounded dovetail wood-to-wood joints; and (iii) linear friction welded joints. The paper briefly summarizes the experimental and numerical investigations to determine the failure modes and capacities of these joints.

The relevant material strengths and their statistical distributions were obtained with small scale specimens. This can be achieved using standardized test specimens that exhibit different shapes and material volumes, and subsequently have to be brought into a coherent mechanical form, i.e. volume. An increase of accuracy can be expected by using a less disparate set of tests; with samples that are equal in their geometry and volume, e.g. a set of off-axis tension tests that allow formulating the failure criterion more straightforwardly.

The experiments for the adhesively bonded and the welded joints were carried out on high quality almost defect free timber which considers an idealized situation, since such a selection is unlikely to occur in practical applications. However, using less strictly selected timber will in a first instance only increase the scattering of the material strength, without altering the principles behind the dimensioning method as shown for the dovetail joints.

Finite element analyses were applied to determine the stress distribution and provide input data for the capacity prediction. The subsequent application of the probabilistic approach proved to be sufficiently accurate for all investigated joints. The paper also shows how characteristic values of joint capacity can be predicted in the framework of current standards. Since brittle failure tends to be well described by extreme value probability density functions distributions, e.g. Weibull, such statistics also lead to good agreement between experimentally and numerically determined characteristic values.

This paper summarizes a new approach by implementing probabilistic concepts in an engineering context. Firstly the method overcomes the difficulties raised by the timber's inherent brittleness and strength variability; secondly, it offers an alternative to much more complex fracture mechanics methods, for which the correct input data is complicated to generate. Furthermore, the probabilistic method allows predicting characteristic values of joint capacities. Its implementation is straightforward, and results are sufficiently accurate for the investigated joints under brittle failure over a large set of parameters. The proposed method has immediate application for the design improvement of the investigated joints and can be extended to other joints; e.g. dowel type connections.

7 References

- [1] Serrano E and Gustafsson PJ (2006) Fracture mechanics in timber engineering – Strength analyses of components and joints. *Materials and Structures*, 40:87–96.
- [2] Gustafsson PJ (2003) Crack propagation in wood and wood products. *Proc. 2nd Int. Conf. of the European Society for Wood Mechanics*, Stockholm, Sweden, 227–236.
- [3] Weibull W (1939) A statistical theory of strength of materials. *Proc. of the Royal Swedish Institute*, Research No.151, Stockholm, Sweden.
- [4] Bohannon B (1966) Effect of size on bending strength of wood members. Research paper FPL 56, *Forest Products Laboratory*, Madison, USA.
- [5] Barrett JD (1974) Effect of size on tension perpendicular-to-grain strength of Douglas-Fir. *Wood and Fiber* 6(2):126-143.
- [6] Foschi RO and Barrett JD (1976) Longitudinal shear strength of Douglas-Fir. *Canadian Journal of Civil Engineering*. 3(2):198-208.
- [7] Smith I, Landis E and Gong M (2003) Fracture and fatigue in wood. *Wiley*, Chichester, England. 242 pp.
- [8] Keller T and Vallée T (2005) Adhesively bonded lap joints from pultruded GFRP profiles; Part I: Stress-strain analysis and failure modes, *Composites Part B* 36(4):331-340.

- [9] Tannert T, Lam F and Vallée T (2010) Strength prediction for rounded dovetail connections considering size effects. *ASCE Journal of Engineering Mechanics*, 136(3):358-366.
- [10] Vallée T, Correia JR and Keller T (2006) Probabilistic strength prediction for double lap joints composed of pultruded GFRP profiles–Part II: Strength prediction. *Composites Science and Technology*, 66(13):1915–1930.
- [11] Tannert T, Lam F and Vallée T (2010) Structural performance of rounded dovetail connections: experimental and numerical investigations. *European Journal of Wood and Wood Products*, DOI 10.1007/s00107-010-0459-1.
- [12] Vallée T, Tannert T and Ganne-Chedville C (2010) Capacity prediction of welded timber joints. Accepted in: *Wood Science and Technology*, WST-10-0086.
- [13] Tannert T, Vallée T and Hehl S (2010) Probabilistic strength prediction of adhesively bonded timber joints, Submitted to: *Wood Science and Technology*. WST-10-0019.
- [14] Vallée T, Tannert T, Murcia J and Quinn D (2010) Influence of stress reduction methods on the strength of adhesively bonded joints composed of brittle adherends. *Int. Journal of Adhesion and Adhesives*. 30(7):583-594.
- [15] Volkersen O (1938) Nietkraftverteilung in zugbeanspruchten konstanten Laschenquerschnitten. *Luftfahrtforschung*, 15:41-47.
- [16] Goland M and Reissner E (1944) The stresses in cemented joints. *Journal of Applied Mechanics*, A17–27.
- [17] Da Silva LFM, Das Neves PJC, Adams RD, Wang A and Spelt JK (2009) Analytical models of adhesively bonded joints - Part II: Comparative study, *Int. Journal of Adhesion and Adhesives*, 29(3):331-341.
- [18] Kasal B and Leichti RJ (2005) State of the art in multiaxial phenomenological failure criteria for wood members, *Progress in Structural Eng. and Materials* 7(1):3-13.
- [19] Norris CB (1962) Strength of orthotropic materials subjected to combined stresses. *Report No.1816, Forest Products Laboratory, Madison, USA*,
- [20] Towse A, Potter KD, Wisnom MR and Adams RD (1999) The sensitivity of a Weibull failure criterion to singularity strength and local geometry variations. *Int. Journal of Adhesion and Adhesives* 19:71-82.
- [21] Broughton JG, Hutchinson AR (2001) Adhesive systems for structural connections in timber, *Int. Journal of Adhesion and Adhesives*, 21:177-186.
- [22] Vallée T, Correia JR and Keller T (2006) Probabilistic strength prediction for double lap joints composed of pultruded GFRP profiles–Part I: experimental and numerical investigations, *Composites Science and Technology*, 66(13):1903–1914.
- [23] Tannert T and Lam F (2009) Self-tapping screws as reinforcement for rounded dovetail connections. *Structural Control and Health Monitoring*, 16(3):374-384.
- [24] Tannert T, Prion H and Lam F (2007) Structural performance of rounded dovetail connections under different loading conditions. *Canadian Journal of Civil Engineering*, 34(12):1600-1605.
- [25] Ganne-Chédeville C, Properzi M, Leban JM, Pizzi A and Pichelin F (2008) Wood Welding: Chemical and Physical Changes According to the Welding Time. *Journal of Adhesion Science and Technology*, 22(7):761–773.

**INTERNATIONAL COUNCIL FOR RESEARCH AND INNOVATION
IN BUILDING AND CONSTRUCTION**

WORKING COMMISSION W18 - TIMBER STRUCTURES

DUCTILITY IN TIMBER STRUCTURES

A Jorissen

University of Technology, Eindhoven and SHR, Wageningen,
THE NETHERLANDS

M Fragiaco

University of Sassari, Dept. of Architecture, Design and Urban Planning, Alghero
ITALY

MEETING FORTY THREE

NELSON

NEW ZEALAND

AUGUST 2010

Presented by A Jorissen

H Larsen: Not in agreement with capacity based concept.

A Palermo: It is good to have presentation like this but what about structural systems?

H Blass: how does one expect to have large moments and ductility in beam as shown in Gerber system?

T Poutanen: Assuming 2 structures and one is brittle and one ductile. How much is the ductile one better? A Jorissen: hard to put a number but the steel and concrete industry are using this concept.

P Quenneville: how to force connections to control this design? M Fragiaco: the ductility is to be forced only through system design, not component design.

A Ceccotti: In EC 8, safety coefficient for timber is to be 1 for brittle, 1.3 ductile.

A Buchanan: Not in agreement with paper. The authors are trying to use seismic concepts in non seismic situations.

Ductility in Timber Structures

André Jorissen⁽¹⁾ and Massimo Fragiaco⁽²⁾

⁽¹⁾ University of Technology, Eindhoven and SHR, Wageningen, the Netherlands

⁽²⁾ University of Sassari, Dept. of Architecture, Design and Urban Planning, Alghero, Italy

1 General notes on ductility

At ultimate limit state, timber structural elements generally fail in a brittle manner. Such behaviour is due to the elastic-brittle stress-strain relationship of the material in both tension and shear. Non-linear load-deformation relationships characterized by some plasticization can only be achieved in timber engineering by elements loaded in compression, both parallel and perpendicular to the grain, and through connections. In bending, the load-deformation relationship is generally close to linear due to the elastic-brittle stress-strain relationship in tension, which hinders extensive plasticization in compression.

Within COST Action E55, modelling of the performance of timber structures (<http://www.cost-e55.ethz.ch/>), research has been undertaken into three main subjects: (1) System identification and exposures; (2) Vulnerability of components; and (3) Robustness of systems. From probabilistic analyses it was demonstrated that ductile structural behaviour positively influences structural robustness [2]. It is therefore of importance to investigate possible ductile behaviour of structural components for implementation into the probabilistic structural robustness analyses. This task has been undertaken by the members of COST Action E55 Working Group 2.

Ductility is an important requirement in structural design. Traditional literature references quote three main reasons for achieving ductile behaviour:

1. to ensure the failure will occur with large deformations, so as to warn the occupants in the case of an unexpected load (e.g. exceptional snow load, etc.);
2. to allow stress redistribution within a cross-section and force redistribution among different cross-sections in statically indeterminate structures (plastic analysis), so as to increase the load-bearing capacity of the structure with respect to the value calculated in elastic analysis. Plastic analysis can only be carried out for structures which exhibit a minimum amount of ductility;
3. to allow energy dissipation under seismic loading. Energy dissipation reduces the effect of the earthquake on a structure, leading to an overall better behaviour. Roughly speaking, the larger the ductility, the lower the seismic action that has to be considered in design. The seismic actions considered in design are therefore related to the ductility of the structure.

In addition, there is another important reason for ductility requirements:

4. to ensure the fulfilment of structural robustness, where the members must be able to accommodate large displacement and rotation demand caused by sudden failure of a single member within the whole structural system. According to analyses carried out in [2], only a little ductility is needed for a significant robustness increase.

It should be noted that stress redistribution in members subjected to bending is traditionally related to ductility. However, this can hardly ever be achieved for timber since it has to be ensured that plasticization in compression occurs before brittle failure in tension; consequently a tensile strength markedly higher than the compression strength is required. For clear wood this is certainly the case. For structural timber containing defects, however, this is only the case when the defects are mainly located in the compression zone. This is also the case for beams strengthened in the tensile area through ductile reinforcement for which some examples are shown in Figure 1.

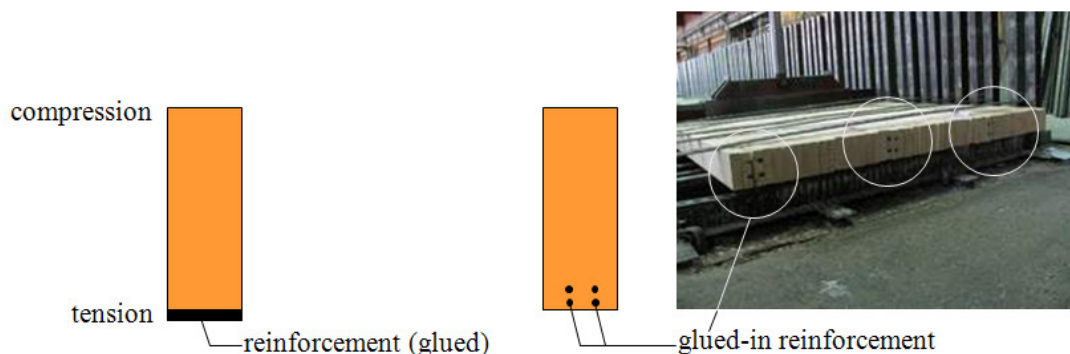


Figure 1: Reinforcement of beams (bending) for stress redistribution purposes

Under static load conditions, design for ductile failure in the connections is desirable because this allows redistribution of forces between components and subassemblies. This is one of the means of avoiding progressive and disproportionate collapse in structural systems. In seismic design, ductile failure in the connections is desirable because mechanical connections are the only significant sources of ductility and energy absorption during cyclic loading [1].

Timber structures are mostly designed as a set of individual statically determinate elements connected to each other. However, most structures end up being highly statically indeterminate due to the (semi) rigidity of most connections modelled as perfectly pinned in the design phase. Consequently, it can be expected that failures in systems initiate and develop in ways that are inconsistent with the design practice or intent. This can be more problematic than, for example, in steel or reinforced concrete systems because mechanical responses of components in timber structures may be completely different from the expectations, as illustrated in Figure 2 [3]. The large differences in component response do not affect the system response at serviceability level. However, the system response at ultimate limit state can be completely different than intended during the design causing unexpected failures at unexpected load levels.

The relevance of understanding the real structural response at ultimate limit states become an important issue when designing “extrapolated structures” (large span structures with several load paths, high rise buildings) for which standard experience is not available. Load paths can “exactly” be predicted for statically determinate structures. This is much more complex for statically indeterminate structures, varying loads and system (material) properties. Due to the varying properties, it is even not certain, although pretty certain, that the intended concept of the connection being the governing parameter (capacity based design), shown in Figure 3, is achieved.

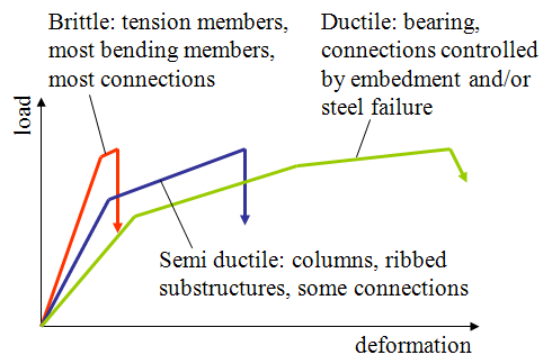


Figure 2: Typical range of responses for components in structural timber systems [3]

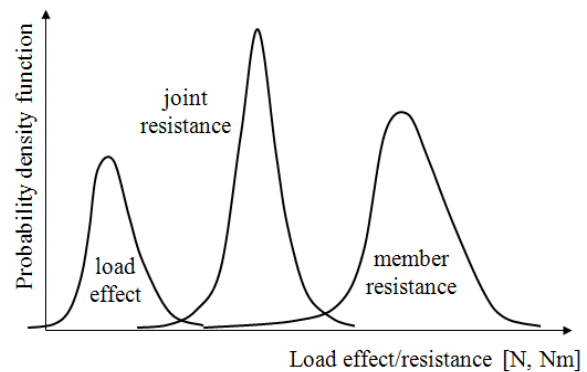


Figure 3: Capacity Based Design

Furthermore, the connections should be regarded as multiple fastener connections in strength, stiffness and ductility analyses and not as a set of single fastener connections. Depending on the connection geometry, the failure mode may change from ductile to brittle as shown in Figure 4 for dowel-type fasteners loaded perpendicular to the grain.

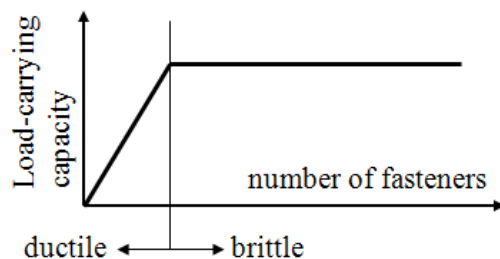


Figure 4: Changing failure mode depending on the connection geometry and on the number of fasteners for dowel-type fasteners loaded perpendicular to the grain

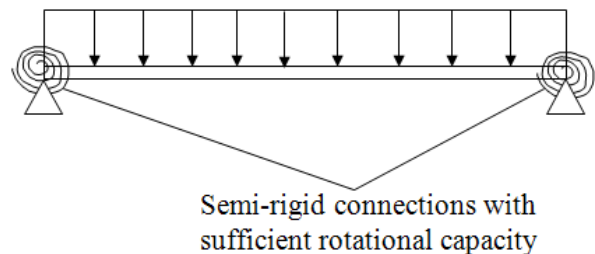


Figure 5: Requirement for a plastic-plastic design

Something similar happens for dowelled connections loaded parallel to the grain, where the failure mode may change from ductile for single dowelled connections to brittle for multiple dowelled connections due to stress perpendicular to the grain accumulation and/or row shear failure. In Eurocode 5, EN 1995-1-1 [4], this is taken into account by introducing an effective number of fasteners (n_{ef}).

2 Elastic versus plastic analysis

Timber elements are usually analysed assuming fully-elastic behaviour: this is the normal case. The plastic-plastic design (PP), where the effects (forces, bending moments) as well as the resistances of cross-sections are calculated with a plastic analysis is usually not applicable for timber structures since the deformations to be achieved in the mechanism are, in most cases, not realistic for timber. The plastic-plastic design is only applicable for timber structures when the rotational capacity of the connections, see Figure 5, is sufficient. Clearly, the members between the connections have to show sufficient deformation capacity if they are part of the mechanism. However, this is not necessary when a capacity based design, as shown in Figure 3, is applied.

Another possibility, more suitable for timber structures, is the so-called elastic-plastic (EP) design, where the calculation of load effects (forces, bending moments) is based on elastic analysis, but the strength capacity is evaluated by accounting for the plastic resistance of

the cross-section. Redistribution of the internal stresses can only be considered in design if the material exhibits a ductile behaviour, i.e. the material can accommodate a large strain demand without significant loss of strength capacity. This reduction in strength capacity is estimated as no more than 20% of the peak strength by the Swiss Timber Code [5], by EN 12512 for timber joints made from mechanical fasteners [6], and by the Italian Regulation for masonry walls [7]. It should be noted, however, that contrary to e.g. metal (steel) elements loaded in tension and/or bending, unreinforced timber elements fail brittle with hardly any redistribution of internal stresses. In these cases plastic behaviour can be exhibited only by cross-sections loaded in compression or subjected to coupled bending and compression with strict limitations on slenderness and M/N ratios, as discussed at by Buchanan [8], Steiger and Fontana [9], and Blass [10].

The plastic capacity of e.g. steel or reinforced concrete structures is incorporated into design codes, with provisions to ensure the achievement of a minimum strain and deformation capacity, so as to make structures more economic, not necessarily more robust. Ductile timber structures can be achieved only if a capacity based design procedure is followed and ductile connections are used as the timber material is inherently brittle. Until now, the ductility of connections (e.g. dowels) is taken into account by determination of the characteristic strength values at a certain displacement level. The ductility limitations yet to define aims at a more robust structure, not necessarily at a more economic structure.

3 Ductility design for statically loaded structures

As discussed above, ductility in timber structures is possible in the connections and in members subjected to compression. For statically determinate structures, ductility may give the possibility to the occupant to see deformations (e.g. due to compression perpendicular to the grain at supports or large deformations in the connection) before failure. Consequently, the ductile regions must govern the design instead of the bending or tensile resistance of the member. In other words, the design strength of the ductile element must be less than the design strength of the brittle elements (basis for capacity based design). Since in a correct design the strength of a support is always larger than the bending strength of a timber beam, ductility cannot be achieved for simply-supported timber beams. The only way to achieve ductile behaviour would be to include a ductile connection within the span of the beam, which would make little sense as it would reduce the load-bearing capacity and increase the cost.

For statically indeterminate systems, “semi-rigid connections” must be designed so as ductile failure for plasticization of the connections can be achieved. An example is given in Figure 6. The timber elements must be overdesigned in order to ensure they will not fail before the plasticization of the connections. This relates to the so-called Capacity Based Design concept, described e.g. by Aziz and Smith [1]. The semi-rigid connections must be designed such that they are able to accommodate the rotation demand due to the redistribution of bending moments.

Looking at the system shown in figure 6, it should be noted that the formation of a complete mechanism is prevented by the brittle failure in bending of the timber member. Once all semi-rigid connections have plasticized, the bending moment will increase within the member until the flexural capacity of the timber member is reached. Since, however, the flexural failure of a timber member is brittle, the full mechanism will not form and, consequently, a plastic-plastic design is not possible. An incremental non-linear analysis

has therefore to be carried out in timber structures with semi-rigid joints in order to exploit the ductility of the connection. This is a significant difference with reinforced concrete and steel structures where, with a proper choice of details, a full failure mechanism can be reached and the plastic-plastic design can be used. A significant consequence of this remark is that in timber structures with semi-rigid joints like the one depicted in Figure 6, a redistribution of forces is possible (#2 in Section 1), but large deformations to warn the occupants in the case of unexpected excessive load may not occur (#1 in Section 1).

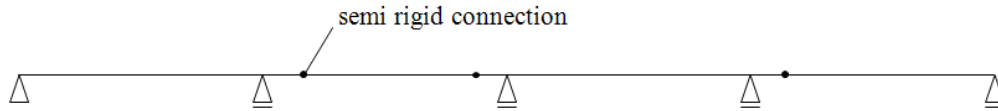


Figure 6: Statically indeterminate beam with semi-rigid connections

The occurrence of a full mechanism is, however, possible for the timber frame shown in Figure 7 if the connections govern the design, which is usually the case. However, the connection shown in Figure 7 only fails ductile when reinforced in order to avoid splitting, otherwise the connection is inherent brittle. Connection A is reinforced with densified veneer wood (DVW), glued on each member, which reinforces the timber elements. The connection is realized with tube fasteners, which behave in an extremely plastic manner. Consequently, connection A shows sufficient deformation capacity at failure and a full mechanism is possible when using this type of connection. However, the efficiency of this connection with respect to the load-carrying capacity is high: the load carrying capacity equals (almost) the load carrying capacity of the timber elements and a capacity based design approach is important to avoid brittle failure in the timber elements. This is not the case for connection B, which has to be reinforced to avoid splitting in the connection area.

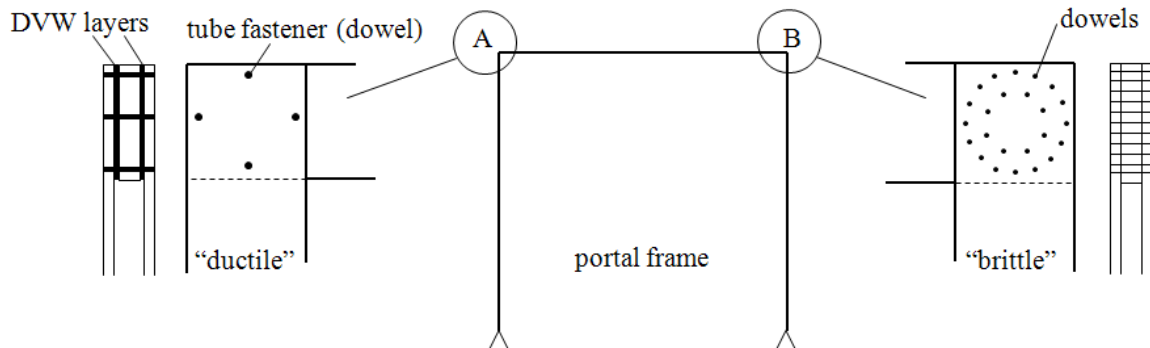


Figure 7: Portal frame; a full mechanism is only possible when the rotational deformation capacity of the connection is sufficient

4 Ductility design for dynamically loaded structures

With respect to dynamically loaded structures, a distinction has to be made between structures subjected to vibrations and fatigue, e.g. bridges, and structures subjected to seismic loading, explosions or other impact loads.

4.1 Ductility design of bridges

Plastic design is generally not allowed for bridges by current design codes due to vibrations and fatigue, for which high stiffness is required. The internal forces are therefore evaluated through an elastic analysis for ultimate limit states of fatigue and strength (flexural, shear, etc.). Ductile analyses are only allowed for exceptional loading

(e.g. unintended collision, earthquake, etc.). Connections must be designed in the elastic range under “normal load conditions” due to progressive damage under cyclic load caused by pinching, but they will be required to be ductile in order to warn users in the case of an unexpected exceptional load (#1 in Section 1). The timber members, on the other hand, will be overdesigned in order to ensure they will fail only after the connection has plasticized. To avoid pinching, some codes such as the Dutch code NEN 6760 [11] prescribe a design load overestimating the actual design load according to equation (1), and require the members to be governing:

$$F_d = F_{d,max} + \frac{1}{3} F_{d,min} \quad (1)$$

where: $F_{d,max}$ = the absolute value of the **maximum** connection load
 $F_{d,min}$ = the absolute value of the **minimum** connection load

Consequently, ductility analyses cannot be applied for bridges under “normal load conditions”, whereas they are allowed at the design load level F_d according to equation (1).

4.2 Ductility design in relation to earthquakes, explosions or other impact loads

Loads like earthquakes, explosions or impact may decrease the internal force demand due to energy dissipation. Structural details must ensure energy dissipation. A behaviour factor which reduces the elastic forces due to the earthquake for seismic design can be evaluated based on the possibility of the structure to dissipate energy and is generally tabled by current codes of practice such as the Eurocode 8 [12].

It must be acknowledged, however, that recently developed design methods such as the Displacement-Based Design, proposed by Priestley et al. [13], and the N2 method proposed by Fajfar [14] mainly focuses on the maximum displacement a structure must be able to undergo during a seismic event. Therefore, it seems that in seismic design emphasis should be placed more on the total displacement than on the ductility ratio. Sway limits such as the ‘drift’ or ‘interstorey drift’ have been therefore implemented in many design codes such as the FEMA [15] and the Eurocode 8 [12].

It should be also pointed out that since seismic actions usually cause the structure to vibrate, the amount of energy dissipated during the seismic cycles will be of great importance as it will significantly affect the dynamic performance of the system. While for static action the most representative quantity to measure the ductility seems to be the strain/rotation/curvature/displacement for material/connection/beam/structure respectively, for dynamic (seismic) loading the most important quantity seems to be the dissipated energy, which can be related to the equivalent viscous damping according to equation (2), and affect the dynamic response of the structure under seismic excitation:

$$v_{eq} = \frac{E_d}{4\pi E_p} \quad (2)$$

with: E_d = energy dissipated in a half hysteresis cycle, see Figure 8;

$E_p = \frac{1}{2} F_{max} u_f$ = potential energy to failure, with $F_{max}=F_{uf}$, as shown in Figure 8.

The quantities E_d and E_p must be determined based on experimental testing [6]. This is a “curve fitting problem” for which a possible approach, shown in Figure 9, is described in [16]. The piecewise-linear (black line) must approximate the experimental hysteretic curve (red line) such that the corresponding dissipated energies are equivalent.

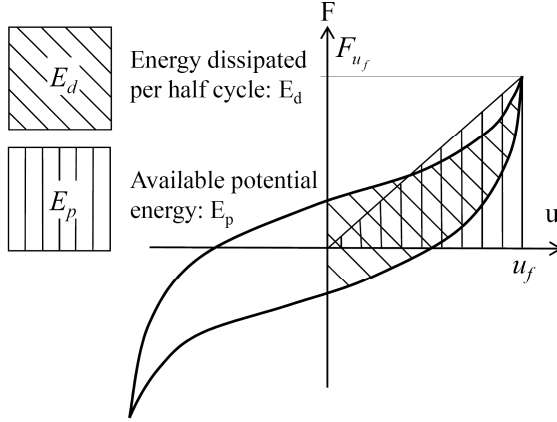


Figure 8: Definition of E_d and E_p for the determination of the equivalent viscous damping ratio for one cycle [6]

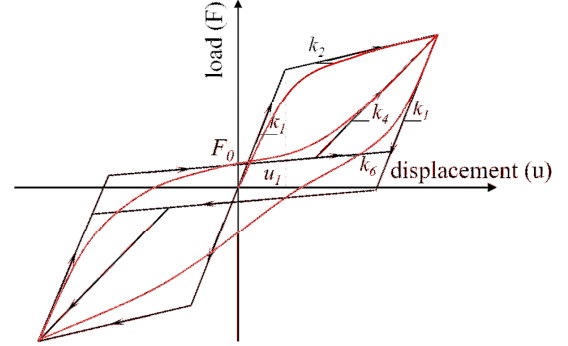


Figure 9: “Curve fitting” problem described in [16], possibly useful for the determination of E_d and E_p

In seismic engineering, the capacity based design approach requires the use of the so-called overstrength factor γ_{Rd} , which is defined as the ratio between the 95th percentile $f_{0.95}$ and the design value f_d of the strength of a structure/member/joint/material:

$$\gamma_{Rd} = \frac{f_{0.95}}{f_d} = \frac{f_{0.95}}{f_{0.05}} \cdot \frac{f_{0.05}}{f_k} \cdot \frac{f_k}{f_d} = \gamma_{Rd,m} \cdot \gamma_{Rd,an} \cdot \gamma_m \quad (3)$$

With simple manipulation it can be seen that the overstrength factor is given by the product of three factors, where $f_{0.05}$ is the actual 5th percentile of the structure/member/joint/ material strength, f_k is the analytical value of the structure/member/joint/material characteristic strength as predicted using analytical formulas, and f_d is the design value of the same property. The factors $\gamma_{Rd,m}$, $\gamma_{Rd,an}$ and γ_m represent, therefore, the experimental scatter of the strength property (see Figure 10), the accuracy of the analytical formula/mode used to calculate that property, and the material safety factor, respectively. The $\gamma_{Rd,m}$ factor should be determined with experimental tests on a sufficient number of specimens to adequately represent the scatter of results (ten specimens at least).

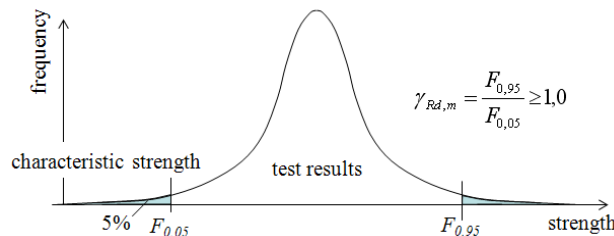


Figure 10: Definition of the coefficient $\gamma_{Rd,m}$ (F is a strength property of a structure/member/joint/ material)

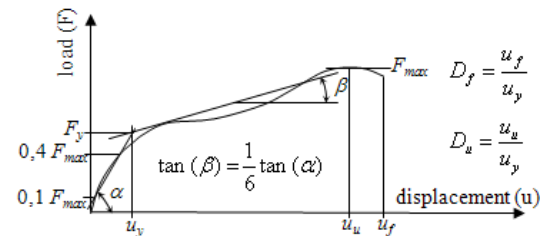


Figure 11: Ductility definitions D_f and D_u suggested by EN 12512 [6]

As an example, for a timber connection $f_{0.95}$ and $f_{0.05}$ represent the 5th and 95th percentiles of the shear strength evaluated in experimental tests, f_k represents the characteristic shear strength predicted using the European Yielding Model. The coefficient $\gamma_{Rd,an}$ measures the

degree of accuracy achievable using a formula/analytical model (e.g. the European Yielding Model). For the flexural strength of a timber beam, $\gamma_{Rd,an}$ would be equal to one as the model used to predict the flexural strength does not contain any approximation or, in other words, is fully consistent with the way of measuring the bending capacity.

The overstrength factor is important for ductile design as it ensures that the brittle member will fail after plasticization of the ductile member with a high probability of occurrence, since reference to the 95th percentile of the ductile member strength is made. Brittle members will therefore have to resist the design load F_d multiplied by the overstrength factor γ_{Rd} of the ductile member. For example, in a timber beam with semi-rigid joints such as that displayed in Figure 5, the timber member will be designed for the design load of the timber joint multiplied by the overstrength factor of the timber joint. In this way it is possible to create a hierarchy of strengths and ensure the ductile behaviour with the selected ductile failure modes.

5 Ductility definitions

An important point of discussion is which parameter can best reflect the ductility of a structure/member/joint/material. On this regard, several suggestions have been done in the past. In EN 12512 [6] the suggestion displayed in Figure 11 is given. Stehn and Björnfot [17] proposed ten different ductility definitions, illustrated in Figure 12.

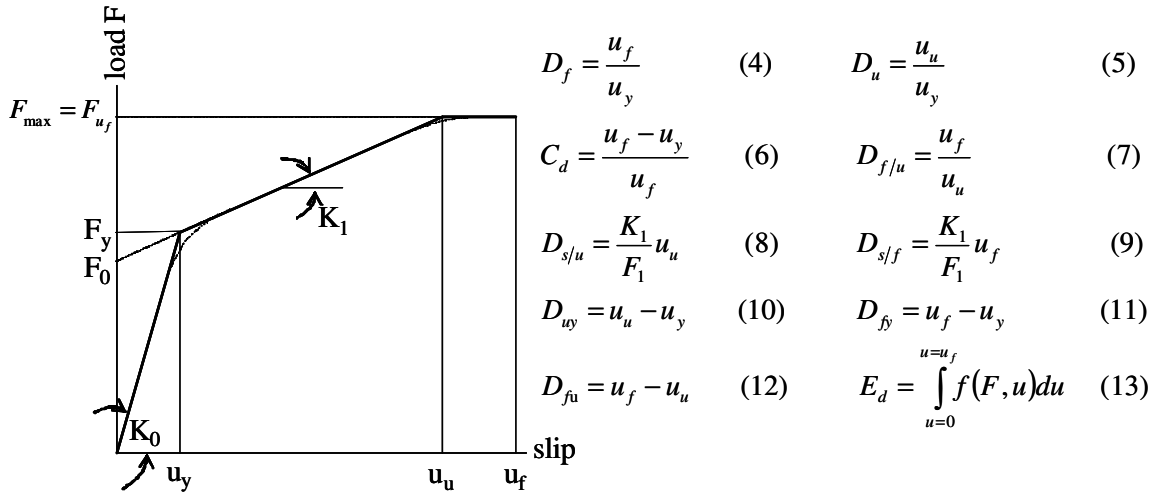


Figure 12: Ductility definitions by Stehn and Björnfot [17]

Ductility definitions (4) to (9) are relative definitions, while definitions (10) to (13) are absolute definitions. Definitions (4) and (5) are similar to those provided in EN 12512 [6] and shown in Figure 11. Definition (4) is incorporated in the Swiss Timber Code, SIA 265 [5], which explicitly allows for a reduction in the material safety factor γ_m for a ductile structure. Such a reduction in material safety factor is not considered in the Eurocode 5, EN 1995-1-1 [4]. The evaluation with respect to ductility of the load-slip curve shown in Figure 12 can be carried out on the experimental curve, or alternatively on an approximated curve, e.g. equation (14) which is applicable for (single) dowelled, bolted and (multiple) nailed connections:

$$F = (F_0 + K_1 u) \left(1 - e^{-\frac{K_1 u}{F_0}} \right) \leq F_{\max} \quad (14)$$

with $K_1 \approx 0$ for parallel to the grain loading. The relative definitions (4) to (6) shown in Figure 12 are in need of the so-called yield slip u_y . A procedure for the evaluation of this quantity is suggested in EN 12512 [6], see Figure 11, and discussed in Muñoz et al. [18], where six different methods commonly used all around the world for the determination of u_y are presented (see Figure 13).

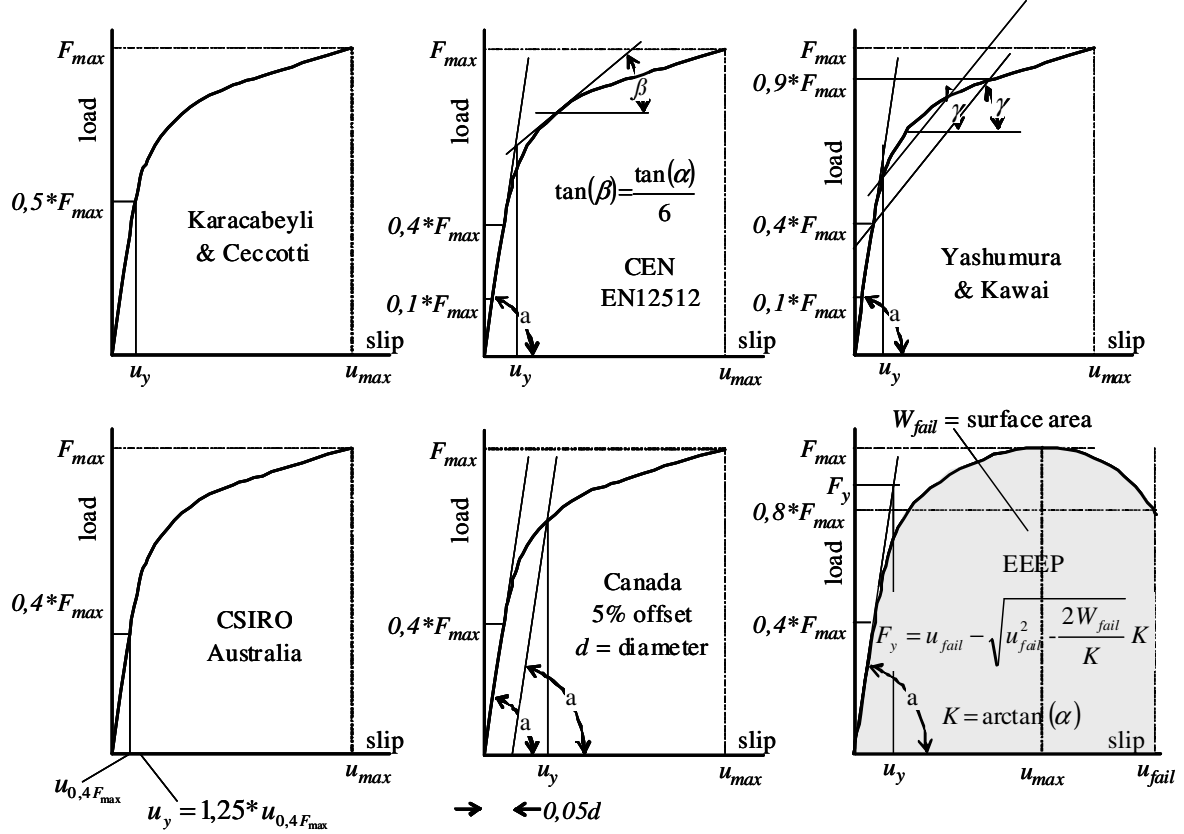


Figure 13: Methods commonly used for estimation of the yield point [18], with $u_{max} = u_u$ (displacement at maximum load; not necessarily the slip at failure)

With reference to equation (14) and Figure 12, a further method for the determination of u_y can be added according to equation (15):

$$u_y = \frac{F_0}{K_0 - K_1} \quad \text{and} \quad u_u = \frac{F_u - F_0}{K_1} \quad (15)$$

where the variables F_0 , K_0 and K_1 , derived on the basis of regression analysis, are explained in Figure 12. The values obtained with equation (15) are similar to the values obtained according to EN 12512 [6] as shown in Figure 13.

Muñoz et al. [18] concluded that the values of the “yield displacement” vary up to 80% depending on the methods displayed in Figure 13 used for their evaluation. In particular, the authors pointed out that the EEEP (Equivalent Energy Elastic-Plastic) method results quite often in unrealistic values. Furthermore, the EEEP method is hardly applicable for bolted connections since these, in particular multiple bolted connections, show little plasticization. When using a relative Ductility Definition, hence, only ONE well-defined criterion for the evaluation of the yield displacement u_y should be chosen to avoid the high variability of such a quantity highlighted above.

Regarding earthquake design, energy dissipation related ductility definition is most probably the most appropriate. The equivalent viscous damping provided by equation (2),

which results in an absolute value, is a possibility. However, a relative definition, e.g. according to equation (16), might be appropriate as well:

$$D_E = \frac{E_d}{E_{py}} \quad (16)$$

with: $E_{py} = \frac{1}{2} F_y u_y$, where u_y is derived from tests according to one of the methods described in Figure 13 or according to equation (15) based on the first cycle, and E_d is defined in Figure 8.

6 Discussion

An important point under discussion in this paper is which quantity should be used to describe the ductility of a timber material/joint/member/structure. An issue designers have to confront with is the possibility of using many ductility definitions, each of which leading to rather different results. The relative definitions, e.g. definitions (4) to (9) shown in Figure 12 (definitions (4) and (5) are suggested by the European standard EN 12512 [6]), are the most commonly used. However, looking at the four main reasons why a structure should be ductile, i.e. deformations to provide sufficient warning due to unexpected excessive load, force and stress redistributions, energy dissipation, and structural robustness, it can be inferred that an absolute definition better represents the ductility concept. In all cases, in fact, what counts is the slip/rotation/displacement at failure u_f or the difference with the yield value $u_f - u_y$, not the ratio u_f/u_y or u_u/u_y . Furthermore, in the plastic analysis of statically indeterminate structures, the load-bearing capacity due to the attainment of a plastic failure mechanism depends upon the ultimate rotation of the plastic hinge as an absolute value rather than on the ratio between the same quantity and the yield rotation.

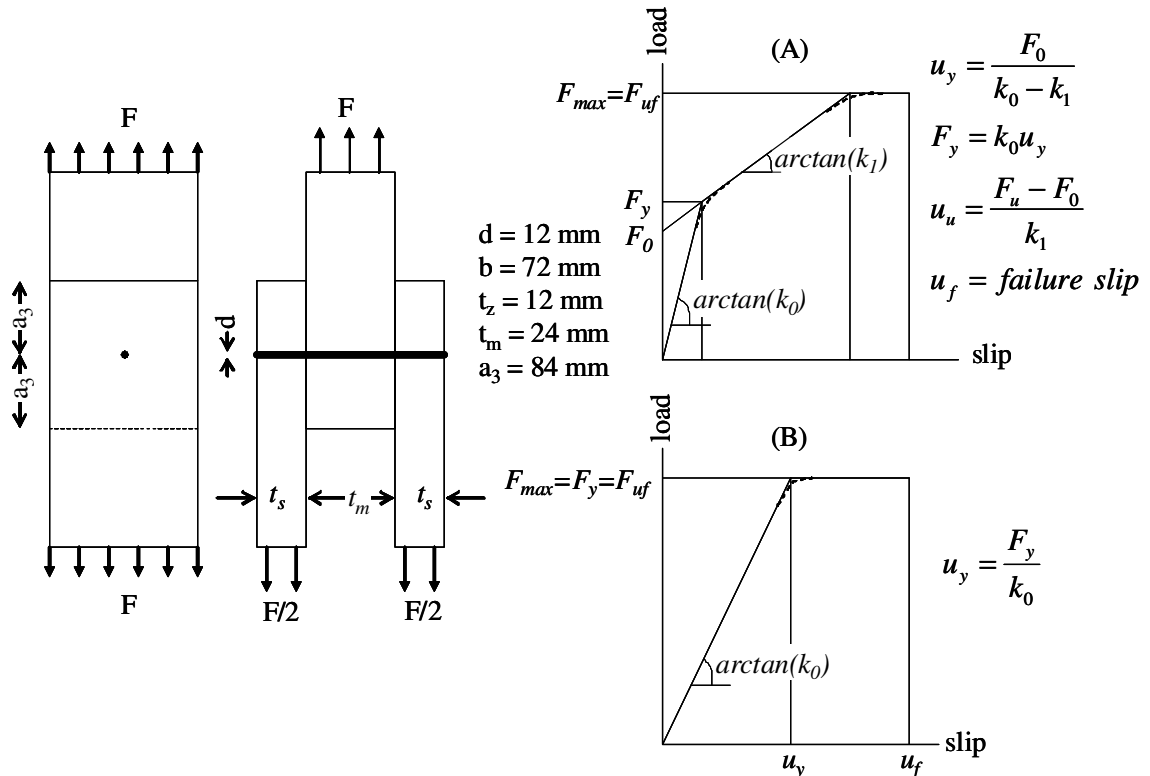


Figure 14: Single bolted (M12), loaded parallel to the grain, connections analysed

As a first investigation for identifying the most appropriate definition for “connection ductility”, at least for statically loaded structures, a data of parallel to the grain loaded single M12 bolted connections, shown in Figure 14, were analysed using equation (15) as an approximation of the experimental load-slip curve. Furthermore, equation (16) was used for determining the “yield” slip u_y and the “ultimate” slip u_u . All the data can be found in Jorissen [19]. Remark: equation (15) for u_u is, obviously, not valid for those connections showing load-slip behaviour type B (Figure 14).

Table 1: Evaluation of the load-slip curves for the single bolted connections shown in figure 14

	Ko [N/mm]	K1 [N/mm]	Fo [N]	u-y [mm]	F-y [N]	F-u [N]	u-u [mm]	u-f [mm]	F-f [N]	figure 14 (case)
D1110701	56215	626	5837	0,105	5902	8610	4,433	12	8610	(A)
D1110702	46742	1227	4283	0,094	4399	8560	3,485	6,747	8560	(A)
D1110703	31008	382	5419	0,177	5487	7290	4,896	6,251	7290	(A)
D1110704	54235	982	3948	0,074	4021	8580	4,719	12	8580	(A)
D1110705	32134	943	4045	0,130	4168	8120	4,320	12	8120	(A)
D1110707	45326	1041	3991	0,090	4085	7550	3,418	8,118	7550	(A)
D1110708	37922	576	4121	0,110	4185	7200	5,346	7,705	7200	(A)
D1110709	44709	747	3886	0,088	3952	7180	4,412	6,516	7180	(A)
D1110710	77619	945	4088	0,053	4138	7380	3,485	4,966	7380	(A)
D1110713	46938	441	5564	0,120	5617	7440	4,251	6,242	7440	(A)
D1110714	68423	647	4559	0,067	4603	6740	3,370	4,718	6740	(A)
D1110715	45869	880	4578	0,102	4668	7070	2,832	3,682	7070	(A)
D1110716	40068	644	4137	0,105	4205	6700	3,983	5,392	6700	(A)
D1110717	39447	802	5165	0,134	5272	7470	2,876	5,200	7470	(A)
D1110718	72626	957	4960	0,069	5026	7470	2,622	5,178	7470	(A)
D1110719	56339	571	5068	0,091	5120	6500	2,507	3,010	6500	(A)
D1110720	41395	871	4464	0,110	4560	7520	3,508	5,18	7520	(A)
D1110722	41325			0,166	6850			10,2	6850	(B)
D1110727	65629	2445	4492	0,071	4666	7570	1,259	3,932	7570	(A)
D1110728	65629	2445	4492	0,071	4666	7570	1,259	3,932	7570	(A)
D1110729	42283	1660	5121	0,126	5330	7240	1,276	3,81	7240	(A)
D1110732	14073			0,511	7190			4,181	7190	(B)
D1110733	14623		6960	0,476	6960			3,868	6960	(B)
D1110734	10951		9230	0,843	9230			7,885	9230	(B)
D1110735	11790		7660	0,650	7660			6,591	7660	(B)

The evaluation of the load-slip curves is shown in Table 1. The calculation of the ductility parameters according to equations (4) to (13) in Figure 12 is displayed in Table 2. The ductility definition according to equations (2) and (16) can only be considered for cyclic loading tests, and is consequently not relevant for the monotonic test results shown in Tables 1 and 2. It can be noted that only ductility definitions according to equations (4), (11) and (13) provide consistent results for all specimens tested

7 Conclusions

The purpose of this paper on ductility is to provide acceptable input for probabilistic robustness analyses. Therefore, the results must be consistent: the ductility parameter of obviously brittle connections (with low deformation capacity) should differ significantly from the ductility parameter of connections showing large deformations. From Table 2 it can be concluded that this is not the case for most ductility definitions. However, this conclusion might be premature since Tables 1 and 2 only refer to tests on single bolted connections loaded parallel to the grain. Many more test results should be analysed with respect to the ductility definitions before final conclusions can be drawn.

It is also pointed out that absolute ductility definitions rather than relative definitions such as the ductility ratio should be used in timber structures and connections.

Table 2: Evaluation of the ductility parameters (equations (4) to (14)) listed in Figure 12

(n.r. signifies not realistic)

	ductility definition (figure 12)										Figure 14 (case)
	Def. (4) $D_f [-]$	Def. (5) $D_u [-]$	Def. (6) $C_d [-]$	Def. (7) $D_{fu} [-]$	Def. (8) $D_{su} [-]$	Def. (9) $D_{st} [-]$	Def. (10) $D_{uv} [mm]$	Def. (11) $D_{fy} [mm]$	Def. (12) $D_{fu} [mm]$	Def. (13) $E_d [Nmm]$	
D1110701	114.3	42	0.991	2.707	0.470	1.272	4.328	11.895	7.6	96866	(A)
D1110702	71.7	37	0.986	1.936	0.972	1.882	3.391	6.653	3.3	50100	(A)
D1110703	35.3	28	0.972	1.277	0.341	0.435	4.719	6.074	1.4	40511	(A)
D1110704	161.9	64	0.994	2.543	1.152	2.930	4.645	11.926	7.3	91884	(A)
D1110705	92.5	33	0.989	2.778	0.978	2.716	4.190	11.870	7.7	88376	(A)
D1110707	90.1	38	0.989	2.375	0.871	2.069	3.328	8.028	4.7	55029	(A)
D1110708	69.8	48	0.986	1.441	0.736	1.060	5.235	7.595	2.4	47020	(A)
D1110709	73.7	50	0.986	1.477	0.834	1.231	4.324	6.428	2.1	39345	(A)
D1110710	93.1	65	0.989	1.425	0.795	1.134	3.431	4.913	1.5	30804	(A)
D1110713	52.2	36	0.981	1.468	0.334	0.490	4.132	6.122	2.0	42119	(A)
D1110714	70.1	50	0.986	1.400	0.474	0.663	3.303	4.651	1.3	27972	(A)
D1110715	36.2	28	0.972	1.300	0.534	0.694	2.730	3.580	0.9	22271	(A)
D1110716	51.4	38	0.981	1.354	0.610	0.825	3.878	5.287	1.4	30806	(A)
D1110717	38.9	22	0.974	1.808	0.437	0.791	2.742	5.066	2.3	35184	(A)
D1110718	74.8	38	0.987	1.975	0.499	0.986	2.553	5.109	2.6	35217	(A)
D1110719	33.1	28	0.970	1.201	0.280	0.336	2.416	2.919	0.5	17540	(A)
D1110720	47.0	32	0.979	1.477	0.670	0.990	3.398	5.070	1.7	33347	(A)
D1110722	61.5	n.r.	0.984	n.r.	n.r.	n.r.	n.r.	10.034	n.r.	69302	(B)
D1110727	55.3	18	0.982	3.123	0.660	2.060	1.188	3.861	2.7	27668	(A)
D1110728	55.3	18	0.982	3.123	0.660	2.060	1.188	3.861	2.7	27668	(A)
D1110729	30.2	10	0.967	2.985	0.398	1.187	1.150	3.684	2.5	25909	(A)
D1110732	8.2	n.r.	0.878	n.r.	n.r.	n.r.	n.r.	3.670	n.r.	28225	(B)
D1110733	8.1	n.r.	0.877	n.r.	n.r.	n.r.	n.r.	3.392	n.r.	25265	(B)
D1110734	9.4	n.r.	0.893	n.r.	n.r.	n.r.	n.r.	7.042	n.r.	68889	(B)
D1110735	10.1	n.r.	0.901	n.r.	n.r.	n.r.	n.r.	5.941	n.r.	47999	(B)
acceptable	yes	no	no	no	no	no	no	yes	no	yes	

8 Relevance for future code development

It should be noted that quantities related to deformation capacity are needed when, for example, plastic design is carried out, as well as for seismic design. Therefore it seems important, for future development in timber engineering, to provide criteria for classification of timber connections depending on their stiffness (rigid, semi-rigid, and pinned), strength (full- and partial-strength) and ductility (ductile and brittle).

A possible parameter to classify connections is the ratio between connection strength and strength of the connected member, as suggested in Eurocode 3 Part 1-8 [20] for steel connections. In fact, ductility can be fully exploited only if the connection is partial-strength, i.e. it can transmit a force (e.g. bending moment) smaller than the strength of the members connected. If this condition is not satisfied, then failure will occur on the member side rather than in the connection and will be inherently brittle. It should be also noted that timber connections are usually regarded as pinned connections in design. However, many are semi-rigid. Only a few connection types, e.g. the connections realised with expanded tubes, are rigid (and ductile), see Figure 7.

9 Acknowledgments

The authors wish to extend their gratitude to Prof. I. Smith, Prof. H. Kreuzinger, Dr. R. Steiger, and Dr. J. Branco for the useful comments provided for this paper.

The facilitating network provided by the COST Action E55 ‘Modelling of the performance of timber structures’ (<http://www.cost-e55.ethz.ch/>) is also gratefully acknowledged.

Literature references

- [1] A. Aziz and I. Smith (2005). New generation of timber design practices and code provisions linking system and connection design. In Proceedings of CIB-W18/38-102-1, Karlsruhe, Germany.
- [2] Poul Henning Kirkegaard (2009). Robustness assessment of timber structures with ductile behaviour. COST E55 meeting, Trondheim, Norway.
- [3] Ian Smith and Andi Asiz (2010). Transition from design of timber components to design of systems. Presented at the IABSE-fib conference in Cavtat (Dubrovnik).
- [4] EN 1995-1-1 (2004). Eurocode 5— Design of timber structures—Part 1-1: General – Common rules and rules for buildings. Comité Européen de Normalisation, Brussels, Belgium.
- [5] SIA 265 (2003). Swiss Code for Timber Structures. Published by Swiss Society of Engineers and Architects, PO Box, CH-8027 Zürich.
- [6] EN 12512 (2001). European Standard. Timber structures. Test methods. Cyclic testing of joints made with mechanical fasteners. Comité Européen de Normalisation, Brussels, Belgium.
- [7] Italian Ministry for the Infrastructures (2009). Commentary to the new technical regulation for construction. Circular 2 February 2009 No. 617 CSLLPP, Rome, Italy.
- [8] A. Buchanan (1984). Combined bending and axial loading in lumber. In: ASCE Journal of Structural Engineering, 112(12), 2592-2609.
- [9] R. Steiger and M. Fontana (2005). Bending moments and axial force interacting on solid timber beams. RILEM Materials and Structures, 38, 507-513, 2005.
- [10] H.J. Blass (1991). Design of columns. In: Proceedings of the 1991 International Timber Engineering Conference, London, U.K. Vol. 1, 1.75-1.81.
- [11] NEN 6760 (2005). Design of Timber Structures. Published by NEN, P.O. Box 5059, 2600 GB, Delft, the Netherlands.
- [12] EN 1998-1 (2003). Eurocode 8: Design of structures for earthquake resistance - Part 1: General rules, seismic actions and rules for buildings. CEN, Brussels, Belgium.
- [13] M.J.N. Priestley (2000). Performance based seismic design. In: Proceedings of the 2th European Conference on Earthquake Engineering, Auckland.
- [14] P. Fajfar (1999). Capacity spectrum method based on inelastic demand spectra. In: Earthquake Engineering and Structural Dynamics, 28:979–993.
- [15] Federal Emergency Management Agency (2009). NEHRP Recommended Seismic Provisions for New Buildings and Other Structures. 2009 Edition. Washington, DC, USA.
- [16] Ario Ceccotti and Carmen Sandhaas (2010). A proposal for a standard procedure to establish the seismic behaviour factor q of timber buildings. In: Proceedings of the 10th World Conference on Timber Engineering, WCTE 2010, Riva del Garda, Italy.
- [17] L. Stehn and A. Björnfot (2002). Comparison of different ductility measurements for a nailed steel-to-timber connection. In: Proceedings of the 7th World Conference on Timber Engineering, WCTE 2002, Shah Alam, Malaysia.
- [18] W. Muñoz, M. Mohammad, A. Salenikovich and P. Quenneville (2008). Need for a harmonized approach for calculations of ductility of timber assemblies. In: Proceedings of CIB-W18/41-15-1, St. Andrews, Canada.
- [19] André Jorissen (1998). Double shear timber connections with dowel-type fasteners. Ph.D. Thesis, Delft University of Technology, ISBN 90-407-1783-4, The Netherlands.
- [20] EN 1993-1-8 (2003). Eurocode 3 - Design of steel structures - Part 1-8: Design of joints. Comité Européen de Normalisation, Brussels, Belgium.

**INTERNATIONAL COUNCIL FOR RESEARCH AND INNOVATION
IN BUILDING AND CONSTRUCTION**

WORKING COMMISSION W18 - TIMBER STRUCTURES

**DESIGN OF MECHANICALLY JOINTED CONCRETE-TIMBER BEAMS TAKING
INTO ACCOUNT THE PLASTIC BEHAVIOUR OF THE FASTENERS**

H J Larsen
DENMARK

H Riberholt
H. Riberholt ApS
DENMARK

A Ceccotti
Ivalsa, Trees and Timber Institute
San Michele al Adige
ITALY

**MEETING FORTY THREE
NELSON
NEW ZEALAND
AUGUST 2010**

Presented by H Larsen

H Blass: Discrepancy between interpretations of some of the behaviour of some connectors. H Larsen: Will be reviewed.

B Walford: Not a good idea to have plastic behaviour of connector for bridges. H Larsen: this is a suggestion for the design, not the actual behaviour.

Design of mechanically jointed concrete-timber beams taking into account the plastic behaviour of the fasteners

H. J. LARSEN

Hans Jørgen Larsen

Denmark

H. RIBERHOLT

H. Riberholt ApS

Denmark

A. CECCOTTI

Ivalsa, Trees and Timber Institute

San Michele al Adige

Italy

1 Introduction

Mechanically jointed built-up members were used to some extent until about 1950 but were then completely replaced by glued members, e.g. glulam and light I-beams with webs of panel materials. Mechanically jointed beams with traditional nail and screw connections have the disadvantage that the slip between the lamellas shall be rather big in order to achieve a composite effect and this typically results in large deflections.

The reason why there is still interest in the topic in CIB W18 is that the same theory applies to composite T-members with wooden web and concrete flange, both in new structures (e.g. bridges) and especially in old buildings where a new concrete slab on top of existing beams can ensure an upgrading of strength, vibration characteristics and sound insulation.

The calculation of the internal forces and moments is generally made assuming elastic behaviour either by the method laid down in Eurocode 5 (beam theory) or by more advanced design methods, e.g. Finite element methods. When the internal forces and moments are determined it is tacitly assumed that the load-carrying may be found by using the usual elastic failure criteria for the individual members. It is shown in this paper that this assumption is in most cases very much on the safe side for the calculation of the shear load-carrying capacity and that a much better estimate may be found by taking into account the plastic properties of most fasteners. A further advantage by the proposed design method is that it can be used to optimise the fastener pattern

This paper will describe the theory and verify it by comparing reported test results to the results from calculations. The requirements for using the method, e.g. fastener stiffness and deformation capacity will be determined.

At the end a proposal for changes in Eurocode 5 is given.

2 Theory

The theory is based on the assumptions that the lamellas are linear-elastic and the fasteners linear-elastic/ideal-plastic. The expressions are derived in Annex A.

3 Tests

3.1 Reported tests

The tests reported in [2], [3], [4], [5], [8], [9] and [10] are briefly described and evaluated.

All tests to failure were made on simply supported beams loaded in the third or quarter points. The verifications have been made with mean material properties. Where these are not reported they are assumed to correspond to characteristic values multiplied by 1,4. In many cases, the basic parameters e.g. timber strength and stiffness, and slip moduli are not well documented, and it has been necessary to estimate them from the general information in the papers. Luckily, the estimates of the shear load-carrying capacity of the composite members, that is the topic of this paper, are rather insensitive to variations in the parameters. Comparisons of the calculated and measured deflections show that the assumed wood and fastener stiffnesses are reasonable.

3.2 Test results

The test results are summarised in Table 1.

3.3 Ceccotti et al, [1]

The test beam is shown in Figure 1 where also the fastener load-slip curve is shown.

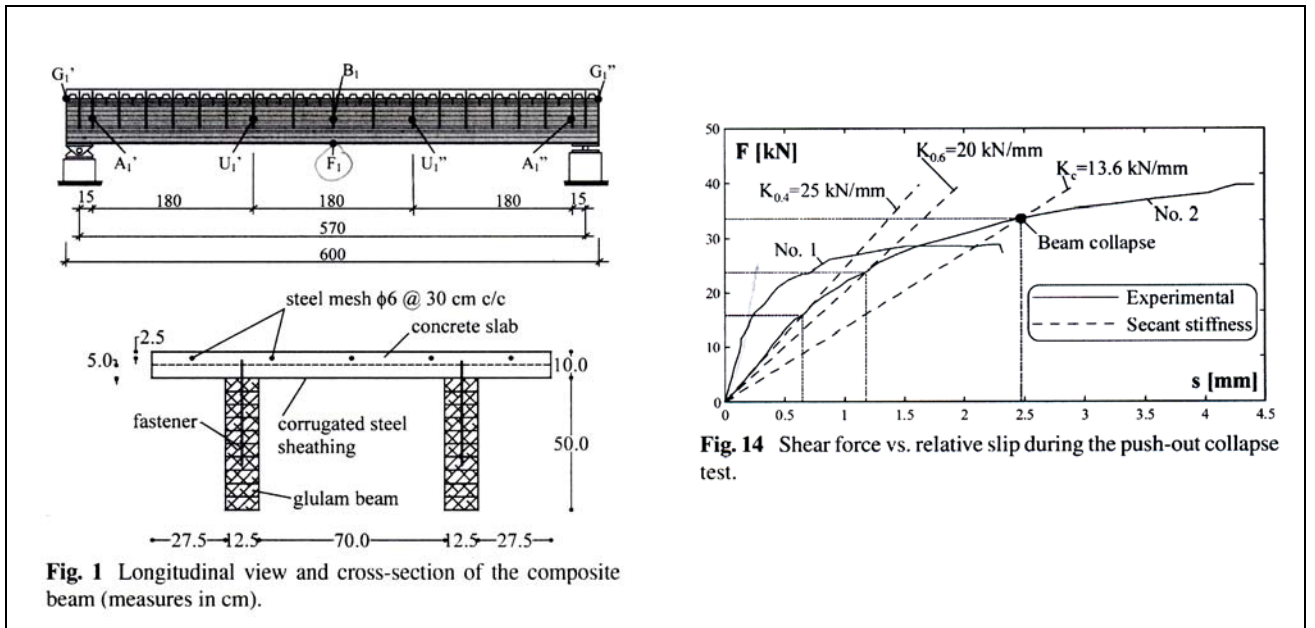


Figure 1. Test beam.

Collapse (failure) occurred under a load of $F_{ult, test} = 125 \text{ kN}$ due to bending/tensile failure in the outermost lamination corresponding to a calculated elastic stress of $23,6 \text{ N/mm}^2$ which is a “surprisingly low value closer to the characteristic bending strength of GL 24 than to the expected mean strength of $29,9 \text{ N/mm}^2$. This may be explained by a weak section caused by a knot or a finger joint”.

The theoretical elastic failure mode was, however shear caused by failure in the fasteners for a load of only 34 kN . Assuming plastic behaviour of the 8 closely spaced fasteners between the support and the load, the theoretical shear failure load is 133 kN , a much better estimate.

The calculated slip at the 8 fasteners at failure is in the range $3,6 \text{ mm}$ to $4,9 \text{ mm}$ to be compared to a slip of less than 3 mm to ensure yield

3.4 Grantham et al, [3]

An existing floor area (A1) was converted to a timber-concrete composite floor that was tested to failure. The connectors were SFS $75 \times 100 \text{ mm}$ connectors (see Figure 8) with spacing and inclinations as shown in Figure 2.

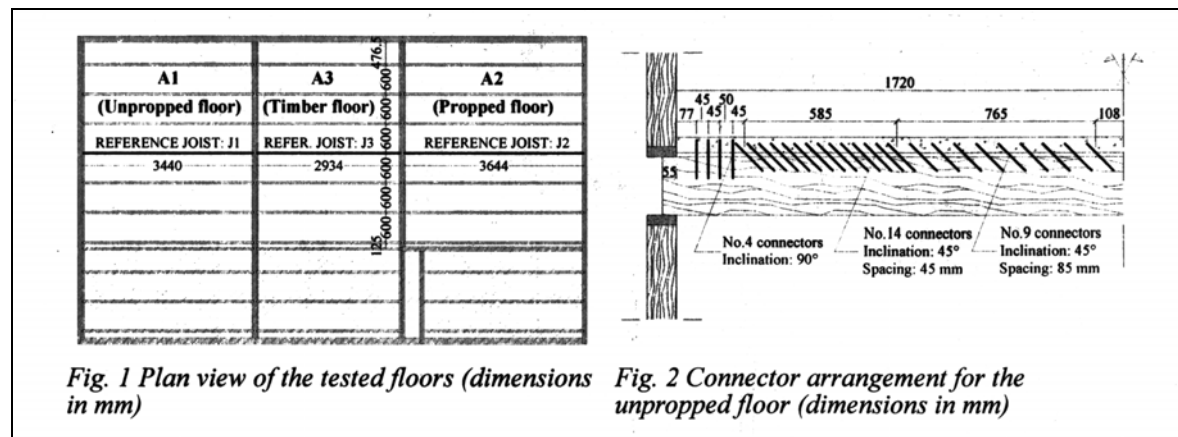


Figure 2. Test beams.

The observed failure mode is bending failure in the web, and the elastic theory correctly predicts the strength: 18 kN . The problem is however that the same theory predicts a shear failure for a much smaller load: 6 kN . The plastic theory predicts a value of 21 kN .

3.5 Godycki et al, [4]

The Test beams are shown in Figure 3. Two types of fasteners were investigated. Type A: Smooth $4,5$ or $5,5 \text{ mm}$ nails together with concrete cast into cut-outs in the beam. Type B: Nails alone .

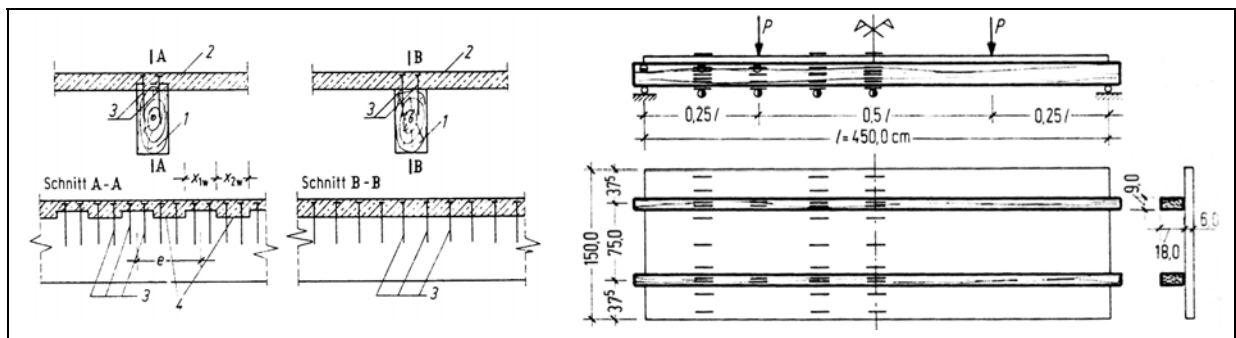


Figure 3. Test beams.

The fastener type A is so stiff that only an elastic analysis is appropriate. Theoretically the bending load-carrying capacity in bending is 38 kN and 30 kN in shear. The test value is 33 kN. The failure mode is not reported.

For beams with type B fasteners the general trend is that the theoretical elastic load carrying capacity in bending is about 30 % higher than the test values, but the predicted elastic shear capacity is only about 25 % of the test values. The theoretical load-carrying capacity assuming plastic behaviour behaviour is between 3 % and 30 %, on average 16 %, higher than the test values. The calculated slip of the fasteners is just sufficient to ensure plasticity.

3.6 Kenel and Meierhofer, [5]

The cross-section of the beams is shown in Figure 4.

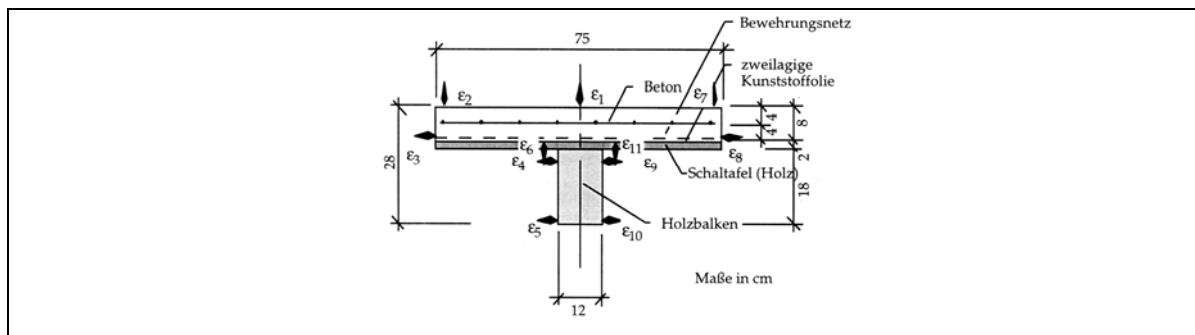


Figure 4. Cross-section. Measurements in mm. The beam is composed of timber beams (Holzbalken) and a concrete slab (Beton) with a reinforcement net (Bewehrungsnetz).

The fasteners were SFS VB-48-7,5x100 mm, see figure 7. Three configurations were investigated, see Figure 5. The strength and stiffness of the fasteners were determined by shear tests. An example of the fasteners used in beams B5 is also shown in Figure 5. The load is for 2 x 4 sets of fasteners.

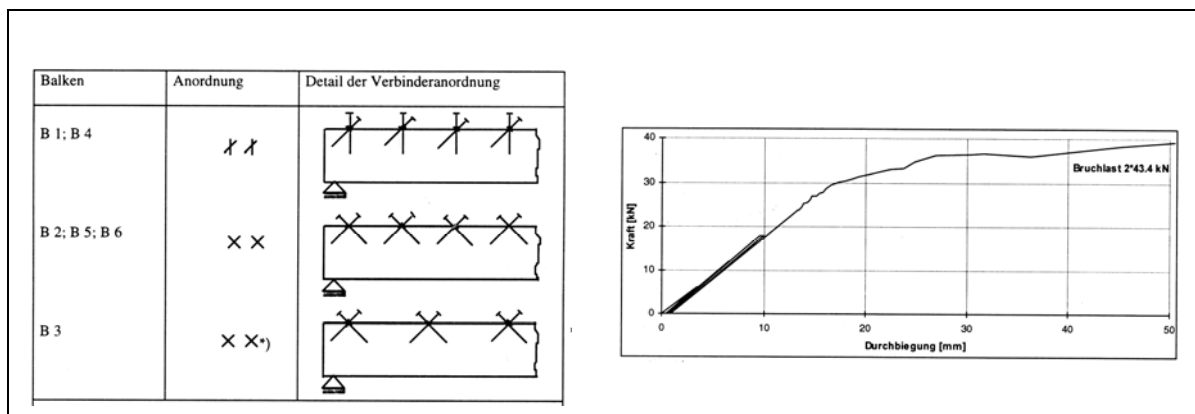


Figure 5: Left: Fastener configuration. Right: Typical load-deflection curve.

Balken = beams. Anordnung = configuration. Bruchlast = failure load. Kraft = load. Durchbiegung = deflection-

In the main test series six beams denoted B1-B6 were short-term tested. The test results for three typical beams (B3, B4 and B5) are shown in Table 1.

The theoretical strength values in bending are 40-90 % higher than found by testing while the theoretical elastic shear strength values are only 65-75 % of the test values. The ratios between the theoretical plastic shear values and the test values are: 1,26 – 0,93 – 1,00.

3.7 Van der Linden, [8]

The test beams are shown in Figure 6. The wood is glulam spruce GL36 with a measured mean bending strength of about $f_{m,mean} = 45 \text{ N/mm}^2$ and a mean modulus of elasticity of $E = 14.000 \text{ N/mm}^2$

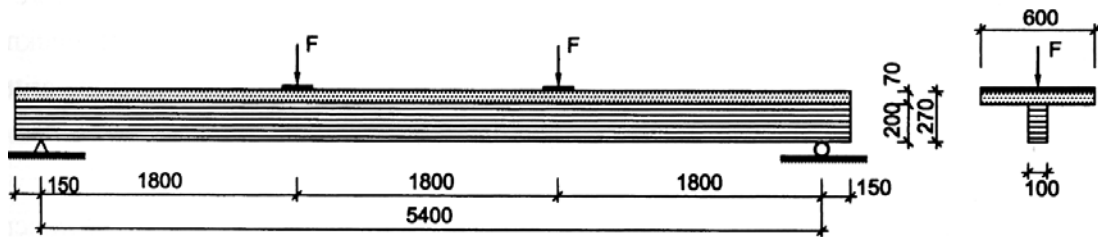


Figure 6 Test beams. Measurements in mm.

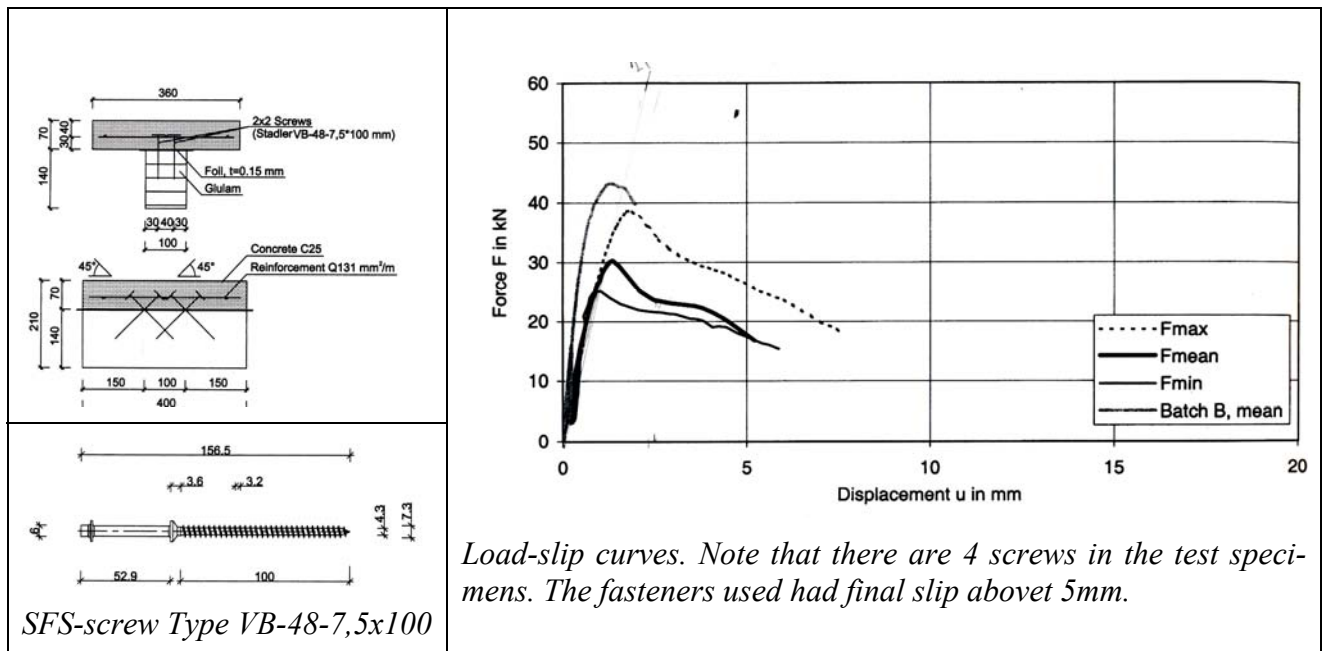


Figure 7. Fasteners type 1, inclined SFS-screws.

Three types of fasteners were investigated, see Figure 7 - 9. Type 1 is inclined (45°) SFS Timber-concrete screws VB-48-7,5x100. Type 2 is punched metal plates bent at an angle of 90°, where one part is pressed into the timber member, the other part embedded in con-

crete. Type 3 is a combination of a concrete notch with diameter 70 mm and a 20 mm reinforcement bar pressed into tight-fitting holes.

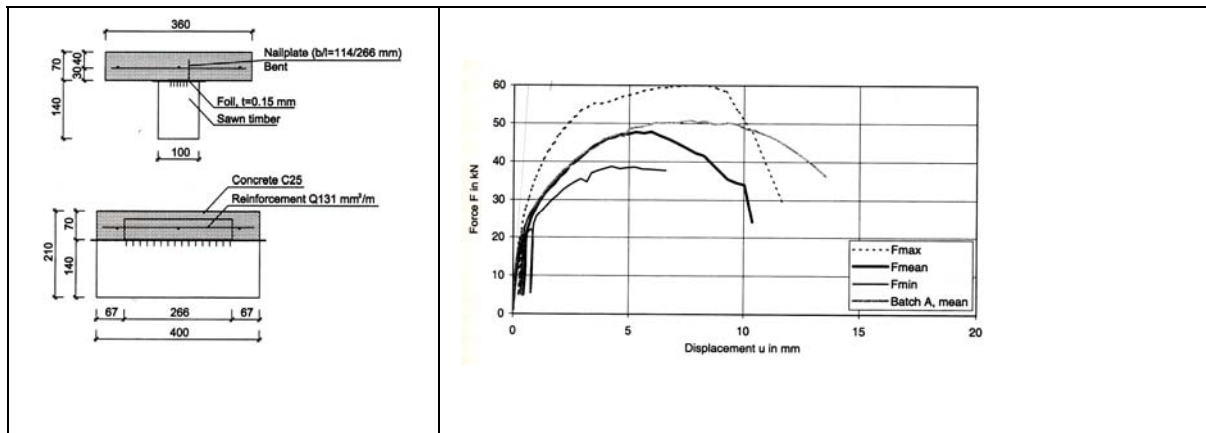
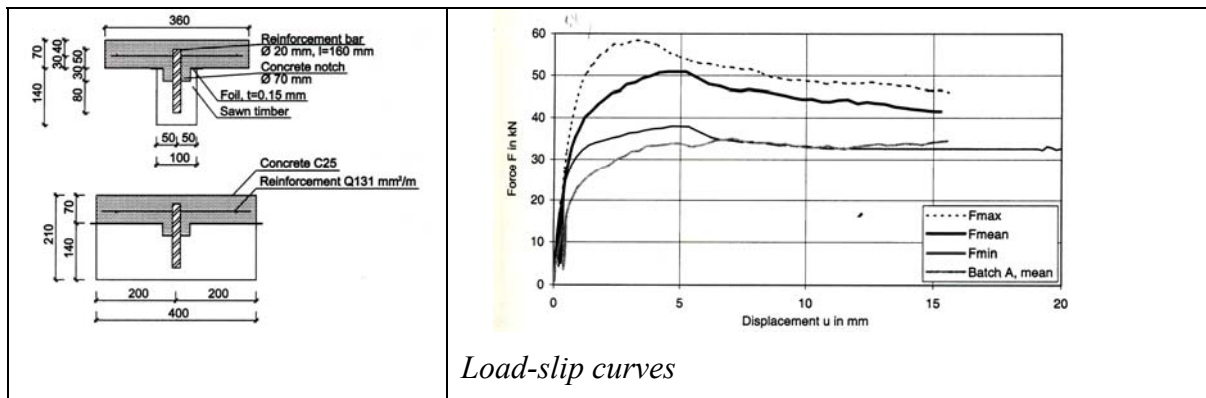


Figure 8. Fasteners type 2, bent punched metal plates.



Load-slip curves

Figure 9. Fasteners type 3, reinforcement bar in concrete notch.

SFS screws: The theoretical bending failure load corresponding to the timber bending strength is 33 kN. This load was, however not reached. At 14-15 kN, a gap occurred between the beam and the concrete plate. With increasing load, this gap moved midspan and widened near the support. Some of the fasteners became plastic. The beam failed in shear at 23 kN. The theoretical shear failure loads are 16 kN (elastic) and 27 kN (3 effective plastic fasteners). The calculated slip was about 2 mm which is sufficient to cause yield.

Nailplate fastener: The calculated bending failure load was 26 kN. Failure took place at 13-31 kN. The lowest value was caused by a badly glued finger joint. Plastic behaviour of the fasteners was observed in the strongest beams at 30-35 kN. The theoretical shear failure loads were 20 kN (elastic) and 31 kN (3 effective plastic fasteners). The calculated slip was about 4 mm which is sufficient to cause yield.

Reinforcement bar with concrete notches: The calculated bending failure load was 39 kN, which was never reached. Shear failure took place at 27-37 kN. Plastic behaviour of the fasteners was observed at 30-35 kN. The theoretical shear failure loads were 20 kN (elastic) and 31 kN (3 effective plastic fasteners). The calculated slip was about 6 mm which is sufficient to cause yield. It is surprising that this fastener type had so good ductile properties. The explanation may be that the system acts as a reinforced concrete cantilever.

3.8 Luciano Nunes Magalhaes, [9]

The test beams are shown in Figure 10.

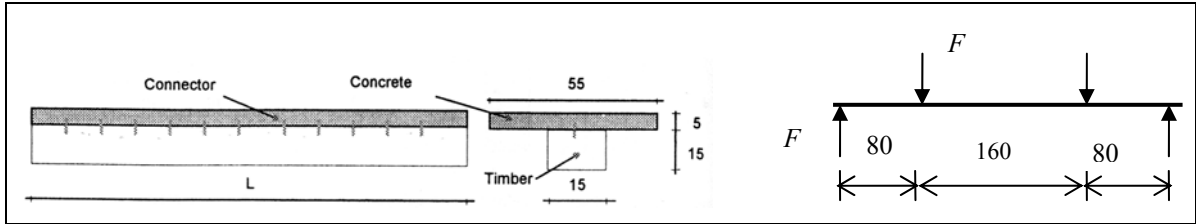


Figure 10. Cross-section and test configuration. Measurements in cm.

The wood is a tropical hardwood Paraju-Masaranduba with density greater than 1000 kg/m³ and correspondingly high strength and stiffness, tensile strength $f_{t,mean} = 183 \text{ N/mm}^2$, $f_{c,mean} = 85 \text{ N/mm}^2$ and $E_{mean} = 21500 \text{ N/mm}^2$. The following estimated bending strength is used $f_{m,mean} = 100 \text{ N/mm}^2$.

The fasteners are 3.6 mm round nails. They are so stiff that only an elastic analysis is appropriate. The calculated load-carrying capacity in bending is 150 kN and 20 kN in shear. The test value is 15 kN. The failure of beams happened in two steps. First the connectors broke – as predicted – then the timber failed in shear.

3.9 Yeoh et al, [10]

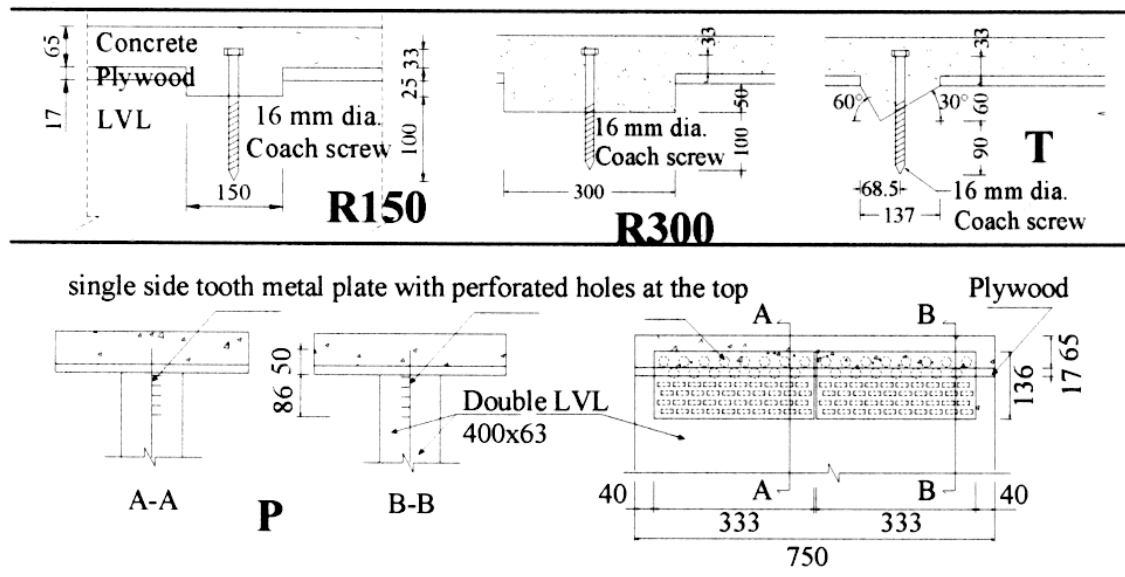


Figure 11. Fasteners.

Four types of fasteners were used, see Figure 11. Type R150, R300 and T are coach screws combined with concrete notches, and they are so stiff that they are not relevant for an plastic analysis. Type P are nail-plates pressed between two LVL beams. The cross-section is shown to the left in Figure 12.

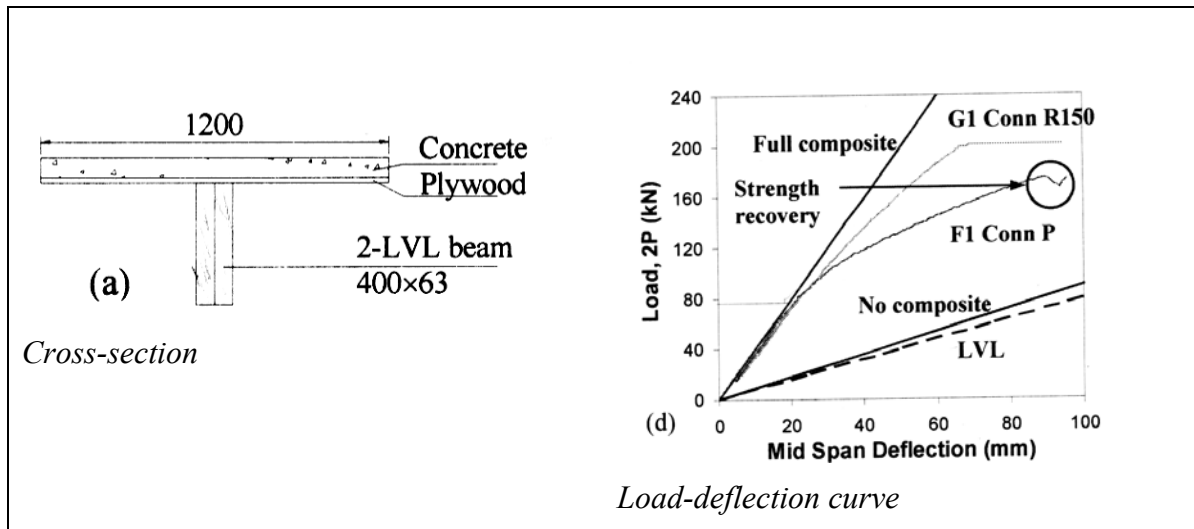


Figure 12. Cross-section and load-deflection curve.

The load-deflection curves are shown to the right in Figure 13. Note the initial failure of F1 followed by a recovery. The test was not continued to complete destruction, and the load at initial failure is taken as the failure load.

The estimated elastic bending strength was 115 kN. The estimated elastic shear strength was 29 kN. The load at initial failure was 87 kN. The estimated plastic shear failure load was 72 kN assuming that 4 of the 5 fasteners are effective. There is not sufficient information to estimate whether the fasteners have sufficient plastic slip capacity,

3.10 Conclusions

There is good agreement between the measured and the elastic deformations calculated according to the linear-elastic method given in Eurocode 5, Annex B.

For stiff, brittle fasteners, there is good agreement between the load-carrying capacity found by testing and the smaller of the bending strength and the fastener shear capacity calculated according to Eurocode 5, Annex B.

For fasteners with plastic properties the predicted load-carrying capacity

- is smaller than the load found by an elastic calculation according to Eurocode 5, Annex B assuming that failure takes place when the stress in the bottom of the web exceeds the bending strength;
- is greater (normally much greater) than found by an elastic calculation according to Eurocode 5 assuming that failure takes place when the shearing force per fastener between the timber web and the concrete web exceeds the fastener shear strength;
- corresponds to the load-carrying capacity calculated by the method described in section 4 assuming that the behaviour of the fasteners is elasto-plastic. The slip at the fasteners shall be checked and shall correspond to the plastic part of the load-slip curve.

4 Eurocode 5-proposal

(1) The cross-section is shown in Figure 13.

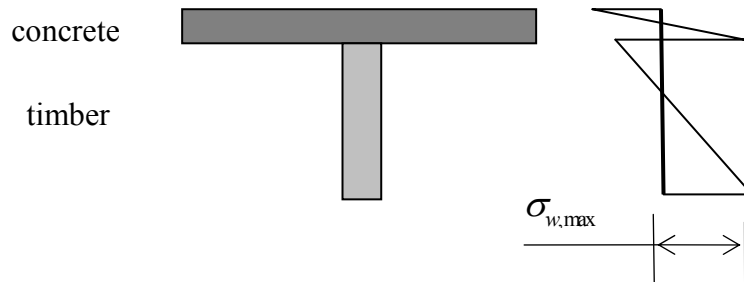


Figure 13. Composite concrete-wood T-cross-section.

(2) For sufficiently ductile fasteners (i.e. fasteners fulfilling (1)) the load-carrying capacity shall be taken as the smaller of

- The load-carrying capacity found by an elastic calculation according to Eurocode 5, Annex B assuming that failure takes place when the stress in the bottom of the web exceeds the bending strength
- The load-carrying capacity found by assuming plastic behaviour in the fasteners assuming that failure takes place when the shearing force per fastener between the timber web and the concrete flange exceeds the fastener shear strength

Only the fasteners for which the slip u_s fulfils the conditions

$$u_y \leq u_s \leq u_u \quad (1)$$

shall be taken into account. u_y is the slip at yielding and u_u is the slip at failure.

(3) If (1) is not fulfilled the load-carrying capacity should be taken as the smaller of

- The load-carrying capacity found by an elastic calculation according to Eurocode 5, Annex B assuming that failure takes place when the stress in the bottom of the web exceeds the tensile strength:
- The load carrying capacity found by an elastic calculation according to Eurocode 5 assuming that failure takes place when the shearing force per fastener between the timber web and the concrete flange exceeds the fastener shear strength.

(4) The concrete grade shall as a minimum have a cube strength of $f_{ck} = 16 \text{ N/mm}^2$ with at least 0,2 % reinforcement.

5 References

- 1 Ceccotti, A, 1995. Timber concrete structures, Timber Engineering, STEP 2, Centrum Hout, The Netherlands.
- 2 Cecotti, A, Fragiaco, M and Giordano, S, 2006. Long-term and collapse tests on a timber-concrete composite beam with glued-in connection. *Materials and Structures* 40.
- 3 Grantham, R, Enjily, V, Fragiaco, M, Nogarol, C, Zidaric, I and Amadio, C, 2004. Potential upgrade of timber frame buildings in the UK using timber-concrete composites. *Proceedings of the World Conference of Timber Engineering*, Lahti.
- 4 Godycki, T, Pawlica, J and Kleszewski, J, 1984. Verbunddecke aus Holzrippen und Betonplatte. *Bauingenieur* 39.
- 5 Kenel, A and Meierhofer, U, 1998. Long-term performance of timber-concrete composite structural elements. Report No. 115/39, EMPA, Abteilung Holz, Dübendorf.
- 6 Larsen, H J, 1974. The design of built-up timber columns, CIB W18 Paper 3-2-1.
- 7 Larsen, H J and Riberholt, H, 2005. Trækonstruktioner, Beregning. SBI-Direction 210. Danish Building Research Institute, Copenhagen.
- 8 van der Linden, M L R, 1999. Timber concrete composite floor systems, Diss. Technical University, Delft.
- 9 Magalhães, N M, Souza, Á J and Chahud, E, *Proceedings of the 5 th World Conference on Timber Engineering*, Montreux, Switzerland.
- 10 Yeoh, D, Fragiaco, M, Buchanan, A and Deam, B, 2010. Experimental performance of LVL-concrete composite floor beams. *World Conference on Timber Engineering*, Riva del Garda, Italy.

Table 1. Summary of tested beams and test results

1			2	3	4	5	6	7	8	9	10	11
Paper			Wood		Fastener		Deflection u for 10 kN		Calculated $R_{ult,calc}$			
			f	E_2	R_{ult}	$K_{in,yield}$	calc	test	bending	elastic. shear	plastic shear	test
			N/mm ²		kN	N/mm	mm		kN			kN
2	Ceccotti et al		33	10.000	34.000	20.000	4 ¹⁾	5 ¹⁾	124	34	133	125
3	Grantham et al		22	8.000	13.000	10.000	2	2	18	6	21	18
4	Godycki et al	B-4,5/6/4	34	12.500	2.050	8000	9	10	38	9	37	30
		B-4,5/4/2	34	12.500	2.050	5300	10	12	37	7	31	30
		B -4,5/2/2	34	12.500	2.050	2700	15	22	33	6	29	25
		B -5,5/6/4P	34	12.500	2.750	12000	9	11	39	12	39	30
		B-5,5/4/2	34	12.500	2.750	8000	10	12	38	6	31	28
		B-5,5/2/2P	34	12.500	2.750	4000	13	14	34	5	29	25
		A-4,5/6/4	34	12.500	59.000	320.000	9	10	38	30	30	33
5	Kenel & Meierhofer	B3	31	13.400	9.000	6.500	7	10	59	22	39	31
		B4	31	13.400	5.100	3.000	7	10	57	27	38	41
		B5	31	13.400	9.000	6.500	6	6	67	32	43	43
8	Van der Linden	Screws	45	14.040	15.000	9.300	20	21	33	16	27	23
		Nail plate	42	12.320	47.000	7.600	15	10-20	26	20	31	32
		Bars	45	13.430	33.000	10.300	12	10-20	39	20	31	33
9	Magalhães		100	21.500	45.000	12.000	3	3	147	20	-	15
10	Yeoh et al	Nail plate	40	11.300	85.000	116.000	5	5	115	29	72	87

Annex A

Theory

A.1 General theory

The theory is described for a symmetric, simply supported beam with T-cross-section, see Figure A.1 and A.2. Expressions for general cross-sections may be found in [6]. The expressions may also be found in [8].

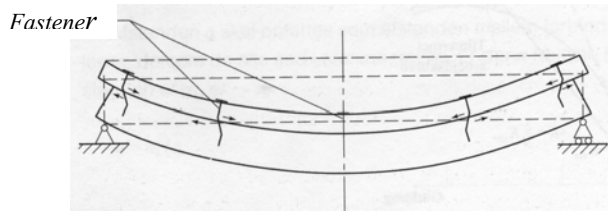


Figure A.1. Simply supported composite (built-up) beam).

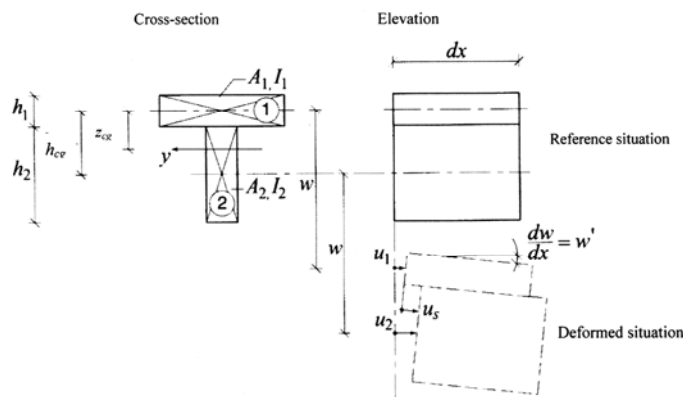


Figure A.2. T-cross-section.

It is assumed that the lamellas are linear elastic. The lamination areas are A_1 and A_2 . The second moments of area (moments of inertia) about their own centres of gravity are I_1 and I_2 . If the moduli of elasticity are different, the theory applies if E_1 is taken as reference and the following geometrical values are used:

$$A_1, \frac{E_2}{E_1} A_2, I_1 \text{ and } \frac{E_2}{E_1} I_2.$$

To transfer load between the lamellas there must be a slip in the joint, increasing from zero in the middle (due to symmetry) to a maximum value at the ends. The theory will be set up both for fasteners having a linear-elastic load-slip curve and for fasteners having an linear-elastic/ideal-plastic behaviour.

The centre of gravity is placed at

$$z_{cg} = h_{cg} \frac{A_2}{A_1 + A_2} \quad (\text{A.1})$$

The total geometrical moment of inertia is

$$I = I_1 + I_2 + A_1 z_{cg}^2 + A_2 (h_{cg} - z_{cg})^2 = I_0 + h_{cg}^2 A_r \quad (\text{A.2})$$

where

$$I_0 = I_1 + I_2 = B^2 I \quad (\text{A.3})$$

$$A_r = \frac{A_1 A_2}{A_1 + A_2} \quad (\text{A.4})$$

The deformation of the beam is described by the three translations u_1 , u_2 and w where

u_1 translation in the beam direction of the centre of gravity of lamella number 1

u_2 translation in the beam direction of the centre of gravity of lamella number 2

w translation perpendicular to the beam axis (the same for both lamellas).

The strains are ('= differentiation with regard to x):

$$\varepsilon_1 = u_1' \quad \text{and} \quad \varepsilon_2 = u_2' \quad (\text{A.5})$$

The curvature is

$$\kappa = -w'' \quad (\text{A.6})$$

For small values of w''

$$u_s = u_2 - u_1 + h_{cg} w' \quad (\text{A.7})$$

or by differentiation

$$u_s' = u_2' - u_1' + h_{cg} w'' \quad (\text{A.8})$$

u_s is the slip in the joint between lamella 1 and 2 taken positive as shown in Figure A.3.

For elastic materials

$$N_1 = EA_1 u_1' \quad \text{and} \quad N_2 = EA_2 u_2' \quad (\text{A.9})$$

$$M_1 = -EI_1 w'' \quad \text{and} \quad M_2 = -EI_2 w'' \quad (\text{A.10})$$

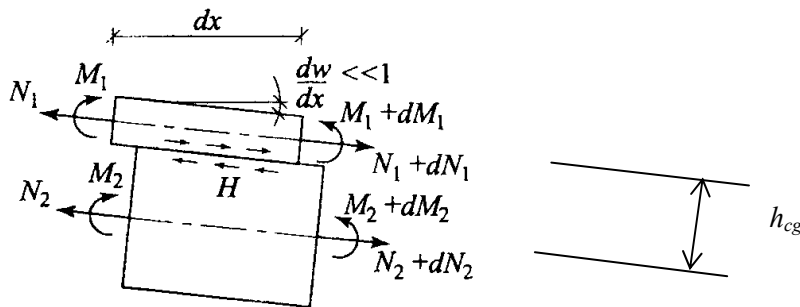


Figure A.3. Forces and moments in the deformed situation.

Since there is no external axial force, equilibrium leads to:

$$0 = N = N_1 + N_2 = EA_1 u_1' + EA_2 u_2' \quad (A.11)$$

$$u_2' = -\frac{A_1}{A_2} u_1' \quad (A.11)$$

Moment equilibrium for the total cross-section:

$$M = M_1 + M_2 - h_{cg} N_1 = -E(I_1 + I_2) w'' - h_{cg} EA_1 u_1' = EI_0 w'' - h_{cg} EA_1 u_1' \quad (A.12)$$

Equilibrium for Lamella 1:

$$H dx + N_1 + dN_1 - N_1 = 0 \quad H = -N_1' \quad (A.13)$$

H is the shearing force per unit length.

Elastic behaviour of fasteners

With a fastener spacing of a , the load on one fastener is Ha and with a fastener stiffness

$$K: Ha = Ku_s \quad H = \frac{K}{a} u_s \quad (A.14)$$

Inserting (14) and (10) differentiated in (13) gives

$$u_1'' = -\frac{K}{aEA_1} u_s \quad (A.15)$$

The following equation is found.

$$w'''' - \left(\frac{\gamma}{B}\right)^2 w'' - \frac{1}{EI_0} (q + M\gamma^2) = 0 \quad (A.16)$$

with

$$\gamma^2 = \frac{K}{EA_r a} \quad (A.17)$$

For a simply supported beam with sinusoidal load

$$w(x) = \frac{M_0}{EI} \left(\frac{l}{\pi}\right)^2 \frac{1 + \left(\frac{\pi}{l\gamma}\right)^2}{1 + B^2 \left(\frac{\pi}{l\gamma}\right)^2} \cos \frac{\pi x}{l} = \frac{1 + \mu}{1 + B^2 \mu} w_0(x) \quad (A.18)$$

where

$$\mu = \left(\frac{\pi}{l\gamma}\right)^2 = \frac{\pi^2 EA_r a}{l^2 K} \quad (A.20)$$

$$\frac{w}{w_0} = \frac{w'}{w'_0} = \frac{w''}{w''_0} = \frac{w'''}{w'''_0} = \frac{1 + \mu}{1 + B^2 \mu} \quad (A.21)$$

The effective moment of inertia is defined as

$$I_{ef} = I \frac{1+B^2\mu}{1+\mu} = I_0 + (I - I_0) \frac{1}{1+\mu} \quad (22)$$

By using the effective moment of inertia, the deflections may be found by the usual methods from the theory of elasticity.

Plastic behaviour of fasteners

It is assumed that the load-slip curve is stiff-elastic/plastic. For structural reasons fasteners are in practice placed over the full beam length, however with a concentration at the length βl near the ends where the slip is biggest. The fasteners over the rest of the beam length are on the safe side disregarded. The derivation is given in [7].

It is assumed that the fastener spacing over the length βl is constant and that the slip at least corresponds to the yield slip u_y , i.e the load per fastener is R_y . The shearing force per unit length is $H_y = R_y/a$ where a is the spacing.

Examples

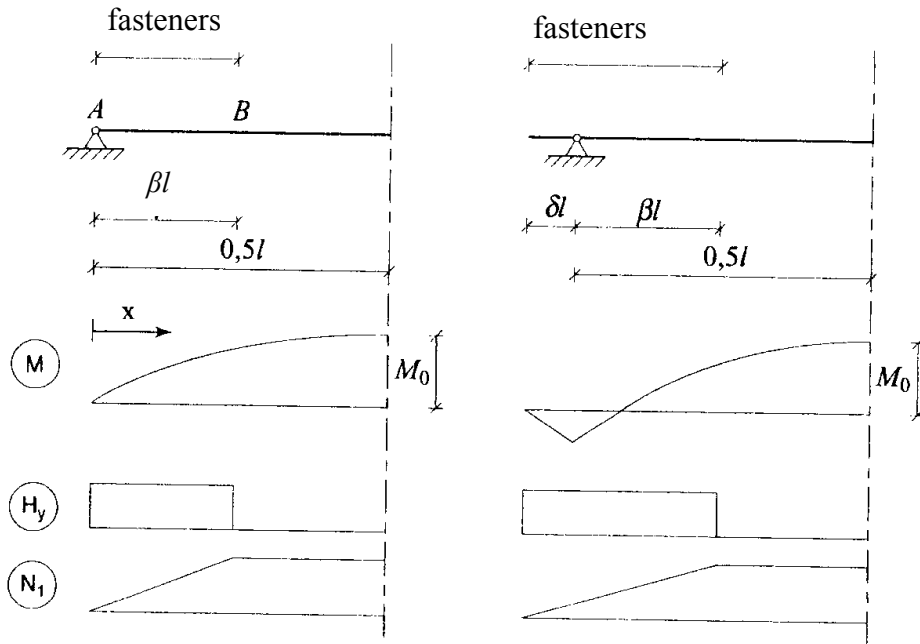


Figure A.4. Simply supported beam with constant uniformly distributed load and plastic fastener over the length βl (left) or $(\delta l + \beta l)$ (right).

A simply supported beams with uniformly distributed load built up of two members jointed by elastic-plastic fasteners with spacing a and yield load R_y is regarded.

No cantilever, $\delta l = 0$

See Figure A.4 left.

$$0 \leq x \leq \beta l \quad N_1 = -\frac{x}{a} R_y \quad (A.23)$$

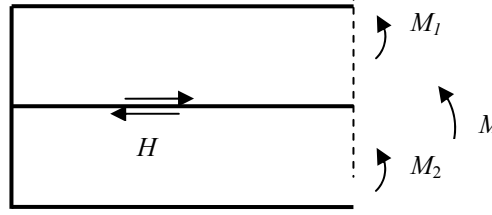
$$\beta l \leq x \leq 0,5l \quad N_1 = -\frac{\beta l}{a} R_y$$

(A.24)

Figure A.5 Forces and moments in lamellas.

The normal stresses in the laminations are, see Figure A.5, found from the external moment M and the axial forces $N_1 = -H$ and $N_2 = H$. The moments in the laminations are

$$M_1 = \frac{I_1}{I_1 + I_2} (M + Hh_{cg}) \quad \text{and} \quad M_2 = \frac{I_2}{I_1 + I_2} (M - Hh_{cg}) \quad (\text{A.25})$$

$$\sigma_{2,\max} = \frac{H}{A_2} + \frac{6M_2}{b_2 h_2^2} \quad (\text{A.26})$$

The slip is found by (A.8):

$$u_s' = u_2' - u_1' + h_{cg} w'' = N_1 \left(\frac{1}{EA_1} + \frac{1}{EA_2} + \frac{h_{cg}^2}{EI_0} \right) - \frac{M}{EI_0} h_{cg} \quad (\text{A.27})$$

Integrating and using

$$u_s = 0 \quad \text{for } x = 0,5l \quad \text{and} \quad u_s^+ = u_s^- \quad \text{for } x = \delta l$$

$$\text{A: } u_s = \frac{l^2}{24E} \left(\frac{h_{cg}}{I_0} ql - 12 \frac{R_y / a}{A_r B^2} (1 - \beta) \beta \right) \quad (\text{A.28})$$

$$\text{B: } u_s = \frac{l^2}{24E} \left(\frac{h_{cg}}{I_0} ql (1 - 6\beta^2 + 4\beta^3) - 12 \frac{R_y / a}{A_r B^2} (1 - 2\beta) \beta \right) \quad (\text{A.29})$$

It shall be verified that

$$u_y \leq u_s \leq u_{\text{failure}} \quad (\text{A.30})$$

where

$$u_{\text{failure}} \sim 4u_y \quad (\text{A.31})$$

If the beam has a cantilever δl , it is a good approximation just to replace βl by $(\delta l + \beta l)$, i.e. to substitute β by $(\beta + \delta)$.

**INTERNATIONAL COUNCIL FOR RESEARCH AND INNOVATION
IN BUILDING AND CONSTRUCTION**

WORKING COMMISSION W18 - TIMBER STRUCTURES

**DESIGN OF TIMBER-CONCRETE COMPOSITE BEAMS WITH
NOTCHED CONNECTIONS**

M Fragiacomò

University of Sassari, Dept. of Architecture, Design and Urban Planning, Alghero
ITALY

D Yeoh

Universiti Tun Hussein Onn Malaysia, Faculty of Civil and
Environmental Engineering
Batu Pahat, Johor,
MALAYSIA

MEETING FORTY THREE

NELSON

NEW ZEALAND

AUGUST 2010

Presented by M Fragiacomò

R Nestic: What about long term? M Fragiacomò: There are long term tests in progress and results will be published.

H Larsen: This concept is hard to use as fasteners are far too strong and stiff. Notches suggested are expensive as well.

H Blass: Some of the data used in reference was done with shear strength of 1/3 the characteristic values for shear.

A Palermo: How will MC and fatigue affect serviceability issues? M Fragiacomò: MC increase is not substantial in wood.

S Franke: Tests in Weimar showed that MC increase is not deep in timber. M Fragiacomò: Increase in MC in wood is not a problem for wood, but loss of moisture from concrete is a problem.

Design of timber-concrete composite beams with notched connections

Massimo Fragiaco⁽¹⁾ and David Yeoh⁽²⁾

⁽¹⁾ University of Sassari, Dept. of Architecture, Design and Urban Planning, Alghero, Italy

⁽²⁾ Universiti Tun Hussein Onn Malaysia, Faculty of Civil and Environmental Engineering, Batu Pahat, Johor, Malaysia

1 Introduction on design of timber-concrete composite beam

Timber-concrete composite (TCC) structures must be designed so as to satisfy both serviceability (SLS) and ultimate limit states (ULS) in the short- and long-term (the end of the service life). The ULS is checked by comparing the maximum shear force in the connection, the maximum stress in concrete, and the combination of axial force and bending moment in timber with the corresponding resisting design values. The most important serviceability verification is the control of maximum deflection, which is used also for an indirect verification of the susceptibility of the floor to vibration, as suggested by Australian/New Zealand Standard 1170 Part 0 [1].

Two problems have to be addressed when evaluating stress and deflection of a TCC beam: (1) the flexibility of connection, which leads to partial composite action and, in general, does not allow the use of the transformed section method in design; and (2) the time-dependent behaviour of all component materials, i.e. creep, mechano-sorption, shrinkage/swelling, thermal and moisture strains of timber and concrete, and creep and mechano-sorption of the connection system.

To account for the first problem, two approaches have been proposed: the linear-elastic method [2] and the elasto-plastic method [3]. The linear-elastic method is based on the assumption that all materials (concrete, timber and connection) remain within the linear elastic range until the first component (generally, either the timber beam or the connection) fails. This is appropriate in many cases of technical interest, particularly for TCC with very strong and stiff connectors such as notches cut in the timber and filled with concrete. A linear-elastic analysis is generally carried out for the short-term (instantaneous) verifications according to the approach suggested by Ceccotti [2], which is based on the use of the gamma method recommended in the Annex B of the Eurocode 5 [4]. According to the gamma method, an effective bending stiffness, $(EI)_{ef}$, given by Eq. (1), is used to account for the flexibility of the timber-concrete shear connection. A reduction factor γ , which ranges from 0 for no composite action between the timber and concrete interlayers to 1 for fully composite action (and rigid connection), is used to evaluate the effective bending stiffness:

$$(EI)_{ef} = E_1 I_1 + E_2 I_2 + \gamma_1 E_1 A_1 a_1^2 + \gamma_2 E_2 A_2 a_2^2 \quad (1)$$

where subscripts 1 and 2 refer to concrete and timber elements, respectively; E is the Young's modulus of the material; A and I are the area and the second moment of area of the element cross-section; a is the distance from the centroid of the element to the neutral axis of the composite section; and γ is the shear connection reduction factor. Using the effective bending stiffness, the maximum stresses in bending, tension and compression for both the timber and concrete elements, and the shear force in the connection can then be calculated [2]. In Eq. (1), γ_1 is calculated from Eq. (2) and γ_2 is taken as one:

$$\gamma_1 = \frac{1}{1 + \frac{\pi^2 E_1 A_1 s_{ef}}{K l^2}} \quad \gamma_2 = 1 \quad (2) \quad (3)$$

where s_{ef} is the effective spacing of the connectors assumed as smeared along the span of the floor beam; l is the span of the TCC floor beam; and K is the slip modulus of the connector. For verifications at ULS and SLS, different values of slip moduli, K_u and K_s , are used, defined by Eqs. (4) and (5), respectively. Such a difference between K_u and K_s arise from the shear force-relative slip relationship of the connection, which is generally non-linear [2,5]. These stiffness properties of connector are evaluated through experimental push-out shear test (Figure 1) carried out as recommended in EN 26891 [6]:

$$K_u = \frac{0.6 F_m}{v_{0.6}} \quad K_s = \frac{0.4 F_m}{v_{0.4}} \quad (4) \quad (5)$$

where F_m is the mean shear strength obtained from a push-out test, $v_{0.4}$ and $v_{0.6}$ are the slips at the concrete-timber interface under a load of 40% and 60% of the mean shear strength F_m , respectively. Figure 1 displays a typical experimental set-up of a push-out test, carried out at the University of Canterbury, New Zealand, to investigate the mechanical properties of notched connectors between LVL joists and concrete slabs [7].

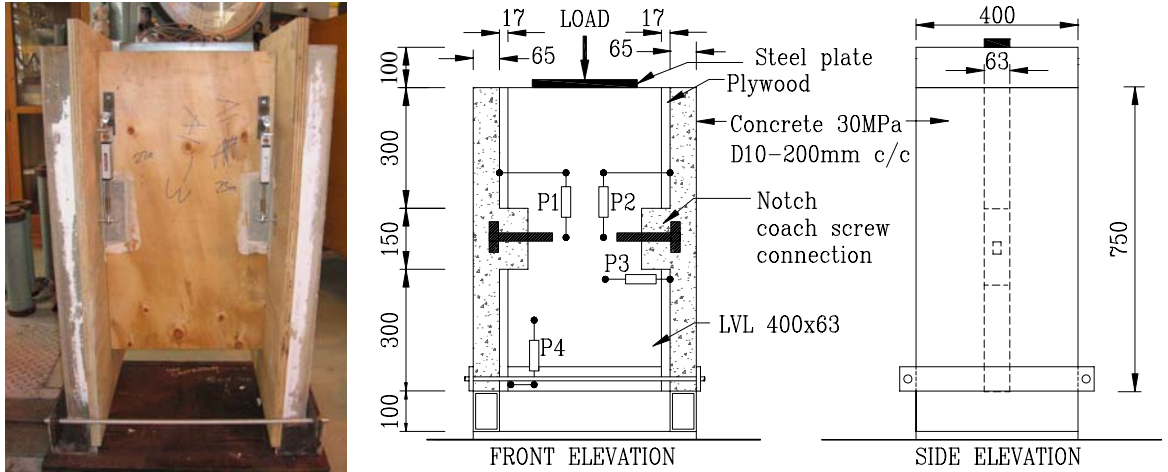


Figure 1: Symmetrical push-out test set-up (dimensions in mm)

The elasto-plastic solution [3] has been proposed specifically for cases where the failure of the TCC is attained after extensive plasticization of the connection system, so as to allow for redistribution of the shear force from the most stressed to the less stressed connectors along the beam. This is fairly common where the connectors are low strength, low stiffness and high ductility, such as for mechanical fasteners. The failure load is evaluated by assuming a rigid-perfectly plastic behaviour of the connection.

For verifications in the long-term, the ‘Effective Modulus Method’ recommended by Ceccotti [2] is used to account for the effect of creep of the different materials. The effective moduli of concrete, E_1 , and timber, E_2 ; and slip modulus of connector, K in Eq. (1) are replaced with their respective effective moduli $E_{1,eff}$, $E_{2,eff}$ and K_{eff} given by:

$$E_{1,eff} = \frac{E_1}{1 + \phi_1(t, t_0)} \quad E_{2,eff} = \frac{E_2}{1 + \phi_2(t - t_0)} \quad K_{eff} = \frac{K}{1 + \phi_f(t - t_0)} \quad (6) \quad (7) \quad (8)$$

where $\phi_1(t, t_0)$, $\phi_2(t - t_0)$ and $\phi_f(t - t_0)$ are, respectively, the creep coefficient of concrete, timber, and connector, t and t_0 are, respectively, the final time of analysis (the end of the service life, usually 50 years) and the initial time of analysis (the time of application of the imposed load). A detailed description of the design of TCC at ultimate and serviceability limit states, with emphasis on the influence of creep in the long-term, including two worked examples, is provided in [8].

The approach discussed above neglects the effect of environmental strains caused by the different thermal expansion and shrinkage of concrete and timber on the internal forces and the deflection of TCC, resulting in an underestimation of the deflection at the end of service life. To resolve this issue, rigorous [9] and approximated [10] closed form solutions were derived to account for the effects of environmental strains and drying shrinkage of concrete on TCC. Such formulas were compared to each other [11] showing good accuracy, and then used to estimate the influence of different environmental conditions, type of exposure, and size of the timber cross-section on the design of TCC beams [12,13]. A significant influence on the design was found, particularly for TCC systems with solid timber decks and rigid connections, and for TCC floors with narrow timber joists exposed to outdoor, sheltered environmental conditions [13].

2 The notched connection

A wide range of connection systems have been developed in different parts of the world and throughout the century. The connectors can be metal or timber fasteners, or notches cut in the timber and filled by concrete. Based on their arrangement along the beam, the connectors can be categorized in discrete/continuous, and vertical/inclined. They can also be categorized in glued/non-glued, and prestressed/non-prestressed, based on the way they are inserted in the timber.

Notches cut in the timber beam and reinforced with a steel screw or dowel, as illustrated in Figure 2, is by far one of the best connection for TCC with respect to strength and stiffness performance although it may not be altogether economical if the notches had to be cut manually [14,15]. The relative slip between the concrete slab and the timber beam can be prevented by direct bearing of the concrete within the notch on the timber of the beam, leading to a strong and stiff connection. Different notch geometries (rectangular, triangular, inverted trapezoidal) have been used with different timber materials (sawn timber, glulam, and LVL), with or without reinforcement.

Inverted trapezoidal notches cut in a timber deck made from sawn timber were tested at Colorado State University, US [16]. The notches were reinforced with a metal anchor which can be tightened after 28 days from the concrete placement to eliminate any gap within the notch due to drying shrinkage of concrete and restore the tight fit at the concrete-timber interface. Rectangular notches, with or without a reinforcement made from

lag screws, were tested at the University of Stuttgart, Germany, on a composite system made from board stacks [14]. Rectangular, triangular and trapezoidal notches cut in LVL joists, with and without a lag screw reinforcement, were tested at the University of Canterbury, New Zealand [15,17,18]. The length of the notch, the presence of a lag screw and its depth of penetration into the timber, were found to be the most important factors affecting the performance of the connection. It was found that the notch length affects the strength and stiffness of the connection while the lag screw improves the post-peak behaviour.

3 Experimental evaluation of mechanical properties of notched connections

The shear strength of a notched connection is an important mechanical property for the design of TCC floors at ULS. Such a quantity can be evaluated by testing to failure small TCC blocks (push-out tests, see for example Figure 1). The outcomes of an extensive experimental programme carried out at the University of Canterbury on several LVL-concrete push-out specimens (9 per connection type) is summarized in Table 1. The tests were carried out on rectangular and triangular notched connections reinforced with a lag screw (see connection details in Figure 2). The concrete slab was 600 mm wide and 65 mm deep, and the concrete had an average compressive strength of 45 N/mm². The LVL joist was 63 mm wide and 400 mm deep, and had a bending strength of 48 N/mm².

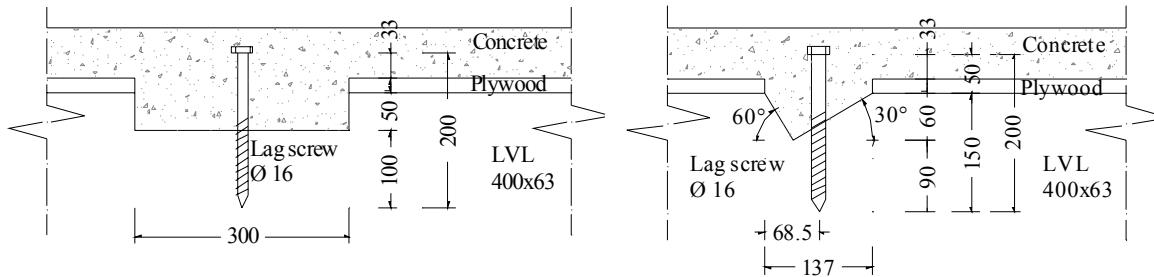


Figure 2: Details of the rectangular (left) and triangular (right) notched connections tested at the University of Canterbury (dimensions in mm) [7,18]

The outcomes of the tests as shear strength (mean value F_m and characteristic value F_k) and mean slip moduli for SLS and ULS verifications, K_s and K_u respectively, are listed in Table 1. More details on the experimental programme can be found in [7,18]. The quantity F_k is used for ULS control of the connection, whilst the quantities K_s and K_u are used in Eqs. (2) and (1) for evaluation of the effective flexural stiffness of the composite beam at SLS and ULS, respectively. From Table 1 it is fairly clear that there is no significant difference between K_s and K_u , hence only one value of the slip modulus could be used for both SLS and ULS verifications.

Table 1: Experimental values of the slip moduli and shear strength of rectangular and triangular notched connections, and analytical predictions of the mean shear strength.

Type of connection	K_s [kN/mm]	K_u [kN/mm]	F_k [kN]	F_m [kN]	F_m [kN]	F_m [kN]	F_m [kN]
	Experim.	Experim.	Experim.	Experim.	Analytic NZS	Analytic EC	Analytic EC*
Rectangular	247.2	241.4	115.3	138.9	186.4	99.1	140.3
Triangular	145.8	138.8	70.4	84.8	94.0	70.7	83.4

4 Analytical evaluation of the shear strength of notched connections

A simplified analytical model for strength evaluation of notch connections reinforced with lag screws is proposed in Eqs. (9) to (12). The formulas were compared with the experimental results and were found to predict the failure load with acceptable accuracy in most cases. The connection is regarded as a concrete corbel protruding into the laminated veneer lumber (LVL) joist subjected to the shear at the concrete-timber interface. The lag screw acts as reinforcement for the concrete corbel, and contributes to the shear transfer from timber to the concrete. The model is based on the control of all possible failure mechanisms that may occur in the connection region (see Figure 3) [19]: (1) failure of concrete in shear in the notch; (2) crushing of concrete in compression in the notch; (3) failure of LVL in longitudinal shear between two consecutive notches or between the last notch and the end of the LVL beam; and (4) failure of LVL in crushing parallel to the grain at the interface with the concrete corbel. Analytical design formulas in accordance with New Zealand Standards and Eurocodes were derived. By comparing the outcomes from the different standards, it was found that the New Zealand Standards method overestimates the maximum shear strength, while the Eurocode method is quite conservative with the actual experimental results in between (see Table 1). An alternative approach based on the introduction of a reduction factor β^* to be used in the Eurocodes formulas was then derived and compared with the experimental results, showing the best accuracy.

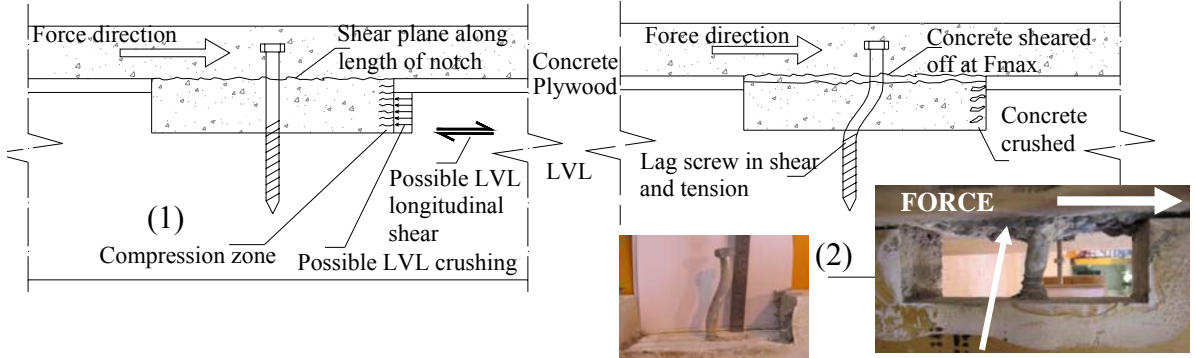


Figure 3: Experimental failure mechanisms and behaviour of a rectangular notch connection reinforced with a lag screw

4.1 Strength evaluation model according to New Zealand Standards (NZS method)

The corresponding formulas, reported herein after, were derived in accordance with provisions from New Zealand Standards for both timber [20] and concrete structures [21] based on the aforementioned four possible failure mechanisms of the notched connection:

$$F_{conc, shear} = 0.2f'_c bl + nk_1 pQ \quad F_{conc, crush} = f'_c A_c \quad (9) \quad (10)$$

$$F_{LVL, shear} = k_1 k_4 k_5 f_s Lb \quad F_{LVL, crush} = k_1 f_c bd \quad (11) \quad (12)$$

where $F_{conc, shear}$ is the nominal shear strength of concrete for a notched connection reinforced with a lag screw, $F_{conc, crush}$ is the nominal compressive strength of concrete in the crushing zone, $F_{LVL, shear}$ is the nominal longitudinal shear strength of LVL between two consecutive notches or between the last notch and the end of the timber beam, and

$F_{LVL,crush}$ is the compressive strength of LVL in the crushing zone. f'_c is the compressive strength of concrete, b and l are the breadth of the LVL joist and the length of notch, respectively, n is the number of lag screws in the notch, k_l is the modification factor for duration of loading for timber, p is the depth of penetration of lag screw in the timber, and Q is the withdrawal strength of the lag screw in Eq. (9). A_c is the crushing zone effective area, i.e. $b \times d$ in Eq. (10) where d is the depth of the notch. k_4 and k_5 are the modification factors for load sharing (taken as 1.0 for material with properties of low variability such as LVL), f_s is the LVL strength for longitudinal shear, and L is the shear effective length, i.e. the distance between two consecutive notches or between the last notch and the end of the timber beam in Eq. (11). f_c is the compressive strength of LVL parallel to the grain in Eq. (12). The design value of the shear strength is obtained by using the characteristic values of material strengths f'_c , Q , f_s and f_c in Eqs. (9) to (12), and by multiplying the minimum among the four values of strength by the strength reduction factor ϕ .

4.2 Strength evaluation model according to Eurocodes (EC method)

Based on the Eurocodes for both timber [4] and concrete structures [22], the shear strength of concrete for a notched connection reinforced with a lag screw when modelled as a corbel can be calculated using the following equation:

$$F_{conc.shear} = \beta 0.5 b_n l_n \nu f_c + n_{ef} (\phi_{cs} d_{ef} \pi)^{0.8} f_w \quad (13)$$

where β is the reduction factor of the shear force for load applied in proximity of the support of the notch regarded as a corbel, which should be assumed as 0.25 in accordance with Eurocode 2 [22] for the case under study; b_n and l_n are the breadth of the joist and the length of the notch, respectively; ν is a strength reduction factor for concrete cracked in shear, assumed as 0.516; f_c is the compressive strength of concrete; n_{ef} is the effective number of lag screws, assumed equal to the actual number of screws in the notch if they are spaced enough; ϕ_{cs} is the diameter of the lag screw, d_{ef} is the pointside penetration depth less one screw diameter; and f_w is the withdrawal strength of the screw perpendicular to the grain. The other three failure mechanisms are governed by design equations similar to Eqs. (10) to (12), the only difference being that the coefficients k_4 and k_5 are replaced by the modification factor for system effect k_{sys} , assumed 1.0 for LVL, and the coefficient k_l is replaced by k_{mod} which denotes the modification factor for duration of load and moisture content. The design value of the shear strength is then obtained by using the design values of the material strengths f_{cd} , f_{wd} , etc., which are obtained by dividing the characteristic values by the material strength coefficients, γ_m , in the design equations, and by taking the minimum of the so obtained four values of design strengths.

4.3 Modified reduction factor method (EC* method)

A new reduction factor, β^* , given in Eq. (14), was introduced to replace the existing reduction factor, β , in Eq. (13) in order to account not only for the loading distance but also for the length of the notch, l_n , which was found to have a significant effect in the experimental tests, and the diameter of the lag screw, ϕ_{cs} .

$$\beta^* = \frac{l_n - 2\phi_{cs}}{2l_n} \quad (14)$$

4.4 Experimental-analytical comparisons

Table 1 provides a comparison of the experimental mean shear strength for the rectangular and triangular notched connections with the three analytical strength evaluation methods discussed above. For all connector types, the governing design formula was found to be Eq. (9) and Eq. (13) for concrete shear, which agrees well with the failure mechanism detected in the experimental tests. The EC method was found to be the more conservative than the NZS method while the EC* method shows a prediction very close to the experimental outcomes in all of the cases.

5 Collapse tests of TCC beams with notched connections

The formulas discussed above allow a reasonably accurate prediction of the shear strength of a notched connection, which can then be used in ULS verifications. More complex is to derive analytical formulas for the mean slip modulus of a notched connection. Such a quantity is needed in Eqs. (1) and (2) to calculate the effective flexural stiffness of the composite beam and, then, all other quantities such as deflections, stresses, etc. needed for ULS and SLS verifications. So far, no accurate formula was proposed for the prediction of the slip modulus, therefore experimental testing is currently the only possible way to evaluate this quantity. For the rectangular and triangular notched connections tested in New Zealand, the values are reported in Table 1.

On the other hand, notched connections were found to be fairly stiff and, therefore, it may be interesting to investigate the possibility to use the transformed section method, which assume fully rigid connection between concrete and timber and, therefore, does not require the slip modulus, in the design of TCC beams with notched connections. To this aim, reference to an extensive experimental programme carried out on full-scale composite beams is made in this paper.

A semi-prefabricated LVL-concrete composite system was developed at the University of Canterbury, New Zealand, comprising of 2400 mm wide M-section panels built with laminated veneer lumber (LVL) beams acting as floor joists and a plywood interlayer as permanent formwork (Figure 4a) [7]. For the purpose of experimental tests to collapse, the M-section was reduced in width from 2400 mm to a T-section of 1200 mm and 600 mm (Figure 4b). Nine beam specimens of 8 and 10 m span were designed, built and tested to failure under four-point bending, with the purposes of measuring the flexural stiffness, identifying the failure mechanisms, and assess the load-carrying capacity. Three types of notched connectors were used to construct the composite beam specimens: (1) Rectangular notches 150 mm long and 25 mm deep reinforced with a lag screw (R150); (2) Rectangular notches 300 mm long and 50 mm deep reinforced with a lag screw (R300) – see Figure 2; (3) Triangular notches reinforced with a lag screw (T) – see Figure 2. All beams had one LVL joist and a 600 mm wide concrete slab, except beam G1 which had two LVL joists and a 1200 mm wide concrete slab.

The beams were designed at ULS and SLS using the gamma method for two design levels: well-designed and under-designed, depending on whether all design inequalities at ULS and SLS were satisfied or not. The most critical design criterion for the well-designed beams was deflection at SLS in the long-term, followed by shear strength of connection at ULS in the short- and long-term. In the under-designed beams, the demand of shear force in the most stressed connector was about 30% more than the design resistance at ULS in the short- and long-term. An imposed load Q of 3 kN/m² for office buildings and a total

permanent load $G = G_1 + G_2$ of 3 kN/m^2 , with G_1 and G_2 signifying the self-weight and the superimposed permanent load, assumed as 2 and 1 kN/m^2 , respectively, were considered in the design. The purpose for the variations in the design level was to investigate the actual strength and composite action achievable by the beam specimens, to verify the accuracy of the analytical gamma method used in design, and to explore the possibility to disregard the connection flexibility and use the transformed section method. The details of the beam tested are summarized in Table 2. More information can be found in [7].

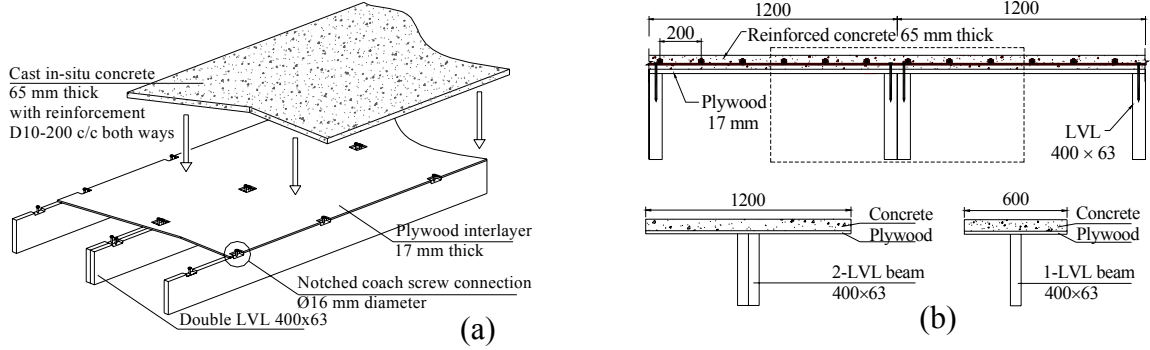


Figure 4: (a) Semi-prefabricated panels; (b) Reduced T-section (dimensions in mm)

Table 2: Details of the beam specimens, failure loads, and experimental (Exp), analytical (gamma method - Anal) and fully rigid (FuC) mid-span deflection at SLS load level (No. conn.=Number of connectors, R150=rectangular notch 150 mm long and 25 mm deep, R300=rectangular notch 300 mm long and 50 mm deep, T=triangular notch)

Beam	Span length [m]	No. conn.	Conn. type	Design level	Failure load $2P_{max}$ [kN]	Deflection Δ at SLS load level [mm]				
						FuC	Exp.	Anal	Exp/FuC	Exp/Anal
A1	8	6	R150	Under	87.3	15.6	22.7	17.5	1.45	1.30
A2	8	6	R150	Under	75.3	13.5	18.0	15.1	1.34	1.19
B1	8	10	R150	Well	105.0	24.3	26.5	26.1	1.09	1.02
B2	8	10	R150	Well	97.5	24.3	27.1	26.1	1.12	1.04
C1	8	10	T	Well	89.7	20.7	23.9	22.1	1.15	1.08
C2	8	10	T	Well	110.0	25.4	28.8	27.1	1.13	1.06
D1	8	6	R300	Well	80.8	18.7	21.1	19.7	1.13	1.07
E1	10	6	R300	Under	79.6	27.8	27.8	28.9	1.00	0.96
G1	8	10	R150	Well	201.0	23.2	25.9	25.5	1.12	1.02

Two types of failure mechanisms were observed: (1) fracture in tension of LVL under loading points at one-third of the span (Figure a) with no apparent sign of failure in connections, for well-designed beams; and (2) for under-designed beams, failure of connection in shear and/or crushing of concrete with plasticization of the lag screw in the case of notched connections (Figure b). The failure pattern of notched connectors was similar to that detected in push-out tests [7] where concrete strength was found to significantly influence the shear strength of the connection and, therefore, the load-carrying capacity of the composite beam. In most cases, the first crack sound was heard at approximately 60% of the collapse load F_{max} indicating the start of connection yielding which was followed by further plasticization as the screeching sound became louder. The failure hierarchy observed for under-designed beams was as follows: (1) crack sound in

one or multiple connections as an early warning; (2) failure of the first connector, usually near the support; (3) consecutive failures of the other connectors moving towards the middle of the beam due to redistribution of the shear force; (4) when all connectors have failed, the load is resisted only by the LVL beams and final fracture of LVL in tension.



Figure 5: Different types of failure mechanisms detected in the composite beams: (a) fracture in tension of LVL; (b) failure for concrete shear and crushing in 300 mm rectangular notched connection

6 Results and discussion

Analytical-experimental comparisons of load-carrying capacity at ULS and SLS in the short-term in terms of imposed load for tested TCC beams and fully composite beams were performed. The analytical design imposed load in kN/m^2 was predicted such that all the ULS and SLS short-term inequalities were satisfied using the gamma method with connection slip moduli K_u and K_s , respectively, where concrete, LVL and connection strength design values were used. For under-designed beams, the connection strength inequality was governing followed by deflection in the short- or the long-term. The design of well-designed beams was governed by either deflection in the short- or long-term [7].

In the ULS comparison, it was found that all well-designed beams exhibited an experimental load-carrying capacity very close to that of a fully composite beam with rigid connection (approximately 0.9 times). This can be clearly appreciated from Figure 6, which displays a typical load-deflection curve of a well-design beam (in this case, specimen B2) and compare such a curve with the cases of fully composite (rigid connection) and non-composite (no connection) beam. In the SLS comparison, the analytical prediction underestimated the experimental imposed load by about 10%. This indicated that the gamma method provided an accurate and conservative prediction of the imposed load at SLS. Furthermore, the experimental load-carrying capacities of well-designed beams were only 10% less than that of fully composite beams implying that these beams have relatively high degree of composite action (87 to 100%) which was quantified according to Eq. (15):

$$DCA = \frac{\Delta_N - \Delta_F}{\Delta_N - \Delta_R} \times 100 \quad (15)$$

where Δ_N , calculated theoretically, signifies the deflection of the composite beam with no connection (lower limit); Δ_R , calculated theoretically, signifies the deflection of the composite beam with fully rigid connection (upper limit); and Δ_F , measured experimentally, signifies the deflection of the composite beam with the actual flexible

connection. This further indicates that the transformed section method can be used with some correction factors to design composite beams with notched connections such as those investigated in this study characterized by a high degree of composite action.

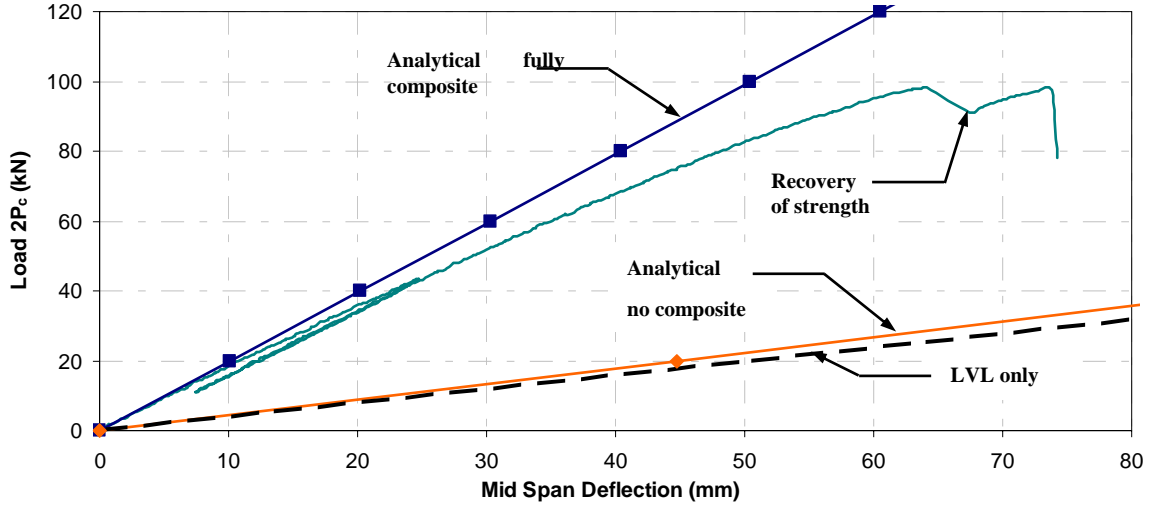


Figure 6: Typical experimental load $2P_c$ vs. midspan deflection curve for well-designed beams (specimen B2)

In an attempt to quantify this correction factor for design, the fully composite beam deflections (FuC) at SLS load level were compared, as presented in Table 2, with the experimental (Exp.) deflections, and with the analytical (Anal) deflections determined using the gamma method with the connection slip modulus K_s experimentally measured in push-out tests on connections. For the well-designed beams, the experimental deflection was 1.09 to 1.15 times the fully composite deflection, and 1.02 to 1.08 times the analytical deflection. Taking a conservative approach, this finding is indicative of a 15% increment correction factor to the deflection or, equivalently, a 13% reduction to the flexural stiffness (EI) calculated using the transformed section method (Eq. (1) with $\gamma_1=1$).

The method of the transformed section can therefore be used in design of TCC beams with notched connections. For evaluation of deflection at SLS, the flexural stiffness (EI) should be conservatively reduced by 13%. For connection design at ULS, it is suggested that no reduction in the flexural stiffness calculated with the transformed section be made, so as to overestimate the demand of shear force in the connection and carry out a conservative design. The connection strength capacity can then be calculated using the analytical formulas proposed in this paper. For timber and concrete design at ULS, the use of the flexural stiffness calculated with the transformed section method may be non conservative, therefore the use of the 13% reduction factor is recommended. It should be noted, however, that these ULS verifications are usually less critical than the ULS of connection and SLS of deflection. Hence, any possible approximation on the correction factor is less critical for such ULS verifications.

7 Conclusions and implications for future code developments

This paper discusses the design of timber-concrete composite beams with notched connections. Analytical formulas for the prediction of the shear resistance of notched connectors were derived, based on four possible failure mechanisms: (i) shearing of the

concrete within the notch, (ii) compression of the concrete within the notch, (iii) shearing of the timber parallel to grain between two consecutive notches or from the first notch to the end of the beam, and (iv) crushing of the timber parallel to the grain at the interface with the concrete. The formulas, derived according to the New Zealand Standards and the Eurocodes, were validated against the results of an extensive experimental programme which involved several push-out specimens to failure carried out on small LVL-concrete composite blocks at the University of Canterbury, New Zealand. Such formulas can therefore be proposed in the new versions of the aforementioned regulations.

Based on an extensive experimental programme carried out at the University of Canterbury which involved tests to failure of full-scale LVL-concrete composite beams with notched connections, it was found only a minor difference between the experimental deflection at serviceability limit state and the analytical value calculated using the transformed section method, i.e. by neglecting the flexibility of the connection. This suggests a possible simplified procedure for design of timber-concrete composite beams with notched connections, i.e.: (1) calculation of the flexural stiffness (EI) of the composite section using the transformed section method; (2) calculation of the shear strength demand of the notched connection at ultimate limit using the flexural stiffness (EI); (3) comparison of the shear strength demand with the strength capacity of the notched connection evaluated using the proposed analytical formulas; (4) evaluation of the deflection at serviceability limit state by reducing the flexural stiffness (EI) by 13%; (5) calculation of the stresses in concrete and timber at ultimate limit state by reducing the flexural stiffness (EI) by 13%.

Although the aforementioned procedure was derived and validated on a particular type of composite floor made from LVL joists with rectangular and triangular notched connections, the procedure is general and can be applied to any type of composite structure with notched connection. Further analytical-experimental comparisons are however warranted, in particular to check the accuracy of the 13% reduction factor of the flexural stiffness used together with the method of the transformed section for different types of composite floors (for example, with solid deck).

Literature references

- [1] AS/SNZ Standards Australia and Standards New Zealand (2002). AS/NZS1170 – Structural design actions – Part 0: General principles. Canberra, Australia.
- [2] Ceccotti A. (2002). Composite concrete-timber structures. *Progress in Structural Engineering and Materials*, 4(3), 264-275.
- [3] Frangi A., Fontana M. (2003). Elasto-plastic model for timber–concrete composite beams with ductile connection. *IABSE Struct. Eng. International*, 13(1), 47–57.
- [4] CEN Comité Européen de Normalisation (2004). Eurocode 5 – Design of timber structures – Part 1-1: General rules and rules for buildings. Brussels, Belgium.
- [5] Lukaszewska E., Fragiaco M., Frangi A. (2007). Evaluation of the slip modulus for ultimate limit state verifications of timber-concrete composite structures. Meeting 40 of the Working Commission W18-Timber Structures, CIB, Bled (Slovenia), 14 pp.
- [6] CEN Comité Européen de Normalisation (1991). EN 26891 – Timber structures – Joints made with mechanical fasteners – General principles for the determination of strength and deformation characteristics. Brussels, Belgium.

- [7] Yeoh D. (2010). Behaviour and design of timber-concrete composite floor system. Ph.D. Thesis, University of Canterbury, New Zealand.
- [8] Ceccotti A., Fragiaco M., Gutkowski R. (2002). Design of timber-concrete composite structures according to EC5-2002 version. Proceedings of the Meeting thirty-five of the Working Commission W18-Timber Structures, CIB. Kyoto, Japan, September, 10 pp.
- [9] Fragiaco M. (2006). Long-term behaviour of timber-concrete composite beams. II: Numerical analysis and simplified evaluation. ASCE J. Struct. Eng., 132(1), 23–33.
- [10] Schänzlin, J. (2003). Time dependent behavior of composite structures of board stacks and concrete. Ph.D. Thesis, University of Stuttgart (in German).
- [11] Schänzlin J., Fragiaco M. (2007). Extension of EC5 Annex B formulas for the design of timber-concrete composite structures. Meeting forty of the Working Commission W18-Timber Structures, CIB, Bled (Slovenia), August 28-31, 10 pp.
- [12] Fragiaco M., Ceccotti A. (2006). Simplified approach for the long-term behaviour of timber-concrete composite beams according to the Eurocode 5 provisions. Meeting thirty-nine of the Working Commission W18-Timber Structures, CIB, Florence (Italy), 12 pp.
- [13] Fragiaco M., Schänzlin J. (2010). The effect of moisture and temperature variations on timber-concrete composite beams. 11th World Conference on Timber Engineering WCTE 2010, Riva del Garda (Italy), June 20-24, 2010, 8 pp., CD.
- [14] Kuhlmann U., Schänzlin J. (2001). Grooves as shear connectors for timber-concrete composite decks. Proc. of the RILEM Conference 'Joints in Timber Structures', Stuttgart, Germany, Sept.12-14, 283-290.
- [15] Deam B.L., Fragiaco M., Buchanan A.H. (2008). Connections for composite concrete slab and LVL flooring systems. RILEM Materials and Structures, 41(3), 495-507.
- [16] Gutkowski R., Brown K., Shigidi A., Natterer J. (2004). Investigation of notched composite wood-concrete connections. ASCE J. Struct. Eng., 130(10), 1553-1561.
- [17] Yeoh D., Fragiaco M., Buchanan A., Gerber C. (2009). Preliminary research towards a semi-prefabricated LVL-concrete composite floor system for the Australasian market. Australasian Journal of Structural Engineering, 9(3), 225-240.
- [18] Yeoh D., Fragiaco M., De Franceschi M., Buchanan A. (2010). Experimental tests of notched and plate connectors for LVL-concrete composite beams. J. of Struct. Eng., submitted
- [19] Kuhlmann U., Michelfelder B. (2006). Optimised design of grooves in timber-concrete composite slabs. In: Proceedings of the 9th World Conference on Timber Engineering, Portland, Oregon (USA), CD.
- [20] SNZ Standards New Zealand (1993). NZ3603 – Design of timber structures. Wellington, NZ.
- [21] SNZ Standards New Zealand (2006). NZ3101 – Concrete structures standard – Part 1: The design of concrete structures. Wellington, New Zealand.
- [22] CEN Comité Européen de Normalisation (2004). Eurocode 2 – Design of concrete structures – Part 1-1: General rules and rules for buildings. Brussels, Belgium.

**INTERNATIONAL COUNCIL FOR RESEARCH AND INNOVATION
IN BUILDING AND CONSTRUCTION**

WORKING COMMISSION W18 - TIMBER STRUCTURES

**DEVELOPMENT OF DESIGN PROCEDURES FOR TIMBER CONCRETE
COMPOSITE FLOORS IN AUSTRALIA AND NEW ZEALAND**

K Crews

C Gerber

Centre for Built Infrastructure Research, University of Technology Sydney
AUSTRALIA

MEETING FORTY THREE

NELSON

NEW ZEALAND

AUGUST 2010

Presented by C Gerber

H Blass: what is an S notch? C Gerber: A notch with rounded edges. A diagram will be added to the paper.

P Quenneville: What is a batten connection? C Gerber: A diagram will be added to the paper.

S Aicher: How to derive the K stiffness for the fasteners? C Gerber: From connection tests.

Linear regression from separate results, not floor test.

S Winter: Hard to get information from paper and presentation. More information is needed to follow procedures. K Crews: An 80 page report will be available.

H Larsen: why would one want a simplified method? C Gerber: in Australia, they want simple methods. K Crews: A design tools is needed and will be made available.

T Tannert: We also teach TCC and suggest getting away from Gamma Method as it is too complicated. K Crews: A method in a design tool (spreadsheet) will be what is used.

M Fragiaco: Length will influence some factors. Some values in tables are not compatible with NZ Design. How to explain? C Gerber: Tabled values were adjusted between Australia and NZ

DEVELOPMENT OF DESIGN PROCEDURES FOR TIMBER CONCRETE COMPOSITE FLOORS IN AUSTRALIA AND NEW ZEALAND PART 1 – DESIGN METHODS

Prof Keith Crews & Dr Christophe Gerber

Centre for Built Infrastructure Research, University of Technology Sydney, Australia

1 Introduction

Timber concrete composite (TCC) floor systems are relatively new to Australia and New Zealand and satisfactory performance requires a rigorous design procedure addressing both ultimate and serviceability limit states. TCC structures have a degree of complexity since they combine two materials that have very different mechanical properties and respond in different ways to their environment. Furthermore, most TCC structures exhibit partial (not full) composite action and this adds to the complexity of the system.

Several design procedures are discussed in the literature. Amongst these, the Eurocode 5 (EC5) procedure is relatively straightforward and has been successfully implemented in Europe. It utilises a simplification for modelling the complex timber - concrete interaction known as the “Gamma coefficients” method, which manipulates properties of the concrete member in order to predict the cross-section characteristics of the structure.

The details of this research are presented in two papers. Part 1 deals with design procedures, whilst Part 2 discusses an extensive R&D program of connection testing and the derivation of characteristic properties.

2 Scope

The EC5 approach has been adopted as the underlying basis for the design procedures presented in this document; modified to comply with current design codes and practices in Australia¹. It comprises normative parameters for the strength and safety (ultimate limit state) and informative guidelines for appearance, deflection limits and comfort of users (serviceability limit states). Whilst the latter must be defined by designers to meet the specific functional requirements of the floor under consideration, it is recommended that the Guidelines in this document should be adopted as a minimum standard for TCC floors.

At the time of publication, there is still considerable uncertainty about some aspects of long term deflection of TCC floors and as such the design procedures contained in this document are limited to floors not exceeding 8m in span and utilising the notched connections prescribed in Table 1.

3 Design requirements

Load type and intensity, load combinations and modification factors for both the ultimate and the serviceability limit states have been defined in accordance with the AS/NZS 1170 series (AS/NZS 2002a; 2002b).

¹ With minor modifications the same approach is relevant for New Zealand.

The limit states that require checking can be summarised as follows:

1. the **short-term ultimate limit state**; where the structure response to the maximum load is analysed. It generally corresponds to short-term exertion of the structure.
2. the **long-term ultimate limit state**. This analysis focuses on the structure response to a quasi permanent loading and aims at avoiding failure due to creep of the timber member in particular*.
3. the **short-term serviceability limit state**. This corresponds to the instantaneous response of the structure to an imposed load.
4. the **long-term serviceability limit state**. This analysis aims to identify the service life behaviour of structure considering the time-dependent variations of the material properties; in particular creep.
5. the **1.0-kN serviceability limit state**. This corresponds to the instantaneous response of the structure to an imposed point load of 1.0 kN at mid-span.

*Checking the end-of-life ultimate limit states corresponds to an attempt to analyse and assess the durability and reliability of the structure.

3.1 Connection behaviour

The structural behaviour of the connection is a significant parameter in the design of a TCC floor. The elastic properties of the connection are used for both limit states and accounted for in the identification of the Gamma coefficients in the design procedure.

4 Design procedure

The design procedure has three fundamental stages:

1. The initial stage of the design procedure focuses on identifying of the characteristics of the TCC cross-section.
2. Assessment of the strength capacity of the structure is completed in the second stage of the procedure; whilst
3. The final stage deals with the serviceability limit state.

4.1 Cross-section characteristics

The effective (apparent) stiffness of the composite cross-section is:

$$(EI)_{ef} = E_c I_c + E_t I_t + \gamma_c E_c A_c a_c^2 + \gamma_t E_t A_t a_t^2 \quad (1a)$$

Note: The subscripts c and t refer to concrete and timber respectively, unless otherwise specified. The contribution of the formwork (if present) is neglected in the design.

where the section properties in (1a) are given by:

$$I_c = \frac{b_c h_c^3}{12}; \quad I_t = \frac{b_t h_t^3}{12} \quad (2a); (2b)$$

$$\gamma_c = \frac{1}{1 + \frac{\pi^2 E_c A_c s_{ef}}{K_t L^2}}; \quad \gamma_t = 1 \quad (3a); (3b)$$

$$A_c = b_c h_c; \quad A_t = b_t h_t \quad (4a); (4b)$$

$$a_c = \frac{\gamma_t E_t A_t H}{\gamma_c E_c A_c + \gamma_t E_t A_t}; \quad a_t = \frac{\gamma_c E_c A_c H}{\gamma_c E_c A_c + \gamma_t E_t A_t} \quad (5a); (5b)$$

The height factor “H” is defined by:

$$H = \frac{h_c}{2} + a_f + \frac{h_t}{2} \quad (6)$$

where:

- the tributary width of the concrete member is assessed with (AS 2001, p. 93):

$$b_c = b_t + 0.2a; \quad b_c = b_t + 0.1a \quad (7a); (7b)$$

- the effective spacing (refer to Figure 1) of the connections is given by:

$$s_{ef} = 0.75s_{\min} + 0.25s_{\max} \quad (8)$$

- where all connectors are evenly spaced within the end quarter spans

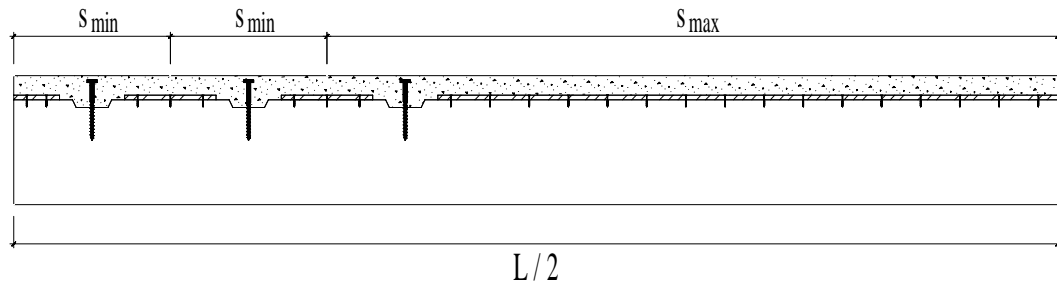


Figure 1: Connection-related distances.

- and the stiffness of the connection corresponds to (refer to TABLE 1):

$$K_{ser} = \frac{0.4R_m}{V_{0.4}}; \quad K_{eff} = \frac{K_{ser}}{j_{2,long}}; \quad K_u = \frac{0.6R_m}{V_{0.6}} \quad (9a); (9b); (9c)$$

Note: Whilst it is understood that the creep behaviour of TCC floors is quite complex, the “creep component” for long term deflections is modelled using the j_2 factor. This is consistent with AS 1720.1 (2010), which uses a simplified multiplier to the initial short term deflection. A value of $j_{2,long}$ between 3.0 and 4.0 is currently recommended for indoor applications.

4.2 Strength of the composite cross-section – concrete & timber members

The load combinations and factors for the ultimate limit state (ULS) must comply with the relevant provisions of AS / NZS1170 series (AS/NZS 2002a; 2002b). The checks imposed on a structure under flexural action or flexural and axial actions are described in Sections 3.2 and 3.6 of AS 1720.1 (AS 1997) respectively. These requirements apply to TCC floor structures as follows:

- bending strength – the concrete and timber members resist a combination of bending moment and/or axial force.
- flexural shear strength – the timber member resists the flexural shear force.
- bearing strength – the timber member resists the support action/reactions.

4.2.1 Strength requirements for Bending strength

At the extreme fibres – upper and lower – the concrete and timber members experience compression and tension stresses which result in combined bending and axial stresses as defined in Equation (10). The check is completed for the upper and lower fibres of the concrete member and for the lower fibre of the timber member².

$$\frac{N^*}{(\phi N)} + \frac{M^*}{(\phi M)} \leq 1.0 \text{ (expressed as stress ratios)} \quad (10)$$

The general expression for bending stress is defined in Equation (11):

$$\sigma_{b,i} = \pm \frac{1}{2} \frac{E_i h_i M^*}{(EI)_{ef}} \quad (11)$$

Specifically, the stresses in the concrete and timber member respectively are:

$$\sigma_{b,c} = \pm \frac{1}{2} \frac{E_c h_c M^*}{(EI)_{ef}}; \quad \sigma_{b,t} = \pm \frac{1}{2} \frac{E_t h_t M^*}{(EI)_{ef}} \quad (11a); (11b)$$

Equations (11a) and (11b) respectively identify the bending moment capacity:

$$\phi M_u = \phi f'_c \frac{2(EI)_{ef}}{\gamma_c E_c h_c}; \quad (\phi M) = \phi k_1 k_4 k_6 k_9 k_{11} k_{12} f'_b \frac{2(EI)_{ef}}{\gamma_t E_t h_t} \quad (12a); (12b)$$

These capacities must be greater than the design moment M^* , which is derived from loading requirements and boundary conditions of the TCC structure. The axial (in-plane) stress is predicted using Equation (13):

$$\sigma_{c/t,i} = \pm \frac{\gamma_i E_i a_i M^*}{(EI)_{ef}} \quad (13)$$

Specifically, the stresses in the concrete and timber member respectively are:

$$\sigma_{c,c} = -\frac{\gamma_c E_c a_c M^*}{(EI)_{ef}}; \quad \sigma_{t,t} = \frac{\gamma_t E_t a_t M^*}{(EI)_{ef}} \quad (13a); (13b)$$

Assessment of the axial stress is derived from the flexural action. However, (13a) and (13b) can be manipulated to identify the (corresponding) design axial force:

$$N_c^* = \sigma_{c,c} A_c; \quad N_t^* = \sigma_{t,t} A_t \quad (14a); (14b)$$

where the allowable axial forces are defined as:

$$\phi N_u = \phi f'_c A_c; \quad (\phi N) = \phi k_1 k_4 k_6 k_{11} f'_t A_t \quad (15a); (15b)$$

² An efficient design of a TCC cross-section occurs when the concrete member is fully under compressive stress and the timber member is mainly subjected to tensile stress. It is possible for the timber beam to experience compression, but this is not critical because the timber material exhibits adequate compression capacity.

4.2.2 Strength requirements for Flexural shear strength

In the absence of structural reinforcement in the concrete member, the flexural shear strength is provided by the timber member, therefore,

$$(\phi V) \geq V^* \quad (16)$$

Where for rectangular sections:

$$(\phi V) = \phi k_1 k_4 k_6 k_{11} f'_s \frac{2A_t}{3} \quad (17)$$

Note: Some conditions, (for example use of a deep notch), may require reducing the shear plane area by using the net area of the (beam) cross-section.

4.2.3 Strength requirements for Bearing strength

The bearing strength is provided by the timber member, therefore,

$$(\phi N_p) \geq N_p^* \quad (18)$$

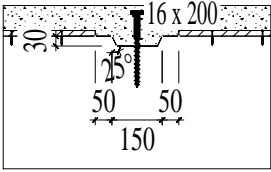
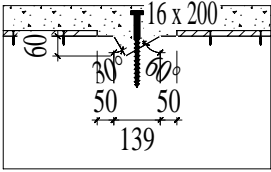
in which:

$$(\phi N_p) = \phi k_1 k_4 k_6 k_7 f'_p A_p \quad (19)$$

4.3 Strength of the composite cross-section – connection capacity

The connection (or notch) transfers the shear force occurring between the members under flexure. The actual mechanics of this force transfer are relatively complex. However a prescriptive approach that defines connection capacities (based on empirical test data - refer TABLE 1) that ensures the design procedure remains user-friendly, has been adopted for this document.

TABLE 1: CHARACTERISTIC PROPERTIES OF THE CONNECTION

Connection type	Beam width ^{*^†} b_t <i>mm</i>	Strength Q_k <i>kN</i>	SLS stiffness K_{ser} <i>kN/mm</i>	ULS stiffness K_u <i>kN/mm</i>
	48	46	81	58
	63	78	105	76
	48	55	35	34
	63	66	96	69

^{*} connection properties for beams 48 mm < b_t < 63 mm, are derived by linear interpolation.

[^]for beam, b_t > 63 mm, a reduction coefficient is applied: $k_{u,red} = \left(\frac{b_t}{63}\right)^{1.42}$ & $k_{s,red} = \left(\frac{b_t}{63}\right)^{0.42}$.

[†]for other connection types, empirical values must be established.

4.3.1 Shear strength of the connection

A global assessment of the connection strength is performed. It includes the assessment of the strength of the first connection, V_{\max}^* , and the connection located at the quarter-span area, $V_{L/4}^*$.

$$(\phi N_j) \geq Q^* \quad (20)$$

NOTE: Refer to TABLE 1, for empirical strengths of the specified connections.

where:

$$(\phi N_j) = \phi k_1 k_4 k_6 Q_k \quad (21)$$

and the effective shear force in the connection located near the support equals:

$$Q_{(V_{\max}^*)}^* = - \frac{\gamma_c E_c A_c a_c s_{\min}}{(EI)_{ef}} V_{\max}^* \quad (22)$$

(where $x = 0$ – refer to **Fehler! Verweisquelle konnte nicht gefunden werden.**, in Appendix Section **Fehler! Verweisquelle konnte nicht gefunden werden.**):

and the effective shear force in the connection located at the ‘quarter’ span:

$$Q_{(V_{L/4}^*)}^* = - \frac{\gamma_c E_c A_c a_c s_{\max}}{(EI)_{ef}} V_{L/4}^* \quad (23)$$

(where $x = L/4$ – refer to **Fehler! Verweisquelle konnte nicht gefunden werden.**, in Appendix Section **Fehler! Verweisquelle konnte nicht gefunden werden.**):

4.3.2 Shear strength of the timber

The shear strength of the timber – tangential shear action in the area located between the support and the first connection is assessed and checked as follows:

$$(\phi N_v) \geq V^* \quad (24)$$

where:

$$(\phi N_v) = \phi k_1 k_4 k_6 f'_s (b_t l_s) \quad (25)$$

4.4 Serviceability verification / assessment of the composite cross-section

The load combinations and factors for the serviceability limit states (SLS) are defined in the AS/NZS 1170 series (AS/NZS 2002a; 2002b). Serviceability of the TCC structure is undertaken by checking the deflections against the limits defined to suit the functional requirements of the building being designed. In the absence of any specific limits the following are recommended:

- Short term Live load only, limited to span / 300
- Short term Point load deflection, limited to 2.0mm

The mid-span deflection under uniformly distributed load is assessed as follows:

$$\Delta = \frac{5(G^* + \varphi w_{imp}^*)L^4}{384(EI)_{ef}} \quad (26)$$

For which the value of φ and $(EI)_{ef}$ are defined to suit the loading condition and duration.

4.4.1 Instantaneous short-term deflection:

The shrinkage and creep effect of the concrete member and the creep of the timber is neglected. Thus, $\varphi = 1.0$ and $(EI)_{ef}$ is approximated as defined in Equations (1a) to (9).

- a) imposed load deflection check under uniformly distributed load, from Eqn (26),
- b) deflection under 1.0 kN (vibration check):

$$\Delta = \frac{P^* L^3}{48(EI)_{ef}} \quad (27)$$

Where $P^* = 1.0$ kN (point load applied at mid-span).

4.4.2 Long-term end-of-life deflection

The shrinkage and creep of the concrete member and the creep of the timber are accounted for.

Thus, $\varphi = 4.0$ and $(EI)_{ef}$ is approximated as per Equations below.

- a) permanent and imposed load (deflection check under uniformly distributed load),
- b) permanent load only (deflection check under uniformly distributed load) Δ , is calculated using Equation: (26)

Where, the effective (apparent) stiffness of the composite cross-section is given by (1b) :

$$(EI)_{ef} = E_{c,lts} I_c + E_{t,lts} I_t + \gamma_{c,lts} E_{c,lts} A_c a_c^2 + \gamma_{t,lts} E_{t,lts} A_t a_t^2$$

I_c and I_t refer to Equations 2a and 2b and the gamma functions are given by Equations 3c and 3d

$$\gamma_{c,lts} = \frac{1}{1 + \frac{\pi^2 E_{c,lts} A_c s_{ef}}{K_{eff} L^2}}; \quad \gamma_{t,lts} = 1$$

A_c and A_t are obtained from Equations (4a) and (4b) and the “distance” factors are given by Equations 5c and 5d.

$$a_c = \frac{\gamma_{t,lts} E_{t,lts} A_t H}{\gamma_{c,lts} E_{c,lts} A_c + \gamma_{t,lts} E_{t,lts} A_t}; \quad a_t = \frac{\gamma_{c,lts} E_{c,lts} A_c H}{\gamma_{c,lts} E_{c,lts} A_c + \gamma_{t,lts} E_{t,lts} A_t}$$

Where:

$$E_{c,ls} = \frac{E_c}{(1 + \varepsilon_{cs})(1 + \phi_{cc})} \quad E_{t,ls} = \frac{E_t}{j_2} \quad (28a); (28b)$$

Note: The recommended creep coefficient for TCC, $j_2 = 3.0$ to 4.0 .

And:

$$\varepsilon_{cs} = k_1 \varepsilon_{cs,b} \quad (29)$$

$$\phi_{cc} = k_2 k_3 \phi_{cc,b} \quad (30)$$

for H refer to Equation (6)

for b_c refer to Equations (7a); (7b).

5 Concluding Comments

The design procedure presented in this paper is adapted from the design procedure of EC5 and modified to suit local practices and reflect research and development recently undertaken in Australia and New Zealand.

The design methodology adequately addresses the complexity of TCC structures, including the partial composite action provided by the connection and imposes a comprehensive series of strength checks on the cross-section components and serviceability checks with consideration to the long term performance of the structure.

Adapting the design procedure to suit Australian practices has been a challenging exercise and where assumptions have had to be made due to uncertainties, these have erred on being conservative. These assumptions are also areas for further research in order to address the uncertainties associated with them.

It is anticipated that further research will include:

- shear strength of the connection – size effect on the connection strength and stiffness,
- shear strength of the concrete notch – effect of the coach screw,
- shear strength wood portions between the notches,
- flexural shear strength of the beam – effect of deep notch and use of the net area of the shear plane,
- short-term serviceability – initial deflection and effect of concrete curing,
- long-term deflection
- influence of wood portions between the notches

Further work will also focus on making the design procedure more user-friendly wherever possible whilst preserving the safety and functionality of the design.

6 References

- Australian StandardTM 1997, *Timber Structures, Part 1: Design Methods*, vol. AS 1720.1–1997, Standards Australia, Homebush (NSW), Australia.
- Australian StandardTM 2001, *Concrete Structures*, vol. AS 3600–2001, Standards Australia, Homebush (NSW), Australia.
- Australian StandardTM 2003, *Composite structures – Part 1: Simply supported beams*, vol. AS 2327.1–2003, Standards Australia, Homebush (NSW), Australia.
- Australian/New Zealand StandardTM 2002a, *Structural Design Actions, Part 0: General Principles*, vol. AS/NZS 1170.0:2002, Standards Australia, Homebush (NSW), Australia.
- Australian/New Zealand StandardTM 2002b, *Structural Design Actions, Part 1: Permanent, Imposed and Other Actions*, vol. AS/NZS 1170.1:2002, Standards Australia, Homebush (NSW), Australia.
- British Standard 1991, *Timber structures. Joints made with mechanical fasteners. General principles for the determination of strength and deformation characteristics*, vol. BS EN 26891:1991, BSI British Standards, London, UK.
- Ceccotti, A. (ed.) 1995, *Timber-concrete composite structures*, Centrum Hout, Almere, The Netherlands.
- Crews, K., Gerber, C., Buchanan, A. & Fragiaco, M. 2008a, *Innovative Engineered Timber Building Systems for non residential applications* University of Technology, Sydney.
- Crews, K., Gerber, C., Choi, F.C., Buchanan, A. & Fragiaco, M. 2007, *Innovative Engineered Timber Building Systems for non residential applications* University of Technology, Sydney.
- Crews, K., Gerber, C., Yeoh, D., Buchanan, A. & Fragiaco, M. 2008b, *Innovative Engineered Timber Building Systems for non residential applications* University of Technology, Sydney.
- European Committee for Standardisation 1995, *Design of Timber Structures — General Rules and Rules for Buildings*, vol. Eurocode 5 (ENV 1995-1-1), European Committee for Standardisation CEN, Brussels, Belgium.
- Möhler, K. 1956, *Über das Tragverhalten von Biegeträgern und Druckstäben mit Zusammengesetzten Querschnitten und Nachgiebigen Verbindungsmitteln*, Universität Karlsruhe, Karlsruhe, Germany.
- Naterer, J., Hamm, J. & Favre, P.-A. 1996, 'Composite wood-concrete floors for multi-story buildings', paper presented to the *International Wood Engineering Conference*, New Orleans (LA), USA.
- Yeoh, D., Fragiaco, M., Buchanan, A. & Gerber, C. 2009, 'Preliminary research towards a semi-prefabricated LVL-concrete composite floor system for the Australasian market', *Australian Journal of Structural Engineering*, vol. 9, no. 3, pp. 225-240.

APPENDIX

Notation

The symbols and letters used in the design procedure are listed below:

A_c	cross-sectional area of the concrete member
A_t	cross-sectional area of the timber member
A_l	bearing area for loading parallel to the grain (timber)
A_p	bearing area for loading perpendicular to the grain (timber)
A_{sl}	shear plane area for shear action parallel to the grain (timber)
A_{st}	cross-sectional area of the coach screw (TCC only)
a	distance between points of zero bending moment
a_c	distance for the concrete member
a_f	thickness of the formwork
a_t	distance for the timber member
b_c	tributary width of the concrete member
b_t	width (thickness) of the timber member
b_v	width of the notch (concrete)
d_o	length of the notch (concrete)
E_c	value of the modulus of elasticity of the concrete member
$E_{c,lts}$	value of the modulus of elasticity of the concrete member for long-term serviceability
E_t	value of the modulus of elasticity of the timber member
$E_{t,lts}$	value of the modulus of elasticity of the timber member for long-term serviceability
$(EI)_{ef}$	effective (apparent) stiffness of the TCC cross-section
f_b'	characteristic strength in bending
f_c'	characteristic strength in compression
f_l'	characteristic strength in bearing parallel to the grain

f_p'	characteristic strength in bearing perpendicular to the grain
f_s'	characteristic strength in shear
f_t'	characteristic strength in tension
G^*	design self-weight
H	factor for the height of the TCC cross-section
h_c	thickness of the concrete member
h_t	depth (height) of the timber member
I_c	second moment of area (moment of inertia) of the concrete member
I_t	second moment of area (moment of inertia) of the timber member
j_2	stiffness modification factor – load duration
K_{eff}	connection (shear key) stiffness for design of the Service Limit State – long-term deflection
K_i	connection (shear key) stiffness
K_{ser}	connection (shear key) stiffness for design of the Service Limit State – short-term deflection
K_u	connection (shear key) stiffness for design of the Ultimate Limit State
k_1	shrinkage strain coefficient (concrete)
k_1	duration of load (timber)
k_2	creep factor coefficient (concrete)
k_3	maturity coefficient (concrete)
k_4	moisture condition (timber)
k_6	temperature (timber)
k_7	length and position of bearing (timber)
k_9	strength sharing between parallel members (timber)
k_{11}	size factor (timber)
k_{12}	stability factor (timber)
L	span of the structure

l_s	length of the horizontal shear plane (timber)
M^*	design action effect in bending
ϕM_u	design capacity in bending (concrete)
(ϕM)	design capacity in bending (timber)
N^*	design action effect produced by axial force
N_p^*	design action effect in bearing produced by reaction at a support
ϕN_u	design capacity in axial stress (concrete)
(ϕN)	design capacity in axial stress (timber)
(ϕN_j)	design capacity of the connection in shear
(ϕN_l)	design capacity in bearing parallel to the grain (timber)
(ϕN_p)	design capacity in bearing perpendicular to the grain (timber)
(ϕN_v)	design capacity in shear parallel to the grain (timber)
(ϕN_θ)	design capacity in bearing at an angle to the grain (timber)
P^*	design action for point load action (Service Limit State)
Q^*	design action effect in shear in the connection
$Q_{V_{L/4}}^*$	design action effect in shear in the connection (at $L / 4$)
$Q_{V_{\max}}^*$	design action effect in shear in the connection (at a support)
Q^*	design action for shear in the connection
Q_k	characteristic strength of the connection in shear
R_m	mean characteristic strength of the connection in shear (test data)
s_{ef}	factor for the connection spacing
s_{max}	distance of the first connector from mid-span
s_{min}	distance between the connectors (inside the external quarter-spans)
V^*	design action effect in flexural shear (also tangential shear)
$V_{L/4}^*$	design action effect in flexural shear (also tangential shear) at $L / 4$
V_{\max}^*	design action effect in flexural shear (also tangential shear) at a support
(ϕV)	design capacity in flexural shear (timber)

ϕV_{uc}	design capacity in shear (concrete)
W_{imp}^*	imposed design load(s)
$\beta_{1,2,3}$	coefficients (concrete)
Δ	deflection at mid-span
γ_c	partial factor for material properties of the concrete member
$\gamma_{c,lts}$	partial factor for material properties of the concrete member – long-term serviceability
γ_t	partial factor for material properties of the timber member
$\gamma_{t,lts}$	partial factor for material properties of the timber member – long-term serviceability
ε_{cs}	design shrinkage strain (concrete)
$\varepsilon_{cs,b}$	basic shrinkage strain (concrete)
$v_{0.4}$	mean slip of the connection measured at $0.4 R_m$ (test data)
$v_{0.6}$	mean slip of the connection measured at $0.6 R_m$ (test data)
ϕ	capacity factor
ϕ_{cc}	design creep factor (concrete)
$\phi_{cc,b}$	basic creep factor (concrete)
φ	creep coefficient (timber)
θ	angle of the notch facet under compression,
σ_b	effective bending stress
σ_c	effective compression stress
σ_t	effective tension stress

DEVELOPMENT OF DESIGN PROCEDURES FOR TIMBER CONCRETE COMPOSITE FLOORS IN AUSTRALIA AND NEW ZEALAND PART 2 – CONNECTION CHARACTERISATION

Prof Keith Crews, Dr Christophe Gerber & Dr Rijun Shestha

Centre for Built Infrastructure Research, University of Technology Sydney, Australia

1 Introduction

The approach adopted for design of timber concrete composite (TCC) floor systems in Australia and New Zealand is based upon extensive testing of the permitted connection types that are specified in the design procedures, identifying strength, serviceability stiffness and so called ultimate stiffness characteristic properties that are required for utilisation of the “Gamma coefficients” method, which manipulates properties of the concrete member in order to predict the cross-section characteristics of the structure. This paper presents an overview of testing undertaken to date and the derivation of characteristic properties (5th percentile for strength and 50th percentile or average for stiffness).

2 Background

An extensive (literature) review of shear connectors used in timber concrete composite structures, covering the period from 1985 to 2004, has been undertaken by Dias (2005). Elsewhere, Ceccotti (2002) also presents an overview of the timber-concrete connectors which are most commonly used to achieve composite action between the concrete and the timber members (Figure 1).

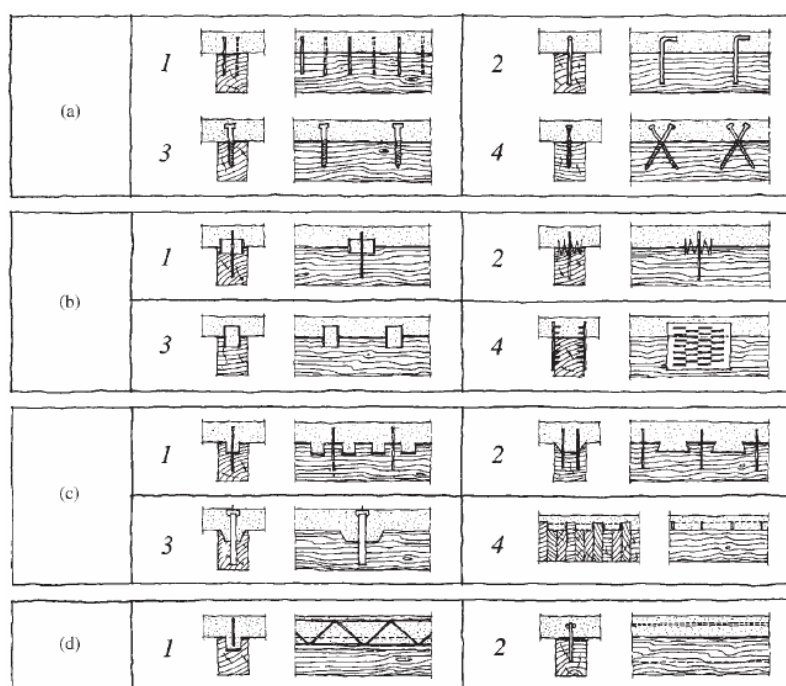


Figure 1 - Examples of TCC connections (Ceccotti 2002)

Notes on Figure 1:

(a1) nails; (a2) glued reinforced concrete steel bars; (a3, a4) screws; (b1, b2) connectors (split rings and toothed plates); (b3) steel tubes; (b4) steel punched metal plates; (c1) round indentations in timber, with fasteners preventing uplift; (c2) square indentations, with fasteners preventing uplift; (c3) cup indentation and prestressed steel bars; (c4) nailed timber planks deck and steel shear plates slotted through the deeper timber planks; (d1) steel lattice glued to timber; (d2) steel plate glued to timber.

The stiffness characteristics of some the shear connectors presented in Figure 1 are plotted in Figure 2. The load-slip plot in Figure 2 indicates that for this group of connector types, the stiffest connections are those in group (d), while the least stiff are in group (a). Connections in groups (a), (b) and (c) allow relative slip between the timber element and the concrete member, that is, the cross-sections do not remain planar under load – and the strain distribution is not continuously linear in the composite cross-section. Only connections in group (d) exhibit a planar behaviour, corresponding thus to fully composite action between timber member and the concrete slab. It can be assumed that TCC structures assembled with connectors from group (a) achieve 50% of the effective bending stiffness of TTC systems constructed with connectors from group (d) Ceccotti (1995).

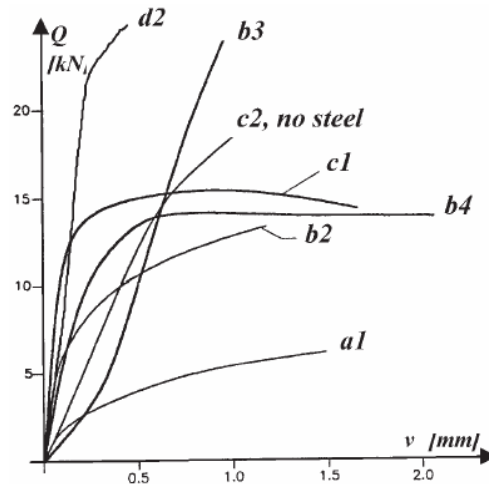


Figure 2 - Schematic of load-slip behaviour of types of connection (Ceccotti 2002)

3 Scope of Testing Program

An extensive experimental investigation has been carried out on shear connections for TCC floors using small scale specimens. The tested connections have been developed over a period of time between 2007 and 2010 and therefore the experimental investigations involved a number series of tests and have been divided more appropriately into different test phases. Experimental study in each phase looked at different connection type which was either an improvement over a preceding test series or investigation on completely new connection type. Details and results for each of the phase are presented elsewhere (Shestha et al 2010).

A number of different types of shear connections were fabricated and tested, including:

1. Nail plates
2. Nail plates with wood screws
3. Nail plates with notch
4. Square notch (with and without coach bolts)
5. Trapezoidal notch (with and without coach bolts)

6. Bird mouth notch (with and without coach bolts)
7. Batten
8. Tri-angled notch (with and without coach bolts)

Typical details for the bird's mouth notched connection are shown in Figure 3.

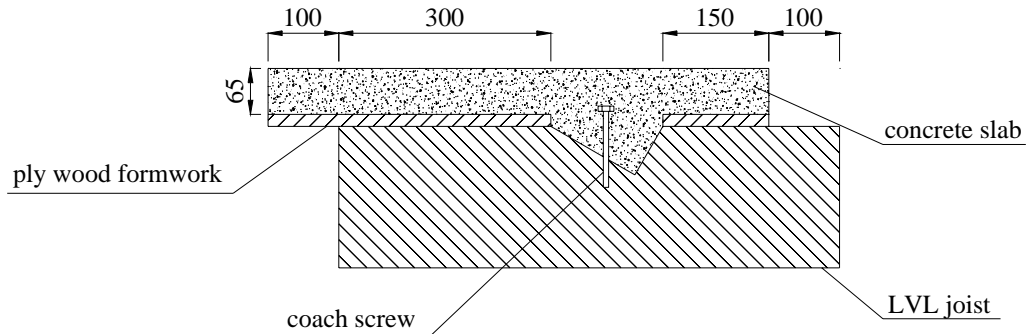


Figure 3- Typical geometry and components of a bird's-mouth shear connection

Analysis of the results from these tests led to the conclusion that the most promising connection types were the trapezoidal and bird's mouth notched connections, with coach bolts. Subsequently, a further study of 100 connections was undertaken in 2010, details of which are summarised graphically in Figure 4.

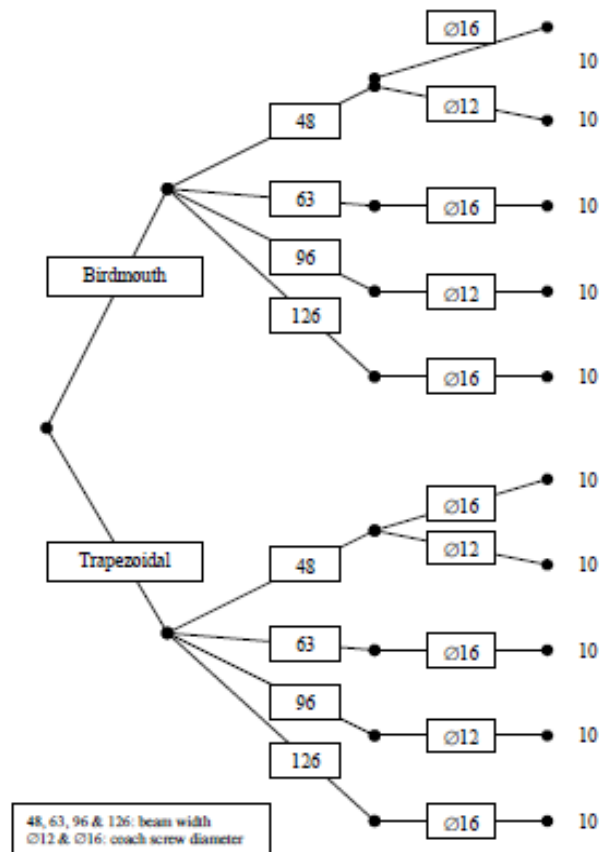


Figure 4- Overview of 2010 research plan for notched connections

Analysis of the test results for this final series of tests has led to the development of the characteristic design properties presented in Part 1 of this paper.

4 Testing Protocol

There are two types of tests that are normally used to study the properties of shear connection and to verify analytical and/or numerical models excluding the consideration of withdrawal test for a dowel-type connection – the shear test and the bending test. The shear test (also called slip test or push out test) can have two types of configurations – either symmetrical or asymmetrical. The asymmetrical configuration has the merits of saving time and cost as concrete is cast on one side of timber beam only. However, there can be an overestimation of strength and stiffness of the connection tested due to the reaction that tends to close any gap that is caused by an eccentric loading force (van der Linden 1999). This can be minimised by appropriate restraint of the specimen to ensure that any eccentric effects are negligible.

The tests on all shear connections in the current study were carried out using an asymmetrical push out test and details of the test rig and setup are presented in Figure 5.

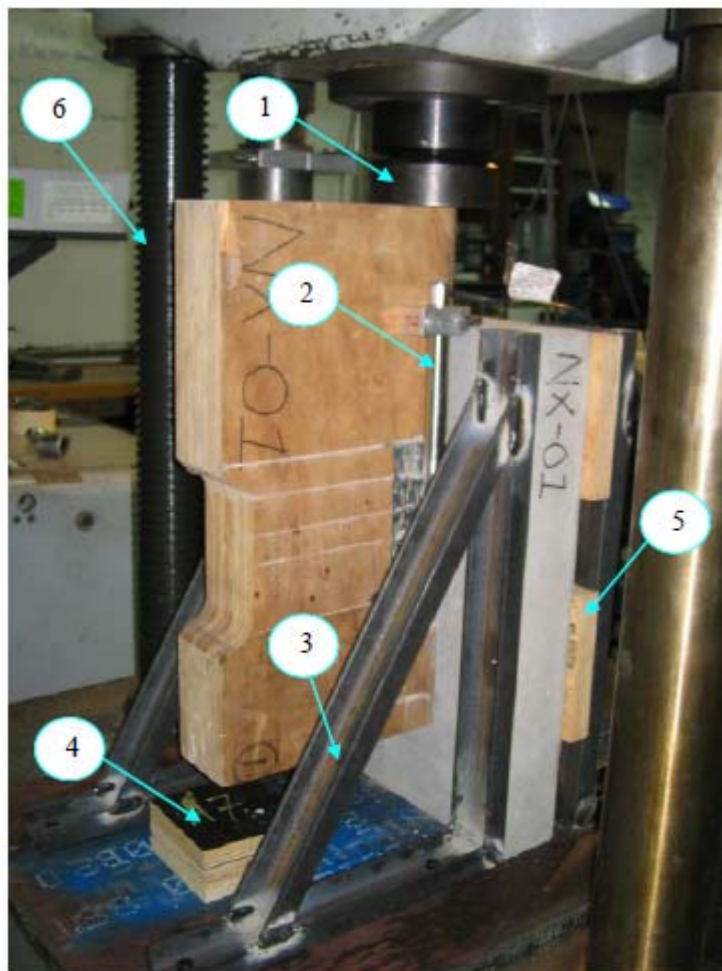


Figure 5 - Setup of a test specimen in the test rig

Notes

1. Spherical seating for loading – top edges were aligned to negate any eccentricity
2. Two LVDTs were screwed onto both sides of the LVL.
3. Steel test rig
4. Several ply boards were placed underneath the LVL to prevent it from causing any damage during the collapse of the specimen.
5. Timber blocks were used to secure the specimen in position during loading.
6. Screw column

**INTERNATIONAL COUNCIL FOR RESEARCH AND INNOVATION
IN BUILDING AND CONSTRUCTION**

WORKING COMMISSION W18 - TIMBER STRUCTURES

**FAILURE BEHAVIOUR AND RESISTANCE OF DOWEL-TYPE
CONNECTIONS LOADED PERPENDICULAR TO GRAIN**

B Franke

P Quenneville

University of Auckland

NEW ZEALAND

MEETING FORTY THREE

NELSON

NEW ZEALAND

AUGUST 2010

Presented by P Quenneville

A Jorissen: Is there still splitting at $a/h = 0.7$? P Quenneville: there could be. Model gives proper load-slip curve and failure criterion is used (first occurrence of splitting or 5% offset).

R Crocetti: Laboratory results may be simulated, but in practice this type of connection should be avoided. P Quenneville: Reinforcement will be avoided due to cost.

T Tannert: Numerical study is 2D. What would be the influence of 3D? P Quenneville: 3D would be more favourable to a ductile behaviour.

R Görlacher: Have you compared results to the C1B- paper of 1989? B Franke: No, comparison was to code equations.

M Yasumura: What is the failure criterion? B Franke: failure (in splitting) is maximum load when crack becomes unstable.

L Daziel: here Steel-Wood-Steel connection is shown, in practice Steel-Wood is often used. What will be the influence? P Quenneville: Possible embedment and 3D model would be needed.

A Palermo: How did you verify the model for the cohesive part? B Franke: No calibration was carried out, average values for Canadian glulam code were used.

A Manoorchehr: What was the thickness of the cohesive elements? B Franke: no thickness at all.

P Schädle: which element type was used? B Franke: Element no.174 in ANSYS.

Failure behaviour and resistance of dowel-type connections loaded perpendicular to grain

Bettina Franke, Pierre Quenneville
University of Auckland, New Zealand

1 Introduction

The load capacity of mechanical connections loaded perpendicular to grain is limited by either a brittle failure, such as splitting of the wood, or ductile failure behaviour, such as the bending of the fasteners and/or the embedding or bearing failure of the wood under the fastener. Most international design standards predict the ductile failure using the accepted European Yield Model (EYM) with good accuracy. However, different design equations are used for the prediction of the splitting failure of the wood. These are, on the one hand, the design equations in the EN 1995-1-1:2004 based on the fracture mechanics and on the other hand, the German design equations in the DIN 1052:2008 based on a strength criterion.

Experimental test series are traditionally used to investigate the load capacities and to develop design concepts. A further option is to use numerical simulations of the failure behaviour of connections. A numerical model developed was used to investigate the non-linear behaviour including the ductile and brittle failure of dowelled connections loaded perpendicular-to-grain with different geometry layouts. The numerical results reached show that important parameters change the load capacities, the stress-strain distribution and the failure behaviour of the connection. The comparison of the numerical load capacities with the EN 1995-1-1:2004 shows that connection parameters such as number of rows and columns or the connection width are not considered. The investigation of these different parameters presented in this paper shows at this stage potential to improve the design methods.

2 Numerical test series

2.1 Numerical model

A 2-dimensional numerical model for the prediction of the load capacity for steel wood steel dowel type connections was developed. The objective was the simulation of a realistic failure behaviour which includes the ductile and splitting failure of the wood member. Therefore the important material definitions used will be explained, where further details of the modelling process are described in [7]. In the numerical simulations, the

4.1 Loading procedure

The loading procedure in European Standard EN26891 described by Dias (2005) and shown in Figure 6 was closely adopted for all tests. The load is applied in following steps.

1. The load is applied until about 40% of the estimated failure load. This stage is normally completed in about two minutes.
2. The load is maintained at this intensity (about 40% of the estimated failure load) for about 30 seconds.
3. The load is released until about 10% of the estimated failure load. This stage aims to last about one and a half minute.
4. The load is maintained at about 10% of the estimated failure load for some 30 seconds.
5. The load is (re-)applied until failure of the specimen. The loading rate should be close to the initial loading rate.

The reason for loading in this way was to eliminate any internal friction in the connections. This is essential to ensure that when the specimen is tested to failure, it does not fail due to initial slip or slack in the connection. A typical test would take approximately 10-15 minutes (600-900 seconds) to complete.

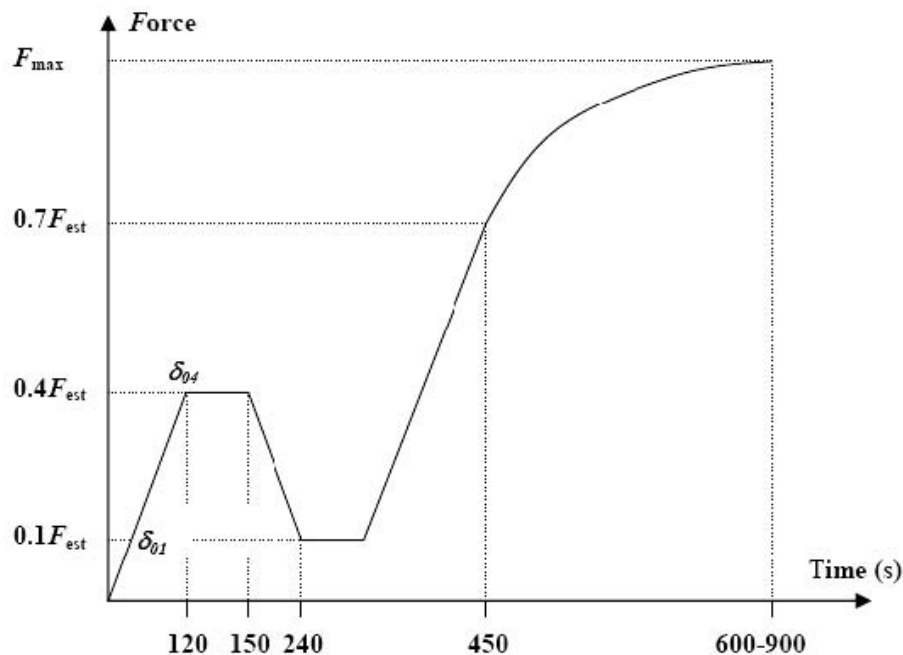


Figure 6 - Loading regime as per EN 26891 (BSI - 1991)

4.2 Test criteria

The behaviour and effectiveness of the tested shear connections were assessed based on their strength (failure load or maximum load), stiffness and failure mode. The strength of the connection specimens was defined as the maximum load that can be applied in the push-out tests before failure. Depending upon the failure mode, the connection specimens may have some load carrying capacity following the maximum load resulting in a ductile behaviour. The failure modes were therefore carefully documented in all tests. The connection stiffness or slip modulus, which represents the resistance to the relative displacement between the timber joist and the concrete slab, is one of the key parameters that define the efficiency of a shear connection. Stiffness for the serviceability limit state (SLS) and ultimate limit state

(ULS) are essential to characterise a shear connection. The stiffness for SLS (K_{ser}) corresponds to the inclination of the load-slip curve between the loading start point (generally taken as 10% of failure load to overcome “settling in”) and the 40% of the failure load. The stiffness for ULS (K_u) corresponds to the inclination of the load-slip curve between the loading start point and the 60% of the failure load. As a general rule, it can be assumed that $K_u = (2/3) K_{ser}$.

5 Test Results

The main results for both connection types (which are described schematically in Figure 7), are presented in Table 1.

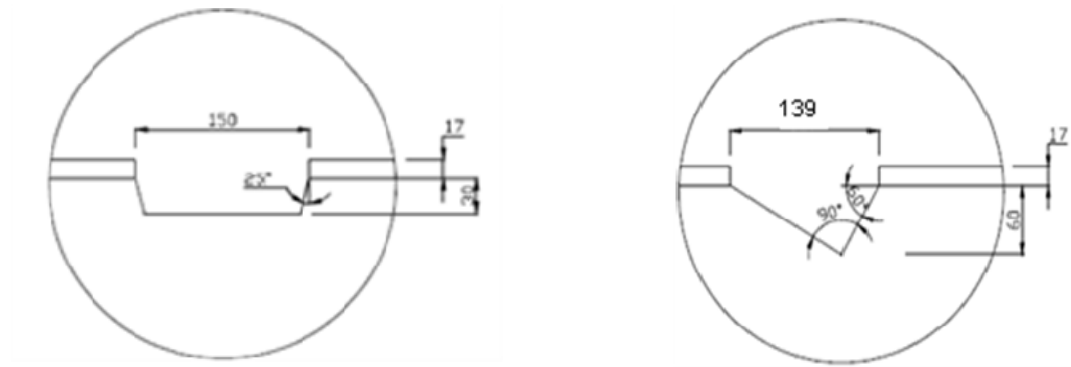


Figure 7 - Connections T3 (left) & B3 (right) – 63mm thick LVL with 16mm coach screw

TABLE 1 – Characteristic Properties of Connectors

Connection Description	Strength Q_k (kN)	K_{serv} (kN/mm)	K_u (kN/mm)
T1 – 48mm LVL, 16mm bolt	46 – 8.7%	87 – 20.5%	60 – 13.0%
T2 – 48mm LVL, 12mm bolt	46 – 6.6%	106 – 15.0%	87 – 17.9%
T3 – 63mm LVL, 16mm bolt	78 – 6.4%	109 – 19.3%	81 – 24.7%
T4 – 96mm LVL, 12mm bolt	89 – 10.0%	110 – 34.8%	93 – 39.3%
T5 – 126mm LVL, 16mm bolt	134 – 4.8%	124 – 41.3%	103 – 30.2%
B1 – 48mm LVL, 16mm bolt	55 – 8.1%	37 – 12.4%	36 – 15.2%
B2 – 48mm LVL, 12mm bolt	51 – 8.4%	115 – 48.4%	46 – 54.0%
B3 – 63mm LVL, 16mm bolt	66 – 7.7%	98 – 12.9%	74 – 27.7%
B4 – 96mm LVL, 12mm bolt	91 – 5.5%	156 – 19.8%	119 – 20.8%
B5 – 126mm LVL, 16mm bolt	120 – 11.6%	213 – 34.2%	150 – 22.7%

NOTES:

- integer = capacity; % = CoV
- Strength – 5th percentile based on a log normal distribution
- Stiffness – 50th percentile

6 Conclusions

A number of shear connections have been tested using push-out tests on full scale specimens and load-deflection plots and stiffness for these connections have been determined. Parameters such as the type of connector, shape of notches, use of mechanical anchors and concrete properties have been investigated and analysis of this data has led to number of conclusions.

- Early research showed that use of nail plates alone as shear connectors did not prove to be effective, whilst a combination of nail plates with either screws or concrete notches was more effective - especially incorporation of concrete notches.
- A number of concrete notch type shear connections were then tested such as trapezoidal, bird-mouth type and tri-angled notch and parameters such as slant angle, use of either coach screw or normal wood screw as mechanical fastener, inclination of the mechanical fastener, inclination of the slanting face and use of low shrinkage concrete were studied.
- Use of coach screws has the advantage of deeper penetration depth inside the concrete slab in comparison to normal wood screws due to their longer length. This resulted in a single coach screw providing higher shear capacity than a combination of four wood screws.
- Interesting results were obtained from the bird-mouth type connections as these connections generally exhibited higher strength and stiffness than the trapezoidal notch connections and especially so for bird-mouth connections using 70-20 and 60-30 angle combinations.
- Tri-angled notch connections were also found to be superior to the trapezoidal notch connections, however, the complex angle sequence makes such connections difficult to fabricate.
- On the other hand, bird-mouth type connections are much easier to fabricate with a simple cutting sequence and do not need special tools for fabrication. Use of a slanted coach screw configuration in the bird-mouth notch connections provided higher stiffness; however, the effect on characteristic strength was not significant, while steel plate placed on top of the coach screw did not provide any additional strength or stiffness. It should however be noted that the coach screws in the bird-mouth notch provided only limited post peak plastic behaviour when compared to trapezoidal notch connections.
- The depth of the notch has a significant effect on both the stiffness and strength of the connections. Connections with 60 mm deep notch had superior strength and stiffness compared to the connections with 90 mm deep notch. Test results also showed that widening the slot dimension had a positive effect on strength and stiffness of the connections.
- The effect of the ratio of coach screw diameter to LVL thickness is one of the parameters that needs to be further investigated. Table 1 highlights the effect of the ratio of coach screw diameter to LVL thickness and suggests that there is no advantage to using 16mm diameter screws in 48mm thick LVL beams

Whilst the variability of maximum load (strength) is considered to be acceptable, the variability of the characteristic stiffness properties highlights some of the uncertainty that is inherent in the performance of notched connections for TCC constructions. It is proposed to use the data generated to date, to refine connection performance and attempt to reduce that stiffness variability to lower levels that could lead to more efficient design of these type of floor structures.

7 References

Ceccotti, A. (1995) *Timber-concrete composite structures*, in Timber Engineering – STEP 2, H. J. Blass, P. Aune, B. S. Choo, R. Görlacher, D. R. Griffiths, B. O. Hilson, P. Racher, and G. Steck, Eds. Almere, The Netherlands: Centrum Hout.

Ceccotti, A. (2002) “Composite concrete-timber structures”, *Progress in Structural Engineering and Materials*, vol. 4, pp. 264-275.

Dias, A. M. P. G. (2005) *Mechanical behaviour of timber-concrete joints*, Technical University Delft.

Shestha, R; Crews, K; Gerber, C (2010) *Characterisation of Shear Connections for TCC Floors – Compendium Report – STIC Report 2010-05 – University of Technology Sydney*

Van der Linden, M. L. R. (1999), *Timber concrete composite floor systems*, PhD Thesis, Technical University Delft.

material behaviour of the wood is assumed as orthogonal anisotropic. Nine independent elastic constants define the element stiffness matrix of wood in the numerical solution. The description of the orthotropic material used does not include a strain or displacement interconnection and considers no influence of the temperature.

For the numerical simulation of the ductile failure behaviour under compression perpendicular to grain, a bilinear elastic plastic material behaviour with hardening after yielding is used. The material law goes back to the generalized anisotropic Hill potential theory and a modified von Mises yield criterion, [1]. The material behaviour is described by the tensile and compressive stress-strain curves in the three orthogonal directions and the shear stress-strain curves in the corresponding planes.

For the brittle failure including the crack initiation and crack propagation, the contact technology corresponding to a defined cohesive zone material was used. This technique directly uses fracture mechanism methods by adopting softening relationships for tension stress perpendicular to grain and shear stress depending on the critical fracture energy, [1]. The cohesive zone material used, considers the single fracture modes I or II as well as the mixed mode using a quadratic fracture criteria. It is characterised by the tensile strength perpendicular to grain $f_{t,90}$, the shear strength f_s , the contact stiffness K and the critical fracture energies \mathcal{G}_c^I or \mathcal{G}_c^{II} .

2.2 Reference solutions for the numerical model

The results for a dowel type connection with 2 rows and 3 columns are presented in this section. According to the experimental test series by Reshke [11], the specimen sizes are $b = 80$ mm, $h = 190$ mm and $l = 620$ mm. The connection is located at midspan of the beam with a loaded edge distance of $h_e = 133$ mm, a connection height of $a_c = 57$ mm and width of $a_r = 175$ mm. The variables are defined as shown in Figure 1.

The material axes are orientated according to the Canadian spruce glulam material used in the test series, so that the model describes a RL-crack system. The contact element pairs are predefined in layers in the assumed crack directions of the numerical model. With regards to the cellular structure of the wood, the crack growth direction of dowel-type connections loaded perpendicular to grain is in parallel direction and at the height of the dowel centre. The dowels and support plates were modelled explicitly as steel components using a linear elastic material description. The contact between the wood and the steel parts is considered by friction. To respect the natural character of the material wood in the simulation, the parameters are probabilistically uniformly distributed. The range of the probabilistic values is assumed at about ± 30 % of the mean values from Table 1.

The comparison of the numerical solution with the mean value describes the main failure behaviour of these connections, as shown in Figure 1: Defined variables of a 3 by 2 dowel-type connection loaded perpendicular to grain and Figure 3. A statistical analysis of the results shows, that after 30 probabilistic loops, the average value of the load capacities

Table 1: Material properties for Canadian Spruce Glulam, mean values [8], [10], [13]

Modulus of Elasticity	$E_L = 10000 \text{ N/mm}^2$	$E_R = 350 \text{ N/mm}^2$	$E_T = 350 \text{ N/mm}^2$
Rigid modulus	$G_{LR} = 410 \text{ N/mm}^2$	$G_{LT} = 410 \text{ N/mm}^2$	
Strength	$f_{c,90} = 4.5 \text{ N/mm}^2$	$f_{t,90} = 2.0 \text{ N/mm}^2$	$f_s = 4.0 \text{ N/mm}^2$
Fracture Energy	$\mathcal{G}_c^I = 0.225 \text{ Nm/mm}^2$	$\mathcal{G}_c^{II} = 0.650 \text{ Nm/mm}^2$	

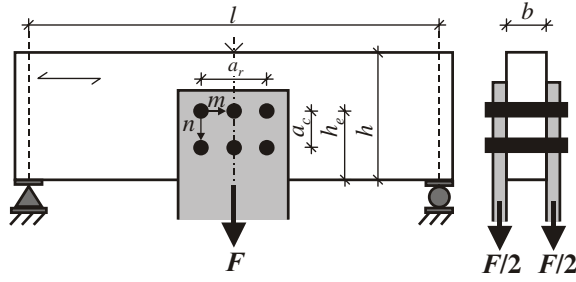


Figure 1: Defined variables of a 3 by 2 dowel-type connection loaded perpendicular to grain

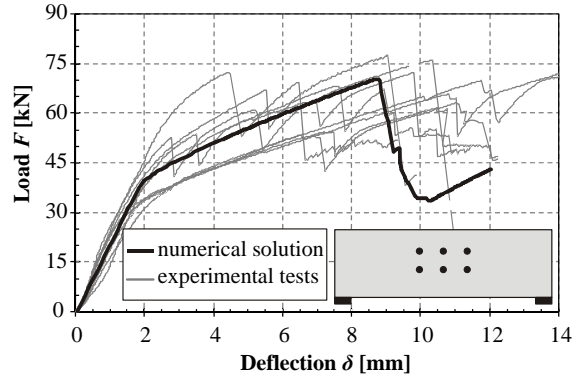


Figure 2: Comparison of experimental test series observed with the numerical solution, mean values

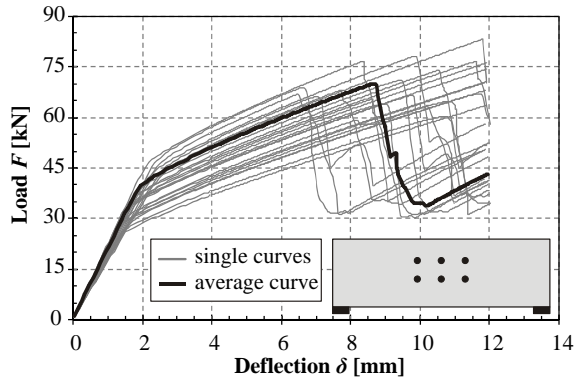


Figure 3: Numerical results for the probabilistic distributed material parameters and the mean values

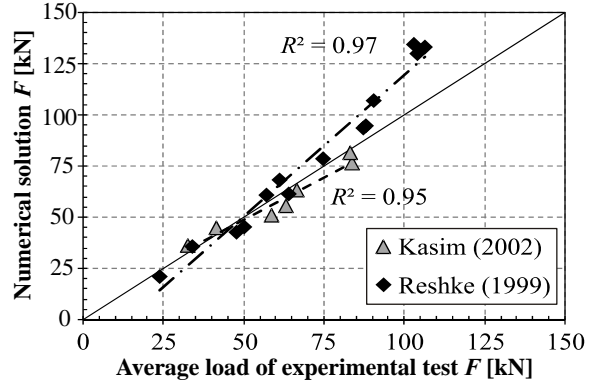


Figure 4: Correlation between numerical loads obtained and experimental test series

reaches a constant level. A further increase of the number of loops of the probabilistic distributed numerical solution does not change the results.

In further numerical solutions, 21 other different connections identical to the ones tested by Reshke [11] and Kasim [9] were modelled in the same way and compared, as shown in Figure 4. The steel-wood-steel dowel type connections vary in the number of rows and columns of dowels as well as the loaded edge distance and the connection width. The correlation between the numerical load capacity reached and the experimental tests observed confirms a good accuracy of the numerical predictions of the failure loads.

2.3 Numerical test series

The numerical model presented allows the extension of experimental test series easily or to investigate important geometry parameters of connections. Based on experimental tests, [9], [11] the loaded edge distances h_e , the connection width a_r , the number of rows n and columns m as well as the position of the dowel along the span were investigated. The parameters of the numerical test series are summarized in Table 2. For all numerical test series, the dowel diameter was constant at 19 mm. The mechanical parameters are based on Canadian glulam, Table 1. For each numerical test series were solved 30 different numerical solutions with uniform probabilistic distributed material parameters to respect the natural distribution of the material wood. The same range of the probabilistic distribution was assumed at about $\pm 30\%$ of each average values from Table 1.

Table 2: Geometry parameters of the numerical test series

Test group	Description	Specimen size $b / h / l$ [mm]	Connection layout		
			$m \times n$	h_e/h [mm]	a_r [mm]
A	loaded edge distance	80/190/610	1 x 1	0.2, 0.4, 0.5,	-
			2 x 1	0.6, 0.7, 0.8	$4d$
B	connection width	80/190/(a_r+8h)	2 x 1	0.2, 0.4, 0.6, 0.7, 0.8	$3d, 4d, 6d, 8d,$ $10d, 15d, 20d,$
C	position of dowel $l_r = (0, 10, 50, 100, 150, 200)$ mm	80/190/610	1 x 1	0.4	-
D	increasing number of rows	80/304/1320	1, 2, 3, 4 x 1, 2, 3	0.44, 0.7	$19d$
E	increasing number of columns	80/304/1320	2, 3, 4 x 1, 2, 3	0.44, 0.7	$19d$

3 Analyses of the load capacities and the failure behaviour

3.1 Load capacities

For each load deflection curve of the 30 numerical solution loops of one test series, the crack initial load, the splitting load and the ductile load were evaluated. The crack initial load corresponds to the crack initiation at the dowels. The splitting load capacity is associated with the maximum load before the first main unstable failure occurs together with a load drop. The ductile load is calculated with the commonly used 5 % offset method, [2]. The ultimate load capacity of the connection is determined depending on which failure occurs at first, the splitting or the ductile failure. The splitting load capacity of a dowel-type connection in wood loaded perpendicular to grain depends mainly on the loaded edge distance h_e , the connection width a_r and the number of rows n or columns m of dowels parallel or perpendicular to grain. The numerical investigation shows, that the load capacity is independent of the position of the connection along the span of the beam, [7]. The diagrams in section 5 show the effect of different parameters using relative load capacities, i.e. for each test group the relative load capacity is determined with the average value of the splitting load capacity for the smallest dependent parameter of this series.

3.2 Investigation of the shear and tension stress perpendicular to grain

For the numerical test series where the position of the connection changes within the span of the member, the stress perpendicular to grain and the shear stress were investigated. Moving the connection in the direction of the support results in a change of the internal structural forces, i.e. a change of the ratio between the shear force and moment. This change of the structural forces has no effect on the splitting load capacity of the connection. The same could be observed for the stress distributions beside the dowel as shown in Figure 5 to Figure 8. For each movement of the connection, the transverse tension stress and the shear stress were plotted onto paths over the complete beam depth at a constant load of $F = 15$ kN. The paths are located on each side of the dowel with a distance of 10 mm and 50 mm to the dowel edge. It shows almost the same stress distribution for each connection before reaching the maximum load capacity.

Each of the following figures includes the investigated positions of the connection between mid position $l_r = 0$ mm and a total moved distance of $l_r = 200$ mm. The stress perpendicular to grain and the shear stress distribution are in a very close range. The stress distribution for a distance of 10 mm beside the dowel show the influence of the dowel to the transverse stress and shear stress distributions over the beam depth. The effect of

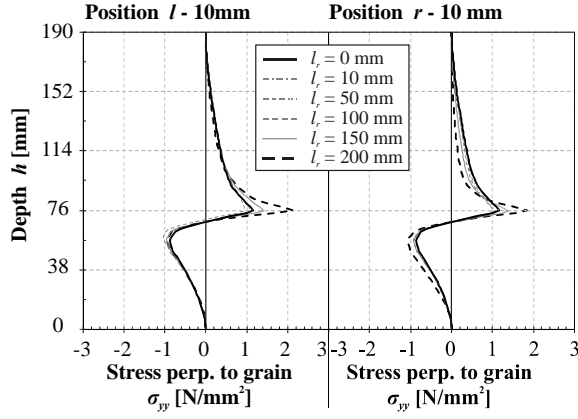


Figure 5: Transverse stress distribution over the beam depth at a distance of 10 mm

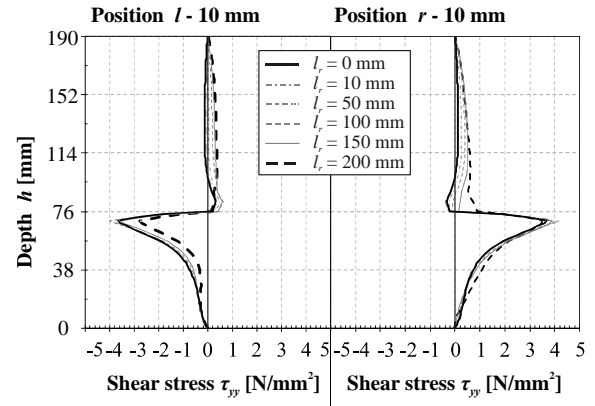


Figure 6: Shear stress distribution over the beam depth at a distance of 10 mm

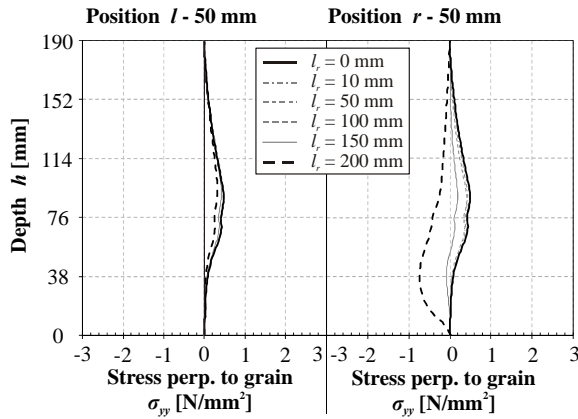


Figure 7: Transverse stress distribution over the beam depth at a distance of 50 mm

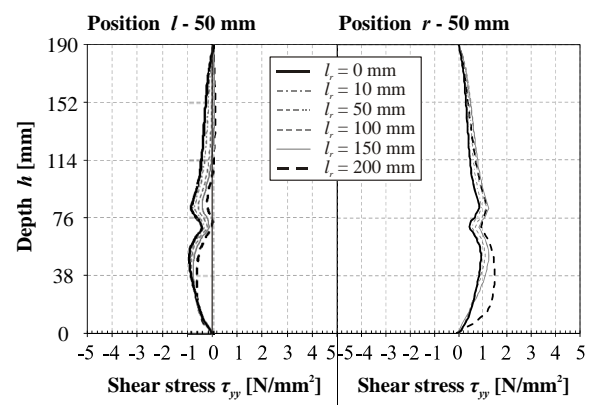


Figure 8: Shear stress distribution over the beam depth at a distance of 50 mm

disturbance is symmetric to each sides of the dowel. At a distance of 50 mm, the curves show nearly the typical distribution over the beam depth. The influence of the disturbance of the dowel is nearly abated. The curves for the stress perpendicular to grain in a distance of 50 mm on the right side of the dowel show more differences for the greater distance l_r . This includes the influence of the prevailing bearing compression stress above the support area.

3.3 Failure behaviour of multiple dowel connections

Multiple dowel connections are one of the standard connections with mechanical fasteners in timber constructions. What happens in the connection when the number of rows or the number of dowels increases per row? These effects were investigated for two different loaded edge distances in the test group D and E (Table 2). At first, the distribution of the load per row was determined at failure of the connection with a first load drop. At this situation, the splitting load capacity of the connection was determined as well. Figure 9 shows the distribution over the displacement of the relative load capacities for the first and second row of different connection layouts, which all have 2 rows in total and a loaded edge distance of $h_e/h = 0.44$. At failure, each row carries the same load proportion of the total load capacity. The summary of all investigated connection layouts shows that at failure, each row always carries the same load proportion of the total load capacity, as shown in Figure 10.

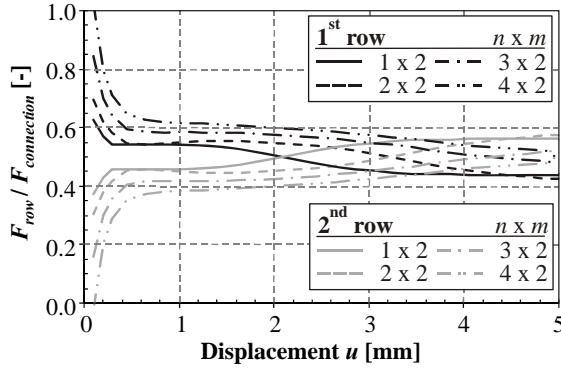


Figure 9: Load capacity of the 1st and 2nd row over the displacement for the test series with a loaded edge distance of $h_e/h = 0.44$

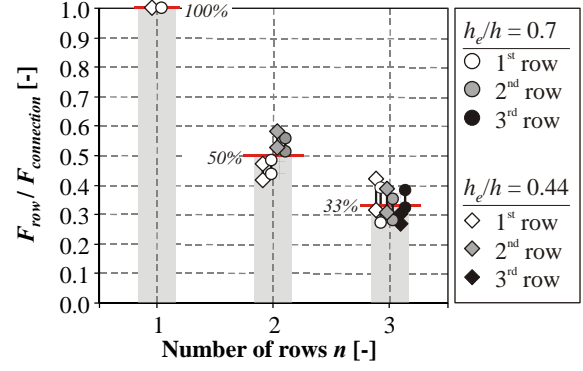


Figure 10: Proportions of the load capacity per row for all test series with 1 to 3 rows and different loaded edge distances

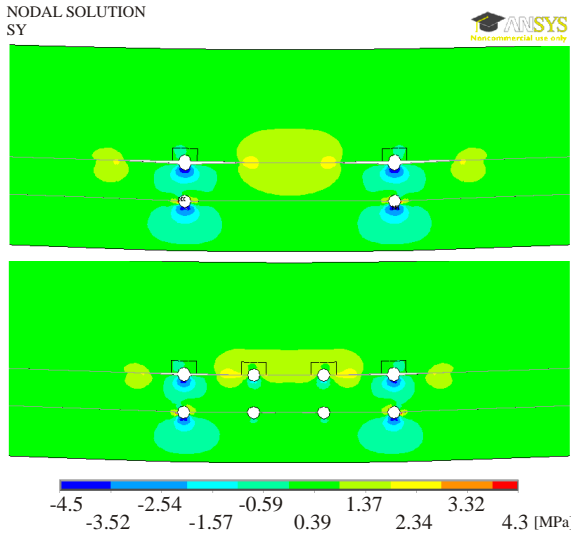


Figure 11: Transverse stress distribution for a connection with 2 columns and 4 columns at a displacement of $u = 4.85$ mm

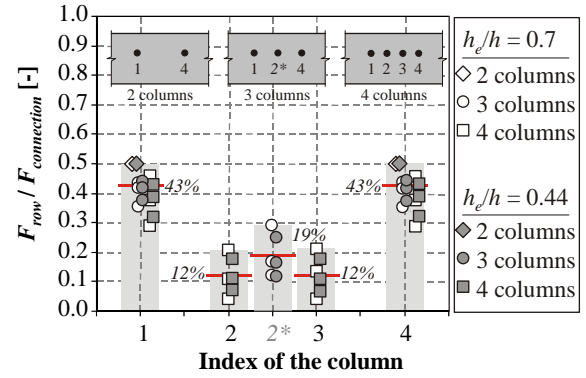


Figure 12: Proportions of the load capacities per column for all test series with 2 to 4 columns and different loaded edge distances

In a further step, the effect of the increase of the number of columns on the failure load of connections was investigated. Figure 11 shows the transverse stress distribution for a connection with 2 and 4 columns. The increase of the number of columns per connections reduces the main tension stress perpendicular to grain besides the outer columns of the connections as well as the crack propagation. The proportions of the load capacities of the number of columns are summarized in Figure 12. The results show that the connection load distribution over the number of columns is not equal. The inner columns carry a lower proportion of the total load capacity.

4 Comparison with design standards

For the comparison of the numerical predictions with the design standards, the two main concepts were used. These are on the one hand, the concept of the European design standard EN 1995-1-1:2004 which is based on fracture mechanics methods and was introduced by v. d. Put and Leijten [12], and on the other hand, the concept of the German design standard DIN 1052:2008 which is based on a strength criterion and was introduced by Ehlbeck, Görlacher and Werner [5]. Figure 13 and Figure 14 show the comparison of the numerical splitting load capacities obtained with the capacities determined using the

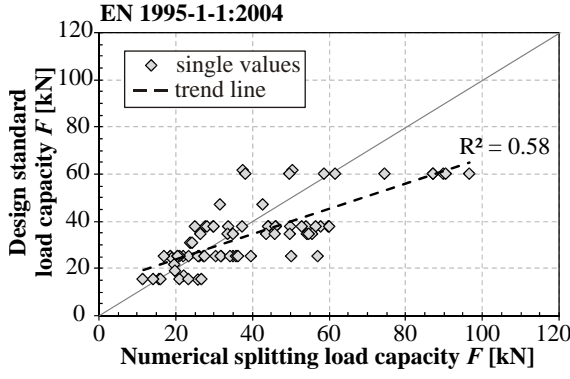


Figure 13: Comparison with the Eurocode design standard EN 1995-1-1:2004

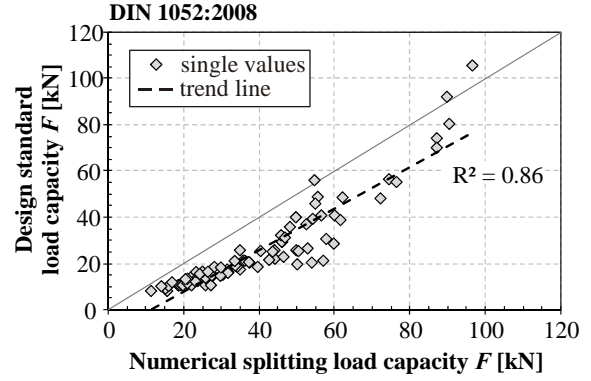


Figure 14: Comparison with the German design standard DIN1052:2008

design equations. The 5-percentile values of the numerical splitting load capacities were calculated and used to compare with the characteristic design values obtained using the equation in the European standard. For the German standard, the characteristic strength $f_{t,90,c} = 0.51$ MPa was used as valid for Canadian spruce glulam, [3]. The connection was assumed as a double shear connection with thick outer steel plates.

As shown in Figure 13 the distribution of the European design standard shows clearly visible constant levels of the design load against the increase of the numerical results. These are caused by the inability of the equation to consider the effect of the connection width, the number of rows parallel to grain and the number of columns perpendicular to grain. In some cases, the designed load capacity increase more than the numerical load and lies on the unsafe side (above the diagonal). As shown in Figure 14 the more comprehensive German design standard reflects the numerical splitting load capacities with a good accuracy and a better correlation. This design equation considers the connection width and the number of rows in addition to the loaded edge distance.

5 Discussion

Detailed investigations of the different effects on the load capacities and the design equations lead to the following relation between the failure behaviour and the design standards, as shown in Figure 15 to Figure 18. For the comparison, the relative load capacity, which is defined as the ratio between the current value and the reference value (the smallest parameter of the test group investigated), is used.

The trend of the effect of the loaded edge distance is respected in both design concepts, whereas the German method predicts the results in average very well, as shown in Figure 15.

As mentioned before, only the German design standard considers the number of rows and the connection width using separate multiplication factors. The factor k_s in equation (1) considers the connection width a_r , but also k_g in equation (2) respects the connection width, which is in this case specifically valid for a 2 dowel connection. The variable l_g is in general the distance between the centres of the connection groups, but for a connection with 2 dowels, $l_g = a_r$. Depending on the current connection width, the factor k_s or k_g is to be used for the design load, which is represented by the two curves in Figure 16 for connections with 2 dowels. The two curves cover mostly the main behaviour of the numerical test results observed for the test group B with 2 dowels. For the cases presented,

the constant load level seems to occur already at a distance of $a_r = 15d \approx 1.5h$ and reaches a level of 1.8.

$$k_s = \max \begin{cases} 1 \\ 0.7 + \frac{1.4 \cdot a_r}{h} \end{cases} \quad (1)$$

$$k_g = \begin{cases} 1 & l_g < 0.5h \\ 2 \left(\frac{l_g}{4h} + 0.5 \right) & \text{for } 0.5h \leq l_g \leq 2h \\ 2 & l_g > 2h \end{cases} \quad (2)$$

The factor k_r in equation (3) increase the load capacity with increasing number of rows. It depends on the loaded edge distance as well as on the distance between the rows. For the investigation in the test group D, a second and third row with a constant spacing were added below the first row, thus the loaded edge distance is kept constant. Furthermore two loaded edge distances and different number of dowels per row were considered. The comparison of the row effect shows that the increase of the factor k_r is higher than the increase of the numerical test results, as shown in Figure 17. In a first step, two adjusted curves are added to the diagrams. The two curves, valid for the two cases presented, reflect the numerical results and depend linearly on the number of rows.

$$k_r = \frac{n}{\sum_{i=1}^n (h_i/h_i)^2} \quad (3)$$

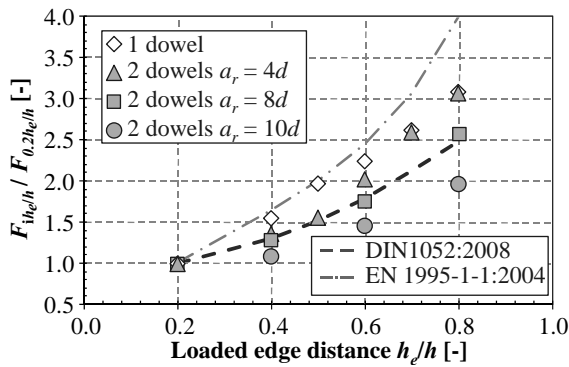


Figure 15: Effect of the loaded edge distance h_e

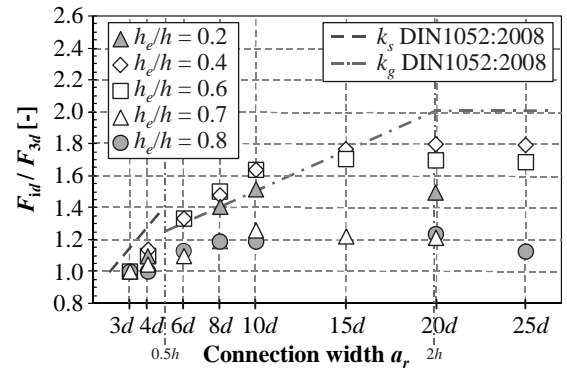


Figure 16: Effect of the connection width a_r and the curves of the factors k_s and k_g

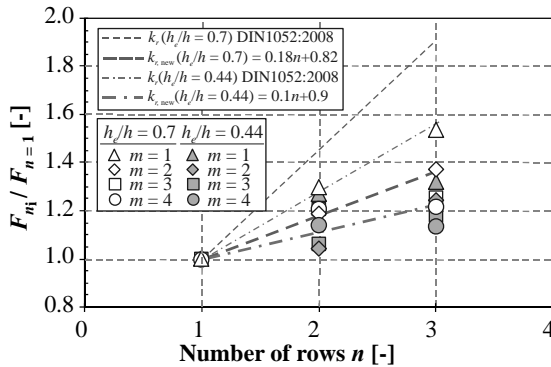


Figure 17: Effect of the number of rows n and the curves of the factor k_r

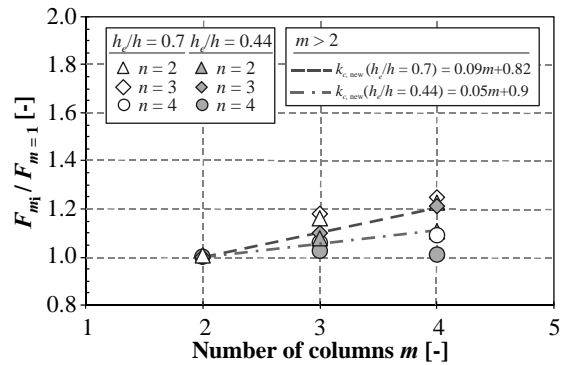


Figure 18: Effect of the number of columns m and trend curves for the two loaded edge distances

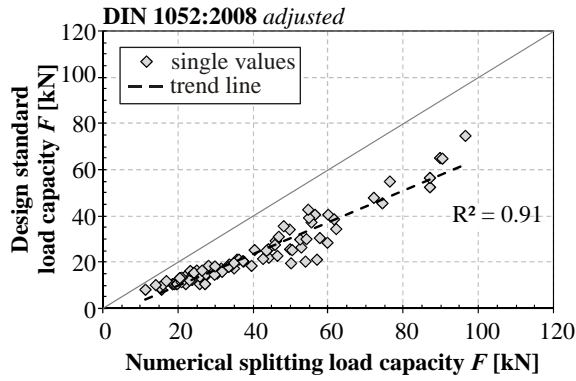


Figure 19: Comparison with the German design standard using the adjusted factors

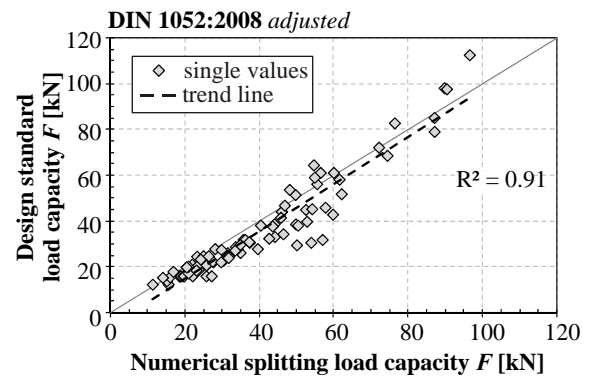


Figure 20: Comparison with the German design standard using the adjusted factors and the calibration factor

Figure 18 shows the effect of the number of columns in a connection on the load capacity. In test group E (Table 2), the connection width was always constant, but the number of columns was increased. A lesser influence on the load capacity could be observed. It seems that the effect also depends on the loaded edge distance, but before introducing an additional factor to the design equation, further investigation is needed.

In a first step, the proposed factors for the row effect are used for the prediction of the load capacities for all test groups. The comparison shows that predictions of the overestimated configurations could be decreased and the final correlation improved, as shown in Figure 19. To further increase the adequacy of the predictions of the trend, a calibration factor ($k = 1.5$) is proposed. The effect of this factor is simply to displace the trend and not the variability of the predictions, as shown in Figure 20.

6 Conclusion

The results show that the German design standard DIN 1052:2008 respect the most important parameters and shows a good agreement with the load capacities reached in the numerical test series and experimental test results. The use of the European design standard EN 1995-1-1:2004 for the prediction of the load capacity of dowel type connections loaded perpendicular to grain should be used very carefully because the effect of important parameters are not taken into account and in some case the load capacities were over predicted.

The German design standard can be improved through calibration of the factors k_s , k_g and k_r which respect the connection width or the number of rows or by introducing a factor taking into account the number of columns. In further research, an extended numerical parameter study with additional geometry parameters as well as experimental test series can complete the results obtained. Further studies are being undertaken to develop analytical solutions considering these parameters.

7 Acknowledgment

The research work is proudly supported by the Structural Timber Innovation Company (STIC).

8 References

- [1] Ansys (2007): Release 11.0 Documentation for Ansys – Theory Reference for Ansys and Ansys Workbench. Canonsburg PA, USA.
- [2] ASTM International (1997): ASTM D 5764-97a Standard test method for evaluating dowel-bearing strength of wood and wood-based products. West Conshohocken, PA, USA.
- [3] Canadian Standards Association (2009): O86-09 Engineering design in wood. Mississauga, Canada.
- [4] Deutsches Institut für Normung e. V. (2008): DIN 1052:2008 Entwurf, Berechnung und Bemessung von Holzbauwerken – Allgemeine Bemessungsregeln und Bemessungsregeln für den Hochbau. Berlin, Germany.
- [5] Ehlbeck, J., Görlacher, R., Werner, H. (1989): Determination of perpendicular to grain tensile stresses in joints with dowel-type fasteners. In: International council for research and innovation in building and construction, CIB-W18, paper 22-7-2, Germany.
- [6] European Committee for Standardization (CEN) (2004): EN 1995-1-1:2004 Design of Timber structures. Brussels, Belgium.
- [7] Franke, B., Quenneville, P. (2010): Analyses of the failure behaviour of transversely loaded dowel type connections in wood. In: Proceedings of 11th World Conference on Timber Engineering, Italy.
- [8] Forest Products Laboratory (1999): Wood Handbook - Wood as an Engineering Material. Gen. Tech. Rep. FPL-GTR-113, U.S. Department of Agriculture, Madison, USA.
- [9] Kasim, M. H. (2002): Bolted timber connections loaded perpendicular-to-grain - Effect of row spacing on resistance. Royal Military College of Canada, Kingston, Canada.
- [10] Larsen, H. J., and Gustafsson, P. J. (1990): The fracture energy of wood in tension perpendicular to grain – results from a joint testing project. In: International council for research and innovation in building and construction, CIB-W18, paper 23-19-2, Portugal.
- [11] Reshke, R. (1999): Bolted timber connections loaded perpendicular-to-grain - Influence of joint configuration parameters on strength. Royal Military College of Canada, Kingston, Canada.
- [12] Van der Put, T. A. C. M., Leijten, A. J. M. (2000): Evaluation of perpendicular to grain failure of beams caused by concentrated loads of joints. In: International council for research and innovation in building and construction, CIB-W18, paper 33-7-7, The Netherlands.
- [13] Vasic, S. (2002): Applications of fracture mechanics to wood. The University of New Brunswick, New Brunswick, Canada.

**INTERNATIONAL COUNCIL FOR RESEARCH AND INNOVATION
IN BUILDING AND CONSTRUCTION**

WORKING COMMISSION W18 - TIMBER STRUCTURES

**PREDICTING TIME DEPENDENT EFFECTS IN UNBONDED
POST-TENSIONED TIMBER BEAMS AND FRAMES**

S Giorgini

A Neale

A Palermo

D Carradine

S Pampanin

A H Buchanan

Department of Civil and Natural Resources Engineering,
University of Canterbury, Christchurch
NEW ZEALAND

MEETING FORTY THREE

NELSON

NEW ZEALAND

AUGUST 2010

Presented by A Palermo

B Yeh: What about moisture effects? A Palermo: Some experimental work is being done where moisture is being monitored but this is taken care in k_{def} .

A Jorissen: You are introducing aging effect. Why? A Palermo: The procedure is borrowed from concrete technology. Integration of pre-stress and losses is taken into account with time and this allows one not to do experimental tests.

T Gibney: What strands are being used? A Palermo: 7-wire strands

S Aicher: any monitoring of pool post-tensioned beams? A Palermo: No. Not allowed.

S Winter: What about corrosion prevention in pool building? A Palermo: Grease and plastic membrane were used.

T Poutanen: Is there economical benefit analysis to this technology? A Palermo: Done for a bridge deck. Same costs. Some reduction in timber section size.

R Crocetti: Should look at what has been done in timber bridge decks to minimize pre-stress losses. A Palermo: Agree. Several stressing cycles may be required and this may be difficult for frames. To be considered.

Predicting Time Dependent Effects in Unbonded Post-tensioned Timber Beams and Frames

S. Giorgini, A. Neale, A. Palermo, D. Carradine, S. Pampanin, A.H. Buchanan
Department of Civil and Natural Resources Engineering, University of Canterbury,
Christchurch, New Zealand

1 Introduction

Development of engineered timber products such as Laminated Veneer Lumber (LVL) have caused a renewal in the development of heavy timber construction. A research programme on the application of unbonded post-tensioned construction techniques similar to concrete have been successfully proven with LVL at the University of Canterbury. This technology has been applied firstly to earthquake resistant frames and then, given the advantages that this solution offers, extended to long span beams for gravity loading. Extensive numerical and experimental research is continuing at the University of Canterbury supported by the Structural Timber Innovation Company (STIC).

Rocking connections in post-tensioned frames and walls allow discrete dissipative devices to be placed in specific locations in the structure, providing energy absorption during seismic loading, with no damage to structural members. This system has been developed throughout the last two decades for precast concrete structures, known as “PRESSS” (Precast Seismic Structural Systems) (Priestley 1991 [1], 1996 [2], Priestley et al., 1999 [3], Pampanin, 2005 [4]), and it has been successfully transferred to timber frames (Palermo et al., 2005 [5], 2006 [6]) and walls (Smith et al., 2007 [7]), known as “Pres-Lam”. Because the moment capacity of post-tensioned timber connections depends on the level of post-tensioning force applied by tendon, losses must be accurately assessed to ensure the structure maintains seismic integrity throughout its life. Generally the largest components of the loss are the effects of creep in the wood and relaxation of the steel tendon. The problem is also complicated by the particular column-to-beam connection where post-tensioning tendons pass through the column, loading it perpendicular to the grain, where the stiffness of the wood is much lower than parallel to the grain, so this effect can lead to considerable losses. This issue has been investigated by Davies (2007, [8]) through experimental tests.

While the Pres-Lam system developed for multi-storey timber buildings (Fig. 1a,b) uses straight tendons in the centroid of the section, the use of post-tensioning with draped or eccentric profiles becomes a suitable solution for long span timber beams, either in post-tensioned frames or as stand-alone beams. Enhanced performance of this solution have been confirmed through experimental investigations [10][11] on two static schemes evaluating different tendon profiles (Fig. 1c)). The major benefit was a displacement only

60% of that for the non-post-tensioned beam. In addition to this, a significant nonlinear stiffening effect due to tendon elongation has been identified. In order to properly quantify the benefits of this technology, long-term issues have to be evaluated. Recent preliminary studies [8][12] have confirmed that post-tensioning losses can be estimated around 25% in the worst environmental scenario. In order to validate the analytical approach, long term tests are ongoing at the University of Canterbury [12].

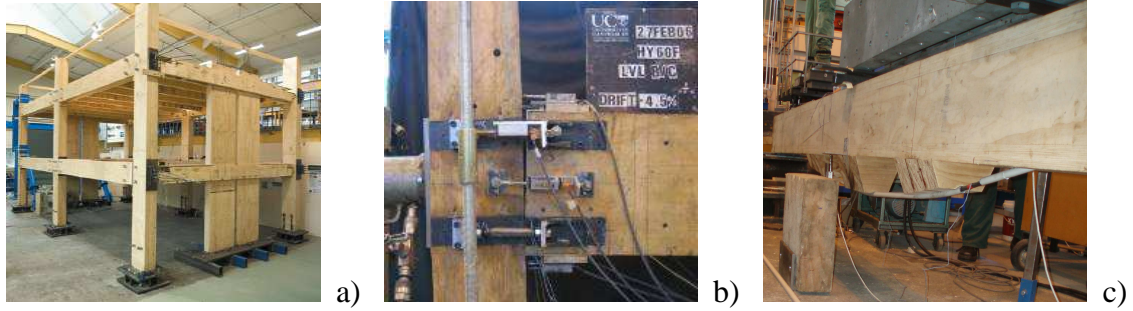


Fig. 1: Unbonded post-tensioned timber frames and beams: a) Pres-Lam timber building tested for earthquake loads [9]; b) Rocking connection; c) Post-tensioned timber beam tested for vertical serviceability loads [11]

The scope of this paper is to propose design procedures and simplified expressions in order to accurately quantify post-tensioning losses in long span beams and timber frames (Pres-Lam system). Both instantaneous elastic and long-term losses are investigated. By applying typical creep formulations [13] to post-tensioned timber members with an eccentric force, some simplified expressions have been developed for beams in a form suitable for standardisation. The analytical formulation is carried out for a simply supported beam in the elastic and long-term ranges. The formulation uses a single dimensionless coefficient \mathcal{O}_p in order to encompass all the involved geometric and mechanical parameters (material properties, beam geometry, steel area and the type of cable profile).

For frame systems, a simplified expression for straight concentric post-tensioning, validated through monitoring of a Pres-Lam timber building [9], is proposed as a viable tool for predicting post-tensioning losses taking into account column joint reinforcement. Simplified design charts are presented in order to facilitate the use of the proposed formula in a design procedure.

2 Long span beams

Simplified analytical expressions for the calculation of elastic and time-dependent (due to creep) losses are herein presented; the latter have been derived using the Age Adjusted Effective Modulus (AAEM) approach, currently used for concrete and suggested by several international codes [14][15][16][17]. In fact, similarly to concrete, the exact solution would be provided by a Volterra's integral equation, too complex for common design practice. Since long term effects due to creep cause shortening of the section and hence losses, the basic approach for the calculation of such losses is the same as for instantaneous elastic losses but including time as a variable. For this reason the proposed expressions are herein shown firstly in the elastic range and then extended over time.

Because the post-tensioning is unbonded, beam analysis is complicated by the possibility of tendon elongation resulting from flexural deformations of the beam, or from gap opening at the beam-column joint of a frame due to lateral loading. Both of these will increase the tendon force. Two alternative ways are presented to take this effect into account, one

involving an iterative procedure and the other one using bond reduction coefficients. Both of them have been already developed for concrete and herein transferred and adapted to timber.

2.1 Elastic losses

The application of a compressive axial force induces a shortening of the beam, depending on the elastic modulus of the material considered. As the first tendon is being stressed, the beam shortens causing elastic loss. Then, the post-tensioning of the second tendon causes further loss on the already post-tensioned first tendon and so on, so that the maximum loss is in the first tendon and the minimum loss is in the last one tensioned.

Since there is no bond between steel and timber, the sectional compatibility of the displacements at the end of the beam relative to the cable gives the amount of the loss caused by the elastic shortening. Two factors contribute to the displacement of the timber section; the axial contribution (pure shortening) and the bending contribution (rotation and thus shortening or elongation depending on the cable position at the end of the beam).

Eq. 1 gives the elastic loss due to post-tensioning of one tendon in a simply supported beam for different profiles (Table 1):

$$\Delta P_{P0} = P_{P0} (1 - \Theta_P) \quad \text{Eq. 1}$$

With Θ_P defined as a mechanical ratio involving all geometrical and mechanical features of the beam (Eq. 2):

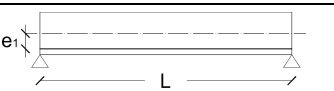
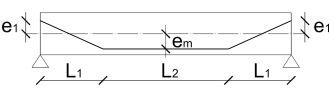
$$\Theta_P = \frac{v_{LP}}{n \cdot \omega_P} \left(\frac{v_{LP}}{n \cdot \omega_P} + \frac{1}{r_f} + \frac{1}{\eta^2 \cdot r_f} \cdot \frac{1}{8} \cdot k_1 \cdot k_2^2 \right)^{-1} \quad \text{Eq. 2}$$

Where n is the ratio between the elastic modulus of the post-tensioning steel and the timber, k_1 is a coefficient that takes into account the influence of the tendon profile on the slope of the section at the end, k_2 is a ratio between the eccentricity at the end of the beam and half height section, v_{LP} is the ratio between the length of the tendon and the length of the beam, ω_P is the mechanical steel ratio, η is the ratio between the radius of inertia of the section and half the height of the section and r_f is the ratio between the strength of steel and timber.

A similar expression of Θ_P has been defined for a statically indeterminate beam with three supports [12] but for sake of brevity is not presented here.

Coefficients k_1 are defined in Table 1, where e_1 and e_m are respectively the eccentricities at the end of the beam and at mid-span (positive if downwards), L is the total length of the beam, L_2 is the length of the central segment of the tendon in the draped configuration.

Table 1: Definition of the coefficient k_1 that takes into account the tendon profile

Tendon profile	k_1
	1
	$\frac{1}{2} \left(\frac{e_m}{e_1} - \frac{L_2}{L} + \frac{L_2}{L} \cdot \frac{e_m}{e_1} + 1 \right)$

The coefficients reported in Table 1 are valid if the end eccentricity e_l is greater than zero, otherwise in both static schemes the coefficient simplifies as follows (Eq. 3):

$$\Theta_p = \frac{v_{LP}}{n \cdot \omega_p} \left(\frac{v_{LP}}{n \cdot \omega_p} + \frac{l}{r_f} \right)^{-1} \quad \text{Eq. 3}$$

The factor Θ_p depend on several parameters; its range of variation has been assessed in [12] in order to quantify elastic and long term losses. It varies between 0.85 and 0.99, where minimum and maximum values depend on the steel area and the ratio between elastic moduli; if the steel area increases and the timber elastic modulus decreases the factors decrease and the losses increase. With such a range of values, elastic losses in one cable/tendon range from 1% to 15%.

Eq. 4 shows the formula from Eurocode 2 [16] used to calculate elastic post-tensioning losses for concrete as an average loss in each cable; this expression can be also applied to post-tensioned timber members.

$$\Delta N_{p0} = A_p \cdot E_p \cdot \sum \left[\frac{n-1}{2n} \cdot \frac{\Delta \sigma_t}{E_t} \right] \quad \text{Eq. 4}$$

Where $\Delta \sigma_t$ is the stress variation in the post-tensioning steel, E_t and E_p are the elastic moduli of timber and post-tensioning steel respectively, A_p is the post-tensioning steel area and n is the number of equal tendons post-tensioned in succession. Therefore, starting from a value calculated for one tendon as previously explained, the average elastic loss in each tendon can be calculated.

2.2 Steel relaxation due to creep

In a prestressed concrete member, subjected to constant stresses over time, strain increases because of creep and shortening of the member causing stress reduction in the post-tensioned steel. This phenomenon similarly happens to timber even if it is more complicated by moisture and temperature variation within the lifetime of the structure [18]. The same compatibility equation used for calculating elastic losses can be extended over time; an algebraic method named AAEM, i.e Age Adjusted Effective Modulus, is herein proposed in order to drastically simplify the solution of the problem. Eq. 5 shows the simplified expression.

$$\Delta P(t) = P_{p0} \left[1 - \frac{\Theta_p \left[1 - (1 - \Theta_p) \cdot \varphi(t, t_0) (1 - \chi(t, t_0)) \right]}{1 + \chi(t, t_0) \cdot \varphi(t, t_0) \cdot (1 - \Theta_p)} \right] \quad \text{Eq. 5}$$

Where $\varphi(t, t_0)$ is the timber creep coefficient and $\chi(t, t_0)$ is the adjusted factor which has been introduced for concrete to take into account the aging effect (assessed at time t for a tension applied at time t_0). There are many models available in literature [19][20][21][22] which can be adopted for the definition of creep coefficients, however for design purposes $\varphi(t, t_0)$ can be substituted by values at infinite time suggested by codes (for example k_{def} referring to Eurocode 5 [23]) and $\chi(t, t_0)$, which for concrete is usually assumed to be 0.8, needs to be calibrated for timber.

Considering Θ_p ranging as previously defined, with the $\chi(t, t_0)$ factor equal to 0.8 and a creep coefficient at infinite time in class 2 (average conditions) as defined in Eurocode 5 [23], long term post-tensioning losses vary from 1% to 10%.

2.3 Geometric non-linearity due to tendon elongation

Geometric non-linearity can complicate the analysis of post-tensioned timber beams. If the deformed configuration of a beam subjected to vertical loads is not negligible, this can cause an additional elongation effect which can affect the internal tendon forces. This elongation depends on beam deflection, and, since there is no bond between steel and timber, the stress variation in each tendon is member-dependent rather than section-dependent.

Moreover, since the elastic modulus of timber is smaller than that of concrete, this contribution is amplified. This affects the final deformed configuration of the beam and hence the final tensile force in the tendons. In addition, the shear contribution in timber is not negligible and this amplifies the above mentioned non-linear effects, starting from the serviceability limit state level. Typically these tendon elongation rates are an additional positive contribution in terms of deformation but a check has to be done in order to avoid possible premature yielding of tendons.

This paper focuses on the serviceability limit state only. Two different approaches can be envisaged, one based on an iterative procedure and one on a coefficient method; the latter is suitable for standardization. Both methods have already been developed for unbonded post-tensioned concrete members [24][25].

Iterative procedure

As Balanguru, 1981 [24], has done in order to determinate the increase of stress in prestressed concrete for various cases, an iterative procedure is herein shown for unbonded post-tensioned timber beams. Since the tendon elongation increases the stresses in the tendons, a new transversal displacement profile $v(x)$ and rotations $\phi(x)$ of the beam ends can be calculated considering the increment of tendon elongation ΔL_i . This procedure requires several iterative steps and is repeated several times until convergence within the tendon force is reached. Fig. 2 briefly summarizes this concept.

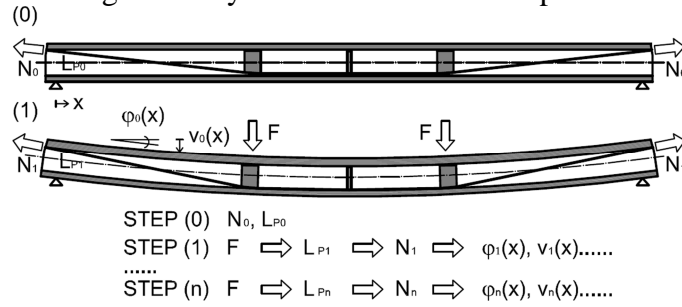


Fig. 2: Non-linear unbonded post-tensioned tendons concept

At step (0) the initial post-tensioning load N_0 is applied; after the application of the forces F , step (1), the beam changes its configuration and the tendon length L_{p0} increases to reach a value L_{p1} ; the additional tendon strain produces an increase of the post-tensioning load to N_1 . Since the beam initial configuration depends on the pre-camber due to the post-tensioning, if the post-tensioning load changes the deformed configuration changes too. Dividing the tendon profile into finite segments, the length of the single elements $l_{p0,i}$ can be calculated with Pitagora's theorem. Calculating the length variation ΔL_n at each step, it is possible to find the increase of strain $\Delta \epsilon_n$ and thus the new force in the tendons N_n^* . However, since this force increase is subjected to instantaneous losses, the force calculated has to be reduced by that amount ($\Delta N_{\Delta N_n^*}^{(inst)}$), obtaining the real force at that step (N_n). At this stage it is possible to determine a new slope $\phi(x)$ and a new displacement profile $v(x)$ of the beam, and repeat the step-by-step procedure until convergence is reached ($N_n \cong N_{n-1}$).

typically after a few iterations. Fig. 3 illustrates the iterative procedure at step n .

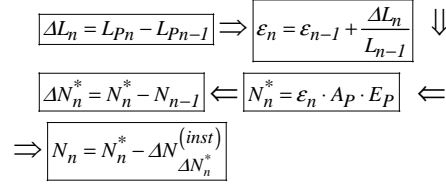


Fig. 3: Iterative procedure at step n

Eq. 6 shows the recurrent formula:

$$N_n = A_P \cdot E_P \cdot \left(\varepsilon_{n-1} + \frac{\Delta L_n}{L_{n-1}} \right) - \Delta N_{\Delta N_n^*}^{(inst)} \quad \text{Eq. 6}$$

Strain reduction coefficient approach

Naaman, 1990 [25], proposed a simplified method which simplifies the analysis of prestressed unbonded post-tensioned concrete beams to that of beams prestressed with bonded tendons through the use of a strain reduction coefficient Ω . He defined the coefficient Ω as the ratio between the average strain increase in the external tendons over the length of the member, calculated at the section of maximum moment ($(\Delta \varepsilon_{ps})_{m \text{ unbonded}}$) and the strain change in the same section with the hypothesis of bond ($(\Delta \varepsilon_{ps})_{m \text{ bonded}}$). This factor depends only on the bending function and on the tendon profile. Naaman calculated values of Ω for several loading cases and profiles in order to properly calculate the increase of stress in the tendon.

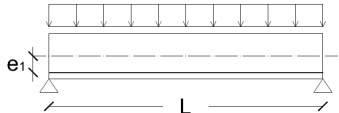
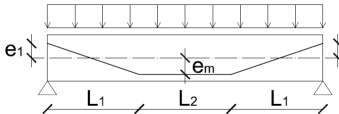
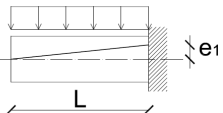
The same approach has been applied to timber; factors Ω are reported for common static schemes suitable for unbonded post-tensioned timber beams. Eq. 7 shows the expression used for the calculation, where M_{max} is the bending moment in the critical section, e is the corresponding eccentricity, L is the length of the beam, $M(x)$, and $e(x)$ are respectively the bending moment, and the eccentricity function along the beam.

$$\Omega = \frac{I}{M_{max} \cdot (e)_{max} \cdot L} \int_0^L M(x) \cdot e(x) dx \quad \text{Eq. 7}$$

The factor Ω apparently depends only on the bending function and on the tendon profile. This approach is able to significantly simplify the problem because no step-by-step procedure is needed.

Table 2 reports values obtained for most common statical schemes.

Table 2: Expressions for the Bond Reduction Coefficients Ω

Scheme	Ω
	$\frac{2}{3}$
	$2 \left(\frac{L_1}{L} \right)^3 \left(\frac{1}{3} \frac{e_1}{e_m} - 1 \right) + \frac{8}{3} \left(\frac{L_1}{L} \right)^2 \left(-\frac{1}{2} \frac{e_1}{e_m} + 1 \right) + \frac{1}{3} \left(\frac{L_2}{L} \right)^3 \left(3 \frac{L}{L_2} - 1 \right) + 4 \frac{L_1^2 \cdot L_2^2}{L^3} \cdot \left(\frac{L}{L_1 \cdot L_2} - \frac{1}{L_2} - \frac{1}{2L_1} \right)$
	$\frac{1}{4}$

For a statically determinate beam, the increase of stress Δf_{ps} in the cable is (Eq. 8):

$$\Delta f_{ps} = \frac{\Omega \cdot \Delta M \cdot e}{E_t/E_{ps} \cdot r^2 \cdot A_t + \Omega \cdot A_p (r^2 + e^2)} \quad \text{Eq. 8}$$

Where ΔM is the bending moment increase in the critical section, e is the corresponding eccentricity, E_t and E_{ps} are the elastic moduli of timber and post-tensioning steel, A_p is the post-tensioning area, r is the radius of inertia along the vertical axis.

Therefore, considering the tendon elongation due to dead load and self weight only, the long term loss $\Delta P(t)$ is reduced down to $\Delta P^*(t)$ as defined in Eq. 9:

$$\Delta P^*(t) = \Delta P(t) - \Delta f_{ps} \cdot A_p \quad \text{Eq. 9}$$

3 Frames

The same approach used for the calculation of long term losses in beams can be extended to Pres-Lam frames; however, the analytical problem is slightly different: the tendons are straight and typically coaxial, while timber is loaded perpendicular to grain in the column and parallel to grain in the beam; thus, there is an additional complexity due to the perpendicular to grain contribution in the compatibility equation [8].

Moreover, since timber loaded perpendicular to the grain has low stiffness, steel components (hollow sections, screws or rods) or wood reinforcing have to be introduced in order to help to bear the load. Armoured columns are the recommended solution and have been successfully proved in early testing although they are expensive to manufacture. After a brief explanation of the analytical approach, simplified design charts are proposed to calculate long-term post-tensioning losses considering the steel reinforcement.

3.2 Analytical approach

An algebraic expression based on the AAEM method for the calculation of long term losses due to the combined effect of creep and steel intrinsic relaxation has been proposed by Davies and Fragiaco (2008 [26]) for post-tensioned frames without reinforcing in the columns. The Davies and Fragiaco formula has been re-written in the same form proposed for beams (Eq. 5), also including the effect of the reinforcement and neglecting steel intrinsic relaxation, which can be easily quantified ranging from 2% to 5%. The effect of the reinforcement has been modelled as a spring in parallel with the column displacement [27]. The factor Θ_p previously defined for beams in Eq. 2 becomes for reinforced frames $\Theta_{p,F}$ (Eq. 10):

$$\Theta_{p,F} = \frac{v_{LP}}{n \cdot \omega_p} \left(\frac{v_{LP}}{n \cdot \omega_p} + \frac{I}{r_f^*} \right)^{-1} \quad . 10$$

Where the term I/r_f^* involves the perpendicular to grain and the reinforcement effects. Eq. 11 shows its expression:

$$\frac{I}{r_f^*} = \frac{I}{r_f} (1 + \alpha) \quad \text{with} \quad \alpha = \frac{\beta_{\perp}}{(1 - \beta_{\perp})} \left[\frac{E_{\perp}}{E_{\parallel}} + \frac{E_s}{E_{\parallel}} \rho_s \frac{L_{\perp}}{L_s} \right]^{-1} \quad \text{and} \quad \beta_{\perp} = \frac{(n_{sp} + 1) \cdot L_c}{(n_{sp} + 1) \cdot L_c + n_{sp} \cdot L_b} \quad \text{Eq. 11}$$

Where the area loaded perpendicular to grain is considered equal to the area loaded parallel to grain ($A_{\perp} = A_{\parallel} = A$), E_{\parallel} and E_{\perp} are respectively the elastic moduli parallel and

perpendicular to the grain, L_{\perp} is the length loaded perpendicular to the grain, L_s is the length of the reinforcement, ρ_s is the steel geometric ratio of the reinforcement and β_{\perp} is defined in function of the number of spans n_{sp} , the beam span L_b and the column width L_c .

While elastic losses can be obtained substituting Θ_p with $\Theta_{p,F}$ in Eq. 1, the calculation of long term losses is more complicated because of the different behaviour of timber in different directions. For frames, Eq. 5 becomes (Eq. 12):

$$\Delta P(t) = P_{p0} \left[1 - \frac{\Theta_{p,F} \left[\alpha_{\Theta} - (1 - \Theta_{p,F} \cdot \alpha_{\Theta}) \cdot (\varphi_{\parallel}(t, t_0) (1 - \chi_{\parallel}(t, t_0)) + \alpha_{\perp}^{EM} - \alpha_{\perp}^{AD}) \right]}{1 + (\chi_{\parallel}(t, t_0) \cdot \varphi_{\parallel}(t, t_0) + \alpha_{\perp}^{AD}) \cdot (1 - \Theta_{p,F} \cdot \alpha_{\Theta})} \right] \quad \text{Eq. 12}$$

Where coefficients α_{Θ} , α_{\perp}^{EM} , α_{\perp}^{AD} are defined as follows (Eq. 13, 14 and 15):

$$\alpha_{\Theta} = \left(\frac{v_{LP}}{n \cdot \omega_p} + \frac{1}{r_f^*} \right) \cdot \left(\frac{v_{LP}}{n \cdot \omega_p} + \frac{1}{r_f} \right)^{-1} \quad \text{Eq. 13}$$

$$\alpha_{\perp}^{EM} = \frac{\beta_{\perp}}{(1 - \beta_{\perp})} \cdot (1 + \varphi_{\perp}(t, t_0)) \left[\frac{E_{\perp}}{E_{\parallel}} + \frac{E_s}{E_{\parallel}} \rho_s (1 + \varphi_{\perp}(t, t_0)) \frac{L_{\perp}}{L_s} \right]^{-1} \quad \text{Eq. 14}$$

$$\alpha_{\perp}^{AD} = \frac{\beta_{\perp}}{(1 - \beta_{\perp})} \cdot (1 + \chi_{\perp}(t, t_0) \cdot \varphi_{\perp}(t, t_0)) \left[\frac{E_{\perp}}{E_{\parallel}} + \frac{E_s}{E_{\parallel}} \rho_s (1 + \chi_{\perp}(t, t_0) \cdot \varphi_{\perp}(t, t_0)) \frac{L_{\perp}}{L_s} \right]^{-1} \quad \text{Eq. 15}$$

Eq. 12, including intrinsic relaxation as in [26], has been verified using the Pres-Lam building [9]. Measurements of deflections, loads and environment were measured over approximately 11 weeks on the two storey, three dimensional post tensioned structure. The tendon force was shown to decrease over time and the loss was less across the steel-armoured connections (compared with the screw-reinforced connections). The expression appeared to give a reasonable correlation to the recorded behaviour.

3.1 Design procedure

The expression developed earlier for long term losses has been implemented in a series of design charts to simplify its application. The presence of timber loaded perpendicular to the grain (β_{\perp}) drastically affects the post-tensioning losses; techniques like screw reinforcement and steel armouring can reduce these losses. For sake of brevity design tables are reported for the unreinforced columns (Table 3). Values have been calculated at infinite time (Service class 1 of Eurocode 5 [22]) for $E_{\parallel}=14400$ MPa, $E_{\perp}=280$ MPa, $E_p=200000$ MPa, $k_{def\parallel}=0.6$, $k_{def\perp}=4$ [8]. E_{\perp} and $k_{def\perp}$ values have been conservatively used for the weaker direction; considering the other direction losses would be lower.

Table 3: Loss Percentage for Unreinforced Column

<i>Unreinforced ($\rho_s=0$)</i>							
ρ_p		0.003	0.006	0.009	0.012	0.015	0.018
β_{\perp}	0%	6.5%	8.3%	9.9%	11.4%	12.7%	13.9%
	1%	21.2%	31.3%	38%	42.8%	46.4%	49.3%
	2.5%	31%	43.2%	50.1%	54.6%	57.7%	60%
	5%	43.3%	55.3%	61.1%	64.5%	66.7%	68.3%
	100%	55.6%	65.1%	69.1%	71.3%	72.7%	73.7%

The correct estimation of post-tensioning losses will also allow prediction of the ultimate moment capacity of Pres-Lam connections (Fig. 4).

In fact, the amount of total losses defines the initial post-tensioning force needed; however since at the beginning of the structure's life the tendon force will be higher than the expected design value (long term losses not yet occurred), a proper check of the hierarchy of strength has to be maintained to ensure the expected and desired collapse modes. In order to avoid the seismic displacement demands being accommodated in less favourable locations (e.g. hinging in the columns and the formation of a soft storey mechanism), it is important, as part of the design procedure to check this early stage overstrength.

Note that the Pres-Lam connections rely on the elastic re-centering provided by the tendons to guarantee negligible residual displacements after an earthquake event. To achieve this, it is necessary in the design process to check that the tendon remains elastic during all lateral loading. This is done in the codes by placing restrictions on the extent of both initial and total tendon stress. Eurocode 2 requires the initial stress at jacking to remain under 75% of the characteristic strength of the tendon. The maximum allowable tendon stress during seismic gap opening is required to remain below 90% of the yield strength.

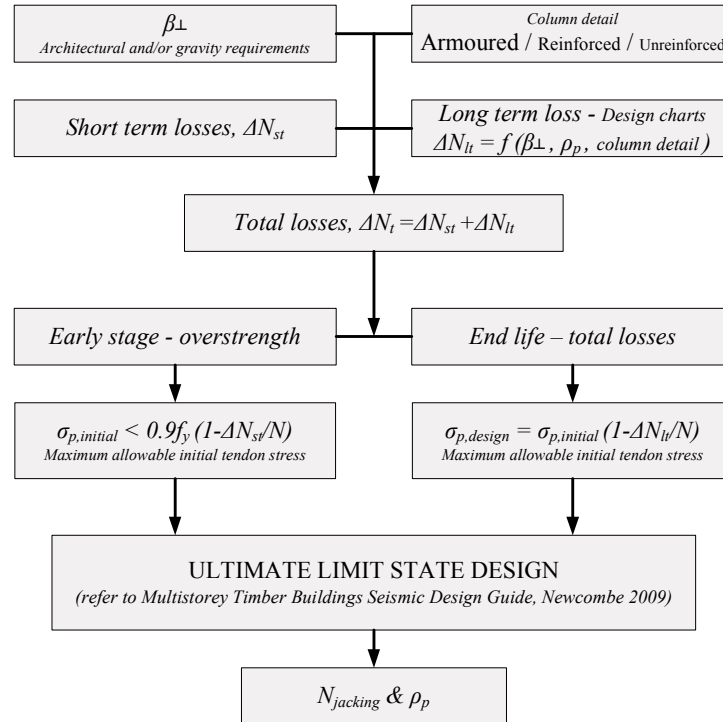


Fig. 4: Ultimate Limit State Design Flow Chart

Conclusions

For design of post-tensioned timber beams, proper assessment of the post-tensioning losses is crucial for establishing the initial post-tensioning force and to maintain the long-term structural performance.

In this paper post-tensioning losses have been expressed for beams and frames in a common analytical formulation, expressed as function of a global mechanical parameter. Solutions based on this method have been proposed, to simplify the calculation of such complicated phenomena by practitioners.

In addition, for frames, the effect of the column reinforcement is taken into account and design charts have been created in order to further simplify the calculations.

Acknowledgements

This research has been funded by the Structural Timber Innovation Company Ltd (STIC).

References

- [1] Priestley, M. J. N. (1991). "Overview of the PRESSS Research Program." *PCI Journal*, 36(4), 50-57.
- [2] Priestley, M. J. N. (1996). "The PRESSS Program—Current Status and Proposed Plans for Phase III." *PCI Journal*, 41(2), 22-40.
- [3] Priestley, M. J. N., Sritharan, S., Conley, J. R. and Pampanin, S. (1999). "Preliminary Results and Conclusions from the PRESSS Five-story Precast Concrete Test-building." *PCI Journal*, 44(6), 42-67.
- [4] Pampanin, S. (2005). "Emerging Solutions for High Seismic Performance of Precast/Prestressed Concrete Buildings." *Jo. of Adv. Concrete Technology*, invited paper "High performance systems", 3(2), 202-223.
- [5] Palermo, A., Pampanin, S., Buchanan, A., and Newcombe, M. (2005). "Seismic Design of Multi-storey Buildings using Laminated Veneer Lumber (LVL)." *NZSEE Annual Conference*, CD-ROM.
- [6] Palermo, A., Pampanin, S., Fragiaco, M., Buchanan, A. H. and Deam, B. L. (2006). "Innovative Seismic Solutions for Multi-storey LVL Timber Buildings". *9th World Conference on Timber Engineering*, CD-ROM.
- [7] Smith, T., Ludwig, F., Pampanin, S., Fragiaco, M., Buchanan, A., Deam, B., and Palermo, A. (2007). "Seismic Response of Hybrid-LVL Coupled Walls under Quasi-static and Pseudo-dynamic Testing". *NZSEE Annual Conference*, CD-ROM.
- [8] Davies, M. (2007). "Long Term Behaviour of Laminated Veneer Lumber (LVL) Members Prestressed with Unbonded Tendons." University of Canterbury, New Zealand, 2007.
- [9] Newcombe, M. P. (2010). "Seismic Design of New Generation Multistorey Timber Buildings (in print)," Doctorate Thesis, University of Canterbury, New Zealand.
- [10] Dal Lago B. A., Di Benedetto C. (2009). "Use of longitudinal unbonded post-tensioning in multi-storey timber buildings". MSc thesis Technical University of Milan, Italy.
- [11] Palermo A., Pampanin S., Carradine D., Buchanan A. H., Dal Lago B., Dibeneditto C., Giorgini S., Ronca P. "Enhanced performance of longitudinally post-tensioned long-span LVL beams." *World Conference Timber Engineering 2010*, Riva del Garda, Italy.
- [12] Giorgini, S. (2009). "Service load analysis and design of long span unbonded post-tensioned timber beams." MSc thesis, Technical University of Milan, Italy.
- [13] Comité Euro-International du Béton (CEB) (1984). "Structural effects of time-dependent behaviour of concrete." CEB design manual.
- [14] Comité euro-international du béton, Federation internationale de la précontrainte (1993). "CEB-FIP model code 1990: Design code." London: T. Telford.
- [15] Fédération internationale du béton (2000). "Structural concrete: textbook on behavior, design and performance: updated knowledge of the CEB/FIP Model code 1990." Lausanne, Switzerland: International Federation for Structural Concrete.
- [16] EN 1992-1-1:2004. "Eurocode 2 – Design of concrete structures - Part 1-1: general rules and rules for buildings."
- [17] NZS 3101:Part1:2006. "Concrete structures standard Part 1 - The design of concrete structures."
- [18] Morlier, P. (1994). "Creep in Timber Structures." Rilem Report 8, E & F Spon (Chapman & Hall).
- [19] Toratti T. (1992). "Creep of timber beams in variable environment." Dissertation, Helsinki University of Technology, Laboratory of Structural Engineering and Building Physics.
- [20] Hanhijarvi A. (1995). "Modelling of creep deformation mechanisms in wood." Dissertation, Helsinki University of Technology, Technical Research Centre of Finland, VTT Publications, Espoo (SF).
- [21] Becker P. (2002). "Modellierung des zeit – und feuchteabhängigen Materialverhaltens zur Untersuchung des Langzeitverhaltens von Druckstäbe aus Holz." Dissertation, Bauhaus – Universität Weimar.
- [22] Martensson A. (1992). "Mechanical behaviour of wood exposed to humidity variations." PhD thesis.
- [23] EN 1995-1-1:2004. "Eurocode 5 - Design of timber structures - Part 1-1: General -Common rules and rules for buildings."
- [24] Balanguru, P. N. (1981). "Increase of stress in unbonded tendons in prestressed concrete beams and slabs." *Canadian Journal of Civil Engineering*, 36, 262-268.
- [25] Naaman, A. (1990). "New Methodology for the Analysis of Beams Prestressed with External or Unbonded Tendons." *External Prestressing in Bridges, SP-120, American Concrete Institute, Detroit*, 339-354.
- [26] Davies, M. and Fragiaco, M. (2008). "Long-Term Behaviour of laminated Veneer Lumber Members Prestressed with Unbonded Tendons." *NZ Timber Design Journal*, Vol. 16 Issue 3.
- [27] Neal A. (2009). "Long term performance of post-tensioned timber buildings." Third Pro Project, University of Canterbury, New Zealand.

**INTERNATIONAL COUNCIL FOR RESEARCH AND INNOVATION
IN BUILDING AND CONSTRUCTION**

WORKING COMMISSION W18 - TIMBER STRUCTURES

**SIMPLIFIED DESIGN OF POST-TENSIONED
TIMBER FRAMES**

M P Newcombe

M R Cusiel

S Pampanin

A Palermo

A H Buchanan

Department of Civil and Natural Resources Engineering, University of Canterbury,
Christchurch
NEW ZEALAND

MEETING FORTY THREE

NELSON

NEW ZEALAND

AUGUST 2010

Presented by M Cusiel

L Daziel: How significant are the plates to limit the crushing at the columns? M Cusiel: It provides a stiffer connection. Better to use flexibility in member than plasticity in connection.

A Ceccotti: Why was this system not used in the NMIT building? A Buchanan: It was not in the winning bid.

A Ceccotti: How much crushing is allowed in seismic design (due to pre-stress)? How much pre-stress losses? M Cusiel: none.

M Fragiaco: Do dissipators help? M Cusiel: connections are stiffer and dissipators are not engaged. Uneconomical.

Simplified Design of Post-Tensioned Timber Frames

M. P. Newcombe, M. R. Cusiel, S. Pampanin, A. Palermo and A. H. Buchanan

Department of Civil and Natural Resources Engineering, University of Canterbury,
Christchurch, New Zealand

1 Introduction

A high performance solid timber frame system has been developed at the University of Canterbury, in collaboration with the Structural Timber Innovation Company (STIC Ltd). The structural system uses post-tensioning tendons or bars to connect large timber sections (see Figure 1). The sections are constructed from engineered wood product, such as Glulam, Laminated Veneer Lumber (LVL) or Cross Laminated Timber (CLT), forming beams, columns, walls or floors. Post-tensioned timber is suitable for a wide range of building types, including commercial structures, and has the potential to compete with existing forms of construction in terms of cost, versatility and structural performance [Newcombe *et al.*, 2010a].

The connection technique [Palermo *et al.*, 2005] was adapted from post-tensioned pre-cast concrete systems [Priestley *et al.*, 1999; Pampanin, 2005]. For seismic design, the combination of timber and post-tensioning is particularly efficient since it avoids potential brittle failure modes that can occur in traditional timber connections [Buchanan and Fairweather, 1993] and prevents excessive frame elongation, avoiding damage to the floor system [Newcombe *et al.*, 2010b]. Hence, the system fits well into recent Performance-Based Seismic Engineering (PBSE) design approaches [Christopoulos and Pampanin, 2004] because structural damage is minimized and, due to restoring action provided by the post-tensioning, residual deformations are insignificant.

Previous research has shown that simply designed post-tensioned timber frames respond essentially elastically to even severe earthquake loading [Newcombe *et al.*, 2010b]. In such cases, for code-based seismic design, the ultimate limit state lateral forces cannot be significantly reduced due to structural ductility or hysteretic damping, in contrast to well designed concrete and steel structures. Even so, the serviceability limit state lateral load design usually governs the size of the members and the amount of post-tensioning, especially if stringent displacement limitations, according to current code provisions, are imposed to protect non-structural partitions inside a building. For an elastic design, for service or ultimate conditions, either force-based [NZS1170.5:2004] or displacement-based [Priestley *et al.*, 2007] design can be used to determine the lateral seismic forces for post-tensioned timber frames. However, for force-based design it is essential that the allowable displacements are used to determine the natural period of the frame [Deam, 2005].

The lateral resistance of post-tensioned timber frames is highly dependent on the behaviour of the beam-column connections [Newcombe *et al.*, 2008b]. Analytical models have been proposed to predict the moment-rotation response of precast concrete beam-column connections with unbonded post-tensioning tendons [Pampanin *et al.*, 2001]. These models have been adapted to timber [Pampanin *et al.*, 2006; Newcombe *et al.*, 2008a] but require further validation as more experimental data is obtained [Iqbal *et al.*, 2010; Newcombe *et al.*, 2010b]. Recent research has demonstrated that the shear deformation of the timber columns in the joint panel region, between the beams, significantly contributes to the overall frame flexibility [Newcombe *et al.*, 2008b]. Such considerations are not required for equivalent precast concrete connections. To enable accurate design of post-tensioned timber frames, to meet specified displacement limitations, all deformation components must be quantified and accounted for.

In some situations additional non-prestressed reinforcement may be added to the beam-column connections (see Figure 1) creating what is termed a ‘Hybrid’ connection [Stanton *et al.*, 1997; NZS3101, 2006]. With careful detailing, this reinforcement can improve the strength of the connections and the energy dissipation capability of the frame at large displacements.

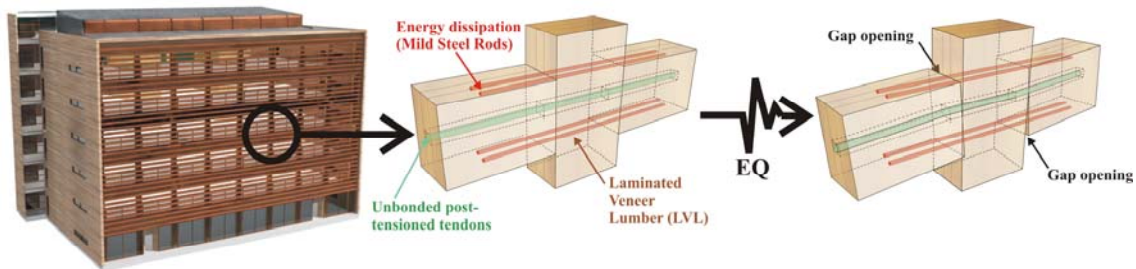


Figure 1. Post-tensioned timber frame concept

While lateral load design methodologies for post-tensioned concrete and steel frames exist [Christopoulos *et al.*, 2002; fib, 2004; NZS3101, 2006], these procedures are not directly applicable to timber frames. This paper describes a simplified design procedure for post-tensioned timber frames (see Figure 2) which builds on previous publications by Pampanin *et al* [2006] and Newcombe *et al* [2008a]. The focus is given to characterisation of frame deformation. For simplicity, hybrid connections are not considered here.

2 Lateral force design

A simplified lateral force design is performed to determine the actions on the frame due to wind or earthquake. The seismic design can be either an equivalent static force-based design [NZS1170.5:2004] or a displacement-based design [Priestley *et al.*, 2007]. For both procedures, the elastic period should be determined considering a secant-stiffness to an allowable design displacement for a given earthquake intensity. Based on recent shake-table experimentation [Pino *et al.*, 2010], the elastic damping of the frame system may be taken as 5% of critical damping. Once the design base shear is determined, the frame actions can be calculated according to an equilibrium-based approach [Priestley *et al.*, 2007].

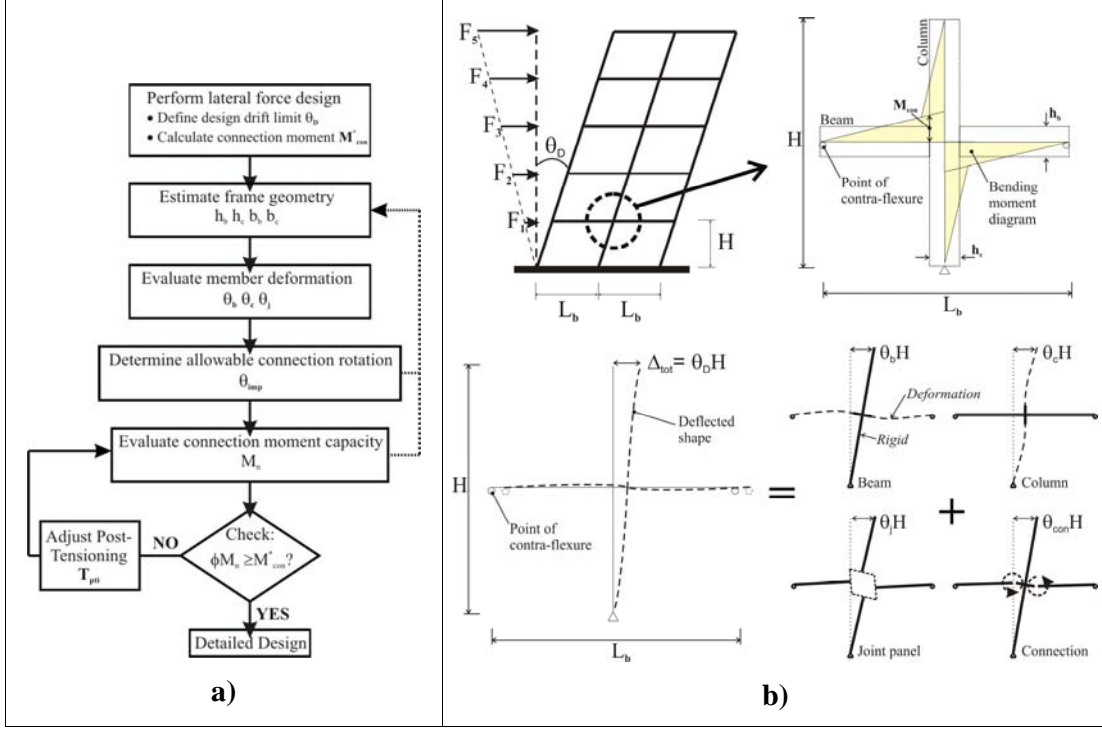


Figure 2. a) Simplified design procedure for post-tensioned timber frames b) Idealization of frame deflection to an internal beam-column subassemblage

3 Member deformation

The deformation of a frame system is often quantified by considering an internal beam-column sub-assemblage that is representative for the rest of the frame system [Buchanan and Fairweather, 1993; Priestley *et al.*, 2007]. If the lateral force design follows the proposed displacement-based design methodologies [Newcombe *et al.*, 2008b], the goal is to achieve uniform risk structures. Hence, the enveloped seismic demand, in terms of interstorey drift, is expected to be uniform up the height of the structure. When the frame response is dominated by the 1st mode, for low-rise structures or wind loading, the interstorey drift of the bottom floor is critical. Therefore, a first floor internal beam-column joint is considered appropriate for maximum deflection calculations (see Figure 2).

The main contributions to the interstorey drift (θ_D) are rotations due to the flexure and shear deformation of the beam (θ_b) and column (θ_c), the joint panel shear deformation (θ_j) and connection rotation at the face of the column (θ_{con}), as expressed in Eq. 1.

$$\theta_D = \theta_b + \theta_c + \theta_j + \theta_{con} \quad (1)$$

3.1 Beam and column deformation

From simple beam theory the deformation of the beams and columns can be determined accurately:

$$\theta_b = \frac{\phi_b}{L_b} \left(\frac{(L_b - h_c)^2}{6} + \frac{E_t h_b^2}{G 4} \right) \text{ And } \theta_c = \frac{\phi_c}{H} \left(\frac{(H - h_b)^2}{6} + \frac{E_t h_c^2}{G 4} \right) \quad (2) \quad (3)$$

Where E_t and G are the bending and shear elastic modulus respectively, L_b is the length of the bay, H is interstorey height, h_b is the depth of the beam and h_c the depth of the column. The curvature in the beam and column is also a function of the applied moment in the connection (M_{con}) and the frame geometry (see Figure 2):

$$\phi_b = \frac{M_{con}}{E_t I_b} \text{ And } \phi_c = \frac{M_{con}}{E_t I_c} \frac{L_b (H - h_b)}{H (L_b - h_c)} \quad (4) \quad (5)$$

Where I_b and I_c are the section moments of area of the beam and column respectively.

3.2 Joint panel deformation

Due to the low shear modulus of timber, the joint panel deformation can significantly contribute to the flexibility of a timber frame. This deformation is predominately caused by shear forces induced by the applied stresses at the rocking interface; hence the joint panel and connection response are implicitly related. In addition, the low shear modulus and low aspect ratio of the joint allow flexural deformations within the joint to be neglected.

The deformation of the column due to joint distortion, γ , is given below:

$$\theta_j = \gamma \left(1 - \frac{h_c}{L_b} - \frac{h_b}{H} \right) \quad (6)$$

Where $\gamma = \gamma_h + \gamma_v$, γ_h and γ_v are shown in Figure 3.

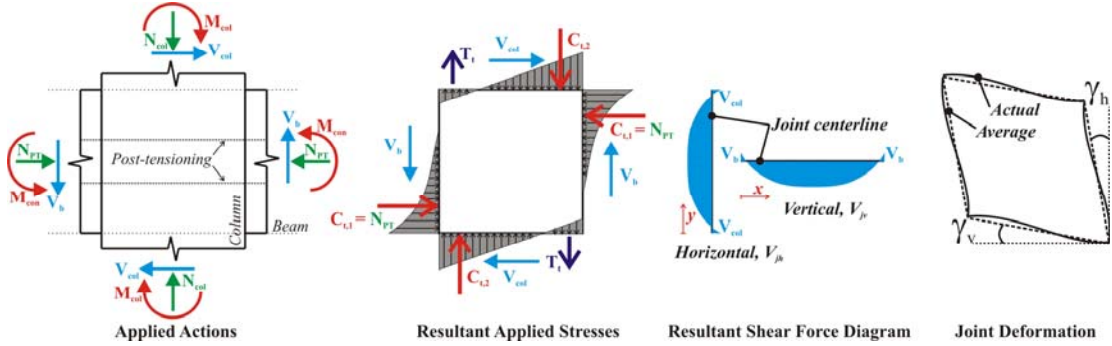


Figure 3. Applied actions and stress resultants for an internal beam-column joint

According to standard beam theory, the total shear deformation of the joint is:

$$\gamma_h = \frac{1}{GA_{sh} h_b} \int_0^{h_b} V_{jh} dy = \frac{\bar{V}_{jh}}{GA_{sh}} \text{ And } \gamma_v = \frac{1}{GA_{sv} h_c} \int_0^{h_c} V_{jv} dx = \frac{\bar{V}_{jv}}{GA_{sv}} \quad (7) \quad (8)$$

Where \bar{V}_{jh} , \bar{V}_{jv} , A_{sh} and A_{sv} are the horizontal and vertical average shear force, and shear area within the joint panel respectively.

Assuming there is no mild steel reinforcement and the beam and column are solid rectangular sections the following analytical expressions apply:

$$\bar{V}_{jh} = \frac{2M_{con}}{h_b} - V_{col} \text{ And } \bar{V}_{jv} = \frac{2M_{con}}{h_c} \frac{L_b (H - h_b)}{H (L_b - h_c)} - V_b \quad (9) \quad (10)$$

For cases where the beam section is not rectangular, numerical integration is required to

find the average horizontal shear force and the joint distortion γ (as shown in Eq. 7 and 8). Although the horizontal and vertical joint shear forces may be similar in magnitude, the vertical shear area continues up the entire height of the column indicating that overall building deformation due to vertical joint shear deformation will be minimal. This has been verified with 2-dimensional finite element analysis (FEM) and experimental results for beam-column sub-assemblages. More information can be found in Newcombe [2011].

4 Allowable connection rotation

The moment capacity of a connection gradually increases as the connection rotation increases. Furthermore, at a certain connection rotation, the moment capacity increases as the force from the post-tensioning increases. Hence, to minimize the required post-tensioning reinforcement the maximum allowable connection rotation should be used for design of the post-tensioning.

$$\theta_{con} = \theta_D - (\theta_b + \theta_c + \theta_j) \quad (11)$$

According to NZS1170.5, the interstorey drift θ_D is limited to 2.5% for the ultimate limit state and ranges from 0.3% to 1% drift for the serviceability limit state. The design moment demand must be achieved without exceeding the allowable connection rotation θ_{con} . If a negative (or near zero) allowable connection rotation is obtained, the beam and column sizes must be increased to reduce the member deformation.

Furthermore, at the column face the allowable imposed connection rotation, θ_{imp} is:

$$\theta_{imp} = \frac{\theta_{con}}{\left(1 - \frac{h_c}{L_b}\right)} \quad (12)$$

5 Evaluation of the connection moment capacity

The connection moment capacity is calculated at the allowable imposed connection rotation. This can be done using existing procedures, or a modified procedure, presented below.

5.1 Existing procedures

As introduced, analytical procedures have been proposed in literature to determine the moment-rotation response of timber rocking connections [Pampanin *et al.*, 2006; Newcombe *et al.*, 2008a]. Because strain compatibility assumptions do not apply, these procedures rely on a *Monolithic Beam Analogy* (MBA) [Pampanin *et al.*, 2001; Palermo, 2004] to determine the strain at the extreme fiber of the rocking sections, ε_t . Applying the MBA to rocking timber connections, the following expression is derived:

$$\varepsilon_t = \left(\frac{3\theta_{imp}}{L_{cant}} + \phi_{dec,para} \right) c \quad (13)$$

Where L_{cant} is the shear span, $\phi_{dec,para}$ is the decompression curvature of the parallel-to-grain timber in the beam and c is the neutral axis depth. Newcombe *et al* [2008] suggested

the use of a calibrated ‘effective connection elastic modulus’ to determine the stress at the extreme fiber:

$$f_t = E_{con} \varepsilon_t \quad (14)$$

Where $E_{con} = 0.55E_{para}$ and E_{para} is the parallel-to-grain elastic modulus.

More recently it has been noted that, while the MBA may be appropriate for concrete or steel structures, where the initial stiffness of the rocking connections is effectively infinite, they can lead to inaccurate predictions of the initial strength of softer (perpendicular-to-grain) timber connections at small rotations [Newcombe, 2010]. Furthermore, the use of a calibrated effective connection modulus leads to under estimation of the stresses in the timber.

5.2 Modified procedure

Modifications to the existing theory have been made by Newcombe [2008] that more accurately account for the stresses in the timber at the interface between the beam and column. The following steps, similar to the aforementioned existing procedures can be followed to determine the moment capacity of the connection within its elastic range:

Step 1: Impose connection rotation

The allowable connection rotation θ_{imp} is applied to the connection.

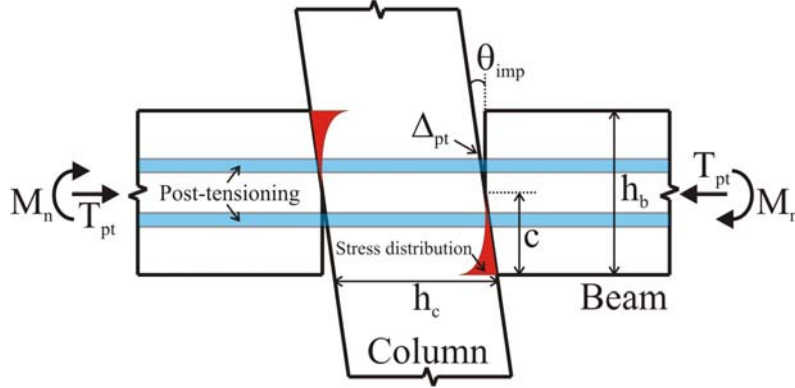


Figure 4. Gap opening mechanism

Step 2: Estimate the neutral axis position

An empirical relationship for the neutral axis depth as a function of the imposed connection rotation has been calibrated within sufficient accuracy. This relationship was verified through parametric analysis, using finite element models with varying frame geometries, initial post-tensioning force and material properties. Again, more information can be found in Newcombe [2011]. The neutral axis position, within the beam depth, is given by:

$$c = \alpha \beta h_b \left(\frac{0.054}{\sqrt{\theta_{imp}}} - 0.12 \right) \quad (15)$$

Where α is a correction factor for the columns transverse elastic modulus, E_{perp} , and is empirically expressed in MPa as:

$$\alpha = \frac{390}{E_{perp}} + 0.42 \quad (16)$$

While β is a correction factor for the initial axial stress in beams, f_i , and is empirically expressed in MPa as:

$$\beta = \frac{f_i}{4.5} \quad (17)$$

Step 3: Choose the post-tensioning

The area, position, applied initial prestressing and number of post-tensioning tendons (or bar) must be chosen. To avoid excessive creep deformation of the frame, it is suggested that the sum of the initial post-tensioning forces in each tendon, $T_{pti,i}$, should be less than 40% of the compressive strength of the timber [Davies and Fragiaco, 2008]:

$$\frac{f_i}{f_c} \leq 0.4 \quad (18)$$

Where f_c is the compressive strength of the column in the transverse direction and the initial axial stress in the beams is defined as:

$$f_i = \frac{\sum_{i=1}^n T_{pti,i}}{A_b} \quad (19)$$

Where A_b is the area of the beam and n is the number of tendons.

Step 4: Determine the force in the post-tensioning tendons

The post-tensioning force will increase during seismic loading, due to opening of the gap at the beam-column interface. Considering Figure 4, the elongation of the tendon due to a gap opening is given below. Only elongation (or positive deformations) should be considered, as indicated by experimental testing [Newcombe *et al.*, 2010c].

$$\Delta_{pt,i} = \theta_{imp} (y_{pt,i} - c) \geq 0 \quad (20)$$

Where $\Delta_{pt,i}$ is the displacement of the i^{th} tendon and $y_{pt,i}$ is the distance from the extreme compression fibre to the i^{th} tendon.

If multiple tendons are positioned symmetrically about the longitudinal axis of the beam, the additional strain in each tendon due to the gap opening on both sides of the column is:

$$\Delta \varepsilon_{pt,i} = \frac{n_{con} (\Delta_{pt,i} + \Delta_{pt,n+1-i})}{2l_{ub}} \quad (21)$$

Where n_{con} is the number of connections and l_{ub} is the unbonded length of the tendons in the frame.

To ensure the tendons remain elastic, the maximum stress should not exceed 90% of yield.

$$\varepsilon_{pt,i} + \Delta \varepsilon_{pt,i} \leq 0.9 \varepsilon_y \quad (22)$$

Where $\varepsilon_{pt,i} = T_{pti,i} / A_{pt,i} E_{pt}$ is the strain due to the initial post-tensioning force; $A_{pt,i}$ is the cross sectional area of the i^{th} tendon, E_{pt} is the elastic modulus of the tendons and ε_y is the tendon yield strain. The total tendon force, T_{pt} , can be determined:

$$T_{pt} = \sum_{i=1}^n T_{pt,i} + E_{pt} \sum_{i=1}^n \Delta \varepsilon_{pt,i} A_{pt,i} \quad (23)$$

Step 5: Calculate peak timber stress

The peak timber stress can be determined as follows:

$$f_t = \chi \frac{2T_{pt}}{cb_b} \leq f_y \quad (24)$$

Where b_b is width of beam at the connection interface and χ is a factor to account for non-linear stress distributions (see Figure 4). A χ -value of 2, matches well with results from numerical modelling [Newcombe, 2010].

If the yield stress of the timber is exceeded, to ensure prediction accuracy the inelastic stress distribution must be integrated to determine the compression centroid. A similar approach is necessary if the beam width is not uniform. More detail can be found in Newcombe [2010].

Step 6: Determine moment capacity

The moment capacity is calculated taking moments from the compression centroid to the centre of each tendon. The centroid of the compressive stress distribution, see Figure 4, is at approximately one-fourth the height of the neutral axis [Newcombe, 2010].

$$\phi M_n = \phi \sum_{i=1}^n T_{pt,i} \left(y_{pt,i} - \frac{c}{4} \right) \quad (25)$$

Where ϕ is the flexural strength reduction factor. A ϕ -value of 0.85 is suggested, as used for precast concrete construction [NZS3101, 2006].

6 Connection capacity versus demand

The reduced connection moment capacity, at the imposed connection rotation, must be greater than the demand.

$$M_{con} \leq \phi M_n \quad (26)$$

If the above inequality is not satisfied then the initial post-tensioning force must be increased. Alternatively, if the allowable initial stress is exceeded (see Eqn. 18) the beam and column sizes may be increased or connection reinforcement may be modified.

7 Detailed design

The flexural and shear capacity of the beam and column must be checked for ultimate limit state loading. For column design, the inclusion of overstrength and dynamic amplification factors is necessary. In addition, a shear key must provide support to the beams when subjected to gravity loading as specified in NZS3101:2006 for precast concrete. Further details can be found in Newcombe [2010] and Newcombe *et al* [2008b].

8 Conclusions

A simplified design procedure has been proposed for the lateral force design of simple post-tensioned timber frames, responding within the elastic range.

The procedure allows the determination of the required section sizes and post-tensioning forces to achieve the lateral strength demand of the frame, without exceeding the total allowable displacements for either serviceability or ultimate limit states. All significant deformation components are accounted for using analytical expressions.

For predicting the moment-capacity of the beam-column connections, a refined methodology is proposed that, when compared to previously published procedures for post-tensioned timber connections, more accurately predicts the peak timber stresses within the connection and can avoid iteration. Empirical relationships have been proposed which were calibrated from detailed finite element modelling and experimental data.

References

- Buchanan, A. H., and Fairweather, R. H. 1993. Seismic Design of Glulam Structures. *Bulletin of the New Zealand Society of Earthquake Engineering*, Vol. **26**: **4**, pp 415-436.
- Christopoulos, C., Filiatrault, A., Uang, C. M., and Folz, B. 2002. Post-tensioned Energy Dissipating Connections for Moment Resisting Steel Frames. *ASCE Journal of Structural Engineering*, Vol. **128** **9**, pp. 1111-1120.
- Christopoulos, C., and Pampanin, S. 2004. Towards performance-based design of MDOF structures with explicit consideration on residual deformations, Special Issue on "Performance-Based Seismic Design". *ISET Journal of Structural Engineering*, Vol. **41**: **1**, pp 53-73.
- Davies, M., and Fragiaco, M. 2008. Long-Term Behaviour of Laminated Veneer Lumber Members Prestressed with Unbonded Tendons *New Zealand Timber Design Journal*, Vol. **16**: **3**, pp. 13-20.
- Deam, B. 2005. A Displacement-Focused, Force-Based Structural Design Procedure. *New Zealand Society of Earthquake Engineering Conference Rotorua*, New Zealand, pp. 8.
- fib. 2004. Seismic Design of Precast Concrete Building Structures. *fib bulliten 27*, ISBN 978-2-88394-067-3, International Federation for Structural Concrete, Fib Commission 7, Federal Institute of Technology, Lausanne.
- Iqbal, A., Pampanin, S., and Buchanan, A. H. 2010. Seismic Performance of Prestressed Timber Beam-Column Sub-Assemblies. *New Zealand Society of Earthquake Engineering Conference*, Wellington, New Zealand.
- Newcombe, M. P. 2008. "Seismic Design of Multistorey Post-Tensioned Timber Buildings," Masters Thesis, University of Pavia, Pavia.
- Newcombe, M. P. 2010. "Seismic Design of New Generation Multistorey Timber Buildings (in print)," Doctorate Thesis, University of Canterbury, Christchurch.
- Newcombe, M. P. 2011. "Seismic Design of New Generation Multistorey Timber Buildings (under preparation)," Doctorate Thesis, University of Canterbury, Christchurch.
- Newcombe, M. P., Pampanin, S., Buchanan, A., and Palermo, A. 2008a. Section Analysis and Cyclic Behavior of Post-Tensioned Jointed Ductile Connections for Multi-Storey Timber Buildings. *Journal of Earthquake Engineering*, Vol. **12**: **Special Issue**, pp. 83-110.

- Newcombe, M. P., Pampanin, S., Buchanan, A., and Palermo, A. 2008b. Seismic design of post-tensioned timber frames. *14th World Conference in Earthquake Engineering*, Beijing, China, pp. 8, Paper No. S12-008.
- Newcombe, M. P., Pampanin, S., and Buchanan, A. H. 2010a. Design, Fabrication and Assembly of a Two-Storey Post-Tensioned Timber Building. *11th World Conference on Timber Engineering*, Trentino, Italy, pp. 9.
- Newcombe, M. P., Pampanin, S., and Buchanan, A. H. 2010b. Experimental Testing of a Two-Storey Post-Tensioned Timber Building. *9th US National and 10th Canadian Conference on Earthquake Engineering*, Toronto, Canada, pp. 8.
- Newcombe, M. P., Pampanin, S., and Buchanan, A. H. 2010c. Numerical Modelling and Analysis of a Two-Storey Post-Tensioned Timber Frame with Floor Diaphragms. *14th European Conference on Earthquake Engineering*, Ohrid, Macedonia, pp. 8.
- NZS1170.5:2004. *Structural Design Actions - Part 5 - Earthquake Actions*, New Zealand Standards, Wellington.
- NZS3101. 2006. *Concrete Structures Standard: Appendix B: Special Provisions for Seismic Design of Ductile Jointed Precast Concrete Structural Systems*, New Zealand Standards, Wellington.
- Palermo, A. 2004. "Use of Controlled Rocking in the Seismic Design of Bridges," Doctate Thesis, Technical Institute of Milan, Milan.
- Palermo, A., Pampanin, S., Buchanan, A., and Newcombe, M. 2005. Seismic Design of Multi-Storey Buildings using Laminated Veneer Lumber (LVL). *2005 New Zealand Society of Earthquake Engineering Conference*, Wairaki, New Zealand, pp. 8.
- Pampanin, S. 2005. Emerging solutions for High Seismic Performance of Precast/Prestressed Concrete Buildings *Journal of Advanced Concrete Technology*, "High Performance Systems" Vol. **3: 2**, pp. 202-223.
- Pampanin, S., Palermo, A., Buchanan, A., Fragiocomo, M., and Deam, B. 2006. Code Provisions for Seismic Design of Multi-Storey Post-Tensioned Timber Buildings. *CIB W18 Workshop on Timber Structures, Florence, Italy*, pp. 12.
- Pampanin, S., Priestley, M. J. N., and Sritharan, S. 2001. Analytical Modelling of the Seismic Behavior of Precast Concrete Frames Designed with Ductile Connections. *Journal of Earthquake Engineering*, Vol. **5: 3**, pp. 329-367.
- Pino, D., Pampanin, S., Carradine, D., Deam, B., and Buchanan, A. H. 2010. Dynamic Response of a Multi-Storey Post-Tensioned Timber Building. *14th World Conference on Timber Engineering*, Trento, Italy.
- Priestley, M. J. N., Calvi, G. M., and Kowalsky, M. J. 2007. *Displacement-Based Seismic Design of Structures*, IUSS PRESS, Pavia, Italy.
- Priestley, M. J. N., Sritharan, S., Conley, J. R., and Pampanin, S. 1999. Preliminary Results and Conclusions from the PRESSS Five-story Precast Concrete Test-Building. *PCI Journal*, Vol. **44: 6**, pp. 42-67.
- Stanton, J. F., Stone, W. C., and Cheok, G. S. 1997. A Hybrid Reinforced Precast Frame for Seismic Regions. *PCI Journal*, Vol. **42: 2**, pp. 20-32.

**INTERNATIONAL COUNCIL FOR RESEARCH AND INNOVATION
IN BUILDING AND CONSTRUCTION**

WORKING COMMISSION W18 - TIMBER STRUCTURES

FATIGUE BEHAVIOUR OF FINGER JOINTED LUMBER

S Aicher

G Stapf

MPA University Stuttgart

GERMANY

MEETING FORTY THREE

NELSON

NEW ZEALAND

AUGUST 2010

Presented by S Aicher

R Crocetti: were failures in joints or in lumber? S Aicher: Mostly (about 90%) in joints. Some were in lumber at knots.

R Crocetti: The ratio is closer to 0 for lumber. Why use 0.5? S Aicher: Design offices for roller coaster asked for testing at this value. Testing currently being done is at 0.1

T Poutanen: for other glues, would results be different? S Aicher: 1 comp. Polyurethane performs better.

J Schmid: for joint failures, are they due to glue? S Aicher: no, always in the fingers.

T Tannert: do you have indication that moisture factor proposed is dependant on moisture cycling? S Aicher: hard to say but moisture content factor is based on average moisture content.

Fatigue behaviour of finger jointed lumber

S. Aicher and G. Stapf
Material Testing Institute
University of Stuttgart, Germany

1 Introduction

Solid lumber is increasingly replaced in engineered timber structures by finger jointed lumber used as studs and beams. There are several reasons for this, being i) the significantly increased yield of higher quality/strength lumber by cutting out the knots and other strength reducing timber defects, ii) a highly increased production flexibility (drying, storage, sizes, delivery) and iii) a considerably higher dimensional stability of sticks of longer length, being a prerequisite of today's wood machining technology.

At present, finger jointed lumber is almost exclusively used in constructions designed for static loads. However, there is a demand for finger jointed lumber to be used as well in dynamically loaded constructions, e.g. bridges, wind mills, roller coasters, etc. The limited existing research data on tension fatigue strength of finger joints in small clear wood and in structural sized lumber indicate a fatigue limit in a very wide range of about 0,30 to 0,55 of static strength. The rather limited knowledge on fatigue loaded finger-jointed lumber contributed to the fact that no difference is made today in Eurocode 5, Part 2, Design of Timber Structures – Bridges, with regard to fatigue of solid lumber without finger joints and with finger joints. As there are no explicit hints on the eventual differences in the fatigue behaviour between both timber materials a design engineer might use them in an alternative manner such as in design of exclusively statically loaded constructions.

In order to get more insight into the fatigue behaviour of finger jointed solid lumber a research project is presently being conducted at the MPA University Stuttgart on fatigue of finger jointed structural sized pine lumber. Hereby, the effects of moisture and preservation treatment are considered, too. The paper presents some results of the research project including the effect of preservation treatment and gives a comparison with the fatigue reduction values k_{fat} of Eurocode 5, Part 2.

2 Literature review

Literature provides only a limited number of papers on the fatigue behaviour of glued (finger) joints. Relevant contributions were especially given by Lewis (1951), Egner und Jagfeld (1964), Bohannon and Kanvik (1968) and von Roth and Noack (1983). Lewis performed a comprehensive investigation with repeated tension fatigue loading at a stress ratio of $R = 0,1$ on glued scarf joints, being very similar to finger joints in many respects, in small clear specimens of Douglas Fir and White Oak. At $2 \cdot 10^6$ stress cycles a mean fatigue tension strength of about 60 % of the ramp load strength was obtained almost equally for both species. The well matched solid wood specimens forwarded similar fatigue results for oak and slightly higher values for fir.

The work of Bohannon and Kanvik is closely related to the investigations of Lewis. In this first, and up to today most extensive investigation on fatigue of finger joints, small clear finger jointed Douglas Fir specimens with rather similar dimensions, as those used by Lewis, were tested in repeated tension fatigue ($R = 0,1$) at 15 Hz up to 10^7 load cycles. Two different finger joint geometries were investigated. At $2 \cdot 10^6$ load cycles the fatigue bound strength reduction vs. the matched static ramp load reference results was about 0,48 for both profiles. The fatigue limit of about 40 % of static strength is in the range of $3 \cdot 10^7$ cycles according to this investigation. Thus, the fatigue reduction of the finger joints was more pronounced as in case of clear solid wood and scarf joints in solid wood.

The only known literature on finger joint fatigue of structural sized specimens stems from Egner and Jagfeld and from von Roth and Noack. Egner and Jagfeld performed repeated tension fatigue tests with finger joints in boards which previously had served for many years at moist/dry climate conditions as parts of flanges in bridge I-beams. The R-ratios of the tests varied from 0,2 to 0,3; the test frequency was 2,7 Hz. At a stress level of 55 % of the ramp load reference tests all (7) specimens survived at 10^6 load cycles. The investigations of von Roth and Noack were performed with finger jointed frame corners made of laminated Sipo Mahagoni subjected to repeated bending with 1 Hz at either positive or negative bending moment to a limit cycle number of $2 \cdot 10^6$. The fatigue bending strength values of the finger joints at $2 \cdot 10^6$ cycles were in average 51 % of the ramp load values. For higher load cycle numbers a further, however undefined strength decrease below 50 % of static strength was predicted, being qualitatively in line with the results of Bohannon and Kanvik.

The effect of moisture on wood in general has been studied by Tsai and Ansell (1990), revealing that moisture is even more detrimental in fatigue as in static loading.

3 Fatigue design according to Eurocode 5 – Part 2

In the following the fatigue design concept of EN 1995-2:2005, Eurocode 5 – Part 2, here termed EC 5-2, for timber components and mechanical connections in timber, is briefly outlined. In this context it has to be stated that EC 5-2 does not specify any hint how glued joints and especially finger joints in solid lumber should be considered. As no design rules are given, finger jointed lumber and glulam with large finger joints could be regarded as excluded from applications subject to fatigue. An engineer who is less rigorous in his approach might adopt, for finger jointed lumber sticks, subject e. g. to bending, the fatigue design rules for the bending of solid lumber.

According to EC 5-2 a simplified fatigue verification can be performed which is based on an equivalent constant amplitude fatigue loading, representing the fatigue effects of the full spectrum of loading events. More advanced fatigue verifications for varying stress amplitudes can be based on a cumulative linear damage theory, i. e. the Palmgren-Miner hypothesis. The stresses/forces due to fatigue relevant actions should be determined by an elastic analysis taking into consideration the (semi-)rigidity of the connections.

The necessity of a fatigue verification is given (EC 5-2), whenever the fatigue ratio

$$K = \frac{\frac{|\sigma_{d,max} - \sigma_{d,min}|}{f_k}}{\gamma_{M,fat}} = \frac{\Delta\sigma_d}{f_k} \quad (1)$$

exceeds the values given in Table 1.

In Eq. (1) the following notations are used:

$\sigma_{d,max}$	numerically largest design stress from the fatigue loading (Note: for determination of R acc. to Eq. (5), $\sigma_{d,max}$ and $\sigma_{d,min}$ have to be employed with signs)
$\sigma_{d,min}$	numerically smallest design stress from the fatigue loading
f_k	characteristic strength
$\gamma_{M,fat}$	partial safety factor for the material subjected to fatigue loading (shall be taken as $\gamma_{M,fat} = 1,0$)
$\Delta\sigma_d$	fatigue design stress range

component	loading or fastener type	fatigue ratio K
timber or wood based member	compression parallel or perpendicular to grain	0,6
	bending, tension, tension-compression	0,2
	shear	0,15
mechanical fasteners	dowel-type fasteners	0,4
	nails	0,1
	other joints	0,5

Table 1: Fatigue ratios K acc. to EC 5-2, Annex A

The fatigue verification criterion for a (quasi-) constant amplitude loading is

$$\sigma_{d,max} < f_{fat,d} \quad (2)$$

where

$$f_{fat,d} = k_{fat} \frac{f_k}{\gamma_{M,fat}} = k_{fat} \cdot f_k \quad \text{design value of the fatigue strength} \quad (3)$$

The fatigue reduction factor k_{fat} representing the reduction of strength at cyclically repeated or reversed loading (compression, tension, shear) dependant on the number of stress cycles N at a given stress ratio R is specified as

$$k_{fat} = 1 - \frac{1-R}{a(b-R)} \log(\beta N_{obs} t_L) \geq 0 \quad (4a)$$

where

$$R = \frac{\sigma_{d, \min}}{\sigma_{d, \max}} = \frac{\sigma_{k, \min}}{\sigma_{k, \max}} \quad \text{with} \quad -1 \leq R \leq 1 \quad \text{stress or R-ratio} \quad (5)$$

and

- a, b coefficients as specified in Tab. 2, defining the type of fatigue action imposed on timber members or connections
- N_{obs} number of constant amplitude stress cycles per year
- t_L design service life of the structure
- β factor (=indirect safety factor) considering the consequences of a fatigue failure ($\beta = 1$: no substantial consequences; $\beta = 3$: substantial consequences)

	a	b
Timber members in		
- compression, perpendicular or parallel to grain	2,0	9,0
- bending and tension, tension-compression	9,5	1,1
- shear	6,7	1,3
Connections with		
- dowels with $d < 12 \text{ mm}^1$	6,0	2,0
- nails	6,9	1,2

¹⁾ details see EN 1995-2:2004

Table 2: Values of fatigue coefficients a and b according to EC 5-2, Table A. 1

Eq. (4a) can be rewritten for reason of comparison with other known approaches (e.g. Mohr (2001) in the format

$$k_{\text{fat}} = 1 + \alpha \lg N \quad (4b)$$

where

$$\alpha = \frac{1 - R}{a (b - R)} \quad (6)$$

Equations (4a, b) specify a linear relationship between the fatigue reduction factor k_{fat} and the logarithm of the number of stress cycles at the end of service life, what represents the most simple assumption / approximation for the fatigue degradation of a material.

Figures 1a-f show an evaluation of Eqs. (4a,b), i. e. the linear $k_{\text{fat}} - \lg N$ relationships, for different discrete R-ratios stretching from -1 to 0,8. Table 3 specifies the k_{fat} values for two distinct numbers of stress cycles, $N = 2 \cdot 10^6$ and 10^7 , at six R-ratios between -1 and 0,8. Figures 2a and b show the nonlinear relationship between k_{fat} and the stress ratio R for the different types of fatigue loadings and fasteners. All graphs in Figs. 1a-f and Figs. 2a, b reveal a considerable difference in the evolution of k_{fat} for the different types of fatigue loading as well as between dowel type fasteners and nails. Repeated

compression fatigue loading delivers the smallest reduction of the short term ramp load strength. On the contrary, shear loading delivers the lowest k_{fat} values in the whole reversed loading range $-1 < R \leq 0$ of all loading types and in most of the repeated fatigue stress range $0 \leq R \leq 0,6$. (Note: mechanical fasteners, forwarded still somewhat more pronounced fatigue degradations are not discussed here.) In between repeated compression and shear loading (reversed/repeated up to $R = 0,6$) the fatigue reduction factor for repeated tension, bending or reversed tension-compression and reversed bending, is found.

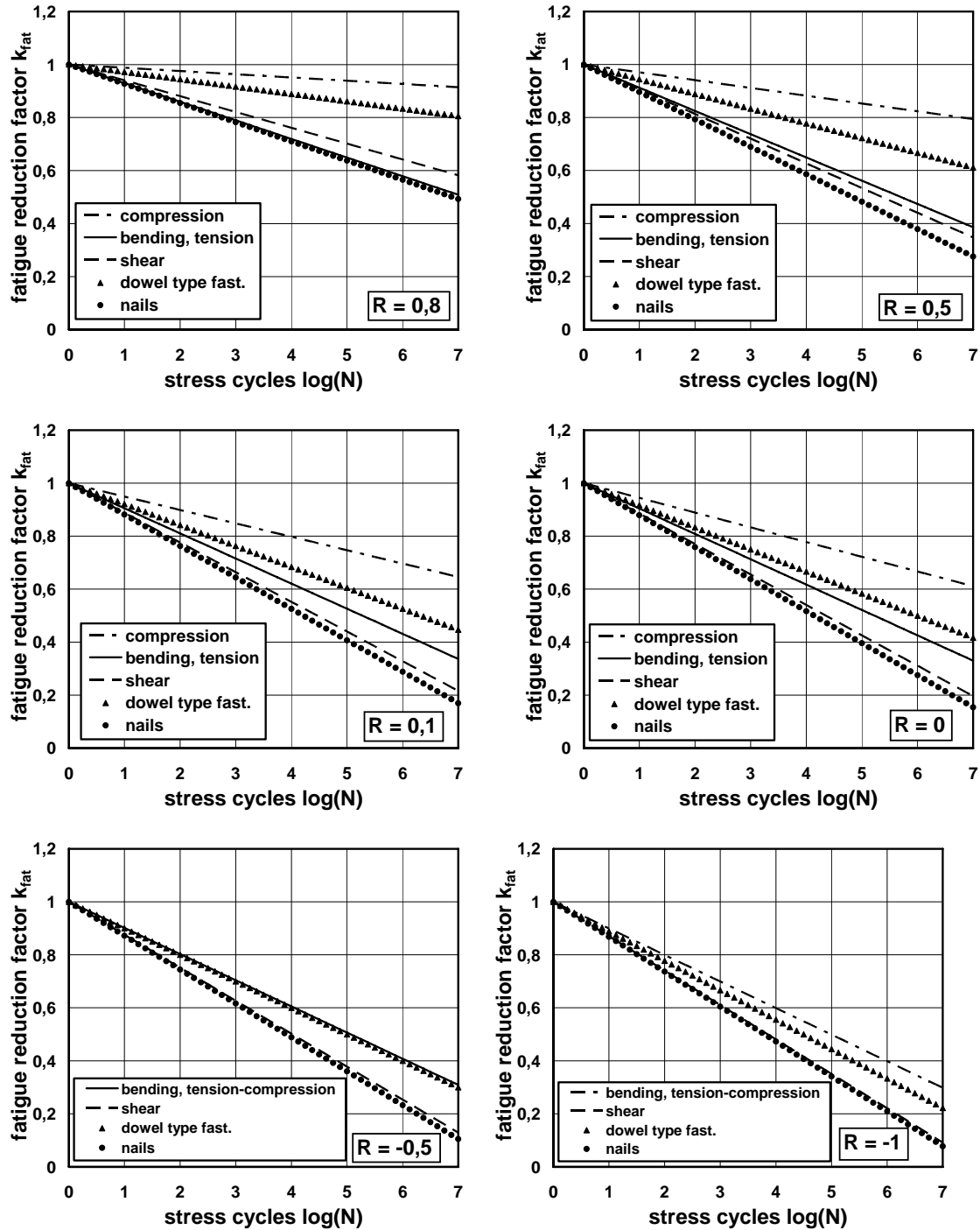


Figure 1a-f: Graphs of fatigue reduction factor $k_{fat}(N, R = \text{const.})$ depending on stress cycles N at discrete stress ratios R for different loading modes of timber members and timber fastener types.

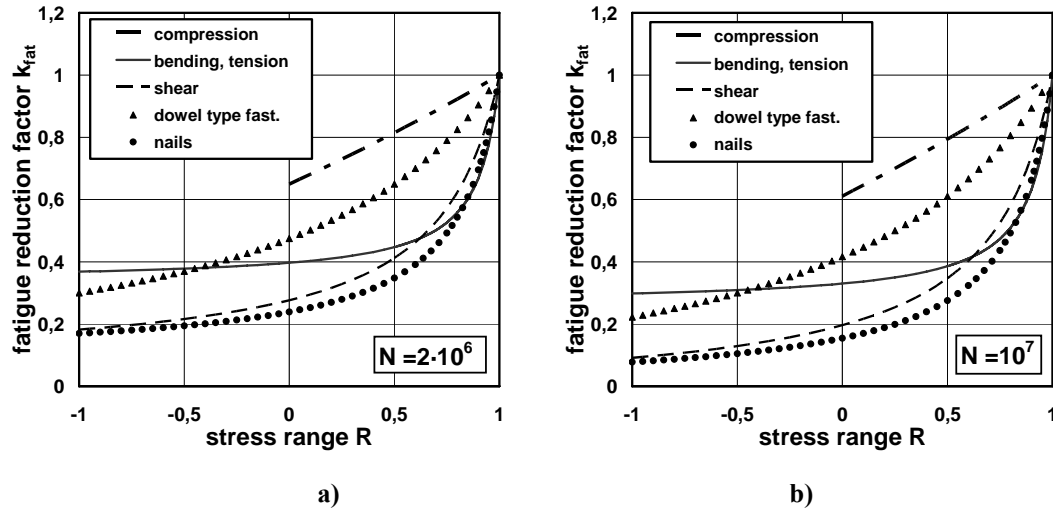


Figure 2a, b: Graphs of fatigue reduction factor $k_{fat}(N = \text{const.}, R)$ acc. to EC 5-2 depending on stress ratio R at discrete stress cycle numbers N for different loading modes and timber fastener types.

materials / fasteners	loading mode or fastener type	stress ratio R and stress cycles N											
		0,8		0,5		0,1		0		-0,5		-1	
		$2 \cdot 10^6$	10^7	$2 \cdot 10^6$	10^7	$2 \cdot 10^6$	10^7	$2 \cdot 10^6$	10^7	$2 \cdot 10^6$	10^7	$2 \cdot 10^6$	10^7
timber members	compression, (parallel or perpendicular to grain)	0,92	0,91	0,81	0,79	0,68	0,65	0,65	0,61	0,50	0,45	0,37	0,30
	bending, tension, tension-compression	0,56	0,51	0,45	0,39	0,40	0,34	0,40	0,33	0,38	0,31	0,37	0,30
	shear	0,62	0,58	0,41	0,35	0,29	0,22	0,28	0,20	0,22	0,13	0,18	0,09
mechanical fasteners in timber components	dowel type fastenes	0,82	0,81	0,65	0,61	0,50	0,45	0,47	0,42	0,37	0,30	0,30	0,22
	nails	0,54	0,49	0,35	0,28	0,25	0,17	0,24	0,15	0,19	0,10	0,17	0,08

Table 3: Compilation of fatigue reduction factors k_{fat} acc. to EC 5-2 for discrete stress cycle numbers and R -ratios

It is evident from Figs. 2a and b that the fatigue bound strength reduction in bending and at tension – compression loading according to EC 5-2 takes place almost entirely in the repeated stress range $0 \leq R < 1$ and hereby predominantly in the range of $0,5 < R < 1$. This is contrary to shear loading where EC 5-2 specifies a rather continuous fatigue degradation over the whole stress ratio range of $-1 \leq R < 1$. A thorough literature review has not forwarded any fundamental publication substantiating the described R -ratio effects. Significantly different R -ratio influences are for instance given by Mohr (2001).

4 Experimental program, specimens

The conducted test program aiming at the determination of the k_{fat} -values in bending of finger jointed structural lumber consisted of three test series B1, B2 and C, all comprising ramp load reference tests, fatigue tests and residual strength tests. The employed

lumber was visually graded European pine (*pinus sylvestris*) of strength class C 24. The visual grading was performed with regard to grade S 10 acc. to DIN 4074-1, which conforms to EN 14081. The cross-sectional dimensions of the lumber were very similar, being 90 mm x 190 mm in test series B1 and B2 and 100 mm x 200 mm in case of test series C. The density of the timber was closely matching in all test series and conformed on average to about 510–540 kg/m³ (see below). The specimens of test series B2 were preservative treated. Table 4 gives a compilation of the test program and specifies the numbers of specimens per test series.

test series	cross-section b x d	preservative treatment	number of specimens		
			ramp load reference tests	fatigue tests	residual strength tests
-	mm x mm	-	-	-	-
B1	90 x 190	no	6	8	1
B2	90 x 190	yes	7	8	1
B=B1+B2	90 x 190	yes/no	13	16	2
C	100 x 200	no	10	24	11
B+C	rd. 100 x 200	yes/no	23	40	15

Table 4: Compilation of test program and number of specimens per test series; all tests were performed in flatwise 4point bending with a finger joint at mid-span (finger profile visible on the wide cross-sectional side)

All bending specimens contained a finger joint at mid-length. The finger profile dimensions conformed to EN 385; the length of the finger was 20 mm, pitch and tip width were 6,2 mm and 1,0 mm, respectively. The finger joints were glued by means of a one-component moisture curing Polyurethane adhesive (HB 530, Purbond AG) approved for structural gluing by a German Technical Building Approval, Z-9.1-616, issued by DIBt, Berlin.

The treated timber sticks were impregnated by means of a salt-based, water-soluble timber preservative “Wolmanit CX-8”, company Dr. Wolman GmbH, conforming to German Technical Building Approval Z-58.1-1510. The amount of salt impregnation, being > 7,5 kg/m³ of wood was oriented on the demands of hazard class 4 of DIN 68800-3, necessitating a pressure vacuum preservative treatment.

5 Test setup and procedure

All tests being static ramp load reference tests, the fatigue tests and the tests for residual strength of the survivors, were performed as 4-point bending tests acc. to EN 408 in flatwise bending. Figures 3a, b give a schematic view of the test set-up and of the specimen dimensions being equal in ramp, fatigue and residual strength tests.

All specimens had a finger joint at mid-span, i.e. in the constant moment range. The orientation/manufacture of the fingers was such that the zig-zag finger profile was visible on the wide sides of the cross-section, also termed “standing fingers”. This finger orientation results in general, in static loading, at higher strengths as compared to so termed “lying fingers” where the zig-zag finger profile is visible along specimen depth. In the latter finger joint configuration, depending on the quality of joint manufacture, a

small groove/notch along full width at the bending tension edge can occur. This groove then acts as a stress raiser what can be considered especially unfavourable in case of fatigue loading.

The ramp load reference tests were performed quasi-force controlled in a test stand with hydraulic pistons. Apart from the applied forces, mid-span deflection was measured at mid-width of the bending compression edge. Moisture content was measured for all untreated specimens (used for ramp load, fatigue and residual strength testing) in three different cross-sectional depths of 1, 2,5 and 4 cm. The moisture content of the treated specimens was obtained by oven dry method. Density of both adherents was throughout determined by weighing cross-sectional slabs.

The fatigue tests were performed in force control, whereby the loads at the 3rd point of the span were applied by a servo-hydraulic actuator acting at mid-span on a steel bar, distributing the loads via steel rollers to the beam. At both supports (rollers) the bearing areas were covered with teflon layers to minimize friction. The failure recognition was programmed as a trespass of a deflection limit of about three times of the initial elastic deformation.

The most important fatigue test parameters were chosen as following:

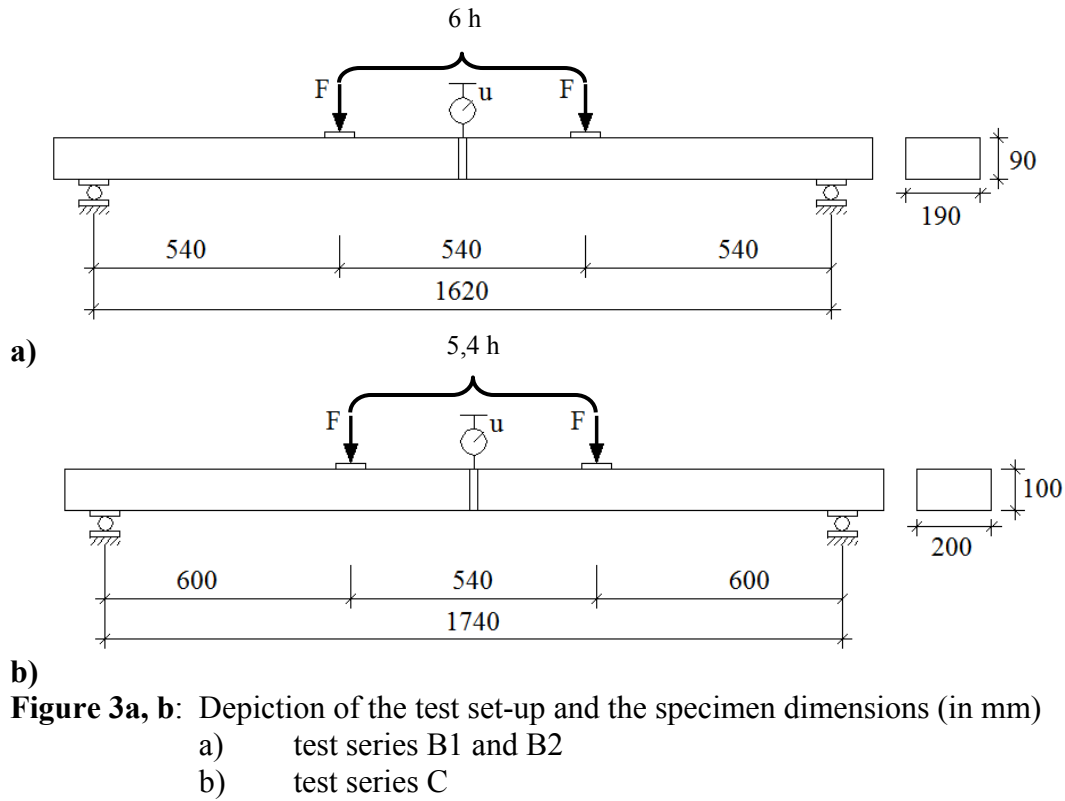
- the stress ratio of the repeated bending tests was set constant to $R = 0,5$. The reason for the rather high R-ratio emanated from the demands of an industrial application of the reported research project results
- the load/stress cycle frequency varied from 1,5 to 3,3 Hz, being 2 Hz for most of the tests (the frequency variation resulted from some test equipment restriction)
- the limit load cycle number (ideally intended to verify the fatigue limit strength) when tests were stopped in case the specimen had not failed (= survivor) was set to the lowest scientifically justifiable number of $N_{\text{limit}} = 2 \cdot 10^6$ load/stress cycles.

The most crucial part in the conception of fatigue tests consists in the determination of the fatigue stress levels. This task heavily depends on the financial limitations/time frame of the project and is inherently bound to the scatter of the material/specimen properties, the latter being very high in case of visually graded, finger jointed lumber. Literature provides several procedures to derive a consistent S-N curve from ramp load strength to the fatigue limit strength. In all approaches one or several specimens are tested in fatigue loading (repeated or reversed loading) at a distinct stress level (SL) of the ramp load reference strength, which in cases of timber in structural dimensions is subject to a rather crude estimate. This is even truer, in case the moisture content of the specimens to be compared varies.

In the three reported test series of the project, all with very or rather small specimen numbers, two different strategies were followed. In test series B1 and B2 the applied stress levels were chosen quite high in order to assess, if possible, the slope of the S – N curve in short time. In the case of test series C an effort was made to assess the fatigue limit strength by testing a high number of specimens at stress levels closer to the estimated fatigue limit strength. The individually chosen nominal and moisture normalized (see below) fatigue stress levels SL are given in Tables 6 and 7 for test series B1, B2 and C, respectively.

All survivors in the fatigue tests (no failure below $2 \cdot 10^6$ stress cycles) were tested in quasi-force controlled ramp load tests for determination of residual bending strength and stiffness.

All tests i. e. ramp load reference tests, fatigue tests and residual strength test were performed at ambient climate in non-climate controlled test rooms at a temperature of about 20 °C to 24 °C and relative humidities of about 40 % to 53 %.



6 Test results

6.1 Results of ramp load reference tests

Table 5 comprises the results (mean values, standard deviation (STD), C.O.V., minimum value) of the ramp load reference tests. Apart from bending strength nominal and moisture normalized ($u = 12\%$), moisture content, density and modulus of elasticity of each test (sub-)series is given.

The results given in Tab. 5 reveal a close agreement of the ramp load bending strength values of all test series. This is especially true for the moisture normalized ($MC = 12\%$) results. Closely related hereto, and mechanically compliant, the densities of all test series were very similar.

In order to compare all strength results and also the stress levels of the fatigue tests on the basis of a unique moisture content ($MC = 12\%$), the relation between ramp load bending strength as well as fatigue stress level (specimen with $u \neq 12\%$) and moisture content of the samples of all test series of the research project was determined as a fourth order bending strength vs. moisture content u equation. In linearized manner, the employed bending strength-moisture relation can be written as (u dimensionless in $\%$) $f_m = 0,0189 \cdot u + 23,86$ [N/mm²].

6.2 Results of fatigue tests

The results of the fatigue tests, being in essence the number of load/stress cycles to failure, if occurred, are given in Tables 6 and 7 for test series B1, B2 and C, respectively.

Additionally, the tables give the nominal and moisture normalized stress levels SL_{nom} and SL_{12} of each fatigued specimen and the type of the respective fatigue fracture.

The fracture modes were, in general, finger joint failures, sometimes in combination with a crack emanating from a knot at admissible distance from the joint. A few failures in test series B1 and B2 were exclusively initiated by a knot; these results were not excluded from the evaluation. Figures 4a and b, and Figure 5 depict the obtained fatigue results of test series B1, B2 and C in semi-logarithmic representation of the nominal stress level SL_{nom} vs. the logarithm of load/stress cycles N to failure (if occurred). The figures also contain the ramp load and residual strength test results, the latter not discussed in this paper.

test series	treatment	Number of specimens	statistical parameter	bending strength f_m		moisture content (MC)	density (mean of both adherents)	Modulus of elasticity
				at moisture (MC) of test	normalized to 12% MC			
				$f_{m,u}$	$f_{m,12}$			
-	-	-	-	N/mm ²	N/mm ²	%	kg/m ³	N/mm ²
B1	no	6	x_{mean}	42,5	39,7	10,3	539	11950
			STD	7,6	7,1	0,7	53	1140
			COV %	17,9	17,9	7,1	9,9	9,6
			x_{min}	34,4	32,8	9,3	487	9820
B2	yes	7	x_{mean}	42,2	41,3	11,4	546	11290
			STD	7	6,9	0,7	36	1300
			COV %	16,7	16,8	6,2	6,6	11,5
			x_{min}	31,7	31,7	10	489	9090
B= B1+B2	no/yes	13	x_{mean}	42,3	40,6	10,9	543	11600
			STD	7	6,8	0,9	43	1230
			COV %	16,5	16,7	8,4	7,9	10,6
			x_{min}	31,7	31,7	9,3	4,87	9090
C	no	10	x_{mean}	38,5	43,2	15,3	522	9830
			STD	5,8	6,3	1,1	34	648
			COV %	15	14,5	7,5	6,5	6,6
			x_{min}	29,1	34,5	13,3	475	8710

Table 5: Compilation of results from ramp load reference bending tests

With regard to an approximation of the fatigue data and a comparison with the EC 5-2 fatigue curves, all test series were comprised in one sample. Figures 6a, b show the stress levels SL , now termed k_{fat} , of all data vs. $\lg N$ together with the ramp load and residual strength values. In detail, Fig. 6a presents the fatigue reduction factor based on the nominal stress level $k_{fat} = SL_{nom}$ and Fig. 6b gives the S-N curve on the basis of the moisture normalized stress levels $k_{fat} = SL_{12}$. Both figures also show the $k_{fat} - \lg N$ relationship of EC 5-2 derived from Eqs. (4b) and (6) for the two loading types bending and shear with $R = 0,5$ what results in

$$k_{fat} = 1 - 0,088 \lg N \quad \text{EC 5-2, bending} \quad (7a)$$

$$k_{fat} = 1 - 0,093 \lg N \quad \text{EC 5-2, shear} \quad (7b)$$

In order to obtain a median S-N (or k_{fat} -N) curve from the $k_{fat} = SL_{nom}$ test results a regression line was computed by a weighted least square fit based on the median times to failure at the different nominal load/stress levels. As usual, the median of the ramp load strengths was included. In a rather crude conservative assumption the median time to failure of stress level $SL_{nom} = 0,39$, which revealed seven survivors out of eight specimens, was set to $2 \cdot 10^6$ cycles. Further, in order to enable a linear regression function (incorrect according to Physics) which incorporates the ramp load median ($k_{fat} = 1$) as closely as possible (correct according to Physics), the results of the very high stress level $SL_{nom} = 0,94$ were excluded (see Fig. 6a)

The data fit was performed twofold as $N = f(SL_{nom})$ being correct according to Physics and by $SL_{nom} = f(N)$ as predominantly given in the literature. In the specific case both approximations yielded the same linear median Wöhler curve

$$k_{fat} = 1 - 0,080 \lg N \quad (8)$$

which, irrespective of the stated deliberate assumptions is in very good agreement with the S-N curves (7a, b) resulting from EC 5-2. Note: The approximation of the moisture normalized stress levels SL_{12} forwarded an almost similar result as eq. (8), when excluding the $SL_{12} = 0,93$ and $0,94$ specimens.

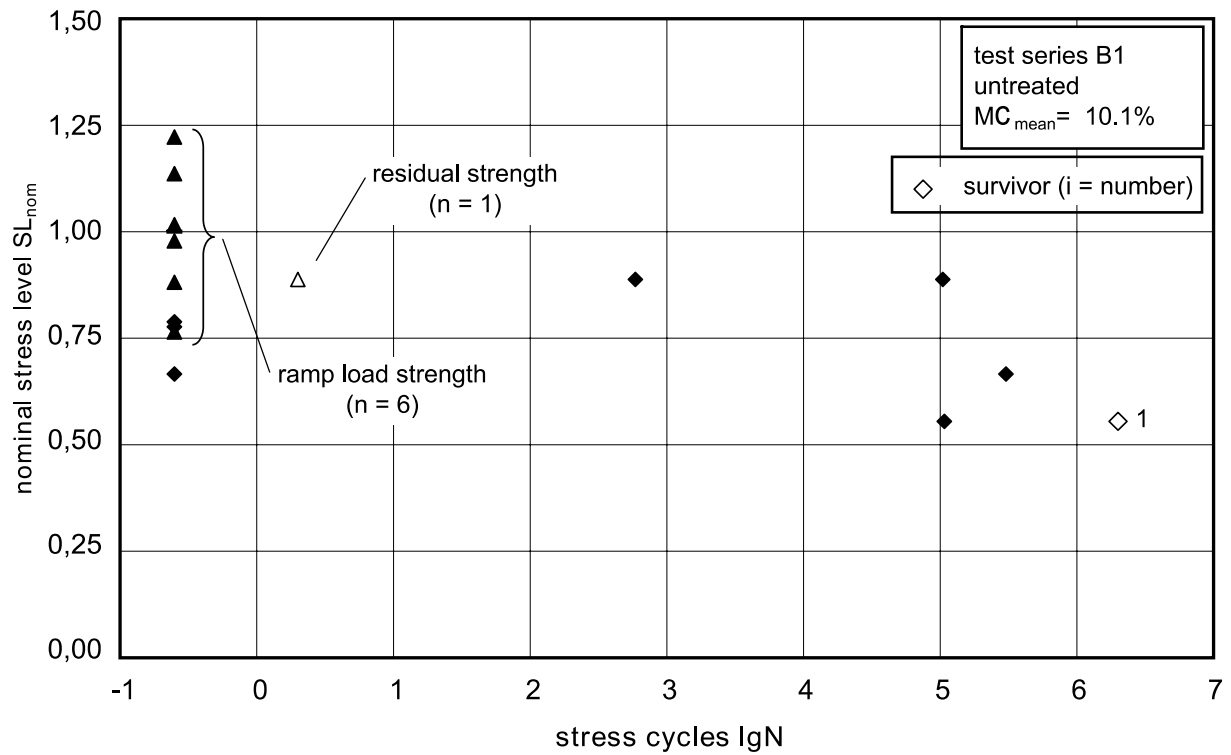
For a stress cycle number of $N = 2 \cdot 10^6$ the EC 5-2 values for k_{fat} are 0,45 and 0,41 in case of bending and shear loading, respectively, whereas Eq. (8) delivers a slightly or moderately higher value of $k_{fat} = 0,47$. In contrary hereto, the hi-linear relationship III specified by Mohr (2001) for fatigue of finger jointed lumber subject to repeated tension (and also proposed for shear of solid wood) results in a k_{fat} -value of 0,60 being considerably higher as the EC-5 predictions and the experimentally derived fatigue reduction factor.

test series	specimen No.	frequency	moisture content	nominal max. stress	moisture normalized max. stress	stress level		fatigue failure cycles	type of failure FJ=finger joint K=knot S=survivor
				$\sigma_{\max, \text{nom}}$	$\sigma_{\max, 12}$	nominal SL_{nom}	moist. norm. SL_{12}		
-	-	Hz	%	N/mm ²	N/mm ²	-	-	-	-
B1 (untreated)	1	1,5	10,4	40	37,7	0,94	0,93	589	FJ
	2	1,5	10,4	40	37,7	0,94	0,93	104288	FJ
	3	2	9,3	35	31,5	0,82	0,78	0	FJ
	9	2	9,9	35	32,3	0,82	0,8	0	K
	4	2	11,1	30	29	0,71	0,71	0	K
	6	2	10,7	30	28,5	0,71	0,7	302152	FJ
	12	2	9,2	25	22,4	0,59	0,55	2000000	S
	15	2	9,4	25	22,6	0,59	0,56	107070	FJ
B2 (treated)	1b	1,5	10,4	40	37,7	0,94	0,93	22000	FJ
	2b	1,5	10,4	40	38	0,94	0,94	173	FJ
	3b	2	12	35	35	0,82	0,86	42729	FJ
	9b	2	9,7	35	32	0,82	0,79	18210	FJ/K
	4b	2	11,1	30	28,9	0,71	0,71	0	FJ/K
	6b	2	10,3	30	28,2	0,71	0,69	97920	K
	12b	2	9,4	25	22,7	0,59	0,56	2000000	S
	15b	3	10,1	25	23,2	0,59	0,57	749297	FK/K

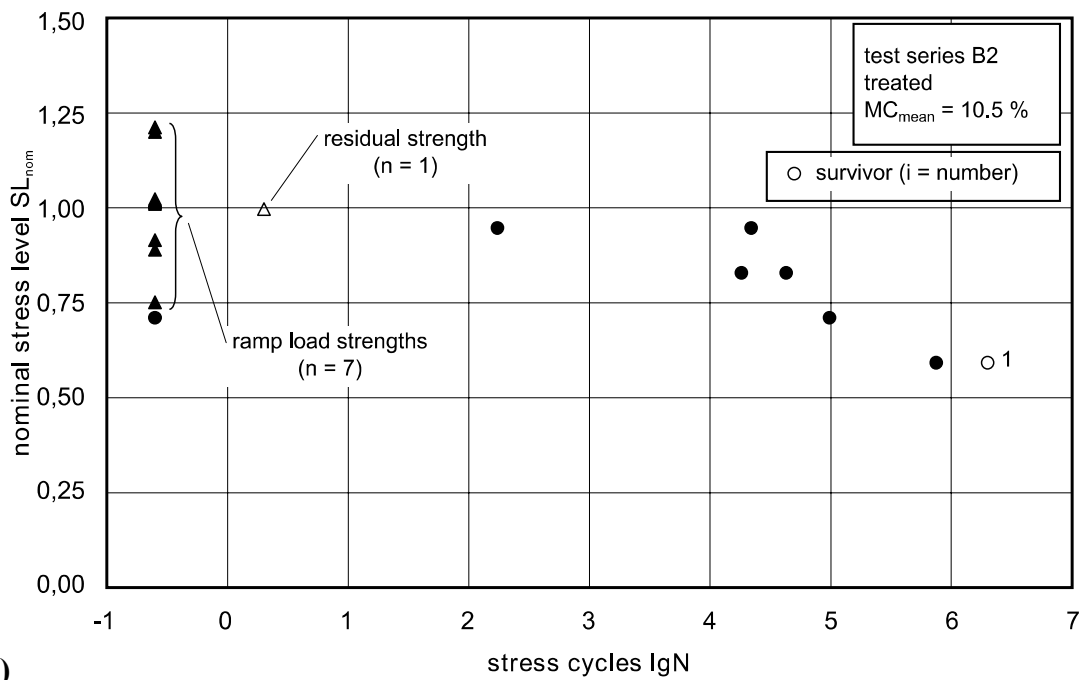
Table 6: Compilation of fatigue stress levels and fatigue results of test series B1 and B2

test series	specimen No.	frequency	moisture content	nominal max. stress	moisture normalized max. stress	stress level		fatigue failure cycles	type of failure FJ=finger joint K=knot S=survivor
				$\sigma_{\max, \text{nom}}$	$\sigma_{\max, 12}$	nominal SL_{nom}	moist. norm. SL_{12}		
-	-	Hz	%	N/mm ²	N/mm ²	-	-	-	-
C (untreated)	1	1,5	18,7	30	37,4	0,78	0,87	5023	FJ/K
	2	2	17	30	35,6	0,78	0,82	691	FJ
	3	2	17,5	30	36,2	0,78	0,84	0	FJ
	4	2	16	30	34,5	0,78	0,8	286	FJ
	5	2	18,5	25	31	0,65	0,72	82700	FJ
	6	2	16,8	25	29,5	0,65	0,68	33900	FJ
	7	2	16,3	25	29,1	0,65	0,67	2059318	FJ
	8	3	14,7	20	22	0,52	0,51	782920	FJ
	9	3	16	20	23	0,52	0,53	1117227	FJ
	10	3	15,7	20	22,7	0,52	0,53	$> 2 \cdot 10^6$	S
	11	3	12,8	20	20,6	0,52	0,48	$> 2 \cdot 10^6$	S
	12	3	14	20	21,5	0,52	0,5	129388	FJ/K
	13	3	13,7	20	21,2	0,52	0,49	$> 2 \cdot 10^6$	S
	14	3	14,2	20	21,6	0,52	0,5	$> 2 \cdot 10^6$	S
	15	3	15	20	22,2	0,52	0,51	814000	FJ
	16	3	13,7	20	21,2	0,52	0,49	1957470	FJ
	17	3,3	15	15	16,7	0,39	0,39	$> 2 \cdot 10^6$	S
	18	3,3	15,2	15	16,8	0,39	0,39	831424	FJ
	19	3,3	13,8	15	16	0,39	0,37	$> 2 \cdot 10^6$	S
	20	3,3	11	15	14,4	0,39	0,33	$> 2 \cdot 10^6$	S
	21	3,3	14,5	15	16,4	0,39	0,38	$> 2 \cdot 10^6$	S
	22	3,3	13,7	15	15,9	0,39	0,37	$> 2 \cdot 10^6$	S
	23	3,3	13,8	15	16	0,39	0,37	$> 2 \cdot 10^6$	S
	24	3,3	13,8	15	16	0,39	0,37	$> 2 \cdot 10^6$	S

Table 7: Compilation of fatigue stress levels and fatigue results of test series C



a)



b)

Fig. 4 a, b: Fatigue results of test series B1 and B2, given as SL_{nom} vs. $lg N$ relationship; additionally ramp and residual strengths are included
a) series B1 (untreated) b) series B2 (treated)

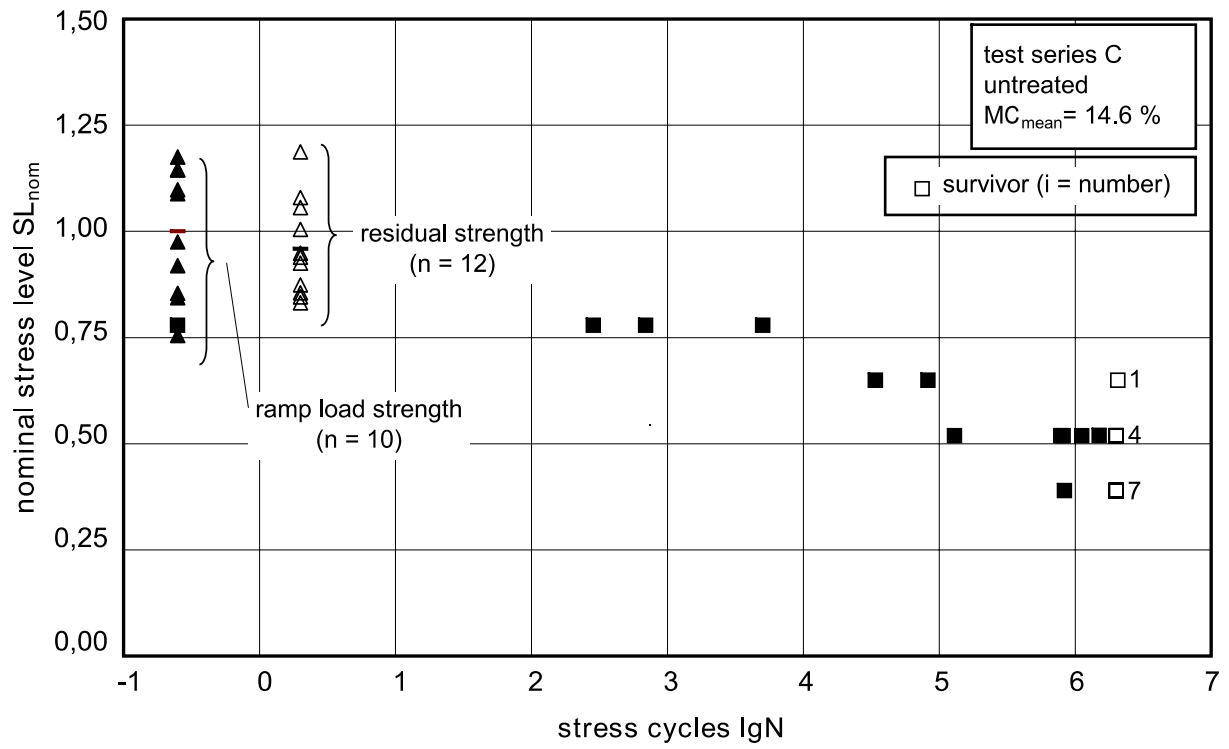
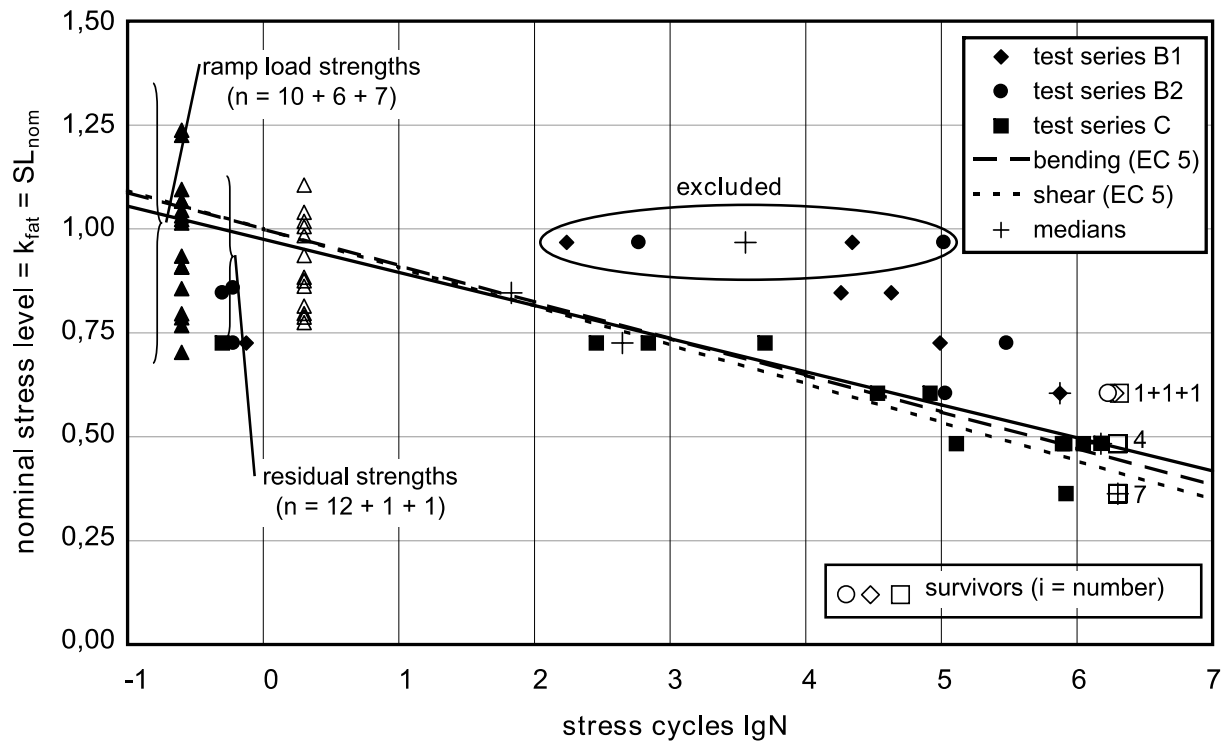
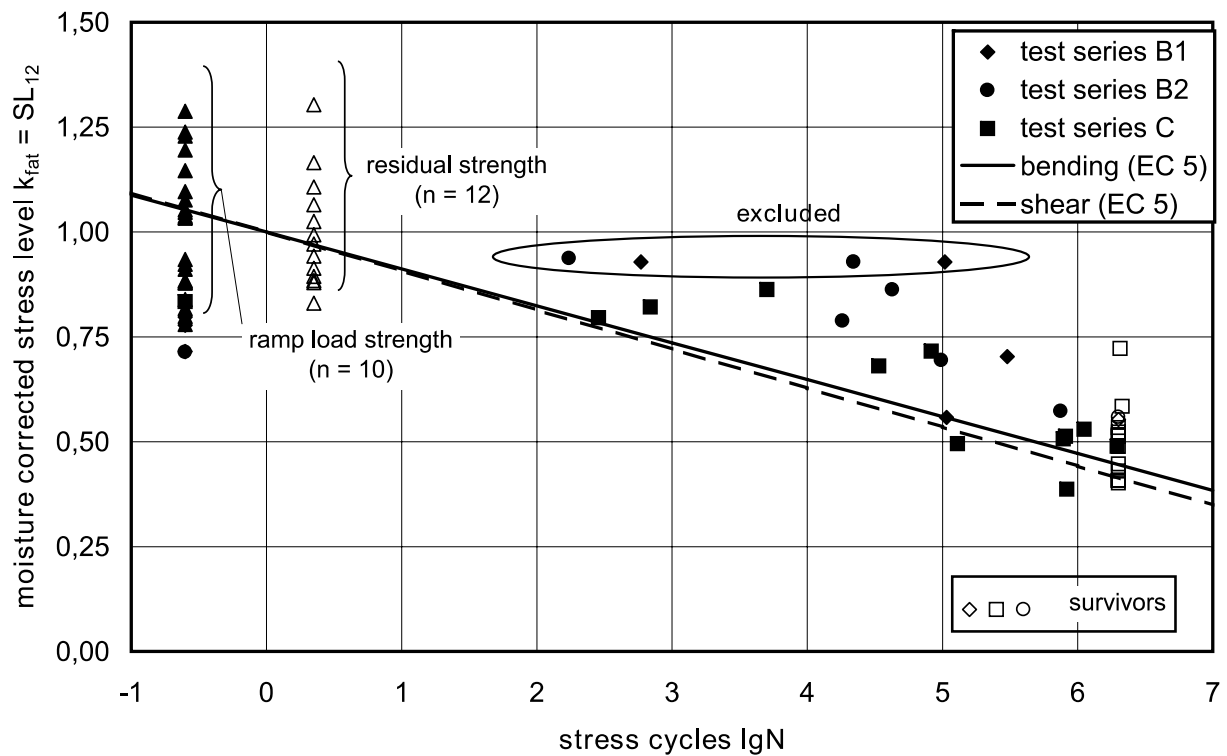


Figure 5: Fatigue results of test series C, given as SL_{nom} vs. $\lg N$ relationship; additionally ramp and residual strengths are included



a)



b)

Fig. 6 a, b: Fatigue reduction factor k_{fat} vs. $lg N$ results (plus ramp load and residual strengths of survivors) of the combined test series B1 and B2 and C. Additionally the EC 5-2 curves (lines) for fatigue in bending and shear and the approximations of the test results are given for the median level

a) $k_{fat} = SL_{12}$

b) $k_{fat} = SL_{nom}$, (note: $SL_{nom} = 0,94$ excluded from linear regression analysis)

7 Conclusions

Fatigue bending tests with finger jointed pine lumber were performed with a stress ratio of 0,5. The nominal cross-section was 100 mm x 200 mm. The tests were conducted up to a maximum (limit) stress cycle number of $2 \cdot 10^6$, beyond which unbroken specimens were considered as survivors and tested in ramp load for determination of residual strength.

The fatigue results were approximated for derivation of a median S-N curve in crude engineering manner by a linear regression including the ramp load results. The obtained linear median Wöhler curve has a slightly less steep slope as resulting from Eurocode 5 – Part 2 for bending and shear loading. Whether these findings hold true for small positive and especially for negative R-ratios is not evident especially as the effect of R ratio is assessed quite different in literature. It has also to be checked whether the more unfavourable finger joint configuration with “lying fingers” elicits similar fatigue results. According to all of the test results (ramp load, fatigue, residual strength data) the median fatigue bending strength limit (for $R \approx 0,5$) should be in the range of 35 % to 45 % of the ramp load strength, to be verified in further investigations.

The limited numbers of results in each of the test series B1 and B2 do not enable a reliable answer as to whether the specific preservative treatment has an impact on the fatigue behaviour or not. On the other hand, the data do not give any indication of a significant difference in the fatigue of treated and untreated finger jointed pine lumber. This statement however, is necessarily related to the very dry moisture state of about 10 % of both test series.

8 References

- EN 1995-2:2005 (2005): Eurocode 5: Design of timber structures – Part 2: Bridges.
- Bohannon, B. and Kanvik, K.J. (1969): Fatigue strength of finger joints. Forest Service Res. Paper FPL No. 114, U. S. D. A., FPL, Madison, WI
- Egner, K. and Jagfeld, P. (1964): Investigations on finger-jointed planks after many years of use – behaviour at pulsating tensile stress (in German). Holz Roh-Werkstoff 22 (3): 107 – 113
- Tsai, K. and Ansell, M. (1990): The fatigue properties of wood in flexure. J. Mat. Science 25:865-878
- Lewis, W. (1951): Fatigue of wood and glued joints used in laminated construction. Forest Prod. Res. Soc. 5 221–229
- Mohr, B. (2001): Zur Interaktion der Einflüsse aus Dauerstands- und Ermüdungsbeanspruchung im Ingenieurholzbau. PhD thesis, Technical University Munich
- Von Roth W. and Noack D. (1983): Studies on the Fatigue Behaviour of Framework Made of Bent Laminated Wood (in German, English abstract). European Journal of Wood and Wood Products 41 (6): 233–240

**INTERNATIONAL COUNCIL FOR RESEARCH AND INNOVATION
IN BUILDING AND CONSTRUCTION**

WORKING COMMISSION W18 - TIMBER STRUCTURES

**EXPERIMENTAL AND NUMERICAL INVESTIGATION ON
THE SHEAR STRENGTH OF GLULAM**

R Crocetti

Division of Structural Engineering, Lund University

P J Gustafsson

H Danielsson

Division of Structural Mechanics, Lund University

A Emilsson

Limträtenik AB, Falun

SWEDEN

S Ormarsson

Department of Civil Engineering, DTU

DENMARK

MEETING FORTY THREE

NELSON

NEW ZEALAND

AUGUST 2010

Presented by R Crocetti

H Larsen: Tests should be done using EN408 so that results can be corrected. Other methods are more complicated and EN408 is the simplest. R Crocetti: You may be right but EN408 method is not always successful.

R Nestic: Have you compared results with ASTM tests? R Crocetti: No, but beam tests method is higher than small specimens' tests

B Yeh: People assume that glulam shear values are for ASTM method but this is not the case. How to induce shear in a beam with overhangs when there are no shear within these parts? R Crocetti: It does occur.

S Aicher: Did you try to evaluate k_{cr} value for specimens with cracks? R Crocetti: It was not our intention.

T Poutanen: Shear values obtained look high in comparison to the ones in use. Do you agree? R Crocetti: No.

A Manoorchehr: How is the notch made in the specimens?

R Crocetti: using band saw. The cracks forces the stresses to start

L Daziel: When putting UDL on un-glued laminations, the same capacity was obtained because of friction. The shear capacity was observed as negligible.

Experimental and numerical investigation on the shear strength of glulam

Roberto Crocetti¹, Per Johan Gustafsson², Henrik Danielsson², Arne Emilsson³, Sigurdur Ormarsson⁴

¹ Division of Structural Engineering, Lund University, Sweden

² Division of Structural Mechanics, Lund University, Sweden

³ Limträtenik AB, Falun, Sweden

⁴ Department of Civil Engineering, DTU, Denmark

1 Introduction

According to EC5, the shear resistance of a structural timber element should be determined on the basis of the characteristic shear strength of the material, along with classical beam theory. For glulam, the characteristic strength values are given by the European standard EN 1194 [3], which assumes a direct relationship between tensile strength and shear strength of the lamination

$$f_{v,k} = 0.32 \cdot (f_{t,0,k})^{0.8}$$

As an example, the characteristic shear strength of glulam class GL28c, consisting of inner laminations with characteristic tensile strength $f_{t,0,k} = 14.5$ MPa, would be $f_{v,k} = 0.32 \cdot (14.5)^{0.8} = 2.9$ MPa.

However, recent investigations both on glulam members [4] and on timber members [5] have shown that the shear strength of spruce is higher than the shear strength obtained by means of the model proposed by EN1194. Moreover, the studies show that the shear strength is nearly constant, regardless the strength class of the timber material.

1.1 Objective

The general objective of this study is to gain a better knowledge on the shear strength of glulam subjected to predominant shear loading and with different boundary conditions. Specific objectives include the following:

- Propose a practical setup for testing glulam in shear which does not generate too large secondary stresses in the specimen, e.g. perpendicular to the grain stresses.
- Investigate the shear strength of glulam specimens both with I-cross section and with rectangular cross section.
- Investigate the influence of growth ring orientation on the shear strength of glulam

1.2 Background

The European standard EN 408 [6] gives indications for the determination of shear strength of timber. The loading arrangement according to EN 408 involves gluing of steel plates to the timber specimens. This method is rather unpractical and it often leads to failure in the glued area at the interface between the steel plate and the timber specimen, due to high perpendicular-to-grain stresses in the vicinity of the point of application of the load, resulting in invalid shear strength values [5]. There are also indications that the shear strength obtained by testing according to EN 408 is lower than the shear strength obtained by means of ordinary beam test methods [10].

Several authors have investigated on the shear strength of timber.

H. Granholm [7] conducted shear tests on I-beams in four-point bending. Totally 19 beams were tested, divided in four main groups. The first three groups consisted of I-beams with nominally identical flanges with cross section 152x 25mm². The results showed that I-

beams with webs consisting of boards placed edgewise (i.e. primarily subjected to shear in radial plane) had considerably greater strength than the I-beams with webs consisting of boards flatwise placed (i.e. primarily subjected to shear in tangential plane). In particular, the I-beams with webs consisting of three edgewise placed boards, showed shear strength values about 70% larger than the shear strength of I-beams with webs consisting of flatwise glued boards.

J.K.Denzler et al. [5] presented the results of 382 shear tests carried out according to EN 408, with specimen size 32 x 55 x 300 mm³. The main results of this research are: *i)* mean shear strength is significantly lower when failure occurs in tangential direction as compared to shear failure in radial direction across the growth rings (radial direction); *ii)* knots do not have remarkable influence on shear strength; *iii)* correlation between density and shear strength; *iv)* no evidence of an increase of characteristic shear strength for higher strength classes.

B. Madsen [8] conducted shear tests on hundreds of timber specimens. The specimens were boards with realistic dimensions (cross section 35x140 mm², and different lengths up to 560 mm). The specimens were loaded by a direct application of a moment couple created by two parallel forces applied to the edge of the specimens. The main results obtained by the author are: *i)* the stressed volume has influence on the shear strength; *ii)* shear strength strongly decreases with increasing moisture content; *iii)* shear strength of specimens loaded in tangential direction is similar to shear strength of specimens loaded in radial direction across the growth rings.

D.R.Rammer [9] investigated the behaviour of glulam beams with rectangular cross section tested in a five-point beam configuration to determine the shear strength capacity. A total of 200 specimens were tested, 100 loaded edgewise about the strong axis (shear in the radial plane) and 100 loaded flatwise about the weak axis (shear in the tangential plane). The specimens had all the same width but different depths, in order to investigate the influence of volume on the shear strength. The main findings obtained by this research are: *i)* shear strength decreases with increasing specimen volume; *ii)* flatwise loaded specimens showed higher shear strength than edgewise loaded specimens, due to “system effect”.

M. Poussa et al. [10] performed some 280 shear tests, of which 200 were performed according to the European standard EN-408, and 80 on beams with I-cross section loaded in a three-point beam configuration. The main result of this research is that the shear strength of beam specimens was about two times that of shear specimens.

K. B. Dahl [11] investigated the shear behaviour of some 83 small scale specimens loaded in different planes: The authors used the so called “Arcan specimen” for their investigations. Such a specimen is butterfly shaped and has the peculiarity of generating a shear distribution that is nearly uniform over the critical cross section. The authors found that the shear strength of specimens loaded in the tangential plane was about 50% higher than the shear strength of specimens loaded in the radial plane.

G. Schickhofer et al [4] conducted tests on glulam beams with I-cross section loaded in a three-point beam configuration to determine the shear strength capacity. Totally, 24 specimens were tested. Different glulam classes, from GL24 to GL36 were used for the manufacture of the specimens. The main findings are: *i)* no clear evidence of relationship between glulam strength class and shear strength; *ii)* a number of failure occurred due to high perpendicular to grain compression between web and flange at the support.

Sundström et al [12] conducted shear tests on 104 glulam beam in a three-point beam configuration to determine the shear strength under varying humidity conditions. The main finding of this research is that variation of humidity does not considerably affect the shear strength of glulam.

2 Test methods and material

Two kinds of specimens were used in the present shear strength tests: specimens similar to those defined in EN408 (here denoted “modified EN408 tests”) and beams. The test setup and test results are in greater detail presented in [1] and [2], respectively. All tests were made as short time ramp loading tests with time to failure in the order of 5 minutes.

The tested specimens were made of glulam “L40”. The raw material used for the laminations was Norway spruce, with characteristic tensile strength $T \geq 22$ MPa and with nominal thickness $t=45$ mm. The mean density and moisture content was 471 kg/m^3 and 11.1%, respectively, for the material used in EN408-test, and 464 kg/m^3 and 10.7%, respectively, for the material in tested beams. The EN408 specimens were conditioned at 60% RH and the beams indoors under plastic cover. The specimens were randomly cut from different beams.

2.2 Modified EN408 test method and test specimens

The test setup and specimen geometry of the modified EN408 tests are shown in Figure 1. These tests comprised 9 test series with 4 nominally equal tests in each series. The test specimen is attached to the two steel parts by a large number of screws, not by glue as proposed in the EN-standard. The use of screws was mainly due to practical reasons. However, the use of screws - instead of glue - may also contribute to a more uniform distribution of the shear load. The use of knee-shaped steel parts, instead of use of straight steel plates and inclined application of the load is partly due to practical reasons and partly to avoid compressive load across the fracture section. The specimens were moreover given a 115 mm long centric cut of width 3 mm in each end. It is believed that this cut is important for the test results. Initial tests of specimens without the cut showed fracture at low load due to significant tensile stress perpendicular to grain at two of the corners of the specimen. Fracture did not develop as a shear failure along the centre line of the specimen, but instead as a combined tensile and shear failure starting in the vicinity of a corner. This experimental observation was verified by finite element stress analysis, showing significant perpendicular to grain tensile stresses in the corner regions. Along the centerline of the specimen is, on the contrary, a stress state with almost pure shear stress due to symmetry. A drawback of the end-cuts could be that they may give shear stress concentration and a more non-uniform shear stress distribution. This is analyzed by non-linear finite element analysis in a following section.

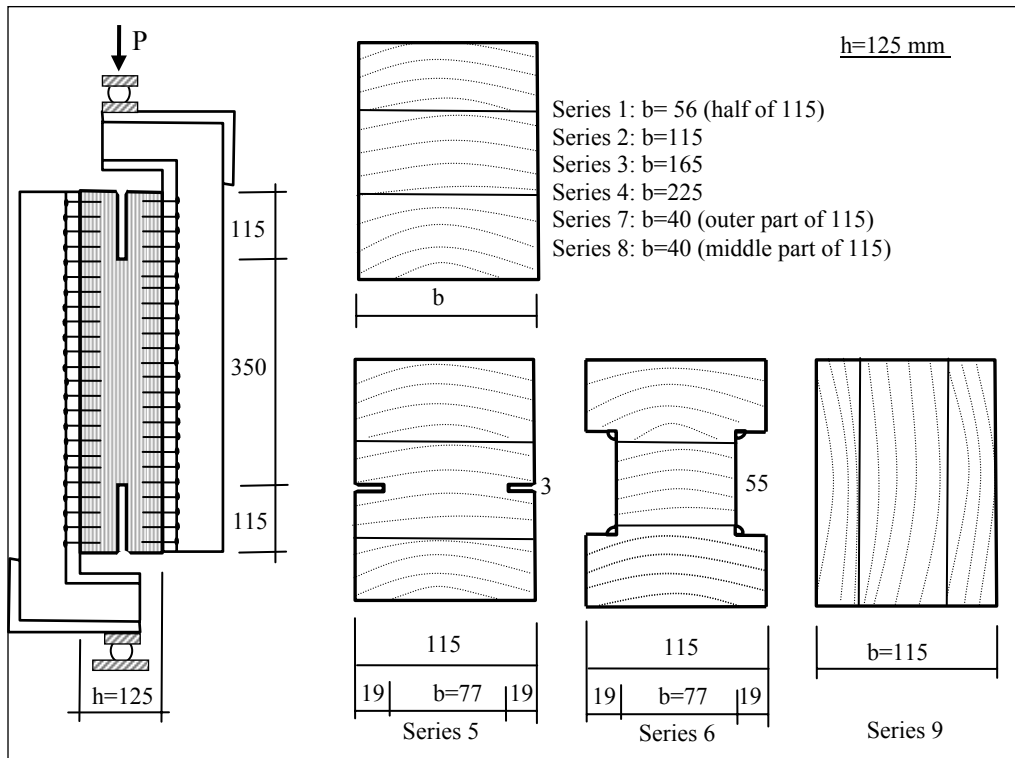


Figure 1. Shear tests by modified EN408 test method: setup and specimens for 9 test series

2.3 Beam test method and test specimens

The beam tests comprised 6 test series with 4 nominally equal tests in each series. Series 1 related to a rectangular beam cross section and series 2-6 to various support and loading conditions for beams with an I-shaped cross section, manufactured by cutting of beams with a rectangular section. Cross sections and loading conditions are shown in Figure 2 and 3. The length of the decisive shear span was in all tests 787 mm, i.e. 2.5 times the beam height, 315 mm. Series 3 related to possible influence of an overhang at support. Series 4 and 5 related to possible influence of increased and decreased perpendicular to grain compressive stress in the wood in the vicinity of the support. The additional compressive and tensile loads were created by a steel beam loading arrangement. The tensile load was applied to the upper surface of the beam by means of a number of screws. Series 6 related to the shear strength of a continuous beam where the bending moment is large at the support. The beam in series 6 is statically indeterminate and the ratio between the recorded load P and the shear force V was calculated by conventional beam theory, giving $V=0.815 P$. Consideration to shear deformation by Timoshenko beam theory would indicate a slightly lower shear force at given recorded load, $V=0.794 P$.

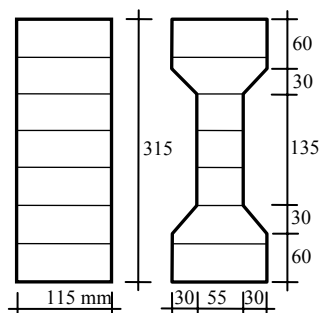


Figure 2 (left). Cross sections of tested beams

Section data:

Section	A, mm^2	I, mm^4	$S_{h/2}, \text{mm}^3$
Rectangular	36225	$299.5 \cdot 10^6$	$1.426 \cdot 10^6$
I-shape	26325	$276.3 \cdot 10^6$	$1.220 \cdot 10^6$

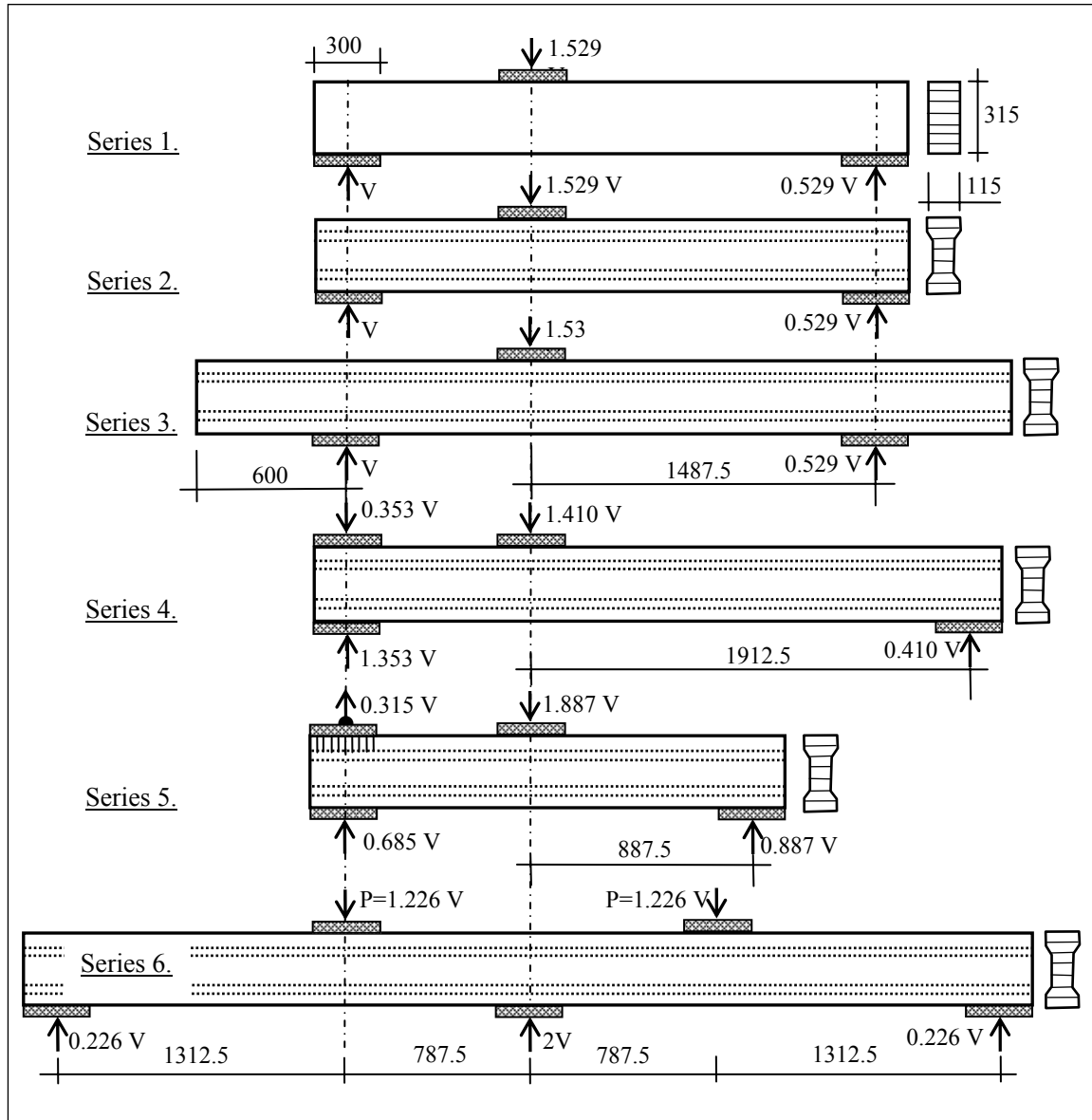


Figure 3. Beam tests

3 Test results

3.1 Modified EN408 test results

Table 1 shows the test results for the modified EN408 tests. The size of the fracture section is denoted A , i.e. $A=350 \times 77 \text{ mm}^2$ for series 5 and 6, and $350 \times 115 \text{ mm}^2$ for the other series. This means that the indicated strength value, P_f/A , is the mean shear stress at failure. Also density and annual ring thickness was measured for the individual specimens, giving average results as indicated in the table. The results show no consistent influence of glulam width and no significant difference between rectangular and I-shaped cross sections. The specimens with a slit similar to a drying crack showed about 10% increase in shear strength. Comparison between series 2 and 9 shows that flatwise loading with standing orientation of the annual rings in shear section gives about 15% decrease in shear strength. Series 2, 7 and 8 shows that sawing of a wide section into thinner sections can reduce the strength by about 10%, but no difference between the middle part and the edge parts was found. Correlation between density and strength was found. Out of the 32 specimens tested, it was found that the two specimens with lowest strength were the two specimens with lowest density. Figure

4 shows strength versus density. Linear regression analysis for all tests considered as one group gave the upper line shown in the figure, which is: $f_v = 0.17 + 0.0102\rho$

where $f_v = P_f/A$ is the shear strength in MPa and ρ the density in kg/m^3 at 11% MC. No correlation between strength and annual ring thickness was found. Mean strength and standard deviation for all 32 specimens were 4.96 MPa and 0.73 MPa, respectively, which gives a coefficient of variation $\text{CoV} = 0.73/4.96 = 15\%$. At the assumption of normal distribution, this gives an estimated 5% fractile characteristic strength $f_{v,k} = 4.96 - 1.64 \cdot 0.73 = 3.76$ MPa.

Table 1. Modified EN408 shear strength test results, density ρ and annual ring width t_a

Test series	Cross section width, mm	Individual test results				Mean results				
		P_f/A , MPa				P_f/A	Std	CoV	ρ , kg/m^3	t_a , mm
1	56	5.05	-	-	-	5.05	-	-	496	1.0
2	115	5.56	5.47	5.79	3.60	5.11	1.01	20%	461	2.7
3	165	5.32	6.23	5.35	5.49	5.60	0.43	8%	477	3.0
4	215	4.94	4.19	5.16	5.25	4.89	0.48	10%	459	2.5
5	77 (115), slit	6.23	6.12	4.53	5.49	5.59	0.78	14%	474	3.0
6	77 (115), I	5.60	4.56	4.82	5.23	5.05	0.46	9%	468	2.3
7	40	4.22	5.38	3.83	-	4.48	0.81	18%	478	2.3
8	40	4.91	4.60	4.09	4.19	4.45	0.38	9%	481	2.0
9	115,	4.15	4.70	3.45	5.07	4.34	0.70	16%	463	2.7
Overall average						4.96	0.63	13%	471	2.5

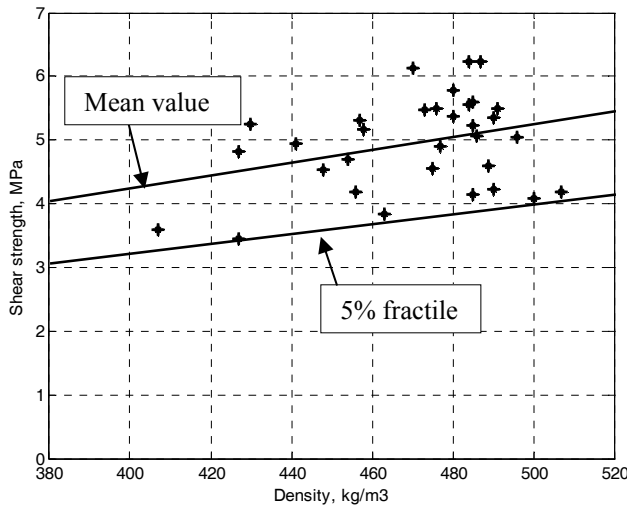


Figure 4. Shear strength, P_f/A , versus density from modified EN408 test results

3.2 Beam test results

The beam shear strength test results are shown in Table 2. The shear strength f_v was calculated according to conventional beam theory from the recorded failure value of the shear force, V_f . Also the compressive stress σ_c perpendicular to grain at the supports is calculated according to conventional Bernoulli-Euler beam theory. All beams failed in a sudden manner and most of them due to sudden development of a shear crack along the beam. Some of the beams did, however, fail in bending or in a combination of shear and bending. These beams are indicated with * in Table 2. For these cases the true shear strength would be equal to or greater than the recorded shear stress at failure. These perhaps somewhat too low recorded shear failure stresses were not excluded when calculating mean strengths and standard deviations. Series 1 and 2 show significantly higher strength for the

I-shaped cross sections than for the rectangular cross section. From series 3 it seems that increased beam length at support has no or only some small beneficial influence. Comparison between series 2, 4 and 5 suggest that increased compressive stress perpendicular to grain may give a slight increase of the shear strength. Comparison between series 2 and 6 suggests that the shear force capacity at an inner support of a continuous beam is greater than shear capacity of a support at the end of a beam. Taking the test results of series 2, 3, 4 and 5 as one group, the mean strength is 6.27 MPa and the estimated 5% fractile characteristic strength $6.76-1.64 \cdot 0.76=5.51$ MPa. The corresponding figures for the rectangular beams, series 1, are 4.57 MPa and $4.57-1.64 \cdot 0.41=3.90$ MPa, respectively. For the continuous beams, series 6, the corresponding figures are 7.22 MPa and $7.22-1.64 \cdot 0.44=6.50$ MPa.

Table 2. Beam shear strength test results

Test series	Test series characteristic	Individual test results				Mean shear strength			Mean σ_c , MPa
		f_v , MPa				f_v	std	cov	
1	Rectan.	4.24 *	4.22 *	4.77	5.06	4.57	0.41	9.0%	1.60
2	I-section	5.86	6.43 *	6.63	5.31	6.06	0.60	9.9%	2.28
3	Overhang	5.42	6.84 *	4.78 *	7.78	6.21	1.36	21.9%	2.33
4	Compression	6.71 *	6.32	6.41	7.06	6.63	0.33	5.0%	4.25
5	Tension	6.30	-	6.57	5.66	6.18	0.47	7.6%	0.87
6	Cont. beam	7.59	6.58	7.37	7.34 *	7.22	0.44	5.4%	5.42
Overall average						6.14	0.58	9.4%	2.78

* bending failure or combined bending and shear failure

4 Stress and strength analysis

4.1 Stress and strength analysis of modified EN408 specimen

Two dimensional plane stress linear elastic finite element analysis of the modified EN408 test setup in Figure 1 was performed, with glulam specimen geometry according to series 2. Both the glulam specimen and the knee-shaped steel parts were included in the model, however ignoring the compliance of the screw connection and instead assigning full interaction between the glulam and steel parts. Stress components $\sigma_{||}$, σ_{\perp} and τ in the glulam specimen are illustrated in Figure 5, for specimens with and without centric end-cuts. Applied external load corresponds to a mean shear stress of 5.0 MPa in the fracture sections. The results are based on material stiffness parameters $E_{||}=13\,700$ MPa, $E_{\perp}=460$ MPa, $G_{||\perp}=850$ MPa, $\nu_{||\perp}=0.46$ for glulam and $E=210\,000$ MPa, $\nu=0.3$ for steel parts. As indicated by preliminary tests of specimen without the end-cuts, the modified EN408 test setup results in significant perpendicular to grain tensile stress σ_{\perp} in two corner regions of the specimen. This stress is reduced by introducing the cuts, but instead stress concentrations arise at the ends of the cuts.

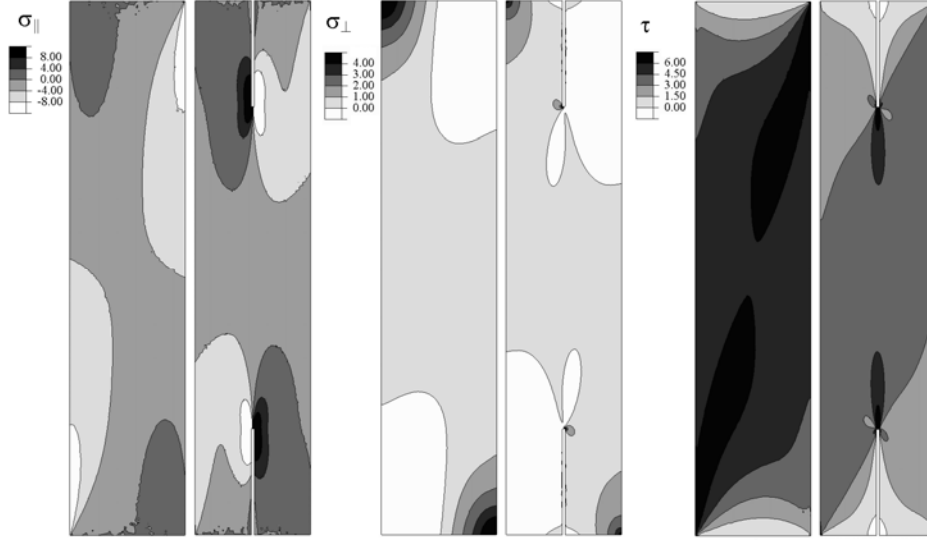


Figure 5. Stress $\sigma_{||}$, σ_{\perp} and τ for modified EN408 specimen with and without end-cuts

Nonlinear fracture course analysis of the specimen with centric end-cuts was also performed using cohesive spring elements in the fracture section with a piecewise linear shear stress-displacement relationship to represent the strain softening properties. The initial stiffness was adjusted to represent linear elastic behaviour up to maximum stress, i.e. local material strength. For increasing displacement, the ability to transfer stress diminishes and the (negative) stiffness is adjusted to represent the fracture energy of the material. Nonlinear stress-strain performance outside the fracture process region contributes however to a more uniform shear stress distribution. The volume of material exposed to the high local stress is furthermore very small: only about 1% of the volume has reached shear stress greater than 95% of the local material strength at maximum load P_f/A . This means that the test results P_f/A may be a reasonably relevant measure of for the actual specimen volume. The mean stress in the fracture area at maximum load P_f/A was by the nonlinear fracture course analysis found to be 60-70% of the local material strength for fracture energies in the range 0.600-1.200 Nmm/mm².

4.2 3D stress analysis of beams

To study how shear stresses vary over cross-sections of the studied glulam beams three dimensional finite element simulations were performed. To illustrate how the simulation results can be presented, Fig. 6 shows deformed geometry of the beams, mesh pattern, load distribution (corresponds to 147.7 kN), boundary conditions, annual ring pattern, colour plots and path plots for the global shear stress τ_{yz} . The wood material is assumed to be an orthotropic material with stiffness parameters: $E_r = 800$, $E_t = 500$, $E_l = 14000$, $G_{rt} = 60$, $G_{rl} = 600$, $G_{tl} = 700$, $\nu_{rl} = 0.02$, $\nu_{tl} = 0.02$, $\nu_{tr} = 0.3$. The pith is assumed to be a straight line along the centre of the bottom surface of each wood member. The interaction between the steel plates and the wood material is modelled as a full contact interaction based on penalty formulation.

The simulation results show clearly how the global shear stress τ_{yz} varies over the cross sections. For the rectangular beam the largest shear stresses occur at the neutral axis, close to the side surfaces whereas for the I-beam they occur in the inner corners where the web and the flange are connected. These results have been compared with hand calculations. The maximum shear stresses became 5% and 9% larger than the hand calculated values for the rectangular respective I-beams. The main reason for this discrepancy is that the simulation takes into account the curved annual rings and it generates stress concentrations in the inner corners of the I-beams.

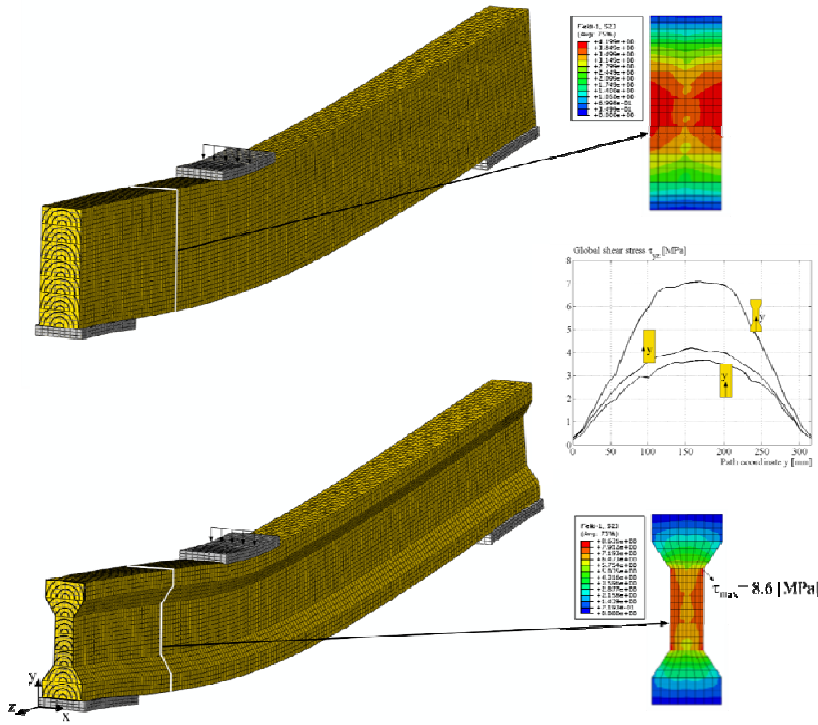


Figure 6. Illustration of bending deformations and related shear stress distribution over a critical cross section (all deformations are magnified 8 times).

5 Discussion and conclusions

The proposed test method, i.e. the modified EN 408 with two 115 mm cuts at the bottom part and at the upper part has the advantage, that it allows for a state of stress in the region between the cut tips characterized by predominant longitudinal shear (i.e. shear parallel to the grain). Moreover, the presence of the cuts significantly reduces the tension perpendicular to grain at the corners of the specimen. The disadvantage of such a test method could be the high stress concentration that occurs at the cut tips, which may *negatively* influence the shear strength of the timber. On the other hand, the cuts “oblige” the failure surface to occur at a given plane, which may *positively* influence the shear strength of timber. Specimens with width between 40 mm and 215 mm were shear tested according to modified EN 408. Similar shear strengths were achieved for all these specimens, indicating that the width of the specimen does not have a remarkable influence on shear strength.

In general it can be stated that testing according to modified EN 408 gives shear strength lower than shear strength obtained by beam testing. However, if the beam specimens with applied compression at the top of the support and the beam specimens on three supports were excluded, the characteristic shear strengths obtained by the two methods would become comparable.

For the modified EN 408 tests, no remarkable shear strength differences between specimens with rectangular cross section and specimens with I-cross section could be observed. On the other hand higher shear strength could be observed for beams with I-cross section than for beams with rectangular cross section. The reason for such a discrepancy could be the possible beneficial influence of higher perpendicular to grain compression in the web of the I-beams. Moreover, it should be observed that 50% of the beam specimens with rectangular cross section failed in bending. Perhaps, if bending failure had been prevented, shear

strength similar to that for I-beams could have been achieved also for beams with rectangular cross section.

Four specimens were tested according to modified EN 408 method, loading in the radial direction instead of loading in the tangential direction – as occurred in all other cases. It was observed that the shear strength in the radial direction was slightly lower than the shear strength for specimens loaded in the tangential direction. This is in line with the results by Dahl et al, but not with the results obtained by all the other authors cited in this paper. However, the number of specimens loaded in the radial direction is too low for drawing any relevant conclusions.

Overhangs do not seem to have any evident effect on the shear strength for the tested timber beams. Neither, has the action of a external tension applied on the upper part of the beam at the support, in the direction perpendicular to grain. On the other hand, external perpendicular to grain compression stress applied on the upper part of the beam at the support seem to affect the shear strength positively. However, this conclusions cannot be extended to cases were the applied external tension or compression are higher than those used for these experiments.

In the case of beam with three supports higher shear strength than the shear strength for simply supported beams was observed. This may be due to the fact that at the intermediate support the transmission of internal forces occurs in a great extent by “strut action” and the zones with pure shear action are rather small.

Acknowledgments

The authors gratefully acknowledge the financial support of the Swedish Glulam Association.

References

- [1] Gustafsson, P.J., Emilsson, E., Crocetti, R. and Ormarsson, S.: ”Provningar av limträskjuvhållfasthet hösten 2009”, Report TVSM-7158, Div. of Struct. Mech., Lund University, Sweden, 2009
- [2] Andersson, D. and Odén, J.: “Träs skjuvhållfasthet och limträbalkars tvärkraftskapacitet – provningar och beräkningar”, Master’s Dissertation, Report TVSM-5159, Div. of Struct. Mech., Lund University, Sweden, 2009
- [3] EN 1194:1999, “Glued laminated timber – Strength classes and determination of characteristic values”, 1999
- [4] Schinkhofer, G and Obermayr, B.: “Development of an optimized test configuration to determine shear strength of glued laminated timber”, CIB-W18/31-21-1
- [5] Denzler, J. K. and Glos, P.: “Determination of shear strength values according to EN 408”, Material and Structures, 2007
- [6] prEN 408:2003 “Timber Structures – Structural Timber and Glued Laminated Timber – Determination of Some Physical and Mechanical Properties”, 2003
- [7] Granholm, H. “Armerat trä”. Transactions of Chalmers University of Technology, Göteborg, 1954
- [8] Madsen, B. “Structural Behaviour of Timber”. Amer Society of Civil Engineers ISBN -10: 0969616201, 1995
- [9] Rammer, D.: “Shear strength of glued-laminated timber beams and panels”. Madison, Forest Products Laboratory, USDA Forest Service. 1996
- [10] Poussa M., Tukiainen P.: “Experimental Study of Compression and Shear Strength of Spruce Timber”, CIB- W18/40-6-2, Bled, Slovenia, 2007
- [11] Dahl, K. “Mechanical properties of clear wood from Norway spruce”. Department of Structural Engineering, Norwegian University of Science and Technology. ISBN 978-82-471-1911-2, 2009
- [12] Sundström, T. Kevarinmäki, A. Toratti, T.: “ Shear strength of Glulam beams under varying humidity conditions, WCTE 2010, Riva del Garda, Italy, 2010

**INTERNATIONAL COUNCIL FOR RESEARCH AND INNOVATION
IN BUILDING AND CONSTRUCTION**

WORKING COMMISSION W18 - TIMBER STRUCTURES

**SYSTEM EFFECTS IN GLUED LAMINATED TIMBER
IN TENSION AND BENDING**

M Frese

H J Blaß

Karlsruhe Institute of Technology (KIT)
GERMANY

MEETING FORTY THREE

NELSON

NEW ZEALAND

AUGUST 2010

Presented by M Frese

A Jorissen: Is the length factor (observed for tension members) valid for bending as well? M Frese: No. Length factor is for tension only.

R Nestic: In the numerical model, did lamination have different behaviour. M Frese: Yes, each 150mm segments behave differently

S Aicher: What is failure? M Frese: Failure in outer lamination (bending) in lumber or finger – joint.

S Winter: Is the effect really a volume effect for which the tension is the main significant one?

T Poutanen: How do you model the timber in compression? M Frese: the behaviour is modelled as linear-elastic.

T Poutanen: do you assume that failure occurs in compression? H Blass: No. It does not make a difference in the 5th% value. Tension failure is critical on the 5%-level.

L Daziel: Is the multiple-span factor a recommendation? M Frese: Yes! What about spans of different length? M Frese: We do not know at this point what the effect of different span length is.

System effects in glued laminated timber in tension and bending

M. Frese and H.J. Blaß
Institut für Ingenieurholzbau und Baukonstruktionen
Karlsruher Institut für Technologie (KIT)

1 Introduction

In 2005, bending tests on full size glulam beams showed that the bending strength values obtained, were far too low compared with the current product standard. For that reason, a new research on glulam was carried out involving a series of numerical studies on the glulam bending strength [1]. This research resulted in a new strength model for the bending strength. The current paper aims at giving a comprehensive overview on recent developments in simulating glulam strength parallel to grain. These developments have arisen from the new research on glulam and a failure analysis on timber hall structures [2] and now cover the tensile-to-bending-strength ratio as well as the size effect in members subject to tension [3] and the load-carrying capacity of simple and continuous beams with up to 5 supports [4]. Therefore, the current paper is a direct continuation of the author's CIB-W18 paper in 2008 [5]. In general, the strength hereinafter refers to characteristic glulam bending ($f_{m,g,k}$) and characteristic glulam tensile strength ($f_{t,0,g,k}$), respectively. Both values are associated with standardised member sizes: 0.6 m times 10.8 m ($h \cdot \ell_m$) in case of bending tests and 0.6 m times 5.4 m ($h \cdot \ell_t$) in case of tensile tests (Fig. 1).

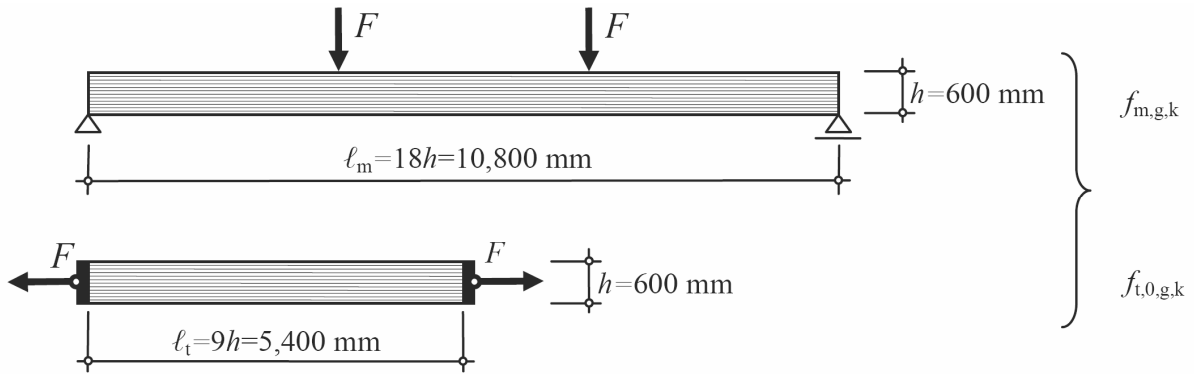


Fig. 1 Test configurations in European test standard EN 408 (2003) with the terms of European standard EN 1194 (1999); bending test (top) and tensile test (bottom)

2 Computer model, methods and simulated materials

All the results of the examinations were conducted using a newly developed and validated finite element based computer model (CM) [6] [7]. Therefore, the following description of the CM is restricted to its crucial properties and modifications for the current studies. The basic models to simulate the bending and tensile strength are shown in Fig. 2.

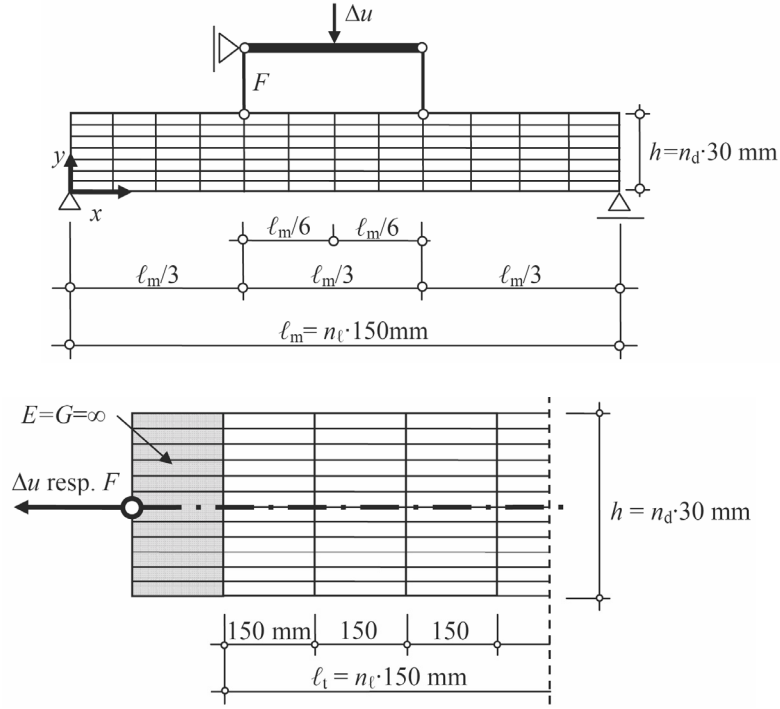


Fig. 2 Basic finite element models to simulate glulam bending strength (top) and glulam tensile strength (bottom). The *grey zone* indicates infinite stiffness of modelled grips

They constitute the test configurations in Fig. 1. The sizes of the simulated members depend on the numbers (n_ℓ and n_d) of elements (150 mm in length and 30 mm in depth) along the length (ℓ_m resp. ℓ_t) and depth (h) of the beams. The stochastically distributed and auto-correlated mechanical properties of glulam are assigned systematically to the elements of the models. The lay-up of the simulated members is homogeneous. The material is orthotropic. In the compressive zone of simple beams under bending, ideal elastoplasticity and in the tension zone, in principle, linear elasticity until tensile failure is assumed (uniaxial failure criterion). To simplify matters, linear elasticity in the spatially limited compressive zones above the supports of continuous beams (cf. Fig. 6) is assumed as well, instead of ideal elastoplasticity; in a preliminary examination, it was shown that the difference between both material models, linear elasticity and ideal elastoplasticity, each assumed in the compressive zone of simple beams under bending has no major influence on the 5th percentile of the bending strength: The corresponding 5th percentiles differ from each other only by one percent. The ultimate failure criterion used is based on the assumption that no further load (F) increase is possible if the locally calculated tensile stress of any element in the outermost laminations equals the individual element tensile strength. In both finite element models, the load is applied through a stepwise displacement (Δu) resulting in a particular number of load steps for a simulated test. During the load steps, element failure in the tension zone outside the outermost laminations is allowed; corresponding elements are identified after each load step and are deactivated by multiplying their stiffness by a severe reduction factor. With that a slight non-linear behaviour in the tension zone is modelled. The bending strength (f_m) as a result of a single simulated test is calculated with the global maximum moment ($M_{1,\max}$, $M_{2,\max}$, $M_{3,\max}$ or $M_{4,\max}$, cf. moment diagrams in Fig. 6) and the section modulus W and, therefore, is denoted as an effective (or apparent) bending strength. The tensile strength (f_t) is calculated with the maximum tensile force (F_{\max}) and the cross-section area.

Nine grading methods, leading to various board tensile strength values, were from case to case employed by the CM to exert a different influence on the glulam strength. The set of grading methods available in the CM is comprehensively given in [1] or briefly in [5]. Visual

methods are denoted as VIS I, II, III, density-based ones as DENS I, II and dynamic-MOE-based ones as EDYN I, II, III, IV. Each grading method is associated with a particular board tensile strength and finger joint tensile strength. Both strength values are adapted to each other resulting in a balanced as well as realistic relation between board and finger joint quality [3].

3 Tensile-to-bending-strength ratio

As the tensile strength is usually given as a portion of the bending strength, comparative simulations of tensile and bending test were performed to determine its relation. In this comparative examination, the nine grading methods were employed. A total of 18,000 simulations were run which corresponds to 1000 simulations per strength type (f_m and f_t) and grading method. Fig. 3 depicts cumulative distributions for the strength values, tensile and bending strength, as an example, for the grading methods VIS II and EDYN I. The target values to draw a comparison between the 5th percentiles are highlighted in boxes; they coincide with the points of intersection between the quasi-empirical cumulative distribution functions and the horizontal reference lines located at 0.05.

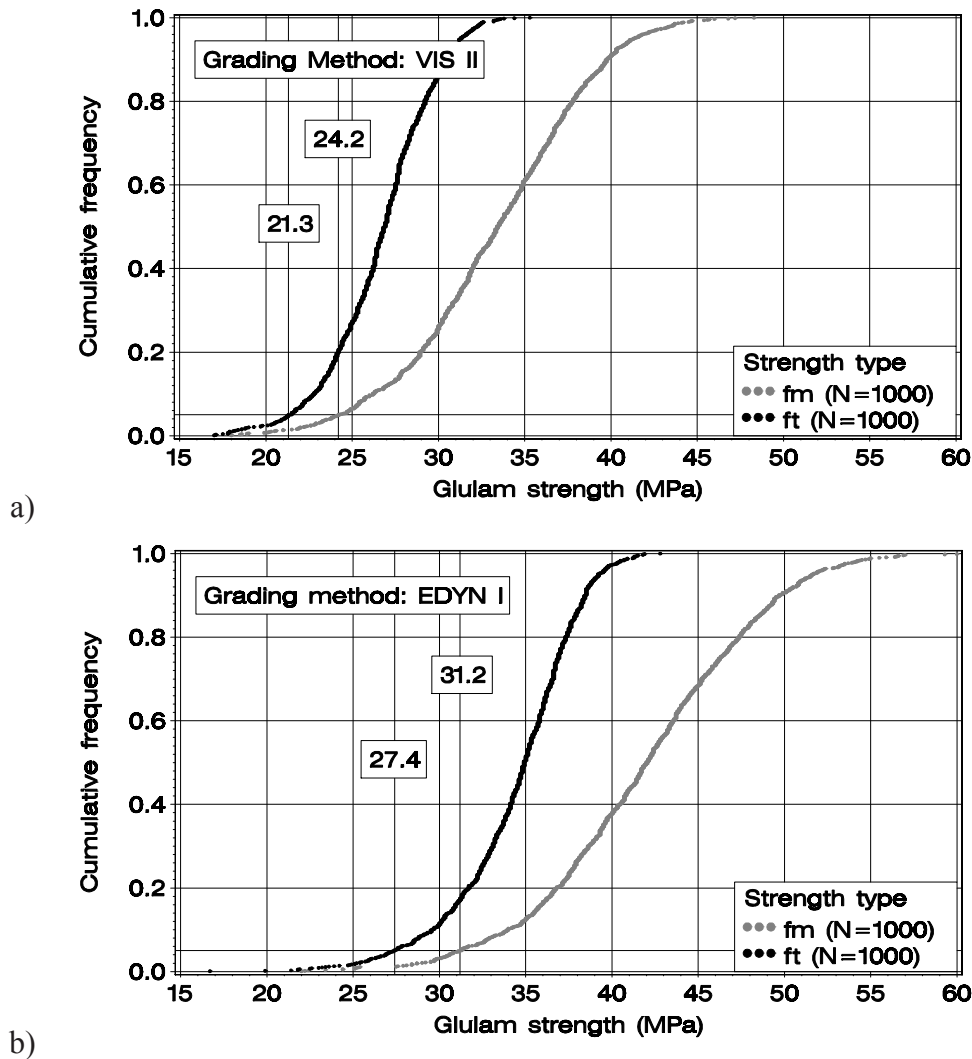


Fig. 3 Cumulative distributions of simulated tensile (f_t) and bending strength (f_m); simulation results exemplified for (a) grading method VIS II and (b) EDYN I

For the two cases exemplified the ratios are $21.3/24.2=0.88$ and $27.4/31.2=0.88$. Even considering the results on the basis of the other seven grading methods, the corresponding coefficients hardly deviate from 0.88 (Table 1). Hence, there is non-significant influence of the grading methods and the material strength, respectively, on the ratio. As a consequence, the comparative examination brought out the relation (1) between the characteristic tensile and characteristic bending strength where both strength values are related to standardised member sizes as depicted in Fig. 1.

$$f_{t,0,g,k} = 0.88 \cdot f_{m,g,k} \quad (1)$$

Table 1 Statistics of the simulated tensile and bending strength and ratio of 5th percentiles

	Tensile strength [MPa]			Bending strength [MPa]			Ratio
Grading method	\bar{X}	s	$f_{t,0,g,k,sim}$	\bar{X}	s	$f_{m,g,k,sim}$	$\frac{f_{t,0,g,k,sim}}{f_{m,g,k,sim}}$
VIS I	25.3	2.97	20.1	31.3	5.19	22.7	0.89
VIS II	26.7	3.02	21.3 ¹	33.3	5.21	24.2 ¹	0.88
VIS III	30.8	3.33	24.6	38.1	5.50	28.7	0.86
DENS I	33.4	3.45	26.9	41.0	6.30	30.6	0.88
DENS II	35.5	3.76	28.0	43.7	6.23	32.7	0.86
EDYN I	34.4	3.63	27.4 ¹	41.9	6.23	31.2 ¹	0.88
EDYN II	35.8	3.79	28.2	43.5	6.64	32.1	0.88
EDYN III	38.6	3.87	32.0	47.1	6.56	36.3	0.88
EDYN IV	40.6	3.67	34.4	49.7	6.74	38.2	0.90

¹ depicted in Fig. 3

4 Size effect in members subject to tension

As in general, the strength depends on the member size subject to tension, different member sizes for tensile tests ($150 \leq \text{free member length } \ell_t \leq 54,000 \text{ mm}$; $120 \leq \text{member depth } h \leq 600 \text{ mm}$) were simulated. In total 70,000 simulations were performed for tension. The high number of simulations for tensile tests is due to an independent variation of the member depth. The member sizes were defined through different numbers of elements along the edges of the rectangular shape (n_ℓ and n_d according to Fig. 2). The simulated strength data (Fig. 4), obtained from a single grading method (EDYN II), were expressed by appropriate strength ratios (dots in Fig. 5) to describe the deviation of the effective strength from the reference value ($f_{t,0,g,k,ref}=28.5 \text{ MPa}$). The reference value is related to the standardised member size $\ell_{t,ref}=5,400 \text{ mm}$ and $h=600 \text{ mm}$ (cf. Fig. 1). The deviation from the reference strength is given by the curve in Fig. 5 brought into line with the simulated strength ratios. This curve represents the size factor $k_{\ell,k}$ described by equations (2) and (3) on the basis of Weibull's theory. The corresponding size depending tensile strength, meaning effective strength ($f_{t,0,g,k,ef}$), can finally be expressed as product of $k_{\ell,k}$ and the characteristic strength. As expected, $k_{\ell,k}$ is 1.0 for the reference size (cf. points of intersection between the curve in Fig. 5 and the corresponding thick vertical reference line). The variation of depth in Fig. 4 showed that there is no major influence of the depth on the effective tensile strength.

$$\begin{aligned}
k_{\ell,k} &= (5400/\ell_t)^{1/10.8} & 150 \text{ mm} < \ell_t < 60,000 \text{ mm} \\
k_{\ell,k} &= 1.40 & \ell_t \leq 150 \text{ mm} \\
k_{\ell,k} &= 0.80 & 60,000 \text{ mm} \leq \ell_t
\end{aligned} \tag{2}$$

$$f_{t,0,g,k,ef} = k_{\ell,k} \cdot f_{t,0,g,k} \tag{3}$$

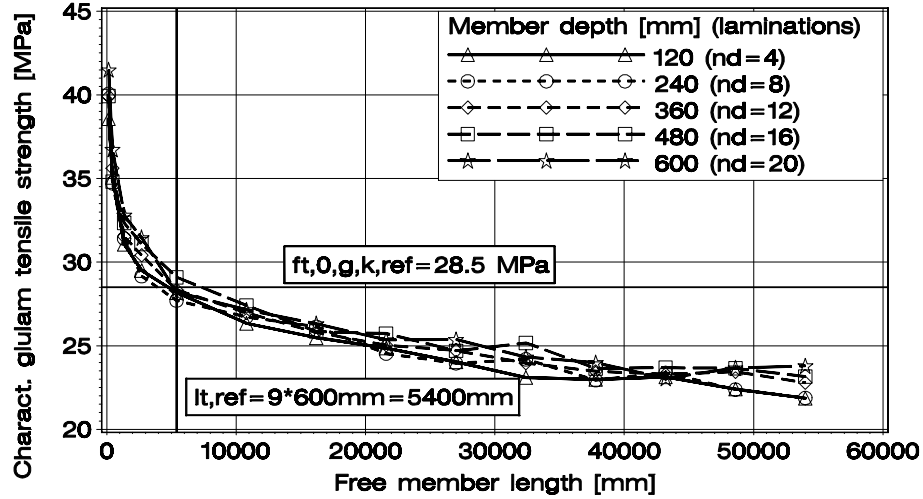


Fig. 4 Simulated characteristic glulam tensile strength and free member length and depth, respectively; reference values $f_{t,0,g,k,ref}$ and $\ell_{t,ref}$ highlighted (*thick lines*)

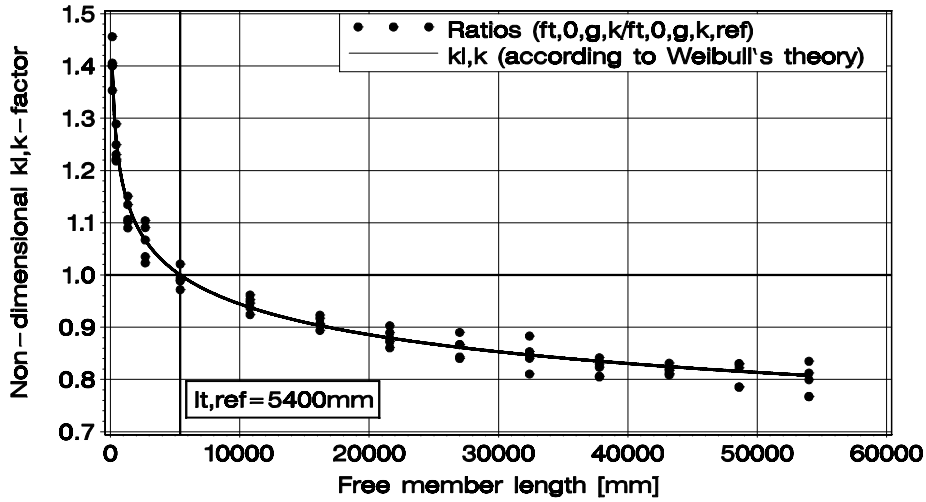


Fig. 5 $k_{\ell,k}$ -factor (*curve*) and strength ratios (*dots*), calculated by the reference value 28.5 MPa, in dependence of free member length; reference length ($\ell_{t,ref} = 5400 \text{ mm}$) and corresponding $k_{\ell,k}$ -factor (= 1.0) highlighted (*thick lines*)

5 Load-carrying capacity, determined by the system

Due to the lower occurrence probability of weak points in the outer tension zone, subject to comparatively high tensile stress, of continuous beams with 3, 4 or 5 supports in contrast to corresponding simple beams, a higher load-carrying capacity is given in those continuous beams, e.g. [8] [9]. In particular, big knots, compression wood and fibre deviation distributed

along the timber constitute typical weak points. Considering the moment diagrams in Fig. 6, it becomes evident that the simple beam depicted, is subject to global maximum stress over a third of its span ($\ell/3$) whereas the continuous beams below are, according to elementary beam theory, subject to global maximum stresses only at single points above the middle supports. The higher load-carrying capacity in continuous beams can be expressed by a particular effective bending strength determined by the system.

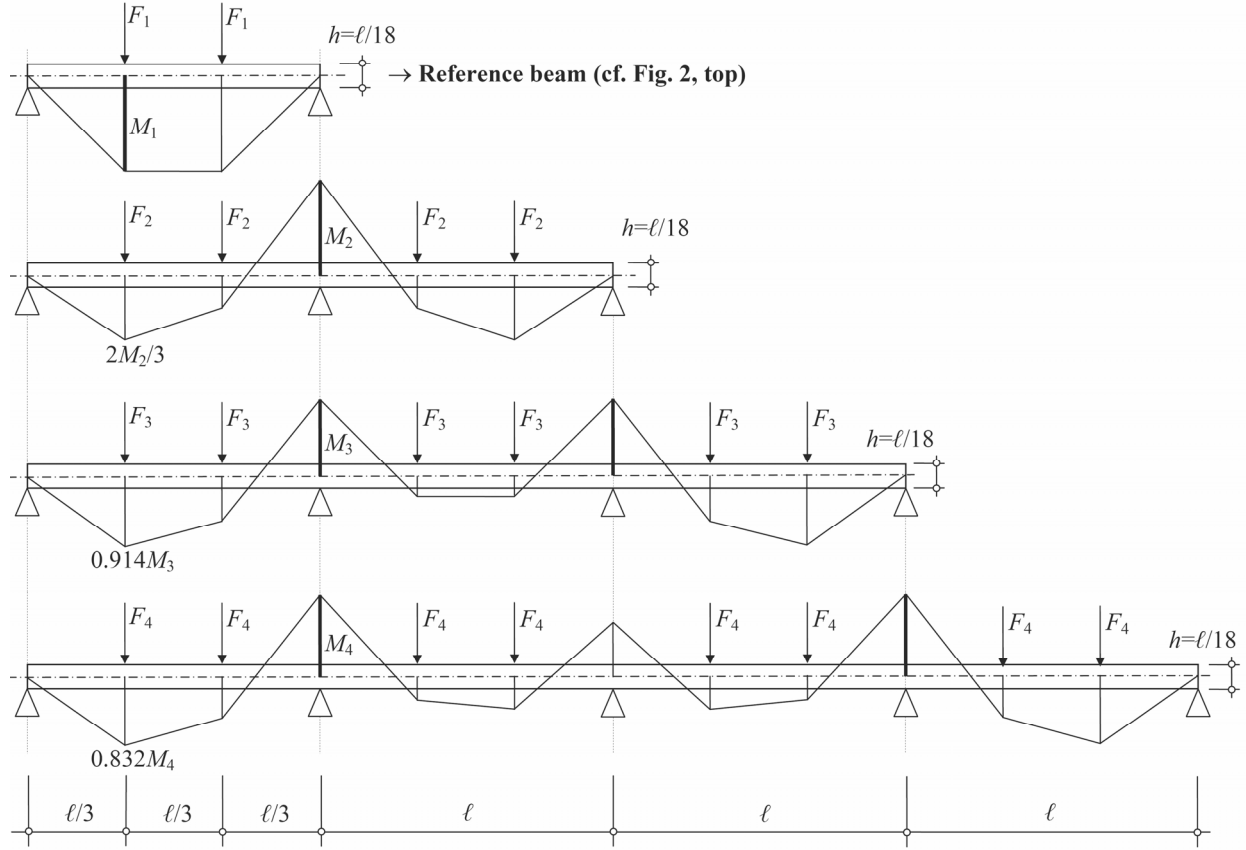


Fig. 6 Beams simulated and moment diagrams; simple beam (top), 2- and 3-span beam (middle), 4-span beam (bottom); moment diagrams scaled for $F_1=F_2=F_3=F_4$

To quantify the effective bending strength in 2-, 3- and 4-span beams, those beams were examined numerically and the strength output was compared with the characteristic strength as reference strength. The nine grading methods were employed to consider a wide range of strength levels. The models used are shown in Fig. 7. The continuous beam models constitute multiples of the basic model. Whereas the bending strength of the reference beam is calculated with the maximum moment $M_{1,max}$ the bending strength values of the continuous beams are calculated with the maximum moments $M_{2,max}$, $M_{3,max}$ and $M_{4,max}$, respectively; maximum moments depend on the maximum load-carrying capacity. 1,000 simulations per grading method and system were performed, which is a total of 36,000 tests (9 times 4 times 1,000) in finally 36 samples.

As an example, Fig. 8a exemplifies the simulation results referring to VIS II for the maximum load-carrying capacity F_{max} and Fig. 8b for the effective bending strength. Fig. 9 depicts the effective strength referring to EDYN I. Only parts of the quasi-empirical cumulative distribution functions of the load-carrying capacity and of the effective bending strength are shown in the diagrams to better identify the 5th percentiles. The comparative cumulative frequencies are between 0 and 10% which corresponds to 100 single values per system.

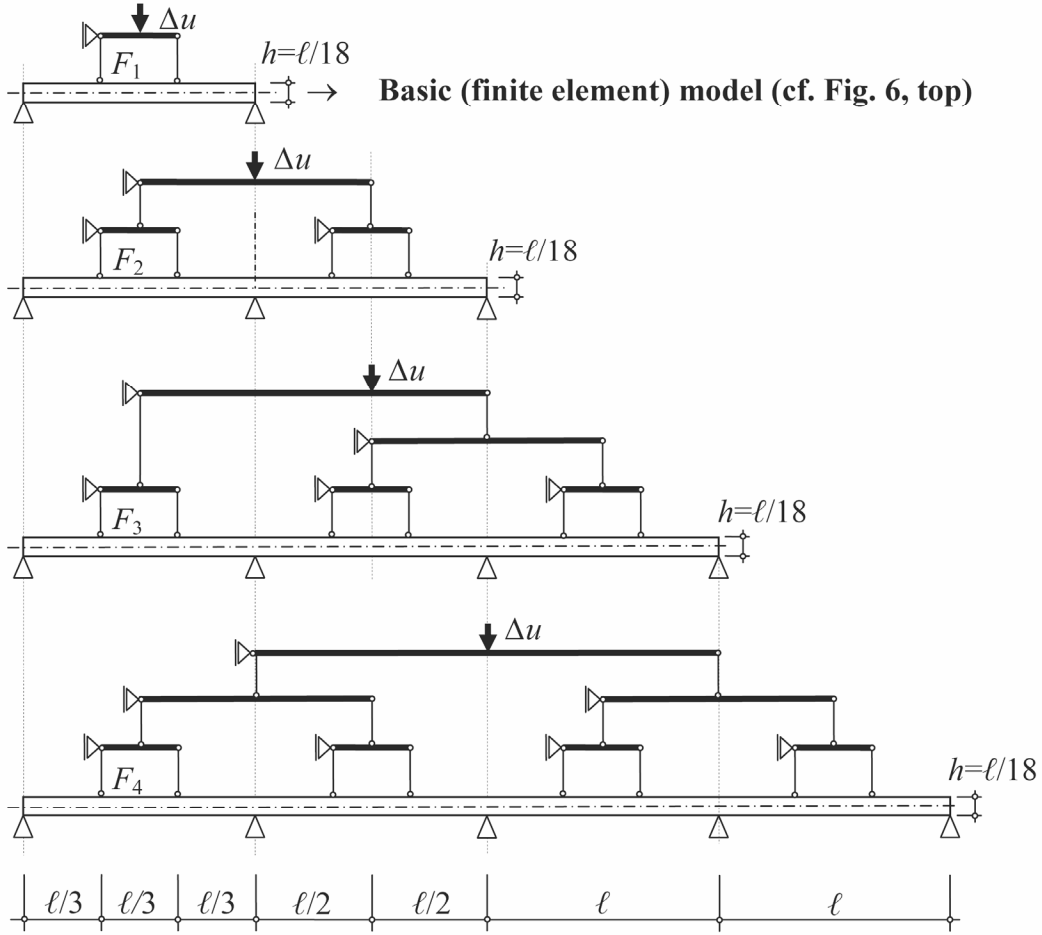


Fig. 7 Models for the analysis; the loading equipment (beam and link elements) enables the load distribution according to Fig. 7

For the grading method VIS II, the connection between Fig. 8a and 8b is explained by the following calculations. The corresponding load-carrying capacities (see additional vertical reference lines in Fig. 8a) and effective strength values are related to the 5th percentile level. In the calculation, the span ℓ is 10.8 m and the section modulus W 0.0066m³.

Simple beam:

$$F_{\max,1} = 44.5 \text{ kN} \rightarrow M_{\max,1} = 0.333 \cdot \ell \cdot F_{\max,1} = 0.160 \text{ MN} \rightarrow f_{\text{m,g,k}} = \frac{M_{\max,1}}{W} = 24.2 \text{ MPa}$$

2-span beam:

$$F_{\max,2} = 55.8 \text{ kN} \rightarrow |M_{\max,2}| = 0.333 \cdot \ell \cdot F_{\max,2} = 0.201 \text{ MN} \rightarrow f_{\text{m,g,k,2-span}} = \frac{M_{\max,2}}{W} = 30.4 \text{ MPa}$$

3-span beam:

$$F_{\max,3} = 58.6 \text{ kN} \rightarrow |M_{\max,3}| = 0.267 \cdot \ell \cdot F_{\max,3} = 0.169 \text{ MN} \rightarrow f_{\text{m,g,k,3-span}} = \frac{M_{\max,3}}{W} = 25.6 \text{ MPa}$$

4-span beam:

$$F_{\max,4} = 59.0 \text{ kN} \rightarrow |M_{\max,4}| = 0.286 \cdot \ell \cdot F_{\max,4} = 0.182 \text{ MN} \rightarrow f_{\text{m,g,k,4-span}} = \frac{M_{\max,4}}{W} = 27.6 \text{ MPa}$$

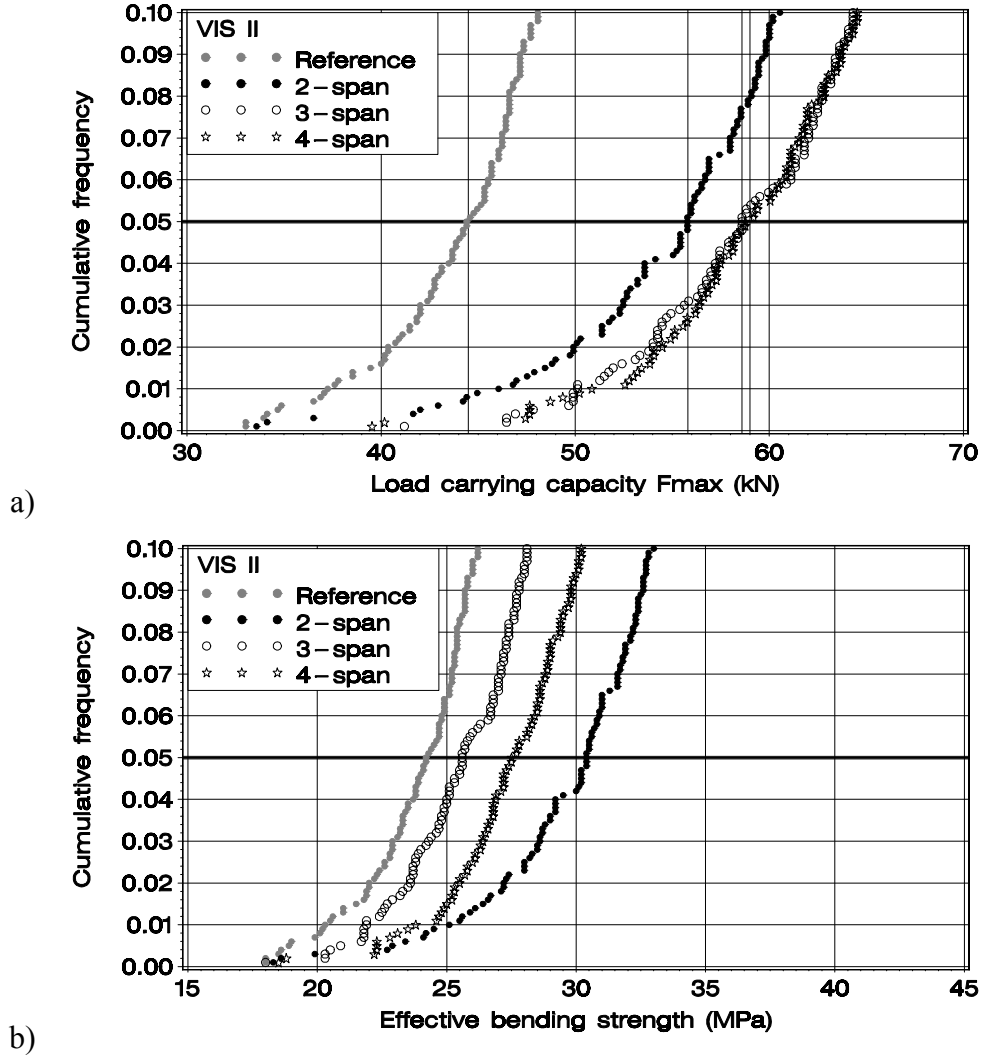


Fig. 8 Cumulative distributions of (a) load-carrying capacity and (b) effective bending strength; grading method VIS II

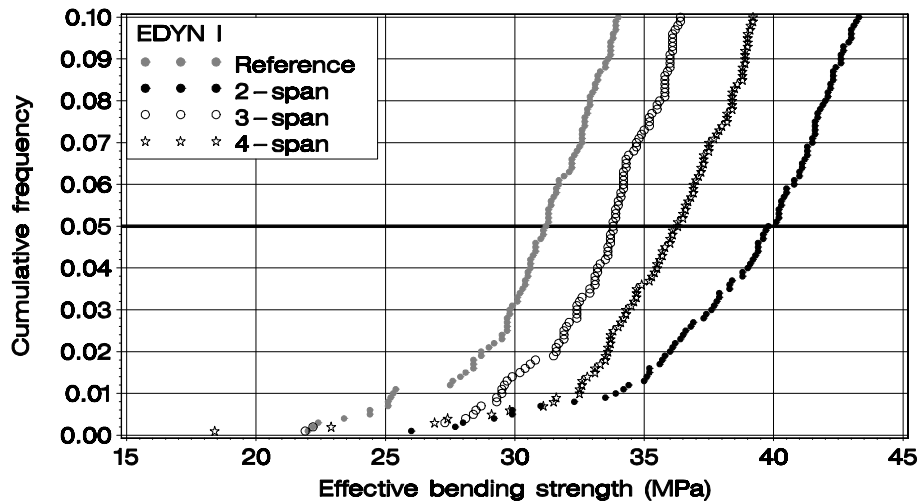


Fig. 9 Cumulative distributions of effective bending strength; grading method EDYN I

For each of the 36 samples, the 5th percentiles were determined and compared to each other. In Fig. 8b and 9 the 5th percentiles coincide with the points of interaction between the quasi-empirical cumulative distribution functions and the horizontal reference lines located at 0.05. A complete comparison is given in Fig. 10. The effective characteristic bending strength of 2-span beams is represented by *dots*, of 3-span beams by *circles* and of 4-span beams by *stars*. The symbols are plotted on top of each other in dependence on the characteristic bending strength as reference. The relations for the grading methods VIS II and EDYN I are, as an example, highlighted through thick vertical reference lines. The regression straight lines, approximately coinciding with the equations (4) to (6), show that for 2-span beams the effective strength ($f_{m,g,k,2\text{-span}}$) is about 25%, for 3-span beams ($f_{m,g,k,3\text{-span}}$) about 8% and for 4-span beams about 15% higher than the reference strength. There is non-significant influence of the grading methods on the coefficients in the examined range of 22 MPa to 39 MPa for the reference strength.

$$f_{m,g,k,2\text{-span}} \approx 1.25 \cdot f_{m,g,k} \quad (4)$$

$$f_{m,g,k,3\text{-span}} \approx 1.08 \cdot f_{m,g,k} \quad (5)$$

$$f_{m,g,k,4\text{-span}} \approx 1.15 \cdot f_{m,g,k} \quad (6)$$

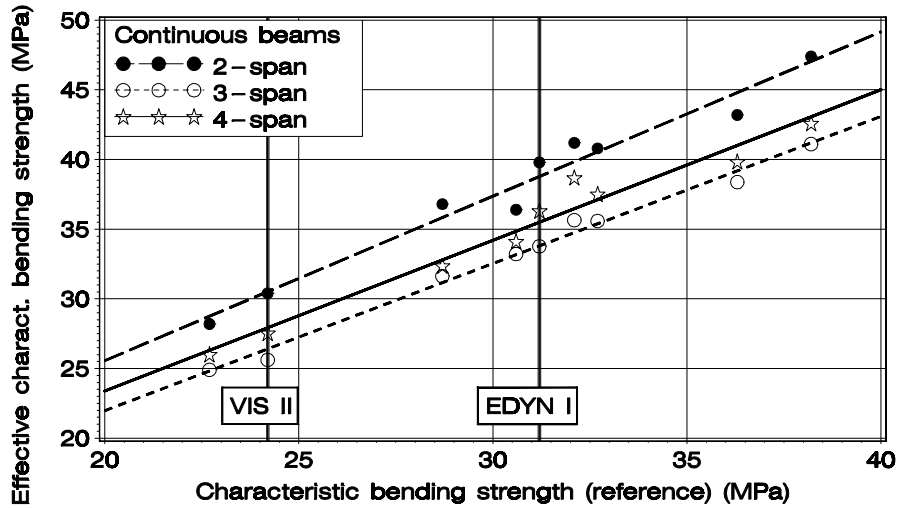


Fig. 10 Effective bending strength present in continuous beams and reference strength

6 Conclusions

- Comparative simulations of tensile and bending tests were performed to revise the tensile-to-bending-strength ratio. According to the study the tensile-to-bending-strength ratio is 0.88. The ratio applies to characteristic values of homogeneous glulam, is independent of the material strength and refers to standardised specimen dimensions for tensile and bending tests. The new found ratio is about 25 % higher than the value of about 0.70 in the European standard EN 1194 (1999). This difference may benefit the glulam industry by increasing the reference value for the characteristic tensile strength.
- A wide range of length-depth-combinations was considered for simulated tension members to create a database describing the size effect in glulam members subject to tension. In the study, the length but not the depth was found to be the dominant factor affecting the tensile strength. The influence of a member depth between 120 and 600 mm on the tensile strength is negligible. Based on Weibull's theory, a non-dimensional length factor was ob-

tained to fit the tensile-to-reference-tensile-strength ratio for characteristic values. The ratio decreases rapidly with increasing length for short members, meaning the tensile strength shows a strong dependence on the length of short members. For a quasi-infinite member length the size effect wears off. The effective strength of a tension member 150 mm in length is about 140% of the reference value whereas the remaining tensile strength for quasi-infinite member length is approximately 80% of the reference value. The consideration of a length-dependent glulam tensile strength may increase economical design of short tension members and the reliability of very long tension members.

- Comparative simulated bending tests on simple, 2-span, 3-span and 4-span beams show that the load-carrying capacity of continuous beams is 30 - 40% higher than of comparable simple beams. In regard to the design of continuous beams the effective (or apparent) characteristic bending strength of 2-span beams is 25%, of 3-span beams 8% and of 4-span beams 15% higher than the corresponding characteristic bending strength referring to simple beams. The 25% increase in case of 2-span beams is in good agreement with analytical results based on Weibull's theory [8][9]. In contrast to the current rule in the German timber design code DIN 1052 (2008) where a 10% increase is allowed on the basis of moment redistribution, the findings of the present study may allow a more economical and consistent design of continuous beams.

7 References

- [1] Blaß HJ, Frese M, Glos P, Denzler JK, Linsenmann P, Ranta-Maunus A (2008) Zuverlässigkeit von Fichten-Brettschichtholz mit modifiziertem Aufbau – Reliability of spruce glulam – modelling the characteristic bending strength, Bd. 11. Karlsruher Berichte zum Ingenieurholzbau. Universitätsverlag Karlsruhe: Karlsruhe
- [2] Blaß HJ, Frese M (2010) Schadensanalyse von Hallentragwerken aus Holz – Failure analysis on timber hall structures. Karlsruher Berichte zum Ingenieurholzbau. In preparation for publication by KIT Scientific Publishing: Karlsruhe
- [3] Frese M, Chen Y, Blaß HJ (2010) Tensile strength of spruce glulam. Accepted for publication in Eur. J. Wood Prod.
- [4] Frese M (2010) System effects in continuous glulam beams. Proceedings of the 11th World Conference on Timber Engineering, Riva del Garda, Italy
- [5] Frese M, Blaß HJ (2008) Bending strength of spruce glulam – new models for the characteristic bending strength. CIB-W18/41-12-2, St. Andrews by the Sea, Canada
- [6] Frese M, Blaß HJ (2009) Bending strength of spruce glulam. Eur. J. Wood Prod. 67: 277-286
- [7] Frese M, Hunger F, Blaß HJ, Glos P (2010) Validation of strength models for softwood glulam. Eur. J. Wood Prod. 68: 99-108
- [8] Colling F (1986) Influence of the volume and the stress distribution on the strength of a beam with rectangular cross section. Holz Roh- Werkst 44: 179-183
- [9] Isaksson T (2003) Structural Timber – Variability and Statistical Modelling. In: Thelandersson S, Larsen HJ (Ed.) Timber Engineering. Wiley & Sons: Chichester
- DIN 1052 (2008) Design of timber structures – General rules and rules for buildings (only available in German)
- EN 408 (2003) Timber structures – structural timber and glued laminated timber – determination of some physical and mechanical properties
- EN 1194 (1999) Timber structures – glued laminated timber – strength classes and determination of characteristic values

**INTERNATIONAL COUNCIL FOR RESEARCH AND INNOVATION
IN BUILDING AND CONSTRUCTION**

WORKING COMMISSION W18 - TIMBER STRUCTURES

**EXPERIMENTAL INVESTIGATIONS ON MECHANICAL BEHAVIOUR
OF GLUED SOLID TIMBER**

C Faye
F Rouger
P Garcia

Institut Technologique FCBA, Bordeaux
FRANCE

**MEETING FORTY THREE
NELSON
NEW ZEALAND
AUGUST 2010**

Presented by C Faye

H Larsen: Why are the E values higher for some of the configuration? C Faye: It may be due to system effect.

H Larsen: Since averages are taken, E should not change.

R Crocetti: In transversely pre-stressed bridge decks, higher E values are also obtained.

Experimental investigations on mechanical behaviour of Glued Solid timber

Carole Faye^a, Frédéric Rouger^b, Patrice Garcia^c

^a Institut Technologique FCBA, Allée de Boutaut, BP227, 33 028 Bordeaux Cedex, carole.faye@fcba.fr

^b Institut Technologique FCBA, Allée de Boutaut, BP227, 33 028 Bordeaux Cedex, frederic.rouger@fcba.fr

^c Institut Technologique FCBA, Allée de Boutaut, BP227, 33 028 Bordeaux Cedex, patrice.garcia@fcba.fr

1 Context and objective:

Glued Solid timber (GS) beams are structural elements with rectangular cross section formed by bonding together two, three, four or five laminations having a thickness between 45 and 85 mm. Laminations can be finger jointed.

GS beams are used in traditional carpentry, timber frame housing, or as bracing elements, etc.

Even if this product is more expensive than solid timber, the use of GS beams is increasing due to the following advantages: a better dimensional stability, moisture content around 12% due to the manufacturing process, cross section until $(260 \times 320) \text{ mm}^2$, directly compatible with CNC machines.

Because their cross section is close to squared section (maximum cross section is $L \times H \leq 260 \text{ mm} \times 340 \text{ mm}$), GS beams can be loaded in flatwise (load is perpendicular to glue lines) or edgewise (load is parallel to glue lines) bending (cf. figure1).

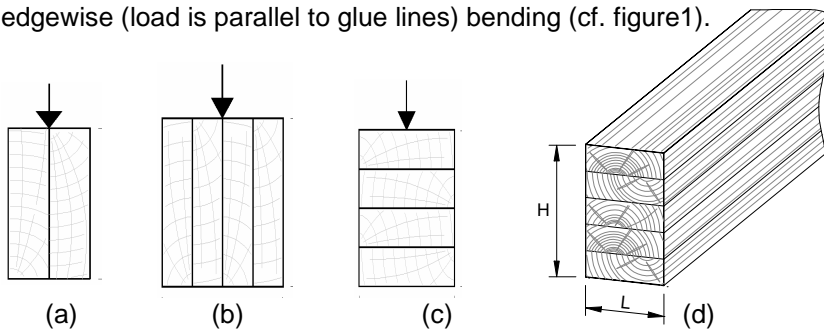


Figure 1 : GS beams with two (a) and four (b) laminations in edgewise bending, GS with four (c) or five (d) laminations in flatwise bending, $H \times L < 260 \text{ mm} \times 320 \text{ mm}$.

In flatwise bending, due to the fact that GS beams are composed of few laminations with large thickness, their mechanical behaviour is different from glulam. Actually, laminations in GS beams loaded in flatwise bending are not only stressed in tension but both in tension and bending.

In edgewise bending, the mechanical behaviour involves system effect: laminations with higher stiffness are more stressed. Since these laminations also have higher strength, this results in a composite product with higher strength.

In this context, the aim of this paper is to determine mechanical performances of GS beams and to propose beam lay ups for GS beams based on an experimental study carried on 180 beams in Spruce and Fir and Douglas Fir (in flatwise and edgewise bending) and on bending tests on finger joints and laminations. This work is the first part of research project of 2 years. These experimental investigations will be completed by additional tests on GS beams with 4 and 5 laminations and a probabilistic finite element model taking into account the variability of the mechanical properties of the laminations (presented in a future paper).

2 Experimental investigations on Douglas fir and Spruce and Fir: Presentation

Tables 2 and 3 present tests performed on laminations, finger joints and GS beams respectively for Douglas fir and Spruce and Fir.

A sampling has been performed to derive two equivalent sub samples:

- Sample A for laminations and finger joints testing,
- Sample B to produce GS beams.

Each lamination was evaluated by two non destructive methods:

- First one: visual method for structural use according to French standard NF B 52 001. This standard determines for French species grades STI, STII or STIII from visual criteria. In this study, GS beams were produced with laminations visually graded because it is representative of the French production.
- Second one: machine method (Goldeneye 702 of Microtec based on X-Ray) to establish two pair matched samples A and B.

This procedure is illustrated in Figure 2.

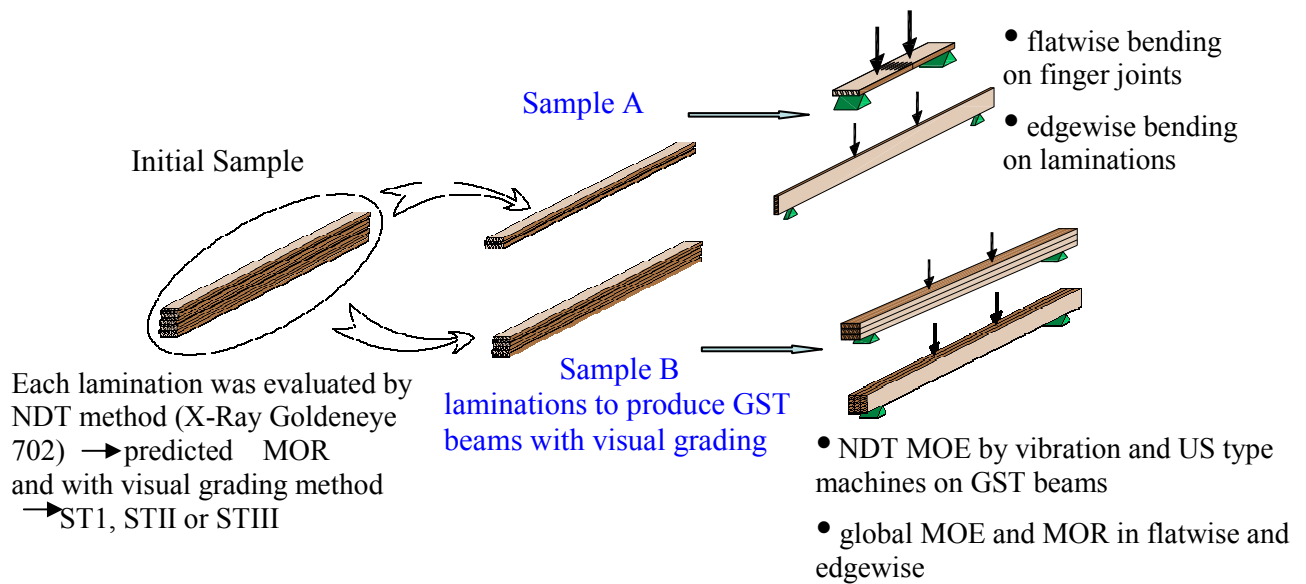


Figure 2 : Procedure to establish two pair matched samples A and B.

Mechanical performances and density required for strength classes C18, C24, C30 for solid timber according EN 338 and correspondance with French visual classes are given in Table 1.

French strength grades based on visual criteria (NF B 52 001)	STIII	STII	STI
Strength Classes for solid Timber (EN 338)	C18	C24	C30
Characteristic value of MOR MPa	18	24	30
Mean value of MOE MPa	9000	11 000	12 000
Characteristic value of density kg/m ³	320	350	380
Mean value of density kg/m ³	380	420	460

Table 1 : strength classes of solid timber Cxx(according EN 338, 2003) and correspondance with French visual structural classes.

Variables	Test Methods	Materials (number/beams or lamination/strength class/cross section)	
dynamic MOE	Ultrason and Vibration method	121 GST beams in flatwise	
global MOE and MOR in edgewise or flatwise for GS beams	EN 408 - 4 points loading bending	15 DUO ST2	130x130mm ² edgewise
		15 DUO ST2	130x130mm ² flatwise
		15 TRIO ST3	195x195mm ² edgewise
		15 TRIO ST3	195x195mm ² flatwise
		15 TRIO ST2	195x195mm ² edgewise
		15 TRIO ST2	195x195mm ² flatwise
global MOE and MOR in edgewise for laminations (Sample A)	EN 408 - 4 points loading bending edgewise	11 TRIO ST1	195x195mm ² edgewise
		10 TRIO ST1	195x195mm ² flatwise
		10 5-lames ST2	320x220mm ² flatwise
		37 ST2 130x66mm ² 60 ST3 195x65mm ² 34 ST2 195x65mm ² 36 ST1 195x65mm ² 41 ST2 230x65mm ²	
f _{m,j,k} in flatwise for finger joints (Sample A)	EN 408 - 4 points loading bending flatwise		5 ST2 130x66mm ² 9 ST3 195x65mm ² 5 ST2 195x65mm ² 12 ST1 195x65mm ² 0 ST2 230x65mm ²

Table 2 : Materials and Methods concerning Douglas fir samples.

Variables	Test Methods	Materials (number/beams or lamination/strength class/cross section)	
dynamic MOE	Ultrason and Vibration method	60 GST beams in flatwise	
global MOE and MOR in edgewise or flatwise for GS beams	EN 408 - 4 points loading bending	15 duo ST2 160x160mm ² edgewise 15 duo ST2 160x160mm ² flatwise 15 duo ST3 160x160mm ² edgewise 15 duo ST3 160x160mm ² flatwise	
global MOE and MOR in edgewise for laminations (Sample A)	EN 408 - 4 points loading bending edgewise	37 ST2 160x80mm ² 28 ST3 160x80mm ²	
f _{m,j,k} in flatwise for finger joints (Sample A)	EN 408 - 4 points loading bending flatwise		8 ST2 160x80mm ² 9 ST3 160x80mm ²

Table 3 : Materials and Methods concerning Spruce and Fir samples.

Edgewise bending tests on laminations were performed to determine strength classes of samples A. As samples A and B were matched, these results will give a good estimation of mechanical performances of laminations constituting GS beams.

To analyse experimental results on GS beams, characteristic values of MOR were calculated with a reference depth value equal to 150 mm (as for solid timber) and with a depth factor equal to 0,1 (as for glulam).

In order to compare results between edgewise and flatwise for a same configuration (given cross section, strength class):

- GS beams were evaluated by vibration methods to separate beams into matched samples,
- furthermore, cross sections of GS tested beams were squared.



Figure 3 : NDT MOE of Glued Solid timber evaluated by UltraSonic method.

3 Experimental investigations on Douglas fir: Results

3.1 Comparison between Samples A and B

The fractile curve presented in Figure 4 shows that NDT MOR of laminations used to produce GS beams (Samples B) are equivalent to NDT MOR of laminations tested in edgewise (samples A).

A fractile curve is established by associating X-values and Y-values having the same probability of occurrence.

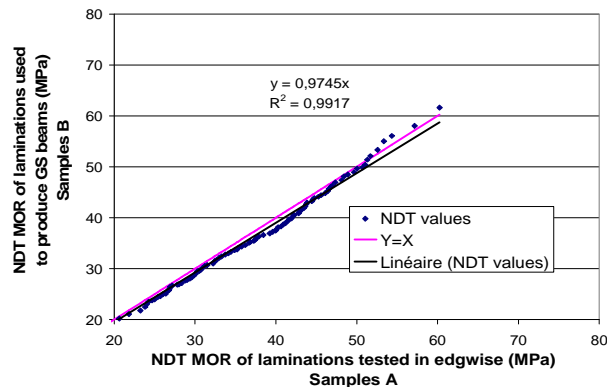
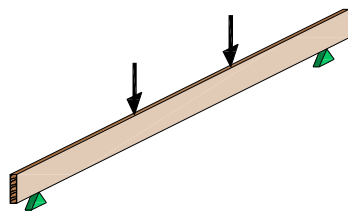


Figure 4 : Fractile Fractile curve of NDT MOR of laminations used to produce GS beams in Douglas Fir with 2, 3 and 5 laminations (sample B) depending on NDT MOR of laminations tested in edgewise (sample A).

3.2 Experimental results for laminations tested in edgewise bending (Sample A)

Statistical values of mechanical performances and density of Douglas fir laminations are presented in Table 4.



lamination cross section			Nb		MOE local	MOE global	MOR	Density
h	b				calculated	measured	h=150 mm	
mm	mm				(MPa)	(MPa)	(MPa)	(kg/m3)
130	65	ST2	37	MEAN	13 900	12 800	42,5	487
				CV		19%	25%	11%
				MIN		8 500	22,0	413
				MAX		18 600	69,9	587
				5% (EN 14358 §5)			24,5	
195	65	ST1	36	MEAN	16 800	15 000	61,7	525
				CV		14%	31%	8%
				MIN		11 168	17,9	455
				MAX		18 800	94,6	630
				5% (EN 14358 §5)			30,1	
195	65	ST2	34	MEAN	14 700	13 400	42	513
				CV		12%	29%	9%
				MIN		10 400	23,4	435
				MAX		17 300	70,8	630
				5% (EN 14358 §5)			24,6	
195	65	ST3	60	MEAN	13 800	12 700	40,7	499
				CV		17%	31%	11%
				MIN		9 200	22,9	392
				MAX		16 900	78,1	722
				5% (EN 14358 §5)			23,4	
230	65	ST2	41	MEAN	14 700	13 400	41	490
				CV		12%	29%	9%
				MIN		9 300	17,9	407
				MAX		15 900	69,8	555
				5% (EN 14358 §5)			23,5	

Table 4 : statistic values of MOE_{global} , MOR and density for Douglas fir laminations tested in edgewise bending (sample A). Mean value of MOE_{local} is calculated from mean value of MOE_{global} according the following relation $MOE_{Local} = MOE_{global} * 1,3-2690$ (EN 384, August 2004).

The main observations are the following:

- laminations visually graded in STI fulfil C30 requirements: mean value of MOE_{local} (=16 800 MPa) is greater by 40% than the required one (12 000 MPa) and experimental characteristic value of MOR (30,1 MPa) is close to required one (30 MPa).
- laminations visually graded in STII, for the 3 different cross sections, fulfil C24 requirements: mean value of MOE_{local} is greater by approximately 25% than the required value and experimental values of MOR (from 23,5 to 24,6 MPa) are close to required one (24MPa).
- laminations visually graded in STIII have higher strength than expected: mean value of MOE_{local} equals 13 800 MPa and characteristic strength is close to 24 MPa. This can be explained by the fact than correlation between visual criteria like size knots, growth ring width and mechanical performances are not relevant for Douglas fir.

3.3 Experimental results for finger joints tested in flatwise bending (Sample A) for Douglas fir

Table 5 presents experimental results of $f_{m,j,k}$, characteristic strength of finger joints in flatwise bending for the four configurations related to GS beams with 2 and 3 laminations. It was not possible to perform test on laminations corresponding to GS beams with 5 laminations because of lack of them.

Cross section of finger joints(mm ²)	130*65 (used for GS beams with 2 laminations)	195*65 (used for GS beams with 3 laminations)	260*65 (used for GS beams with 5 laminations)
$f_{m,j,k}$ (MPa) pour STIII		23,7 (min=27,5)	
$f_{m,j,k}$ (MPa) pour STII	25,9 (min=29,1)	27,5 (min=33,1)	No data
$f_{m,j,k}$ (MPa) pour STI		28,3 (min=28,2)	

Table 5 : Characteristic and minimum values bending strength in flatwise for Douglas Fir finger joints.

According to EN 14 080 draft (discussed in June 10 in CEN TC 124/ WG3), the required performance on finger joints for GS beams is given by the following relation: $f_{m,j,k} \geq 1,2 f_{m,l,k}$.

As the number of finger joint tested is low, the statistical evaluation of the characteristic strength is conservative; therefore an additional check on minimum values has been performed.

Finger joints involving STII or STIII laminations have a characteristic (or minimum) strength close to the required one (28,8 MPa).

Finger joints involving STI laminations have a characteristic (or minimum) strength much lower than required one (36 MPa). For this reason, strength of GS beams made with high strength class laminations will be limited by finger joints.

3.4 Experimental results for GS beams tested in bending

Main statistical values of mechanical properties and density corresponding to the Douglas fir GS beams are presented in Table 6.

For each geometrical configuration of GS beams, mechanical properties obtained in edgewise bending are higher than these obtained in flatwise bending. We can notice that, for each geometrical series, dynamic MOE of matched series (respectively in flatwise and edgewise) are very similar.

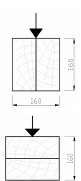
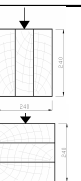


	L	H			MOE vibration (MPa)		MOE local calculated (MPa)	MOE global (MPa)	MOR H (MPa)	MOR h=150 mm k=0,1 (MPa)	Density (kg/m3)
 STII	130	130	DUO	15	MEAN CV 5% (EN 14358 §4)	13 400 12% 14358 §4	edgewise	14 100 13%	43,4 21% 28,1	42,8 27,7	499 7%
	130	130	DUO	15	MEAN CV 5% (EN 14358 §4)	13 800 14% 14358 §4	flatwise	13 100 11%	41,0 22% 25,2	40,5 24,8	500 6%
						0,97	edgewise/flatwise	1,06		1,12	1,00
 STI	195	196	TRIO	10	MEAN CV 5% (EN 14358 §4)	14 100 12% 14358 §4	edgewise	15 500 7%	45,4 18% 29,8	46,6 30,7	522 4%
	196	195	TRIO	10	MEAN CV 5% (EN 14358 §4)	14 200 13% 14358 §4	flatwise	13 200 12%	44,3 34% 21,0	45,4 21,5	513 5%
						0,99	edgewise/flatwise	1,15		1,42	1,02
 STII	195	196	TRIO	15	MEAN CV 5% (EN 14358 §4)	12 700 11% 14358 §4	edgewise	13 600 8%	41,8 21% 27,8	42,9 28,5	503 4%
	196	195	TRIO	15	MEAN CV 5% (EN 14358 §4)	12 900 10% 14358 §4	flatwise	12 100 14%	37,9 28% 22,6	38,9 23,2	505 4%
						0,98	edgewise/flatwise	1,10		1,23	1,00
 STIII	193	193	TRIO	15	MEAN CV 5% (EN 14358 §4)	12 700 10% 14358 §4	edgewise	13 600 9%	37,3 17% 26,8	38,3 27,5	514 3%
	193	193	TRIO	15	MEAN CV 5% (EN 14358 §4)	12 900 8% 14358 §4	flatwise	12 800 10%	35,1 12% 27,2	36,0 27,9	517 5%
						0,98	edgewise/flatwise	1,05		0,99	0,99
5-Lamination: STII	211	322		10	MEAN CV 5% (EN 14358 §4)	13 700 11% 14358 §4	flatwise	13 900 11%	32,1 19% 21,0	34,6 22,6	505 5%

Table 6 : statistical values of MOE_{global}, MOR and density for Douglas fir GS beams tested in edgewise and flatwise bending; MOR for H_{ref}=150mm is calculated from MOR for actual H with a depth factor equal to 0.1.

3.4.1 Edgewise bending

As expected, characteristic strengths for GS beams made with STII or STIII laminations are very similar. The increase of strength of GS beams in comparison with STII laminations strength is around 15%. Concerning GS beams made with STI laminations, the increase is lower (around 5%); this can be explained by the weak performance of finger joints.

3.4.2 Flatwise bending

Characteristic strength for GS beams with STI laminations, obtained from 10 experimental values equals 21,5 MPa ; this calculated value is penalized due to the fact that coefficient of variation is very high (=34%) in comparison with the other configurations (around 20%).

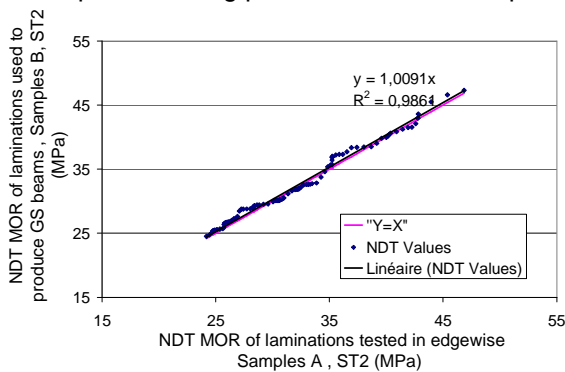
Characteristic strength for GS beams made with STIII laminations (=27,9 MPa) is higher than the strength obtained for GS beams made with STII laminations (around 24 MPa). This is unexpected because (as it is shown in paragraph 3.2), STIII and STII laminations are equivalent. Actually, the increase in strength is due to a lower coefficient of variation (12%).

4 Experimental investigations on Spruce and Fir: Results

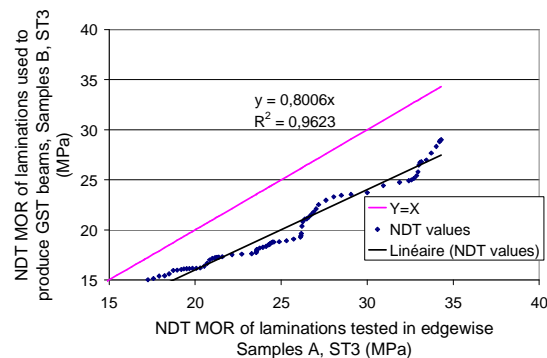
4.1 Comparison between Samples A and B

Fractile Fractile curves presented in Figures 5 show that:

- NDT MOR of STII laminations used to produce GS beams (Sample B) are equivalent to NDT MOR of STII laminations tested in edgewise (sample A) (cf. figure 6-1),
- NDT MOR of STIII laminations used to produce GS beams (Sample B) are lower than NDT MOR of STIII laminations tested in edgewise (sample A) (cf. figure 6-2); a further investigation showed that the pair matching procedure was not respected.



5-1



5-2

Figures 5-1 et 5-2: fractile fractile curves of NDT MOR of laminations used to produce DUO in Spruce and Fir (Sample B) depending on NDT MOR of laminations of Sample A, respectively for STII (6-1) and STIII (6-3).

4.2 Experimental results for laminations tested in edgewise bending (Sample A)

Statistical values of mechanical properties and density corresponding to sample A of Spruce and Fir laminations are presented in Table 7.

We can observe than, for both strength classes STII and STIII, mechanical properties are lower by approximately 10% than the expected values respectively for C24 and C18.

Such properties can be explained by the resource from which the boards are sampled: timber originating from young trees will have a weaker mechanical behaviour, despite a lower knottiness. This type of relation cannot be predicted by a visual grading method.

	Lamination cross section			Nb		MOE local	MOE global	MOR	Density
	h	b				calculated	measured	h=150mm	
	mm	mm				MPa	MPa	MPa	kg/m ³
	160	80	STII	37	Mean	9700	9500	36	390
					CV		18%	24%	7%
					5%			22,1	
	160	80	STIII	38	Mean	7600	7900	28,2	360
					CV		14%	27%	7%
					5%			16	

Table 7 : statistical values of MOE_{global}, MOR and density for Spruce and Fir laminations tested in edgewise bending (sample A).

4.3 Experimental results for finger joints tested in flatwise bending (Sample A) for Spruce and Fir

Table 8 presents experimental results of $f_{m,j,k}$, characteristic strength of finger joints in flatwise bending for both configurations related to GS beams with two laminations.

Cross section of finger joints (mm ²)	155*80 (used for GS beams with 2 laminations)
$f_{m,j,k}$ (MPa) pour $f_{m,l,k}$ =16 MPa	21,7 (min=22,5)
$f_{m,j,k}$ (MPa) pour $f_{m,l,k}$ =22 MPa	24,8 (min=28,8)

Table 8 : Characteristic and minimum values bending strength in flatwise for Spruce and Fir finger joints.

Finger joints involving STII or STIII laminations have a characteristic (or minimum) strength close to the required ones.

4.4 Experimental results for GS beams tested in bending

Main statistical values of mechanical properties and density corresponding to Spruce and Fir GS beams are presented in Table 9.

For both configurations of GS beams, MOE obtained in edgewise bending is higher than the one obtained in flatwise bending by approximately 15%. We can notice that, for each configuration, dynamic MOE of matched series (respectively in flatwise and edgewise) are similar.

4.4.1 Edgewise bending

The strength increase, in comparison with solid timber is :

- around 10% for GS beams with 2 STII laminations,
- around 30% for GS beams with 2 STIII laminations.

4.4.2 Flatwise bending

Characteristic values for GS beams made with STII or STIII laminations are very similar (respectively 20,5 MPa and 20, 6 MPa).

This unexpected result can be explained by the following reasons:

- for GS beams made with STII laminations, the minimum strength of the series (=22,4 MPa) corresponds to a failure in a finger joint including a knot; this is not allowed,
- for GS beams made with STIII laminations, the characteristic value (=20,6 MPa) is statistically increased due to a low coefficient of variation (=11%).

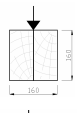

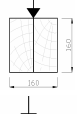
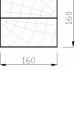
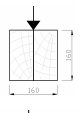

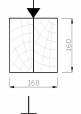
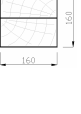
		L		H			MOE vibration (MPa)		MOE local calculated (MPa)	MOE global measured (MPa)	MOR H (MPa)	MOR H _{ref} =150 mm (MPa)	Density (kg/m ³)
 	STII	156	156	DUO	15	MEAN	10600	edgewise	10900	10400	37,0	37,3	406
						CV	14%			11%	21%	24,0	6%
						5%						24,2	
 	STIII	156	156	DUO	15	MEAN	10400	flatwise	9500	9400	29,7	29,9	404
						CV	14%			13%	18%	20,3	6%
						5%	1,01	edge/flat		1,12	1,25	20,5	
 	STII	156	156	DUO	15	MEAN	9200	edgewise	9000	9000	30,9	31,1	398
						CV	11%			10%	19%	20,7	5%
						5%						20,9	
 	STIII	156	156	DUO	15	MEAN	9000	flatwise	7300	7700	25,3	25,5	388
						CV	10%			10%	11%	20,4	5%
						5%	1,02	edge/flat		1,17	1,01	20,6	

Table 9 : statistical values of MOE_{global}, MOR and density for Spruce and Fir GS beams tested in edgewise and flatwise bending; MOR for H_{ref}=150mm is calculated from MOR for actual H with a depth factor equal to 0.1.

5 Proposal for beam lay-ups for Glued Solid Timber

In the aim to determine relations between mechanical properties of GS beams and laminations, the following fractile curves were established:

- fractile curve of all data concerning MOR GS beams (obtained on Douglas, Spruce and Fir GS beams with 2, 3 or 5 laminations) depending on actual laminations MOR tested in edgewise bending (sample A) (cf. figures 6 and 8 for MOR GS beams respectively in edgewise and flatwise bending).
- fractile curve of all data concerning MOE GS beams (obtained on Douglas, Spruce and Fir GS beams with 2, 3 or 5 laminations) depending on actual laminations MOE tested in edgewise bending (sample A) (cf. figures 7 and 9 for MOE GS beams respectively in edgewise and flatwise bending).

The analysis on the whole data set avoids statistical artefacts which are due to limited sub sample sizes. Furthermore, proposal for beam lay-ups must be done without distinction of wooden species. But this approach cannot be used to estimate the influence of the number of laminations.

5.1 GS beams in EDGEwise bending

As illustrated in Figure 6, GS beams produced with laminations with a strength lower than 35 MPa exhibit an increase in strength as compared to the laminations. This increase is less significant for high strength classes because the finger joints strength in that case becomes predominant.

Figure 7 also exhibits an increase in stiffness for GS beams as compared to laminations. This increase is less significant for high strength classes. This can be partly explained by a lower coefficient of variation which tends to decrease the system effect (cf. table 10).

SAMPLE A Cross sections		Spruce and Fir STII (80*160) mm ²	Douglas fir STIII (65*195) mm ²	Douglas fir STII (65*130) mm ²	Douglas fir STII (65*195) mm ²	Douglas fir ST2 (65*260) mm ²	Douglas fir STI (65*195) mm ²
MOEg	Mean (MPa)	9500	12700	12800	13400	13400	15000
	CV%	18%	17%	19%	12%	12%	14%

Table 10 : mean value and coefficient of variation for sample A.

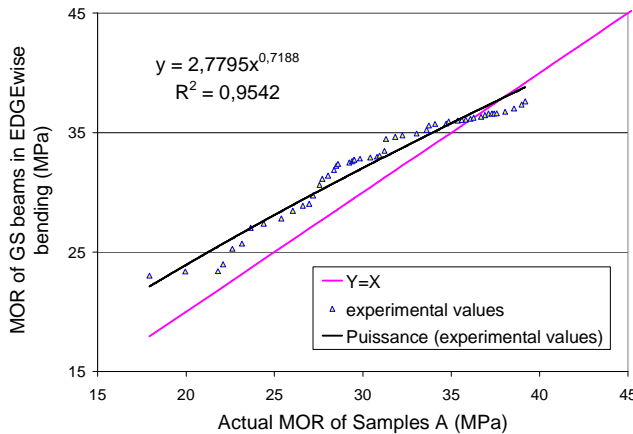


Figure 6

Figure 6 : fractile curve of MOR GS beams tested in edgewise bending depending on actual laminations MOR tested in edgewise bending (sample A).

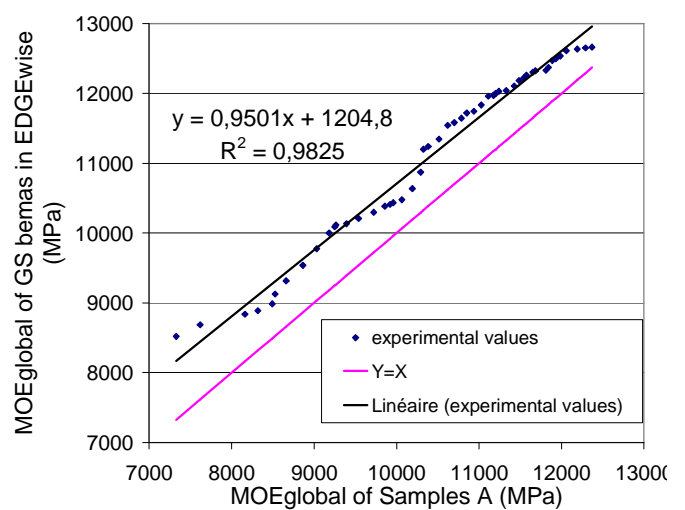


Figure 7

Figure 7 : fractile curve of MOE GS beams tested in edgewise bending depending on actual laminations MOE tested in edgewise bending (sample A).

By using regression functions fitted on fractile curves, mechanical properties of GS beams were calculated from the laminations for C18, C24, C30. Calculated values are presented in tables 11 and 12 respectively for strength and modulus of elasticity.

MOR of laminations	18 MPa	24 MPa	30 MPa
edgewise MOR of GS beams (test results)	22,2 MPa	27,3 MPa	32 MPa
Experimental ksys	1,23	1,14	1,07

Table 11 : relationship between laminations strength and GS beams strength in edgewise for C18, C24, C30, obtained on all experimental data (Douglas, Spruce and Fir GS beams with 2 and 3 laminations).

The system factor (between 1,23 and 1,07) obtained from experiments is larger than the one given by Eurocode 5, namely $k_{sys}=1,03$ for beams with 2 laminations and $k_{sys}=1,06$ for beams with 3 laminations.

MOE of laminations	9 000 MPa	11 000 MPa	12 000 MPa
edgewise MOE of GS beams (test results)	9 700 MPa	11 700 MPa	12 600 MPa

Table 12 : relationship between laminations MOE and GS beams MOE in edgewise for C18, C24, C30, obtained on all experimental data (Douglas, Spruce and Fir GS beams with 2 and 3 laminations).

5.2 GS beams in flatwise bending

According fractile fractile curve presented in Figure 8, GS beams produced with laminations with strength lower than 24 MPa have higher strength than laminations one.

According fractile fractile curve presented in Figure 9, MOE of GS beams and laminations are close.

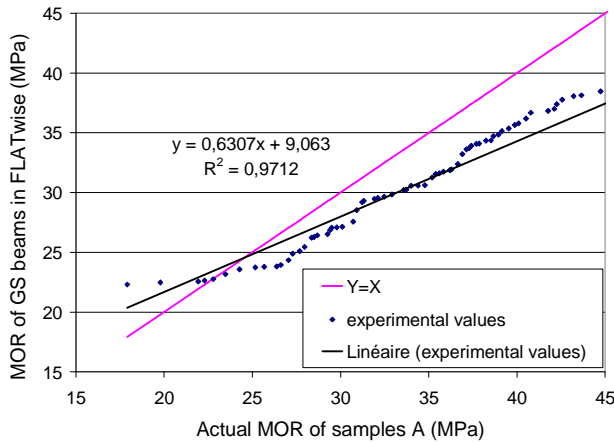


Figure 8

Figure 8 : fractile fractile curve of MOR GS beams tested in flatwise bending depending on actual laminations MOR tested in edgewise bending (samples A).

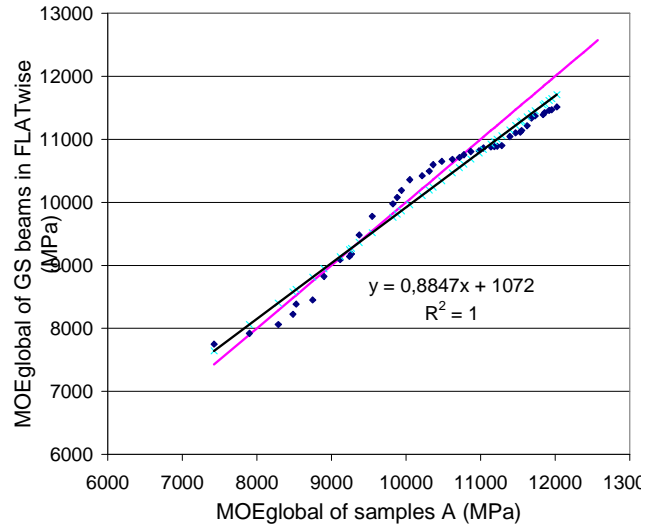


Figure 9

Figure 9 : fractile fractile curve of MOE GS beams tested in flatwise bending depending on actual laminations MOE tested in edgewise bending (samples A).

From regression functions fitted on fractile fractile curves, mechanical properties of GS beams in flatwise were calculated from laminations ones for C18, C24, C30. Calculated values are presented in tables 13 and 14 respectively for strength and modulus of elasticity.

MOR of laminations	18 MPa	24 MPa	30 MPa
flatwise MOR of GS beams (test results)	20,4 MPa	24,2 MPa	28 MPa

Table 13 : relationship between laminations strength and GS beams strength in flatwise for C18, C24, C30, based on all experimental data (obtained on Douglas, Spruce and Fir GS beams with 2, 3 and 5 laminations).

MOE of laminations	9 000 MPa	11 000 MPa	12 000 MPa
flatwise MOE of GS beams (test results)	9 000 MPa	10 800 MPa	11 700 MPa

Table 14 : relationship between laminations MOE and GS beams MOE in flatwise for C18, C24, C30, based on all experimental data (obtained on Douglas, Spruce and Fir GS beams with 2, 3 and 5 laminations).

5.3 Proposal for beam lay-ups

According to the results presented in paragraphs 5.1 and 5.2, a proposal for beams lay-ups for GS beams is given in table 15 for which the corresponding mechanical properties and density are presented in table 16.

Strength class of laminations	Strength class of Glued Solid timber
C18	GS 20
C24	GS 24
C30	GS 28

Table 15 : Beam lay up of homogeneous glued solid timber beams.

For bending, two values for strength and stiffness properties are given depending if glued solid timber is stressed respectively flatwise or edgewise.

For tension parallel to the grain, the characteristic strength is taken as 70% of the characteristic values of the bending strength in flatwise. This is an intermediate reduction factor between solid timber (60%) and glulam (80%).

For compression parallel to the grain, the characteristic strength is taken as the characteristic bending strength of GS beams (as for glulam).

For tension and compression perpendicular to the grain and shear, the characteristic strengths are the same for the 3 classes GSxx and equal to the characteristic strengths of C24.

Density values for GS beams are the same as for laminations.

GS strength class		GS 20	GS 24	GS 28
Bending strength (1)	$MOR_{gs,flat}=f_{m,gs,k,flat}$	20,4	24,2	28
	$MOR_{gs,edge}=f_{m,gs,k,edge}$	22,2	27,3	32
Tensile strength	$f_{t,0,gs,k}$	14,3	17	19,6
	$f_{t,90,gs,k}$	0,5		
Compression strength	$f_{c,0,gs,k}$	20,4	24,2	28
	$f_{c,90,gs,k}$	2,5		
Shear strength	$f_{v,g,k}$	2,5		
Modulus of elasticity (1)	$MOE_{0,g,mean,flat}$	9 000	11 000	12 000
	$MOE_{0,g,mean,edge}$	9 700	11 700	12 600
Density	$\rho_{gs,k}$	320	350	380
Density	$\rho_{gs,m}$	380	420	460

Table 16 : homogeneous glued solid timber: characteristic strength, stiffness properties in N/mm² and densities in kg/m³. (1) For bending, two values for strength and stiffness properties are given depending if glued solid timber is stressed respectively flatwise or edgewise.

6 Conclusions

Based on an experimental study carried on 180 GS beams, strength and stiffness were determined in flatwise and edgewise bending.

In edgewise bending, system effect induces an increase of strength for GS beams in comparison with laminations. This increase is less significant for high strength classes due to the weak strength of the finger joints tested in this study. System factor obtained from experiments is larger than the one given by Eurocode 5, namely $k_{sys}=1,03$ for GS beams with 2 laminations and $k_{sys}=1,06$ for GS beams with 3 laminations.

In flatwise, the correspondence between the strength of laminations and the strength of GS beams is given for a reference depth of 150 mm and a depth factor of 0,1, and it is similar than the correspondence existing for glulam with a reference depth of 600 mm and a depth factor of 0,1.

The beam lays-up presented in paragraph 5 are actually discussed into working group WG3 of CEN TC124 in charge of the revision EN 14 080 which will integrate Glued Solid timber beams.

This first study will be completed by:

- Additional tests on GS beams with four and five laminations,
- A probabilistic finite element model taking into account the variability of the mechanical properties of the laminations and finger joints.

Aknowledgments

The study was supported by the French association France Bois Forêt, French Regions Limousin, Midi-Pyrénées, Auvergne, Bourgogne and Franche Comté, Agriculture Ministry, CODIFAB in collaboration with Manufacturers Monnet Sève, Cosylva, Prolignum, Barlet and Microtec.

**INTERNATIONAL COUNCIL FOR RESEARCH AND INNOVATION
IN BUILDING AND CONSTRUCTION**

WORKING COMMISSION W18 - TIMBER STRUCTURES

**INFLUENCE OF THE BOUNDARY CONDITIONS ON THE
RACKING STRENGTH OF SHEAR WALLS WITH AN OPENING**

M Yasumura
Shizuoka University
JAPAN

**MEETING FORTY THREE
NELSON
NEW ZEALAND
AUGUST 2010**

Presented by M Yasumura

L Dalziel: What are consequences of multiple openings? M Yasumura: would be more complicated. Not being studied.

L Dalziel: Software was developed for multiple openings.

S Franke: does model allow “negative” uplift? M Yasumura: negative uplift is for sheeting only.

H Blass: springs elements for sheeting connections? M Yasumura: yes, and polygonal.

T Gibney: Where tie-down forces measured and what were they? M Yasumura: No, forces where not measured.

T Gibney: were lateral displacements measured? M Yasumura: Yes and always good correlation with model.

S Aicher: Why tension force is approximately constant? M Yasumura: Longer walls can resist higher lateral forces and tensile forces are more or less constant.

Influence of the boundary conditions on the racking strength of shear walls with an opening

Motoi YASUMURA

Shizuoka University, Japan

1 Introduction

It is well known that the boundary conditions such as the vertical restraints of wall panel and the vertical loads due to live and dead loads, snow load, etc. have considerable effects on the mechanical properties of wooden shear walls¹⁾. These effects are to be considered specially for the design of timber structures and the racking tests on shear walls. In this context, International Standard on the static and reversed cyclic lateral loading test method²⁾ proposes two boundary conditions that is designed to ensure the full shear capacity of the wall is achieved (Method I), and that to reflect the intended actual construction details (Method II). This study reviews the experimental results and Finite Element analysis of wood-framed shear walls with various opening configuration and aims at clarifying the effects of boundary condition and the vertical loads on the shear capacity of shear walls with opening to propose its design method.

2 Background

Racking resistance of panel sheathed shear wall with an opening can be estimated by introducing a simple model that have panel zones and an opening as shown in Fig.1. The apparent shear forces per length of each panel zone and the reaction forces at the bottom of the wall panel are shown in the diagram. The total force of the vertical perimeter of the wall panel (Q_{VT}) is expressed by the equation (1).

$$Q_{VT} = Q \cdot \frac{(h_1 + h_2)}{L} + Q \cdot \frac{h_w}{(l_1 + l_2)} \quad (1)$$

where, Q : lateral force, L : wall length, h_1 , h_2 : heights of shear panel zone above and under the opening, l_1 , l_2 : lengths of side walls, h_w : height of opening.

Assuming that the wall panel fails with the nail connection at the end stud of the side wall³⁾, vertical critical force (Q_{VT}) at the end stud is expressed by the equation (2).

$$Q_{VT} = (n-1) \cdot f_{cr} \quad (2)$$

where, f_{cr} is the yield or ultimate shear resistance of a nail joint connecting sheathing material to the stud, n : number of nails at the vertical perimeter of the wall panel.

Equation (2) becomes;

$$Q = (n-1) \cdot f_{cr} \cdot \frac{L}{H} \cdot \frac{1}{1 + \frac{h_w \cdot l_w}{H \cdot L} \cdot \frac{L}{l_1 + l_2}} = Q_0 \cdot r \quad (3)$$

where, Q_0 : racking resistance of a wall without opening which has the same size as the opening wall, r : *Sugiyama's* opening coefficient⁽⁴⁾ defined by the equation (4).

$$r = \frac{1}{1 + (\alpha/\beta)} \quad (4)$$

$\alpha = (l_w \cdot h_w)/(L \cdot H)$, $\beta = (L - l_w)/L$
and l_w : length of opening.

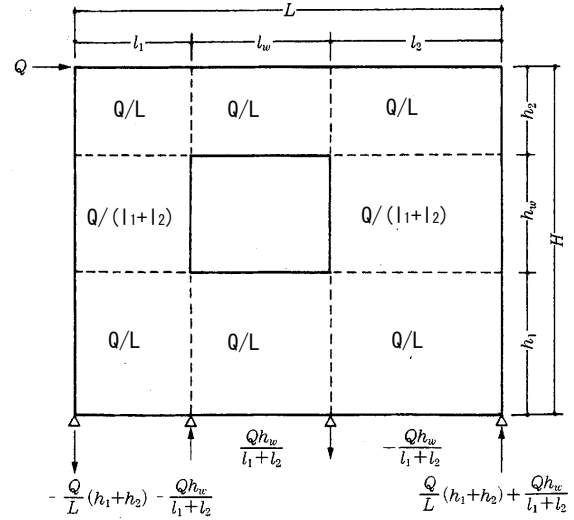


Fig.1 Assumed Shear force distribution in wood-framed shear wall with an opening.

3 Experiments

3.1 Specimens

Racking tests on wood-framed shear walls with various opening configuration and vertical restraints were conducted to investigate the effects of opening and the vertical restraints of studs beside the opening on the shear resistance of wall panel. Specimen had wood-framed shear walls of 2.73 and 3.64m lengths and 2.44m height sheathed with 9.5mm thick spruce plywood on one side of the frame as shown in Fig. 2. Sheathing materials were connected to frames of nominal two-by-four lumbers of S-P-F Standard with JIS A5508 CN50 nails (50.8mm length and 2.87mm diameter). Nails were spaced 100mm in the perimeters of a sheet material and 200mm on the central support. Studs were spaced 455mm and connected to bottom and double top plates with CN90 nails (88.9mm length and 4.11mm diameter). End studs were doubled or tripled and connected each other with CN75 nails (76.2mm length and 3.76mm diameter) spaced 300mm. Specimens had an opening of window configuration of 910mm or 1820mm length and 900mm height and door type configuration of 910 or 1810mm length and 1800mm height as shown in Fig.3. The bottom plates of wall panels were connected to 89mm by 89mm sill and steel foundation with four

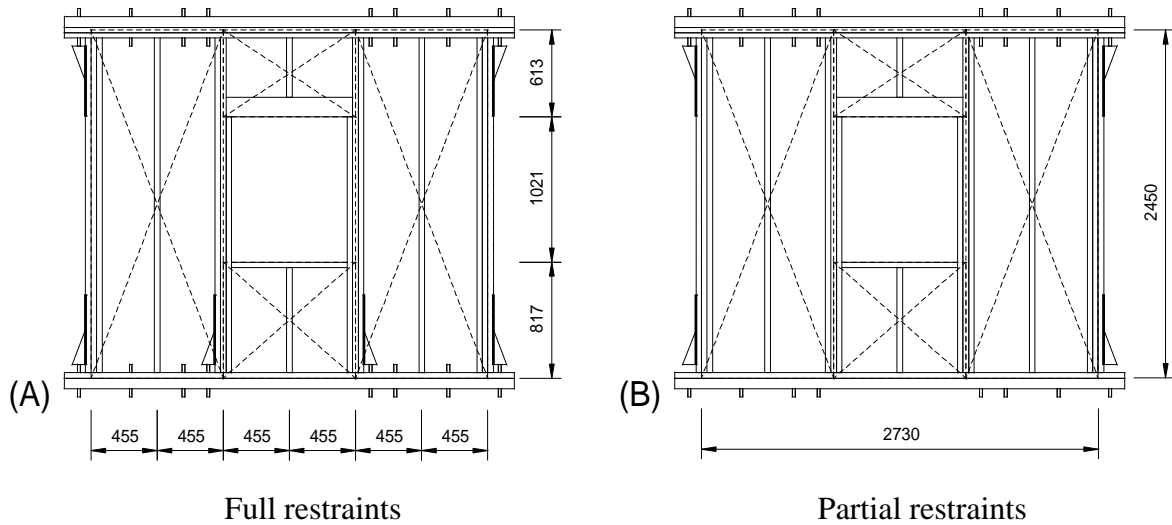


Fig.2 Specimens with **full vertical restraints** (A) and **partial vertical restraints** (B).

Table 1 Outline of specimens

Specimen	Hold-down connections	Opening size (l x h)(m)	Panel size (L x H)(m)
B4P-FH	Full	----	3.64 x 2.44
W4P-FH	Full	1.82 x 0.91	
W4P-PH	Partial		
D4P-FH	Full	1.82 x 1.82	
D4P-PH	Partial		
S4P-FH(*)	Full	1.82x2.42	
S4P-PH(*)	Partial		
B3P-FH	Full	----	2.73 x 2.44
W3P-FH	Full	0.91 x 0.91	
W3P-PH	Partial		
D3P-FH	Full	0.91 x 1.82	
D3P-PH	Partial		
S3P-FH(*)	Full	0.91 x 2.42	
S3P-PH(*)	Partial		

* only numerical analysis conducted

bolts of 16mm diameter. Double top plates were connected to 89mm by 89mm girder with four bolts of 16mm diameter. Hold-down connection of HDB20 were applied to both ends of wall connected to the studs with four bolts of 12mm diameter, and one was applied at the top of end studs to connect to 4-by-4 western hemlock girder located at the top of wall. For the walls with opening, both specimens with full restraints of the foot of studs and partial restraints were prepared for all types of opening configuration. For the walls with partial restraints, hold-down connections beside the opening were removed. The outline of specimens is shown in Table 1.

3.2 Test methods

Monotonic and reversed cyclic loads were applied at the end of girder by a computer controlled actuator. Horizontal and vertical displacements were measured by electronic transducers. Specimens (4P) subjected to only the monotonic loadings, and specimens (3P) were tested under the monotonic and reversed cyclic loading. Single shear test of nail joint (CN50) was also conducted to model the joint connecting plywood sheathing to frame members.

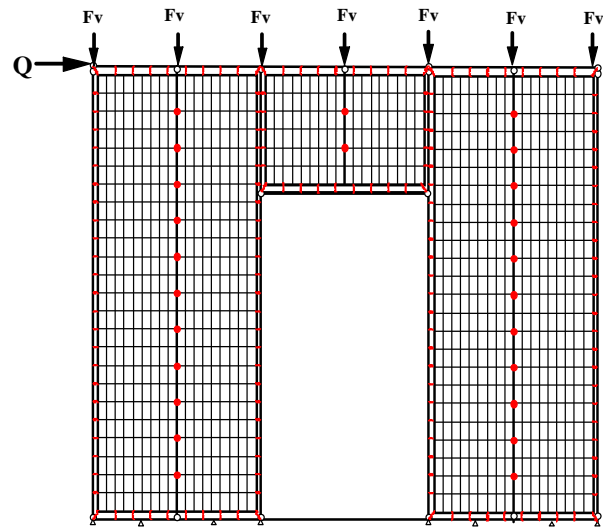


Fig.3 Finite Element model for opening wall

4 Numerical analysis

4.1 Finite Element analysis

Shear walls were modelled with beam, plate and spring elements representing the framing members, sheathings and fasteners connecting sheathings to framing, respectively. The framing elements were modelled with isotropic linear 2D beam elements. The sheathings were modelled with 2D plane stress elements that were elastic and orthotropic. The fasteners between sheathings and framing beams were modelled with a non-linear spring system. The force-displacement curves of fasteners followed a tri-linear curve. The nodal forces were related to the relative nodal displacements. Finite element codes CASTEM 2000 was applied to the modelling and calculation. The joints connecting frame members were modelled with spring elements that had different stiffness in compression and tension. Flexibility of hold-down connections was modelled by replacing the tension stiffness of the particular framing joints with the hold-down stiffness obtained from single shear tests of hold-down connectors. At the locations of the hold-down connections, the bottom plate was assumed to be rigidly connected to the foundation. Bearing between adjacent sheathings was not considered in this time⁵.

4.2 Material properties

Poisson's ratio and modulus of elasticity of the framing members were assumed to be 0.2 and 10,000 N/mm², respectively. For the panel elements Poisson's ratio, the modulus of elasticity and shear modulus were assumed to be 0.5, 5,300 N/mm² and 700 N/mm², respectively. The nail properties used for the fastener elements were determined by single shear tests of nail joints. Tri-linear approximation was adopted to the analysis. The embedding stiffness of the framing joints and the tension stiffness of the hold-downs were determined by tests performed with static compression loading. The embedding and hold-down tests were performed with three specimens for each configuration. In the hold-down test, performed with symmetrically specimens, HDB-20 hold-downs with four lag-screws of 12mm diameter and 75mm length were used. Two hold-down connections were placed on a stud package of four 38-by 89 mm studs. Assuming that the displacement is primarily assigned to the slip of the joints, the joints were tested in compression instead of tension. The embedding tests were also performed with three different configurations, made up of one, two or three. The results from the tests were evaluated to find a suitable linear approximation to be implemented in the finite element model. The approximations of embedding stiffness were 12.8, 21.2 and 23.7 MN/m for one, two and three studs, respectively. The stiffness for the three-studs specimen was chosen in the model since the largest forces arises where three studs are mounted together. The hold-down stiffness was determined to be 13.1 MN/m.

5 Results and discussions

5.1 Test results and FE analysis

Figs.5 shows the comparison of the calculated yield and maximum loads by FEM with the experimental results. Calculated maximum loads showed good agreement with the experimental results. There were some dispersion in relation between calculated yield load and the experimental results. Considering the dispersion of materials and construction of

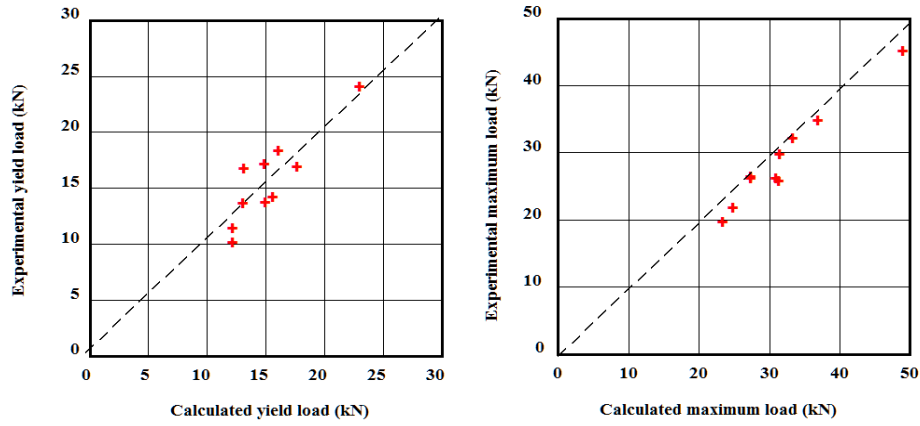


Fig. 5 Comparison of the calculated yield and maximum loads with the experimental results.

specimen, these dispersions may be within the permissible range. Therefore, this model was applied to the analysis mentioned later-on.

5.2 Influence of vertical loads

Tables 2 and 3 show the calculated yield and maximum loads of the specimen under vertical loads (F_v) of 0, 2 and 4 kN per 455mm length (total vertical loads of 14 and 28kN in 3P specimen and 18 and 36kN in 4P specimen). They were compared also with specimen with full restraint of studs. There were few differences in yield and maximum loads in Specimen (W) between the wall with the partial restraints (WPH) and that with full restraints (WFH) regardless of the vertical loads. This result indicates that the restraints such as hold-down connections of the studs beside the opening may be removed in some conditions if the shear wall has only a small opening of window configuration and the end studs are connected tightly to the foundation. Wall with door opening and partial restraints (DPH) showed lower lateral resistance than that with full restraints (DFH) if there were no vertical compressive loads at the top of the wall. However, there were less differences of the lateral resistance between wall with the vertical restraints and that without restraints when the sufficient vertical loads were applied. This indicates that the vertical restraints of studs beside the opening may be removed, but some reduction of lateral resistance shall be considered if the vertical loads are not sufficiently large. There were large differences in yield and maximum loads of Wall (S) between the specimen with the partial restraints (S-PH) and that with full restraints (S-FH) if there were no vertical compressive loads at the top of the wall. The shear resistance increased with the increase of the vertical loads and close to those with full restraints when total vertical loads were 28kN or 36kN. This indicates that it is not recommended to remove the vertical restraints of studs beside the opening if there are no small walls above and below the opening and the studs of the both sides of side walls should be tightly connected to the foundation and horizontal members at the top and the bottom.

Table 2 Calculated yield load (value in parenthesis is the ratio of the yield load with partial restraints to that with full restraints.

Yield load (kN)	Vertical load per stud (kN)	W3P	W4P	D3P	D4P	S3P	S4P
Partial restraints	0	14.91 (1.0)	15.51 (0.97)	12.07 (0.93)	12.12 (0.94)	9.16 (0.77)	9.04 (0.76)
	2	14.91 (1.0)	15.98 (1.0)	13.19 (1.0)	12.63 (0.98)	10.63 (0.90)	11.02 (0.94)
	4	14.80 (1.0)	16.24 (1.0)	13.17 (1.0)	13.02 (0.99)	11.73 (0.99)	11.75 (1.0)
Full restraints	0	14.82 (1.0)	15.96 (1.0)	13.02 (1.0)	12.94 (1.0)	11.82 (1.0)	11.78 (1.0)

Table 3 Calculated maximum load (value in parenthesis is the ratio of the maximum load with partial restraints to that with full restraints.

Maximum load (kN)	Vertical load per stud (kN)	W3P	W4P	D3P	D4P	S3P	S4P
Partial restraints	0	30.83 (0.98)	31.15 (0.94)	23.29 (0.85)	24.68 (0.91)	17.56 (0.71)	18.18 (0.73)
	2	31.20 (0.99)	32.59 (0.98)	27.33 (1.0)	25.83 (0.95)	21.02 (0.85)	22.40 (0.90)
	4	31.15 (0.99)	33.20 (1.0)	27.27 (1.0)	26.80 (0.99)	23.76 (0.96)	24.10 (0.97)
Full restraints	0	31.36 (1.0)	33.21 (1.0)	27.26 (1.0)	27.15 (1.0)	24.79 (1.0)	24.79 (1.0)

Table 4 Calculated yield and maximum loads (value in parenthesis is the ratio of the values with partial restraints to that with full restraints.

Yield load (kN)	Vertical load per stud (kN)	0.01*EI	1.0*EI	100*EI	Maximum load (kN)	Vertical load per stud (kN)	0.01*EI	1.0*EI	100*EI
Partial restraints	0	8.14 (0.69)	9.04 (0.77)	11.27 (0.96)	Partial restraints	0	16.37 (0.66)	18.18 (0.73)	23.05 (0.93)
	2	9.66 (0.82)	11.02 (0.94)	11.50 (0.98)		2	19.20 (0.77)	22.40 (0.90)	24.58 (0.99)
	4	11.10 (0.94)	11.75 (1.0)	11.60 (0.98)		4	21.7 (0.88)	24.1 (0.97)	24.75 (1.0)
Full restraints	0	---	11.78 (1.0)	---	Full restraints	0	---	24.79 (1.0)	---

5.3 Influence of loading beam stiffness

Influence of the loading beam stiffness was studied on the specimen (S4P) which did not have any small walls either above or below the opening except for two pieces of 2-by 6 inches lintel above the opening. This wall configuration was chosen as it was supposed that the loading beam stiffness influence the most on this type of wall. For the standard

stiffness of loading beam, two pieces of 2-by 6 lumbers, MOE of 10,000N/mm² was assumed, and the MOE of loading beam varied 100 times and 1/100 times. Table 4 shows the yield and maximum loads with the loading beam stiffness of 1/100 and 100 times of the standard stiffness. They show that the yield and maximum loads increased as the bending stiffness were higher, and this trend was more significant when the vertical loads were small. When the bending stiffness of loading beam was very high, the influence of the vertical loads were very small and showed the performace close to wall with full restraints. This means that the vertical restraints of studs are very important for the walls without small walls above and below the opening if the stiffness of beams above the opening is not rigid enough, and the vertical loads over the wall is not sufficiently large. These results also indicate the importance to consider the loading beam stiffness and the vertical compressive load over the wall if the wall has an opening and the studs beside the opening are not connected to the foundation, while these incidents do not affect on the mechanical properties of shear walls if the studs are fully connected to the foundation and horizontal members.

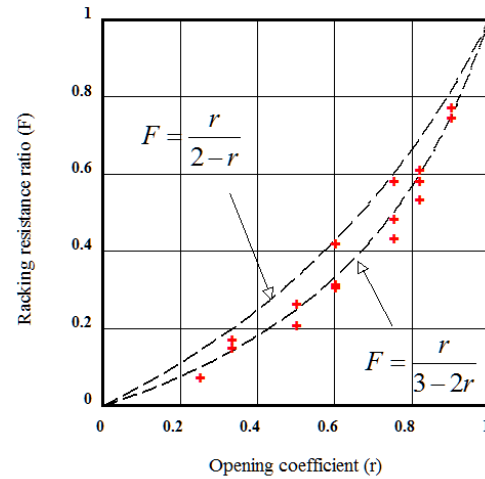


Fig. 6 Racking resistance ratio and opening coefficient^{4,6,8)}

5.4 Application of opening coefficient

5.4.1 Opening coefficient

In 1981, Sugiyama⁴⁾ presented the opening coefficient and conception of the shear resistance ratio which represent the ratio of shear resistance of wall panel with openings to that of the blind wall of the equivalent size. The opening coefficient (r) is expressed by the formula (4). Yasumura and Sugiyama⁶⁾ conducted the experiment using one-third models of the wood framed shear wall which had the opening of the window, door and slitting configurations and approximated the relation between the opening coefficient and the shear strength ratio. ASTM E72⁷⁾ which used tie rods to prevent the up-lift of end studs were applied to the racking test.

Although the rocking of the wall panel was restrained by the steel rods in this test method, some vertical displacements of studs were produced as there were no connection between the foot of studs and the foundation. This caused in particular the decrease of the shear stiffness and strength of the wall panel which had a vertically large opening. Therefore, Yasumura and Sugiyama obtained the following formula by approximating the relation between the shear resistance ratio (F) and opening coefficient (r) from the experimental results with wall panels having a single opening of various configuration⁶⁾.

$$F = \frac{r}{3 - 2r} \quad (5)$$

This formula is related to the shear resistance ratio at 1/100rad shear deformation and the ultimate load. Moreover, Sugiyama continued this research with long walls with multiple openings and proposed the following formula for the shear deformation of 1/300rad. and 1/100 – 1/60 rad., respectively⁸⁾.

$$F = \frac{3r}{8-5r} \quad (\text{at } H/300 \text{ displacement}) \quad (6)$$

$$F = \frac{r}{2-r} \quad (\text{at } H/100 \text{ and } H/60 \text{ displacement}) \quad (7)$$

5.4.2 Varidation

Fig.7 shows the relation between the calculated shear resistance ratio (F) and the opening coefficient (r) for the opening wall panel with the full vertical restraints of studs. It shows that the shear resistance ratio has very good correlation with the opening coefficient, and it is possible to design the shear strength of wall panel with an opening from the shear strength of shear wall without opening which has the same length and height as the opening wall panel multiplied by the opening coefficient (r) obtained from the formula (4).

Fig. 7 also shows the relation between the calculated shear resistance ratio (F) and the opening coefficient (r) for the opening wall panel with the partial vertical restraints of studs. It shows that the shear resistance ratio of opening wall panel whose studs beside the

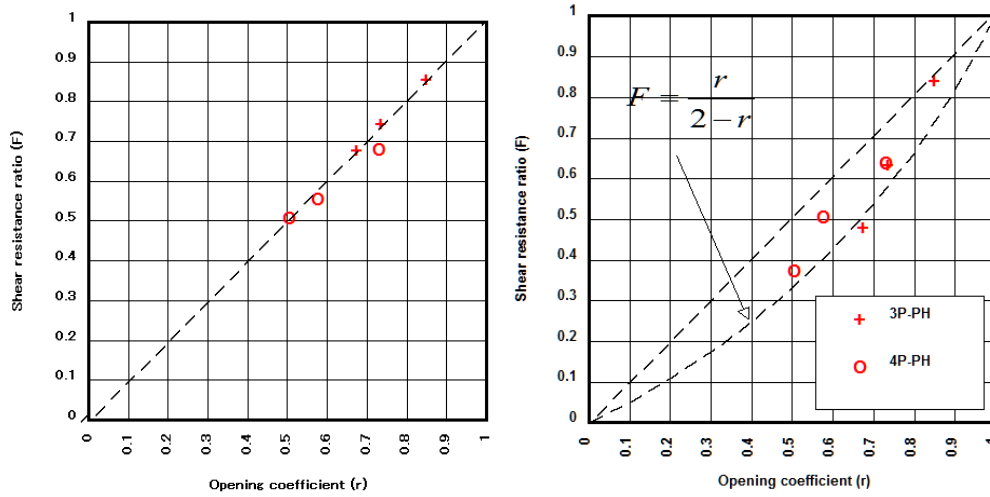
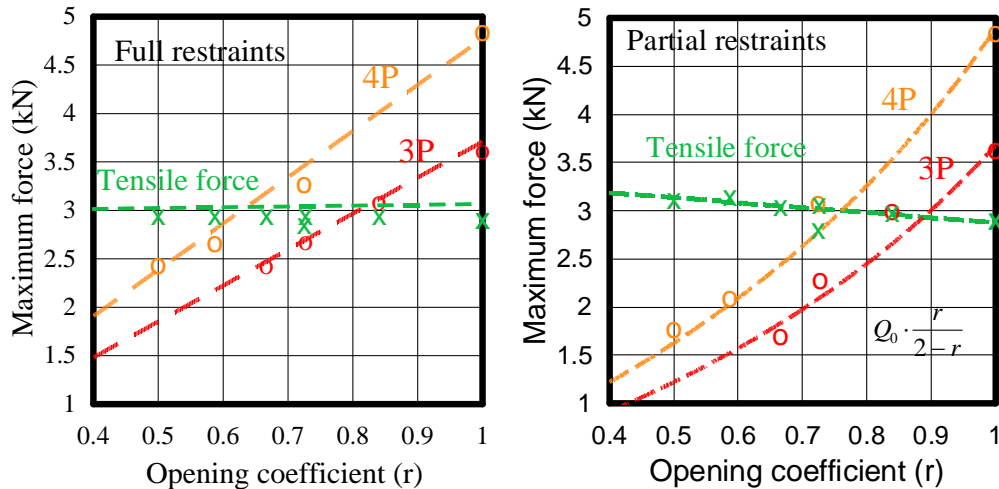


Fig. 7 Relation between Shear resistance ratio and Opening coefficient and in FH(left) PH(right).



opening are not connected to the foundation or horizontal members shows slightly inferior values than the opening coefficient, and superior to the curves defined by Sugiyama's approximation. This result indicates that it is possible to design the racking resistance of

opening wall panel whose studs beside the opening are not connected to the foundation or horizontal members from the shear strength of shear wall without opening which has the same length and height as the opening wall panel by multiplying the racking resistance ratio defined by the formula (7).

5.5 Shear resistance and tensile forces of end studs

Fig. 8 shows the maximum lateral forces and tensile forces at the end stud in function of the opening coefficient. The maximum forces of the wall panel with full restraints decrease linearly as the decrease of the opening coefficient in both 3P and 4P walls. The maximum tensile forces showed almost constant values of 30kN regardless of the wall length and opening area and configuration. The maximum lateral forces of the wall panel with partial restraints decreased as the decrease of the opening coefficient following the *Sugiyama's* reduction factor for long wall with multiple openings. The maximum tensile forces decreased slightly as the increase of the opening coefficient within the range of 29 to 31kN.

6 Design proposal

It is concluded that the racking resistance of plywood-sheathed shear walls with an opening can be obtained from the following formula.

$$Q = F \cdot Q_0 \quad (8)$$

where,

$$F = r \quad (\text{Full vertical restraints of studs}) \quad (9)$$

$$F = \frac{r}{2 - r} \quad (\text{Partial vertical restraints of studs}) \quad (10)$$

$$r = \frac{1}{1 + \alpha/\beta} \quad ; \quad \alpha = \frac{a \cdot b}{L \cdot H} \quad ; \quad \beta = \frac{\sum l_i}{L}$$

Q: racking resistance of wall with an opening, Q_0 : racking resistance without openings which has the same size with the opening wall, a, h: length and height of an opening, L, H: length and height of a wall panel, l_i : length of side wall.

7 Conclusion

The following conclusions are derived from the racking tests of plywood-sheathed wood-framed shear walls and the Finite Element analysis.

- 1) Racking resistance of shear wall with an opening and full vertical restraints can be estimated from that of the shear wall of the same size without openings by multiplying the reduction factor defined by the formula (9) .
- 2) Restraints of studs (e.g. hold-down connections) beside the opening can be removed if the shear wall has an opening of window or door configuration with small walls above and/or below the opening and the end studs of the wall are connected tightly to the foundation and horizontal member above or below the shear wall.
- 3) Racking resistance of shear wall having an opening and partial vertical restraints (in which vertical restraints beside an opening are removed) can be estimated from that of the shear wall of the same size without openings by multiplying the reduction factor defined by the formula (10) .

- 4) It is important to consider the loading beam stiffness and the vertical compressive load over the wall if the wall has an opening and the studs beside the opening are not connected to the foundation or horizontal members, while these incidents do not affect on the mechanical properties of shear walls if the studs are fully connected to the foundation and horizontal members.
- 5) Maximum tensile forces of the end stud of the wall with full restraints showed almost constant values of 30kN regardless of the wall length, opening area and configuration. That of the wall with partial restraints decreased slightly as the increase of the opening coefficient within the range of 29 to 31kN.

Acknowledgment

The author would like to express his thanks to Prof. Daudeville and Dr. Davenne for the basic development of FE codes, Mr. Andreasson for his assistance of developing the shear wall model, and Mr. Nagata and Ms. Suzuki for their assistance of conducting racking tests of shear walls..

References

1. Yasumura M, Karacabeyli E, International Standard Development of Lateral Load Test Method for Shear Walls, Proceedings of CIB-W18, 40-15-5, 2007
2. International Organization for Standardization, ISO 21581-Timber structures- Static and cyclic lateral load test method for shear walls, 2010
3. Yasumura M, Murota T, Design procedure for wood-framed shear walls, Proceedings IUFRO S5.02, Bordeaux, 1992
4. Sugiyama H, Evaluation of wood-based shear walls with opening, Wood Industry, 36(7): 3-8, 1981
5. Andreasson S, Yasumura M, Daudeville L, Sensitivity study of the finite model for wood-framed shear walls, J Wood Sci 48:171-178, 2002
6. Yasumura M, Sugiyama H, Shear Properties of plywood-sheathed wall panels with opening, Trans. of A.I.J., No.338, 1984
7. ASTM E72 - 05 Standard Test Methods of Conducting Strength Tests of Panels for Building Construction, 2005
8. Sugiyama H., Matsumoto T., Empirical equations for the estimation of racking strength of plywood-sheathed wall with openings, summary of Annual Meeting of AIJ, C, Sept. 1994

**INTERNATIONAL COUNCIL FOR RESEARCH AND INNOVATION
IN BUILDING AND CONSTRUCTION**

WORKING COMMISSION W18 - TIMBER STRUCTURES

**INFLUENCE OF DIFFERENT STANDARDS ON THE DETERMINATION
OF EARTHQUAKE PROPERTIES OF TIMBER SHEAR WALL SYSTEMS**

P Schädle

H J Blaß

Karlsruhe Institute of Technology (KIT)

GERMANY

MEETING FORTY THREE

NELSON

NEW ZEALAND

AUGUST 2010

Presented by P Schädle

A Ceccotti: Congratulations for nice work. H Blass should ask TC250 for a new proposal for timber construction for EC 8.

A Jorissen: Is it possible to have a uniform test method for timber elements? P Schädle: Yes, two tests are needed – connector and entire wall.

A Palermo: One should not refer to 1st cycle, only to 2nd and 3rd because of strength degradation. Were simulated earthquakes reflecting the requirements of EC 8? P Schädle: Yes.

A Palermo: Why use force-based analysis? P Schädle - test standard in Germany is still force based.

M Fragiaco: were tests performed with wall components? P Schädle: No, with entire shear walls.

Influence of different standards on the determination of earthquake properties of timber shear wall systems

Patrick Schädle, Hans Joachim Blaß

Timber structures and building construction

Karlsruhe Institute of Technology, Germany

1 Introduction

Shear wall tests on two modern timber construction systems were carried out by Karlsruhe Institute of Technology (KIT). Regarding test results such as stiffness, horizontal load-carrying capacity, hysteresis shape and hysteresis equivalent viscous damping ratio, all results are similar to or even better than the well-known timber frame system. This means that both systems should also be suitable for the use in seismic active areas.

Innovative systems usually do not fit into the design concepts according to Eurocode 8 (EC8, [1]), thus their behaviour factor cannot be found there. The only approach to classify systems into a ductility class specified in EC8 is the declaration of a static ductility. This is insufficient because important characteristics like the energy dissipation and the boundary conditions of the tests are not taken into account. Since no uniform standard for the determination of seismic properties of timber construction systems exists, several problems are identified.

Following from the insufficient static-ductility-approach, the ductility classes for the systems would be too conservative. Thus the evaluation of the behaviour factor q for the tested systems was carried out using a numerical simulation, taking into account the essential properties of the system considered. Difficulties when determining q are described in this paper since several standards influence the value of the behaviour factor. A possible solution of this problem is proposed.

2 Experimental study of shear wall systems

Most of today's timber residential houses are timber frame constructions. A great multitude of studies concerning almost any aspect of construction with timber frame systems exists. New ideas regarding building physics or simple assembling and finishing timber construction systems led to innovative constructions. In some cases (X-lam), manufacturing progress led to a general possibility of using innovative materials. The systems studied and several tests carried out with these are presented in the following.

2.1 X-Lam massive panel system

The X-lam massive panel system is made up of cross-laminated timber panels of 0.625 m x 2.5 m (length x height) with different thicknesses. Crosswise lamination of sawn timber members results in a closed load bearing layer on the outer panel side, an open grid on the inner side can be used for installation (Fig. 1 a)). To produce an entire wall, the panels are mounted between associated top and bottom rails. The outermost vertical boards of each panel are omitted to attach the so called shear (or connection) boards. These are attached to

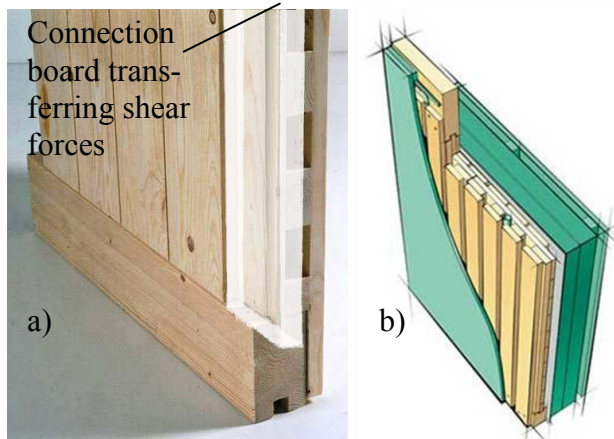


Fig. 1 a) Close-up view of the bottom of a single X-lam massive panel, b) Panel with inner finish plus installation and outer insulation

Ready made installation channels contribute to low costs and high flexibility for the completion of the interior (Fig. 1 b)).

2.1.1 Joints of X-Lam massive panel system

Looking at a timber framed wall, the dissipative zones are firstly the connections between the sheathing and the framing as well as the hold-downs. Hence, when investigating the earthquake behaviour of a timber framed wall, these connections should be considered as it is stated in EC8: “The properties of dissipative zones should be determined by tests either on single joints, on whole structures or on parts thereof in accordance with EN 12512 [2]” and it is also stated that “the dissipative zones shall be located in joints and connections, whereas the timber members themselves shall be regarded as behaving elastically.”

Looking at the X-Lam massive panel system, it is obvious that the dissipative zones are the fasteners at the connector boards as well as the connections to the top and bottom rails. To

both panels with mechanical fasteners (such as staples, grooved coil-nails or screws) to transfer shear forces between the panels when the wall is loaded horizontally.

The vertical timber boards of the panels overlap on both, top and bottom side, where they are connected to the bottom and top rail with the same fasteners that are used for the shear boards. Openings for doors and windows are spared in the factory, so pre-assemblage is possible to a great extent. Wall sizes are primarily limited by transportation requirements; the erection of buildings thus is very fast.

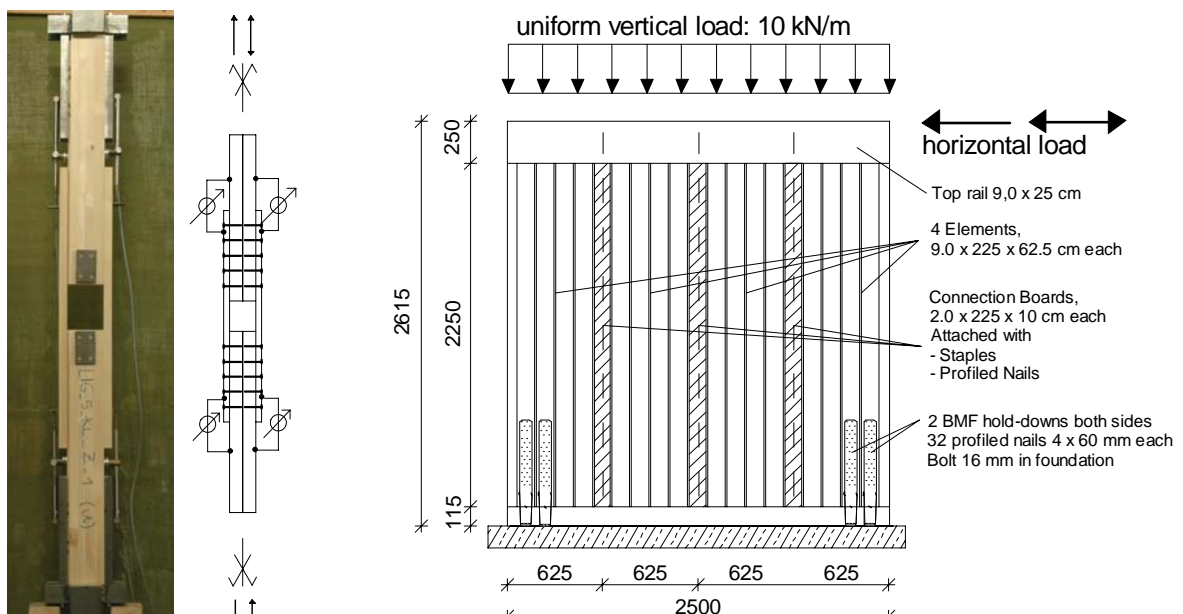


Fig. 2 Tension-Compression-Test for the X-Lam massive panel system using 5 connectors (left), Shear wall test specimen for X-Lam massive panel system (right)

gain information on the cyclic behaviour of the described joints, a test setup as shown in Fig. 2 (left) was chosen. This tension-compression test represents the geometry of the panel and the connector boards. Lateral supports to avoid bending and buckling of the specimen are not shown in Fig. 2 (left) but were used during the tests. A number of 2,5 and 10 connectors in a row were chosen for the tests to consider potential splitting effects as well as to gain calibration data for numerical models.

2.1.2 Shear wall tests on X-Lam massive panel system

A test specimen of a X-Lam massive panel shear wall can be seen in Fig. 2 (right). A total of 25 shear wall tests with the X-Lam massive panel system was carried out, however only cyclic tests with staples and grooved nails are shown in Table 1, since the application of screws is very time-consuming and hence not practicable. The numerous mechanical fasteners in combination with the stiffness of the X-lam panels promised favourable results when subjected to cyclic loading. During the tests the use of 1.83 x 64 mm staples showed to be most efficient for the quick erection of the panels, 2.8 x 65 mm grooved nails were used as an alternative.

The behaviour under cyclic loading is strongly affected by the fastener type. While staples showed pronounced ductile behaviour in all tests, nails tended to break apart at multiple repeated cycles. Softwood boards can be used when only minor horizontal loads, thus low shear forces have to be transferred by the connection boards. To avoid splitting caused by the alignment of fasteners, plywood panels were used. Due to the fact that realistic bound-

Table 1 Shear wall test matrix for X-Lam massive panel system

No.	Description	Connector Boards	Connectors	Connector spacing	Hold-downs
1	ZYK 0 3	Softwood	Staples 1,53 x 55	$a_1 = 40$ mm	2 KR
2	ZYK 0 4	Softwood	Staples 1,53 x 55	$a_1 = 50$ mm	2 KR
3	ZYK 0 5	Softwood	Grooved Nails 2,8 x 65	$a_1 = 60$ mm	2 KR
4	ZYK 10 4	Softwood	Staples 1,53 x 55	$a_1 = 50$ mm	2 KR
5	ZYK 10 5	Softwood	Grooved Nails 2,8 x 65	$a_1 = 60$ mm	2 KR
6	ZYK 10 6	Plywood	Staples 1,83 x 63,5	$a_1 = 50$ mm	2 x HTT 22
7	ZYK 10 8	Plywood	Staples 1,83 x 63,5	$a_1 = 50$ mm	2 x HTT 22
8	ZYK 10 12	Plywood	Staples 1,83 x 63,5	$a_1 = 50$ mm	2 x HTT 22
9	ZYK 10 9	Plywood	Grooved Nails 2,8 x 65	$a_1 = 50$ mm	2 x HTT 22
10	ZYK 10 10	Plywood	Grooved Nails 2,8 x 65	$a_1 = 50$ mm	2 x HTT 22
11	ZYK 10 11	Plywood	Grooved Nails 2,8 x 65	$a_1 = 50$ mm	2 x HTT 22

ary conditions are postulated in the standard used for the testing (ISO/CD 21581 [3], based on [4]), commercially available hold-downs, which were connected to the panels by ringed-shank nails, were used. According to the high load-carrying capacity

of the wall, two hold-downs on either side of the wall had to be employed in the cyclic tests.

2.1.3 Outcomes: Comparison between cyclic tests on joints and shear wall tests

Comparing the hysteresis shape for the joints tests and for the shear wall tests (Fig. 3), significant differences are observed. Pinching is more pronounced in the joint tests while the slope of the pinched part tends towards zero. The unloading part of the curve is nearly vertical in the joint tests, with the hysteresis equivalent damping being high in the first cycles and getting lower in the following cycles (Fig. 4 (top)). The contrary is observed in the shear wall tests: Exhibiting lower damping ratios in the first cycles, and increasing in the following (Fig. 4 (bottom)). It is obvious that the hysteresis shape and also equivalent damping for a connection cannot be used to assess the hysteresis obtained in shear wall tests.

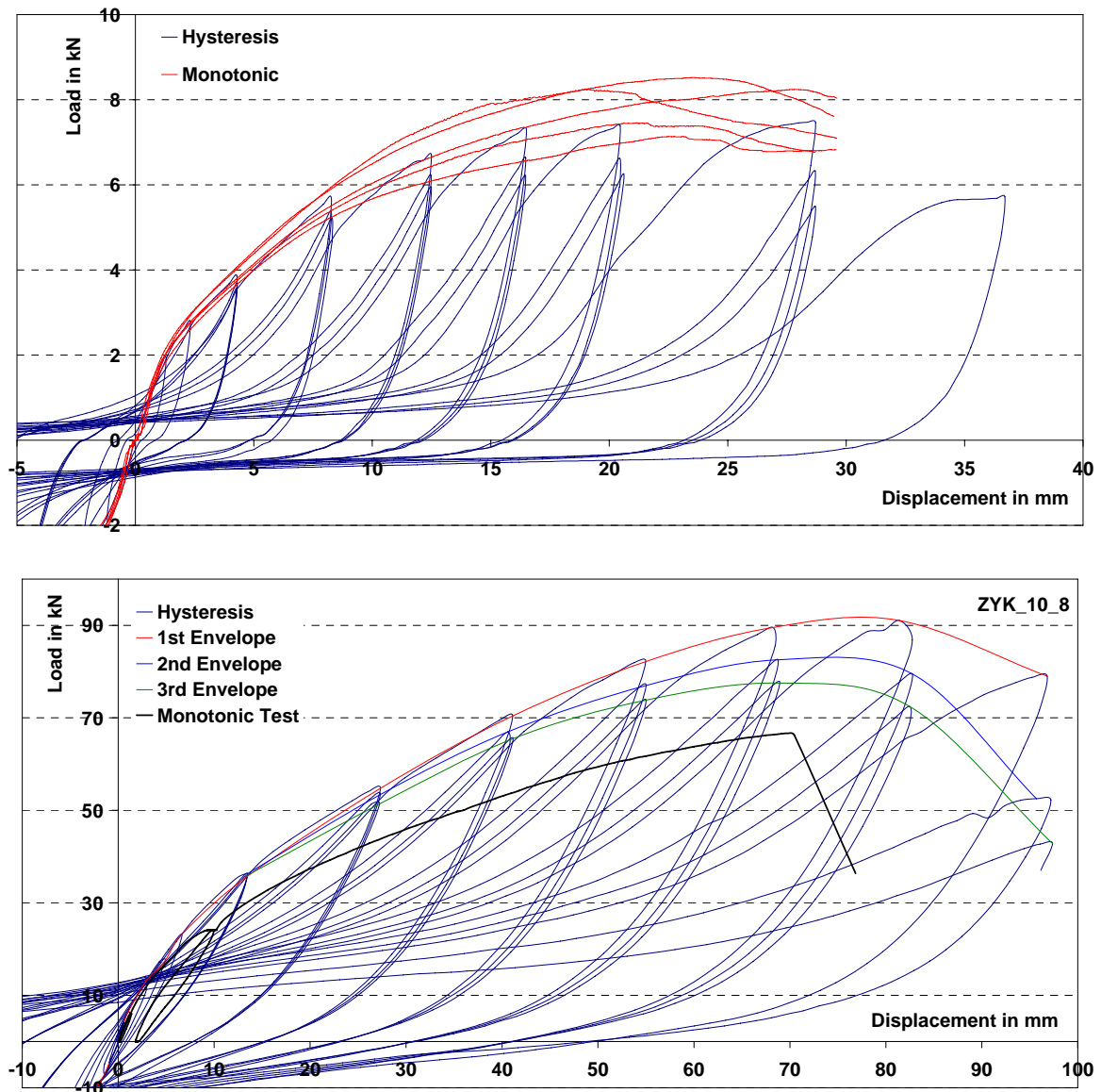


Fig. 3 Comparison of hysteresis of X-Lam massive panel system. Hysteresis of joint test with 5 staples (top), hysteresis of shear wall test with staples (bottom)

The described effect is getting even more pronounced when testing other connectors in e.g. brittle materials like gypsum wall boards.

2.2 Prefabricated timber wall elements (PFTE)

Prefabricated Timber Wall Elements (PFTE) represents a simple, easy to handle and sustainable construction system. The brick-like elements can be easily transported to the building site and are easy to handle due to their low weight. In its basic dimensions the “wooden brick” measures 1,0 m x 0,5 m (length x height) with different thicknesses. (Fig. 5). The wood columns are connected by dove tails to the (inner) chipboard layers. The overlapping of columns and sheathing provides initial stability. The hollow spaces between the columns are used for insulation or installation.

When erecting a wall with PFTE, the layers are simply laid by stacking the wooden “bricks”, where the offset of the outer layers and the offset of the studs of lower and upper elements slide into the next one (Fig. 5). When the planned wall height is reached, a continuous vertical stud is inserted from the top at least every 3 m of wall length. After finish-

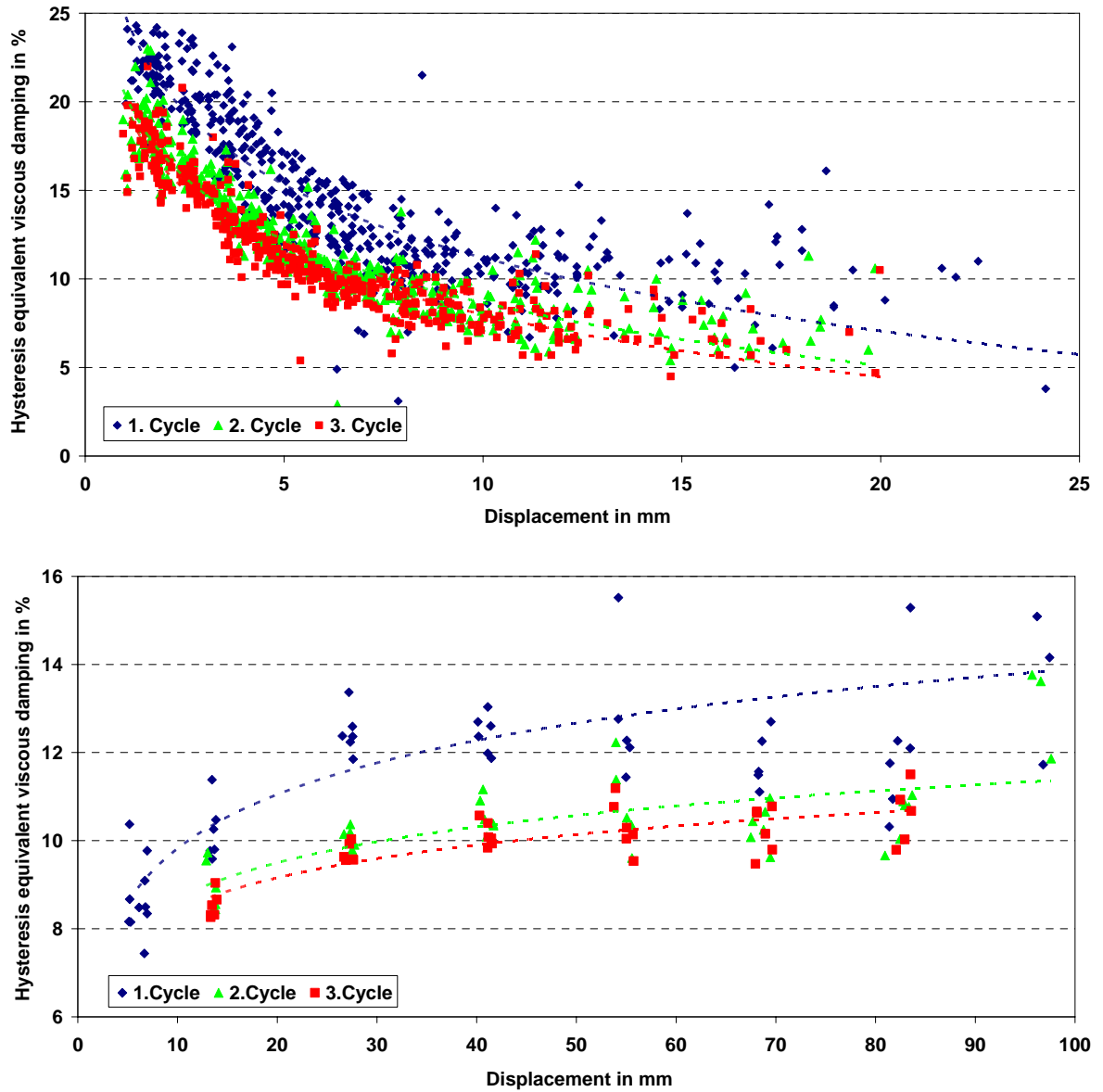


Fig. 4 Hysteresis equivalent viscous damping ratio for X-Lam joints tests (staples)(top), for X-Lam massive panel shear walls connected with staples (bottom)

ing erection, the overlapping parts of the sheathing are connected on the inner side of the building by staples to create a continuous shear wall. The system and several outcomes were already presented in [5].

2.3 Other novel systems and “conventional” timber framed walls

Several other novel systems were developed recently, probably best-known is the “pure” X-lam system, which in an excellent manner uses the advantages of timber construction: Cross-wise lamination nearly prevents swelling and shrinking, the amount of massive timber leads to excellent load-carrying capacities and good climate properties. When building in seismic active regions, dissipative zones can be designed by cutting the X-lam and to reconnect the elements using mechanical fasteners.

Several advantages are offered by conventional timber frame constructions. Flexibility in construction is also given as well as good building physics and sustainability. When sub-

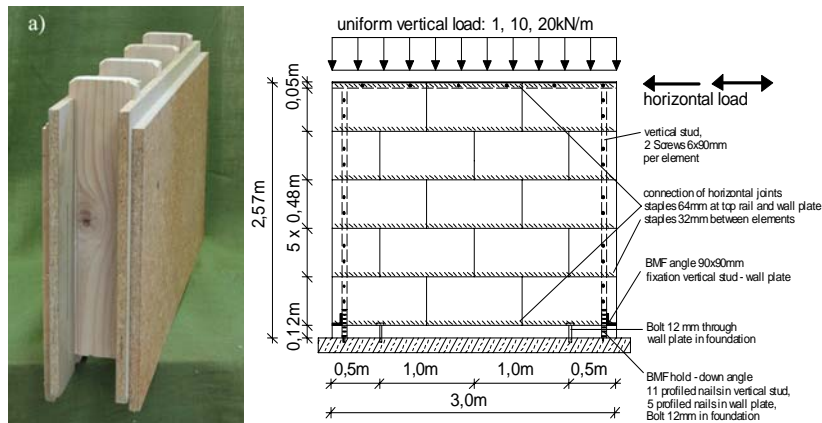


Fig. 5 PFTE (left), Shear wall specimen (right)

jected to seismic loads, the behaviour of timber frame construction is favourable. Three tests on timber framed shear walls were performed at Karlsruhe and were presented in [5].

3 Determination of earthquake properties of timber systems

3.1 EC8 approach

In terms of using the investigated systems in seismic active areas, EC8, the European code for the design of structures for earthquake resistance, provides some guidance. Apart from the general rules for the design of buildings for seismic active zones, specific rules for timber buildings are given.

EC8 includes 3 design concepts where “Depending on their ductile behaviour and energy dissipation (*) capacity, under seismic actions, timber buildings shall be assigned to one of the three ductility classes L, M or H as given in Table 2, where the corresponding upper limit values of the behaviour factors are also given”.

It is obvious that Table 2 does (and maybe cannot and should not) cover all systems. The question when using an unlisted system is which ductility class applies to the construction system. Therefore EC 8 states that “In order to ensure that the given values of the behaviour factor may be used, the dissipative zones shall be able to deform plastically for at least three fully reversed cycles at a static ductility ratio of 4 for ductility class M structures and a static ductility ratio of 6 for ductility class H structures without more than a 20% reduction of their resistance.” Notice that the specification of a static ductility does not take into account the energy dissipation of the system as it was requested before (*).

Table 2 Design concept, Structural types and upper limit values of the behaviour factors for the three ductility classes according to EC8

Design concept and ductility class	q	Examples of structures
Low capacity to dissipate energy - DCL	1,5	Cantilevers; Beams; Arches with two or three pinned joints; Trusses joined with connectors
Medium capacity to dissipate energy - DCM	2	Glued wall panels with glued diaphragms, connected with nails and bolts; [...]; Mixed structures consisting of timber framing (resisting the horizontal forces) and non-load-bearing infill
	2,5	Hyperstatic portal frames with doweled and bolted joints
High capacity to dissipate energy - DCH	3	Nailed wall panels with glued diaphragms, connected with nails and bolts; Trusses with nailed joints
	4	Hyperstatic portal frames with doweled and bolted joints
	5	Nailed wall panels with nailed diaphragms, connected with nails and bolts

3.2 Cross-reference to EN 12512 – lack of shear wall test standard

As stated in 2.1.1, “Dissipative zones shall be located in joints and connections [...]”, and should be tested according to EN 12512 [2]. The tests described in 2.1.1 are used to determine if the ductility ratio required in EC8 can be fulfilled and if DCH can be reached with the systems. In the EC8 definitions, the static ductility is defined as the “ratio between the ultimate deformation and the deformation at the end of elastic behaviour evaluated in quasi-static cyclic tests.”

Consequently, the definition of the ductility ratio is very important. Discussions on how to determine “the deformation at the end of the elastic behaviour” – the yield displacement – are ongoing. Four well-known procedures are 1) the 1/6 method according to EN 12512 (CEN Method), 2) the equivalent energy elastic-plastic method (EEEP), 3) the $0,5 \cdot F_{\max}$ -Method and 4) the 10-40-90-Method. A detailed description of the methods can be found in [6].

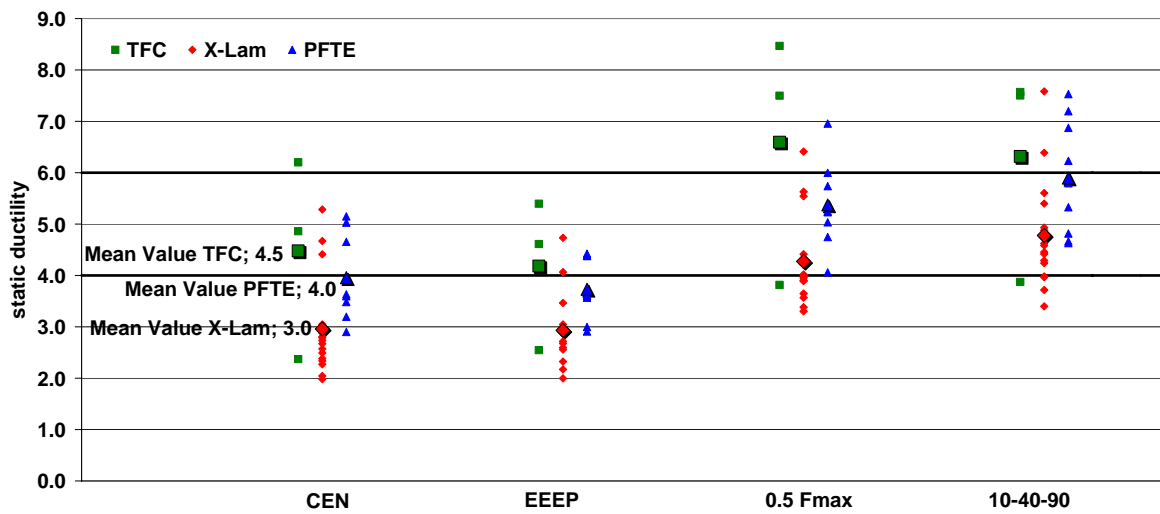


Fig. 6 Static ductility ratio of three different shear wall systems using four different methods of determination

This paper is not intended to contribute to any yield-displacement-discussion, however since the CEN method is specified in EC8 it is interesting to compare the static ductility using different methods. As can be seen in Fig. 6, the mean values for PFTE and X-Lam system using CEN method do not match a static ductility ratio of 4 what means that both systems have to be classified into DCL. Timber frame construction does “only” match DCM, certainly the test basis for the calculation (having three tests only) is weak. As it was proven in the past, nearly all kinds of timber buildings can resist strong earthquake actions, hence the investigated systems should also show better performance. Fig. 6 shows that the declaration of static ductility according to EC8 plus using the CEN method leads to (very) conservative results.

At this point it is important to state that the boundary conditions (BC) applied in all Karlsruhe tests correspond to “Shear cantilever mechanism” as described in [7] and [1]. Because of the lightweight structure of such buildings, rotation of the wall is possible. This BC is regarded as the conservative one, meaning that using other BC’s may lead to significantly higher values for the static ductility. Until today no uniform standard for the monotonic and cyclic testing of shear wall specimen exists. Since the importance of proper earthquake design is obvious especially in southern Europe, a uniform test standard is needed. The proposal of the authors again is to use ISO/CD 21581 [3], which combines in

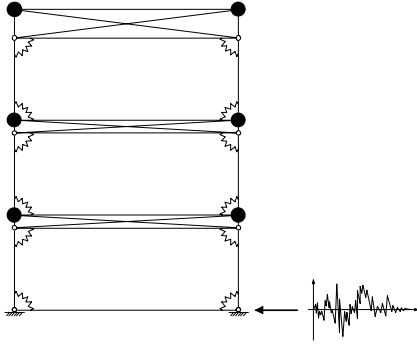


Fig. 7 Two-dimensional model

it to the hysteresis envelope data. According to ISO/CD 21581, the maximum displacement (u_{max}) gained in a monotonic test is used to calculate the amplitudes of the cyclic test protocol. As can be seen in Table 3, the HED at 100% of u_{max} gives useful information about the behaviour what is later verified when calculating the q -value.

Taking into account system properties e.g. in a standardized simulation, it has to be assured that the test data is sufficient and consistent as much as possible. This, again, can only be reached using a test method which is appropriate for shear wall testing such as [3].

a great manner the freedom of engineering as well as it is regulative in the right way. One possible addition would be the definition of a standard vertical load. Common tests carried out at Karlsruhe use a “standard” upload of 10 kN/m, which is considered comparatively small.

3.3 Possible interpretation of test results

Due to the problematic interpretation of the hysteresis equivalent viscous damping (HED), as shown in (Fig. 4) it is suggested to determine HED for each cycle and add

4 Evaluating the q -value of investigated timber systems

The evaluation of the behaviour factor q for all systems is carried out with a model of a sample house reduced to a two-dimensional frame as shown in Fig. 7. The ratio of design ground acceleration to scaled ground acceleration at “near collapse” status equals the behaviour factor q .

Table 3 HED of investigated systems. Values determined at 100% of u_{max}

	Hysteresis equivalent viscous damping 1 st cycle	Hysteresis equivalent viscous damping 2 nd and 3 rd cycle
X-lam, staples	9.6% - 13.4%	8.4% - 10.9%
X-lam, nails	9.6% - 12.7%	9.3% - 11.9%
PFTE	13.9% - 15.7%	14.1% - 14.8%
Timber frame	10.9% - 12.9%	7.9% - 9.2%
Hysteresis equivalent damping $\eta_{ed} = \frac{E_d}{2\pi \cdot E_p}$		
where E_d = Dissipated Energy, E_p = Potential Energy		

The essential properties of the system (ductility and energy dissipation) are taken into account in the simulation. The hysteretic behaviour of the shear walls was modelled with DRAIN-2DX [8] using the Florence pinching hysteresis model [9]. This procedure is described in [10], [11], [12]. The behaviour factors q for a XLAM building in [10] were calculated numerically with a model calibration solely based on the hysteresis shape gained from cyclic testing. Comparing the numerical data with the results of the shake table tests, the excellent quality of the model can be seen.

To calculate the behaviour factor q , the model will be designed for a certain ground acceleration using force based design methods according to EC8 [1]. Thereafter the structure will be excited in each case by ten natural as well as ten artificial earthquakes and the response of the system will be calculated. The division of the ground acceleration reached in the simulation and the calculated one represents the behaviour factor q , where $PGA_{u,eff}$ is the maximal ground acceleration at “near-collapse” status and $PGA_{u,code}$ is the maximal ground acceleration given in the correspondent code. The “near-collapse” status was taken to be 2,5% of storey height (≈ 65 mm), which was reached in all tests. No values were calculated for timber frame construction system since a data basis of 3 tests is insufficient.

When subjected to cyclic loads the systems showed favourable characteristics and a large amount of energy dissipation (see Table 3). The q -values for the PFTE- System only in three cases are lower than $q = 4$, while the 5 %-fractile is 3.7 (Table 4). In the chosen configuration the maximum interstorey drift is always reached in the first storey. Regarding the first floor of a three-storey building, the assumption of an upload of 10 kN/m is again conservative, since first floor walls usually have higher vertical loads. Because of the higher amount of energy dissipation when subjected to higher vertical loads a value of $q = 4.0$ was recommended for the PFTE-system. The q -value for the X-lam massive panel system never falls below a value of $q = 3$ while the 5%-fractile is 3.3. Therefore a value of $q = 3.0$ is recommended for the X-lam massive panel system. Choosing a multiplicity of 20 earthquakes, the statement of q with the 5%-Fractile is once more conservative. Stating q with the average value would also be possible, however then more importance should be attached to reliability analysis, which was not considered in this paper.

Comparing the q -values from Table 4 to the hysteresis equivalent damping in Table 3, one can see that the hysteresis equivalent viscous damping gives valuable information about the q -values derived with the numerical simulation.

5 Discussion

The research on two innovative timber construction systems is presented in this paper. Both systems as well as the established timber construction system have been tested under reversed-cyclic loading and showed a good performance. Since the behaviour of the systems can be classified similar to the well-known timber frame system, this means that they

Table 4 Calculated q -values for the different systems

Earthquake	$PGA_{u,code}$	PFTE $PGA_{u,eff}$	X-lam $PGA_{u,eff}$	PFTE q -value	X-lam q -value
natural earthquakes	0.35	1.29 to 3,77	1.10 to 3.38	3.7 to 10.8	3.1 to 9.7
artificial earthquakes	0.35	1.16 to 1.58	1.15 to 1.55	3.3 to 4.5	3.3 to 4.8
$q = \frac{PGA_{u,eff}}{PGA_{u,code}}$		average value		5.1	4.7
		5% fractile		3.7	3.3
		=> suggested q -value		4.0	3.0

are well suitable for the use in seismic prone areas.

The classification of the earthquake properties of the systems using current

European standards is not ideal at the moment since there is a major lack of information in EC8. The first step to correct this would be the establishment of a uniform standard for shear wall testing like ISO/CD 21581. Thereafter, rules for the interpretation of test results like the hysteresis equivalent viscous damping or static ductility should be more precise, and it should be stated that extended methods like a numerical simulation may be used to evaluate the behaviour factor q . The numerical simulation is more precise than the declaration of a static ductility as given in EC8 because the energy dissipation of the structure is taken into account. Comparison of different parameters suggests that the assumptions in EC8 are conservative.

Using a numerical simulation, the properties of the systems subjected to earthquake loading were reproduced and the behaviour factor q was calculated. Market opportunities for the systems can be seized quicker using these investigations. Based on few and common tests on shear walls an essential statement regarding the behaviour of the system can be given. Complex testing can be omitted. Looking at innovative timber systems, design fundamentals can be given in a short time.

The q -values are verified through the conservative testing on which the model is calibrated. The calculation is carried out using 20 accelerograms. Using this multiplicity of accelerograms, the calculated value has a broad basis. The chosen methodology may be widened to a 3d-Model [10] if needed. Torsion effects and other details can be taken into account. Further reliability analysis is not yet considered in this paper.

6 References

- [1] EC8: Design of structures for earthquake resistance – Part 1: General rules, seismic actions and rules for buildings; German version EN 1998-1:2004
- [2] EN 12512, 2001. Timber Structures – Test methods – Cyclic testing of joints made with mechanical fasteners.
- [3] Committee Draft ISO/CD 21581, 2007: Timber Structures – Static and cyclic lateral test method for shear walls
- [4] Yasumura, M., Karacabeyli, E. (2007): “International Test Standard development for lateral load test method for shear walls”. In: Proceedings of CIB-W 18, paper 40-15-5, Bled, Slovenia, 2007.
- [5] Schädle, P.; Blaß, H. J. (2008): “Behaviour of prefabricated timber wall elements under static and cyclic loading.” In: Proceedings of CIB-W18, paper 41-15-5, St. Andrews, Canada, 2008
- [6] Munoz, W.; Mohammad, M.; Salenikovich, A.; Quenneville, P. (2008): “Need for a Harmonised Approach for Calculations of Ductility of Timber Assemblies”. In: Proceedings of CIB-W18, paper 41-15-5, St. Andrews, Canada, 2008
- [7] Dujic, B., Aicher, S., Zarnic, R., 2005. „Investigations on in-plane loaded wooden elements – influence of loading and boundary conditions.“ Otto-Graf-Journal Vol. 16, 2005, pp 259 – 272.
- [8] Prakash et al. (1993): DRAIN-2DX Base Program Description and User Guide, Version 1.10, University of California, Berkeley, 1993
- [9] Ceccotti, A.; Vignoli, A. (1989): “A hysteretic behavioural model for semi-rigid joints.” European Earth-quake Engineering, 3, 1989
- [10] Ceccotti, A. (2008): “New Technologies for Construction of Medium-Rise Buildings in Seismic Regions: The XLAM Case.” In: Structural Engineering International (IABSE), May 2008, S. 156 -165
- [11] Ceccotti, A.; Follesa, M.; Lauriola, M.; Sandhaas, C. et al (2006): “Which Seismic Behaviour Factor for Multi-Storey Buildings made of Cross-Laminated Wooden Panels?” Proceedings CIB-W 18, paper 39-15-2, Florence, Italy, 2006
- [12] Ceccotti, A.; Sandhaas, C. (2010): “A Proposal for a Standard Procedure to Establish the Seismic Behavior Factor q of Timber Buildings.” Proceedings of WCTE 2010, Session 65, ID 834, Riva del Garda, Italy, 2010

**INTERNATIONAL COUNCIL FOR RESEARCH AND INNOVATION
IN BUILDING AND CONSTRUCTION**

WORKING COMMISSION W18 - TIMBER STRUCTURES

**FULL-SCALE SHEAR WALL TESTS FOR FORCE TRANSFER
AROUND OPENINGS**

T Skaggs

Borjen Yeh

APA – The Engineered Wood Association

U.S.A.

F Lam

University of British Columbia,
CANADA

D Rammer

J Wacker

Forest Products Laboratory

U.S.A.

MEETING FORTY THREE

NELSON

NEW ZEALAND

AUGUST 2010

Presented by T Skaggs

L Daziel: Are the forces measured in the opening where the strap is loaded in compression only? T Skaggs: No. sometimes in tension and also shear as well. It is also a cycle test. When in compression, the straps are not mobilized.

R Crocetti: Are straps only on one side (outside)? T Skaggs: Yes, only on the outside

P Schädle: Testing method. How much time does it take for the entire test? T Skaggs: from 2 sec – 2 mins. At slow rate, strap forces are a bit less but this is not due to rate.

G Beattie: Modelling wood and earthquake. I recommend the fast loading.

L Daziel: was there any difference in strap forces for different opening size? T Skaggs: this effect has not been analyzed yet. It will be available in the future.

Full-Scale Shear Wall Tests for Force Transfer Around Openings

Tom Skaggs and Borjen Yeh
APA – The Engineered Wood Association, U.S.A.

Frank Lam
University of British Columbia, Canada
Doug Rammer and James Wacker
Forest Products Laboratory, U.S.A.

Abstract

Wood structural panel sheathed shear walls and diaphragms are the primary lateral-load-resisting elements in wood-frame construction. The historical performance of light-frame structures in North America are very good due, in part, to model building codes that are designed to preserve life safety, as well as the inherent redundancy of wood-frame construction using wood structural panel shear walls and diaphragms. As wood-frame construction is continuously evolving, designers in many parts of North America are optimizing design solutions that require the understanding of force transfer between load-resisting elements.

The North American building codes provide three solutions to walls with openings. The first solution is to ignore the contribution of the wall segments above and below openings and only consider the full height segments in resisting forces, often referred to as segmented shear wall method. The second approach, which is to account for the effects of openings in the walls using an empirical reduction factor, is known as the “perforated shear wall method”. The final method, which has a long history of practical use with surprisingly little research and testing, is the “force transfer around openings method”. This method is accepted as simply following “rational analysis”. Typically walls that are designed for force transfer around openings result in the walls being reinforced with nails, straps and blocking in the portions of the walls with openings. The authors are aware of at least three techniques which fall under the definition of rational analysis. These techniques result in prediction of the internal forces in the walls as differing by as much as 800% in extreme cases. This variation in predicted forces is resulting in either some structures being over-built or some structures being less reliable than the intended performance objective.

A joint research project of APA – The Engineered Wood Association, the University of British Columbia (UBC), and the USDA Forest Products Laboratory (FPL) was initiated in 2009 to examine the variations of walls with code-allowable openings. This study examines the internal forces generated during these tests and evaluates the effects of size of openings, size of full-height piers, and different construction techniques by using the segmented method, the perforated shear wall method and the force transfer around openings method. Full-scale wall tests as well as analytical modelling were performed. The research results obtained from this study will be used to support design methodologies in estimating the forces around the openings. This paper provides test results from 2.4 m x 3.6 m (8 feet x 12 feet) full-scale wall configurations, which will be used in conjunction with the analytical results from a computer model developed by UBC to develop rational design methodologies for adoption in the U.S. design codes and standards.

1. Introduction

The North American building codes provide three solutions to walls with openings. The first solution is to ignore the contribution of the wall segments above and below openings and only consider the full height segments in resisting forces, often referred to as segmented shear wall method. The second approach, which is to account for the effects of openings in the walls using an empirical reduction factor, is known as the “perforated shear wall method”. The final method, which has a long history of practical use with surprisingly little research and testing, is the “force transfer around openings method”. This method is accepted as simply following “rational analysis”. Typically walls that are designed for force transfer around openings result in the walls being reinforced with nails, straps and blocking in the portions of the walls with openings. The authors are aware of at least three techniques which fall under the definition of rational analysis. The “drag strut” technique is a relatively simple rational analysis which treats the segments above and below the openings as “drag struts”. This analogy assumes that the shear loads in the full height segments are collected and concentrated into the sheathed segments above and below the openings. The second simple technique is referred to as “cantilever beam”. This technique treats the forces in the openings as a series of moment couples, which are sensitive to the height of the sheathed area above and below the openings. A graphical representation of these two techniques are given in Figure 1, the mathematical development of these two techniques is presented in Martin (2005).

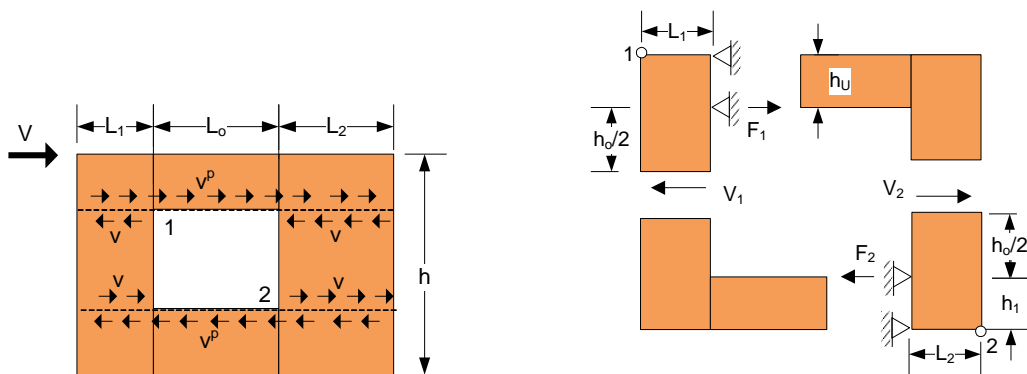


Figure 1. Representation of the drag strut technique (left), and the cantilever beam technique (right) for estimating forces around wall openings (Martin, 2005)

Finally, the more rigorous mathematical technique is typically credited to a California structural engineer, Edward Diekmann and well documented by Breyer et al. (2007). This technique assumes that the wall behaves as a monolith, and internal forces are resolved by creating a series of free body diagrams as illustrated in Figure 2. This is a common technique used by many west coast engineers in North America; however, it can become tedious for realistic walls that include multiple openings.

Of the three common techniques, the predicted internal forces can vary significantly, based on wall geometry. In extreme cases discussed below, the differences in the predicted internal forces may vary by 800%. The purpose of this research is to provide tangible data for comparison and perhaps improvement to the rational analysis methods.

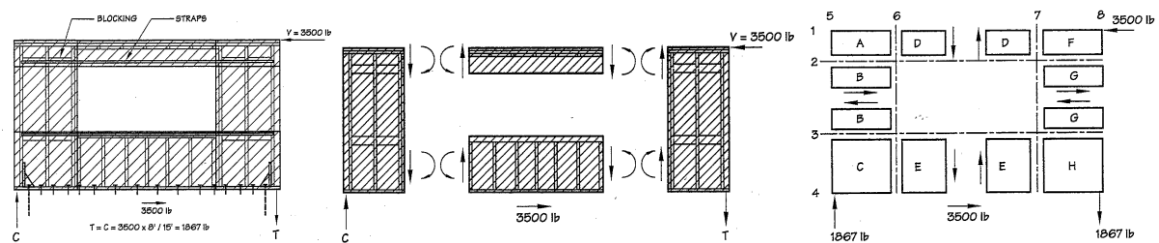


Figure 2. Representation of the Diekmann technique (1998) and drawings from Breyer et al. (2007). Global free body diaphragm of wall with openings (left), beam behaviour of various sheathed areas (center) and, horizontal and vertical cuts for establishing internal shears (right, 1 lbf = 4.45 N)

2. Test Plan

In an effort to collect internal forces around openings of loaded walls, a series of twelve walls were tested, Figure 3. This series was based on North American code permitted walls, nailed with 10d common nails (3.68 mm diameter by 76 mm long) at a nail spacing of 51 mm. The sheathing used in all cases was 12 mm (15/32-inch nominal) oriented strand board (OSB) APA STR I Rated Sheathing. All walls were 3.66 m long and 2.44 m tall. Wall 1 was based on the narrowest segmented wall (height-to-width ratio of 3.5:1) permitted by the code, with overturning restraint (hold-downs) on each end of the full height segments. The window opening of Wall 1 is common to many of the walls in this plan, at 0.91 m. Walls 2 and 3 are based on the perforated shear wall method, $C_o = 0.93$. Hold-downs are located on the ends of the wall and no special detailing, other than compression blocking for Wall 3, were built into the walls. Wall 4 is a force transfer around openings wall which has identical geometry to Walls 1, 2 and 3, and is to compare the various methods for designing walls with openings.

Wall 5 has the same width of piers as the first four walls; however, the opening size was increased to 1.52 m. Wall 6 was common to Wall 4, with the exception that the typical 1.2 x 2.4 m sheathing was “wrapped around” the wall opening in “C” shaped pieces. This framing technique is commonly used in North America. It is considerably more time efficient to sheath over openings, and remove the sheathing in the openings area via hand saw or router. Wall 7 is a segmented wall with height-to-width ratio of the full height segments to 2:1. Wall 8 is a match to Wall 7 but designed as a force transfer around openings wall. The window in Wall 9 is increased from 0.91 m to 1.53 m.

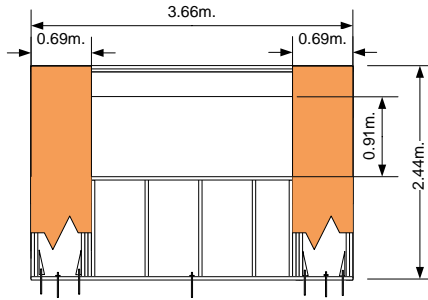
Walls 10 and 11 are very narrow wall segments, for use in large openings such as garage fronts. The two walls are designed with openings on either side of pier, and only on wall boundary, respectively. Finally, Wall 12 is an examination of a wall with two asymmetric openings.

Each tested wall was subjected to a cyclic loading protocol following ASTM E 2126, Method C, CUREE Basic Loading Protocol. The reference deformation, Δ , was set as 61.1 mm. The term α was 0.5, resulting in maximum displacements applied to the wall of +/- 122 mm. The displacement-based protocol was applied to the wall at 0.5 Hz, with the exception of Wall 8b, which was loaded at 0.05 Hz.

For walls detailed as force transfer around openings, two hold downs in line (facing seat-to-seat) were fastened through the sheathing and into the flat blocking (See Figure 3, Wall 4 and Figure 5 illustrating this detail). The hold-downs were intended to simulate the more typical detailed flat strapping around openings. The hold-downs were connected via a calibrated tension bolt for measuring tension forces.

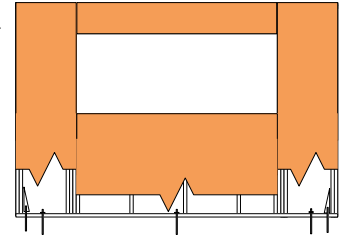
Wall 1

Objective:
Est. baseline case for
3.5:1 segmented wall



Wall 2

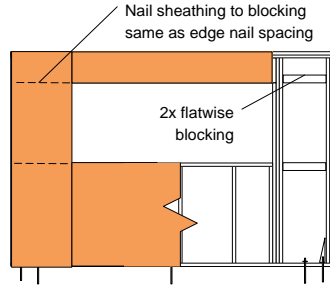
Objective:
No FTAO, compare to Wall 1.
 $C_o = 0.93$. Examine effect of
sheathing above and below
opening w/ no FTAO. Hold
down removed.



Wall 3

Objective:
No FTAO, compare to
Wall 1 and 2. Examine
effect of compression
blocking.

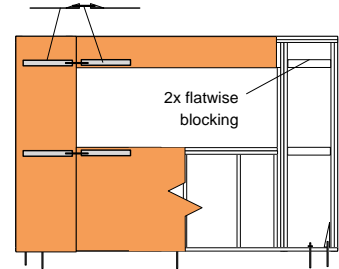
Wall is symmetric,
sheathing on right pier
not shown for clarity



Wall 4

Objective:
FTAO, compare to Wall 1.
Examine effect of straps

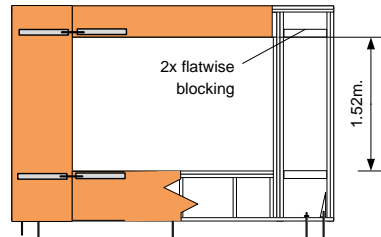
Wall is symmetric,
sheathing and force transfer
load measurement on right
pier not shown for clarity



Wall 5

Objective:
FTAO, compare to Wall
4. Examine effect of
straps with larger
opening

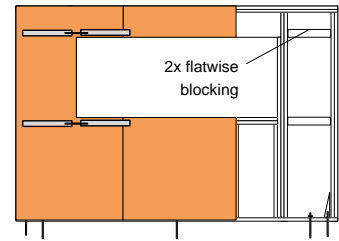
Wall is symmetric,
sheathing and force
transfer load
measurement on right
pier not shown for clarity



Wall 6

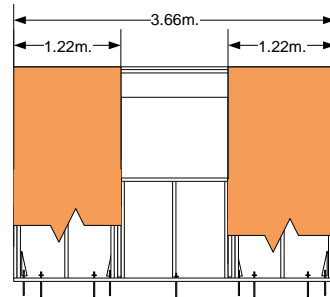
Objective:
Compare to Wall 4. Examine
effect of sheathing around
opening

Wall is symmetric,
sheathing and force
transfer load
measurement on right
pier not shown for clarity



Wall 7

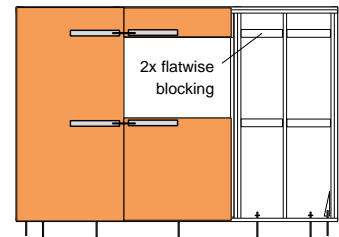
Objective:
Est. baseline case for 2:1
segmented wall



Wall 8

Objective:
Compare FTAO to Wall 7

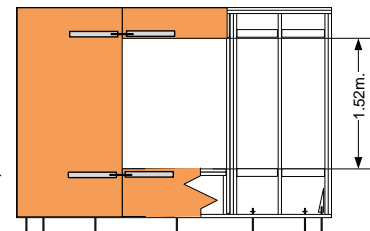
Wall is symmetric,
sheathing and force
transfer load
measurement on right
pier not shown for clarity



Wall 9

Objective:
Compare FTAO to Wall 7
and 8. Collect FTAO data
for wall with larger
opening

Wall is symmetric,
sheathing and force
transfer load
measurement on right pier
not shown for clarity



Wall 10

Objective:
FTAO for 3.5:1 Aspect ratio
pier wall. No sheathing below
opening. Two hold downs on
pier (fixed case)

Wall is symmetric, sheathing
and force transfer load
measurement on right pier
not shown for clarity

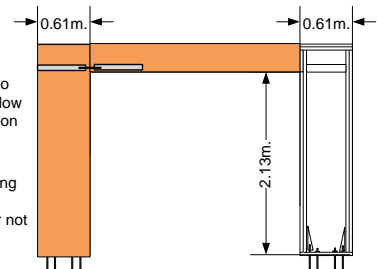
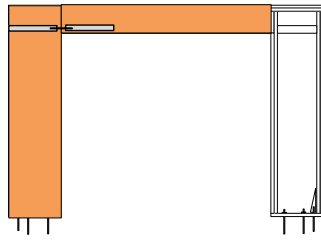


Figure 3. Test schematics for various force transfer around openings assemblies

Wall 11

Objective:
FTAO for 3.5:1 Aspect
ratio pier wall. No
sheathing below
opening. One hold
downs on pier (pinned
case)
Wall is symmetric,
sheathing and force
transfer load
measurement on right pier
not shown for clarity



Wall 12

Objective:
FTAO for asymmetric
multiple pier wall.

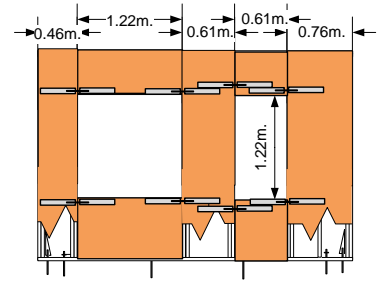


Figure 3 (continued). Test schematics for various force transfer around openings assemblies

3. Results

3.1 Global Response

Figure 4 are hysteric plots of the applied load versus the displacement of the walls. The response curves are representative for all walls tested. One can observe the relatively increased stiffness of perforated shear walls (Wall 2) versus the segmented walls (Wall 1); however, also note the relatively brittle nature of the perforated walls. As one might expect, the walls detailed for force transfer around openings (Wall 4d and 5d) demonstrated both increased stiffness and strength over the segmented walls. In addition, the response of the walls was related to opening sizes, with the larger openings resulting in both lower stiffness and lower strength.

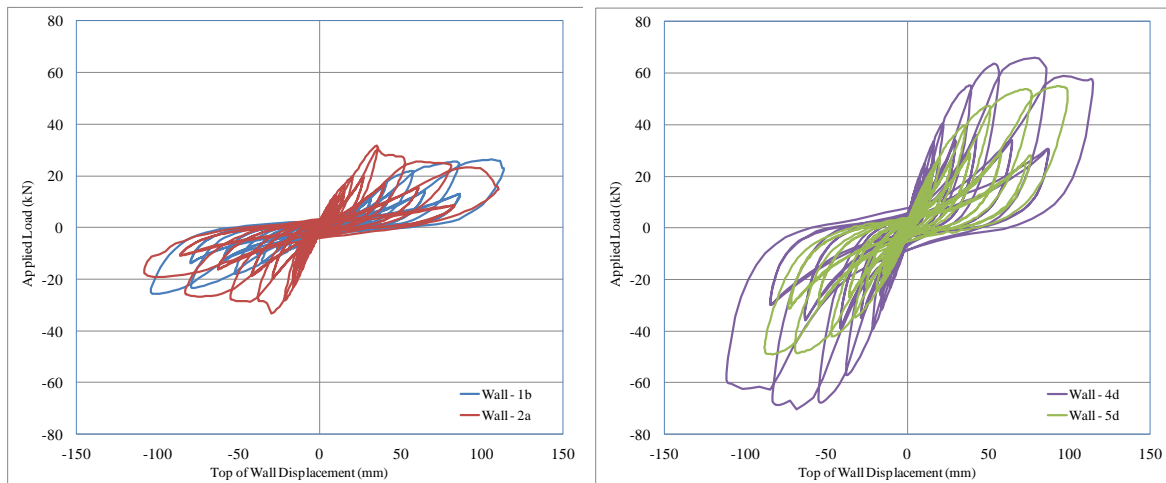


Figure 4. Hysteric behaviour of various walls, typical of the cyclic tests

Table 1 represents the maximum loads resisted by the various walls and calculated load factors. The expected wall capacity is based on the code listed allowable stress unit shear multiplied by the length of the wall. For the perforated shear walls, a further factor of C_o was included.

Table 1. Global response of tested walls

Wall ID	ASD Unit Shear ⁽¹⁾ , v (kN/m)	Effective Wall Length ⁽²⁾ (m)	Wall Capacity ⁽³⁾ (kN)	Maximum Applied Load to Wall			ASD Load Factor ⁽⁴⁾
				negative (kN)	positive (kN)	average (kN)	
Wall 1a	12.7	1.37	17.4	-23.9	24.4	24.1	1.4
Wall 1b	12.7	1.37	17.4	-25.7	26.3	26.0	1.5
Wall 2a	12.7	1.37	16.2	-33.3	31.6	32.5	2.0
Wall 3a	12.7	1.37	16.2	-43.2	49.1	46.1	2.9
Wall 4a	12.7	1.37	17.4	-62.7	70.2	66.4	3.8
Wall 4d	12.7	1.37	17.4	-70.4	66.0	68.2	3.9
Wall 5d	12.7	1.37	17.4	-49.1	54.9	52.0	3.0
Wall 6a	12.7	1.37	17.4	-47.1	59.2	53.1	3.1
Wall 7a	12.7	2.44	31.0	-54.7	56.8	55.8	1.8
Wall 8a	12.7	2.44	31.0	-66.3	70.6	68.5	2.2
Wall 8b ⁽⁵⁾	12.7	2.44	31.0	-66.0	72.1	69.0	2.2
Wall 9a	12.7	2.44	31.0	-66.2	69.4	67.8	2.2
Wall 10a	12.7	1.22	15.5	-31.2	35.3	33.2	2.1
Wall 11a	12.7	1.22	15.5	-29.5	28.1	28.8	1.9
Wall 12a	12.7	1.83	23.2	-76.0	66.7	71.3	3.1

⁽¹⁾ Typical U.S. tabulated values are based on allowable stress design (ASD) unit shear.

⁽²⁾ Based on sum of the lengths of the full height segments of the wall.

⁽³⁾ The shear capacity of the wall, V , is the sum of the full height segments times the unit shear capacity. For “perforated shear walls” (Walls 2 & 3), this capacity was multiplied by $C_o = 0.93$.

⁽⁴⁾ Wall capacity divided by the average load applied to the wall.

⁽⁵⁾ Loading time increased by 10x.

In general, the segmented walls (Wall 1 and Wall 7) resulted in the lowest load factors of the walls tested. The perforated shear wall (Wall 2) also performed at a lower level than the walls specifically detailed with force transfer around openings. Surprisingly, the compression blocking with no straps (Wall 3a) resulted in a significantly improved performance over Wall 2. Another general observation is that the larger the wall opening, the lower the load factors. The wall global behaviour seemed to be insensitive to the different loading rate (Walls 8a and 8b). Finally, for walls with typical window openings with sheathing both above and below openings, the walls with the narrowest piers (height-to-width ratios of 3-1/2:1) based on minimum pier width in North American codes, resulted in higher load factors than walls with full width piers (height-to-width ratio of 2:1).

3.2 Local Response

The internal forces around openings were measured with calibrated tension bolts, as discussed in the test plan above. Although data is not presented in this paper, the tension forces in the hold-downs were also collected. Figure 5 illustrates the notation of the force gages as well as a typical response curve of wall load versus internal force around opening. The response curves show hysteretic behaviour, which is likely due to cumulative damage of the wall as well as the orientation of the bolt recording tension forces, which may be influenced by the differential displacement of the hold-down seats in the vertical direction. Deflection measurements were taken which could potentially be used to correct the load to “pure horizontal tension”. However, in the range of the ASD capacity, the internal load response was relatively linear elastic. Table 2 provides a summary of measured internal forces at the allowable stress capacity of the walls. Test results on Wall 12 are not included in this paper due to the need for additional analysis and will be reported in a future paper.

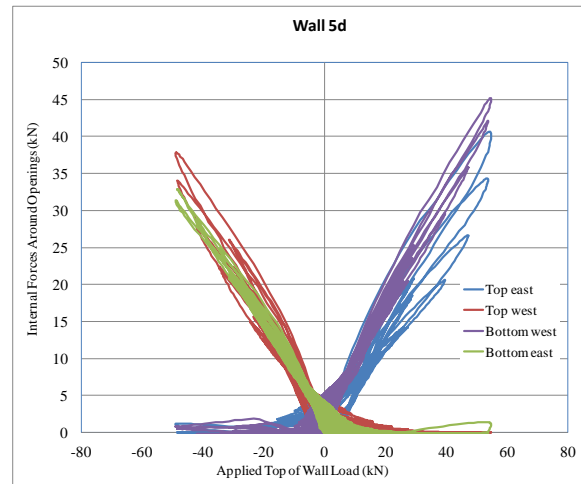
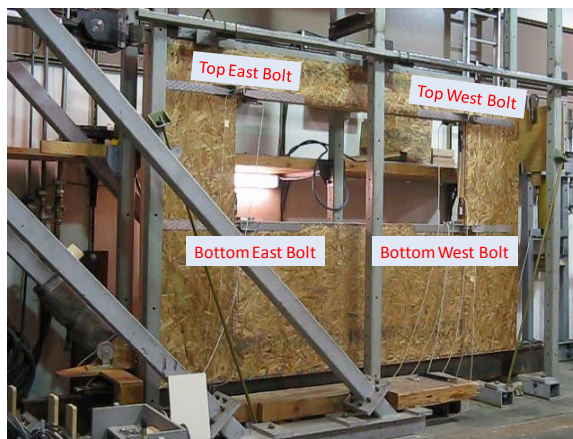


Figure 5. Notation of internal force gages (left), and typical response curve (right)

Table 2. Internal forces of tested walls at the design capacity (ASD) of the walls as compared to various predictions of strap forces

Wall ID	Measured Strap Forces (kN) ⁽¹⁾		Predicted Strap Forced at ASD Capacity (kN)				
			Drag Strut Technique		Cantilever Beam Technique		Diekmann Technique
	Top	Bottom	Top	Bottom	Top	Bottom	Top/Bottom
Wall 4a	3.3	6.6	5.4	5.4	19.9	12.1	8.7
	Error (%) ⁽²⁾		165%	83%	603%	184%	132%
Wall 4d	4.2	6.8	5.4	5.4	19.9	12.1	8.7
	Error (%) ⁽²⁾		131%	80%	478%	177%	128%
Wall 5d	7.7	10.5	5.4	5.4	27.4	20.6	14.5
	Error (%) ⁽²⁾		71%	52%	355%	197%	139%
Wall 6a	2.1	2.0	5.4	5.4	19.9	12.1	8.7
	Error (%) ⁽²⁾		262%	268%	957%	597%	419%
Wall 8a	4.4	6.3	5.2	5.2	35.4	21.5	8.3
	Error (%) ⁽²⁾		117%	82%	802%	344%	132%
Wall 8b ⁽³⁾	3.1	4.4	5.2	5.2	35.4	21.5	8.3
	Error (%) ⁽²⁾		167%	116%	1145%	486%	186%
Wall 9a	7.9	8.3	5.2	5.2	35.4	28.1	13.8
	Error (%) ⁽²⁾		65%	62%	449%	340%	166%
Wall 10a	8.2		5.2		34.8	--	41.3
	Error (%) ⁽²⁾		63%		423%		502%
Wall 11a	9.6		5.2		34.8	--	41.3
	Error (%) ⁽²⁾		54%		362%		429%
Wall 12a	Further analysis required						

⁽¹⁾ Reported strap forces were based on the mean of the “East” and “West” recorded forces at the capacity of the walls as tabulated in Table 1.

⁽²⁾ Error based on ratio of predicted forces to mean measured strap forces. For Diekmann method, the larger of the top and bottom strap forces was used for calculation. Highlighted errors represent **under-conservative** predictions and significant **ultra-conservative** prediction (arbitrarily assigned as 300%).

⁽³⁾ Loading time increased by 10x.

As shown in Table 2, the measured strap forces were based in the mean east and west strap forces for the top of the opening and the bottom of the opening. As demonstrated in Figure 5, the strap forces were symmetric about the y-axis, thus averaging strap forces was justifiable. Also shown in Table 2 are the predicted strap forces at wall capacity for the three techniques discussed above. The calculation of these forces is beyond the scope of

this paper. However, Martin (2005) covers the drag strut and cantilever beam calculations, and Breyer (2007) covers the Diekmann calculations.

The Diekmann technique assumes symmetric forces at the top and the bottom of the wall; hence the maximum of the two measured strap forces was used for the error calculation. Also included in Table 2 is the error, in percent, of the calculated strap forces. There is shading for predictions that fall below 100% of the observed strap forces, which would be considered under-conservative. The errors are also shaded when the predictions exceed the measured forces by three times (300%), which are considered excessively conservative.

Several items may be observed from the test results reported in Table 2. First, in general, the forces at the bottom of the window openings were higher than the forces at the top of the window opening in all cases except for Wall 6. The measured strap forces for Wall 6 were the smallest strap forces of any of the walls tested. This is due to the fact that the forces were transferred through the wrap-around OSB sheathing, thus little demand was placed on the straps at this low load level. Also, as one would expect, as the openings in the walls increased, the strap forces increased. In addition, as the width of the full height pier decreased, the relative magnitude of the strap forces increased. The largest strap forces, relative to the applied load, were observed for the large garage type openings, Wall 10 and Wall 11. Other observations are that the strap forces are reasonably repeatable (Walls 4a and 4b, Walls 8a and 8b), and that the strap forces are relatively insensitive to loading rate (Walls 8a and 8b).

Several observations can also be made about the three methods for predicting strap forces. First, the drag strut technique, arguably the simplest method for estimating strap forces, resulted in predicted strap forces that were less than the observed strap forces for nearly every wall. The cantilever beam technique was, by far, the most conservative method. For every wall tested, the cantilever beam technique over predicted at least one of the strap forces by more than 300 percent. It should also be noted that although the cantilever beam technique decouples the strap forces at the top and the bottom of the window, it always predicted the strap forces at the top of the wall as higher than the bottom of the wall, which is based on the underlying assumption of the moment couples, since the height of the sheathed area above the wall was consistently less than the height of the sheathing below the opening.

Finally the Diekmann technique provided reasonable predicted results (within 190 percent) for all walls with the exception of Walls 6, 10, and 11. As discussed above, Wall 6 was an atypical wall since the sheathing wrapped around the opening, thus the forces were transferred through the sheathing as opposed to the strap forces. For the large openings, it is believed that the Diekmann technique was very conservative due to the assumption that the walls behave as a homogeneous monolith. However, much wood crushing, separation between ends of header and pier studs and compression between adjacent pieces of OSB resulted in the observed forces as being significantly less than the predicted strap forces for all three techniques.

4. Summary and Conclusion

Twelve different wall assemblies were tested to study the effects of openings on both the global and local response of walls. Several of these assemblies were tested with multiple replications. The replications showed good agreement between each other, even when test duration was extended to ten times greater the original duration. In terms of global response, the segmented wall approach resulted in walls with the lowest load factors (based on observed global load divided by allowable capacity of the walls), followed by walls built as perforated shear walls (i.e. no special detailing for forces around openings), and

finally the walls specifically detailed for force transfer around openings. In general, as opening sizes increased, the wall strength and stiffness values were negatively impacted. An observation that was not expected is that for walls with typical window openings, the walls with the narrowest piers based on minimum pier width in North American codes, resulted in higher load factors than walls with full width piers (height-to-width ratio of 2:1).

Of the twelve walls tested, internal forces were collected on eight of the assemblies. For the walls tested, the measured forces at the bottom of the windows were greater than the measured forces at the top of the window. Also, as expected, as the window opening increased and as the pier width decreased, the strap forces increased relative to the global applied force to the wall. Of these eight assemblies, one can conclude that the drag strut technique consistently underestimated the strap forces, and the cantilever beam technique consistently overestimated the strap forces. The Diekmann technique, the most computationally intensive, provided reasonable strap force predictions for the walls with window type openings. The Diekmann technique significantly over predicted the strap forces for large garage type openings.

5. Acknowledgements

This work is a joint research project of APA – The Engineered Wood Association, the University of British Columbia, and the USDA Forest Products Laboratory. This research was supported in part by funds provided by the Forest Products Laboratory, Forest Service, USDA.

6. References

1. ASTM International. 2009. *Standard test methods for cyclic (reversed) load test for shear resistance of vertical elements of the lateral force resisting systems for buildings*. West Conshohocken, PA.
2. Breyer, D. E., K. J. Fridley, K. E. Cobein and D. G. Pollock. 2007. *Design of Wood Structures ASD/LRFD, 6th ed.*, McGraw Hill, New York, NY.
3. Diekmann, E. F. 1998. *Diaphragms and Shearwalls*, Wood Engineering and Construction Handbook, 3rd ed., K. F. Faherty and T. G. Williamson, eds, McGraw-Hill, New York, NY.
4. Martin, Z. A. 2005. *Design of wood structural panel shear walls with openings: A comparison of methods*. Wood Design Focus. 15 (1): 18 – 20.

**INTERNATIONAL COUNCIL FOR RESEARCH AND INNOVATION
IN BUILDING AND CONSTRUCTION**

WORKING COMMISSION W18 - TIMBER STRUCTURES

**OPTIMIZED ANCHOR-BOLT SPACING FOR STRUCTURAL PANEL SHEARWALLS
SUBJECTED TO COMBINED SHEAR AND WIND UPLIFT FORCES**

Borjen Yeh

E Keith

T Skaggs

APA – The Engineered Wood Association

U.S.A.

MEETING FORTY THREE

NELSON

NEW ZEALAND

AUGUST 2010

Presented by B Yeh

P Quenneville: what is the effect of doubling the sill plate? B Yeh: it would work but construction industry does not want to trim all studs.

M Yasumura: In tests, how do you control the vertical forces? B Yeh: Lateral and vertical forces can be controlled to remain constant. There are no standard test methods but perhaps ISO can initiate this.

H Morris: Was the 1.2m spacing tested? B Yeh: It has been in use for almost 50 years.

Optimized Anchor-Bolt Spacing for Structural Panel Shearwalls Subjected to Combined Shear and Wind Uplift Forces

Borjen Yeh, Ed Keith, and Tom Skaggs
APA – The Engineered Wood Association, U.S.A.

Abstract

Wood structural panels, such as plywood and oriented strand board (OSB), have been used to construct shearwalls with a long history of success. However, most wood panel shearwalls are designed as lateral load resisting elements and their capability of resisting uplift forces induced by wind forces has been frequently overlooked. In high wind areas, such as the Gulf Coast in the U.S., the use of wood structural panel shearwalls to resist combined shear and uplift forces has gained attention in recent years due to the reduction in the need for expensive and labor-intensive metal tension straps between studs and the foundation.

The U.S. building codes and design standards have established provisions for using wood panel shearwalls to resist combined shear and uplift forces. Unfortunately, the provisions contained in the U.S. building codes and design standards require a very close spacing, 406 mm (16 in.) on center, for anchor bolts that tie bottom wall plates to the foundation regardless of the magnitude of the shear and uplift forces. This conservatism was largely due to the concern over the cross-grain bending failure on the bottom wall plate, which is a predominant failure mode when subject to combined shear and uplift forces, and the lack of full-scale wall test data to optimize the anchor bolt spacing as a function of the shear and uplift forces.

In response to the desire of builders to reduce the costs associated with the unnecessary close anchor bolt spacings prescribed in the codes and standards, and to promote the concept of advanced framing of Optimal Value Engineering (OVE) of green building movement, APA conducted a research with intent to optimize the anchor bolt spacing for wood panel shearwalls when designed for combined shear and uplift forces. Supported by the results of 26 full-scale combined shear and uplift tests, the research shows that the anchor bolt spacing can vary between 406 mm (16 in.) and 1219 mm (48 in.), depending on the magnitude of the shear and uplift forces. This paper presents the test results from the research and proposes a change to the design standards.

1. Introduction

Wood structural panels, by definition of the U.S. International Building Code (IBC) [1] and International Residential Code (IRC) [2], include plywood manufactured in accordance with Voluntary Product Standard PS1, *Structural Plywood* [3], and oriented strand boards (OSB) and plywood manufactured in accordance with Voluntary Product Standard PS2, *Performance Standard for Wood-Based Structural-Use Panels* [4]. While most wood structural panels are specified based on their span rating, the mechanical properties of wood structural panels have been published by APA – The Engineered Wood Association in the *Panel Design Specification* [5]. When used as a lateral force resisting element, wood structural panels can be designed in accordance with the shearwall design values established by APA and published in the IBC.

Most buildings designed for lateral forces induced by wind are usually subjected to simultaneous wind uplift forces. Shearwalls constructed with wood structural panels have been used to resist combined shear and wind uplift forces for years in the U.S. For example, the Southern Building Code Congress International (SBCCI) published SSTD 10-99, *Standard for Hurricane Resistant Residential Construction* [6], which provided not only the shear resistance, but the wind uplift resistance of wood structural panels. When wood structural panels are designed to resist combined shear and wind uplift forces, SSTD 10-99 tabulated the wind uplift resistance of wood structural panels with a minimum thickness of 12 mm (15/32 inch) when used in conjunction with the shear resistance table.

The SSTD 10 wind uplift table was developed based on the principle of engineering mechanics. It assumes that the nails installed in the shearwall assembly are used primarily to resist the lateral shear forces. If there are extra nails that exceed the demand for the lateral shear resistance, they can be used to resist wind uplift forces. The through-the-thickness shear and tensile strength of the sheathing are checked, but they typically do not govern the capacity of the wall. While this principle seems straightforward, a major concern in this application is the possible cross-grain bending of the bottom wall plates due to the non-concentric uplift forces acting on one face of the wall. This cross-grain bending can split the bottom plate, usually 2x4 lumber, and the design value for this property is unavailable in the code. Therefore, a practical solution to avoid this failure mode is to specify anchor bolts at a tight spacing with large plate washers that are thick and wide enough to hold the bottom plates in place without inducing splitting.

Due to the merger of three regional U.S. model building codes into the IBC in 2000, SBCCI was no longer in existence and the SSTD 10 has not been maintained. In 2005, the Institute for Business & Home Safety (IBHS) published the *Guidelines for Hurricane Resistant Residential Construction* [7] based on the SSTD 10. In the meantime, the International Code Council (ICC) published the ICC 600, *Standards for Residential Construction in High Wind Regions* [8] in 2008 and the American Forest & Paper Association (AF&PA) also revised the ANSI/AF&PA *Special Design Provisions for Wind and Seismic* (SDPWS) [9] at the same year. All of the referenced standards mentioned above contain provisions for combined shear and wind uplift using wood structural panels. The SDPWS revisions included the re-calculation of the mechanics-based uplift resistance using the nail yield model specified in the 2005 *National Design Specification for Wood Construction* (NDS) [10] and supported by the research results provided by APA [11, 12]. Tables 1 and 2 show the nominal capacities of wood structural panel shearwalls for the combined shear and uplift, and uplift only, respectively, in accordance with the 2008 SDPWS.

A substantial restriction exists in the 2008 SDPWS by requiring the anchor bolts be installed at a maximum of 406 mm (16 inches) on center. This requirement is conservative in many cases, but was adopted because of the lack of supporting data to justify otherwise. Further investigation in optimizing the anchor bolt spacing has been conducted by APA after the publication of the 2008 SDPWS, which allows for varying anchor bolt spacing based on the magnitude of the lateral shear and uplift forces. This paper provides full-scale combined shear and uplift test data to support the development of the optimized anchor bolt spacing for the combined shear and uplift applications using wood structural panels.

2. Optimization of Anchor Bolt Spacing

A number of assumptions were made in the development of the anchor-bolt spacing matrix, as illustrated in Table 3 and discussed below.

Table 1. Nominal Uplift Capacity of Wood Structural Panels for Combined Shear and Wind Uplift^(a)

	Nail Spacing Required for Shearwall Design ^(d)											
	6d @ 152 & 305 mm			8d @ 152 & 305 mm			8d @ 102 & 305 mm			10d @ 152 & 305 mm		
	Alternate Nail Spacing at Top and Bottom Plate Edges (mm)											
	152	102	76	152	102	76	152	102	76	152	102	76
	Nominal Uplift Capacity (kN/m) ^(b,c)											
Nails-Single Row ^(d)	0.0	2.5	4.9	0.0	3.2	6.3	NP	0.0	3.2	0.0	3.8	7.6
Nails-Double Row ^(e)	4.9	9.8	14.7	6.3	12.6	18.9	3.2	9.5	15.8	7.6	15.3	22.9

1 mm = 0.0394 in., 1 kN/m = 68.5 lbf/ft

- (a) Minimum 11-mm (7/16-inch) OSB. The framing species shall have a published specific gravity of 0.42 (spruce-pine-fir) or greater. Anchor bolts shall be installed at 406 mm (16 in.) on center.
- (b) For framing with a specific gravity of 0.49 or greater, multiply the listed uplift values by 1.08.
- (c) Where nail size is 6d or 8d, the tabulated uplift values are applicable to 11 mm (7/16 in.) minimum OSB panels. Where nail size is 10d, the tabulated uplift values are applicable to 12 mm (15/32 in.) minimum OSB or plywood with a species of plies having a specific gravity of 0.49 or greater. For plywood with other species, multiple the tabulated uplift values by 0.90.
- (d) OSB panels shall overlap the top member of the double top plate and bottom plate by 38 mm (1-1/2 in.) and a single row of fasteners shall be placed 19 mm (3/4 in.) from the panel edge.
- (e) OSB panels shall overlap the top member of the double top plate and bottom plate by 38 mm (1-1/2 in.). Rows of fasteners shall be 13 mm (1/2 in.) apart with a minimum edge distance of 13 mm (1/2 in.). Each row shall have nails at the specified spacing.

Table 2. Nominal Uplift Capacity of Wood Structural Panels for Wind Uplift Only^(a)

	6d @ 152 & 305 mm			8d @ 152 & 305 mm			10d @ 152 & 305 mm		
	Alternate Nail Spacing at Top and Bottom Plate Edges (mm)								
	152	102	76	152	102	76	152	102	76
	Nominal Uplift Capacity (kN/m) ^(b,c)								
Nails-Single Row ^(d)	4.7	7.0	9.3	6.1	9.1	12.1	7.3	10.9	14.6
Nails-Double Row ^(e)	9.3	14.0	18.7	12.1	18.2	24.3	14.6	21.9	29.2

1 mm = 0.0394 in., 1 kN/m = 68.5 lbf/ft

- (a) Minimum 9.5-mm (3/8-in.) OSB. The framing species shall have a published specific gravity of 0.42 (spruce-pine-fir) or greater. Anchor bolts shall be installed at 406 mm (16 in.) on center.
- (b) For framing with a specific gravity of 0.49 or greater, multiply the listed uplift values by 1.08.
- (c) The tabulated values are applicable to 9.5 mm (3/8 in.) minimum OSB panels or plywood with species of plies having a specific gravity of 0.49 or greater. For plywood with other species, multiple the tabulated uplift values by 0.90.
- (d) OSB panels shall overlap the top member of the double top plate and bottom plate by 38 mm (1-1/2 in.) and a single row of fasteners shall be placed 19 mm (3/4 in.) from the panel edge.
- (e) OSB panels shall overlap the top member of the double top plate and bottom plate by 38 mm (1-1/2 in.). Rows of fasteners shall be 13 mm (1/2 in.) apart with a minimum edge distance of 13 mm (1/2 in.). Each row shall have nails at the specified spacing.

- a) The “Nominal Unit Shear” values were selected from the shearwall design values of the SDPWS to cover a range of values from the “Nail Spacing Required for Shearwall Design” columns in Table 1. An intermediate shear value of 5.8 kN/m (400 plf) with the SG = 0.50 was added to facilitate utilization for low-shear applications.
- b) The “Nominal Unit Uplift” values were selected from 0 to 31.5 kN/m (2,160 plf) with SG = 0.50, or 29.2 kN/m (2,000 plf) with SG = 0.42 based on a range of values for uplift-only in Table 2 (note that the tabulated values in Table 2 are based on SG = 0.42). Intermediate increments were chosen for tabulation purposes.
- c) The shear-only values in the table (“Nominal Unit Uplift” value of 0) were calculated based on the 2005 NDS for 13-mm (1/2-inch) anchor bolts and single shear (two-member) connection. The table provides for the anchor bolt to be fixed (embedded in concrete), and values for a compressive load parallel to the grain ($Z_{//}$) for SG = 0.50








were used ($Z_{//} = 2.9$ kN/bolt or 650 lbf/bolt). A duration of load of 1.6 was applied to the allowable load, yielding:


$$2.9 \text{ kN/bolt} \times 1.6 = 4.6 \text{ kN/bolt}$$

Note that the anchor bolt spacings for shear-only were truncated at 1219 mm (48 inches) on center as this is the most conservative prescriptive anchor-bolt spacing required in the 2009 IBC and IRC.


- d) Testing conducted previously by APA and others at the upper bound levels of high shear and high uplift illustrated that anchor bolt spacing at 406 mm (16 inches) on center and the use of 5.8- x 76- x 76-mm (0.229- x 3- x 3-inch) plate washers between nut and bottom plate were required to prevent a tension-perpendicular-to-grain (cross-grain bending) failure of the bottom plate. These prior results were confirmed by this latest series of tests. As the maximum shear and uplift testing conducted by APA for the other upper-bound shear and uplift cells of the matrix was successfully completed with an anchor bolt spacing of 406 mm (16 inches), this value was used for all other upper-bound values in Table 3.
- e) With values fixed on the left hand side of Table 3 by Item c above and on the right hand side by Item d, the intermediate values were interpolated based on the “Nominal Unit Uplift” values. The “missing” upper-bound value in Table 3 for 8d nails at 21.3 kN/m (1,458 plf) uplift and 14.3 kN/m (980 plf) shear, both SG = 0.50, was assumed to be 406 mm (16 inches). This was later confirmed by Test B5 that will be discussed later.
- f) The above model yields the anchor bolt spacings shown in Table 4 by linear interpolation.

Table 3. Development of anchor bolt spacing (mm) based on lumber framing specific gravity (SG)


Nail (Common)	Nominal Unit Shear (kN/m)		Nominal Unit Uplift (kN/m)											
	SG 0.50		0	3.2	6.3	9.5	12.6	15.8	18.9	21.3	25.2	28.4	31.5	
	SG 0.42		0	2.9	5.8	8.8	11.7	14.6	17.5	19.7	23.4	26.3	29.2	
8d @ 102 mm (11- mm panel)	0	0										406		
	5.8	5.4									406			
	9.8	9.0									406			
	14.3	13.2			<div>Linear interpolation – Item (e) below</div>									
10d @ 152 mm (12- mm panel)	0	0									406	406	406	
	5.8	5.4								406				
	12.7	11.7							406					




Shears based on
the SDPWS shear
table – Item (a)
above



Shear-only values
based on the NDS
Table 11E – Item
(c) below



Range based on
Table 1 – Item (b)
below



406 mm (16 in.)
oc based on
previous testing –
Item (d) below

1 mm = 0.0394 in., 1 kN/m = 68.5 lbf/ft

3. Material and Methods

3.1 Test Frame

Testing was conducted on a test frame designed for combined shear and uplift testing at the APA Research Center in Tacoma, WA, as shown in Figure 1. This test frame consists of a free-standing rigid rectangular steel frame designed to act as a reaction frame for both horizontal and vertical forces. For this study, the horizontal hydraulic cylinders were set

up to apply a positive pressure to the assembly (place the wall in shear) and the vertical hydraulic cylinders were configured to pull upwards (place uplift on the wall). Lateral restraints were provided by steel box sections with a low friction contact surface placed near the top of the assembly. Lateral restraints at the base were provided by the assembly attachment to the rigid base plate. The test frame was designed to permit a number of different wall configurations from 1219 mm x 2438 mm (4 feet x 8 feet) to 3048 mm x 3658 mm (10 feet x 12 feet). For this study, an assembly size of 2438 mm x 2438 mm (8 feet x 8 feet) was used.

Table 4. Proposed anchor bolt spacing (mm) based on model^(a)

Nail (Common)	Nominal Unit Shear (kN/m)		Nominal Unit Uplift (kN/m)										
	SG 0.50		0	3.2	6.3	9.5	12.6	15.8	18.9	21.3	25.2	28.4	31.5
	SG 0.42		0	2.9	5.8	8.8	11.7	14.6	17.5	19.7	23.4	26.3	29.2
8d @ 102 mm (11- mm panel)	0	0	1219	1118	1016	914	813	711	610	533	406		
	5.8	5.4	1219	1118	1016	914	813	711	610	533	406		
	9.8	9.0	940	864	813	737	686	610	533	483	406		
	14.3	13.2	635	610	559	533	508	457	432	406 ^(b)			
10d @ 152 mm (12- mm panel)	0	0	1219	1118	1016	914	813	711	610	533	406	406	406
	5.8	5.4	1219	1118	1016	914	813	711	610	522	406		
	12.7	11.7	711	660	610	584	533	483	432	406			

1 mm = 0.0394 in., 1 kN/m = 68.5 lbf/ft

(a) Shaded cells are outside the range of the SDPWS. Boxed cells were chosen to be tested for model verification. See Tables 5 and 6 for specific details.

(b) This cell is outside the range of the SDPWS, but was tested for model verification.

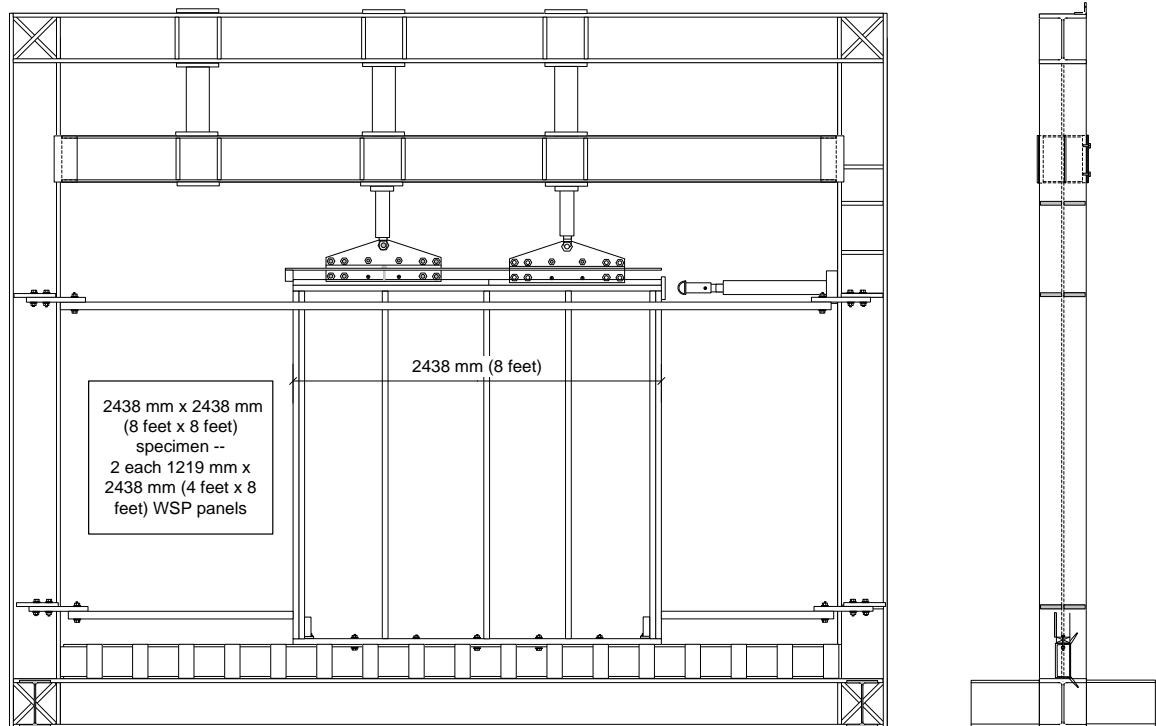


Figure 1. Combined shear and uplift test frame

The test assemblies were attached to the base of the test frame with anchor bolts in predrilled holes. For unusual anchor bolt spacing, machine clamps were utilized to attach the test assembly to the base of the test frame. When used, these clamps secured the wall

through short bolt sections consisting of a bolt head with a 38-mm (1-1/2-inch) shank. The clamp was placed over the head of the bolt section and attached to the flange of the rest frame bed. This provided virtually identical restraint conditions as provided by flat plate washers and anchor bolts.

The vertical and horizontal hydraulic cylinders were set up to provide independent control along each axis but were linked by a computer to synchronize them to meet their independent targeted test loads within the same time period. Load data were recorded electronically as a function of time for motion in both directions.

3.2 Test Assemblies

Combined shear and uplift test assemblies were constructed in accordance with Figure 2 using materials listed in Table 5. Hold-downs sized in accordance with Table 5 were provided at each end of the specimen and attached to the inside of the double studs with 6.4-mm (1/4-inch) Simpson SDS screws. The targeted assembly capacities are shown in Table 6. Table 7 illustrates the position of the test assembly in the final anchor bolt spacing matrix.

3.3 Instrumentation and Installation of Test Assemblies

Simultaneous shear and uplift loads were measured and recorded continuously by commercial data acquisition software in both the vertical and horizontal directions for the duration of each test.

Test assemblies were loaded into the test apparatus and anchored to the base in accordance with the details in Table 5. Anchor bolts of 12.7 mm (1/2 inch) in diameter and 5.8- x 76- x 76-mm (0.229- x 3- x 3-inch) plate washers were used to resist the uplift component along with hold downs to resist overturning. The rectangular plate washers were approximately aligned with the flat sides parallel to the sheathing. Hold downs were bolted to the base of the test apparatus in predrilled holes when the holes were present. When predrilled holes were not available to accommodate the anchor bolt spacing required, machine clamps were provided at the required locations, as discussed before. Hold downs were attached to the double end studs in accordance with the hold down manufacturer's recommendations with the exception that only sufficient fasteners (6.3- x 76-mm or 1/4- x 3-inch SDS screws) were used to develop the required overturning capacity resulting from the shear forces on the assembly.

At the top of the test assembly, a 12.7- x 178-mm (1/2- x 7-inch) metal plate was attached. This plate was attached with metal angles located at 406 mm (16 inches) on center. These angles were predrilled to provide an attachment pattern and schedule. In lieu of the nails required to attach the framing anchor, screws were used (#9 x 51-mm or 2-inch square drive flat-head screws) to facilitate disassembly. The 12.7- x 178-mm (1/2 x 7-inch) plate was engaged by the vertical loading heads when the uplift force was applied thus putting tension on the test assembly via the metal angles and framing anchors in a manner similar to a walls reaction to high wind loads within a structure.

At the edge of the assembly adjacent to the horizontal hydraulic cylinder, a metal bearing plate was applied at the center over the double top plates. The hydraulic cylinder engaged the metal plate via a series of steel rollers. These were used to permit the assembly to move laterally and rotate during loading without introducing any additional constraints other than the vertical and horizontal loads applied into the wall system.

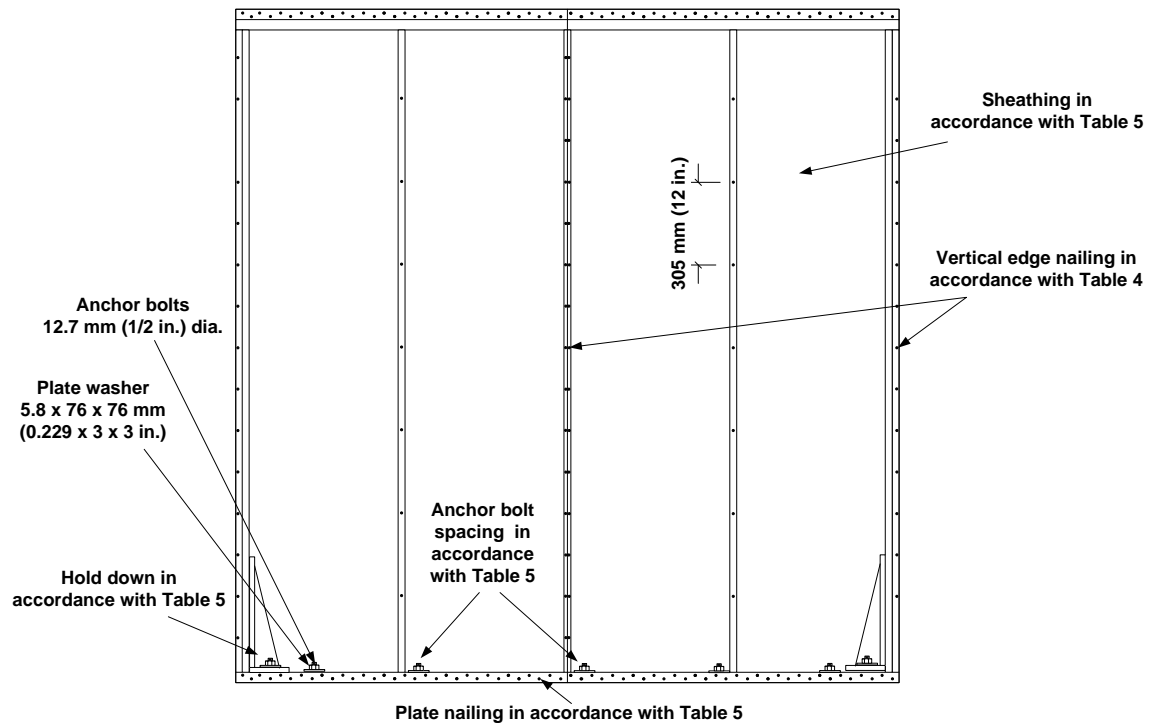


Figure 2. Configuration for shear and uplift assemblies

Table 5. Materials used for test assemblies

Test Series	Framing	Sheathing ^(a) (mm)	Nail (Common)	Nail Pattern on Top and Bottom Plates	Hold Down		Anchor Bolts ^(b)	
					Type	# SDS Screws	Dia. (mm)	Tested Spacing (mm)
A0	All framing DF #2 or better, 610 mm (24 in.) oc with a single center stud (SG = 0.50)	11	8d	2 rows @ 152 mm	PHD6	7	12.7	813
A2		11	8d	2 rows @ 102 mm	PHD6	9	12.7	610
A3		11	8d	1 row @ 102 mm & 1 row @ 152 mm	PHD6	12	12.7	813
B1		11	8d	1 row @ 152 mm	—	—	12.7	1219
B4		11	8d	2 rows @ 76 mm	PHD6	9	12.7	406
B5		11	8d	2 rows @ 76 mm	PHD6	16	12.7	406
B9		12	10d	1 row @ 102 mm	—	—	12.7	813
B10		12	10d	2 rows @ 152 mm	PHD6	11	12.7	610
C1 ^(c)		11	8d	1 row @ 76 mm & 1 row @ 102 mm	—	—	12.7	406
C3 ^(c)		11	8d	2 rows @ 102 mm			12.7	610
C4 ^(c)		12	10d	2 rows @ 102 mm			12.7	406
C5 ^(c)		12	10d	2 rows @ 76 mm			12.7	406
C6 ^(c)		12	10d	1 row @ 76 mm & 1 row @ 102 mm	PHD5	11	12.7	406
C7 ^(c)		12	10d	2 rows @ 76 mm	—	—	12.7	406

1 mm = 0.0394 in.

(a) APA Rated OSB Sheathing meeting the DOC PS2.

(b) 5.8- x 76- x 76-mm (0.229- x 3- x 3-inch) plate washers were used between nut and bottom plate.

(c) Multiple tests in this series.

3.4 TEST METHODS

The test assemblies were tested in accordance with Section 14 of ASTM E 72 [13] and Figure 1. The assemblies were loaded to the targeted loads, as shown in Table 6 in two minutes.

Table 6. Targeted assembly capacities (framing SG = 0.50)

Test Series	Nominal Shear		Nominal Uplift	
	Target Unit Shear (kN/m)	Target Total Shear (kN)	Target Unit Uplift (kN/m)	Target Total Uplift (kN)
A0	5.8	14.2	9.5	23.1
A2	9.8	23.8	15.8	38.4
A3	14.3	34.9	3.2	7.7
B1	—	—	3.2	7.7
B4	9.8	23.8	25.2	61.5
B5	14.3	34.9	21.3	51.9
B9	—	—	12.6	30.7
B10	12.7	31.0	6.3	15.4
C1 ^(a)	—	—	25.2	61.5
C3 ^(a)			18.9	46.1
C4 ^(a)			25.2	61.5
C5 ^(a)			28.4	69.2
C6 ^(a)	12.7	31.0	21.3	51.9
C7	—	—	31.5	76.9

1 kN/m = 68.5 lbf/ft, 1 kN = 224.8 lbf

(a) Multiple tests in this series.

Table 7. Test assembly location in the final anchor bolt spacing matrix^(a)

Nail (Common)	Nominal Unit Shear (kN/m)		Nominal Unit Uplift (kN/m)										
	SG 0.50		0	3.2	6.3	9.5	12.6	15.8	18.9	21.3	25.2	28.4	31.5
	SG 0.42	0	2.9	5.8	8.8	11.7	14.6	17.5	19.7	23.4	26.3	29.2	
8d @ 102 mm (11- mm panel)	0	0	(c)	B1					C3		C1		
	5.8	5.4	(c)			A0							
	9.8	9.0	(c)					A2			B4		
	14.3	13.2	(c)	A3						B5 ^(b)			
10d @ 152 mm (12- mm panel)	0	0	(c)				B9				C4	C5	C7
	5.8	5.4	(c)										
	12.7	11.7	(c)		B10					C6			

1 mm = 0.0394 in., 1 kN/m = 68.5 lbf/ft

(a) Shaded cells are outside the range of the SDPWS. Boxed cells were chosen to be tested for model verification.

(b) This cell is outside the range of the SDPWS, but was tested for model verification.

(c) This cell represents the shear-only value.

4. Results and Discussion

Test results of this study are shown in Table 8. The targeted combined shear and uplift load factor is 2.0. Note that the target uplift and shear values shown in Table 8 are nominal values. When calculating load factors, the nominal value is divided by 2.0 to yield the allowable design value. As such, the load factor is calculated in accordance with Eq. 1.

$$Load\ Factor = \frac{Test\ Result}{\left(\frac{Nominal\ Targeted\ Value}{2.0} \right)} \quad (1)$$

The average load factor shown in Table 8 is calculated based on the average of the uplift and shear load factor.

Table 8. Test results (framing SG = 0.50)

Test ID	Shear (kN/m)		Uplift (kN/m)		Load Factor ^(a)		Average Load Factor ^(b)
	Nominal Target	Test Results	Nominal Target	Test Results	Shear	Uplift	
A0	5.8	6.5	9.5	20.7	2.2	4.4	3.3
A2	9.8	11.7	15.8	17.8	2.5	2.3	2.4
A3	14.3	18.4	3.2	4.4	2.6	2.8	2.7
B1	–	–	3.2	10.5	–	6.7	6.7
B4	9.8	10.3	25.2	24.9	2.1	2.0	2.1
B5	14.3	20.1	21.3	23.3	2.8	2.2	2.5
B9	–	–	12.6	19.0	–	3.0	3.0
B10	12.7	16.4	6.3	8.1	2.6	2.6	2.6
C1A	–	–	25.2	25.5	–	2.0	2.0
C1B				25.6		2.0	
C3A			18.9	25.0		2.7	2.8
C3B				26.4		2.8	
C4A			25.2	25.8		2.0	2.3
C4B				33.2		2.6	
C5A			28.4	30.7		2.3	2.3
C5B				35.6		2.6	
C5C				30.5		2.2	
C5D				28.9		2.1	
C5E				29.1		2.2	
C6A	12.7	12.1	21.3	23.1	1.9	2.2	2.0
C6B		12.2		22.7	1.9	2.2	
C6C		11.9		21.8	1.9	2.1	
C6D		12.6		22.8	2.0	2.2	
C6E		11.0		20.5	1.8	2.0	
C7A	–	–	31.5	46.4	–	2.9	3.0
C7B				50.1		3.2	

1 kN/m = 68.5 lbf/ft

(a) Load Factors were calculated in accordance with Eq. 1.

(b) Average Load Factor is based on the average of the uplift and shear load factors.

As shown in Table 8, the load factors for those 26 assembly testes in this study are typically in the range of 2 to 3. One exception is Wall B1, which is uniaxial (uplift-only) at a very low targeted uplift force. In some critical load cases (high uplift-only or combined shear and uplift), such as Walls C5 and C6 series, additional replicates were tested to increase the data confidence.

It should be noted that all tests reported in Table 8 used 12.7-mm (1/2-in.) diameter anchor bolts, which are different from the current requirements of 15.9-mm (5/8-in.) anchor bolts specified in the SDPWS and the ICC-600. Test results obtained from this study showed that the 12.7-mm (1/2-in.) diameter anchor bolts are adequate for use in the combined shear and uplift applications when the design loads are within the range permitted in the current U.S. national design standards.

4.1 Failure Modes

The typical failure modes for uniaxial tests, such as Walls B1, C1A through C5E, C7A and C7B (uplift only), were the nail withdrawal from the top and bottom plates, and panel edge tear-out, as shown in Figure 3. For biaxial tests (combined shear and uplift), the failure modes were more complicated. At the high combined loading, such as Walls C6A through C6E, it was usually a combination of nail withdrawal from the top and bottom plates, panel edge tear-out, and the bottom plate failure, as shown in Figure 4. The 5.8- x 76- x 76-mm (0.229- x 3- x 3-inch) plate washers performed adequately to avoid cross-grain bending failure on the bottom plate in most cases. It is important, however, to pay attention to the

anchor bolt spacing as the cross-grain bending is a possibility if the anchor bolts are not properly spaced.



Figure 3. Nail withdrawal from bottom and top plates, and panel edge tear-out from uniaxial (uplift-only) tests



Figure 4. A combination of nail withdrawal, panel edge tear-out, and bottom plate failure from biaxial (combined shear and uplift) tests

5. Conclusion

As shown by the results in Table 8, load factors of 2.0 or greater were achieved by the assemblies selected to verify the model used to develop Table 4. As the anchor bolt spacings listed in Table 4 may be difficult to construct in the field, Tables 9 and 10 were developed. Table 9 provides anchor bolt spacings rounded down from Table 4 to 152-mm (6-inch) increments on center. The anchor bolt spacing of 406 mm (16 inches) on center were unchanged in Table 9 as this spacing is a commonly used construction spacing interval in North America, is widely published, and currently exclusively recommended for combined shear and uplift anchor bolt spacing. For practical use, Table 10 further rounds the anchor both spacing from Table 4 down to traditional spacing intervals of 406, 488, 610, 813, 914, 1067, and 1219 mm (16, 19.2, 24, 32, 36, 42, and 48 inches) used in the conventional construction in North America.

Table 9. Anchor bolt spacing (mm) rounded down to spacing with 152-mm (6-inch) increments

Nail (Common)	Nominal Unit Shear (kN/m)		Nominal Unit Uplift (kN/m)										
	SG 0.50		0	3.2	6.3	9.5	12.6	15.8	18.9	21.3	25.2	28.4	31.5
	SG 0.42		0	2.9	5.8	8.8	11.7	14.6	17.5	19.7	23.4	26.3	29.2
8d @ 102 mm (11- mm panel)	0	0	1219	1067	1016	914	762	610	610	457	406		
	5.8	5.4	1219	1067	1016	914	762	610	610	457	406		
	9.8	9.0	914	762	762	610	610	610	457	457	406		
	14.3	13.2	610	610	457	457	457	457	406				
10d @ 152 mm (12- mm panel)	0	0	1219	1067	914	914	762	610	610	508	406	406	406
	5.8	5.4	1219	1067	914	914	762	610	610	508	406		
	12.7	11.7	610	610	610	457	457	457	457	406			

1 mm = 0.0394 in., 1 kN/m = 68.5 lbf/ft

Table 10. Anchor bolt spacing (mm) rounded down to common construction spacings

Nail (Common)	Nominal Unit Shear (kN/m)		Nominal Unit Uplift (kN/m)										
	SG 0.50		0	3.2	6.3	9.5	12.6	15.8	18.9	21.3	25.2	28.4	31.5
	SG 0.42		0	2.9	5.8	8.8	11.7	14.6	17.5	19.7	23.4	26.3	29.2
8d @ 102 mm (11- mm panel)	0	0	1219	1067	914	914	813	610	610	488	406		
	5.8	5.4	1219	1067	914	914	813	610	610	488	406		
	9.8	9.0	914	813	610	610	610	610	488	488	406		
	14.3	13.2	610	610	488	488	488	406	406				
10d @ 152 mm (12- mm panel)	0	0	1219	1067	914	914	813	610	610	488	406	406	406
	5.8	5.4	1219	1067	914	914	813	610	610	488	406		
	12.7	11.7	610	610	610	488	488	488	406	406			

1 mm = 0.0394 in., 1 kN/m = 68.5 lbf/ft

Results presented in Table 10 have been incorporated into the APA System Report SR-101, *Design for Combined Shear and Uplift from Wind* [14], which may be used by design engineers on a voluntary basis before the provisions can be adopted into the U.S. national design standards, such as the SDPWS and the ICC-600. Since the installation details are critical to the combined shear and uplift applications, APA SR-101 also provides many practical details to ensure the wall assemblies are properly designed and constructed. It would be prudent to follow the APA SR-101 construction details closely when designing and constructing wood structural panel shearwalls for the combined shear and wind uplift applications.

While APA SR-101 still recommends the use of 15.9-mm (5/8-in.) anchor bolts as specified in the SDPWS and the ICC-600, test results obtained from this study showed that the 12.7-mm (1/2-in.) diameter anchor bolts are adequate for use in the combined shear and uplift applications when the design loads are within the range permitted in the current U.S. national design standards.

6. References

- [1] International Code Council. International Building Code. Country Club Hills, IL, 2009.
- [2] International Code Council. International Residential Code. Country Club Hills, IL, 2009.
- [3] National Institute of Standards and Technology. Voluntary Product Standard PS1-07, Structural Plywood. Gaithersburg, MD, 2007.

- [4] National Institute of Standards and Technology. Voluntary Product Standard PS2-04, Performance Standard for Wood-Based Structural-Use Panels. Gaithersburg, MD, 2004.
- [5] APA – The Engineered Wood Association. Panel Design Specification. Tacoma, WA, 2008.
- [6] Southern Building Code Congress International. Standard for Hurricane Resistant Residential Construction. Birmingham, AL, 1999.
- [7] Institute for Business & Home Safety. Guidelines for Hurricane Resistant Residential Construction. Tampa, FL, 2005.
- [8] International Code Council. Standards for Residential Construction in High Wind Regions, ICC-600. Country Club Hills, IL, 2008.
- [9] American Forest & Paper Association. Special Design Provisions for Wind and Seismic. Washington, D.C., 2008.
- [10] American Forest & Paper Association. National Design Specification for Wood Construction. Washington, D.C., 2005.
- [11] B. Yeh and T. Williamson. Combined shear and wind uplift resistance of wood structural panel shearwalls. In Proceedings of the 41st International Council for Research and Innovation in Building and Construction, Working Commission W18 on Timber Structures (CIB W18) held on August 23 through August 29, 2008 in St. Andrews, NB, Canada, 2008.
- [12] B. Yeh, T. Williamson, and E Keith. Combined shear and wind uplift resistance of wood structural panel shearwalls. In Proceedings of the 2009 Structural Congress held in Austin, TX, 2009.
- [13] ASTM International. Standard Test Methods of Conducting Strength Tests of Panels for Building Construction, ASTM E72. West Conshohocken, PA, 2005.
- [14] APA – The Engineered Wood Association. Design for Combined Shear and Uplift from Wind, APA System Report SR-101. Tacoma, WA, 2010.

**INTERNATIONAL COUNCIL FOR RESEARCH AND INNOVATION
IN BUILDING AND CONSTRUCTION**

WORKING COMMISSION W18 - TIMBER STRUCTURES

**LIGHT TIMBER FRAME CONSTRUCTION WITH SOLID TIMBER MEMBERS –
APPLICATION OF THE REDUCED CROSS-SECTION METHOD**

J König

J Schmid

SP Trätek/Wood Technology

SWEDEN

MEETING FORTY THREE

NELSON

NEW ZEALAND

AUGUST 2010

Presented by J Schmid

No Questions

Light timber frame construction with solid timber members – Application of the reduced cross-section method

Jürgen König, Joachim Schmid
SP Trätekt/Wood Technology, Sweden

Abstract

In timber members exposed to fire a zone of about 35 to 40 mm depth below to the char layer, although unburned, is heated above ambient temperature. Due to the elevated temperature this zone, strength properties and the modulus of elasticity of the residual cross-section must be reduced. Two methods, known as reduced properties method and reduced cross-section method, respectively, are used in practice. In the first one the strength and stiffness properties of the cross-section, e.g. bending strength or modulus of elasticity, are multiplied by modification factors for fire, while in the second one, the residual cross-section is reduced by a so-called zero-strength layer, whereas the strength and stiffness properties remain unreduced.

For the calculation of the mechanical resistance of wall and floor assemblies in fire consisting of light timber frame members with rectangular cross-sections of solid timber and cavities filled with insulation, EN 1995-1-2 gives a design model using the reduced properties method. In order to simplify the calculation the original data were re-evaluated and expressions for zero-strength layers were derived to allow the use of the reduced cross-section method. For bending, the zero-strength layers were calculated to achieve the best fit of bending resistance in the range of load ratios between 0,2 and 0,4. Only for load ratios smaller than 0,2 the results are slightly non-conservative. For axially loaded members, the zero-strength layers were determined to give the same or lower bending stiffness than according to the reduced properties method. The axial resistance of studs, however, calculated using the method of EN 1995-1-1 with properties relevant for the fire situation, is somewhat greater when the reduced cross-section method is used.

1 Introduction

1.1 General

In timber members exposed to fire a zone of about 35 to 40 mm depth below the char-layer of the residual cross-section, although unburned, is heated above ambient temperature. This elevation of temperature gives rise to reduced strength and stiffness properties of the timber in this zone. EN 1995-1-2 [1] gives design values for strength and stiffness properties for timber members (e.g. beams or columns) as:

$$f_{d,fi} = k_{mod,fi} \frac{f_{20}}{\gamma_{M,fi}} \quad (1.1)$$

$$S_{d,fi} = k_{mod,fi} \frac{S_{20}}{\gamma_{M,fi}} \quad (1.2)$$

where:

- $f_{d,fi}$ design strength in fire (bending strength, compressive strength etc of timber members);
- $S_{d,fi}$ design stiffness property (modulus of elasticity $E_{d,fi}$ or shear modulus $G_{d,fi}$) in fire;
- f_{20} 20 % fractile of a strength property at normal temperature;
- S_{20} 20 % fractile of a stiffness property (modulus of elasticity or shear modulus) at normal temperature;
- $k_{mod,fi}$ modification factor for fire taking into account the reduction in strength and stiffness properties at elevated temperatures;
- $\gamma_{M,fi}$ partial safety factor for timber in fire ($\gamma_{M,fi} = 1$).

The 20 % fractile of a strength, and correspondingly of a stiffness property, is derived from the characteristic (5 % fractile) value as

$$f_{20} = k_{fi} f_k \quad (1.3)$$

where k_{fi} is dependent on the coefficient of variation of the material. For example, for solid timber $k_{fi} = 1,25$, for glued laminated timber $k_{fi} = 1,15$.

For the design procedure for mechanical resistance, for the determination of cross-section properties, i.e. the determination of strength and stiffness properties, EN 1995-1-2 [1] gives two alternative methods:

- the reduced cross-section method
- the reduced properties method.

The reduced properties method is a direct application of the general expressions given above for design values for strength and stiffness properties. For specific structural members modification factors for fire, $k_{mod,fi}$, are given (beams, columns, timber frame members in insulated wall and floor assemblies). The reduced strength and stiffness properties are to be applied to the residual cross-section, i.e. the original cross-section reduced by the depth of the char-layer. In order to simplify the calculation, notional charring depths are used and the residual cross-section is therefore rectangular.

As an alternative, for beams and columns, the effective cross-section method allows for further simplification of the design. This method, permitting the designer to use “cold” strength and stiffness properties (with $k_{mod,fi} = 1$ in equations (1.1) and (1.2)) and an effective residual cross-section, taking into account the reduction of strength and stiffness in the heat affected zones by removing a further 7 mm thick layer from the residual cross-section. It is assumed that this zero strength layer is built up linearly with time during the first 20 minutes of fire exposure, or, in case of a fire protective layer being applied to the timber member, during the time period until the start of charring.

1.2 Timber frame studs and joists

Designers in practice seem to prefer the reduced cross-section method since it is simpler to use. For the design of timber frame wall and floor assemblies with cavities filled with insulation, however, EN 1995-1-2 [1] only gives modification factors $k_{mod,fi}$. The application of the 7 mm zero-strength layer is not permitted since the results would be unsafe. The modification factors $k_{mod,fi}$ are dependent on the cross-section properties and state of stress on the fire exposed side, i.e. tension or compression, and the charring depth. They are given as linear expressions of shape

$$k_{mod,fi} = a_0 + a_1 \frac{d_{char,n}}{h} \quad (1.4)$$

with parameters a_0 and a_1 given for specific member depths h in a number of tables. For simplicity, the values for $b = 38$ mm were assumed also for other values of b . For other depths these parameters are determined by linear interpolation. In [2] more comprehensive data are given for widths of 38, 45 and

60 mm, and depths of 95, 145, 195 and 220 mm.

The notional charring rate, $d_{\text{char},n}$, is determined as

$$d_{\text{char},n} = k_n d_{\text{char}} \quad (1.5)$$

with

$$k_n = 1,5$$

see Figure 1.1.

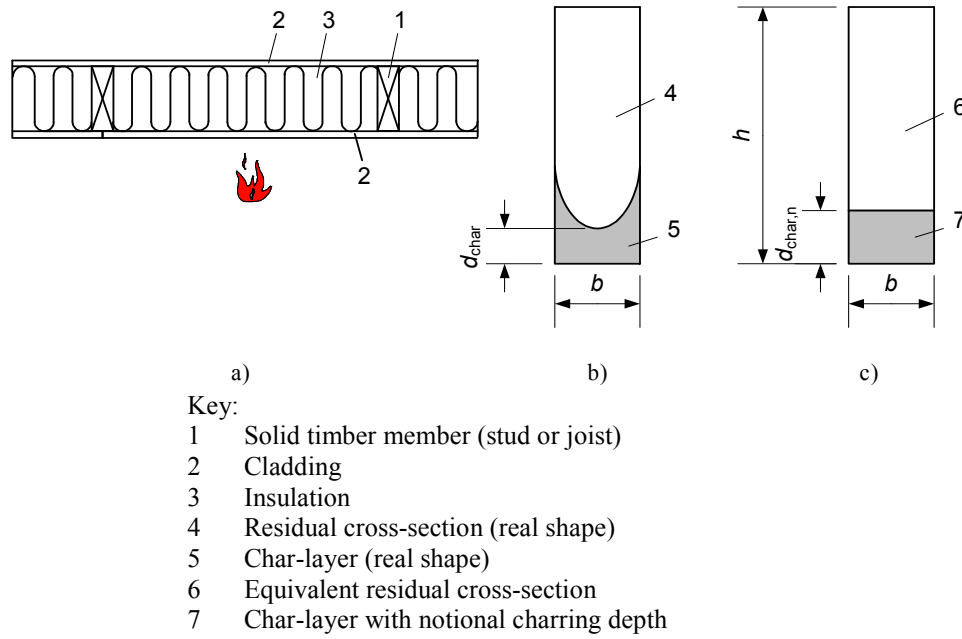


Figure 1.1 – Charring of timber frame member (stud or joist): a. Section through assembly. b. Real residual cross-section and char-layer. c. Notional charring depth and equivalent residual cross-section.

The background of the method given above is given in [3]. In the following section the results of calculations in [3] are re-evaluated with the aim of deriving zero-strength layers for the application of the reduced cross-section method to timber frame members with rectangular cross-sections.

2 Zero-strength layers of timber frame members

2.1 General

The effective cross-section used in the following is defined in Figure 2.1, i.e. it is obtained by increasing the notional charring depth by the zero-strength layer d_0 :

$$d_{\text{ef}} = d_{\text{char},n} + d_0 \quad (2.1)$$

No further reduction of the cross-section is done on the wide sides of the cross-section.

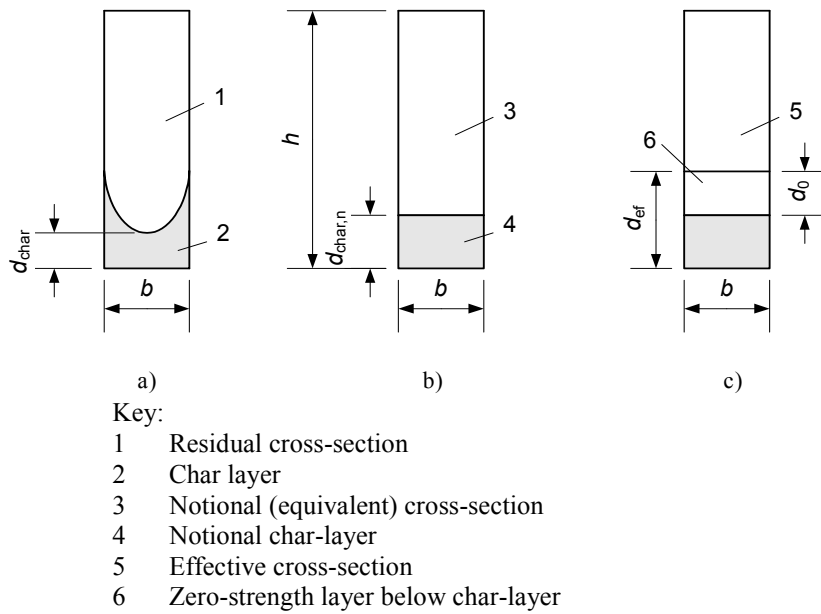


Figure 2.1 – Definition of charring depth, notional charring depth, effective charring depth and zero-strength layer.

2.2 Members in bending (floor joists)

The modification factors $k_{\text{mod,fi}}$ given in [1] were derived in [3]. For simplicity, the non-linear relationships of $k_{\text{mod,fi}}$ versus the relative charring depth d_{char}/h were replaced by linear trendlines, see Figure 2.2. It can be seen that the linear relationship is slightly non-conservative in the range of load levels between 20 and 40 %, which is most relevant in practice. In order to obtain a better agreement, in the following the zero-strength layer was determined from the relationships of relative bending moment versus relative charring depth.

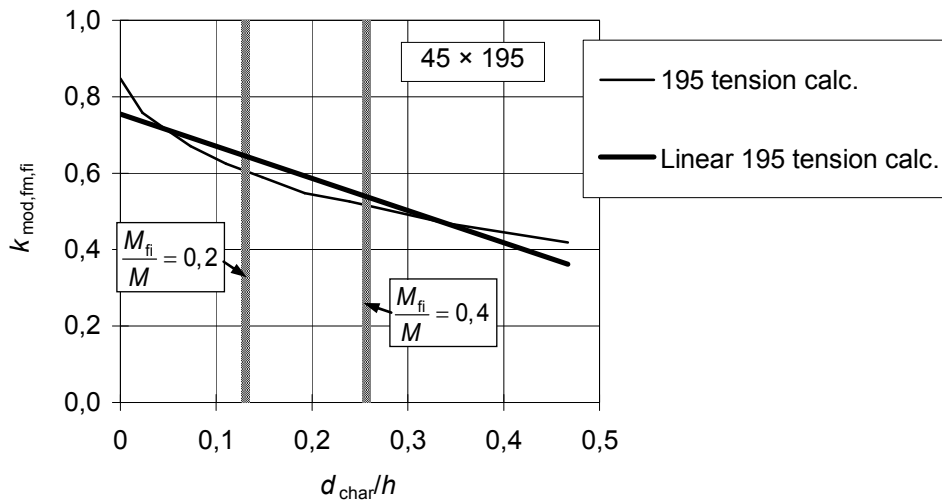


Figure 2.2 – Determination of simplified relationship of modification factor $k_{\text{mod,fi}}$ versus relative charring depth for a cross-section of 45 mm \times 195 mm [3].

Using the background data of [3], for each of the cross-sections with widths b of 38, 45 and 60 mm and depths h of 95, 145, 195 and 220 mm the relationship of bending resistance ratio M_{fi}/M versus relative charring depth d_{char}/h were calculated and plotted in Figure 2.3 to 2.4. In the calculations it was assumed that either the tensile or compressive side was exposed to fire. The temperature in the timber member was calculated under the assumption that the fire protective gypsum plasterboard

cladding remained in place after the start of charring. In such scenario, the rate of heat transfer is slower, the temperature gradient in the timber member is smaller and therefore the reduction of strength and stiffness is greater compared to the case of unprotected timber members. For the stage after failure of the cladding, the assumption made is conservative.

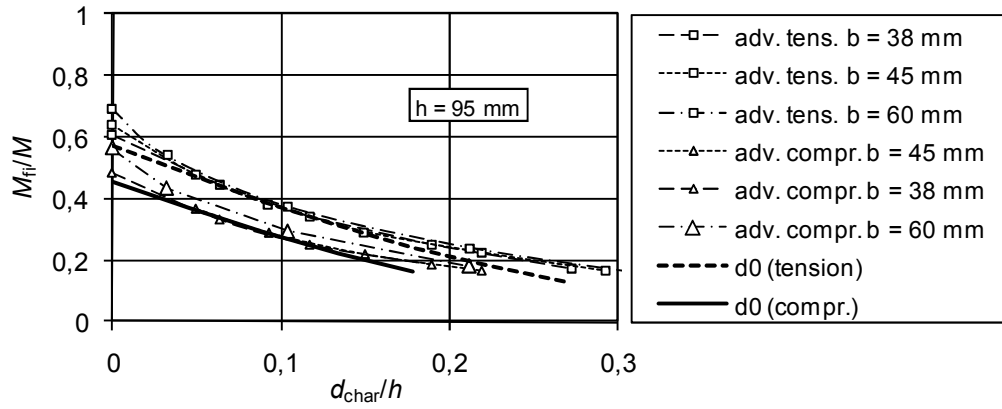


Figure 2.3 – Moment resistance ratios versus relative charring depth according to advanced calculations and reduced cross-section method.

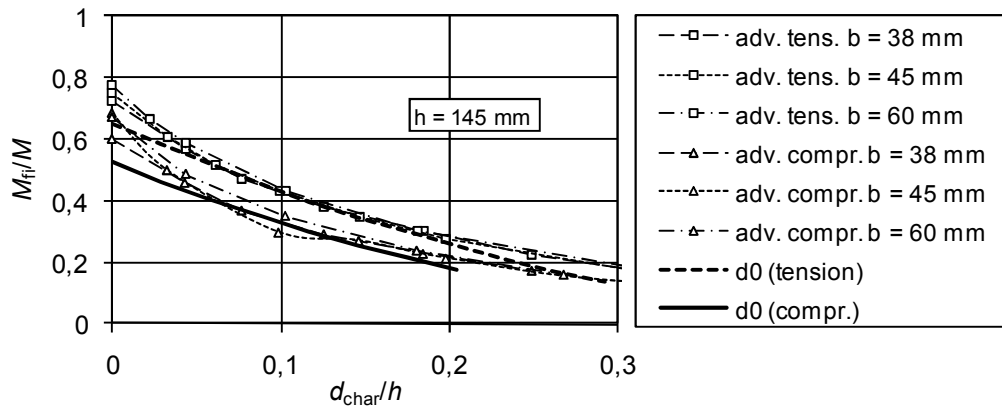


Figure 2.4 – Moment resistance ratios versus relative charring depth according to advanced calculations and reduced cross-section method.

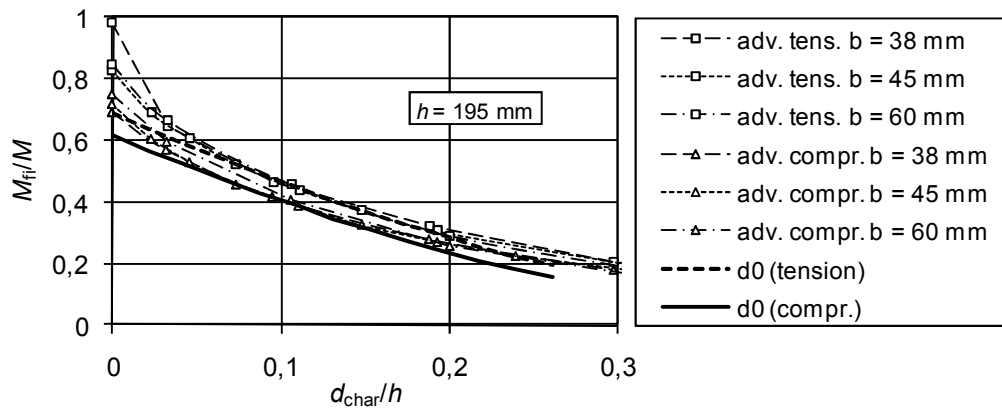


Figure 2.5 – Moment resistance ratios versus relative charring depth according to advanced calculations and reduced cross-section method.

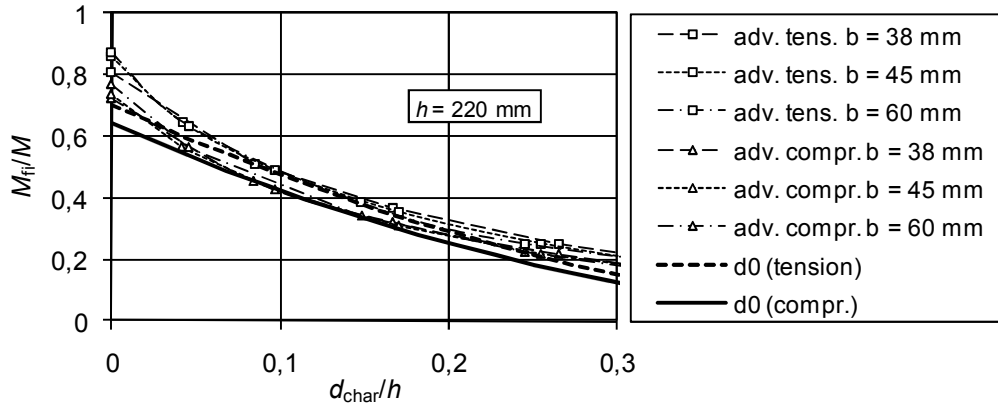


Figure 2.6 – Moment resistance ratios versus relative charring depth according to advanced calculations and reduced cross-section method.

By trial and error, zero-strength layers d_0 (see Figure 2.1) were determined such that the corresponding moment resistance ratio curves gave the best fit for load resistance ratios between 0,2 and 0,4. In these calculations, the charring depth was replaced by the notional charring depth according to expressions (1.5) and (1.6). Since the influence of the width b is small, the zero-strength layer d_0 can be expressed as a function of depth h :

- For members with the fire exposed side in tension

$$d_0 = 13,5 + \frac{h}{10} \quad (2.2)$$

- For members with the fire exposed side in compression

$$d_0 = 21,5 + \frac{h}{10} \quad (2.3)$$

For members with the fire exposed side in tension, for cross-section depths between 95 and 220 mm, d_0 varies from 23 to 35,5 mm, while it is further 8 mm greater when the fire exposed side is in compression.

2.3 Axially loaded members (wall studs)

For axially loaded members column buckling is the relevant failure mode and therefore bending stiffness EI is the most relevant design parameter. Therefore, for the cross-sections studied in [3],

relationships of the relative bending stiffness $\frac{(EI)_{fi}}{EI}$ versus the charring ratio $\frac{d_{char}}{h}$ were determined

for the following cases (for the definition of the y and z-axis see Figure 2.7):

- Fire exposure on one side for deflection in the z-direction (Figure 2.8 to 2.9)
- Fire exposure on one side for deflection in the y-direction (Figure 2.11 to 2.12)
- Fire exposure on two sides for deflection in the z-direction (Figure 2.14)
- Fire exposure on two sides for deflection in the y-direction (Figure 2.15).

In these calculations, the linear expressions for the modification factors $k_{mod,E,fi}$, derived from advanced calculations in [3], were used.

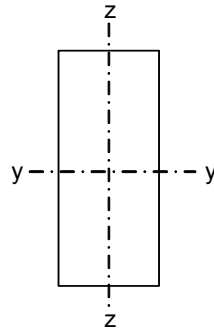


Figure 2.7 – Definition of axes.

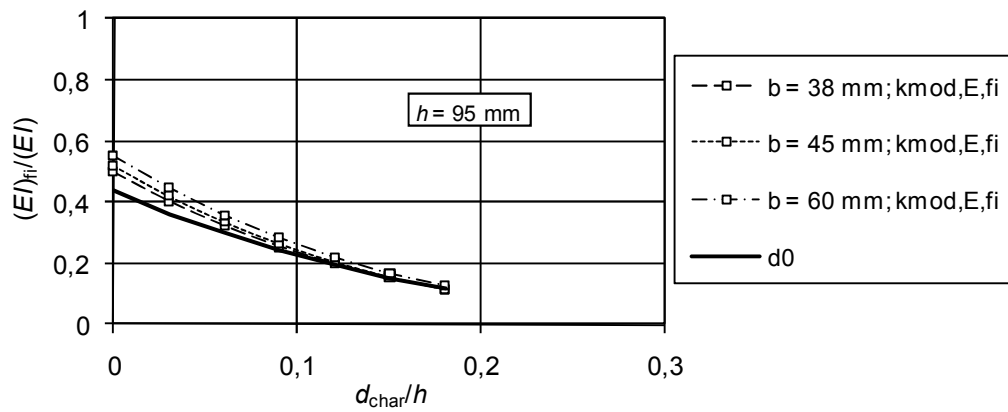


Figure 2.8 – Comparison of relative bending stiffness versus relative charring for deflection in z-direction.

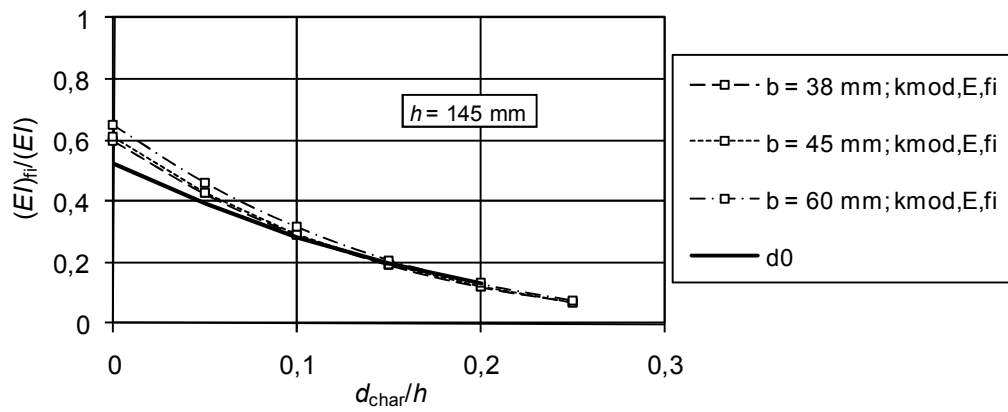


Figure 2.9 – Comparison of relative bending stiffness versus relative charring for deflection in z-direction.

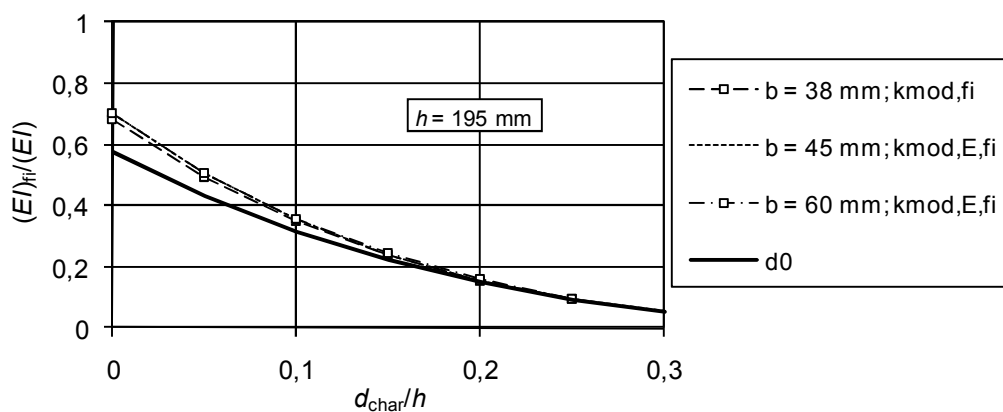


Figure 2.10 – Comparison of relative bending stiffness versus relative charring for deflection in z-direction.

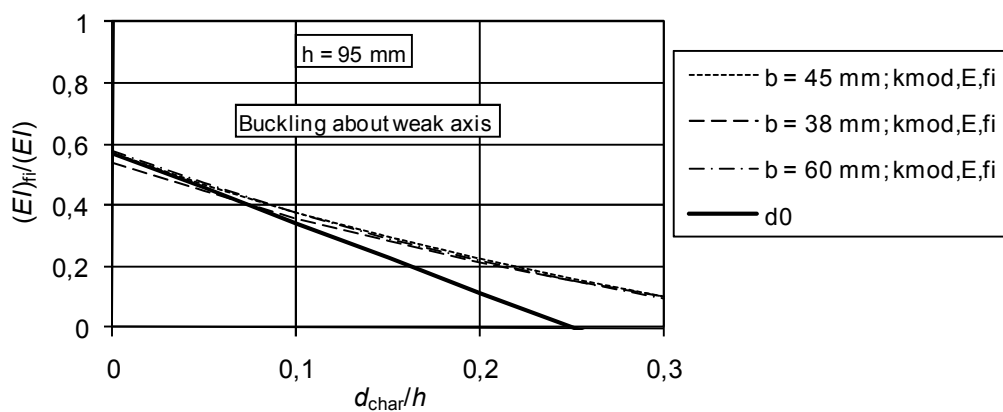


Figure 2.11 – Comparison of relative bending stiffness versus relative charring for deflection in y-direction.

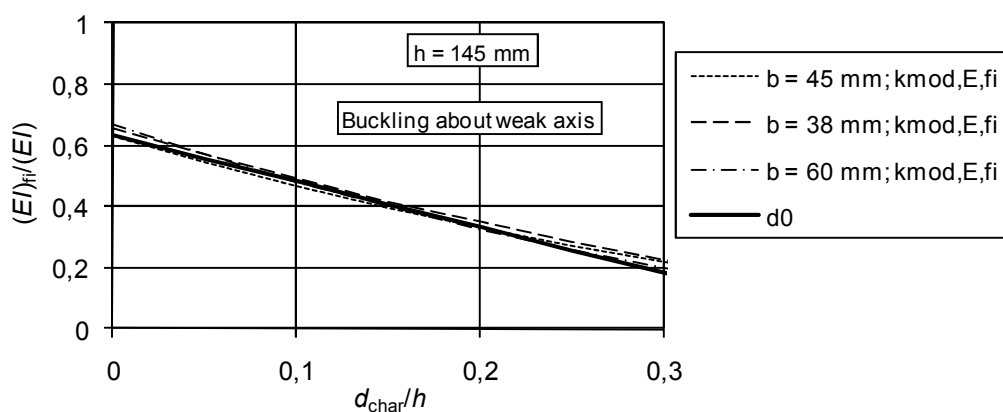


Figure 2.12 – Comparison of relative bending stiffness versus relative charring for deflection in y-direction.

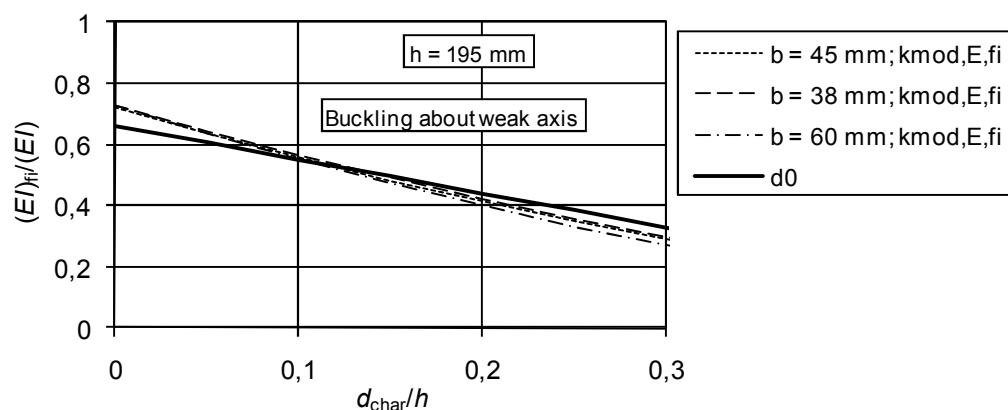


Figure 2.13 – Comparison of relative bending stiffness versus relative charring for deflection in y-direction.

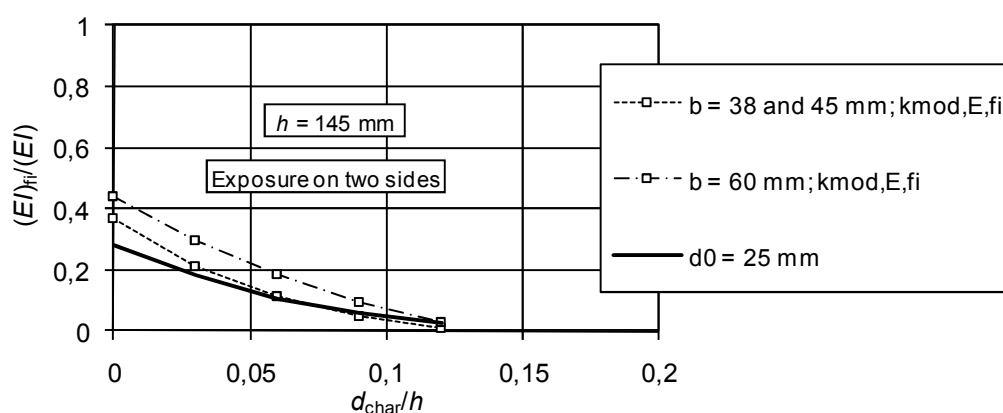


Figure 2.14 – Comparison of relative bending stiffness versus relative charring for deflection in z-direction and fire exposure on both sides.

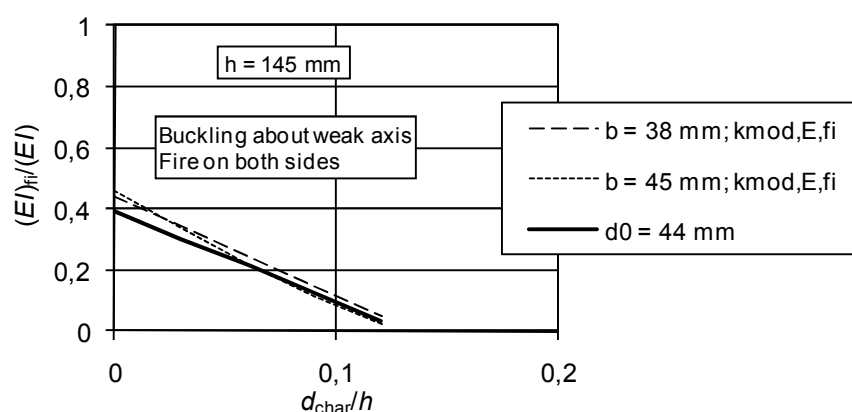


Figure 2.15 – Comparison of relative bending stiffness versus relative charring for deflection in y-direction and fire exposure on both sides.

Calculating the relative bending stiffness using an effective cross-section, the following expressions and values give reasonable agreement with the curves obtained from $k_{\text{mod},\text{fi}}$ -values:

- For fire exposure on one side for deflection in the z-direction (relevant for buckling about the y-axis perpendicular to the wall):

$$d_0 = 13,5 + \frac{h}{10} \quad (2.4)$$

(the same as expression (2.2))

- For fire exposure on one side for deflection in the y-direction (relevant for buckling about the z-axis parallel to the wall):

$$d_0 = 17 + \frac{h}{4} \quad (2.5)$$

- For fire exposure on both sides for deflection in the z-direction (relevant for buckling about the y-axis perpendicular to the wall):

$$d_0 = 25 \text{ mm} \quad (2.6)$$

- For fire exposure on one side for deflection in the y-direction (relevant for buckling about the z-axis parallel to the wall):

$$d_0 = 44 \text{ mm}$$

2.4 Comparison with reduced properties method

2.4.1 Members in edgewise bending

For two cross-sections, 45 mm × 145 mm and 45 mm × 195 mm, the relationships of relative bending moment resistance versus relative charring depth are shown for members with fire exposure on the tension side, see Figure 2.16 and 2.17. It can be seen that the linear model for $k_{\text{mod},\text{fm},\text{fi}}$ gives moment resistance values that are slightly non-conservative for relative resistance values greater than 0,2. The values calculated using a zero-strength layer agree well with the non-linear model for $k_{\text{mod},\text{fm},\text{fi}}$.

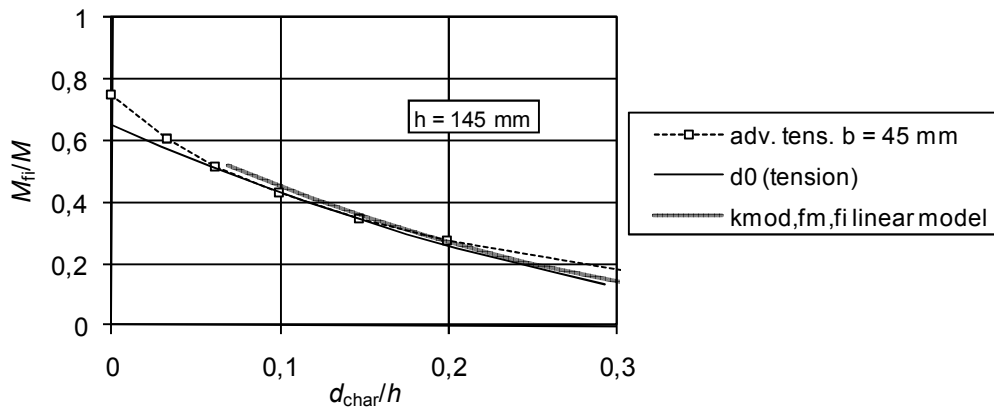


Figure 2.16 – Comparison of models

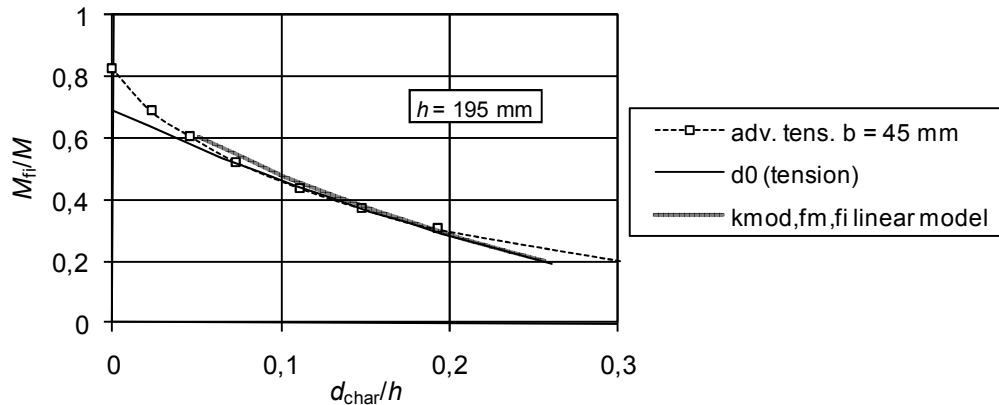


Figure 2.17 – Comparison of models

2.4.2 Axially loaded members

Verification of mechanical resistance in fire means, in terms of EN 1995-1-2 [1], that the design method or model is the same as for the design at ambient temperature, however with material and cross-section properties that are relevant for the fire exposed members. Applying the reduced properties method to axially loaded members, different modification factors for fire are applied to modulus of elasticity and compressive strength. As an approximation, the modification factor for compressive strength was replaced by the modification factor for bending strength, $k_{mod, fm, fi}$ when the fire exposed side of the member is in compression. This approximation is justified since the calculated axial resistance is only slightly sensitive to variations of $k_{mod, fm, fi}$. Since the reduced cross-section method cannot assume different zero-strength layers for the same member, the most relevant value of d_0 relevant for bending stiffness was used.

Figure 0.1 shows a comparison of both methods, carried out for a timber stud of size 45 mm × 145 mm protected by gypsum plasterboards which remain in place during the fire. The axial resistance was calculated according to EN 1995-1-1 [4] with the relevant model parameters taking into account the effect of charring and reduced strength and stiffness properties. The axial resistance calculated using the effective cross-section method is between 2,5 and 10 % larger for relative resistance values between 0,4 and 0,2.

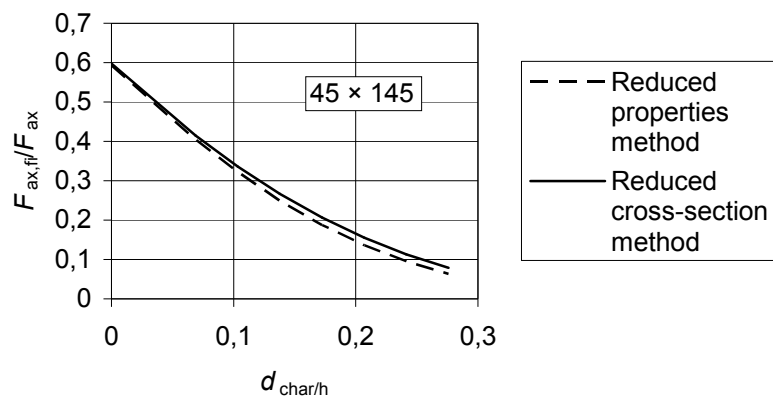


Figure 0.1 – Comparison of models: Timber stud protected by gypsum plasterboard

2.4.3 Conclusions

It has been shown that the reduced properties method for the calculation of the mechanical resistance of timber frame members (studs or joists) in wall and floor assemblies can be replaced by the reduced cross-section method using zero-strength layers instead of modification factors for fire. This will simplify design work. For members in bending, the bending resistance according to the reduced cross-section agrees well with results from the reduced properties method since the zero-strength layers were determined to achieve the best fit for load ratios in the range between 0,2 and 0,4 which is most important in practice. Only for load ratios smaller than 0,2 the results are slightly non-conservative. For axially loaded members the calculated resistance is somewhat greater according to the reduced cross-section method when the method for axially loaded members given in EN 1995-1-1 [4] is used, however with properties relevant for the fire situation. Since the zero-strength layer is equivalent to the modification factors for fire, the difference between the calculated axial resistances is mainly due to the different weighting of parameters (such as slenderness ratios, relative slenderness ratios, area, etc.) in the expressions given in EN 1995-1-1.

3 References

- [1] EN 1995-1-2:2004 Eurocode 5: Design of timber structures – Part 1-2: General – Structural fire design. European Standard. European Committee for Standardization, Brussels, 2004.
- [2] Östman, B., König, J., Mikkola, E., Stenstad, V., Carlsson, J., and Karlsson, B., Brandsäkra trähus. Version 2. Trätek, Swedish Institute for Wood Technology Research, Publ. No. 0210034, Stockholm, 2002.
- [3] König, J, Timber frame assemblies exposed to standard and parametric fires. Part 2: A design model for standard fire exposure. Trätek, Swedish Institute for Wood Technology Research, Report nr 0001001, Stockholm, 2000.
- [4] EN 1995-1-1:2004 Eurocode 5: Design of timber structures – Part 1-1: General – Common rules and rules for buildings. European Standard. European Committee for Standardization, Brussels, 2004.

**INTERNATIONAL COUNCIL FOR RESEARCH AND INNOVATION
IN BUILDING AND CONSTRUCTION**

WORKING COMMISSION W18 - TIMBER STRUCTURES

**FIRE EXPOSED CROSS-LAMINATED TIMBER
- MODELLING AND TESTS**

J Schmid

J König

SP Trätek/Wood Technology

SWEDEN

MEETING FORTY THREE

NELSON

NEW ZEALAND

AUGUST 2010

Presented by J Schmid

H Blass: one dimensional model should not apply to lintel. J Schmid: It does not.

S Winter does not agree with statement that EC5 is unsafe. Fire design always is rough prediction and 10% difference should be acceptable. In multi-span, d_0 would be different for tension and compression portion; this would be too complicated. J Schmid: this is what is done for concrete design.

S Winter: predictions are for strength. What about deflection governed designs?

S Aicher: do figures apply to CLT with glued edges? J Schmid: if edges are opened, charring rate increases.

S Winter: charring rate is hard to establish. Higher if edges are open but char expands and closes gaps.

B Yeh: is the delamination layer important? J Schmid: Yes, as the charring rate will increase for a while.

Fire Exposed Cross-Laminated Timber - Modelling and Tests

Joachim Schmid, Jürgen König,
SP Trätekt/Wood Technology, Sweden
Jochen Köhler,
ETH Zurich, Switzerland

1 Abstract

This paper presents a simple design model using the effective cross-section method for the structural fire design of CLT, i.e. the determination of the mechanical resistance with respect to bending (floors).

Performing advanced calculations for a large number of lay-ups of various lamination thicknesses, using the thermal and thermo-mechanical properties of wood, charring depths and the reduction of bending resistance of CLT were determined as functions of time of fire exposure. From these results zero-strength layers were derived to be used in the design model using an effective residual cross-section for the determination of mechanical resistance.

The model also takes into account different temperature gradients in the CLT in order to include the effect of slower heating rate when the CLT is protected by insulation and/or gypsum plasterboard. The paper also gives results from fire-tests of CLT in bending using beam strips cut from CLT with adequate side protection in order to achieve one-dimensional heat transfer. Reference tests at ambient temperature were performed to predict the moment resistance of the beams being tested in fire.

2 Introduction

2.1 General

When EN 1995-1-2 [1] was drafted, it was believed that the reduced cross-section method could be applied to timber slabs exposed to fire on one side using a zero-strength layer of 7 mm originally calculated for three sided fire exposure by Schaffer et al. [2]. It was not intended that the reduced cross-section method could be applied to this new type of construction without further investigation. In a preliminary study [3] on timber decks in bending, it was shown that the application of a zero-strength layer of 7 mm would give unsafe results in many applications.

2.2 The reduced cross-section method for CLT

For structural fire design EN 1995-1-2 [1] introduces a simplified method for large timber members exposed to fire on three or four sides, the residual cross-section method. Although, for unprotected cross-sections, as approx. 40 mm below the char layer are affected by elevated temperature, the depth of the zero-strength layer, assumed immediately below the char layer, is only 7 mm which compensates strength reduction in the heated zone of the member. For the remaining effective residual cross-section ambient strength and stiffness properties are to be applied.

Since the zero strength layer in general is a function of the temperature profile and the geometry of the cross-section, appropriate values were derived for the reduced cross-section method for CLT. In the fire situation the joints between two adjacent CLT panels are assumed to be capable of transferring shear forces but not bending moments. Therefore CLT panels are assumed to be supported on two opposite edges resulting in that layers in the transverse direction are not regarded as load-bearing in the longitudinal direction.

The charring for CLT may show larger depths than the depth of the exposed outer layer of the CLT which may lead to a zero-strength layer immediately below the char layer which may also comprise a part of a non load bearing cross layer. This leads subsequently to the need of higher values for the zero-strength layer in some cases, see Figure 1. The latter explains parts of the increase of the values for the zero-strength layer for CLT.

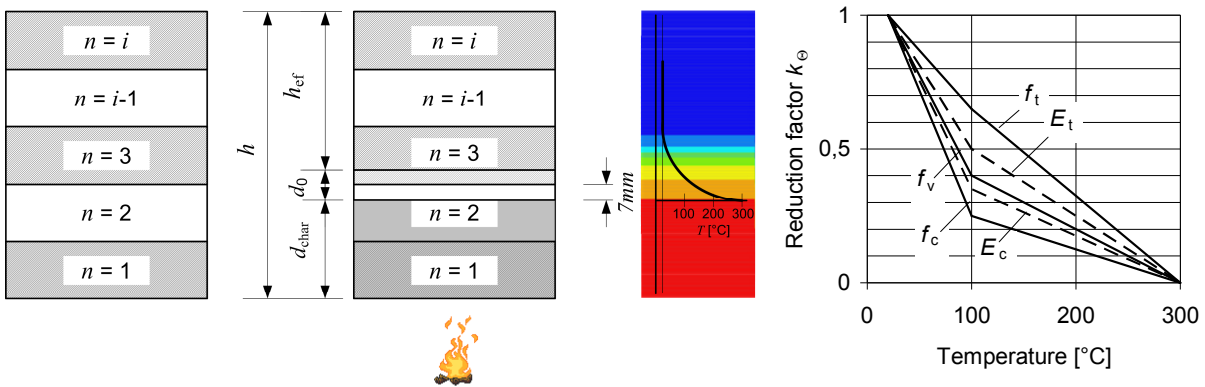


Figure 1: Effective residual cross-section obtained after reduction of original cross-section (left) with charring depth d_{char} and zero strength layer d_0 (middle) with a schematic temperature profile for unprotected CLT if 7 mm of a cross layer remain uncharred. Reduction factors for strength and stiffness properties according to EN 1995-1-2 [1] (right).

The cross-section and the corresponding temperature profile in Figure 1 show that a zero-strength layer of 7 mm would lead, obviously, to unsafe design for CLT panels in this case since the heated zone reaches already into the next load bearing layer. Table 1 gives selected results for zero-strength values for CLT in floors exposed on one side. For CLT in walls and protected CLT see [4]. As given in [1] values for the zero-strength layer of Table 1 rise linearly during the first 20 minutes of fire exposure.

Table 1: Zero strength layer d_0 in mm for CLT where h is in mm.

Exposure on	3 layers	5 layers	7 layers
Tension side	$\frac{h}{30} + 3,7$ (1)	$\frac{h}{100} + 10$ (2)	For $h > 175$ mm: $\frac{h}{35} + 6$ (3)
Compression side	$\frac{h}{25} + 4,5$ (4)	$\frac{h}{20} + 11$ (5)	For $h > 175$ mm: 10

3 Determination of model parameters

3.1 Thermal analysis

The thermal analyses were performed using SAFIR 2007 [5] using thermal properties of wood given by EN 1995-1-2 [1]. The thermal properties of gypsum plasterboard were similar to those given in [6], however further calibrated to fit test results, see [4].

3.2 Structural analysis

For the structural analysis, a computer program CSTFire, written as a Visual Basic macro embedded in Excel, was developed, using the temperature output from the heat transfer calculations and the relative strength and stiffness values given by EN 1995-1-2 [1], i.e. compressive and tensile strengths, f_c and f_t , and moduli of elasticity in compression and tension, E_c and E_t . These values are given as bi-linear functions of temperature from 20 to 300°C with breakpoints at 100°C, also taking into account the effects of transient moisture situations and creep, see Figure 1. The software takes into account the possibility of permitting ductile behaviour of wood under elevated temperature. Contrary to ambient conditions where failure on the tension side of a beam is brittle, in the fire situation tensile failure of the outermost fibres won't cause immediate collapse of the member since a redistribution of internal stresses will take place as long as equilibrium is maintained.

Since the reduction of strength and stiffness properties is different for tension and compression, CSTFire uses an iteration process, increasing the curvature of the member until the maximum moment resistance is reached. The element size used for the thermal and structural analysis was chosen as 1 mm × 1 mm.

The calculations were conducted assuming material properties that are representative for timber deck plates used in practice, using a bi-linear stress-strain relationship. Since the values of tensile and compressive strength of solid timber given in design or product standards, e.g. EN 338 [7], are values related to the whole cross-section and were determined on the assumption of a linear relationship between stress and strain until failure, the use of these values in a finite element analysis would not be correct [6]. Therefore, compressive strength values were determined using the data from Thunell [8] dependent on density and moisture content as shown in [5]. For the timber slabs assumed here the compressive strength was $f_c = 30 \text{ N/mm}^2$, while the tensile strength was taken as $f_t = 27 \text{ N/mm}^2$, that is the ratio of f_t/f_c is 0,9. The results of simulations of cross-laminated timber slabs were taken from [4]. These calculations were made assuming $f_t/f_c = (0,92)$. Since the ratio has only a small influence on the results, it can be neglected for practical application. For layers with the grain direction perpendicular to the longitudinal direction of the plate (cross-layers), the modulus of elasticity was assumed to be zero, while these layers were assumed to be completely effective with respect to shear stiffness, i.e. complete composite action of the longitudinal layers was assumed. This assumption is justified by the slenderness ratios of CLT occurring in practice. For deck plates of thickness 150 mm and a span of 5,5 m, the slenderness ratio is 30. Due to shear deformations the maximum bending stress is increased by about 3 % [9]. Since the slenderness ratio in fire – due to charring – is somewhat greater than under ambient conditions, the increase of bending stresses due to shear deformations would be less than 3 %. This influence is neglected in the model presented here.

The calculations were carried out for members in bending with depths from 45 to 315 mm, layer thicknesses from 15 to 45 mm and layer numbers from 3 to 7, both for unprotected and protected CLT, and both for the fire-exposed side in tension or compression. Both regular and irregular lay-ups were studied, i.e. regular lay-ups with equal layer thicknesses of longitudinal

and cross-layers, and irregular ones where layer thicknesses of longitudinal and cross-layers were different. In all cases, however, all longitudinal layers had the same thickness and the lay-ups were symmetrical.

3.3 Results

In the following, for unprotected CLT with five layers of 20 mm thickness, the results of the computer simulations are shown as relationships between the bending moment ratio M_{fi}/M and time t and charring d_{char} , respectively and zero-strength layer d_0 and time and charring d_{char} , respectively, see Figure 2.

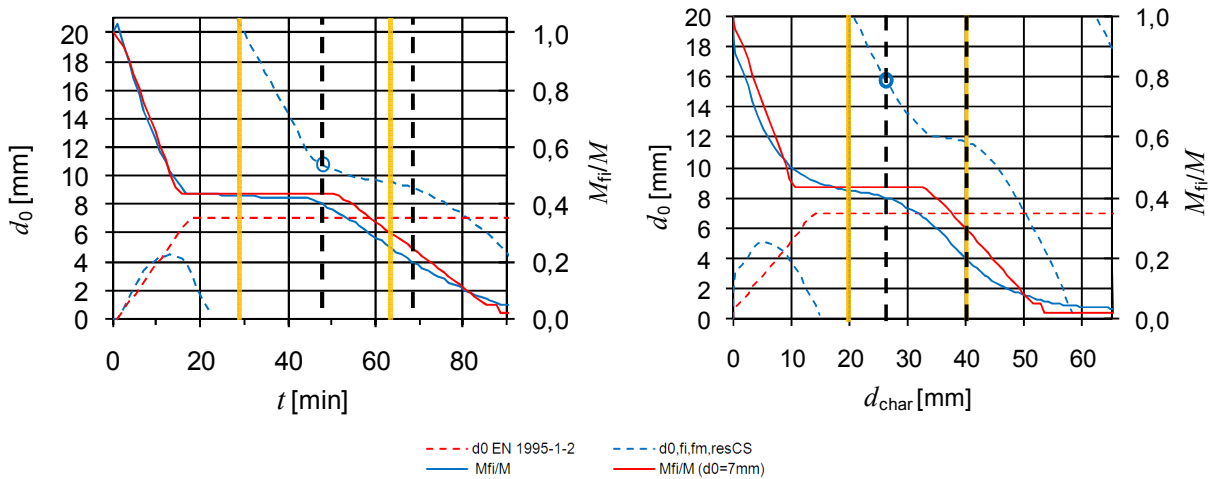


Figure 2 – Results for CLT with 5 layers of thickness 20 mm with the fire-exposed side in tension (left) and compression (right); results given as function of time (left) and charring (right). The yellow bars indicate charring of bondlines. The black broken bars indicate the 20 and 40 % levels of bending resistance.

For the examples shown here, during the first charring phase when charring takes place in the first layer, the bending resistance is reduced to approximately forty percent of ambient resistance. During charring in the second (non load-bearing) layer the bending resistance falls under forty percent: the decay is very slow, but increasing considerably before the char front has reached the second bond line and the next load bearing layer, respectively. At that stage the bending resistance has dropped to twenty-five to twenty percent, depending on the state of stress on the fire-exposed side. When the fire-exposed side is in compression, the reduction of bending resistance is greatest. The charts also show the corresponding zero-strength layers d_0 that should be applied to the cross-section to get the same results using ambient strength and stiffness properties for the effective residual cross-section. Since the value of d_0 varies considerable with time (or charring depth d_{char}), in order to simplify the design model, the largest value within the bending resistance interval between 20 and 40 percent was chosen. In Figure 2 these values are marked as rings: For the CLT panels shown, $d_0 = 10,5$ mm for the fire-exposed side in tension and $d_0 = 15,9$ mm for the fire-exposed side in compression. From the charts can be seen that, for the most relevant stage of relative resistances from 0,2 to 0,4, $d_0 = 7$ mm given by EN 1995-1-2 [1] for beams and columns would give non-conservative results in comparison with the results from the simulations.

This calculation was carried out for a large number of lay-ups with three, five and seven layers. The data for d_0 where the plotted as functions of the depth h of the CLT plate depending on the number of layers, for five layer CLT see Figure 3.

The trendlines, somewhat modified and simplified, are given for unprotected CLT with five layers where the fire-exposed side is in tension and compression as:

$$d_0 = \frac{h}{100} + 10 \quad (2) \quad \text{and} \quad d_0 = \frac{h}{20} + 11 \quad (5) \quad (d_0 \text{ and } h \text{ in millimetres}).$$

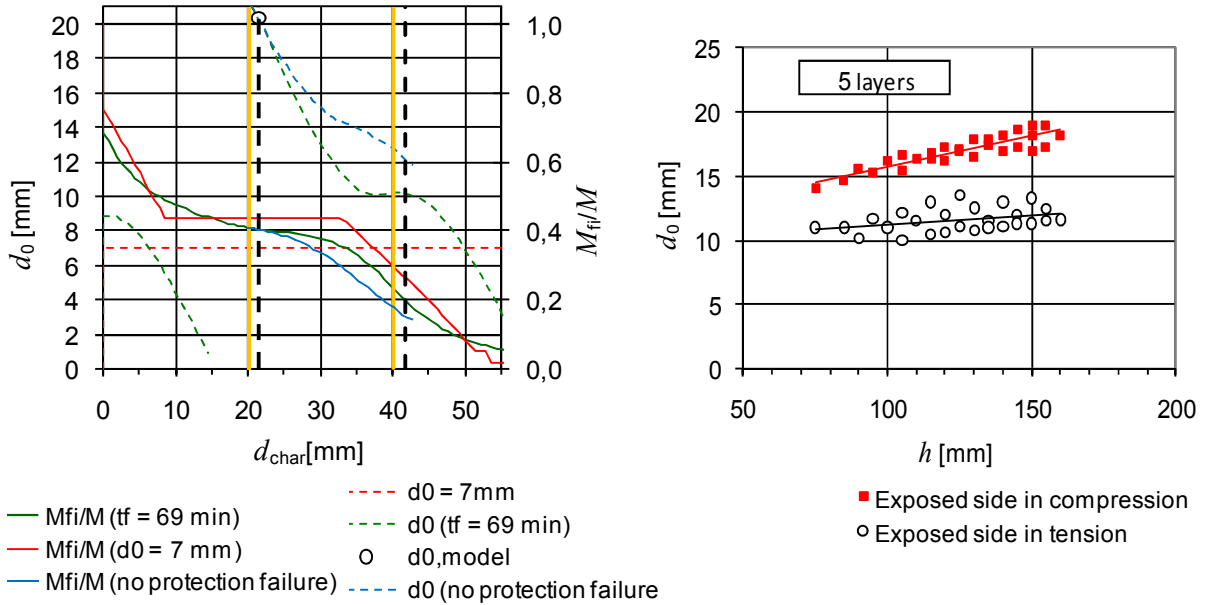


Figure 3 – Same CLT as before but protected, exposed side in compression, results given as functions of charring depth d_{char} (left). Determination of linear expression for zero-strength layer d_0 vs. plate depth for unprotected CLT (right).

The simulations for protected CLT were carried out for a large number of regular lay-ups and protective claddings consisting of one layer (12,5 mm or 15,4 mm thick) or two layers 12,5 + 15,4 mm thick gypsum plasterboard considering different failure times. Long protection times lead to small temperature gradients where ambient temperature is reached in larger depths which may result in higher values for d_0 . Contrary char ablation which exposes following layers directly to fire without a protective char layer would lead to high gradients which may lead to lower values for d_0 . It can be assumed that the presented functions for d_0 would lead to conservative design in these cases, a decrease of d_0 should not be considered since char ablation may be a local effect.

4 Tests

In order to verify the model by tests, two five layer CLT products currently being on the market were chosen. The width of all specimens was 150 mm. The specimens of series M had layers of equal thickness (regular lay-up), i.e. the total thickness was 95 mm, while the lay-up of series S with a thickness of 150 mm was irregular, see Figure 4. Series M was produced without joints in lamellas, series S had no finger joints in the lamellas on the exposed side to avoid influence of finger joints on bending resistance in fire [10].

The width and length of the specimens chosen was governed by the test conditions in the fire situation. Both are considerably smaller than required for testing of CLT products. EN 789 [11] requires a span of 32 times the depth of the CLT panel, while the minimum width required by the standard is 300 mm. A sample of each product was subdivided into two groups, one of which was tested in fire (series MF and SF) while the other was tested at ambient conditions (series MR and SR) in order to provide data for the prediction of the

ambient bending moment resistance of the specimens to be tested in fire. All test specimens were conditioned at 20°C and 65 % relative humidity before reference and fire tests.

4.1 Reference Tests under ambient conditions

The ambient reference tests were carried out as four-point ramp load tests. For series SR the span was 2,7 m and the two point loads were acting at the third points (0,9 m + 0,9 m + 0,9 m). For series MR, in order to reduce the risk of shear failure, the distances were chosen to be equal as in the fire tests (0,9 m + 1,5 m + 0,9 m), see Figure 5. The number of reference tests was 10 (series MR) and 15 (series SR), respectively.

Two different failure modes were observed, either tensile failure in the outer lamella or shear failure in one or two of the cross-layers. The results are shown in Figure 4. In series MR one out of 10 specimens failed due to shear failure while the rest failed due to tensile failure. In Series SR seven specimens failed due to tensile failure and eight specimens due to shear failure. Since shear failure was not expected in the fire tests and is not a relevant failure mode in the simulations and the design model, the results of series SR and MR were evaluated with respect to the relevant failure mode “failure of tensile lamella”. The parameters of a lognormal distribution have been estimated by using the censored using the Maximum Likelihood Method [12].

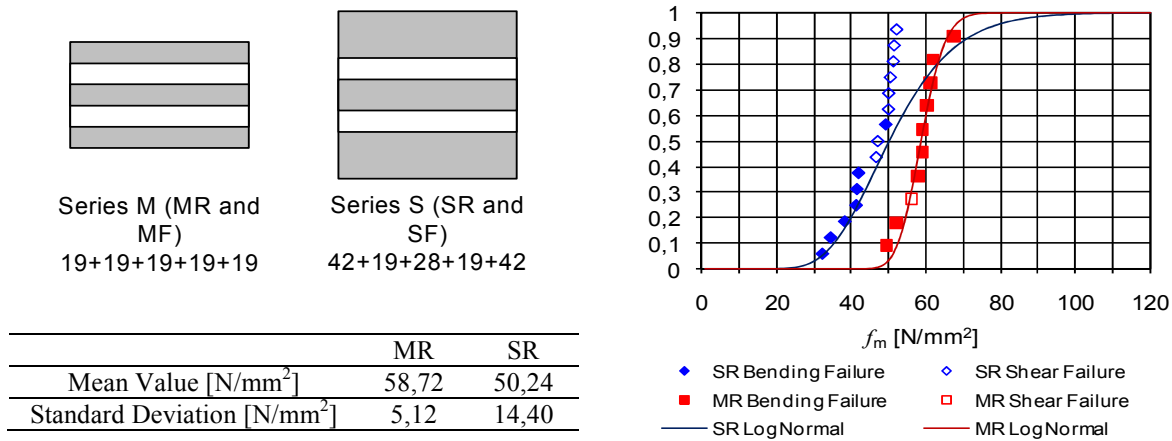


Figure 4 – Build up of the two test series M and S, results from ambient reference tests for series MR and SR plotted together with the corresponding probability distributions (LogNormal, parameters obtained with censored maximum likelihood).

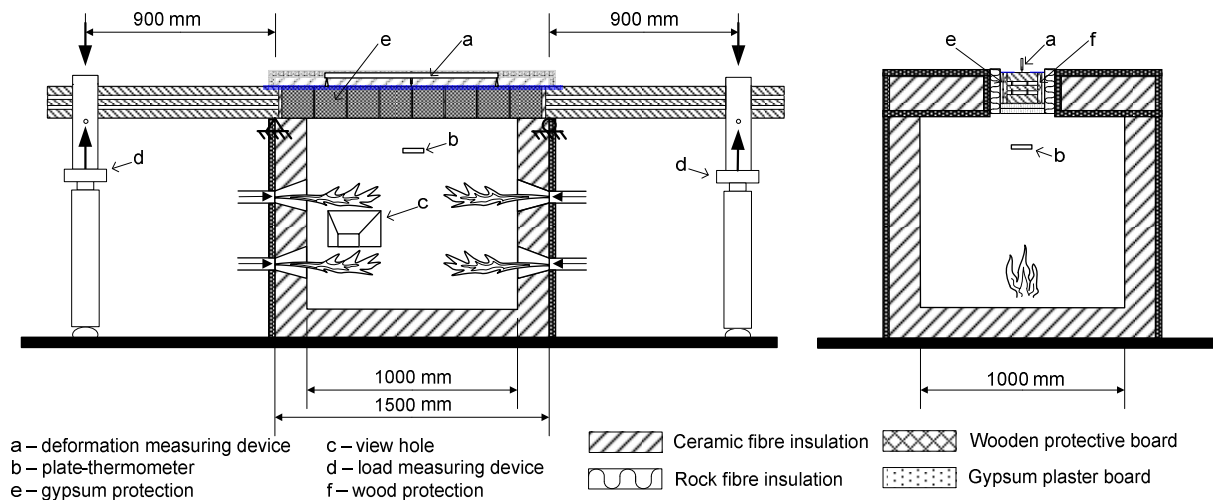
4.2 Fire tests under standard fire exposure

Fire tests of specimens in bending were performed for the following cases:

- Unprotected timber; fire-exposed side in tension (tsw);
- Unprotected timber; fire-exposed side in compression (csw);
- Protected timber; fire-exposed side in tension (tsw);
- Protected timber; fire-exposed side in compression (csw).

In order to simulate the thermal conditions in a CLT plate in fire, i.e. the one-dimensional heat flux, and consequently one dimensional charring, the edges of the beam specimens were protected by a first layer of 20 mm thick pieces of wood with the grain in longitudinal direction and a second layer of 15 mm thick pieces of gypsum plasterboard type F, all of them fixed with nails. These layers were discontinuous in order to prevent composite action, with gap widths of 1 mm. Where the CLT beams were protected, 150 mm long pieces of gypsum plasterboard type F were screwed to the bottom face of the beams with 1 mm gaps between

the pieces. The supports of the specimens were located on the furnace walls outside the heated zone of one metre, see Figure 5. The loads could be applied in upward or downward direction. A measuring device was placed on top of the specimens for measuring the deflection within a gauge length of 900 mm.



At bending failure or when the load could not be held constant, the burners were turned off, the specimen removed from the furnace and the fire in the wood extinguished with water. The time elapsed from turning off the burners to extinguishing the fire was normally from 1 to 1,5 minutes.

From each of the test specimens, at five locations, photographs were taken of the cross-section after the fire test, see two examples shown in Figure 6. Specimen SF 11 (left) was unprotected while specimen SF 12 (right) was protected. Especially for protected beams it was difficult in some cases to achieve one-dimensional heat flux and charring over the whole width of the beams, due to opening of wide gaps between the bottom and side protection.

Comparisons of test results with the simulations using the dimensions of the test beams are shown in Figure 7 and Figure 8 with relationships of the bending resistance ratio versus charring depth.

model was fitted to give best results in the range of a relative bending resistances between 0,2 and 0,4, the values are only shown for this interval.

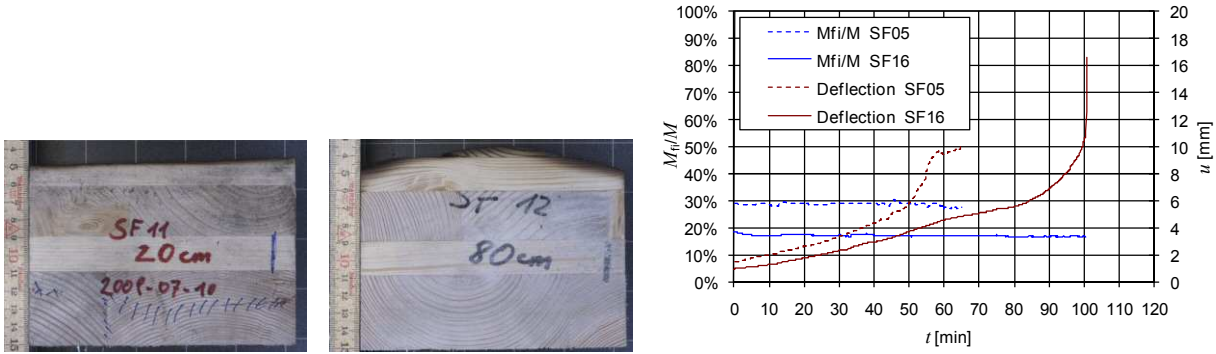


Figure 6 – Examples of residual cross-sections after fire test (left, middle), recorded deflection and load for an excluded test (SF05) and included test (SF16) (right).

In general, the test results agree fairly well with the simulations. Some deviations are, however, noticeable. A more in-depth analysis of the specimens after fire tests showed that some specimens exhibited local deficiencies of charring depth, caused by char ablation or other (excluded test results are marked with not filled dots in Figure 6).

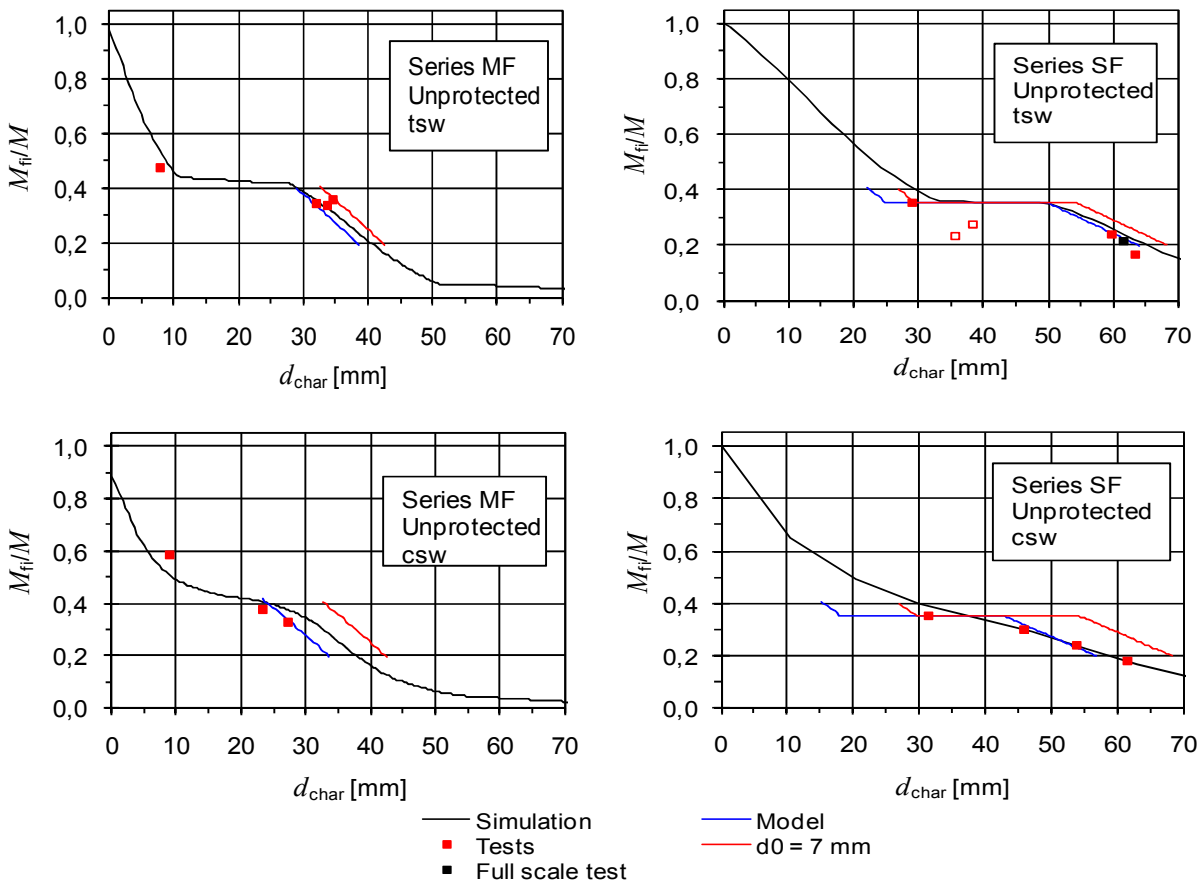


Figure 7 – Comparison of test results for unprotected CLT with simulation and the simplified design model for series MF (left column) and series SF (right column). Exposed side in tension (tsw) at the top row and exposed side in compression (csw) below.

This may have caused lower bending resistances of some tests shown in Figure 7 (SF, unprotected, tsw). Such local deficiencies are more effective in narrow beams; it can be

argued that CLT of sizes used in practice are less vulnerable to local defects. Furthermore the load and deflection measurements were used to detect outliers see Figure 6.

The university of Trieste performed one full scale test with CLT of series S, including eight reference tests and a fire test with a free span of 5,0 m. In the fire test the CLT was loaded with 21,6 % of the load bearing capacity. The result confirms the value of the model scale tests and the simulation result with a failure at ca. 100 minutes, see Figure 8.

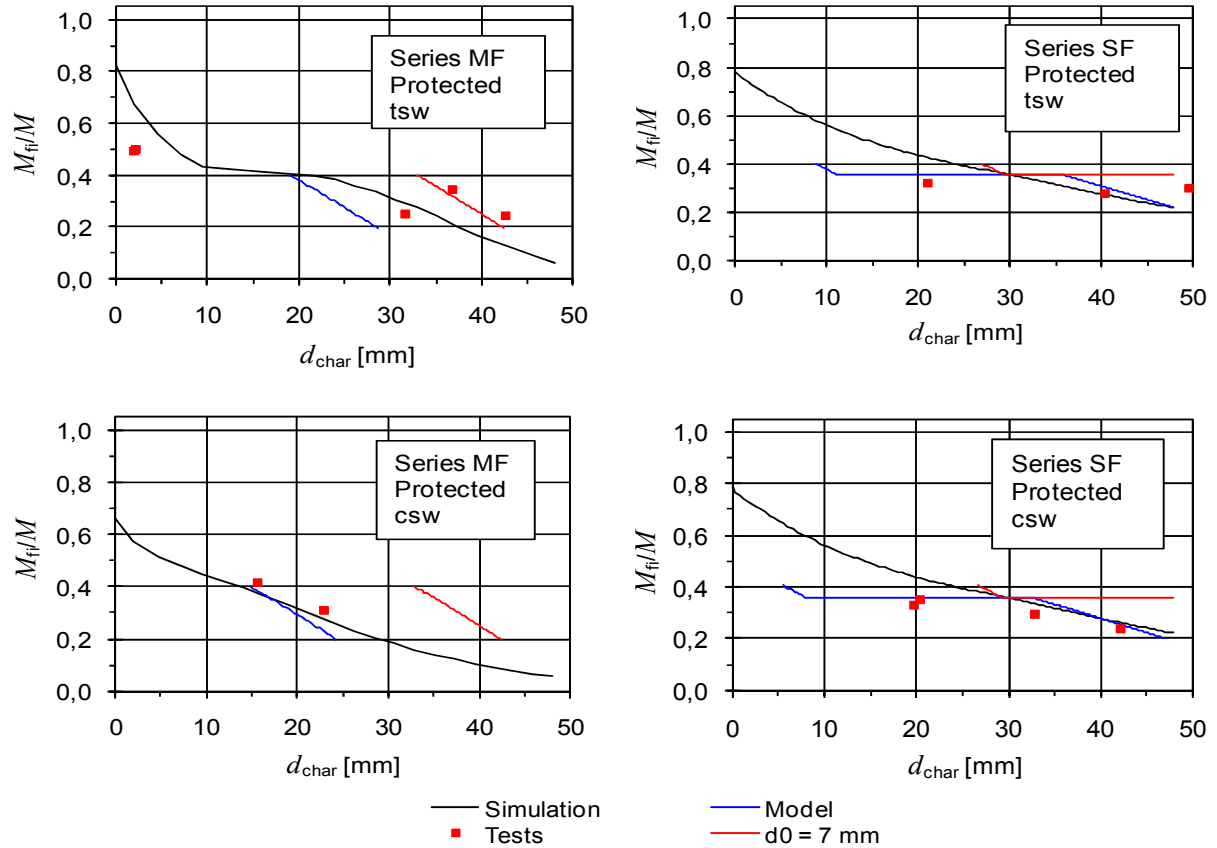


Figure 8 – Comparison of test results for protected CLT with simulation and design model for series MF (left column) and series SF (right column). Exposed side in tension (tsw) at the top row and exposed side in compression (csw) below.

The simplified model for the zero-strength layer normally gives conservative results compared with the simulations, except for protected CLT. Non-conservative deviations are due to the assumption that the cladding would fall off after some time; during the fire tests, however, the protective cladding remained in place during the fire tests. The assumption of a zero-strength layer equal 7 mm gives unsafe results, especially when the fire-exposed side is in compression.

5 Conclusions

It has been shown that the complex performance of CLT exposed to fire can be described by advanced computer simulations, using the thermal and thermo-mechanical properties of wood given by EN 1995-1-2 [1] and that the simulation results are verified by test results from fire tests. In order to present a user-friendly easy-to-use design model for members in bending, the concept of the reduced cross-section method given in [1] was adopted and zero-strength layers determined for consideration of the reduced strength and stiffness properties at elevated

temperatures. The simplified model gives reliable results, while the adoption of the zero-strength layer equal to 7 mm, as given in EN 1995-1-2 [1] for beams and columns, normally gives non-conservative results.

6 Acknowledgement

The research described here was conducted at SP Trätekt, Stockholm, as a part of the FireInTimber project within the European Wood-Wisdom-Net framework. It is supported by industry through the European Initiative Building With Wood and public funding organisations. The test specimens were produced and delivered by Martinsons Trä (Sweden) and Stora Enso Austria. A part of the fire tests were assisted, evaluated and reported by Per Willinder to be included in his Bachelor thesis.

7 References

- [1] EN 1995-1-2:2004, Eurocode 5: Design of timber structures – Part 1-2: General – Structural fire design. European Standard. European Committee for Standardization, Brussels, 2004.
- [2] Schaffer E.L., Marx C.M., Bender D.A. , Woeste F.E, Strength Validation and Fire Endurance of Glued-Laminated Timber Beams, Research Paper FPL 46 US Department of Agriculture, 1986
- [3] König, J, Schmid, J, Bonded timber deck plates in fire. CIB W18, Meeting 40, Bled, Slovakia. Lehrstuhl für Ingenieurholzbau, University of Karlsruhe, Karlsruhe, Germany, 2007.
- [4] Schmid, J, König, J, Cross-laminated timber in fire. In preparation, SP-Report 2010:11, Stockholm, 2010.
- [5] Franssen, J.M, Kodur, V.K.R., Mason, J., User's manual for SAFIR 2004 – A computer program for analysis of structures subjected to fire. University of Liege, Department Structures du Génie Civil – Service Ponts et Charpentes. Liege, Belgium, 2005.
- [6] Källsner, B. and König, J., Thermal and mechanical properties of timber and some other materials used in light timber frame construction. Proceedings of CIB W18, Meeting 33, Delft, Lehrstuhl für Ingenieurbau, University Karlsruhe, Karlsruhe, Germany, 2000.
- [7] EN 338:2003, Structural timber – Strength classes. European Standard. European Committee for Standardization, Brussels, 2003.
- [8] Thunell, B., Hållfasthetsegenskaper hos svenskt furuvirke utan kvistar och defekter. Royal Swedish Institute for Engineering Research, Proceedings No. 161, Stockholm, 1941.
- [9] Blass, H, Görlacher, R, Brettsperrholz – Grundlagen. Holzbau-Kalender 2. 2003 (2002) S. 580-598.
- [10] König, J, Norén, J, Sterley, M, Effect of adhesives on finger joint performance in fire. CIB W18, Meeting 41, St. Andrews, Canada. Lehrstuhl für Ingenieurholzbau, University of Karlsruhe, Karlsruhe, Germany, 2008.
- [11] EN 789:2004, Timber structures – Test methods – Determination of mechanical properties of wood based panels. European Standard. European Committee for Standardization, Brussels, 2004.
- [12] Steiger, R, Köhler, J. Analysis of censored data – examples in timber engineering research. Proceedings of CIB W18, Meeting 38, Karlsruhe, Lehrstuhl für Ingenieurbau, University Karlsruhe, Karlsruhe, Germany, 2005.
- [13] Fiori, S., Analisi Numerico-sperimentale di pannelli di solaio in legno lamellare incrociato esposti al fuoco, Master Thesis, University of Trieste, 2009.

**INTERNATIONAL COUNCIL FOR RESEARCH AND INNOVATION
IN BUILDING AND CONSTRUCTION**

WORKING COMMISSION W18 - TIMBER STRUCTURES

TIMBER-CONCRETE COMPOSITE FLOORS IN FIRE

J O'Neill

D Carradine

R Dhakal

P J Moss

A Buchanan

University of Canterbury

NEW ZEALAND

M Fragiacomio

University of Sassari, Alghero,

ITALY

MEETING FORTY THREE

NELSON

NEW ZEALAND

AUGUST 2010

Presented by D Carradine

S Winter: how were LVL beams connected? D Carradine: screwed together

S Winter: where were screws located? D Carradine: too low! ~ 75 mm from the bottom. It is also important to use fully-threaded screws.

B Yeh: why use size of LVL and not 200 mm to verify theory developed? D Carradine: users of this technology wanted to verify the fire rating for cold designs.

B Yeh: fire regulation would not let extrapolation of results from 400 to 200. A Buchanan: in NZ, extrapolation is possible.

T Gibney: why use so much reinforcing steel in concrete topping? A Buchanan: to satisfy seismic design.

A Palermo: what about continuous slabs and the connection concrete/wood? D. Carradine: not to be considered at the moment (Need to assess priority of next variable).

Timber-Concrete Composite Floors in Fire

James O'Neill*, David Carradine*, Rajesh Dhakal*, Peter J. Moss*, Andy Buchanan*,
Massimo Fragiaco⁺

^{*}University of Canterbury, New Zealand

⁺University of Sassari, Alghero, Italy

1 Introduction

Timber-concrete composite floors are a combination of timber joists and concrete topping, creating a flooring system best utilising the advantages each material has to offer. Timber is used as the main tensile load bearing material due to its high strength-to-weight ratio, while concrete is used in floor slabs for its advantages in stiffness and acoustic separation. The strength of the system is dependent on the connection between timber and concrete, thus the connection must be strong, stiff, and economical to manufacture, to ensure that the flooring system is economically viable. The benefits in aesthetics, sustainability and economical savings due to fast erection time will undoubtedly be a significant factor to their widespread use in the future. Timber-concrete composite structures are not a new technology, and arose in Europe in the early twentieth century as a means of strengthening existing timber floors by the addition of a concrete slab. Due to the many advantages they possess over traditional timber floors, they are now being used in new construction [1-3]. This is currently under investigation in many parts of the world such as Sweden [1-3], the United States [4], Germany [5, 6], Switzerland [7] and New Zealand [8-11].

There are many different types of composite flooring design, the main two categories being either solid timber slab type designs or beam type designs.

Beam type designs consist of timber beams (either sawn timber, glulam or LVL) being used as floor joists, upon which a solid membrane (usually a plywood sheathing or steel deck) is fixed and a concrete slab is cast above. The forms of connections between the timber and concrete are extremely varied, some of which are glued, non-glued, and notched connections [8]. Glued connections consist of a form of steel reinforcement (rebars, punched metal plates, steel lattices) which is glued into the timber members and continues out into the concrete slab. Non-glued connections can consist of screws partially screwed into pre-drilled holes in the timber, inclined steel bars driven into tight holes, or shear studs screwed into the timber member. Notched connections consist of a notch cut out of the timber member which the concrete is cast into, and a stud can be incorporated in the notch for better performance. A number of these different types of connections have been investigated by Ceccotti [12], Lukaszewska et al. [1, 2] and Yeoh et al. [10].

Solid timber slab designs are generally composed of a solid timber decking from nailed timber planks with a concrete slab cast directly on top. Slab type floors generally utilise a grooved connection, the concrete is cast into grooves or trenches in the top of the timber

decking which allows a large shear area of concrete to timber to be utilised, resulting in a very stiff and complete composite connection. Kuhlmann and Michelfelder [5] have conducted extensive research on the strength and stiffness of grooved timber slabs.

The type of composite floor under study was a semi-prefabricated beam type system comprising of "M" panels that were built with laminated veneer lumber beams sheathed in plywood as permanent formwork for the concrete. The plywood had holes cut to accommodate the shear connection between the beams and the concrete slab. Both notched connections and toothed metal plates were used in this research. The panels can be prefabricated off-site then transported to site and craned into position, allowing the concrete slab to be cast in-situ.

2 Timber-Concrete Composite Floors in Fire

With the development of any new structural system, it is important to assess the fire safety of the system to ensure it can be used safely for its intended purpose. This is vital for timber systems, as a fire safety assessment can be a deciding factor in determining success or failure in the international market. Many countries have strict regulations and guidelines regarding the use of timber materials, hence it is important to have conducted fire safety tests on the system to ensure it can meet a required level of fire safety.

In the past, research has been conducted on the fire performance of many different types of timber-concrete composite floors, for instance Frangi and Fontana [13] have conducted fire tests on both beam and slab type composite floors. However the differing types of composite systems available in terms of material composition and structural design mean that different aspects of these systems will govern failure in fires. It is therefore important to identify what differences are present between tested and untested systems to determine what degree of scrutiny is required when researching the fire performance of a new system. This generally applies to beam type floors, as the fire performance of solid timber slab floors can generally be simplified down to the charring rate of the timber decking due to the one dimensional surface presented to the fire, as was found by Frangi and Fontana [13] when they fire tested a solid timber slab floor.

3 Test Specimen Details

The specimen construction and testing was carried out at the Building Research Association of New Zealand (BRANZ), located in Porirua, New Zealand. The full scale testing involved two floor units tested under scaled loads, the dimensions of each floor unit being identical apart from the beam depth and design load. A 300 mm deep LVL beam floor was designed with a nominal span of 5 m, and a 400 mm deep LVL beam floor was designed with a nominal span of 7 m. Although smaller and larger sizes of beams are available, and the floor spans can be designed up to 11 m, the floor designs tested were limited by the loading capabilities of the full scale furnace at BRANZ. A modification on the usual number of connections also had to be made to accommodate the 4 m span of the furnace, having only four notches or eight plates per beam, as opposed to the usual six notches or twelve plates. The general design of the composite floors used in the testing was based on the semi-prefabricated system under development at the University of Canterbury.

Each floor unit consisted of two 4.6 m long double Laminated Veneer Lumber beams spaced 1200 mm apart and fixed together with type 17 self-drilling screws. Two different connection types were used in each test specimen. The result of previous short and long term testing by Yeoh [10] and O'Neill [14] was a 50 mm deep by 300 mm long rectangular notch cut into each beam, with a 16 mm coach screw installed 100 mm into the centre of the notch. A detail of this notch type is shown in Figure 1(a). The other connection tested was toothed steel plates pressed between the double beams, protruding into the concrete slab. This is shown in Figure 1(b).

A 17 mm thick plywood sheathing was nailed to the top of the beams providing permanent formwork for the concrete topping. Upon this a 65 mm thick 30 MPa concrete topping was cast in the forms and through the steel reinforcement, filling the notched connections and through the steel plate connections. The addition of a concrete slab greatly enhances the acoustic separation of the floor, and also provides a more rigid floor diaphragm. For testing purposes the slab was separated at 1200 mm centres over the beams to ensure that each set of beams would act independently once the plywood had burned through.

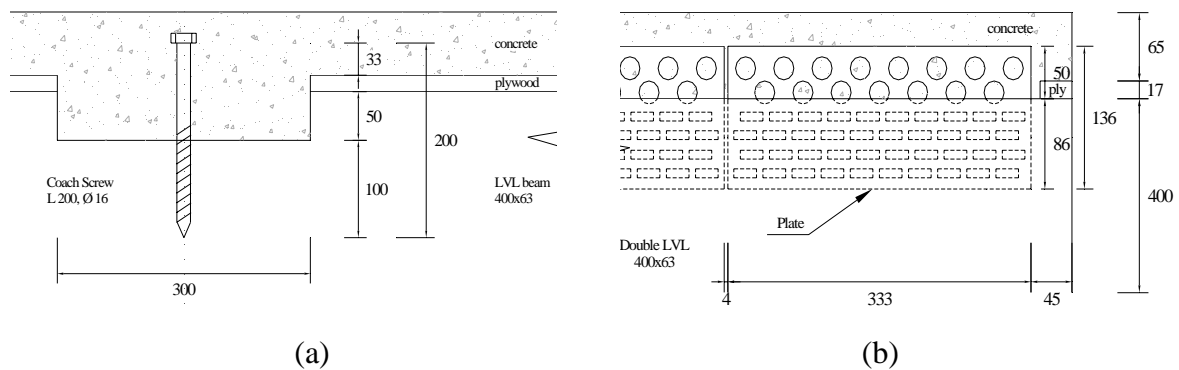


Figure 1: Design Detail of the Connections (dimensions in mm)

Thermocouples were placed in critical areas to allow for temperature data to be recorded at points of interest. The set of thermocouples to measure the temperature distribution through the beams were installed between the double beams. Thermocouples were also installed in the concrete, the connections, various composite interfaces and on the steel mesh. Six potentiometers were fixed to the loading rig and drawn down to the slab surface to measure the vertical displacement of the floors. These were approximately in line with the centrelines of the beams and spaced at third points across the floors.

4 Furnace Testing

4.1 Observations

The primary objective of the full scale testing was to investigate the failure behaviour of timber-concrete composite floors when exposed to fire. The failure mode of the floors was an important part of this as it would identify the critical component of the floor that governs the design for fire safety, whether it was a failure in the beams, the concrete slab or the connections between the two. Other important areas of interest were the charring behaviour of the timber beams, the spalling behaviour of the concrete, the fire damage about the connections and the performance of the plywood sheathing. The test fire was the ISO 834 standard test fire [15]. Due to their combustibility, timber beams cannot be scaled down in size as their fire behaviour is dependent on the actual cross-section present. This

required that the loads on the floor units be scaled up in such a way that similar stresses were induced in the load bearing members of the floor and the same bending moment at the midspan of the floors was obtained. Design loads for the test specimens were based on a live load of 2.5 kPa and the self weight of the floor only with no additional superimposed dead load.

The 300 mm beam floor failed at 75 minutes in the timber beam under the ISO 834 design fire and applied design load, and is shown in Figure 2 directly after furnace testing. The side with notched connections failed first, and the testing was terminated. The 400 mm beam floor test was stopped shortly after 60 minutes to assess the damage at that time and to provide insight into how the beams were charring before complete destruction. The initial and remaining section sizes are shown in Table 1. Measurements represented in the tables were taken from intermediate regions in the beams as the char depth across the beams was very uniform along the beams from inspection of the charred remains.



Figure 2: The Underside of the 300 mm Floor after Furnace Testing



Figure 3: Residual Section of the 400 mm Floor

5.2 Char Damage

Calculated average charring rates for each floor are shown in Table 2. The charring rate for the 400 mm floor beams were slightly higher than the 300 mm floor beams from both directions, and this was attributed to a deeper layer of char providing better insulation on the smaller floor beams, as deeper layers of char will reduce the charring rate of the timber. The deeper floor beams also exhibited centreline separation at the midline to a much greater degree than the smaller beams, allowing further charring to penetrate the bottom surface.

Table 1: Residual Beam Sizes Before and After Furnace Testing

Test Specimen	Size Before Furnace Testing (mm)		Size After Furnace Testing (mm)		Burn Time (min)
	Width	Depth	Width	Depth	
300 mm	126	300	44	130	75
400 mm	126	400	52	255	60

Table 2: Calculated Average Charring Rates for the Floor Beams

Test Specimen	Side Charring Rate (mm/min)	Bottom Charring Rate (mm/min)	Overall Charring Rate (mm/min)
300 mm	0.55	2.27	1.12
400 mm	0.62	2.42	1.22

The charring rate on the sides of the LVL beams was found to be 0.58 mm/min on average, lower than reported values of 0.72 mm/min based on research conducted by Lane [16] on similar LVL at the BRANZ facilities. This was most likely due to the double-tee configuration of the floor beams such that convection of flames and hot gases throughout the space was slightly impeded, and the nearest beam was spaced far enough away that re-radiation off this surface was not significant.

The charring rate on the underside of the beams was very high, being on average four times as large as the charring rate from either side of the beams. The majority of this charring occurred in the latter stages of burning once the residual section had been reduced to such a size that the central area of the timber beams had increased above the initial ambient temperature, thus increasing the rate of heating and burning of the remaining section.

Another important observation was the separation of the double beams after significant burning, that is each beam tended to splay outwards which induced extra charring on the insides of the beam sections and exposed the connections to further fire damage (Figure 3). This phenomenon was primarily caused by uneven drying of the timber beams and loss of integrity of fixing around the fasteners holding the beams together, and would have had a greater impact on the floor performance in the latter stages of testing when the residual section was smaller and closer to failure.

This means that slender beam members are obviously much more susceptible to structural failure earlier in fires as the core heating would be more rapid than a larger timber member. An inherent advantage of structural timber members is that much more redundancy can be designed into members without a major increase in material costs, when compared to other structural materials such as steel and concrete. Larger beam member sizes (especially width-wise) in the case of timber-concrete composite floors serve to drastically increase expected fire resistance. The overall charring rates shown in Table 2 are the average charring rates for three sided exposure for each beam.

It should be noted that the heat flow within the furnace was not entirely uniform across the floor unit, in that the action of pumping of fuel into the compartment via the sides of the furnace and extracting hot gases through the bottom at the centre of the compartment tended to induce hotter burning in the central region of the furnace. This was observed on the residual beam sections after furnace testing, as the char damage was more prevalent on the side of the beam facing the centre of the furnace. It was also reflected in the spall patterns on the underside of the concrete, as it was much more prevalent in the middle of the floor units compared with the edges.

5.3 Vertical Displacement

Average vertical displacement measurements of the potentiometers on the top of the slab at mid-span can be seen in Figure 4 and Figure 5.

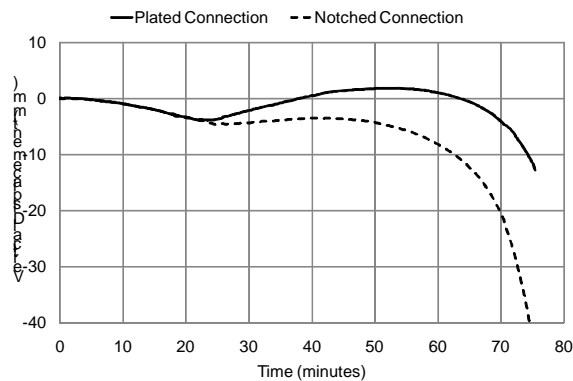


Figure 4: 300 mm Floor Displacement Results

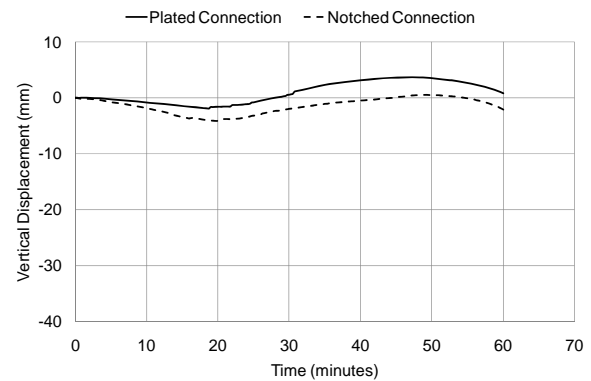


Figure 5: 400 mm Floor Displacement Results

From these measurements it is clear the 300 mm floor sections sagged for the first 23 minutes of testing due to applied loads and reduction in timber beam cross section. However, it can be seen for both sides of the floor that vertical displacement begins to decrease back towards the initial rest position. This behaviour is concurrent with the almost complete burning through of the plywood sheathing, and is probably due to heating of the underside of the concrete slab.

As a significant thermal gradient was introduced across the depth of the concrete, the bottom of the slab expanded due to the temperature increase. This behaviour was restrained by the LVL beam however due to the connections and resulting composite action, therefore a thermal bowing action was induced in the concrete slab that tended to hog the entire floor. This thermal bowing aided in resisting gravity loads imposed on the floors, and was essentially similar to the thrust force that can be developed via axial restraint [17]. This behaviour was more apparent on the side of the floor with plated connections, as the reduction in slip modulus due to fire exposure was much less than for the notched connections as the plates were well insulated from fire and therefore the effect of slab elongation was more significant. This resulted in less floor displacement, a more marked thrust force being developed and better fire resistance overall.

As seen for both floors tested, the displacement up to structural failure was less than 1/20 of the span (200 mm) and the rate of increase of displacement was low. Some common structural requirements specify deflections of less than 1/20 of the span or a limiting rate of deflection when deflection is 1/30 of the span [17], and on comparison the test floors were within these ranges. It should also be noted that for the 400 mm floor displacement measurements diverged at approximately 5 minutes. This was most likely attributed to the higher loads this floor, and coupled with a fast initial charring of plywood it is very likely that the plywood fractured at this time allowing each side of the floor specimen to separate along the structural gap.

6 Spreadsheet Design Tool

The spreadsheet design tool has been developed as a tool to aid in the understanding of how certain timber-concrete composite systems can perform in fires, and to provide a fast method of estimating the expected fire resistance time of a floor under user defined load

conditions and floor geometries. Design equations used for evaluating the strength of the composite floor in the spreadsheet was based on methods presented in Chapter 25 of the Timber Design Guide [8], which was developed in accordance with the Australian/New Zealand AS/NZS 1170 loading standard [18] and the New Zealand Timber Structure Standard NZS 3603 [19]. The spreadsheet tool, however, can be easily modified to incorporate the Eurocode 5 equations [20]. Due to the modular nature of the semi-prefabricated system, the most likely method of construction is to be craned in place and simply supported for their lifetime; hence the spreadsheet currently only takes into account a simply-supported floor. However, as the spreadsheet has been written to be relatively user friendly, modifications to allow the evaluation of different forms of support conditions can be easily made without a breakdown of the spreadsheet coding. The general design methodology of the spreadsheet is as follows:

The load combination for the floor system under fire is:

$$w = 1.0G + 0.4Q \quad (1)$$

G and Q being the permanent and imposed loads, respectively. The design bending moment at midspan, shear force at the supports and shear force at the span/4 from the supports are then calculated, L being the span length:

$$M^* = \frac{wL^2}{8} \quad V^* = \frac{wL}{2} \quad V_{L/4}^* = \frac{wL}{4} \quad (2) \quad (3) \quad (4)$$

The timber strength capacity at midspan is also found for tension and bending:

$$\phi N_R = \phi k_1 k_2 f_t A_t \quad \phi M_R = \phi k_1 k_4 k_5 k_8 f_b Z \quad (5) \quad (6)$$

where ϕ is the strength reduction factor, k_1 is the load duration factor, k_4 and k_5 are the load sharing factors, k_8 is the reduction factor for flexural buckling, f_t and f_b are the tensile and bending strength, A_t and Z are the cross-sectional area and section modulus, respectively. The effective flexural stiffness of the composite is evaluated by first calculating the concrete gamma coefficient γ_c [19] to evaluate the slip between the composites:

$$\gamma_c = \frac{1}{1 + \frac{\pi^2 E_c A_c s_{ef}}{K_{SL} L^2}} \quad \alpha_c = \frac{E_t A_t H}{\gamma_c E_c A_c + E_t A_t} \quad \alpha_t = H - \alpha_c \quad (7) \quad (8) \quad (9)$$

$$(EI)_{ef} = E_c I_c + E_t I_t + \gamma_c E_c A_c \alpha_c^2 + E_t A_t \alpha_t^2 \quad (10)$$

where E , A , I signify the modulus of elasticity, cross-sectional area, and second moment of area of the concrete (subscript c) and timber (subscript t), respectively, s_{ef} is the effective spacing among connectors, estimated as $s_{ef} = 0.75s_{min} + 0.25s_{max}$, s_{min} and s_{max} signifying the minimum and maximum spacing of connectors along the span length of the beam, respectively, H is the distance between the centroids of concrete and timber, K_{SL} is the slip modulus of the connector, and $(EI)_{ef}$ is the effective flexural stiffness of the composite section to allow for the flexibility of the connection. The timber stress σ_t due to the axial force is then calculated, along with the timber axial force N_t^* and bending moment M_t^* :

$$\sigma_t = \frac{E_t \alpha_t M^*}{(EI)_{ef}} \quad N_t^* = \sigma_t A_t \quad M_t^* = \frac{E_t I_t M^*}{(EI)_{ef}} \quad (11) \quad (12) \quad (13)$$

The combined bending and tension ratio of the composite floor is then found:

$$\frac{N_t^*}{\phi N_R} + \frac{M_t^*}{\phi M_R} < 1.0 \quad (14)$$

To evaluate the shear strength of the floors, the timber design shear strength can be found, and compared with the demand of shear force at the supports:

$$\phi V_s = \phi k_1 k_9 f_s \frac{2A_t}{3} \quad \phi V_s > V^* \quad (15) (16)$$

The connection profile used in the spreadsheet is a 300 mm long by 50 mm deep notch with an incorporated 16 mm coach screw implanted in the centre. From previous work conducted at the University of Canterbury on the shear strength of notched connection types, the shear strength at ultimate limit state Q_K was found [11,14]:

$$\phi Q_d = \phi k_1 Q_R \quad (17)$$

The demand of shear force in the connection at maximum shear, and at the span/4 from the supports is then calculated:

$$F_{max} = \frac{\gamma_c E_c A_c \alpha_c s_{min}}{(EI)_{ef}} V_{max} \quad F_{L/4} = \frac{\gamma_c E_c A_c \alpha_c s_{max}}{(EI)_{ef}} V_{L/4} \quad (18) (19)$$

The connection design shear strength must exceed the shear force demand:

$$\phi Q_d > F_{max} \quad \phi Q_d > F_{L/4} \quad (20) (21)$$

It should be noted that strength reduction factors k for the connection design strength and for other strength evaluations are different. These can also change depending on the situation, as in fire conditions the strength reduction factor is specified by NZS 3603 [19] as 1.0 for shear and bending, whereas it would be 0.9 for LVL in normal conditions.

To incorporate the effects of fire conditions into the spreadsheet the major portion of the calculations are set to run in a quasi steady state analysis. That is, mechanical properties of the floor are evaluated iteratively over a number of equal time intervals (in this case each minute) during which time t the effects of fire reduce the residual size of the timber beam and, consequently, the cross-sectional area $A_{t,res}$ and second moment of area $I_{t,res}$ to use in the aforementioned equations. No reduction in timber properties (strength f and modulus of elasticity E_t) was assumed inside the residual cross-section. Charring is based on an initial charring rate $v_c = 0.55$ mm/min, which is increased when the beam width drops to 60 mm. This bi-linear relationship was derived from full scale testing where increased bottom surface charring occurred during the latter stages of burning, and further details can be found in the relevant thesis [21].

A degradation of the slip modulus K_{SLS} and shear strength Q_K of the notched connection was assumed over the time of exposure to the fire t , based on the reduction of the vertical bearing area inside the notch at the timber-concrete interface due to timber charring:

$$K_{SLS}(t)/K_{SLS} = (b_t - 2v_c t)/b_t \quad Q_K(t)/Q_K = (b_t - 2v_c t)/b_t \quad (22) (23)$$

The spreadsheet requires the input of floor geometry, material properties, loading conditions and corresponding safety factors, and outputs an expected fire resistance time for the floor to fail. The spreadsheet was used to derive a number of resistance span tables for varying spans of these composite floors with regard to the varying section sizes available, and different combinations of live and superimposed dead loads. An example of this is shown in Table 3 for timber-concrete composite beams with the notch type connection discussed before and displayed in Figure 1(a).

Table 3: FRR Span Table from Spreadsheet Design Tool for Notched Connections

Fire Resistance Time (min) SDL = 0.5 kPa, Q = 2.0 kPa									
Beam Dimensions (mm)	Span (m)								
	4	5	6	7	8	9	10	11	12
200x45x2	39	37	-	-	-	-	-	-	-
240x45x2	43	41	-	-	-	-	-	-	-
300x45x2	48	46	39	-	-	-	-	-	-
360x45x2	-	50	44	40	-	-	-	-	-
400x45x2	-	-	47	43	39	-	-	-	-
450x45x2	-	-	-	46	42	39	-	-	-
600x45x2	-	-	-	-	52	48	45	42	39
200x63x2	70	68	62	-	-	-	-	-	-
240x63x2	74	72	66	-	-	-	-	-	-
300x63x2	80	77	71	66	-	-	-	-	-
360x63x2	-	81	76	71	67	-	-	-	-
400x63x2	-	-	79	74	70	67	-	-	-
450x63x2	-	-	-	78	74	70	67	-	-
600x63x2	-	-	-	-	84	80	77	74	71

Using a better form of connecting the double beams together, such as adhesives or fully threaded screws would serve to reduce the splaying effect previously mentioned and increase the expected fire resistance.

7 Conclusions

A design method has been proposed for timber-concrete composite floor systems with different types of connections. With the input of floor geometry, material properties, loading conditions and corresponding safety factors, the design method outputs an expected fire resistance time for the floor to reach structural failure. It was used to derive a number of resistance span tables for varying spans of these timber-concrete composite floor systems with regard to section sizes available and different combinations of live and superimposed dead loads. Two full-scale floors were fire tested. The reduction in section size of the timber beams due to charring governed the failure of the floors. Due to the composite action achieved by the connections, the floor units were able to withstand prolonged exposure to the test fire, well exceeding one hour. The effect of reduced section properties due to elevated timber temperatures was found to have a small impact on the overall performance of the test floors. Test data and visual observations aided in the development of an analytical model that is able to predict the expected fire resistance of these floors, taking into account some major time dependent variable properties, loading conditions, material properties and floor geometries.

In conclusion this research has shown that the fire performance of unprotected timber-concrete composite floor is excellent. A large degree of safety is possible without risking structural collapse, and this research should serve as a guideline to the expected performance. Further means of fire protection to these floors such as passive protection (fire rated suspended ceilings, gypsum plasterboard encasement) or active protection (sprinkler systems) will serve to further increase the fire resistance of these floors.

8 References

- [1] Lukaszewska, E., Fragiaco, M., Frangi, A.: Evaluation of the Slip Modulus for Ultimate Limit State Verifications of Timber-Concrete Composite Structures. Meeting 40 of the Working Commission W18-Timber Structures, CIB, International Council for Research and Innovation, Bled (Slovenia), paper No. CIB-W18/40-7-5, 14 pp., August 28-31, 2007.
- [2] Lukaszewska, E., Johnsson, H., and Fragiaco, M.: Performance of Connections for Prefabricated Timber-Concrete Composite Floors. *Materials and Structures*, RILEM, Vol. 41 No. 9, pp. 1533-1550, 2008.
- [3] Lukaszewska, E., Fragiaco, M., and Johnsson, H.: Laboratory Tests and Numerical Analyses of Prefabricated Timber-Concrete Composite Floors. *ASCE Journal of Struct. Engrg.*, Volume 136, Issue 1, pp. 46-55, 2010.
- [4] Fragiaco, M., Gutkowski, R.M., Balogh, J., Fast, R.S.: Long-Term Behavior of Wood-Concrete Composite Floor/Deck Systems with Shear Key Connection Detail. *ASCE Journal of Struct. Engrg.*, Volume 133, Issue 9, pp. 1307-1315, 2007.
- [5] Kuhlmann, U., Michelfelder, B.: Optimized Design of Grooves in Timber-Concrete Composite Slabs. *Proc. The 9th World Conference on Timber Engineering WCTE 2006*, Portland, Oregon, USA, CD, 2006.
- [6] Bathon, L., Bletz, O., Schmidt, J.: Hurricane Proof Buildings-An Innovative Solution using Prefabricated Modular Wood-Concrete-Composite Elements. *Proc. 9th World Conference on Timber Engineering*, Portland, Oregon, USA, 2006.
- [7] Frangi, A., Knobloch, M., and Fontana, M.: Fire Design of Timber-Concrete Composite Slabs with Screwed Connections. *ASCE Journal of Struct. Engrg.*, Volume 136, Issue 2, pp. 219-228, 2009.
- [8] Buchanan, A.H.: *Timber Design Guide*. Third Edition. New Zealand Timber Industry Federation Inc., Wellington, New Zealand, 2007.
- [9] Buchanan, A.H., Deam, B., Fragiaco, M., Pampanin, S., and Palermo, A.: Multi-Storey Prestressed Timber Buildings in New Zealand. *Structural Engineering International*, IABSE, Special Edition on Tall Timber Buildings, Volume 18, Issue 2, pp. 166-173, 2007.
- [10] Yeoh, D., Fragiaco, M., Buchanan, A., and Gerber, C.: A semi-prefabricated LVL-concrete composite floor system for the Australasian market. *Australian Journal of Struct. Engrg.*, Special Issue on Timber, Vol. 9 No. 3, pp. 225-240, 2009.
- [11] Yeoh, D., Fragiaco, M., De Franceschi, M., and Buchanan, A.: Experimental tests of notched and plate connectors for LVL-concrete composite beams. Submitted for possible publication in *ASCE Journal of Struct. Engrg.*, 2010.
- [12] Ceccotti, A.: Composite Concrete-Timber Structures. *Prog. Struct. Engng Mater.*, Vol. 4, Issue 3, pp. 264-275, 2002.
- [13] Frangi, A., Fontana, M.: Fire Behaviour of Timber-Concrete Composite Slabs. *Proc. The 5th World Conference on Timber Engineering*, Switzerland, August 17-20, 1998.
- [14] O'Neill, J.W.: A Study of the Connections in Timber-Concrete Composite Systems. Project Report in Civil Engineering, University of Canterbury, Christchurch, New Zealand, 2007.
- [15] ISO: Fire Resistance Tests - Elements of Building Construction. ISO 834: 1975, International Organisation for Standardisation.
- [16] Lane, W.P.: Ignition, Charring and Structural Performance of Laminated Veneer Lumber. Fire Engineering Research Report 05/3, University of Canterbury, 2005.
- [17] Buchanan, A.H.: *Structural Design for Fire Safety*. John Wiley & Sons Ltd., West Sussex, England, 2002.
- [18] AS/NZS: Structural Design Actions, Part 0: General Principles. AS/NZS 1170.0: 2002, Standards New Zealand.
- [19] NZS: Timber Structures Standard. NZS 3603: 1993, Standards New Zealand.
- [20] Eurocode 5: Design of Timber Structures, Part 1-1: General - Common Rules and Rules for Buildings. EN 1995-1-1: 2004, European Committee for Standardisation, Brussels.
- [21] O'Neill, J.W.: The Fire Performance of Timber-Concrete Composite Floors. Masters Thesis in Fire Engineering, University of Canterbury, Christchurch, New Zealand, 2009.

**INTERNATIONAL COUNCIL FOR RESEARCH AND INNOVATION
IN BUILDING AND CONSTRUCTION**

WORKING COMMISSION W18 - TIMBER STRUCTURES

**COMPARISON OF API, RF AND MUF ADHESIVES USING A
DRAFT AUSTRALIAN/NEW ZEALAND STANDARD**

B Walford

Timber Engineering Laboratory, Rotorua
NEW ZEALAND

**MEETING FORTY THREE
NELSON
NEW ZEALAND
AUGUST 2010**

Presented by B Walford

S Aicher: why re-invent new classification system and not adapt from European ones? B Walford: not reinvention but borrowing from others.

COMPARISON OF API, RF AND MUF ADHESIVES USING A DRAFT AUSTRALIAN/NEW ZEALAND STANDARD

Bryan Walford¹

ABSTRACT: Tests were done using MGP15 slash pine (i.e. non-standard) with an aqueous polymeric isocyanate (API), a resorcinol (RF) and a melamine-urea (MUF) adhesive to AS/NZS4364:2007 (Int)[1], for hydrolytical stability, shear block strength, delamination and creep. The API was found to have a durability intermediate between that of the RF and the MUF adhesives. The draft standard needs to be improved by deletion of the hydrolytic test that involves water bath and oven treatment of specimens. The delamination test could also be deleted as it gives information that is essentially the same as the boil/freeze/dry shear block test. The creep test needs modification to prevent specimens buckling.

KEYWORDS: Adhesives, durability, testing standard, Australasia

1 INTRODUCTION

An interim version of AS/NZS 4364 has been published. This standard is for use by manufacturers to classify glues for durability. Previously it was specific to phenolic and aminoplastic adhesives which are the traditional resorcinol and melamine-based adhesives but it has been amended to include a test for creep. This test was introduced with polyurethane and isocyanate adhesives in mind as these are believed to be susceptible to creep at elevated temperatures. The standard gives options from American and European standards and the tests selected from AS/NZS4364 were:

- Hydrolytic stability, using the method of ASTM 4502.
- Resistance to shear in the dry and wet states by compression.
- Hydro-mechanical response or resistance to delamination during exposure to wetting.
- Resistance to creep under static shear loading during exposure to high humidity, heat and combined heat and moisture.

2 SPECIMEN PREPARATION AND TESTING

Timber supplied for the tests was 600mm lengths of MGP15 [2] radiata and slash pines in 90x35mm

dimension. To achieve members of the required size, some initial lamination using resorcinol adhesive was necessary.

Briefly, the tests involve the following:

2.1 HYDROLYTICAL TESTS

280 modified conventional shear block specimens are made, each consisting of two pieces of timber 38mm along the grain, 25mm across the grain and 8mm thick, glued together with a 6mm overlap. Groups of 50 of these specimens are placed in water baths at temperatures of 60, 70, 77.5, 85 or 100 °C, or in ovens at 120, 130, 145, 160 or 170 °C. Groups of 10 specimens are removed at intervals, reconditioned to EMC (except the water bath specimens are tested wet), and tested in shear.

2.2 SHEAR BLOCK TESTS

90 conventional shear block specimens are made, each consisting of two pieces of timber 45mm along the grain, 50mm across the grain and 20mm thick, glued together with a 5mm overlap. 30 specimens are tested dry, 30 are wetted by vacuum/pressure soaking, and 30 are subjected to 7 boil/dry/freeze cycles with a final boil cycle. They are tested in shear in the condition they are when the conditioning is complete

2.3 DELAMINATION TESTS

6 specimens are made, each consisting of 6 laminations 19mm thick, 140mm across the grain and 75mm along the grain. The specimens are subjected to three cycles of vacuum/pressure wetting and oven drying. Delamination in the gluelines on the end grain surfaces is measured.

¹ Bryan Walford, Timber Engineering Laboratory, Scion, PB 3020, Rotorua, New Zealand 3046, Email: bryan.walford@scionresearch.com

2.4 CREEP TESTS

6 specimens are prepared as described in AS/NZS4364. These are placed under a constant compressive load using a spring loaded cage. Two loaded specimens are conditioned at 20°C and 95% relative humidity (RH) for 7 days then loaded (treatment A), two are conditioned at 20°C and 65% RH then loaded at 70°C and ambient RH for 7 days, (treatment B) while two are vacuum/pressure soaked, wrapped in clear flexible film to prevent moisture loss and loaded at 50°C for 28 days, (treatment C). Creep in the gluelines is measured.

3 RESULTS

3.1 HYDROLYTICAL TESTS

The relative decrease in strength in shear strength is shown in Figures 1 to 6 for the three adhesives in the dry and wet conditions.

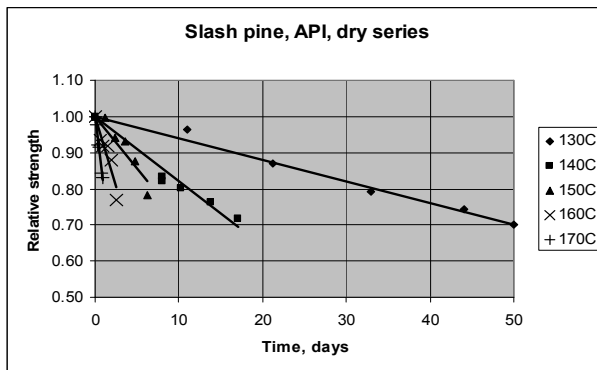


Figure 1: API adhesive, dry tests

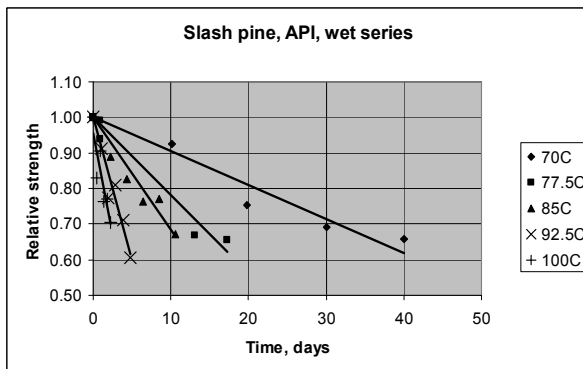


Figure 2: API adhesive, wet tests

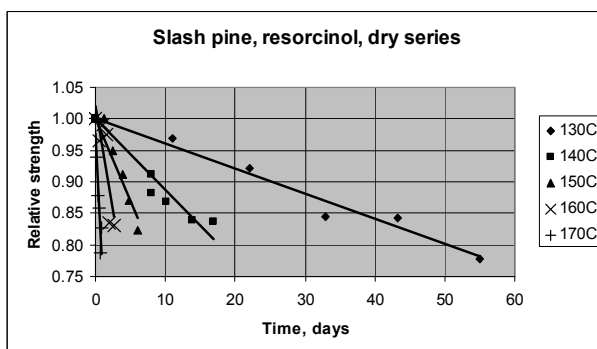


Figure 3: Resorcinol adhesive, dry tests

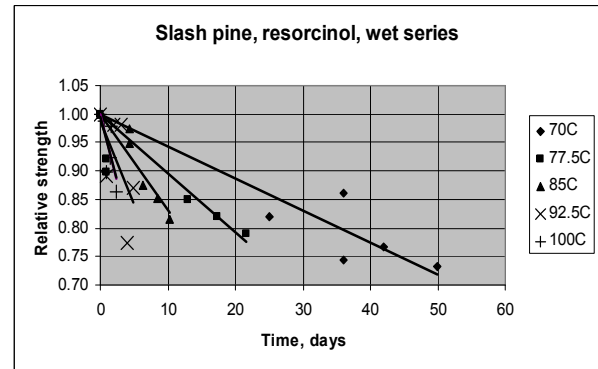


Figure 4: Resorcinol adhesive, wet tests

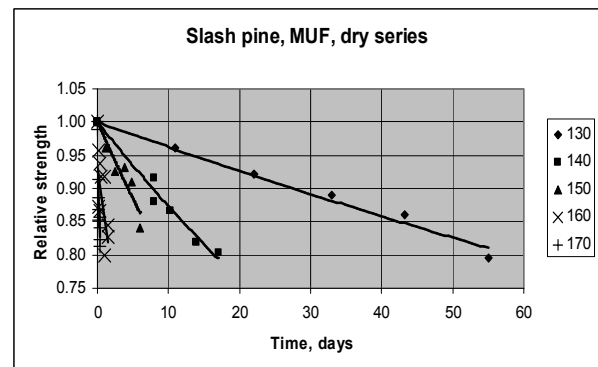


Figure 5: Melamine-urea adhesive, dry tests

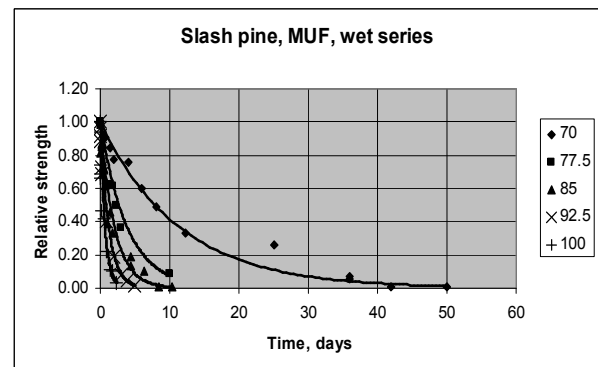


Figure 6: Melamine-urea adhesive, wet tests

Times to 75% of control strength were calculated from the regressions fitted to the strength/time data. The regressions were forced to an intercept value of unity as shown in Figures 7 to 9.

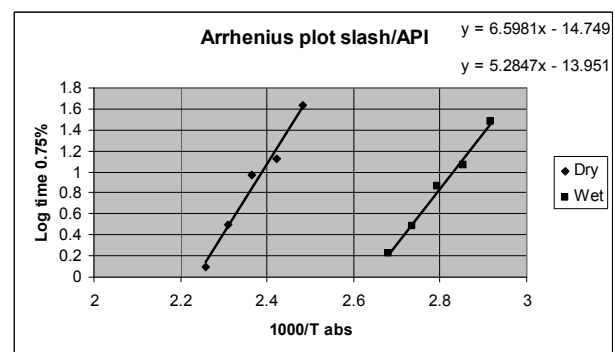


Figure 7: Arrhenius plot for API adhesion

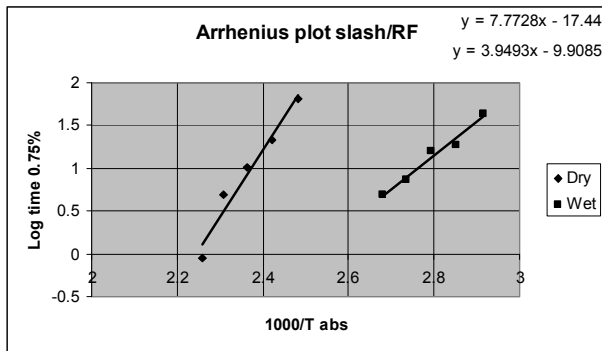


Figure 8: Arrhenius plot for resorcinol adhesion

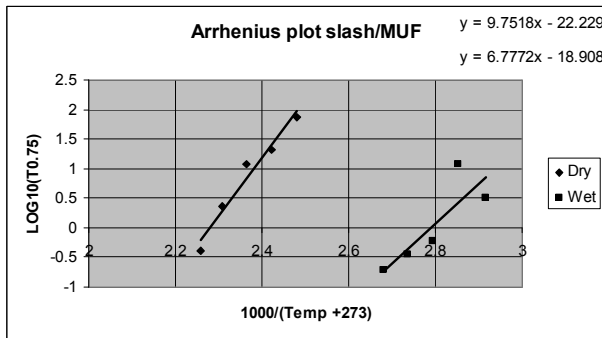


Figure 9: Arrhenius plot for melamine-urea adhesion

Table 1 gives the times to 25% strength loss at 20°C as predicted from the Arrhenius plots. These results are not credible because a life of 310 million years is not believable, even for solid wood. Also, MUF yielded better life predictions than did RF. There is a further problem when it comes to interpolating between the dry

and wet estimates for intermediate moisture contents because the moisture condition for the wet tests is unknown. Therefore this test is not recommended.

Table 1: Estimation of times to 25% strength loss at 20°C

		Slope	Intercept	Time to 75% strength at 20°C
		years		
Dry	API	6.5984	-14.7488	161,462
	RF	7.7728	-17.44	3,360,401
	MUF	9.7518	-22.229	310,244,217
Wet	API	5.2847	-13.9509	33.4
	RF	3.9493	-9.9085	10.2
	MUF	6.7772	-18.908	45.7

3.2 SHEAR BLOCK TESTS

The median strengths and median and lower quartile wood failure results from the shear block tests are given in Table 2. Table 2 shows that the MUF adhesive could not withstand the boil/dry/freeze treatment, otherwise all three adhesives passed these tests.

Table 2: Shear block results summary

	Strength, MPa			Wood failure, %		
	Median	Standard	Lower quartile	Standard	Median	Standard
API						
Dry	13.50	10	100	85	100	75
Vac/press soak	4.52	5.6	100	85	100	75
Boil/dry/freeze	3.08	3.5	100	85	100	75
RF						
Dry	13.88	10	100	85	100	75
Vac/press soak	5.92	5.6	100	85	100	75
Boil/dry/freeze	2.40	3.5	100	85	100	75
MUF						
Dry	13.71	10	100	85	100	75
Vac/press soak	5.61	5.6	100	85	100	75
Boil/dry/freeze	0	3.5	0	85	0	75

3.3 DELAMINATION TESTS

The observed delamination results are given in Table 3

Table 3. Delamination results summary

Maximum delamination in any one bond line, mm			
Adhesive	API	RF	MUF
Max	64	20	130

The maximum delamination permitted in any one glueline is 1% of the total glueline length, i.e. 13mm, so none of the adhesives passed but the use of a non-standard species would have had an effect. However it is apparent that the RF performs better than API which performs better than MUF.

3.4 CREEP TESTS

Under conditions A and B all the specimens of all adhesives showed zero creep but under condition C they collapsed as shown in Figure 10. The API-glued specimens showed some failure in the gluelines while the RF- and MUF-glued specimens showed failure only in the timber adjacent to the gluelines



Figure 10: The API creep specimens that collapsed under 50°C conditions.

The specimens that collapsed showed no creep, i.e. where the gluelines were intact there was no displacement of the knife cuts that had been made across the gluelines prior to loading. The specimens that had survived treatment A were given treatment C and these collapsed. The specimens from treatment B were given treatment C but in the loading cage shims were inserted to prevent buckling. These specimens survived.

4 DISCUSSION

4.1 HYDROLYTICAL TESTS

These tests are not difficult to do but they are very time-consuming and give unrealistic answers. As commented earlier, the analysis requires an assumption to be made as to what is the relevant moisture content

of the specimens in the water bath tests. The observation that the MUF adhesive gave longer predicted life than the RF adhesive is also a puzzle. There is an alternative method specified in ASTM D 4502 where the specimens are placed in sealable aging jars above saturated salt solutions and subjected to heat. This may be more realistic in that the specimens are not subjected to liquid water and thus the treatment is more representative of actual environmental condition. It is recommended that this test be deleted from the draft standard.

4.2 SHEAR BLOCK TESTS

These tests are simple to perform and give definite answers.

4.3 DELAMINATION TESTS

These tests are also simple to perform and gave answers which agreed with those from the shear block tests.

4.4 CREEP TESTS

It appears that this test may need modification to ensure that the specimens cannot buckle under treatment C.

4.5 COMPARISON BETWEEN TESTS

The standard aims to define accelerated tests to determine how adhesives will perform under three service class conditions of:

- Service class 1: Indoor, subject to seasonal fluctuations of temperature and humidity but not subject to wetting.
- Service class 2: Indoor or outdoor, subject to seasonal fluctuations of temperature and humidity but protected from direct sun and rain.
- Service class 3: Outdoors or in ground contact subject to outdoor climate.

The tests do not enable a decision to be made as to whether an adhesive is suitable for Service Classes 1 and 2, only whether or not it is suitable for Service Class 3. This is a deficiency in the draft standard that needs to be addressed.

Another problem with these tests is that a variety of species may be used. This brings in an unnecessary unknown effect. In these tests slash pine was used so it begs the question as to whether or not the results were affected by the timber. If results are to be compared internationally then the same species of timber must be used for all adhesives.

The shear block tests and the delamination tests both ranked the adhesives as RF being more durable than API which was more durable than MUF. Both the API and MUF were affected by treatments that used water baths rather than high humidities. The shear block and delamination tests can be considered to provide the

same information and therefore one of these could arguably be deleted.

The creep test was introduced specifically for adhesives like API and PUR which do not set hard and are believed to creep under conditions of high temperatures. The creep tests conducted in this study show that the details of the equipment need to be modified to prevent buckling. Apart from that, under treatment C, the API appeared to fail in the gluelines as well as in the wood adjacent to the gluelines, while the RF and MUF appeared to fail in the wood only. This test is very time-consuming, mainly because of the intricacy of the specimens. A simpler specimen design is desirable.

5 CONCLUSIONS

- The hydrolytical test involving ovens and water baths should not be an option in the draft standard because it is open to different interpretations, is very time-consuming, and gives unrealistic answers.
- The shear block and delamination tests are quick and simple to do and give answers that are essentially equivalent which suggests that one of the tests could be deleted.
- The creep test needs modification to prevent specimens buckling.
- The API adhesive showed durability intermediate between that of RF and MUF.
- The durability of both the API and the MUF adhesives were significantly reduced in the presence of liquid water.
- The API and MUF may have performed better at high temperatures if they were subjected to water vapour rather than liquid water. This is a matter for further research

REFERENCES

- [1] Anon, Timber – Bond performance of structural adhesives. Interim Australian/New Zealand Standard AS/NZS 4364:2007
- [2] Anon, Timber structures Part 1: design methods, Australian Standard AS 1720.1 - 1997

**INTERNATIONAL COUNCIL FOR RESEARCH AND INNOVATION
IN BUILDING AND CONSTRUCTION**

WORKING COMMISSION W18 - TIMBER STRUCTURES

**THE LONG TERM INSTRUMENTATION OF A TIMBER BUILDING IN NELSON NZ -
THE NEED FOR STANDARDISATION**

H W Morris

P Omenzetter

M Worth

The University of Auckland

S R Uma

K Gledhill

GNS Science

NEW ZEALANDd

MEETING FORTY THREE

NELSON

NEW ZEALAND

AUGUST 2010

Presented by H W Morris

B Yeh: how is segregation of vertical movement done? H W Morris: can't be done in current set up.

B Yeh: history of vertical movement?

A Buchanan: is moisture content of wood measured?

A Ceccotti: how do dissipating devices work? H W Morris describes the principle and refers to explanations during the visit of the building site.

A Palermo: moisture and creep measurements? H W Morris: will be difficult.

M Fragiaco: long-term measurements of MC for LVL and experience are available at Canterbury.

P Schädle: Is a performance-based or a force-based design in use? A Palermo: displacement-based design has been used in this case.

M Fragiaco comments about flexibility of joint at portal frames and his experience at University of Canterbury.

M Frese asks about slide 18 – compression stress distribution at bottom of shear wall?

A Palermo states that a uniform stress under pre-stress and a linear distribution under rocking were assumed.

S Aicher: maximum stress at corner. Design or ultimate strength? A Buchanan: ask designer in afternoon presentation

The Long Term Instrumentation of a Timber Building in Nelson NZ - the need for standardisation

H.W. Morris¹, S.R. Uma², K. Gledhill², P.Omenzetter¹, M.Worth¹

¹The University of Auckland, ²GNS Science, New Zealand

1 Introduction

High quality data on building performance is needed as timber is increasingly used for medium and large commercial, industrial and multi-residential structures in New Zealand and around the world. Timber buildings 6 to 9 storeys high have been constructed in Germany, England, Canada and Sweden. In New Zealand we expect that a 3 storey post-tensioned building in Nelson will be the trailblazer for taller structures here. Performance based standards require an understanding of building response at a range of serviceability levels as well as for life safety.

Large scale earthquake shake table experiments, such as those undertaken in the USA, Italy and Japan, provide very good initial response data for timber structures (Filiatrault, Christovasilis et al. 2010). Multi-storey timber structures in seismic regions are designed for structural ductility with the response analysis based on assumptions for damping which will be different from the laboratory to fully fitted out buildings. It is important that monitoring is used to collect in-situ performance data, particularly in seismic areas, to provide a solid basis for standards for a range of fully finished structures.

For long span structures the timber deformation is a significant serviceability design parameter so the long term deformations need to be predictable. Monitoring provides understanding of the reliability of these design values.

Instrumentation of buildings takes considerable effort and standardisation is necessary to maximise the comparability of data. Timber has a smaller research base than the major structural materials so early standardisation of approach and instrument parameters will maximise the international usefulness of a performance database. Monitoring is discussed in reference to the GNS Science GeoNet network and the Nelson Marlborough Institute of Technology (NMIT) timber building in Nelson and is used to pose the challenge as to how to develop a standard approach for wider application.

1.1 GeoNet Network

GNS Science collects and manages real-time monitoring and data collection on geological hazards in New Zealand. Their accelerograph network enables the study of ground motion characteristics in our highly seismic context.

There are national scale and regional scale networks, and a structural monitoring programme. The national scale network comprises a National Strong-Motion Network and a well distributed National Seismograph Network giving a total of over 220 recording locations.

The performance-based earthquake engineering approach aims for ‘safer’ structures that can perform satisfactorily to match the expectation of owners and engineers including reference to socio-economic variables including dollar loss and down time of facilities. The relationship of structural responses to earthquakes such as floor accelerations, inter-storey drift and damage to the socio-economic parameters needs to be established on the basis of reliable data. In this regard, instrumentation in buildings will enable improved understanding of performance of buildings and to verify the design assumptions.



Figure 1. New Zealand strong-motion recording sites. Green symbols are National Strong-Motion Network sites and red symbols are National Seismograph Network sites

Since 2007 the structure monitoring programme has seen modern instrumentation systems implemented in 4 buildings in Wellington (GNS Science Avalon, Wellington Hospital, BNZ CentrePort, and Victoria University) and in Christchurch (Canterbury University Physics Building). Currently, several buildings are at different stages in their instrumentation process. Figure 2 shows the proposed locations and the facilities considered for instrumentation. Details on the GeoNet building instrumentation programme can be found elsewhere (SR Uma et al, 2010 NZSEE)

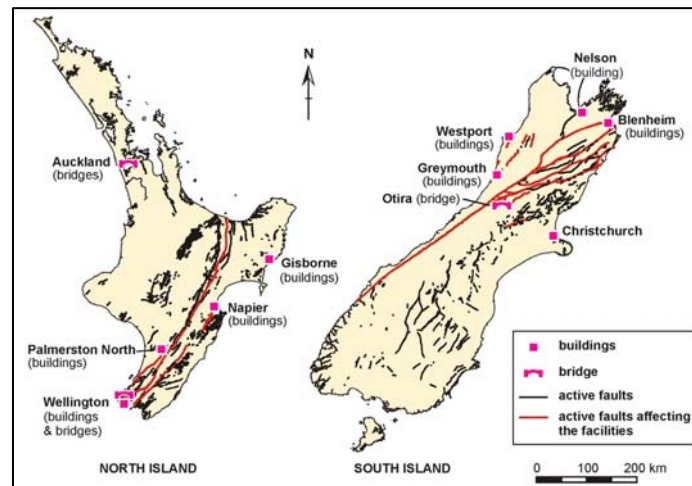


Figure 2. Active faults in the country and proposed GeoNet locations and facilities for seismic instrumentation

Figure 3 illustrates the typical network configuration adopted in building instrumentation. Seismic sensors are distributed within the building and a GPS unit is configured for precise timing. A central datalogger collects the data from the distributed sensors through ethernet wiring and stored data is continuously transmitted to GeoNet data Centre through a dedicated IP connection. The system was designed to be robust, moderate cost, low maintenance and protected against component obsolescence.

Figure 3. Schematic of typical components (CSI Ltd)

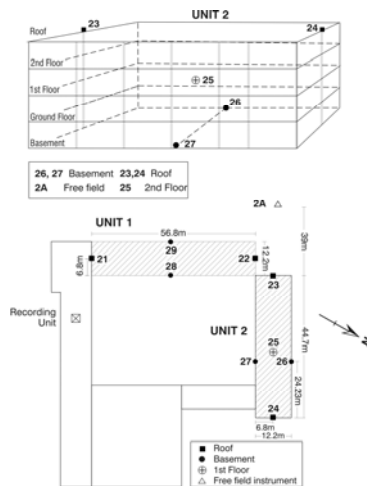
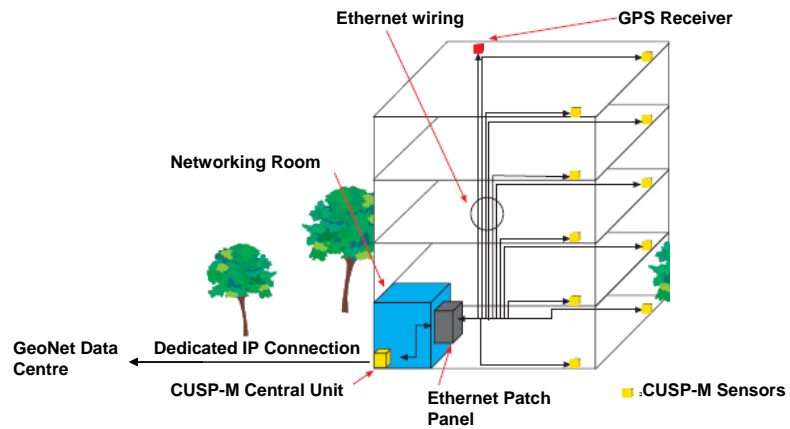


Figure 4a. GNS Science –the first instrumented building to be completed

Figure 4b Photograph of GNS Science building

Figure 4a shows the building layout of GNS Science office at Avalon, Lower Hutt with sensor locations marked on two of the seismically separated sections of the building. The data from this building can be obtained by approaching GeoNet.

The locations and azimuth for each sensor are available from the GeoNet DELTA database, accessed via the GeoNet website (GNS Science, GeoNET). Direct Access is available with identification numbers given to the sensors are identical to that given in the website. Further details on instrumentation of GNS Science building can be obtained elsewhere (SR Uma et al., 2010 – Science report).

2 The NMIT Building

In New Zealand a 3 storey timber building is under construction for the Nelson Marlborough Institute of Technology (NMIT). The preliminary design concept won a Ministry of Agriculture and Forestry (MAF) competition for \$1M of funding for a government owned timber building at a commercial scale. Subsequent competitive MAF funding was obtained to install instrumentation into the building investigating the wind and seismic dynamic response and long term deformations.

The NMIT building complex has 3 separate sections, the Media building, Workshop building and the 3 storey Arts building. The building architects are Irving Smith Jack, Aurecon are the overall project engineers who also undertook the structural design. An independent specialist peer review was done for the structure.



Figure 5. NMIT Arts complex - workshop building on the left, media building on the right, arts at the back

The workshop building is a simple single storey timber structure, the media building is an LVL portal frame which has an epoxy dowel moment connection. It has a haunched rafter member to allow for airconditioning ducts.

2.1 Arts building

The NMIT Arts building is a 3-storey Pinus Radiata LVL frame structure that resists lateral load with post tensioned shear walls. The shear walls use the Pres-lam[®] system proposed by the University of Canterbury (Newcome et al., 2010, NZSEE, Newcome et al., 2010 WCTE) and developed within the Structural Timber Innovation Company (STIC) research consortium.

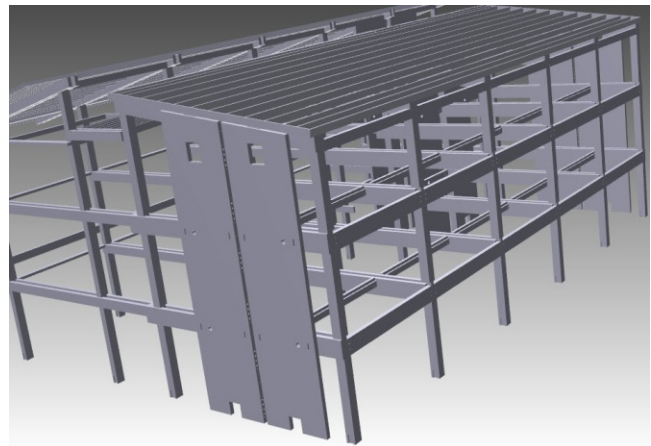


Figure 6. Arts building LVL structural members showing the coupled shear walls (Model by Design Base)

The walls are built in two panels that are designed to rock from side to side in a major seismic event with each panel edge lifting up to maximum of 50mm. The pairs of panels are coupled with energy dissipating (yielding steel) devices to limit damage during a severe event.

The 12m high shear walls are two parallel panels 3.0m wide and 189mm thick. The walls were made by laminating three 63mm thick LVL sections leaving a 600mm void for the full wall height. As shown in figure 6 an opening near the top of the wall allowed the post tensioning of the four 32mm Macalloy rods, an opening at the bottom allowed for a connecting coupler. A post tensioning load of 340kN per rod was applied after the floors were poured.

A cylindrical connection transfers the lateral loads from the structure to the shear wall while minimising moment transfer at maximum deformation.



Figure 7. Shear walls showing the cylindrical shear connector with Teflon spacer, slotted location bolts, and U shaped yielding steel energy dissipaters

The floor of the building was constructed using the local propriety Potius system which uses a 32mm LVL floor with integral LVL beams 360mmx90mm which are top hung from the main frame beams. The concrete floor topping was poured over a polyethylene sheet, the initial concrete pour was stopped short of the main beams, this means the floor is non-composite and concrete shrinkage does not impact on the deformation. The topping for the main beams was poured later with shear studs for composite action in the frame direction.

3 NMIT Structural Monitoring

The 3 storey NMIT Arts building in Nelson is a regular frame structure that is monitored for changes in the post tension, compression deformation, joint deformation, rocking uplift, energy dissipater deformation, wind loads, ground accelerations as free field, and floor accelerations at different locations of the building. The building is seismically separated from the other parts of the complex. The portal frame Media building is monitored for joint rotation and long term deformation near mid span. Both buildings have reference temperature and humidity measurements.

The responses include rocking uplift of shear walls, deformation in energy dissipating devices, and floor accelerations. Wind related parameters are captured using a weather station on the roof of the building.

3.1 Seismic instrumentation

GNS Science is primarily monitoring seismic response of the building. Triaxial accelerometers are placed on all three floors and in the roof to measure accelerations. Figure 8 only shows the ground floor plan with 3 acceleration sensors located to capture ground motions input to the building.

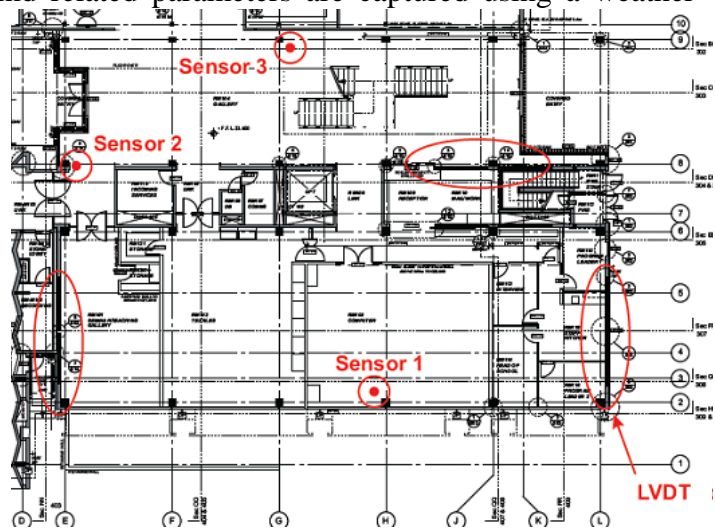


Figure 8. Accelerometers placed in ground floor of the building. (Base plan by Irving Smith Jack)

Note that the upper floors are also provided with sensors vertically aligned across the floor levels as much as possible. The locations of LVL shear walls are circled in Figure 8. The details of instrumentation in these walls are illustrated in Figure 9, where mainly the uplift of the walls while rocking and the deformation of U-shaped metallic energy dissipating devices are of interest. LVDT (linear variable differential transducer) are used for this purpose. Due to practical constraints only two LVDTs could be placed at two far ends of the wall. LVDTs are placed within the dissipation devices at all three levels to monitor their deformation history.

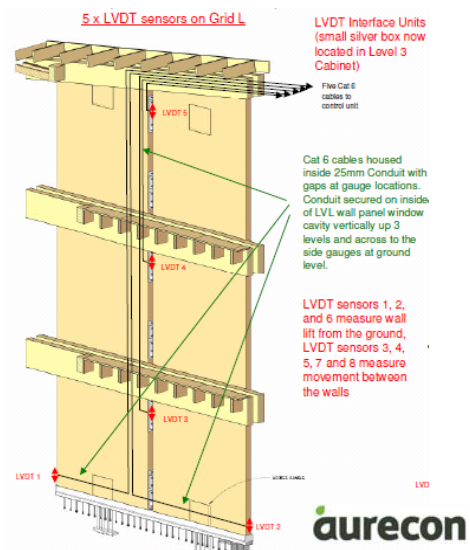


Figure 9. GNS Science typical configuration of LVDT's in a LVL shear wall. (Base illustration by Aurecon)

3.2 Long term and floor monitoring

The University of Auckland (UoA) are installing a complementary array of instruments for the NMIT Arts building. The overall objective is to understand the dynamic and long term response of the structure and particularly for the post tensioned walls. The installation also is being used to monitor dynamic floor performance; in timber structures this is often problematic.

Temperature and humidity is monitored which will be important in understanding the material performance leading up to and during a major wind or seismic event.

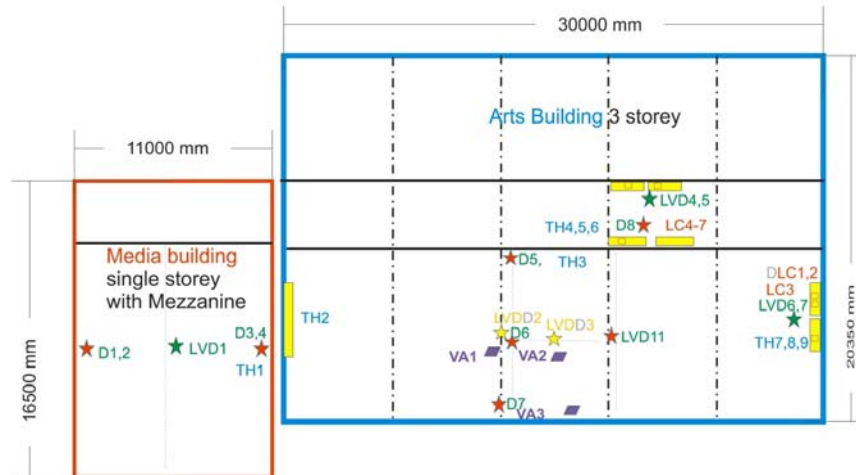


Figure 10. University of Auckland overall instrumentation plan

Figure 10 shows the UoA instrumentation on all levels of the Arts and Media buildings. The temperature and humidity gauges, are designated TH, small deformation gauges - D, larger LVDT deformations - LVD, Loadcells - LC. Long term instruments are monitored every 30 minutes, dynamic instruments are monitored at 200Hz including the vertical floor accelerometers - VA, the amplified loadcells - DLC, and the floor LVDT's -DLVD.

A detailed analysis of the floor dynamics was undertaken by Varun Kohli (Kohli,V. 2010) which has identified the locations of maximum dynamic displacement of the floors and recommended optimal sensor placement.

3.2.1 Shear Wall Stress and Compressive Deformation

As noted above the Pres-lam[®] post tensioned shear walls are the key innovation in the Arts building. The long term change in post tensioning is monitored and the compressive deformation and creep under high stress. As shown in figure 11, custom made 450kN loadcells were installed to monitor the tension in the rods. Given that there is no reference point at the top of the wall the vertical deformation is measured from a hanging weight and will be temperature compensated.

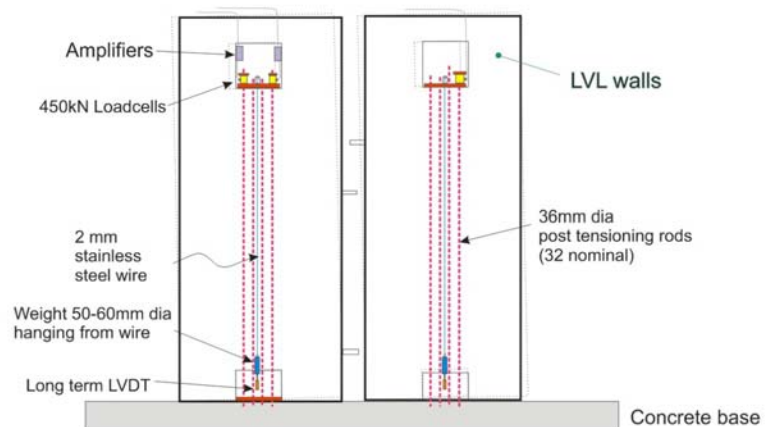


Figure 11. University of Auckland conceptual illustration of Loadcells and vertical displacement measurement.

3.2.2 Floor Deflections

The long term floor sag is monitored using a baseline system for the measurement reference (Stanton et al., 2003). As shown in figure 12a and 12b, a catenary wire is hung over a pulley, in between the 750mm deep frame members, with a 40kg mass to maintain constant tension so temperature compensation is not necessary. Also between the beams, a small trolley (Figure 12c) reduces dynamic wire flutter for the LVDT contact. A separate system monitors deformation for the 6m span Potius floor system.

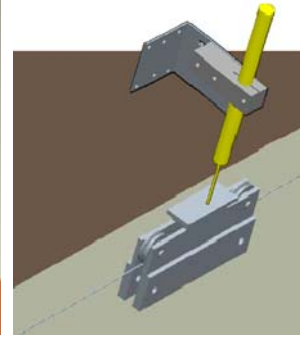
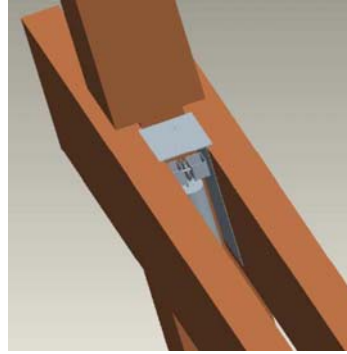
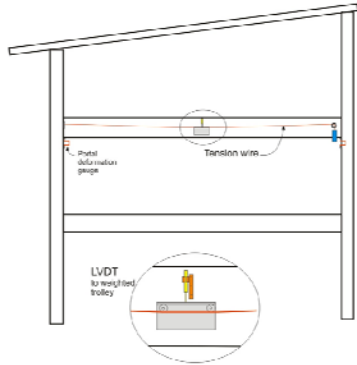


Figure 12a. Long term reference system onto baseline wire

Figure 12b. Detail of pulley and weight between beams

Figure 12c. LVDT setup onto the trolley

3.2.3 Media Portal Frame Deformations

The media building has four simple portal frames that are a modest span. As shown in figure 13 the instrumentation uses linear deformation gauges (“portal” type gauges) to determine crushing and joint rotation with a vertical LVDT connected to a baseline wire to monitor deformation. Clearance limits mean that a trolley could not be used.

In the detail view in figure 13 the LVDT will pass through the “Gib” gypsum board ceiling in order to have adequate clearance to measure the expected deformation.

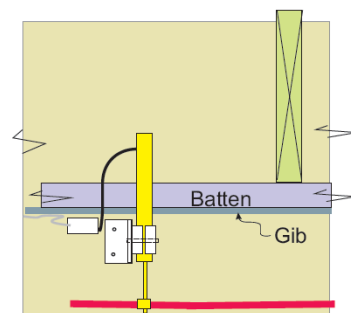
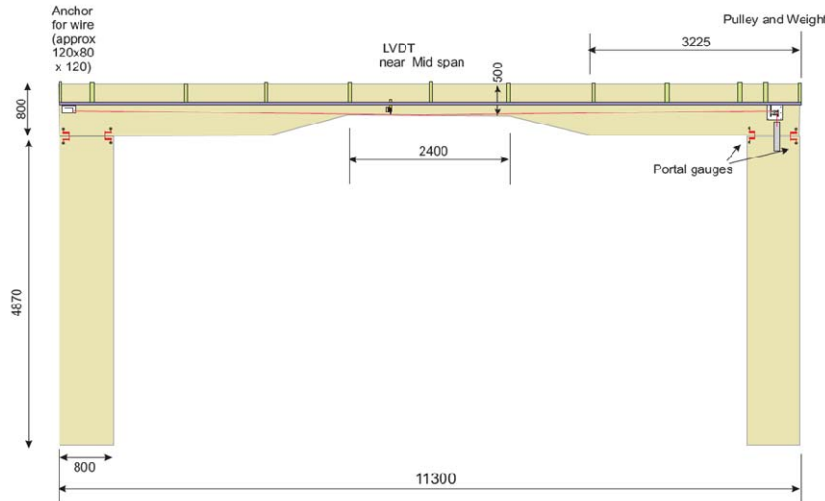


Figure 13. Media portal frame instrumentation for joint rotation and deformation. The mid span detail is also shown. The baseline reference wire is shown in red.

4 Preliminary Dynamic Testing

In-situ testing of the NMIT building is being performed to determine design parameters from testing a ‘real building’ under construction. Canterbury University developed a Direct Displacement Design procedure for the design of the post-tensioned shear walls. The damping values used in this procedure are based on the laboratory testing of light-frame timber buildings and are quite conservative. This testing aims to determine more realistic design parameters for damping.

The research needs to be undertaken within the normal construction context so has to cope with considerable variability in building configuration. The dynamic performance of the building can only be examined within the linear range. This linear range is significant because the serviceability limit state dominates much of the design. The dynamic properties of the NMIT building are being evaluated during different stages of construction; ambient vibrations are being measured using portable accelerometers. The influence of the structural and non-structural components will be analysed to quantify the difference between the stiffness and damping values of the bare frame, bare frame with the concrete floors, with cladding, with the stairway and the completed building.

The data from the ambient testing will be processed using the stochastic subspace identification method to find modal frequencies, stiffness and damping values (Peeters and Roeck 2001). Forced vibration testing may also be performed, as timber buildings show amplitude dependence for both fundamental frequencies and damping values (Camelo 2003). The results from the testing will be updated into a finite element model of the building. An updated model will build a more accurate understanding of the performance and provide a model that can be used to interpret dynamic measurements once the building is complete.

5 Standards for Performance Based Design and Monitoring

5.1 Existing Requirements and Minimal Seismic Monitoring

Because of the valuable data obtained from buildings instrumented at the time of the 1994 Northridge earthquake in the USA, the Uniform Building Code 1997 required owners to install a minimum of 3 sensors into all buildings over 10 storeys high, or over 6 storeys high if they have an aggregate floor area greater than 60,000 square feet. (Celebi, M. 2000)

With the increase in high rise timber construction there is an opportunity to specify appropriate instrumentation schemes and enable timber building owners in seismic zones to install a consistent reliable base level of instrumentation. Standards would make it cost effective for equipment manufacturers to propose simple base level systems at a moderate and predictable cost.

5.2 Comprehensive Building Monitoring

Based on the experience in the USA it is anticipated that much will be learnt from the response of instrumented timber buildings. Opportunities should be actively sought for such instrumentation and wherever possible the data should be consistent with other building installations around the world.

For comprehensive monitoring systems such as those installed by GNS Science the layout of instruments needs to account for the key features and building geometry in every different building. Ideally a dynamic analysis would be undertaken to determine optimal locations within the architectural constraints.

Guidelines for consistent data monitoring would need to include specifications for the accuracy, precision, responsiveness and stability, and data capture rates needed over the lifetime of the system. Suggested requirements are:

- A minimum number of accelerometers to adequately specify building dynamic response, based on building type, size and ground conditions; locations and orientations of all sensors need to be fully documented;
- A free field accelerometer that is measuring the input ground motions away from the building; if possible this sensor should be on bedrock;
- Additional sensor types, where practical, to measure inter-storey drift and slow deformation;
- Meteorological data, where practical, such as wind speed should be recorded; where wind is measured the best and minimum anemometer positions should be specified;
- Installed accelerometers with a minimum sensitivity of 50 - 100 μg so ambient vibrations can give indicative building performance with the maximum acceleration recorded at least 2 g;
- Accelerometers should be sampled at 200 samples per second with a minimum effective resolution of 17 to 19 bits (100 – 115 db);
- Synchronous accelerometer array event triggering should be employed on all sensors, with a data length long enough (up to 5 minutes depending on event size) to give good numerical results;
- The ability to record continuously on site for a period of time to ensure full operation and provide data for research;
- Building drawings be made available with adequate detail to allow independent engineers and researchers to develop and calibrate models for further analysis;
- It is desirable to have data communications to a data centre for data collection and system monitoring

6 Discussion and Conclusions

More data on real building responses to earthquake and strong wind events will mean better verification of design assumptions. The impacts, effects and costs of high level serviceability events would significantly contribute to better performance based design. This requires a number of buildings to be available to collect useful data. GNS Science have experience with modern installations and a comprehensive but modest plan for New Zealand wide installations. A compatible international programme would significantly strengthen such a database, particularly for timber structures 4 storeys or higher.

At the time of writing instrumentation is only partly installed in the NMIT buildings. The timescale for design and installation was very tight to fit the realities of construction project scheduling. The project has considerable complexity as well as design parameters to be determined. At the University of Auckland it became clear that a set of guidelines and standards for would have made for better early decisions. In the longer term such standards including resolution and sampling rates would mean direct comparability between projects.

We recommend that key parameters used in our studies be promoted to others proposing instrumentation, that guidelines be developed with international collaborators, and these be used to form the basis for future monitoring standards.

7 Acknowledgments

We would acknowledge funding from MAF, installations by the GeoNet programme funded by the Earthquake Commission, and also thank NMIT and Arrow International for assistance and access; Aurecon the structural and engineering consultants, Irving Smith Jack Architects; Russell Kells of Design Base for his computer model; students Wasim Sidiyot, and Ahmed Motara, Dr David Carradine from University of Canterbury and Contech post-tensioning specialists, and technicians John Young and Mark Twiname.

References

- Camelo, V. (2003). "Dynamic Characteristics of Woodframe Buildings". California, California Institute of Technology: 255.
- Celebi, M. (2000). "Seismic Instrumentation of Buildings". U.S. Geological Survey, USGS Open-File Report 00-157
- Filiatrault, A., H. Isoda, et al. (2003). "Hysteretic damping of wood framed buildings." *Engineering Structures* 25(4): 461-471.
- GNS Science (www.geonet.org.nz/resources/network/index.html). Sept 2010 direct access link [http://magma.geonet.org.nz/delta/app?service=direct/0/Home/\\$Border.searchSeismicStation](http://magma.geonet.org.nz/delta/app?service=direct/0/Home/$Border.searchSeismicStation).
- Kohli, V. (2010). "Optimal Sensor Placement for Measuring Floor Vibrations", The University of Auckland. Student internship report- unpublished.
- Nelson Marlborough Institute of Technology. (2010). "NMIT Arts & Media Building", Arts & Media Building Information Sheets April 2010, <http://www.nmit.ac.nz/schools/artsmedia/artsandmediabuilding.aspx>
- Newcombe, M.P., Pampanin, S., and Buchanan, A.H. (2010). "Design, Fabrication and Assembly of a Two-storey Post-tensioned Timber Building." Conference Proceedings, World Conference on Timber Engineering WCTE 2010, Trentino, Italy June 2010.
- Newcombe, M. P., Pampanin, S., and Buchanan, A.H.(2010). "Global Response of a Two Storey Pres-Lam Timber Building." New Zealand Society of Earthquake Engineering Conference, NZSEE, Wellington, New Zealand.
- Peeters, B. and G. D. Roeck (2001). "Stochastic System Identification for Operational Modal Analysis: A Review." *Journal of Dynamic Systems, Measurement, and Control* 123(4): 659-667.
- Stanton, J., Eberhard, M. and Barr, P. (2003). "A weighted stretched wire system for monitoring deflections." *Engineering Structures*, 25, 347-357.
- Uma, S.R., King, A., Cousins J., Gledhill K. (2010). "The GeoNET Building Instrumentation Programme", *Bulletin of the New Zealand Society for Earthquake Engineering, NZSEE*, 2010 submitted.
- Uma, S.R., Cousins, W.J, Baguley, D. (2010). "Seismic instrumentation in GNS Science building at Avalon", *GNS Science Report* 2010/26 20 p.

**INTERNATIONAL COUNCIL FOR RESEARCH AND INNOVATION
IN BUILDING AND CONSTRUCTION**

WORKING COMMISSION W18 - TIMBER STRUCTURES

**ESTIMATION OF LOAD-BEARING CAPACITY OF
TIMBER CONNECTIONS**

J Munch-Andersen
Danish Timber Information

J D Sørensen
Dept. of Civil Eng., Aalborg University

F Sørensen
ITW Construction Products
DENMARK

**MEETING FORTY THREE
NELSON
NEW ZEALAND
AUGUST 2010**

Presented by J Munch-Andersen

A Jorissen: Questioned non-safety of D-8 in EC. J Munch-Andersen: Eurocode method allows connections to be taken into account.

H Blass: how to standardize smart, honest and stupid sampling? J Munch-Andersen: that is impossible and to be avoided.

H Larsen: that proposal is too late as new approach (unsafe) is already adopted.

Estimation of load-bearing capacity of timber connections

Jørgen Munch-Andersen
Danish Timber Information, Denmark

John Dalsgaard Sørensen,
Dept. of Civil Eng., Aalborg University, Denmark

Flemming Sørensen,
ITW Construction Products, Denmark

Introduction

Experimental determination of the characteristic value of the properties used to calculate the load-bearing capacity of timber connections involves 3 steps. There is a standard which covers each step:

1. Selection of timber specimens (ISO 8970 = EN 28970)
2. Performing the tests according to the standard relevant for the property
3. Deriving the characteristic value (EN 14358)

This paper is discussing step 1 and 3 which are general for estimation of all properties. The standards are not referring to or in accordance with the principles in EN 1990, Basis of design.

Examples are given for withdrawal of threaded connector nails, where the tests should be carried out according to EN 1382. It is assumed that the withdrawal load-bearing capacity can be expressed as

$$F_{ax} = b(\rho/\rho_0)^c d l_{thr} \quad (1)$$

where

- | | |
|-----------|--|
| d | nail diameter |
| l_{thr} | length of the threaded part of the shank |
| ρ | timber density |
| ρ_0 | a reference density |
| c | a power determining the dependency on the density |
| b | the withdrawal strength f_{ax} at density ρ_0 |

The parameters b and c should be estimated from the test results.

Present method

The present version of ISO 8970 from 1994 is focused on using timber with density as close as possible to the characteristic density for the strength class the results should be used for. It provides a choice between two methods.

According to Method 1 the densities of the test specimens shall be chosen not too much higher than the characteristic value for the strength class the results are aimed for, e.g. 350 kg/m³ for strength class C24. The idea of this method is to use the results without correcting for the density. The method is quite difficult to use as timber with density below and around 350 kg/m³ is very difficult to find.

Higher densities can be used with Method 2, but the measured values should then be corrected to the characteristic density by means of a power c on the density. How this power should be chosen is not very accurately described.

EN 14358 provides a straightforward method for estimating the characteristic load-bearing capacity or strength from test results. But it will be the characteristic capacity for the characteristic density, rather than the characteristic capacity for the natural distribution of the density. This means that the estimated characteristic capacity becomes quite conservative.

On the other hand the coefficient of variation obtained from the measurements only reflects the variations represented by the specimens used for the tests. In principle, a series of e.g. withdrawal tests could be performed with timber specimens cut from the same board so the variation becomes very small. When a more random sampling is used, as most test institutes will probably do, the coefficient of variation increases so the results are safe. But it is quite impossible to know how safe and to which degree the problems of the two standards outweigh each other.

ISO 8970:2010 proposal

The first step towards a better method is taken by the 2010 proposal for a new ISO 8970 where the average density of the specimens should be near to the mean value for the strength class in question and all densities within some limits. The results are not to be corrected for density, which means that all specimens can be chosen so that their density is just below the upper limit. They could still be taken from the same board so it is possible to obtain a very small coefficient of variation, which reflects neither the variation of strength between specimens with the same density nor the variation in density for the strength class.

If the specimens represent the natural variation of properties, the characteristic capacity can be estimated correctly by EN 14358, but this is very difficult to ensure. The mean value approach therefore needs to be accompanied by a new method to derive characteristic values from the test results which especially takes the variation of the density into account. Such a method is given in Annex D of EN 1990. Its use for timber connections is discussed below.

The proposal offers no solution to the problem of choosing the power c if the estimated capacity should be used for another strength class.

In the following a suggestion for improvement is given.

Suggestion for selection of specimens

Ideally the timber specimens to be used for testing should be selected so that the density variation covers the relevant span for the timber strength classes for which the results should be valid. This span could be from the lower characteristic density of the lowest class to the mean value of the highest. But since specimens with density below 350 kg/m³ are almost impossible to find, a realistic range for structural timber might be 370 - 470 kg/m³ - the latter just above the mean value for C30 (460 kg/m³). The median of the range - 420 kg/m³ - equals the mean density for C24 which could be a reasonable reference density for all capacities.

The specimens should be about evenly distributed over the density range, i.e. not representing the real distribution for the strength class. Such data would permit for estimating the mean value of the capacity for a given density, expressed as the capacity at a chosen reference density *and* the power c to correct to other densities. Then the variation of the density should be added to the variation of the mean value obtained from the tests.

The latter is usually termed *model uncertainty* and should represent the variability of other parameters than the density that would affect the capacity, such as the width of the growth rings and the species, because it is unrealistic to quantify the influence of these parameters. In principle, this requires a random sampling, but because these parameters tend to be correlated to the density it might be sufficient to ensure that the density of the specimens is distributed over the required range. It could be required that the timber should originate from different saw mills to ensure a sufficiently random sampling.

If reliable values of the power c are supplied in Eurocode 5 or in other standards, fewer tests are needed. The specimens still need to be randomly sampled except their density, but it is easier to ensure the randomness when different densities are represented. The required range of densities could be narrowed when c is predefined - in order to ease the sampling - but there is no reason to maximize the range.

If there is doubt about the value of c for example for a connector where only a few tests are carried out, a safe choice will be to use a lower limit (e.g. $c = 1$) when estimating the load-bearing capacity for a higher strength class than focused on in the test and an upper limit (e.g. $c = 2$) when the capacity for a lower strength class is calculated.

Deriving the characteristic capacity

Section D8 of EN 1990 describes a method to derive the mean value of the capacity x as a function of a basic parameter t and how the characteristic value can be determined. In the following it is assumed that the model can be written as

$$x = b t^c \quad (2)$$

where b and c should be estimated. The method can also be used for more complicated models.

The estimated values are

$$x_{est,i} = b t_i^c \quad (3)$$

where t_i is the values of the basic (deterministic) variable. t could be a product of several basic variables. The observed values are called $x_{obs,i}$.

EN 1990 states that b should be chosen so that the least square best-fit of the slope of the straight line through the pairs $[x_{est}; x_{obs}]$ is 1 which means that

$$b = \frac{\sum x_{obs} x_{est}}{\sum x_{est}^2} \quad (4)$$

The model error is defined as $\delta_i = x_{obs,i}/x_{est,i}$. c is chosen (by trial-and-error) so that the standard deviation s_Δ of $\Delta_i = \ln \delta_i$ is minimized. For practical use the coefficient of variation of δ can be taken as

$$V_\delta \approx s_\Delta \quad (5)$$

But there is also a variation of the basic variables, which is not accounted for in V_δ because the model is applied with known values of the basic parameters. The total variation of x_{est} can for practical purposes be estimated as

$$V_x^2 = V_\delta^2 + V_T^2 \quad (6)$$

where V_T is the coefficient of variation of t^c . It is related to the variation V_t of t as

$$V_T^2 = c V_t^2 \quad (7)$$

If t is a product of two basic variables u and v it yields that

$$V_t^2 = V_u^2 + V_v^2 \quad (8)$$

The variation of the basic variables must be taken from prior knowledge, e.g. from specifications or standards.

The 5% characteristic value of x can now be determined. For practical application the expression in EN 1990 can be rewritten as

$$x_k = b t^c \exp \left(-1,64 \frac{V_T^2}{V_x} - k_n \frac{V_\delta^2}{V_x} - 0,5 V_x^2 \right) \quad (9)$$

where t is the mean value of the basic parameter and k_n is a factor depending on the number n of tests used to estimate V_δ (e.g. $k_{10} = 1,92$; $k_{30} = 1,73$). The factor approaches 1,64 when n gets large. It is presupposed that the variation of the basic variables is well determined so $k_n = 1,64$ is used for V_T . The last term is a correction because x is assumed to be LogNormal-distributed.

The statistical basis for Annex D is Bayesian statistics and is different from the basis for EN 14358, which uses classical statistics with a 75% confidence interval. The equivalent of k_n in EN 14358 is higher than in Annex D so using Annex D will increase the characteristic value.

$f_{ax,k}$ for connector nails

Two test series have been carried out with ITW GALVPLUS ® connector nails with dimensions as shown in Table 1. The dimensions are defined as:

l	total length of nail
l_{thr}	length of threaded part
l_p	length of point
l_g	$l_{thr} + l_p$

Table 1. Properties of the connector nails used for withdrawal tests.

d	l	l_{thr}	l_p	l_g
4 mm	35 mm	24 mm	5 mm	29 mm
4 mm	40 mm	28 mm	5 mm	33 mm
4 mm	50 mm	39 mm	5 mm	44 mm
4 mm	60 mm	49 mm	5 mm	54 mm

Series 1

Series 1 was designed to fulfil the requirement to use Method 1 in ISO 8970:1994. 10 specimens were used and two 50 mm nails were inserted in each specimen, one tangential and one radial to the growth rings as required in EN 1382. The penetration length was larger than l_g so the entire threaded length was embedded. The observed withdrawal strength parameter is calculated as

$$f_{ax,obs} = F_{ax,obs} / (d l_{thr})$$

The observations are given in Table 2 and shown in Figure 1.

Table 2. Observed withdrawal capacities and strengths for Series 1.

$\rho, \text{kg/m}^3$	$F_{ax,obs}, \text{N}$		$f_{ax,obs}, \text{N/mm}^2$	
	tangential	radial	tangential	radial
345	1516	1546	9,8	10,0
350	1741	1674	11,3	10,8
376	1885	2273	12,2	14,7
394	2390	2452	15,5	15,9
398	2283	2495	14,8	16,1
419	2005	2210	13,0	14,3
420	2095	1972	13,6	12,8
421	2340	2020	15,1	13,1
423	2948	2517	19,1	16,3
426	3046	2598	19,7	16,8

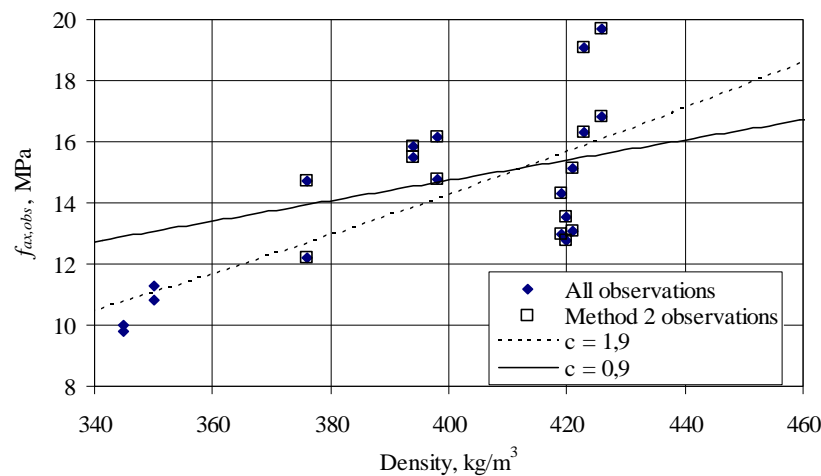


Figure 1. Observed withdrawal strengths versus density. The curves represent the best value of c for all observations ($c = 1,9$) and for the observations used for Method 2 ($c = 0,9$).

Table 3. Estimates of the characteristic withdrawal strength using different methods.

		$f_{ax,k}$ (C24)	Coeff. of Var.	ρ_{mean}
Method 1	$n = 20$	9,6 MPa	19,4 %	397 kg/m ³
Method 2 [#]	$n = 16, c = 1$	9,9 MPa	13,2 %	410 kg/m ³
Method 2 [#]	$n = 16, c = 2$	8,3 MPa	14,0 %	410 kg/m ³
New ISO*	$n = 16$	11,5 MPa	13,8 %	410 kg/m ³
Annex D	$n = 20, c = 1$	10,9 MPa	18,2 %	397 kg/m ³
Annex D	$n = 20, c = 2$	11,0 MPa	20,1 %	397 kg/m ³

[#] The four observations with the two specimens with the lowest density are disregarded in order to fulfill the conditions for using Method 2.

* The four observations with the two specimens with the lowest density are disregarded in order to approach the idea behind the new ISO.

Table 3 gives the estimate for $f_{ax,k}$ using Method 1 and Method 2 in the old ISO-standard, the new ISO-standard and the above proposed new method based on Annex D in EN 1990.

Method 1 requires no correction so the calculation of the characteristic value is straightforward. In Figure 1 it is seen that f_{ax} is clearly increasing with the density. The power best describing the dependency is $c = 1,9$ ("best" meaning the power which minimizes coefficient of variation of the corrected values).

When using Method 2, the observations from the specimens with the lowest density must be disregarded in order to fulfil the requirements. The remaining 16 observations shall be corrected to the characteristic reference density taken as 350 kg/m³. The best power for correcting those 16 observations is about $c = 0,9$. This demonstrates that estimating c from a limited number of tests is very uncertain. In Table 3 the characteristic value is given for both $c = 1$ and $c = 2$.

$c = 1$ - which is often assumed to be the best value - ends up giving a slightly higher characteristic value than Method 1, mostly because the variation is much smaller after correction. Using $c = 2$ - as Eurocode 5 says for smooth nails - gives a smaller value because the fit to the observation is not as good as using $c = 1$.

The new ISO requires no correction and differs mainly from Method 1 by requiring densities around the mean value (420 kg/m³ for C24) instead of close to the characteristic density (350 kg/m³ for C24). This will naturally give a higher characteristic strength, in case 20%. But if the specimens were chosen with densities near to the upper boundary, an even higher characteristic value could have been obtained. It is therefore obvious that the new ISO cannot replace the old without any other alterations of the chain to determine the characteristic strength.

Table 3 also shows the result of using Eq. (9) with $c = 1$ and $c = 2$ on all 20 observations. The equations are used with $t_i = \rho_i / 420 \text{ kg/m}^3$, $x_{obs} = F_{ax,obs} / (d l_{thr})$ and $V_t = 11\%$. The latter is the coefficient of variation of the density within a given strength class implicitly given in EN 338 when the density is LogNormal-distributed and $\rho_{mean} / \rho_k = 420 / 350 = 1,2$. The intermediate calculations necessary to use Eq. (9) are given in Table 4, and Figure 2 shows the observed values versus the estimated.

For the actual observations it is obvious that $c = 2$ gives the best model (smallest V_δ), but the characteristic value ends up being almost the same for $c = 1$ and $c = 2$. This is due to the increase of V_T when using $c = 2$. It suggests that the model is robust and it makes little difference if the value is prescribed as e.g. $c = 1$ in a standard.

From Table 3 is seen that the characteristic strength gets higher using the proposed method derived from Annex D in EN 1990 than when using the present method. The increase is somewhat due to no longer determining the characteristic strength for the characteristic density but for the natural variation of the density and is therefore a just increase.

It should be noted that the density of the test specimens is not at all evenly distributed over the relevant range as suggested above. The proposed method is not very sensitive to the distribution, but the possibility - perhaps unintentionally - of influencing the results when choosing the specimens is minimized when the densities are evenly distributed over the relevant range.

The method is also well suited for testing assemblies where no knowledge of c is available in advance. The larger span of densities included in the tests, the better the determination of c .

Table 4. Estimation using Eq. (2) to (9) for all data in Table 2.

c	b (Eq 4)	V_δ (Eq 5)	V_T (Eq 7)	V_x (Eq 6)	$f_{ax,k}$ (Eq 9)
1	15,1 N/mm ²	14,5 %	11,0 %	18,2 %	10,9 N/mm ²
2	15,8 N/mm ²	12,7 %	15,6 %	20,1 %	11,0 N/mm ²

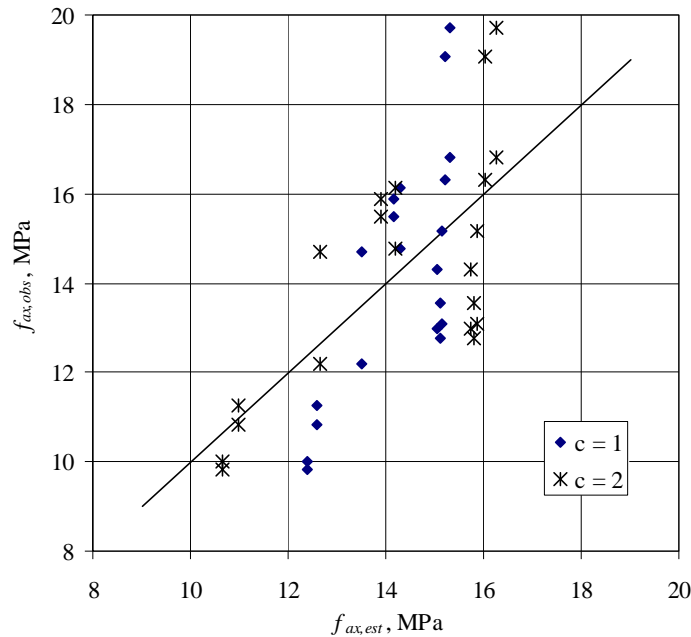


Figure 2. Observed versus estimated values of f_{ax} for $c = 1$ and $c = 2$. Ideally the points should lie on the line with slope 1.

Series 2

Series 2 was aimed at determining the influence of the length of the nail so tests with four nail lengths were carried out. Each nail length was tested 18 times. In order to reduce the uncertainty related to the wood properties, all tests were carried out with timber from three pieces so that each nail length was tested 6 times with each piece. These pieces were from another source than the used for Series 1 and assumed to be of low quality.

Apparently there is doubt whether f_{ax} should be calculated using the actual threaded length l_{thr} or l_g which includes the point. The tests in Series 2 confirm the authors' belief that the point should not be included as this ensures an $f_{ax,k}$ which is independent of the nail length. Figure 3 shows the observations corrected to $\rho_0 = 420 \text{ kg/m}^3$ using $c = 1$ when using l_{thr} (upper) and l_g (lower).

For the three longer nails it is clearly seen that a constant f_{ax} is obtained when using l_{thr} . For the shortest nail the strength seems to be slightly lower. An analysis of variance on these and other data shows that it is on the border of being statistically significant that the shorter nail has a smaller f_{ax} than the longer. The figure also demonstrates that after correcting for density there is still a considerable model uncertainty due to the variability of other parameters.

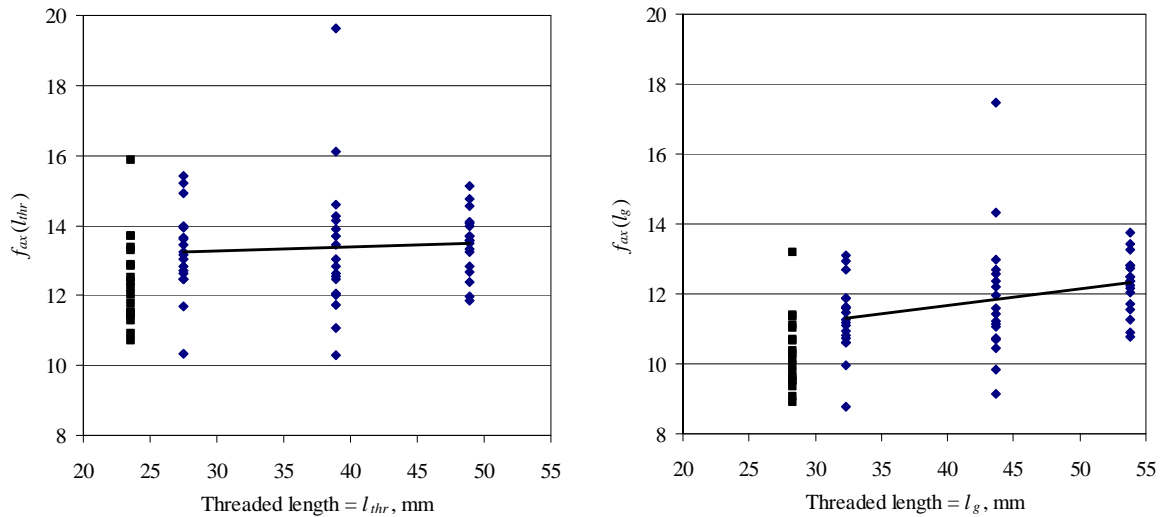


Figure 3. Observations normalized with l_{thr} or l_g . f_{ax} is corrected to $\rho_0 = 420 \text{ kg/m}^3$ using $c = 1$.

Eurocode 5 requires that the load-bearing capacity of threaded nails should be reduced if the pointside penetration depth is smaller than $8d$ and the capacity is zero at $6d$. Since Eurocode 5 uses the same symbol for the penetration depth of the point and the threaded length in the pointside member, it is not clear which length should be compared to $8d$ and $6d$.

If the penetration depth of the point is meant, the short nail with a length of 35 mm has a penetration length just below $8d = 32 \text{ mm}$. This is in good accordance with Eurocode 5 as the observed reduction of the capacity seems to start just at the length where Eurocode starts to require reduction.

If l_{thr} is meant the 35 mm nail which has $l_{thr} = 6d$ gets no withdrawal strength and for the 40 mm nail with $l_{thr} = 7d$ the strength should be halved. These lengths are widely used in Europe for fastening connectors and there is no experience that indicates it should be necessary with such a large reduction.

Figure 4 shows the observed load-bearing capacity F_{ax} for both Series 1 and 2 (excluding the shortest length) versus the estimated $F_{ax,est} = 13,9 \text{ MPa } d \ l_{thr} (\rho/420)^1$. (For more complex data it is advantageous to plot the load-bearing capacity rather than the strength parameter). The characteristic strength becomes $f_{ax,k} = 10,4 \text{ MPa}$ and $V_\delta = 12,6\%$. The best value for density correction is close to $c = 1$.

The strength is somewhat smaller than 10,9 MPa or 11,0 MPa as obtained from Series 1 alone, see Table 4. The difference illustrates the importance of selecting timber from different sources in order to minimize the effect of those properties that cannot be quantified but affects the strength.

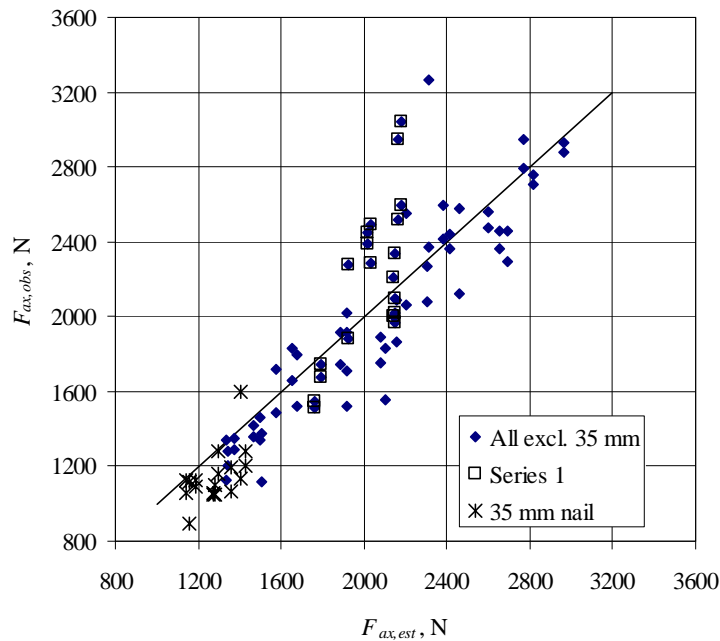


Figure 4. Observed versus estimated values of F_{ax} for Series 1 and Series 2 together (the shortest nails are not included in the estimate).

Conclusions

The present method for estimating strength properties of fasteners based on ISO 8970:1994 suffers from several drawbacks. It aims at determining the characteristic strength for timber with the characteristic density, which is too safe. For Method 1 it is quite difficult to find test specimens with sufficiently low density, and for Method 2 it is not clear which power should be used to correct for variations in density. Both methods are quite dependent on how the specimens are chosen, even though the standard gives no guidance except for the density.

The new ISO 8970:2010 focusses on determining the strength property at the mean value of the density but allows the test specimens to have the same density, so the influence of variation of the density is ignored. This causes unsafe values when estimating the characteristic strength as before using EN 14358.

Instead it is proposed to select test specimens so their densities are evenly distributed over the relevant range of densities, perhaps even requiring that timber from different sources is used. The observed values then have to be corrected to a reference density proposed as 420 kg/m^3 (mean value for C24). The correction should preferably take place using a power c fixed in a standard, but if c is to be determined from the observations, the estimate will be much better when the observations represent a wide range of densities. If fixed values of c are used, they shall of course be identical in the test standards and in Eurocode 5 when the strength for another strength class than C24 is determined by calculation.

There is no single safe choice for c . When shifting to a higher strength class a lower bound is the safe value, but when shifting to a lower class it should be the upper bound. That might be utilized when sufficient information to fix a single value is not available.

When a model for the mean value of the load bearing capacity is established, the parameters including the variation of the model error can be estimated using Annex D in EN 1990. The Annex also offers a method to include the effect of the natural variation of the density (and other parameters such as dimensional tolerances). Simplified equations are presented and their use illustrated for two test series with connector nails.

The examples suggest that the proposed method is quite robust but the selection of test specimens still is important. The characteristic withdrawal strength becomes higher when using the present method but lower if the new ISO 8970 is used together with EN 14358. This is desirable as the old and new ISO 8970 were believed to be too safe and unsafe, respectively.

It is demonstrated that a constant withdrawal strength f_{ax} for different nail lengths can be obtained only if it is determined using a threaded length not including the point. The tests also suggest that the minimum length of threaded nails required by Eurocode 5 should be taken as the real penetration length, not the threaded length as it might be read.

**INTERNATIONAL COUNCIL FOR RESEARCH AND INNOVATION
IN BUILDING AND CONSTRUCTION**

WORKING COMMISSION W18 - TIMBER STRUCTURES

**A NEW METHOD TO DETERMINE SUITABLE SPACINGS AND
DISTANCES FOR SELF-TAPPING SCREWS**

T Uibel

H J Blaß

Timber Structures and Building Construction

Karlsruhe Institute of Technology (KIT)

GERMANY

MEETING FORTY THREE

NELSON

NEW ZEALAND

AUGUST 2010

Presented by T Uibel

B Walford: Did he check crack growth and weathering? T Uibel: No, only cracks due to insertion and short term behaviour were studied.

A Jorissen: Will distances recommendation be made? H Blass: This procedure is already in place in a CUAP for ETAs for self-drilling screws.

P Quenneville: what about multi-screw in a row? T. Uibel: Procedure works also for multiple screws in rows or columns.

S Aicher: Crack growth and in-service crack growth: have you addressed this? H Blass: no, only short term behaviour was studied.

J Schmidt: effect of density? Why results not symmetrical? T. Uibel: density is not known in service. The screw was inserted between the end grain and the second screw.

H Morris: dye in split sample - How is it done? T Uibel: remove screw and insert ink.

S Franke: diagram difference between predicted and actual split. T Uibel: caused by natural variability.

R Harris: EC rule about row screw offset and effect. H Blass: No influence of offset.

R Harris: effect of grain direction - is it investigated? T Uibel: tests were performed with different grain directions. Influence is about 10%.

F Rouger: how to simulate split area? T Uibel: Using springs representing cracking behaviour.

J Munch-Andersen: drilling tips and effect. T Uibel: not significant.

S Winter: good method and danger of providing very detailed spacing recommendations. H Blass: producers want detailed rules for non-pre-drilled screws.

S Aicher: single screw results and offset effect: he recommends offset. H. J. Blass: The offset certainly does not harm and is beneficial for nails and screws in non-predrilled holes.

A New Method to Determine Suitable Spacings and Distances for Self-tapping Screws

T. Uibel, H.J. Blaß

Timber Structures and Building Construction

Karlsruhe Institute of Technology (KIT), Germany

1 Introduction

In recent years self-tapping screws have been increasingly used for connections or reinforcements in timber engineering. Most self-tapping screws can be arranged maintaining only small spacings and distances without risking a consequential splitting failure of the timber member. To avoid significant crack growth and splitting failure minimum values for spacings, end and edge distances as well as for the corresponding minimum timber thickness have to be determined. These requirements are important for the design of joints with self-tapping screws and have to be defined in technical approvals or to be examined regarding structural design codes [1] [2]. Fig. 1 shows typical splitting failure due to too small spacings and distances. The determination of spacing, edge and end distance requirements for self-tapping screws requires numerous and comprehensive insertion tests. Yet the results of such tests cannot be transferred to other types of screws or even to screws of different diameter because of differences in shape or geometry. To reduce the effort of insertion tests a new method was developed which allows the estimation of required spacings, distances and timber thickness.



Fig. 1: Typical splitting failure caused by the insertion of self-tapping screws

2 Conventional insertion tests

Concerning spacing and distance requirements self-tapping screws are usually treated like nails without pre-drilled holes. Often, self-tapping screws may be arranged with smaller spacings, end and edge distances than currently specified in the German design code DIN 1052 [1] or in EN 1995-1-1 [2] without risking a splitting failure. Fig. 2 shows the minimum values which are provided by the German design code DIN 1052 [1]. For many types of self-tapping screws reduced spacings and distances are possible as e.g. for nails with predrilled holes. This particularly depends on the shape of the screw tip and head and on the existence of special features decreasing the torsional resistance to insertion. Fig. 3 shows the great variety of screw tips and heads.

As yet insertion tests (here called “conventional insertion tests”) are carried out in order to determine suitable spacings and distances. For a conventional insertion test the examined self-tapping screw is inserted without pre-drilling as usual in practice. The screw head should be flush with the timber surface. The test specimens have to be made of sawn timber of higher density. After the insertion the crack growth has to be evaluated. To identify possible combinations of spacings, end distances and cross-sections it is necessary to test different configurations iteratively. Table 1 shows the results of 326 conventional insertion tests with five types of self-tapping screws of four manufacturers [3]. The tests were carried out with different configurations so that altogether 1125 screws were used. It was the aim of the tests to determine the minimum timber thickness necessary to avoid undue splitting by arranging the self-tapping screws with the same spacings, end and edge distances as for nails with predrilled holes (last column of the table given in Fig. 2).

Spacing or distance	without predrilled holes ¹⁾		with predrilled holes
	$d < 5 \text{ mm}$	$d \geq 5 \text{ mm}$	
a_1	$(5+5 \cos \alpha) d$	$(5+7 \cos \alpha) d$	$(3+2 \cos \alpha) d$
a_2	$5 d$	$5 d$	$3 d$
$a_{3,t}$	$(7+5 \cos \alpha) d$	$(10+5 \cos \alpha) d$	$(7+5 \cos \alpha) d$
$a_{3,c}$	$7 d$	$10 d$	$7 d$
$a_{4,t}$	$(5+2 \sin \alpha) d$	$(5+5 \sin \alpha) d$	$(3+4 \sin \alpha) d$
$a_{4,c}$	$5 d$	$5 d$	$3 d$

1) for timber of a characteristic density $\rho_k \leq 420 \text{ kg/m}^3$

Fig. 2: Minimum spacings, end and edge distances according to German DIN 1052 [1]



Fig. 3: Different tips and heads of self-tapping screws

The mean density (at normal climate, 20°C/65% RH) of all specimens made of European spruce (*Picea abies*) or fir (*Abies alba*) was $\rho_m = 484 \text{ kg/m}^3$ and the mean moisture content $u_m = 12,0 \%$. The determined minimum timber thickness for each screw type and diameter is given in Table 1. The test results show that the intended spacings and distances are possible for all types of examined self-tapping screws. For some types of screws minor restrictions concerning the end distance $a_{3,c}$ and the spacing a_1 need to be set. The determined corresponding minimum timber thickness is very different depending on the screw type and diameter. The reasons for these discrepancies are differences in screws' geometry or in special features decreasing the torsional resistance e.g. the shape of the screw tips and their effects of pre-drilling. In consequence the results of conventional insertion tests cannot be transferred to other types of screws or even to screws of different diameter. Furthermore the evaluation of insertion tests is ambiguous because it is only based on externally visible cracks. For these reasons the extent of insertion tests and the effort involved in these tests is large.

Table 1: Results of conventional insertion tests with five types of self-tapping screws

Producer / Type	d mm	ρ_{mean} kg/m ³	n_{test}	t_{min} mm		End distance and spacing restrictions
A	5	487	51	24	$4,8 \cdot d$	$a_{3,c} \geq 12 \cdot d; a_1 \geq 5 \cdot d$
A-2	5	483	56	30	$6 \cdot d$	$a_{3,c} \geq 12 \cdot d; a_1 \geq 5 \cdot d$
A	8	477	35	80	$10 \cdot d$	-
A	10	497	12	100	$10 \cdot d$	$a_{3,c} \geq 12 \cdot d; a_1 \geq 5 \cdot d$
A	12	449	42	96	$8 \cdot d$	$a_{3,c} \geq 12 \cdot d; a_1 \geq 5 \cdot d$
B	8	497	13	40	$5 \cdot d$	$a_{3,c} \geq 12 \cdot d; a_1 \geq 5 \cdot d$
C	6	504	51	42	$7 \cdot d$	-
C	8	484	44	64	$8 \cdot d$	-
D	8,9	494	22	127	$14,3 \cdot d$	$a_{3,c} \geq 12 \cdot d; a_1 \geq 5 \cdot d$

3 Test method for determining screw-specific influences

In order to reduce the effort involved in determining suitable spacings, end and edge distances as well as the corresponding timber thickness for self-tapping screws it was the objective of a research project [4] to develop a calculation method which allows an estimation of the splitting behaviour of timber during the insertion process. Therefore the influences which are important for the splitting behaviour have to be taken into account. They may be classified into three groups: Material-specific influences (e.g. wood species, density, width of growth rings and their orientation, moisture content), geometry-specific influences (spacings, end and edge distances in relation to the screw diameter, position and number of screws), fastener-specific influences (e.g. shape of the screw tip, screw head, further features to decrease the torsional resistance). By using a numerical calculation model on the basis of the Finite Element Method almost all of the material-specific and geometry-specific influences on the splitting behaviour can be covered. But so far it is not possible to model the insertion process directly using the Finite Element Method, particularly with regard to the screw-specific influences.

In order to determine the fastener-specific influences on the splitting behaviour a new test method was developed for measuring forces affecting the member perpendicular to the grain during the insertion process [4]. Fig. 4 shows the test set-up. For the test a two-part specimen of solid wood, glued laminated timber or laminated veneer lumber is required.

The two-part specimen is made of one cross-section by sawing it parallel to the grain, as shown in Fig. 5. The two parts of the test specimen are connected with bolts which are used as measuring elements. These measurement bolts are tightened with a defined force. A strain gauge is bonded into a hole drilled at the centre of the measurement bolt. By calibrating the strain gauge bonded in the measurement bolt it is possible to measure axial forces. The examined screw is driven into the interface of the two parts of the test specimen. For the insertion process a screw-testing machine (Fig. 4) is used, so that the rotation speed is constant. Furthermore it is possible to measure the screw insertion moment and to control the penetration depth. The screw is inserted using a template to avoid an inclination of the screw. After the insertion the indentation depth of the root of the screw thread should be similar on both parts of the test specimen, as shown in the example of an opened test specimen in Fig. 5.

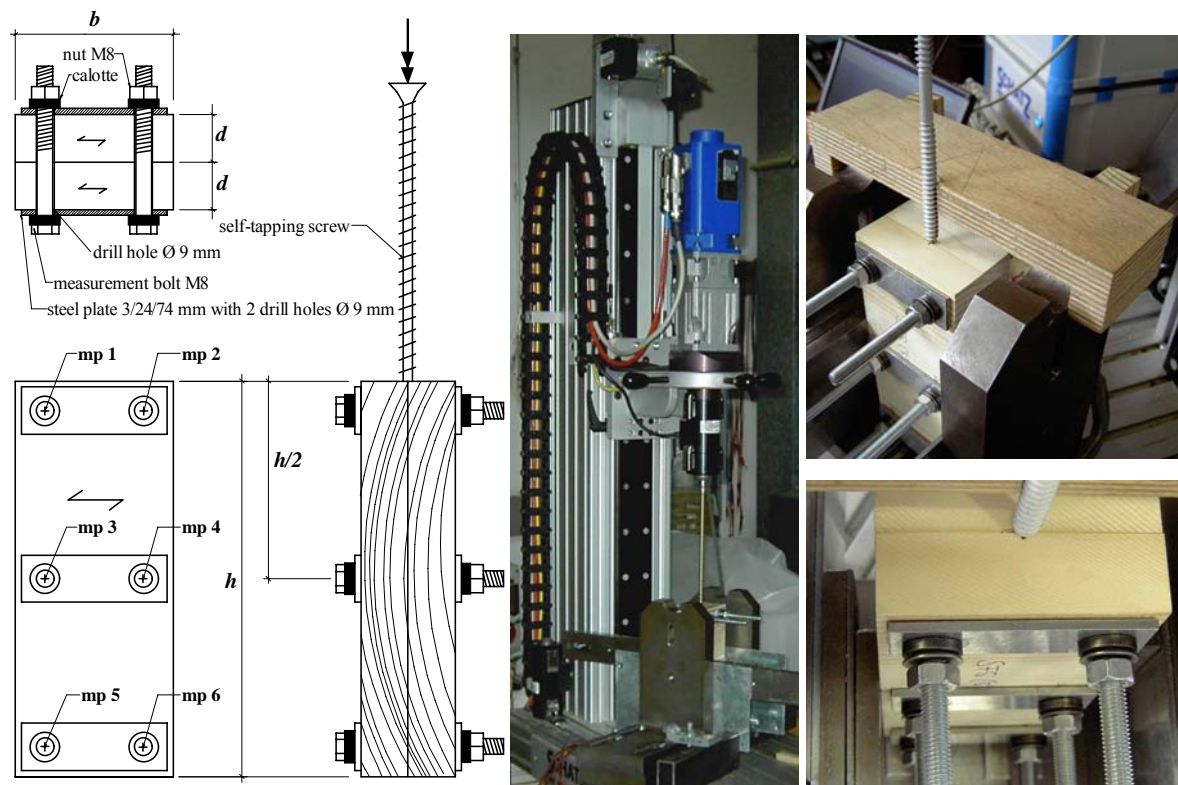


Fig. 4: Test set-up with position of measurement points (mp) 1 to 6

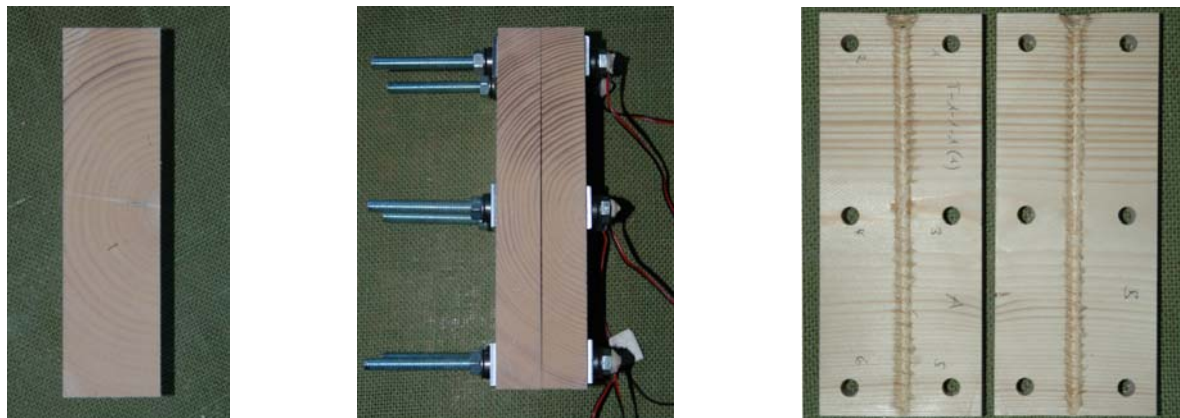


Fig. 5: Two-part test specimen connected with measurement bolts (middle) made of one cross section (left), opened specimen after the test (right)

The test method allows displaying the forces acting on the test specimen, measured at the measuring points, over the penetration depth during the insertion process. The positions of the measurement bolts (measuring points) 1 to 6 are marked in Fig. 4. To compare the splitting behaviour of screws from three manufactures (A, B, C) three test series with altogether 97 tests were carried out. In each series screws of the three different types (A, B, C) with 8.0 x 200 mm in dimension were tested. The parameter of the specimens and the test results are presented in Table 2. It was possible to determine significant force-penetration depth curves for the different types of screw. Fig. 6 shows the results of one test series (series 1). In order to compare the test results directly specimens with the same material properties were used in the different sub-series (e.g. 1-A, 1-B, 1-C). This was realised by using one scantling for the production of several specimens, which were allocated to the different sub-series.

For further comparisons the mean total force $F_{m,tot}$ is defined. This is the sum of all measured forces ($F_{mp,i}$) exerted on the six measurement bolts ($i = 1$ to 6) over the penetration depth (ℓ_{pd}), divided by the nominal screw length ($\ell_{sr,nom}$):

$$F_{m,tot} = \frac{1}{\ell_{sr,nom}} \int_0^{\ell_{pd}} (F_{mp,1}(x) + \dots + F_{mp,i}(x) + \dots + F_{mp,n}(x)) dx \quad \text{in N} \quad (1)$$

with

$F_{m,tot}$ mean total force in N ℓ_{pd} total penetration depth in mm
 $F_{mp,i}$ force at the measuring point i in N $\ell_{sr,nom}$ nominal screw length in mm

Instead of the nominal screw length $\ell_{sr,nom}$ the forces can be set in relation to the real screw length $\ell_{sr,real}$ or the total penetration length ℓ_{pd} .

To facilitate a comparison between the test results of the different series the mean total force for screw type A is used as a reference value, as shown in Table 2. The chosen comparison of indices also allows contrasting the results of the new test method with the minimum timber thickness determined by conventional insertion tests. A visualisation of this comparison is given in the bar chart in Fig. 7. It shows the good correspondence between the results of the two test methods. Thence the method allows a direct evaluation of a screw's effect on the splitting behaviour by comparing it with the results of parallel tests involving reference screws whose influence on the splitting behaviour has already been established.

Table 2: Results of tests with screw types A, B and C, 8.0 x 200 mm, series 1 to 3

Series	Screw type	Number of tests		Specimen dimensions $d/b/h$ mm	ρ_{mean} kg/m ³	$E_{0,\text{dyn},m}$ N/mm ²	Mean total force			Minimum timber thickness	
		absolute	usable				$F_{m,\text{tot}}$ N	CoV %	Index %	t_{\min} mm	Index %
1	A	10	9	24/80/180	453	12511	1646	9,67	100	$10 \cdot d$	100
	B	10	8		454	12659	886	10,0	54	$5 \cdot d$	50
	C	10	7		460	13102	1466	10,9	89	$8 \cdot d$	80
2	A	14	9	24/80/200	378	10249	1003	12,1	100	$10 \cdot d$	100
	B	10	10		391	11195	595	15,8	59	$5 \cdot d$	50
	C	10	10		387	11195	908	11,7	91	$8 \cdot d$	80
3	A	13	6	24/80/200	506	13691	1689	5,49	100	$10 \cdot d$	100
	B	10	7		507	13688	1013	8,06	60	$5 \cdot d$	50
	C	10	8		502	13898	1576	12,5	93	$8 \cdot d$	80
$E_{0,\text{dyn},m}$ Mean value of the dynamic MOE from longitudinal vibration											

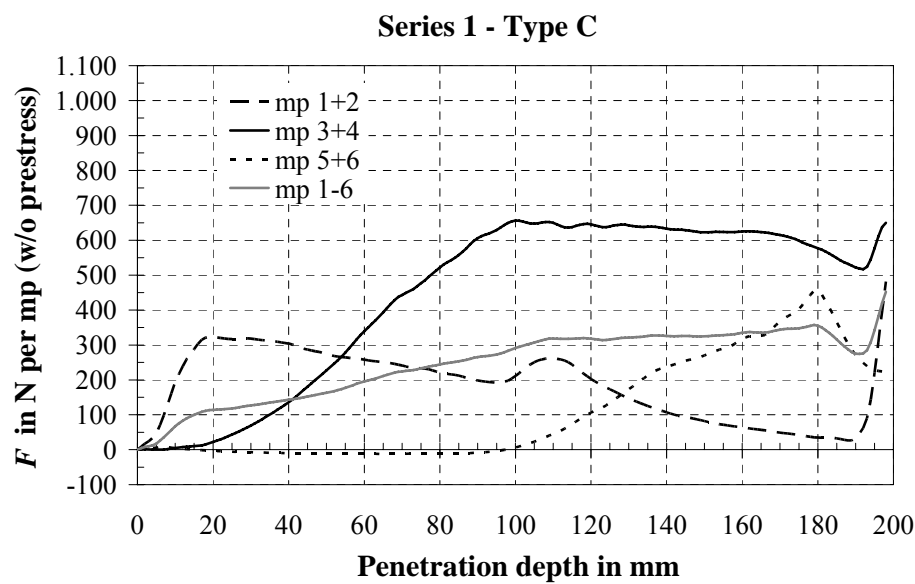
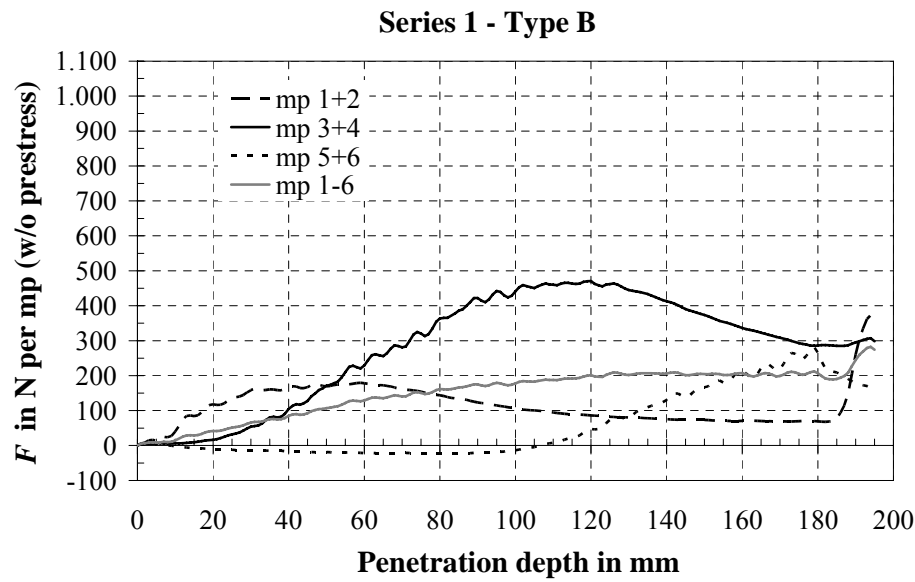
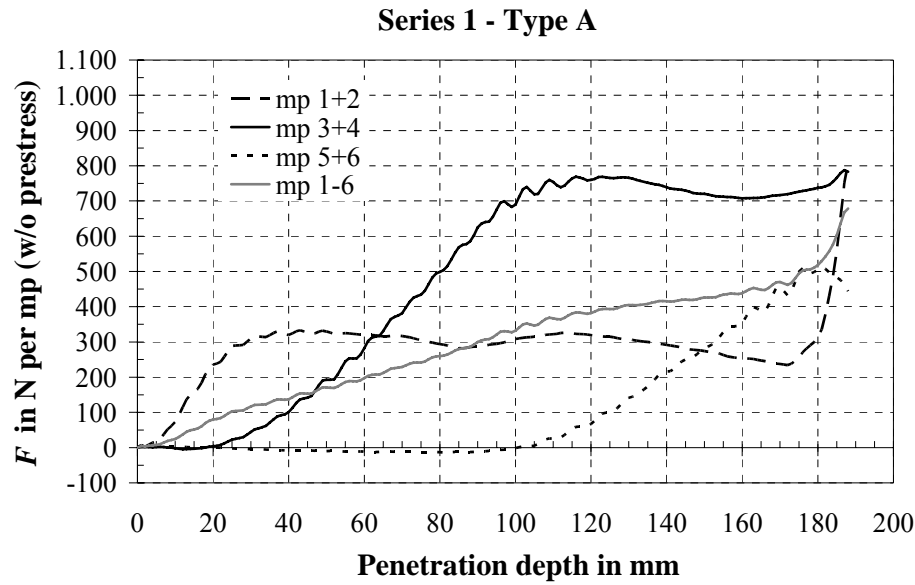


Fig. 6: Forces at the measurement points (mp) over penetration depth for screw types A, B and C, mean values of sub-series (1-A, 1-B, 1-C)

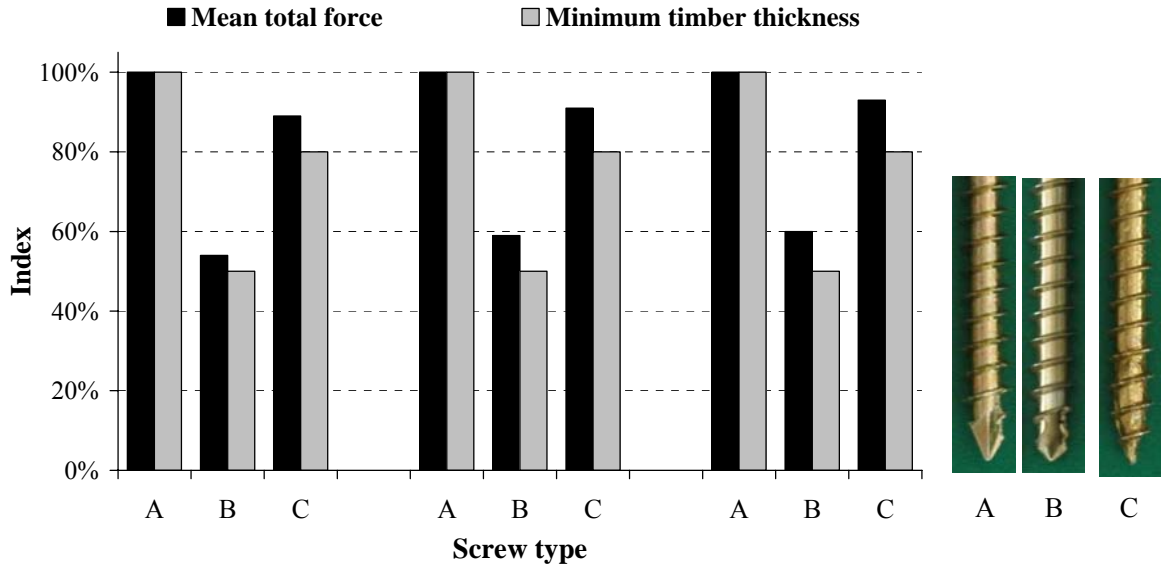


Fig. 7: Bar chart of indices of mean total force $F_{m,tot}$ and minimum timber thickness t_{min} for Series 1 to 3

The following parameters were examined systematically to analyse their influence on the forces acting on the timber during the insertion: geometry of the specimen (width b , height h , depth d as defined in Fig. 5), number of measurement bolts (6, 8, 10), screw length, ratio between screw length and specimen height, insertion speed, pre-stress of measurement bolts. Furthermore the following influences on the splitting forces or mean total forces were the focus of parameter studies: type and diameter of screws, density of the specimen, angle between screw axis and grain direction, angle γ between screw axis and growth ring tangent (Fig. 8) and moisture content of specimen.

The tests performed with specimens of sawn timber are not sufficient to determine the influences of the angle γ between the screw axis and the growth ring tangent. In the case of these specimens the angle γ varied between 0° and 90° depending on the position in specimen height. For an explicit analysis of the influence of γ special specimens of glued laminated timber produced in the laboratory from one lamella (Fig. 8) are used. For these specimens the angle γ is nearly constant over the full height.

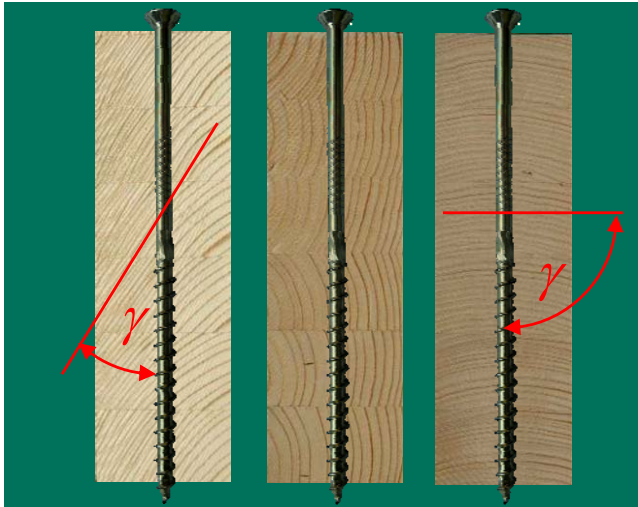


Fig. 8: Specimens to determine the influence of γ

4 Numerical and experimental analysis of split areas

4.1 Numerical model

Knowing the size of the resulting split area is important to evaluate the risk of splitting during the insertion process and hence to determine the required minimum timber thickness and minimum spacings, end and edge distances. Therefore a numerical model was developed to calculate the resulting crack area. For the numerical analysis the finite element program ANSYS 11.0 is used. Taking advantage of the symmetry conditions in the finite element model the timber member is modelled with volume elements. Fig. 9 shows a schematic sketch of the finite element model. In order to model the insertion process an equivalent moving load is used. The tensile strength perpendicular to the grain, which represents a relevant factor for splitting, is simulated by using non-linear spring-elements whose material behaviour was determined on the basis of tests using CT-specimens (Fig. 10) carried out by Schmid [6]. Therefore the tests with CT-specimens were calculated by using a two-dimensional FE model. Because of the symmetry only half the specimen was modelled and the spring elements were placed in the crack area. The parameters of the springs' force-deflection curve were varied until the best fit between test results and FE-calculation of the CT-specimens was reached. Fig. 10 shows a comparison of force-deflection curves of the test and of the FE-calculation for one CT-specimen (Fi02b). Altogether 47 CT-specimen made of *Picea abies* were used to calibrate the spring elements. The calculations resulted in the stress-deflection curve given in Fig. 11.

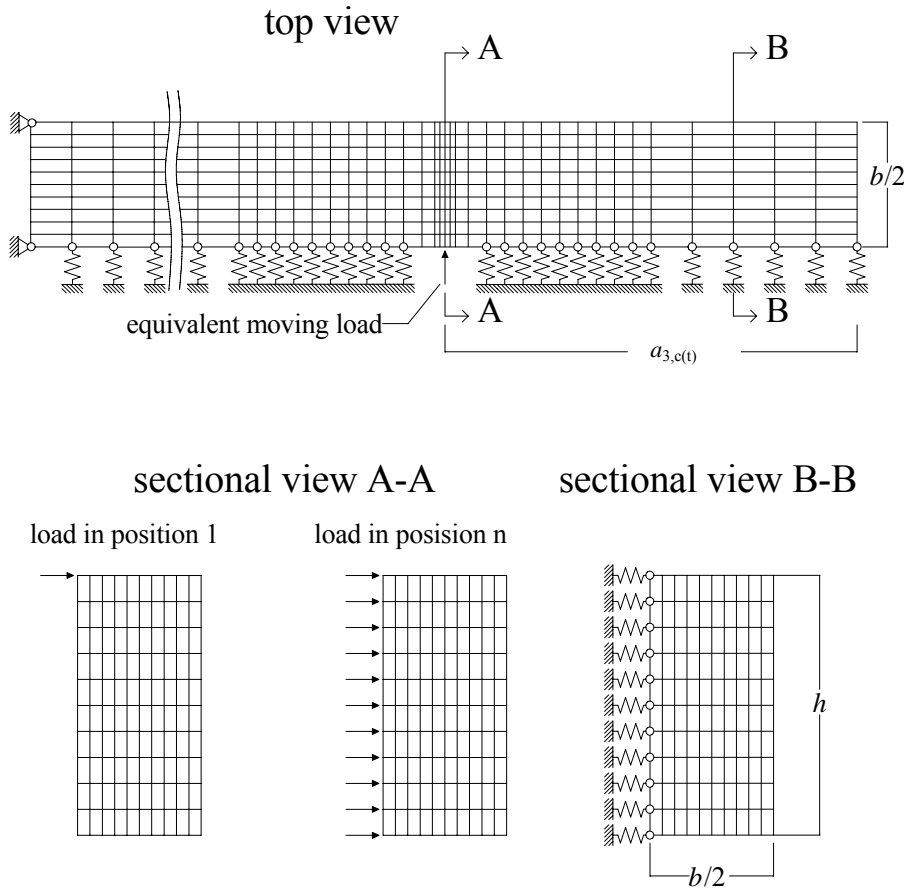


Fig. 9: Schematic sketch of the FE-model used to calculate split areas

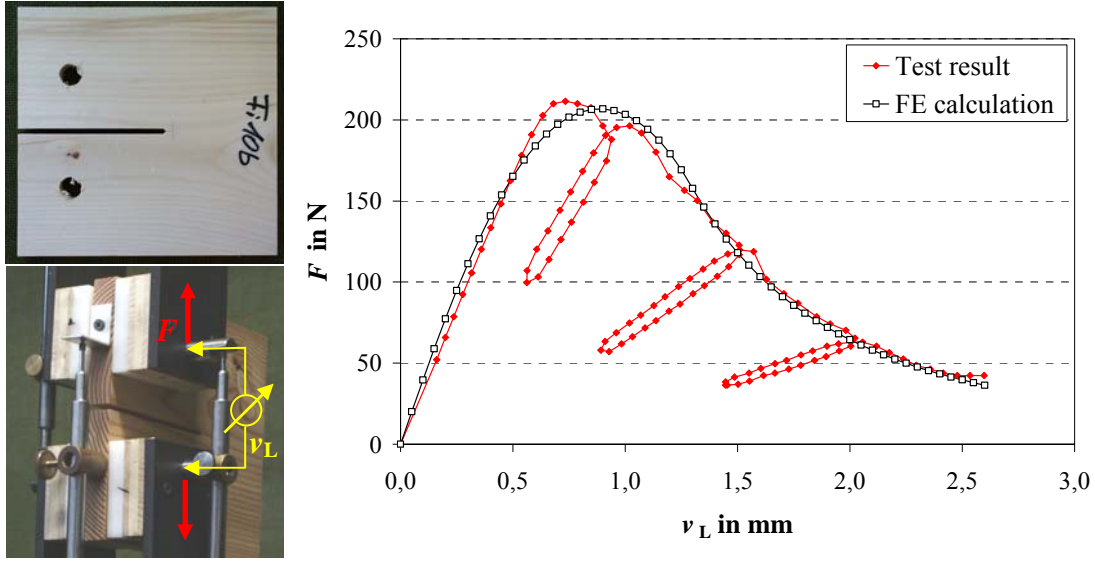


Fig. 10: CT-specimen and test set-up [6] (left), force-deflection curve of one test with a CT-specimen (Fi02b) and of the corresponding calculation

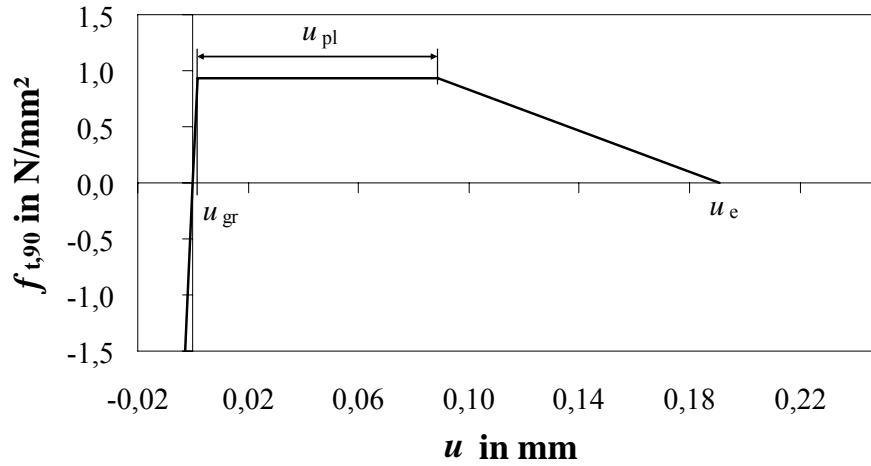


Fig. 11: Stress-deflection curve of the spring elements

4.2 Modelling the insertion process

So far it is not possible to model the insertion process directly using the Finite Element Method. To solve this modelling problem the forces exerted on the timber during the insertion process were meant to be determined on the basis of tests of the new method described in chapter 3. For this purpose the tests are simulated with a three dimensional finite element model. The insertion of the screw is modelled by an equivalent moving load (Fig. 8). This load has to be determined iteratively. Therefore the function of the load $q(x_{sr})$ is varied until the best fit between the force-penetration depth curves of calculations and test results is reached for each pair of measuring points. Fig. 8 (right) shows a comparison between calculated force-penetration depth curves and the test results for measuring points 1 to 6.

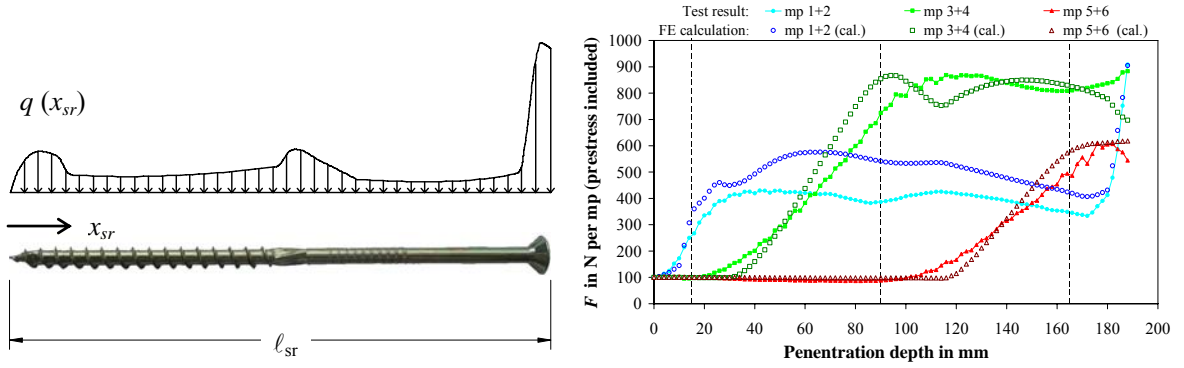


Fig. 12: Schematic representation of an equivalent moving load for screw type C to simulate the insertion process (left) and comparison of calculated force-penetration depth curves and test results for screw type A (right)

4.3 Determining the size of split areas by experimental studies

The calculation model which is used to determine the split areas has to be calibrated and to be verified. To that purpose the cracks were visualized in insertion tests by dyeing the relevant areas. Lau [5] used this method in a similar way for tests with nails. For these tests the screw is driven into and through the timber. The screw should be inserted using a template to avoid an unwanted inclination of the screw. Friction effects reducing the splitting tendency should be eliminated. After the insertion the screw is unscrewed. The screw has produced a hole in the timber. This hole is sealed where the screw tip exits the specimen at the timber surface, e.g. by using a tape. Subsequently a low-viscosity dye is filled into the hole. The dye is distributed by capillary action into the cracks and colours the split area. After the dye has dried, the coloured split areas are made visible by opening the specimens along the split surface. At the opened specimen the size of the split area caused by the insertion of the screw can be quantified e.g. using a digital measuring projector. Fig. 13 shows a typical split image of a specimen with black lines showing the borders of the split area.

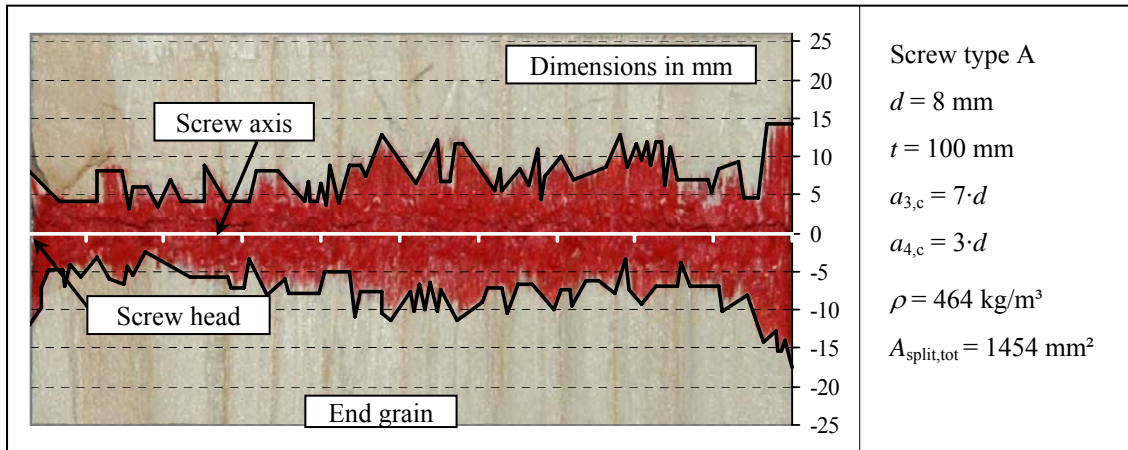


Fig. 13: Opened specimen with red coloured split image, black lines indicating the borders of the split area

4.4 Simulation results and verification

The FE model described in 4.1 is used to calculate the split area for an individual specimen. Therefore it is necessary to adapt the material properties of the volume elements and the spring elements to take into account the specimen's parameters. Additionally the equivalent moving load has to be adjusted. Influences on the equivalent moving load are covered by correction factors:

$$q_{\text{corr}}(x_{\text{Sr}}) = q(x_{\text{Sr}}) \cdot k_{\rho} \cdot k_r \cdot k_{\gamma} \cdot k_{\text{spl}} \quad (2)$$

with

k_{ρ} correction factor for density

k_r correction factor for insertion speed

k_{γ} correction factor for the angle between screw-axis and mean growth ring tangent

k_{spl} split area calibration factor

On the basis of test series with the new test method for screw-specific influences - presented in chapter 3 - it was possible to determine the factors k_{ρ} and k_r :

$$k_{\rho} = \left(\frac{\rho}{\rho_{\text{ref}}} \right)^2 \quad (3)$$

with

ρ density of the specimen in kg/m³

ρ_{ref} density of the specimen used to determine mean total forces in kg/m³

$$k_r = \left(\frac{U}{U_{\text{ref}}} \right)^{0,063} \quad (4)$$

with

U mean insertion speed in rpm,

U_{ref} insertion speed (rpm) at the tests for mean total forces

An exact calculation of k_r is only possible if the rotation speed can be measured e.g. using a screw-testing machine with a known constant and load-independent rotation speed. For customary electric screw drivers the rotation speed under loading is not known and depends on the torsional resistance.

The correction factor for the angle between screw-axis and mean growth ring tangent k_{γ} can be derived by using the special test specimen shown in Fig. 8. As long as k_{γ} is not identified exactly for a screw type by these tests $k_{\gamma} = 1,0$ is assumed.

The factor k_{spl} is used to cover further influences and is determined in the process of the model calibration. For the calibration all known parameters and correction factors are calculated and included in the model. By comparing the calculated split areas with the result of calibration test series the factor k_{spl} is derived. Because of the still existent imprecision of the factors k_r and k_{γ} the correction factors k_r , k_{γ} and k_{spl} were merged to form the factor k_{corr} for the calculations presented here. k_{corr} is determined by using calibration test series as shown in equation (5).

$$k_{\text{corr}} = k_r \cdot k_{\gamma} \cdot k_{\text{spl}} = 1,35 \cdot \left(\frac{\rho_{\text{ref}}}{\rho} \right)^{0,8} \quad (5)$$

With equation (5) the equivalent moving load (2) can be calculated as following:

$$q_{\text{corr}}(x_{\text{Sr}}) = q(x_{\text{Sr}}) \cdot k_p \cdot k_{\text{corr}} \quad (6)$$

Fig. 14 illustrates the resulting split area for one specimen (B.1-01) in comparison to the simulated split area. The results of test and simulation correspond in shape and size.

To verify the calculation model calculated split areas are compared with test results. Fig. 15 shows test results over simulated split areas for three series and three types of screws in each series. The simulated crack areas mostly proved to correspond with the test results.

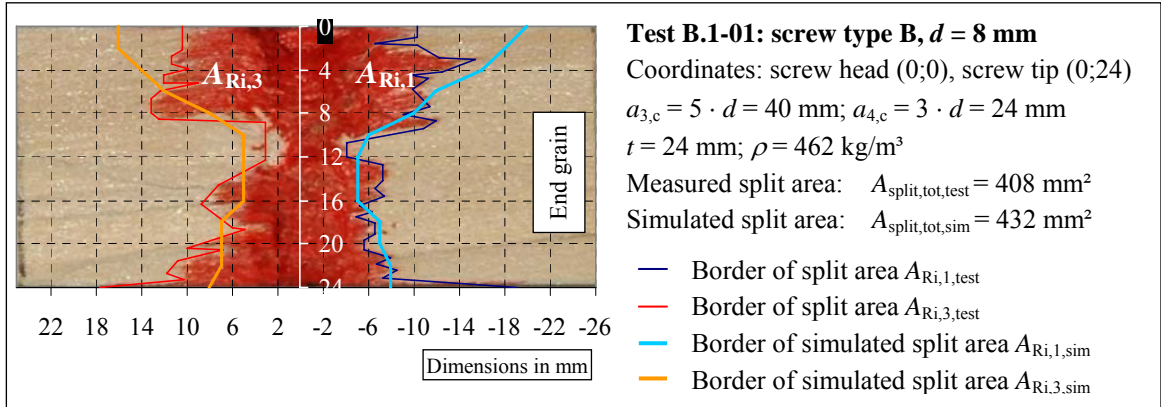


Fig. 14: Split area of test and of calculation for one specimen

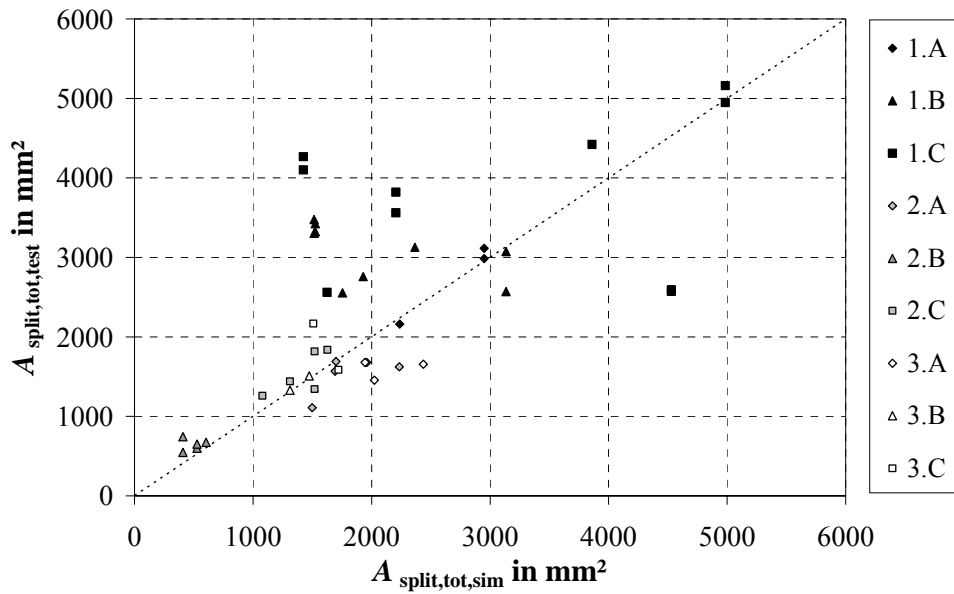


Fig. 15: Measured split areas of tests vs. simulated split areas for nine series

5 Conclusions

To estimate the splitting behaviour of timber during the insertion process a new calculation method was developed. It represents a combination of a FE calculation and a new test method. The FE model allows the calculation of the resulting crack area for screws in different end distances as well as for different cross-sections of timber. In the finite element model the tensile strength perpendicular to the grain that represents a relevant factor for splitting was simulated by using non-linear spring-elements whose material behaviour was determined on the basis of tests using CT specimens.

In order to determine the fastener-specific influences on the splitting behaviour a new test method was developed for measuring forces affecting the member perpendicular to the grain during the insertion process. This method also allows a direct evaluation of a screw's effect on the splitting behaviour by comparing it with the results of parallel tests involving reference screws whose influence on the splitting behaviour has already been established. For the calibration and verification of the model the crack area was visualized in insertion tests by means of dyeing the relevant areas. The simulated crack areas mostly proved to correspond with the test results.

Using the new method reduces the effort of conventional insertion tests and offers a basis for a realistic calculation of the load carrying capacity of joints in the case of failure by splitting.

In the continuation of the research project the parameters influencing the splitting behaviour like e.g. the angle between screw axis and tangent to the annual rings will be determined in greater detail. Besides the influences of the angle between screw axis and grain direction will be examined. In addition, parameters to facilitate the evaluation of the splitting behaviour and their limits (e.g. limits for the dimension of split areas) will be derived.

6 References

- [1] DIN 1052:2008-12: Entwurf, Berechnung und Bemessung von Holzbauwerken – Allgemeine Bemessungsregeln und Bemessungsregeln für den Hochbau
- [2] EN 1995-1-1:2008-09: Eurocode 5: Design of timber structures – Part 1-1: General – Common rules and rules for buildings.
- [3] Blaß H. J., Bejtka I., Uibel T.: Tragfähigkeit von Verbindungen mit selbstbohrenden Holzschrauben mit Vollgewinde. *Karlsruher Berichte zum Ingenieurholzbau*, Band 4, Universitätsverlag Karlsruhe, Germany, 2006
- [4] Blaß H. J., Uibel T.: Spaltversagen von Holz in Verbindungen - Ein Rechenmodell für die Rissbildung beim Eindrehen von Holzschrauben. *Karlsruher Berichte zum Ingenieurholzbau*, Band 12, Universitätsverlag Karlsruhe, Germany, 2009, ISBN 978-3-86644-312-915
- [5] Lau, P.W.C.; Tardiff, Y.: Progress report: Cracks produced by driving nails into wood – effects of wood and nail variables. Forintek Canada Corp., 1987
- [6] Schmid, M.: Anwendung der Bruchmechanik auf Verbindungen mit Holz. Berichte der Versuchsanstalt für Stahl, Holz und Steine, Universität Karlsruhe (TH), Karlsruhe, Germany, 2002.

**INTERNATIONAL COUNCIL FOR RESEARCH AND INNOVATION
IN BUILDING AND CONSTRUCTION**

WORKING COMMISSION W18 - TIMBER STRUCTURES

DEPENDANT VERSUS INDEPENDENT LOADS IN STRUCTURAL DESIGN

T Poutanen

Tampere University of Technology
FINLAND

MEETING FORTY THREE

NELSON

NEW ZEALAND

AUGUST 2010

Presented by T Poutanen

T Poutanen said that there are mistakes in the paper but that the presentation content is correct.

A Buchanan asked whether the author had this discussion about dependant and independent loads with other materials organizations. What was the response? T Poutanen answered he had presented it in May but without response and dialogue.

J Munch-Andersen: I still do not understand that loads are to be dependant on strength. T Poutanen: those do not believe in this can have a look at reliability book and will see that loads are not independent. Loads are dependent on the structure.

T Tannert: if considering loads independent is unsafe, why are we not experiencing more failures? T Poutanen: At most 20% unsafe. Therefore failures are not observe in practice.

S Winter: Will the paper be corrected? T Poutanen: Yes.

Dependant versus independent loads in structural design

T. Poutanen¹

Abstract

In current structural codes loads are sometimes assumed correlated and sometimes non-correlated. Occasionally, when the load includes more than two loads, both assumptions may be applied in the same load combination.

Permanent loads G (e.g. permanent loads of multi storey buildings) are always assumed correlated in the serviceability and in the failure design.

A permanent load and a variable load are always assumed non-correlated in the failure design but correlated in the serviceability design.

Variable loads Q are assumed correlated except in the case of two variable loads where a constant combination factor ψ_0 is applied. This denotes an approximate non-correlated combination as the combination factor ψ_0 is variable.

The current hypothesis is that all loads are non-correlated and combined independently. However, the code literature includes no explanation as to why the loads are often assumed correlated.

This paper establishes that two loads may be correlated or non-correlated. The loads may be proportions of a third load and therefore correlated or correlated for some other reason. On the other hand, most loads are non-correlated.

This paper illustrates that loads are combined dependently in structural design if the strength or deflection constraint is considered and independently if these constraints are not considered.

The author has set out in a previous paper [4] how correlated and non-correlated loads are combined independently. However, the conclusions of the paper [4] are wrongly based on an assumption that all loads are correlated.

A method of combining non-correlated and correlated loads dependently has not previously been published. This paper includes results of a Monte Carlo calculation and concludes that the independent combination seems to be a good and safe approximation to combine dependent loads.

¹ Tampere University of Technology
P.O. Box 600, FIN 33101 Tampere, FINLAND
p: +358408490900, f: +358331152811, e: tuomo.poutanen@tut.fi

1 Introduction

Dependent and independent loads are named in this paper correlated and non-correlated loads to avoid misunderstanding with dependent and independent load combination.

The current structural load combination theory holds that loads are independent, i.e. non-correlated and combined independently. However, in current codes loads are sometimes combined without a combination factor, which corresponds to correlated loads and either a dependent or independent combination. If the load combination includes more than two loads the overall combination may be a mixture of correlated and non-correlated combinations.

If two loads are combined non-correlated, the combination load should include an explicit or an implicit combination factor ψ_0 . If the loads are correlated, no combination factor ψ_0 is applied.

In current codes two permanent loads, G_i and G_j , are always combined without a combination factor denoting that two permanent loads, as well as all permanent loads, are currently calculated correlated.

When one permanent load G and one variable load Q are combined, no combination factor is applied. These loads are assumed correlated in the serviceability state but in the failure state a fictitious combination factor exists as the material safety factors are reduced corresponding to the combination factor ψ_0 i.e. the loads are assumed non-correlated and combined independently.

When two variable loads Q_i and Q_j are combined and if there are two variable loads only, a constant combination factor ψ_0 is applied, i.e. the loads are assumed non-correlated and combined independently in the serviceability and in the failure state. However, the combination is made approximately as the combination factor ψ_0 is variable and depends on the proportion of the combined loads and the current material.

If the action includes more than two variable loads, each added load should have a new combination factor, which is less than the previous one, if the loads are assumed non-correlated. However, in current codes the new added load does not alter the combination factor i.e. the third, the fourth etc. load is assumed correlated.

This paper explains that the loads may be correlated or con-correlated and may be combined regarding or disregarding the constraint of strength or deflection i.e. dependently or independently.

1.1 Probability theory

According to the probability theory events A_1 and A_2 are independent if and only if [3]:

$$P[A_1 \cap A_2] = P[A_1]P[A_2] \quad (1)$$

This is expressed in verbal form as: two distributions, 1 and 2, are independent if a selected value of distribution 1 does not affect the probability of the value of distribution 2.

Assume that distribution 1 is a permanent load and distribution 2 a variable load. Consequently, a value x_1 of the permanent load effects on the probability of x_2 of the variable load as the total load must be less than the strength (or in the serviceability design a

corresponding limit e.g. the deflection); that is, the permanent and the variable loads are not independent i.e. they are dependent.

One may argue against this view, claiming that the loads are independent as the combination defines the constraint. However, this argument means that the strength is infinite during the combination, which is not true. When the loads are combined, a finite constraint exists and the definition of the independent distribution is valid.

1.2 The rule of combining loads

The basic rule in structural engineering to combine loads dictates that the loads must be combined to obtain the maximum load. If the correlation or the combination of the loads is imprecise, the option resulting in a bigger load should be selected. Correlated loads result in a bigger combination load than those non-correlated, and the independent combination results in a bigger load than the dependent combination.

1.3 Monte Carlo

If the Monte Carlo simulation is used to combine two or more loads and corresponding to the quantile of the load, each load i has its free seed number $0 \dots 1$ which is converted to the actual load $0 \dots \infty$ from the selected distribution function and the proportion of the load α_i , it will correspond to non-correlated loads and independent combination and the current load combination hypothesis.

If one seed number is used for all loads, it corresponds to correlated loads and independent combination.

If the loads are non-correlated and combined dependently, the Monte Carlo simulation is modeled as follows: Each load i is given a random seed number between 0 and S_f where S_f is the target survival probability corresponding to the quantile of the load. The related load value is calculated from the actual distribution function resulting in a load between $0 \dots \alpha_i x_{max,i}$, where α_i is the proportion of the load i in the total load and $x_{max,i}$ is the maximum load when the load i acts alone at the target survival probability.

If one seed number $0 \dots S_f$ is given for all loads, it corresponds to correlated loads and dependent combination.

2 Options

There are four options to combine loads in structural design:

1. The current theory assumes that the loads are non-correlated and combined independently. Such combination is an unambiguous abstraction defined by the convolution equation and has been disclosed in detail e.g. in an earlier paper by the author [4].
2. If non-correlated loads are combined dependently, a method to combine these loads has not yet been published. Some Monte Carlo results presented in this paper show that the independent combination seems to be a good and safe approximation.
3. Some loads in structural design are correlated. They may be proportions of another load or are correlated for some other reason, e.g. the loads may be equal. These loads are combined in an opposite way as they are divided: the combination quantile is obtained by adding up the partial quantiles. This combination method is referred to here as “the quantile sum method”. These loads follow the same distribution function and

do not cross (or cross in the infinity).

If this combination method is applied to two distributions, which cross, and the distributions are combined in proportions α and $1 - \alpha$, $\alpha = 0 \dots 1$, the combination distribution of the proportion loads crosses the crossing point of the partial distributions in all proportions of α .

The quantile sum method is difficult to calculate, and thus we can use an alternative simpler method here called “the crossing point method”. This method has been explained in the author’s earlier paper [4]. The main idea of this method is that the loads are combined by using the convolution equation, but the deviation is changed to make the combination distribution cross the crossing point of the partial distributions. The quantile sum method and the crossing point method obtain equal results if the partial distributions relate to the normal distribution function. If the distribution functions are other than normal, the methods deviate slightly, e.g. if one load follows normal distribution and the other gumbel, the maximum deviation is less than 1.5 %. From the actual design point of view both methods may be considered equal and called “correlated independent combination”.

4. Correlated loads may also be combined dependently. Such a combination method has never before been published. This paper includes some Monte Carlo results and concludes that the independent combination is a good and safe approximation.

There may also be other options e.g. some loads may fall between options 2 and 3, i.e. the correlation between the loads lies between 0 and 1. If such loads exist, surveillance data should confirm the correlation. As the correlation data is missing, the assumption of non-correlated and correlated loads as explained above is feasible.

3 Correlated loads

Some loads in structural design are correlated as they are proportions of another load or the loads are correlated due to other reasons. The loads are combined simply by adding up the characteristic or design values without combination factors. This can be demonstrated by use of an example:

Assume a brick has a normal permanent load distribution of $N(x, \mu, \sigma) = N(x, 1, 0.1)$ and it is divided into two equal parts. Thus, either part has the distribution of $N(x, 0.5, 0.05)$. Assume there is an ideal adhesive to glue the parts to attain the original brick. It is obvious that the combination of the parts is equal to the distribution of the undivided brick. If the parts are combined according to correlated distributions, the original combination is obtained, and if combined non-correlated the distribution is $N(x, 1, 0.071)$.

This example is analogous to the loads of structural design. The snow load of a roof girder, for instance, can be divided into two parts acting on the right and the left side of the girder. According to the example, these loads must be combined correlated.

In the author’s view, the example is analogous to the imposed loads of a multi storey building too, as the loads on the floors are proportions of the total imposed load on the house. Regardless of whether the loads are distributed to the floors randomly, the loads are correlated and combined without combination factors. The total load acting on the vertical supporting structures on the first floor is the total imposed load on the house. The current codes apply in this case a combination factor ψ_0 , which is incorrect.

Permanent loads of a multi storey house are combined without the combination factor ψ_0 in current codes. These loads are correlated, or at least nearly correlated, as they are the same loads. When one load has a high value all others have the same or at least ap-

proximately the same high value as the values arise from the same origin. These loads are combined correctly, i.e. without a combination factor ψ_0 , in current codes.

4 Non-correlated loads

Most loads in structural design are non-correlated. As will be demonstrated later, the independent load combination is a good and safe approximation in combining such loads.

5 Demonstration

Four options – independent and dependent combination with correlated and non-correlated loads – to combine loads are demonstrated adapted to the current eurocode with the subsequent basis:

- the design point is set at unity
- permanent load G and variable load Q is combined in the proportion 0.3/0.7, $\alpha = 0.7$, i.e. the combination load includes 30 % G and 70 % Q
- target reliability is $\beta = 3.826$, corresponding to survival probability $S_f = 0.99993496$
- coefficient of variation of G is $V_G = 0.0915$ (corresponding to $\gamma_M = 1.35$, $\beta = 3.826$, $V_M = 0$) safety factor is $\gamma_G = 1.35$, design point value is $d_G = 0.5$
- coefficient of variation of Q is $V_Q = 0.4$, safety factor is $\gamma_Q = 1.5$, design point value is $d_Q = 0.98$ i.e. it is so called “50-year value”
- coefficient of variation of material M is $V_M = 0.2$, (the material is e.g. glue lam), design point value is $d_M = 0.05$

The calculation results are presented in Table 1.

Table 1 Material safety factors γ_M calculated for the eurocode load combination $\alpha = 0.7$ (variable load 70 % of the total) in four ways: $\gamma_{M,ND}$ = Monte Carlo calculation of non-correlated dependent loads, $\gamma_{M,NI}$ = non-correlated and independent calculation according to current hypothesis, $\gamma_{M,CI}$ = correlated and independent calculation, $\gamma_{M,CD}$ = correlated and dependent calculation

Coefficient of variation V_M	Material safety factor			
	$\gamma_{M,ND}$	$\gamma_{M,NI}$	$\gamma_{M,CI}$	$\gamma_{M,CD}$
0.1	0.97	1.002	1.078	1.04
0.2	1.01	1.024	1.092	1.07
0.3	1.12	1.127	1.188	1.17

The Monte Carlo values of Table 1 has been calculated assuming that the load case $\alpha = 0.7$ has the target reliability, $\beta = 3.826$. This is not precisely true in the current eurocode as $\gamma_Q = 1.5$ corresponds to less reliability than the target. Therefore the Monte Carlo values are inexact. We see in this Table that the material safety factors calculated by using the Monte Carlo method dependently are almost the same, ca 1...3 % less, as the values calculated independently i.e. the independent calculation seems to be a feasible and safe method to combine loads in structural design.

Correlated loads result in ca 7 % higher values than those non-correlated.

The calculation result is also presented in Figure 1 where the lines are drawn as follows:

- permanent load G at the serviceability state with 0.5 value at the design point: solid black line
- permanent load G at the failure state i.e. $G/1.35$: solid thick black line
- proportion load of the permanent load G at the failure state i.e. $0.3G/1.35$: dash-dot black line
- variable load Q at the serviceability state with 0.98 value at the design point: dashed red line
- variable load Q at the failure state i.e. $Q/1.5$: dashed thick red line
- proportion load of the variable load Q at the failure state i.e. $0.7Q/1.5$: dash-dot red line
- material property M at the serviceability state with 0.05 value at the design point: dash-dot blue line
- material property M at the failure state derived by using the Monte Carlo method calculated dependently and non-correlated i.e. $1.01M$, dash-dot thick blue line
- material property M at the failure state calculated independently and non-correlated according to the current theory i.e. $1.024M$, solid blue line
- material property M at the failure state calculated dependently and correlated i.e. $1.07M$, dashed blue line
- material property M at the failure state calculated independently and correlated i.e. $1.092M$, dotted blue line
- combination load GQ_i of $0.3G/1.35$ and $0.7Q/1.5$ calculated non-correlated and independently according to the current hypothesis: solid brown line
- combination load GQ_d of $0.3G/1.35$ and $0.7Q/1.5$ calculated correlated and independently: dotted brown line

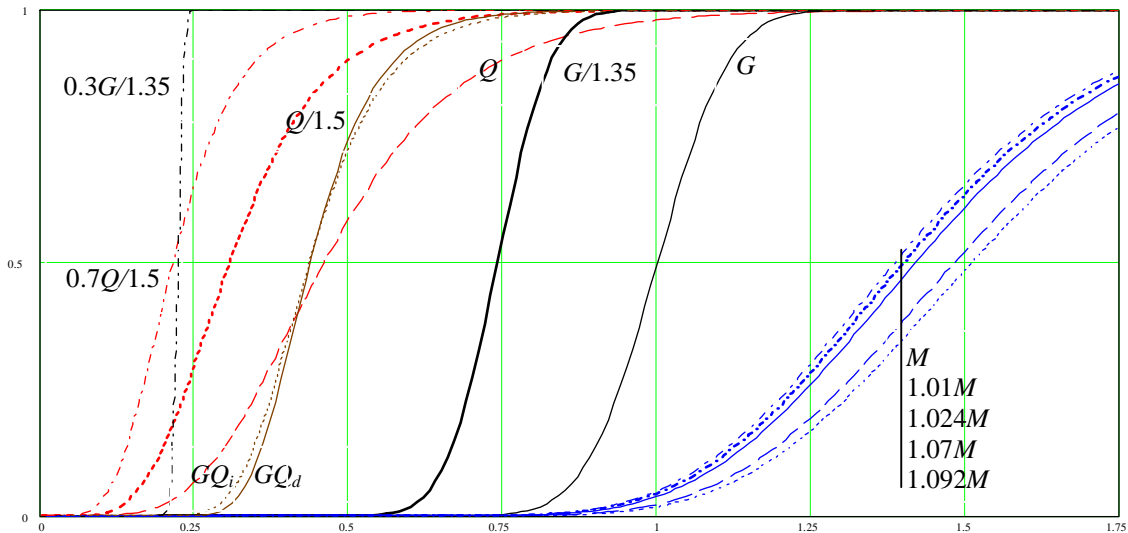


Figure 1 Demonstration of independent/dependent correlated/non-correlated load combination 30 % permanent load 70 % variable load of the eurocode, load-material property at the horizontal axis, cumulative frequency at the vertical axis.

6 Discussion

As seen in Table 1 the Monte Carlo calculation for dependent combination and the independent calculation deviates slightly, 1...3 % with independent calculation being safe. Therefore we may consider the independent calculation feasible to combine loads.

The eurocode includes combination rules 6.10a,b and 6.10a,mod which come from independent load combination and denote a fictitious combination factor ψ_0 . These combination rules are questionable and in the author's view wrong, at least in some cases, as they denote a second consideration of independent loads after considering them first when defining material safety factors i.e. the combination factor ψ_0 is considered twice: The Finnish eurocode has the material safety factor for steel $\gamma_M = 1$. This safety factor is at least almost correct, if the combination rule 6.10 is used, but with rule 6.10a,mod, the factor $\gamma_M = 1$ is unsafe in comparison with the target reliability.

The correlated and independent load combination is simple and safe, and therefore we may investigate as to if this method can be used to simplify the codes.

The eurocode is rather complicated even if it includes a rather significant reliability error i.e. the excess safety margin is ca 65 % in some load cases. This error can be mainly attributed to two factors: material safety factors are constant i.e. not dependent on the load proportion of the permanent and variable load and the design point value of the variable load is constant i.e. not dependent on the coefficient of variation of the variable load. Various options to simplify the code and improve its accuracy may be clarified as follows:

An easy way to make the code simpler is to delete the load factors i.e. set $\gamma_G = \gamma_Q = 1$. There are several alternative methods to achieve this.

- Firstly, we may increase characteristic variable load values in the load tables by 11 % ($1.5/1.35 = 1.11$) when the material safety factor γ_Q becomes 1.35 i.e. the same as γ_G . Then we may divide the design equation by 1.35 when the $\gamma_G = \gamma_Q = 1$ state is obtained. This option corresponds to changing the characteristic variable load to a 103-year load from the 50-year load. This method needs no other changes to the code. The design results are precisely the same as in the current eurocode.
- The second method is to make the material safety factors variable and dependent on the load proportion of variable load to all loads α . The current eurocode is based on $\gamma_G = 1.35$, $\gamma_Q = 1.5$, γ_M . Precisely equal calculation results are obtained if the calculation is based on $\gamma_G = 1$, $\gamma_Q = 1$, $\gamma_{MM} = 1.35(1 + 0.15\alpha)\gamma_M$, where γ_{MM} is a modified material safety factor corresponding to $\gamma_G = \gamma_Q = 1$.
- The third method is to set $\gamma_G = \gamma_Q = 1$ and calculate γ_M -factors accordingly. Load tables and all other factors are kept intact. The overall accuracy remains unchanged and the calculation results are approximately equal to results obtained by using the current eurocode but the accuracy of the steel design is decreased somewhat and the design accuracy of all other materials is increased.

If the γ_M -factors are made variable the calculation accuracy increases by ca 20 % and all materials have about equal design accuracy. The design work does not increase significantly as in all cases of glue lam and concrete, $V_Q \approx 0.2$, γ_M -factors are constant in all load cases. γ_M -factors are also constant in all cases of sawn timber $V_Q \approx 0.3$ when $\alpha > \approx 0.5$ i.e. in all normal cases. The design work increases only in some cases when designing steel $V_Q \approx 0.1$, as the γ_M -factor depends on the load proportion when $\alpha > \approx 0.5$.

The third option to make the code more accurate is to make the design point value d_p of the variable load variable. The coefficient of variation of the variable load V_Q fluctuates from ca 0.2 to ca 0.5 but the current eurocode is based on a constant value ca 0.4 and $d_p = 0.98$. If the design point value were set variable $d_p = 0.96 \dots 0.98$, the calculation of $V_Q = 0.2$ loads would be much more accurate. The design work would not increase. The only change would be to adjust the load tables for variable loads with $V_Q < 0.4$.

These options would decrease the greatest excess safety of the current eurocode from ca 65 % to less than 15 %.

If the combination factors ψ_0 were deleted it would simplify calculation considerably. The excess reliability due to this reason would normally be less than 5 % but in an extreme case, e.g. with low permanent load and equal wind and snow load, up to ca 20 %. Such load cases are rare and the excess reliability is tolerable. Therefore the option $\psi_0 = 1$ is feasible. The approximation $\psi_0 = 1$ allows us to simplify the code further and disregard some minor load cases e.g. wind friction.

If $\psi_0 = 1$ option is selected, the permanent and the variable load should be combined non-correlated as this combination does not increase the design work.

7 Conclusion

The current practice in combining loads is inconsistent as it does not differentiate between correlated and non-correlated loads and assumes all loads to be non-correlated.

Some loads, e.g. the permanent and live loads of multi storey buildings, are correlated and these loads should be combined without a combination factor ψ_0 . Live loads are combined currently with a combination factor i.e. wrongly according to this study, but permanent loads are combined without a combination factor i.e. correctly.

Loads may be combined dependently or independently. Independent combination results in a bigger load and therefore this method should be used in structural design.

If the eurocode is changed to apply correlated and independent load combination i.e. $\psi_0 = 1$ and at the same time subsequently changed, load safety factors are deleted, i.e. $\gamma_G = \gamma_Q = 1$, material safety factors are made variable, design point values of variable load are made variable, the overall accuracy i.e. the maximum excess reliability, would be less than in the current eurocode with less design work.

Literature

- [1] EN 1990:2002 Eurocode – Basis of structural design
- [2] Gulvanessian H., Calgaro J-A., Holicky M., Designer's Guide to EN 1990, Eurocode: Basis of structural design, Thomas Telford Publishing Ltd, London 2002
- [3] Milton J., S, Arnold J., C., Introduction to probability and statistics: principles and applications for engineering and the computing sciences, 3rd ed, New York: McGraw-Hill, 1995
- [4] Poutanen T., Safety factors and design codes, Joint IABSE – fib Conference, Dubrovnik, Croatia, May 3-5, 2010